Research reactor core conversion guidebook

Volume 2: Analysis
(Appendices A–F)

INTERNATIONAL ATOMIC ENERGY AGENCY

FOREWORD

In view of the proliferation concerns caused by the use of highly enriched uranium (HEU) and in anticipation that the supply of HEU to research and test reactors will be more restricted in the future, this guidebook has been prepared to assist research reactor operators in addressing the safety and licensing issues for conversion of their reactor cores from the use of HEU fuel to the use of low enriched uranium (LEU) fuel.

Two previous guidebooks on research reactor core conversion have been published by the IAEA. The first guidebook (IAEA-TECDOC-233) addressed feasibility studies and fuel development potential for light-water-moderated research reactors and the second guidebook (IAEA-TECDOC-324) addressed these topics for heavy-water-moderated research reactors. This guidebook, in five volumes, addresses the effects of changes in the safety-related parameters of mixed cores and the converted core. It provides an information base which should enable the appropriate approvals processes for implementation of a specific conversion proposal, whether for a light or for a heavy water moderated research reactor, to be greatly facilitated.

This guidebook has been prepared and coordinated by the International Atomic Energy Agency, with contributions volunteered by different organizations. The IAEA is grateful for these contributions and thanks the experts from the various organizations for preparing the detailed investigations and for evaluating and summarizing the results.

EDITORIAL NOTE

PLEASE BE AWARE THAT
ALL OF THE MISSING PAGES IN THIS DOCUMENT
WERE ORIGINALLY BLANK

PREFACE

Volume 2 consists of detailed Appendices A-F. Summaries of these appendices can be found in Chapters 2-6 of Volume 1 (SUMMARY) of this guidebook. Included in Volume 2 are example analyses and results for cores with HEU and LEU fuels showing differences that can be expected in the safety parameters and radiological consequences of postulated accidents. Also discussed are methods for preventing loss-of-coolant accidents. There are seven examples of licensing documents related to core conversion and two examples of methods for determining power limits for safety specifications.

The topics which are addressed in Volume 2, the appendices in which detailed information can be found, and the summary chapters in Volume 1 are listed below.

Topic	VOLUME 2 APPENDIX	VOLUME 1 SUMMARY Chapter
Safety Analyses for Generic 10 MW Reactor	A	2
Safety Analysis - Probabilistic Methods	B	2
Methods for Preventing LOCA	C	3
Radiological Consequence Analyses	D	4
Examples of Safety Report Amendments	E	5
Safety Specifications	F	6

CONTRIBUTING ORGANIZATIONS

Argonne National Laboratory	ANL	United States of America
Athens Univ. of Agr. Sciences - Physics Lab.	P.L. AUAS	Greece
Atomic Energy Research Establishment	HARWELL	United Kingdom
Australian Atomic Energy Commission	AAEC	Australia
Chalk River Nuclear Laboratories	CRNL	Canada
Commissariat a l'Energie Atomique	CEA	France
Eidg. Institut für Reaktorforschung	EIR	Switzerland
GA Technologies Inc.	GA	United States of America
GEC Energy Systems, Ltd.	GEC	United Kingdom
GKSS-Forschungszentrum Geesthacht GmbH	GKSS	Federal Republic of Germany
Greek Atomic Energy Commission	GAEC	Greece
Internationale Atomreaktorbau GmbH	INTERATOM	Federal Republic of Germany
Japan Atomic Energy Research Institute	JAERI	Japan
Joint Research Centre - Petten Establishment	JRC - Petten	Netherlands
Kyoto University Research Reactor Institute	KURRI	Japan
Netherlands Energy Research Foundation	ECN	Netherlands
Oak Ridge National Laboratory	ORNL	United States of America
Safety and Reliability Directorate-UKAEA	SRD-UKAEA	United Kingdom
University of Michigan - Ford Nuclear Reactor	FNR	United States of America

CONTENTS

APPENDIX E. EXAMPLES OF SAFETY REPORT AMENDMENTS

APPENDIX F. SAFETY SPECIFICATIONS

Appendix A

SAFETY ANALYSES
FOR GENERIC 10 MW REACTOR

Abstract

Typical safety analyses are provided for conversion of a
generic 10 MW reactor from plate-type HEU fuel to both
plate-type (U_3Si_2-Al and U_3O_8-Al) LEU fuel and rod-type
(UZrH) LEU fuel.

Equilibrium cores and HEU-LEU transition cores are studied
with plate-type fuel and a fresh core is studied with rod-
type fuel. The safety parameters analyzed include power
peaking, thermal-hydraulic safety margins, control rod
worths, shutdown margins, and several types of transients.

All of the safety margins studied are shown to be fully
satisfactory to ensure the safety of the facility in each
case.

Appendix A-1

SAFETY ANALYSES FOR THE IAEA GENERIC 10 MW REACTOR

INTERATOM*
Bergisch Gladbach,
Federal Republic of Germany

Abstract

Design criteria, thermal-hydraulic performance, and selected safety analyses are provided for conversion of the IAEA generic 10 MW reactor from HEU to LEU fuel. The LEU fuel element design that was studied contains 20 plates with 1.0 mm thick U_3O_8-Al fuel meat, a uranium density of 3.0 g/cm^3, and 446 g ^{235}U. Detailed results are also provided for the transition phase from HEU to LEU fuel (mixed cores) based on specific safety criteria.

Basis of Calculations

According to the agreement of the advisory group the investigations of the safety aspects should be based on the generic 10-MW-Core of the first IAEA Guidebook (IAEA-TECDOC-233). Within the German contribution to this Guidebook there exist only conversion calculations with MEU-fuel. So in the first step a suitable LEU-fuel for the HEU→ LEU-conversion of the 10-MW-Core has to be determined.

On basis of the criterion to have the same percentage of loss of U-235 in the core at the begin of cycle (BOC) as well as at the end of cycle (EOC) we found the restriction to a maximum meat thickness of 1 mm the following specifications of the LEU-fuel. (All geometrical values of the element which are neglected are the same as for the HEU-fuel; see also fig. 1.)

Enrichment	19.75	w/o
Plate Thickness	1.76	mm (inner)
	1.99	mm (outer)
Water Channel Thickness	2.217	mm
Meat Thickness	1.0	mm
Plates/Standard Fuel Element	20	
Plates/Control Element	14	
Fuel	U_3O_8-Al	
U-Density	3.0	g/cm^3
U-235-Loading/FE	446	g
U-235-Loading/CE	312.2	g

---

20 plates

cladding thickness: inner plates: .38
                    outer plates: .495
          Uran Density/Meat 3.0g/cm³

meat thickness: 1.0

all dimensions in mm
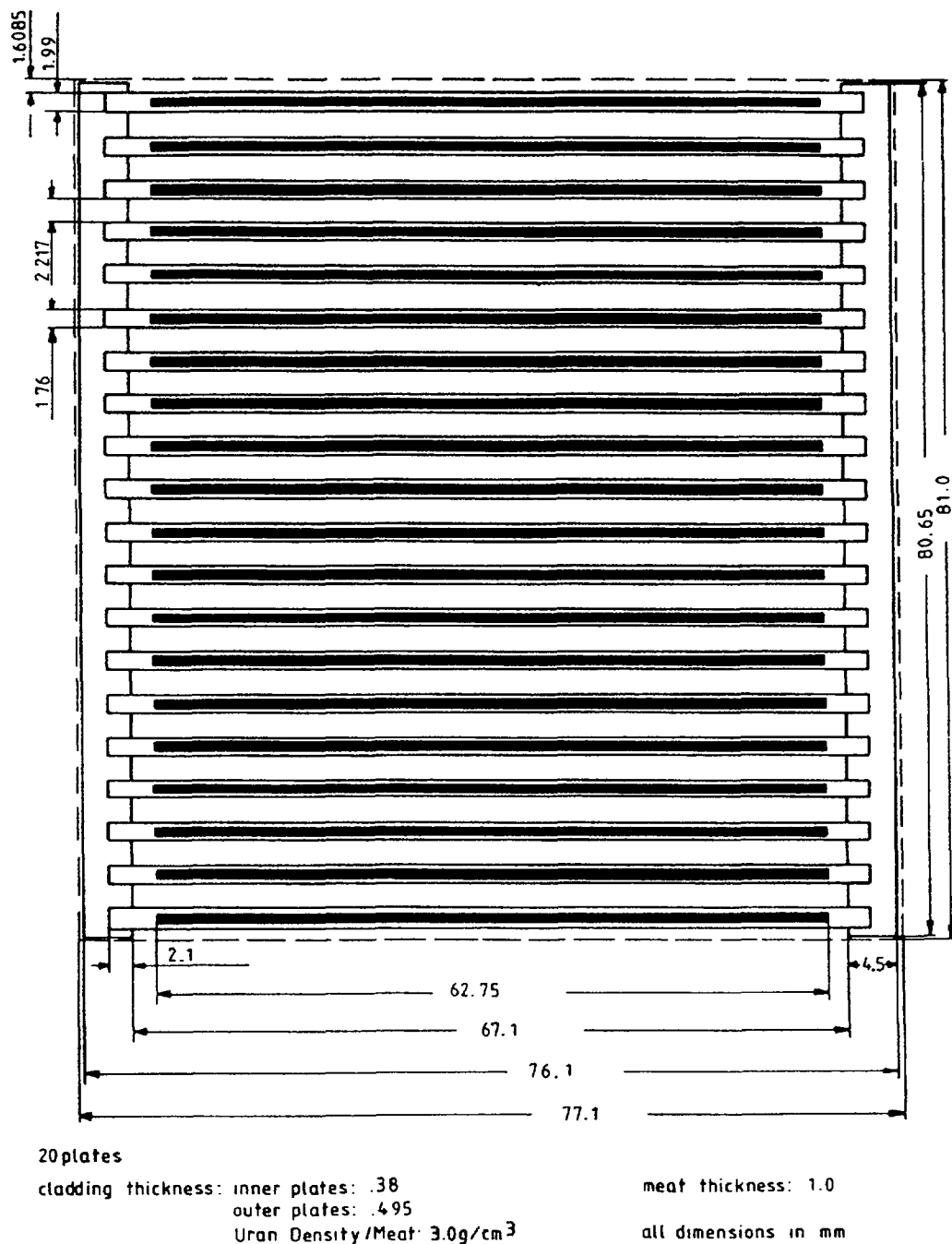
FIG. 1. Fuel element cross-section for LEU fuel (^{235}U loading 446g).

Figure 1 presents a horizontal section of the fuel element with LEU-fuel. It should be mentioned here, that the restriction to 1 mm meat thickness is according to the fuel development program in Germany, the so-called AF-Program.

The core set-up, i. e. specifically the distribution of the different burn-ups within the core area is presented in fig. 2. The upper part gives the status BOC, the lower the status EOC. The average burn-ups are at BOC 24 % and at EOC 36 %. The burn-up step of the cycle is 12 % loss of U-235, which corresponds to a cycle length of 118 FPD. The reactivity behaviour of the core during the equilibrium cycle is given

HEU-Fuel BOC

C	C	C	C	C	C
0	24	0	36	12	0
12	36	48	48	36	12
24	48	48	◯	36	24
0	24	48	48	24	12
◯	0	12	36	24	0
C	C	C	C	C	C

LEU-Fuel BOC

C	C	C	C	C	C
0	24	0	36	12	0
12	36	48	48	36	12
24	48	48	◯	36	24
0	24	48	48	24	12
◯	0	12	36	24	0
C	C	C	C	C	C

HEU-Fuel EOC

C	C	C	C	C	C
10.8	34.5	16.2	46.7	23.3	10.5
23.8	47.5	59.7	61.3	48.9	23.8
35.5	59.8	62.5	◯	50.4	35.4
12.9	36.1	59.3	60.9	38.2	23.6
◯	12.9	25.8	46.3	34.0	10.3
C	C	C	C	C	C

LEU-Fuel EOC

C	C	C	C	C	C
11.1	34.1	16.8	46.4	23.1	11.2
23.6	46.5	57.7	61.0	49.2	24.1
35.5	59.6	62.0	◯	50.6	35.6
13.6	35.3	58.4	60.8	38.6	24.1
◯	13.6	26.6	46.1	33.9	11.0
C	C	C	C	C	C

FIG. 2. 10 MW generic core — burnup distributions.

by fig. 3, which compares the HEU-fuel and the LEU-fuel during the cycle with each other. With these specifications the basis for all the following calculations is defined.

Results

Basic Evaluation of the Thermal-Hydraulic Performace of HEU- and LEU-Core

The thermal-hydraulic performance has been examined for the proposed core design. The safety margins against the occurence of excursive flow instability were determined on the basis of the data specified in Table 1 for steady state operation.

The commonly accepted design criterion for research reactors of the MTR-type is the phenomenon of excursive flow instability. Numerous experiments at conditions typical for this type of

13
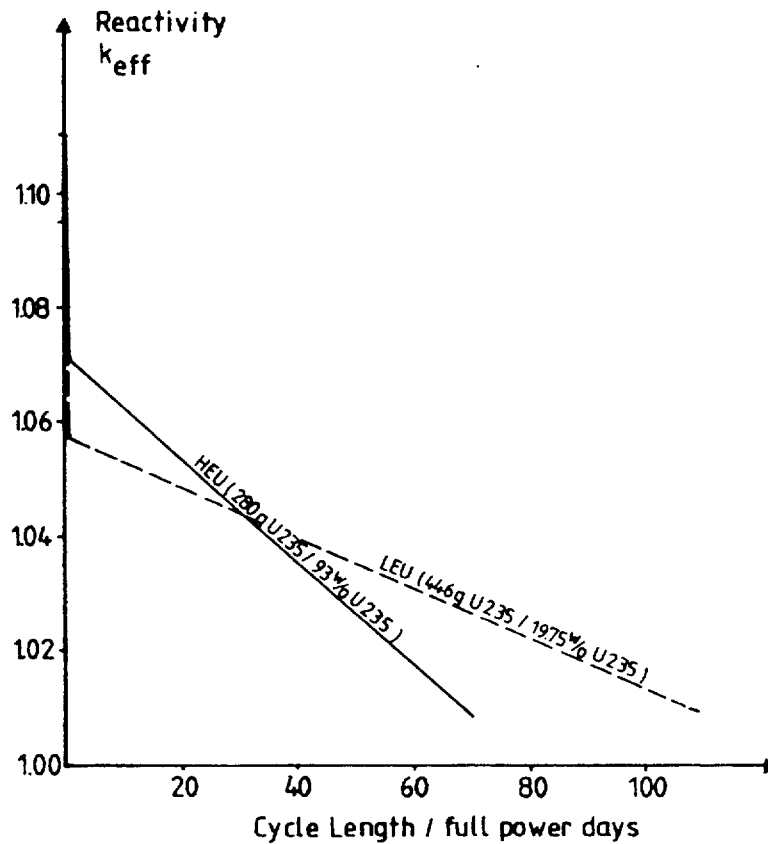
FIG. 3. 10 MW generic core — reactivity vs cycle length.

Table 1: Comparison of Thermal-Hydraulic Parameters of HEU- and LEU-Core

		HEU	LEU
Core Power	MW	10	10
Volumetric Flow Rate	m³/h	1000	1000
Mass Flow Rate	kg/s	275.97	275.97
Core Mass Flow Rate	kg/s	248.38	248.38
Core Flow Area	m²	0.0918	0.0788
Average Coolant Velocity	m/s	2.73	3.18
Core Inlet Temperature	°C	38	38
Core Outlet Temperature	°C	47.6	47.6
Temperature Rise Across Core	K	9.6	9.6
Pressure at Core Midplane	bar	1.7	1.7
Saturation Temperature	°C	115.1	115.1
Number of Fuel Plates		614	530
Heat Transfer Area	m²	46.234	39.909
Average Heat Flux	W/cm²	21.63	25.06

reactor have been performed, see reference 1. They show that for a channel with an imposed constant pressure drop and a constant coolant inlet temperature the channel power can only reach a certain maximum value. If this critical value is exceeded the flow through the channel will be drastically reduced due to the sudden increase of the friction pressure drop when the steam bubbles detach from the channel wall. The

Table 2: Assumptions for Evaluation of Acceptable Nuclear Hot Channel Factors

Maximum Overpower Factor	1.15
Enthalpy Rise Hot Channel Factor	1.20
Heat Flux Hot Spot Factor	1.20
Axial Power Distribution	skewed to the bottom of the core
Safety Margin against Flow Instability (Whittle & Forgan)	1.95
Axial Nuclear Hot Channel Factor	1.6
Acceptable Radial Nuclear Hot Channel Factor (HEU- and LEU-Core)	3.9

same situation exists in the few hot channels in the core, which operate with the pressure drop imposed by the large number of average channels.

A parameter η which governs the stability of the flow is defined as follows:

$$\eta = \frac{V \times \Delta T_{sub}}{q''}$$

V	local coolant velocity
ΔT_{sub}	local subcooling of the coolant
q''	local heat flux

The physical meaning of η is that it controls the behaviour of the steam bubbles formed at active sites of the heating surface. If η exceeds a certain value the steam bubble will detach from the wall, otherwise it will stay there.

A statistical evaluation of the data of ref. 1 shows that in order to be sure with a probability of 95 % that 95 % *) of the maximum power channels are protected against the occurence of excursive flow instability the parameter η must be at least 32.5 $cm^3 K/Ws$.

For this basic evaluation the margin against flow instability was arbitrarily increased by an additional safety factor of 1.5, i. e. the parameter η was assumed to be 47.8 $cm^3 K/Ws$.

Table 2 lists additional assumptions used for the calculation of the maximum acceptable nuclear hot channel factors. For the design axial nuclear hot channel factor of 1.6 a radial nuclear hot channel factor of 3.9 can be accepted without

---

*) Requirement defined in KTA 3101.1 for power reactors

violating the stability criterion for both the HEU- and the LEU-core. The fact, that both cores can be operated with the same nuclear hot channel factors can be explained by looking at the definition of the parameter η.

The increase in average heat flux is compensated by the higher coolant velocity, since both are inversely proportional to the number of fuel plates. This conclusion holds of course only as long as the core mass flow rate is equal in both cores.

The LEU-core will have a higher core pressure drop than the HEU-core. Because the core pressure drop is only a fraction of the primary system pressure drop, the reduction in flow rate will be small. For a decrease of the core flow of 5 % the acceptable radial nuclear hot channel factor will decrease for example from 3.9 to 3.7.

It should be pointed out, that in the case of a loss of flow accident the acceptable nuclear hot channel factors will decrease sizably.

A rough estimate shows that the maximum radial hot channel factor will be limited to about 3.0.

Power Peaking Factors

A further result of some interest is the power distribution across the core. The results of suitable XY-calculations are presented by fig. 4 for the BOC-Xenon-free state as well as for the EOC-Xenon-Equilibrium state and for both fuels under investigation.

The highest power peaking factor occurs at the fresh control element. The changes of the power peaking factors are comparatively small when LEU-fuel is used instead of HEU. For the transition phase from HEU- to LEU-fuel the separate chapter below should be taken into consideration.

Kinetic Parameters

The next calculational results are the kinetic parameters. They are needed for the transient analyses planned. All core calculations hereto were done with a four group structure.

The two values calculated are

- the prompt neutron lifetime l and
- the delayed neutron fraction β_{eff}.

The results are

	l, µs	β_{eff}
HEU	54.5	0.00756
LEU	40.5	0.00723

16
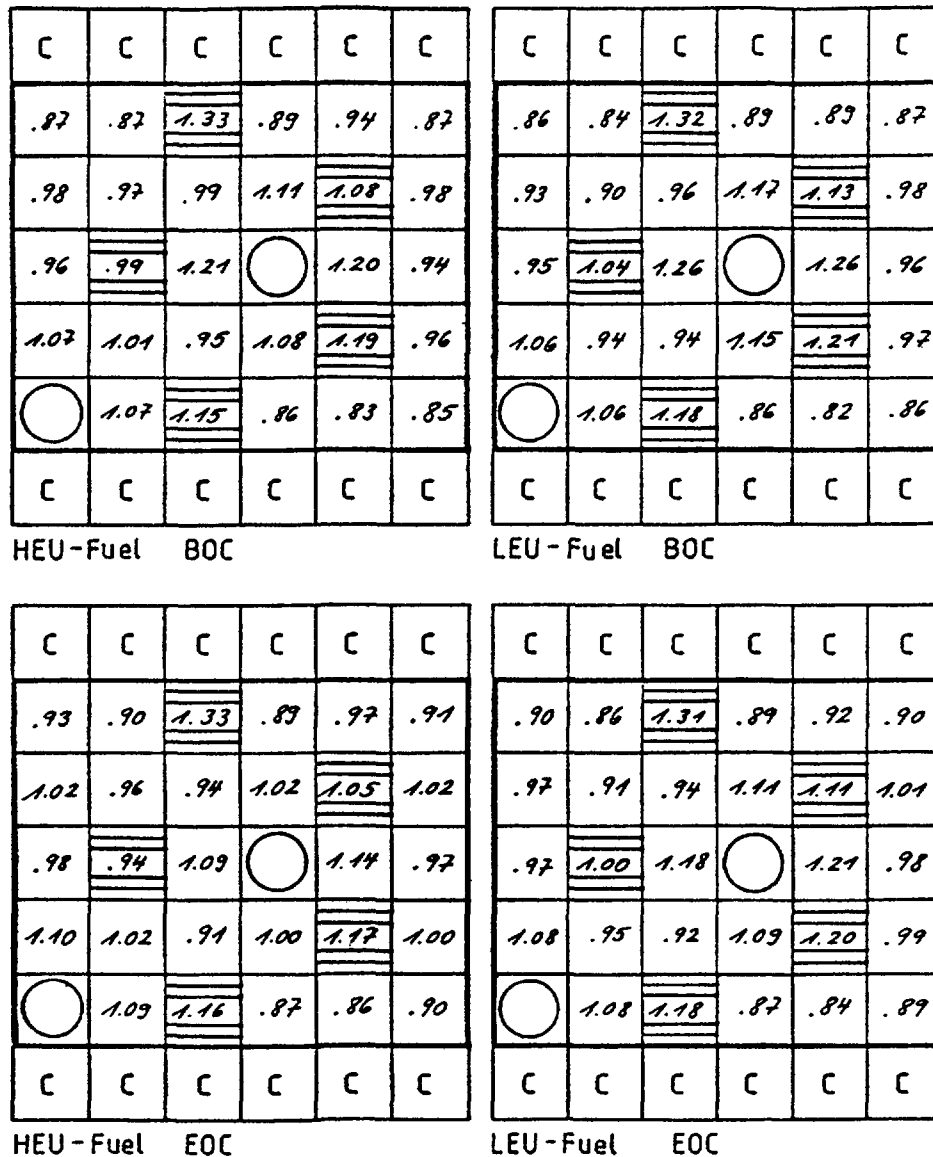
FIG. 4. 10 MW generic core — power peaking factors.

HEU-Fuel BOC

C	C	C	C	C	C
.87	.82	1.33	.89	.94	.82
.98	.97	.99	1.11	1.08	.98
.96	.99	1.21	◯	1.20	.94
1.02	1.04	.95	1.08	1.19	.96
◯	1.07	1.15	.86	.83	.85
C	C	C	C	C	C

LEU-Fuel BOC

C	C	C	C	C	C
.86	.84	1.32	.89	.89	.87
.93	.90	.96	1.17	1.13	.98
.95	1.04	1.26	◯	1.26	.96
1.06	.94	.94	1.15	1.21	.97
◯	1.06	1.18	.86	.82	.86
C	C	C	C	C	C

HEU-Fuel EOC

C	C	C	C	C	C
.93	.90	1.33	.89	.97	.94
1.02	.96	.94	1.02	1.05	1.02
.98	.94	1.09	◯	1.14	.97
1.10	1.02	.94	1.00	1.17	1.00
◯	1.09	1.16	.87	.86	.90
C	C	C	C	C	C

LEU-Fuel EOC

C	C	C	C	C	C
.90	.86	1.31	.89	.92	.90
.97	.91	.94	1.11	1.11	1.01
.97	1.00	1.18	◯	1.21	.98
1.08	.95	.92	1.09	1.20	.99
◯	1.08	1.18	.87	.84	.89
C	C	C	C	C	C

Isothermal Reactivity Feedback Coefficients

For the cores with the two different fuels specified above, i. e. the HEU-fuel with 280 g U-235-loading per element and the LEU-fuel with 446 g U-235-loading per element, the isothermal reactivity feedbacks were computed separately for

- the change in the fuel temperature (Doppler-effect),
- the change in the moderator temperature at constant water density (ϱ = .9924 g/cm^3),
- the change in the moderator density at constant moderator temperature (T_M = 20 °C), and
- the change in the moderator voidage in the whole core volume.

Fig. 5 demonstrates the results got from the calculations. The status of the core taken as a basis for the feedbacks was the core with homogeneous Xenon at the begin of the
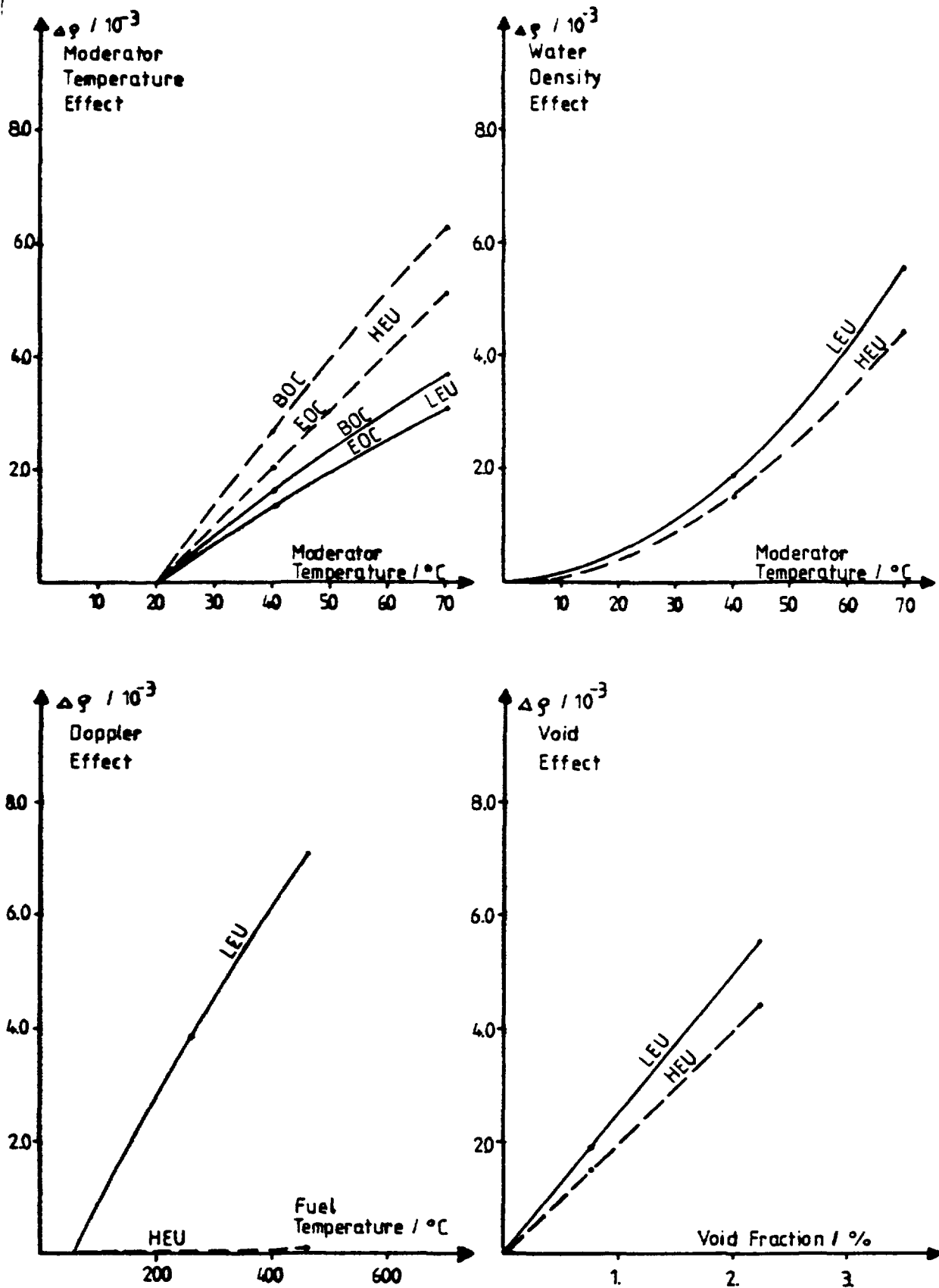
FIG. 5. Isothermal reactivity feedbacks for HEU and LEU fuels:
Changes in moderator temperature only
fuel temperature only
water density only
water voidage only.

equilibrium cycle, the corresponding burn-up-distribution is given by fig. 2.

The results of fig. 5 are in principal agreement with what is to be expected from the physical effects of the exchange of the fuel such as the harder spectrum of the LEU-fuel, the large concentration of U-238 in LEU with its advantageous Doppler-coefficient etc. Just to bring the results of fig. 5 in numbers the slopes of the feedbacks are compiled below:

	$\partial\rho/\partial$ T(HEU) /°C	$\partial\rho/\partial$ T(LEU) /°C
Doppler-Effect (60 °C → 260 °C) BOC	$-0.004 \cdot 10^{-4}$	$-0.019 \cdot 10^{-3}$
Moderator Temperature (40 °C → 70 °C) BOC	$-0.102 \cdot 10^{-3}$	$-0.058 \cdot 10^{-3}$
Moderator Density (40 °C → 70 °C) BOC	$-0.097 \cdot 10^{-3}$	$-0.122 \cdot 10^{-3}$

Besides that a methodical check was carried out by recalculating experiments such as the FRG-0-III-Experiment (D. Bünemann et al., ATKE-Bd. 19/1972, p. 97; GKSS-Report 70/37, p. 18 ff.) which have shown agreement within 5 % for the homogeneous core void coefficient.

Transition Phase from HEU- to LEU-Core

A transition phase from HEU- to LEU-fuel including the mixed cores was calculated taking into account the following boundary conditions:

- The shut down system in case of stuck rod must provide a subcriticality with a sufficient safety margin in the worst case.

- The power density distribution with respect to its maximum peaking factors has to be within an acceptable range.

- At EOC a suitable reactivity reserve for control purpose and experiments should be available.

Fig. 6 shows the reactivity as a function of time for the HEU-equilibrium-cycle, the transition phase, and the first full LEU-cycle. Moreover the related subcriticality in case of stuck rod as well as the number of charged fresh LEU-elements (fuel elements/control elements) are indicated. The cycle length is increasing continuously according to the increase of U-235-content in the core. The conversion from HEU- to LEU-fuel is completed at the beginning of the 5th cycle, i. e. after a transition phase of 351 fpd. Figs. 7 to 9 show the burn-up-distributions as well as the power peaking factors (averaged per element, absorbers withdrawn) for the calculated cycles at BOC and EOC, resp.
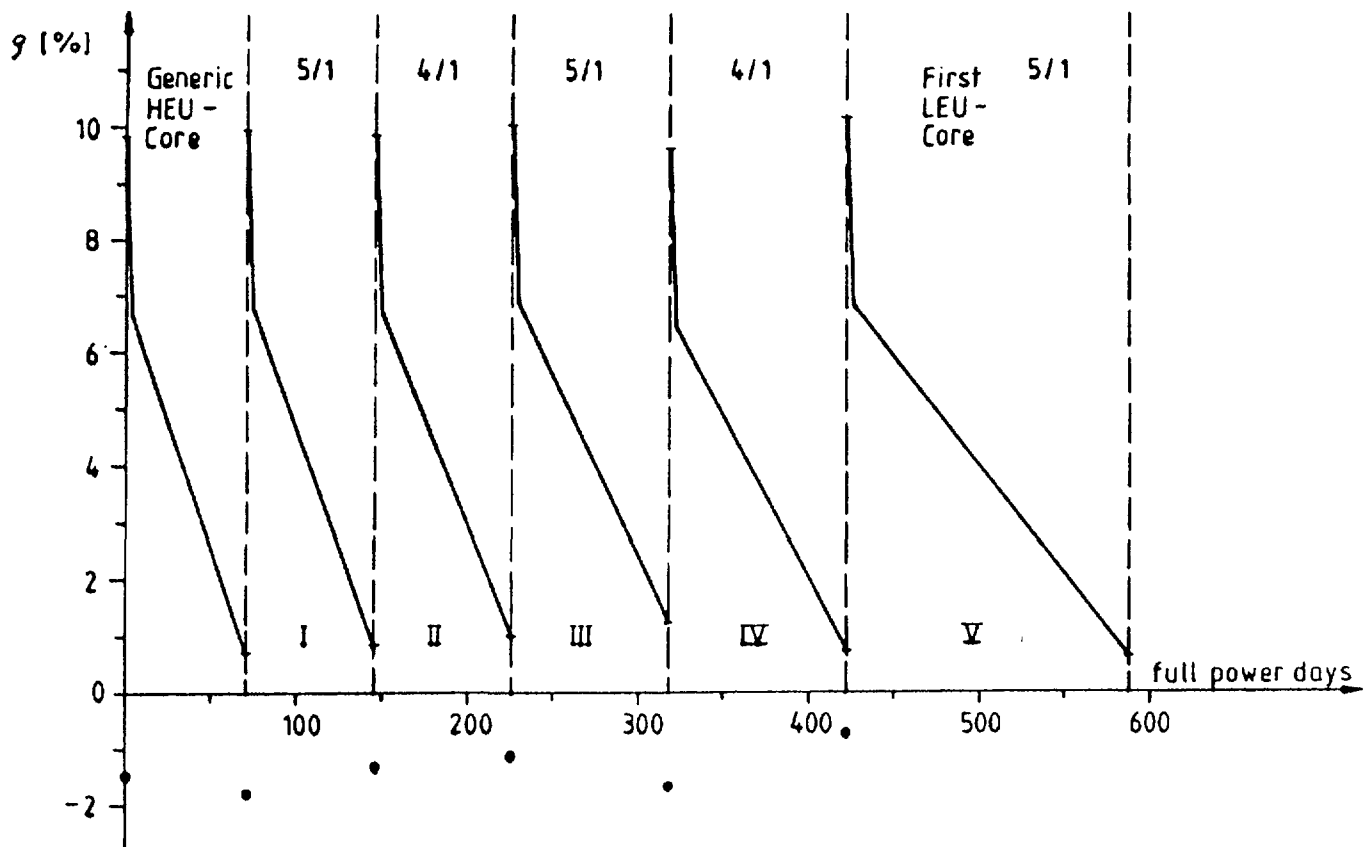
FIG. 6. Reactivity in dependance on time and stuck rod values for the transition phase.

The large difference in U-235-loading of HEU- and LEU-elements generated some difficulties concerning the stuck rod and the power peaking factors. When inserting the first LEU-elements into the core at the begin of the transition phase the stuck rod condition could not simply be fulfilled with a sufficient safety margin. Consequently one HEU-fuel-element with low burn-up has to be replaced by a reflector element. This discharged HEU-element is reinserted at the begin of the second cycle replacing the reflector element used during the foregoing cycle. Moreover the fuel elements have to be arranged carefully during the first cycles of the transition phase with respect to radial power peaks occuring. Even when using such a careful arrangement based on precalculations a maximum radial power peaking factor of about 1.50 occurs for the first two cycles. Whereas for the given coolant throughput no restriction to the 10 MW operation will arise from this enlargement of the radial power peaking factor, for cores which operate near to the limits of their heat removal system this enlargement has to be considered with due care. In case of less careful charging, e. g. if there is a single fresh LEU-control-element surrounded by HEU-elements, radial power peaking factors of 1.70 to 1.80 will be obtained.

It should be noticed likewise that high discharge burn-ups (about 70 %) of the residual HEU-elements occur at the end of the transition phase caused by the large difference in U-235-content.
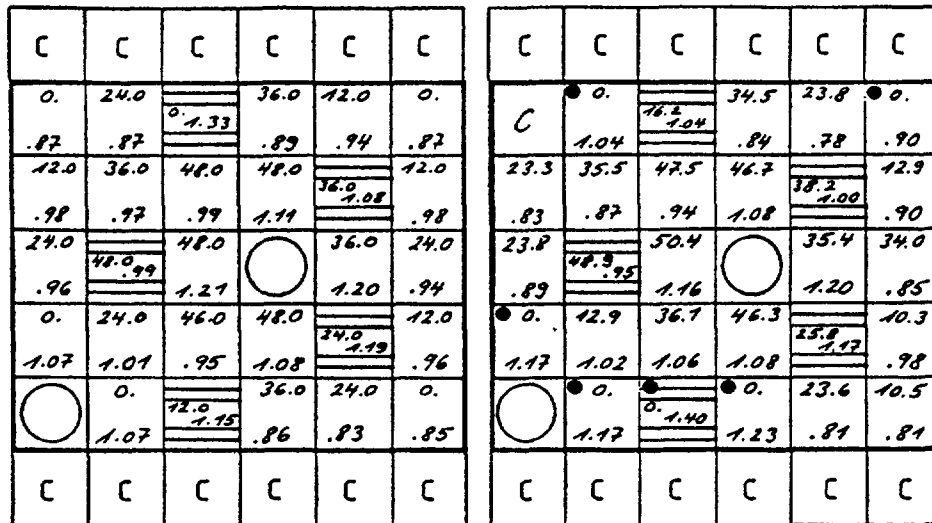
Generic HEU-Core BOC

1st Mixed Core BOC
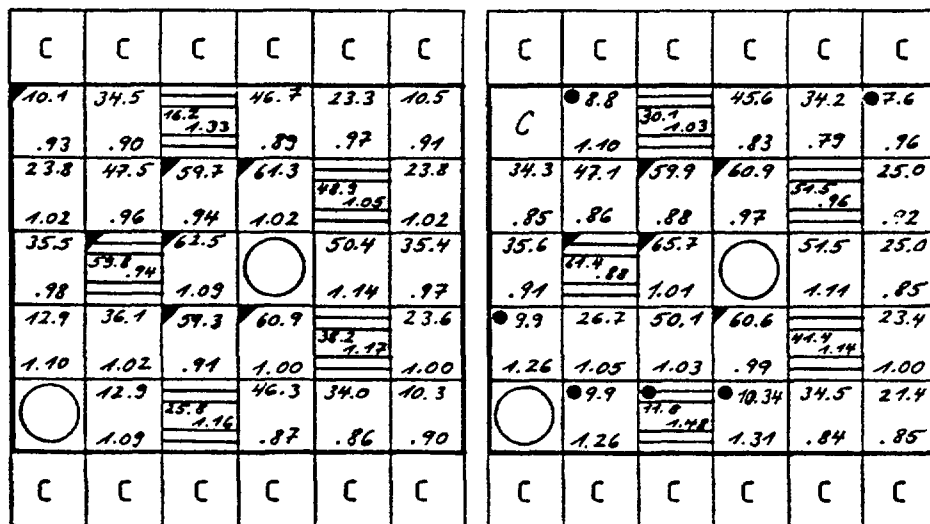
Generic HEU-Core EOC

1st Mixed Core EOC

☐ HEU-Element   ◪ Discharged HEU-Element   ◼ LEU-Element

FIG. 7. Transition phase from HEU to LEU fuel — burnup distributions and power peaking factors.

Finally characteristic data of the calculated transition phase can be summarized as follows:

maximum discharge burn-up   71 %
maximum radial power peaking factor   1.48
(averaged per element)
conversion completed   5th cycle
length of transition phase   351 fpd

Accident Analyses

Two types of accidents were investigated:

-   complete loss of flow
-   inadvertent control rod withdrawal

2nd Mixed Core BOC

3rd Mixed Core BOC

2nd Mixed Core EOC

3rd Mixed Core EOC

☐ HEU-Element   ◢ Discharged HEU-Element   ◼ LEU-Element
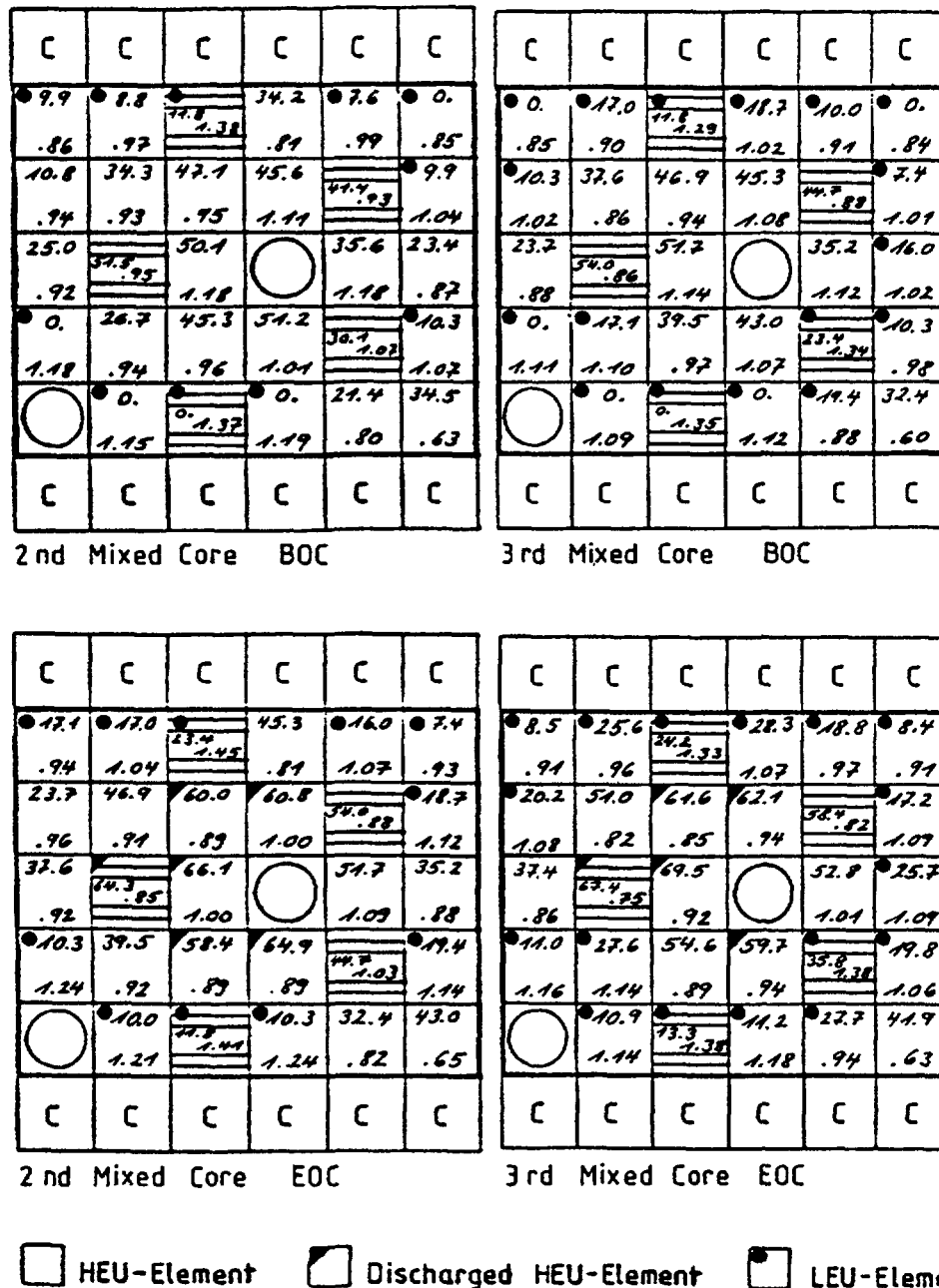
FIG. 8. Transition phase from HEU to LEU fuel — burnup distributions and power peaking factors.

The calculations were performed for the HEU- and the LEU-core specified in Table 1 for a radial design nuclear hot channel factor of 2.6.

Complete Loss of Flow

It was assumed that the reactor is operating at its maximum power level of 115 % and the maximum core inlet temperature of 42 °C when the accident occurs. The coastdown of the primary flow rate is approximated by an exponential function with a time constant of 1 s respectively 10 s. The trip occurs at a relative flow rate of 85 %, the control rods start to drop

22

4 th Mixed Core BOC

1 st LEU - Core BOC

4 th Mixed Core EOC

1 st LEU - Core EOC

☐ HEU-Element   ▰ Discharged HEU-Element   ▣ LEU-Element
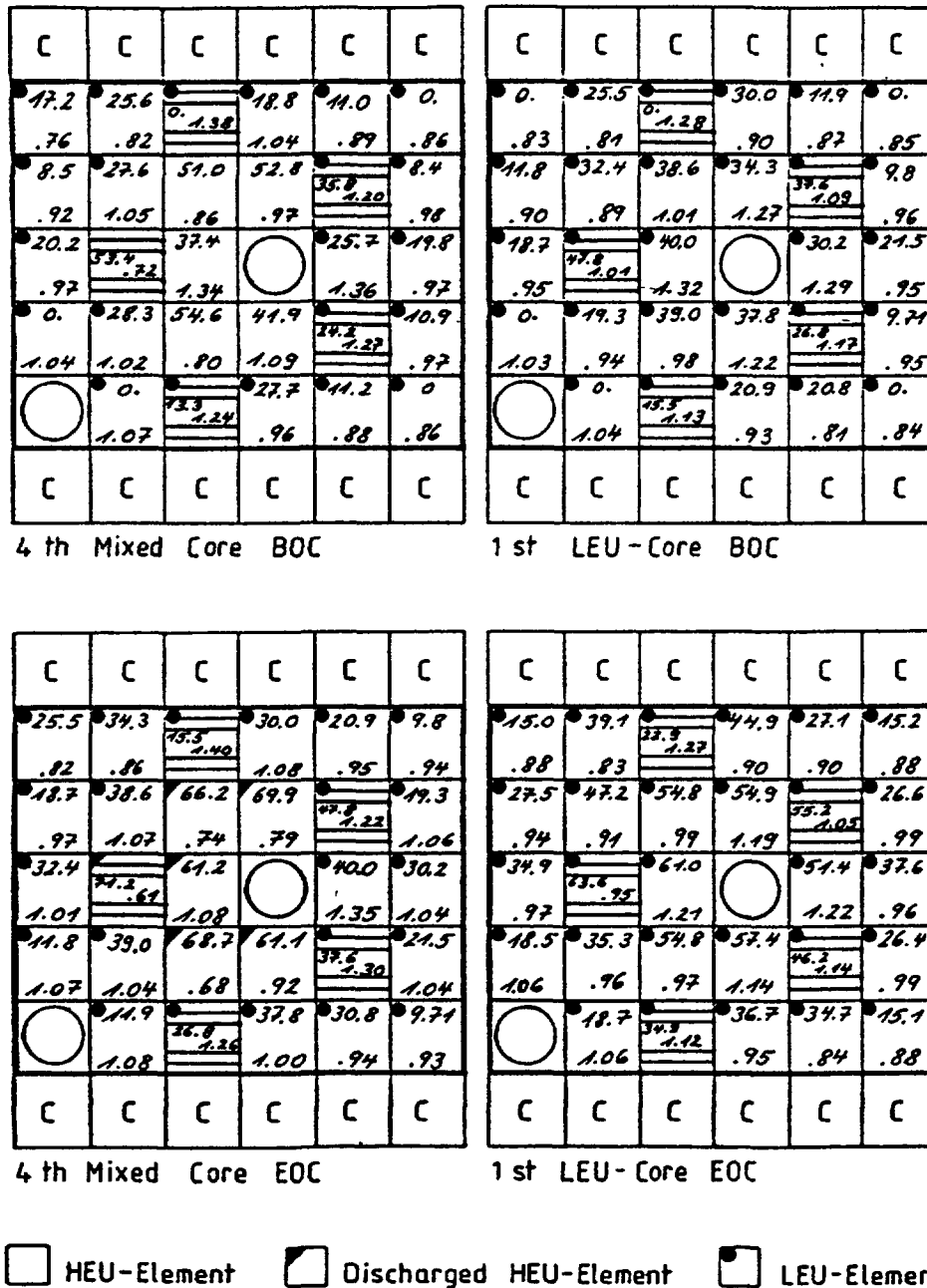
FIG. 9. Transition phase from HEU to LEU fuel — burnup distributions and power peaking factors.

after a delay of 0.2 s. The nominal shut-down reactivity is inserted within 0.5 s into the core. The calculations are terminated at a relative flow rate of 15 % because then the natural circulation flaps are assumed to open automatically causing a flow reversal.

Table 3 and 4 give the results of the calculations for the two cores for the fast and the slow loss of flow accident. Besides the peak values the values at a flow rate of 15 % are given. Fig. 10 to 13 show the relative core power and the relative flow rate, the maximum fuel plate temperature and coolant exit temperature as a function of time.

Table 3: Fast Loss of Flow Transient

Fuel	HEU	LEU
Initial Power, MW	11.5	11.5
Initial Flow Rate, m³/h	1000	1000
Time Constant for Flow Decay, s	1.0	1.0
Flow Trip Point, %	85	85
Time Delay, s	0.2	0.2
Power Level at Scram, %	107.4 (0.363)*	106.1 (0.363)
Peak Fuel Temperature, °C	144.1 (0.363)	167.4 (0.363)
Peak Clad Temperature, °C	141.1 (0.363)	141.9 (0.363)
Peak Outlet Temperature, °C	80.1 (0.42)	80.1 (0.42)
Min. Bubble Detachment Parameter, cm³K/Ws	75.4 (0.38)	77.3 (0.38)
At ~ 15 % Relative Flow:		
Fuel Temperature, °C	66.7	67.5
Clad Temperature, °C	66.5	66.0
Outlet Temperature, °C	51.1	51.2

*) Quantities in parentheses indicate time (in seconds) at which values occur

Table 4: Slow Loss of Flow Transient

Fuel	HEU	LEU
Initial Power, MW	11.5	11.5
Initial Flow Rate, m³/h	1000	1000
Time Constant for Flow Decay, s	10	10
Flow Trip Point, %	85	85
Time Delay, s	0.2	0.2
Power Level at Scram, %	108.4 (1.825)*	107.7 (1.825)
Peak Fuel Temperature, °C	140.1 (1.825)	164.3 (1.825)
Peak Clad Temperature, °C	137.2 (1.825)	138.2 (1.825)
Peak Outlet Temperature, °C	78.1 (1.825)	77.9 (1.825)
Min. Bubble Detachment Parameter, cm³K/Ws	94.7 (1.825)	96.2 (1.825)
At ~ 15 % Relative Flow:		
Fuel Temperature, °C	51.4	51.3
Clad Temperature, °C	51.3	50.9
Outlet Temperature, °C	45.9	45.7

*) Quantities in parentheses indicate time (in seconds) at which values occur
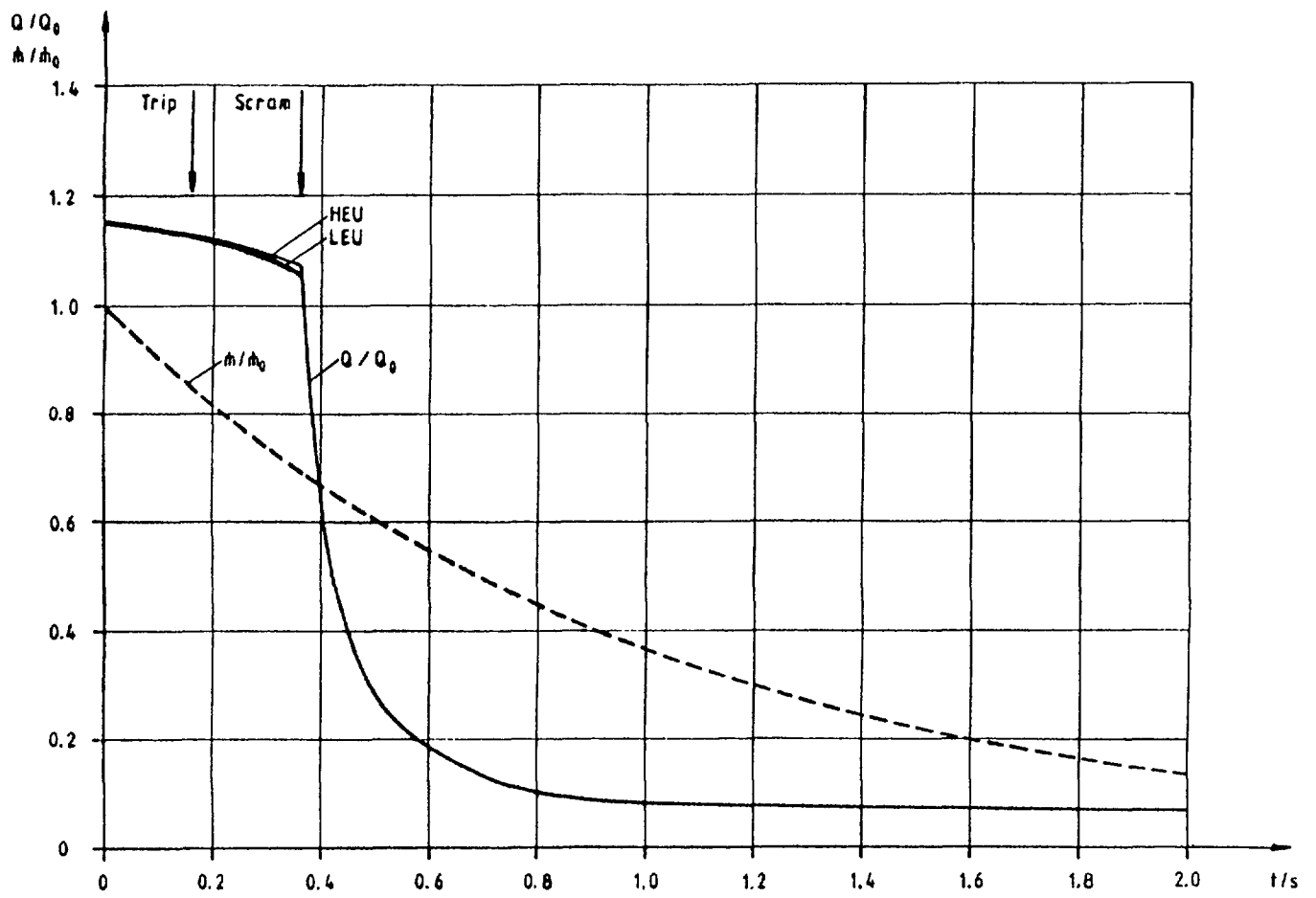
FIG. 10. Fast loss-of-flow transient.

FIG. 11. Fast loss-of-flow transient.

FIG. 12. Slow loss-of-flow transient.
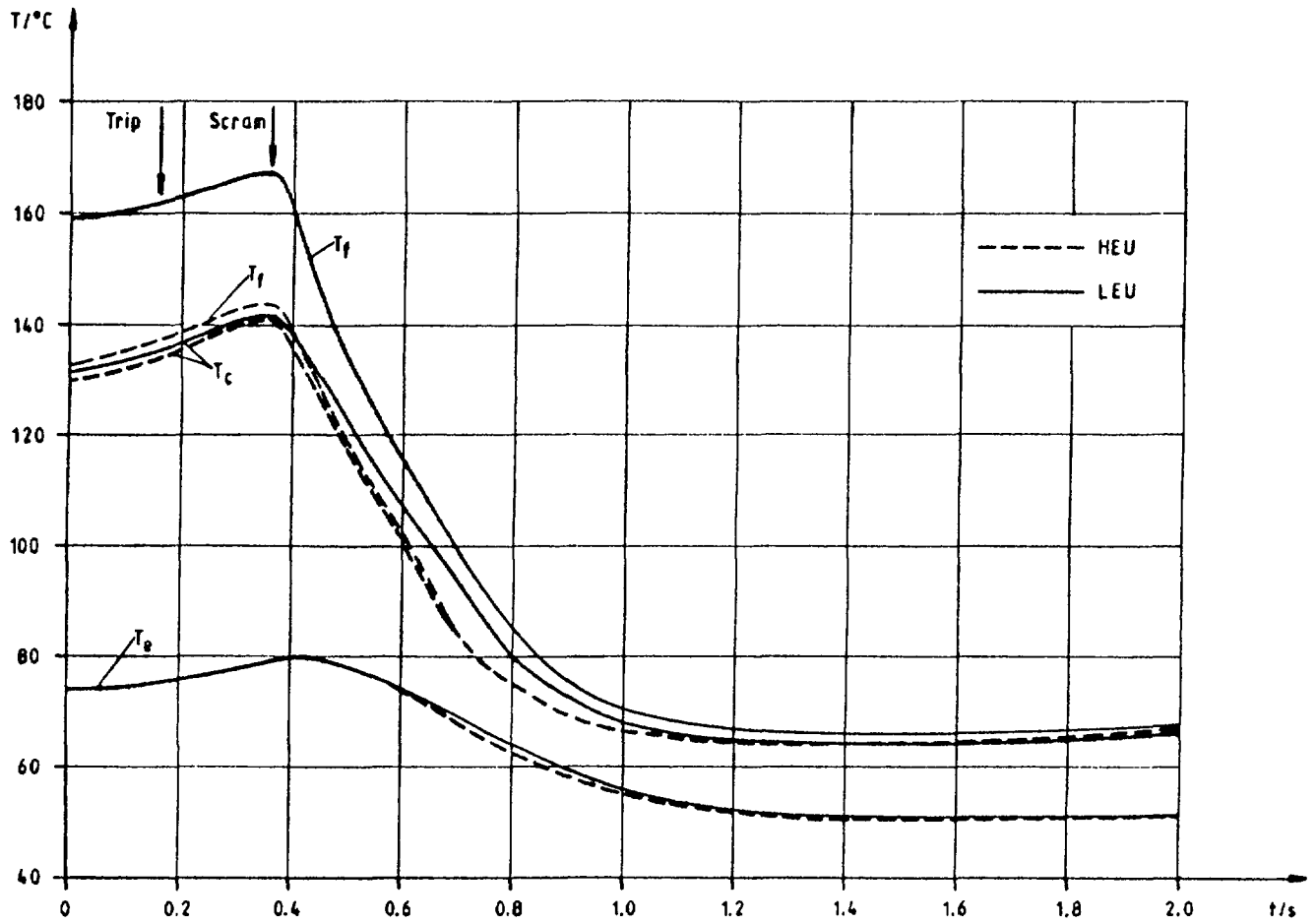
FIG. 13. Slow loss-of-flow transient.
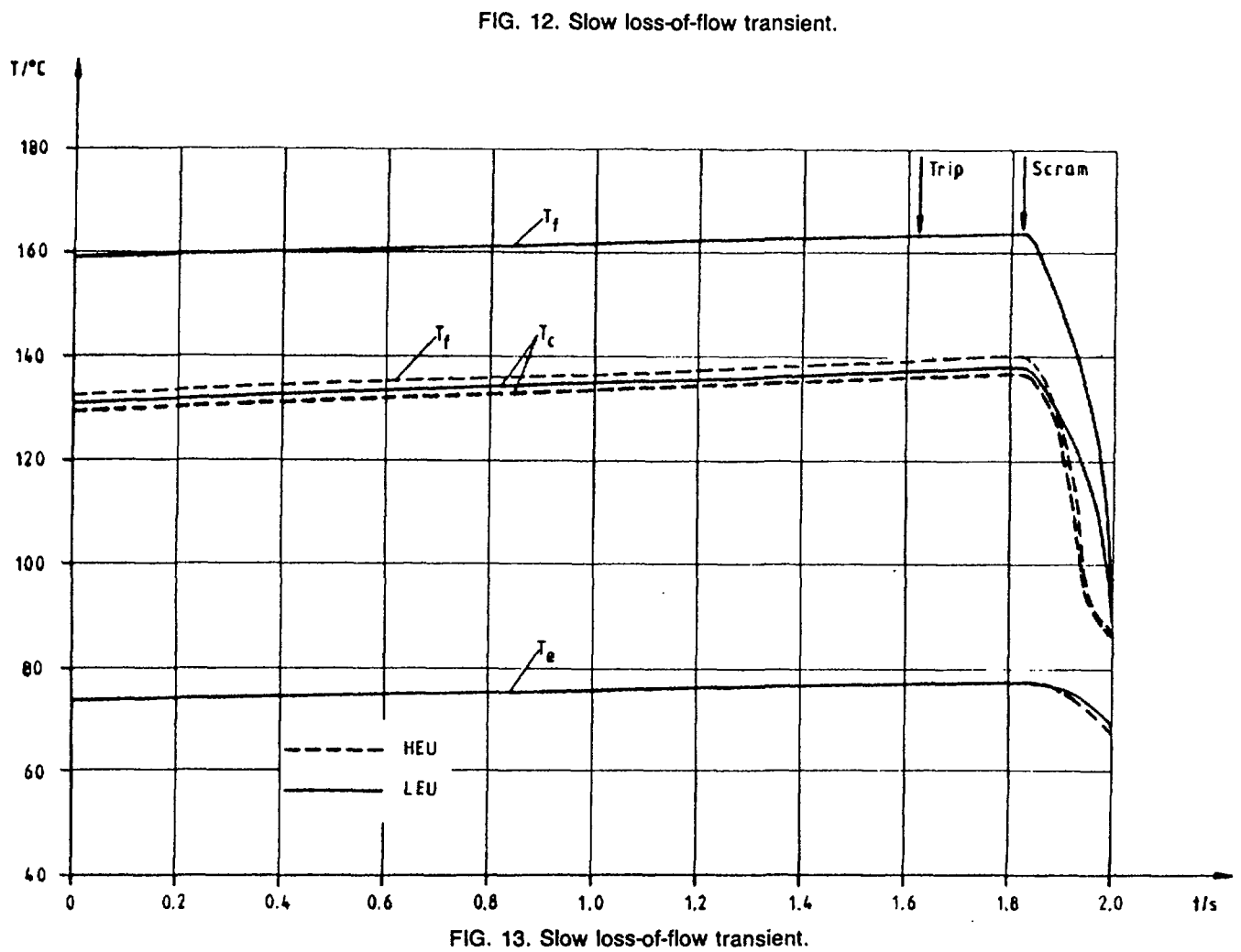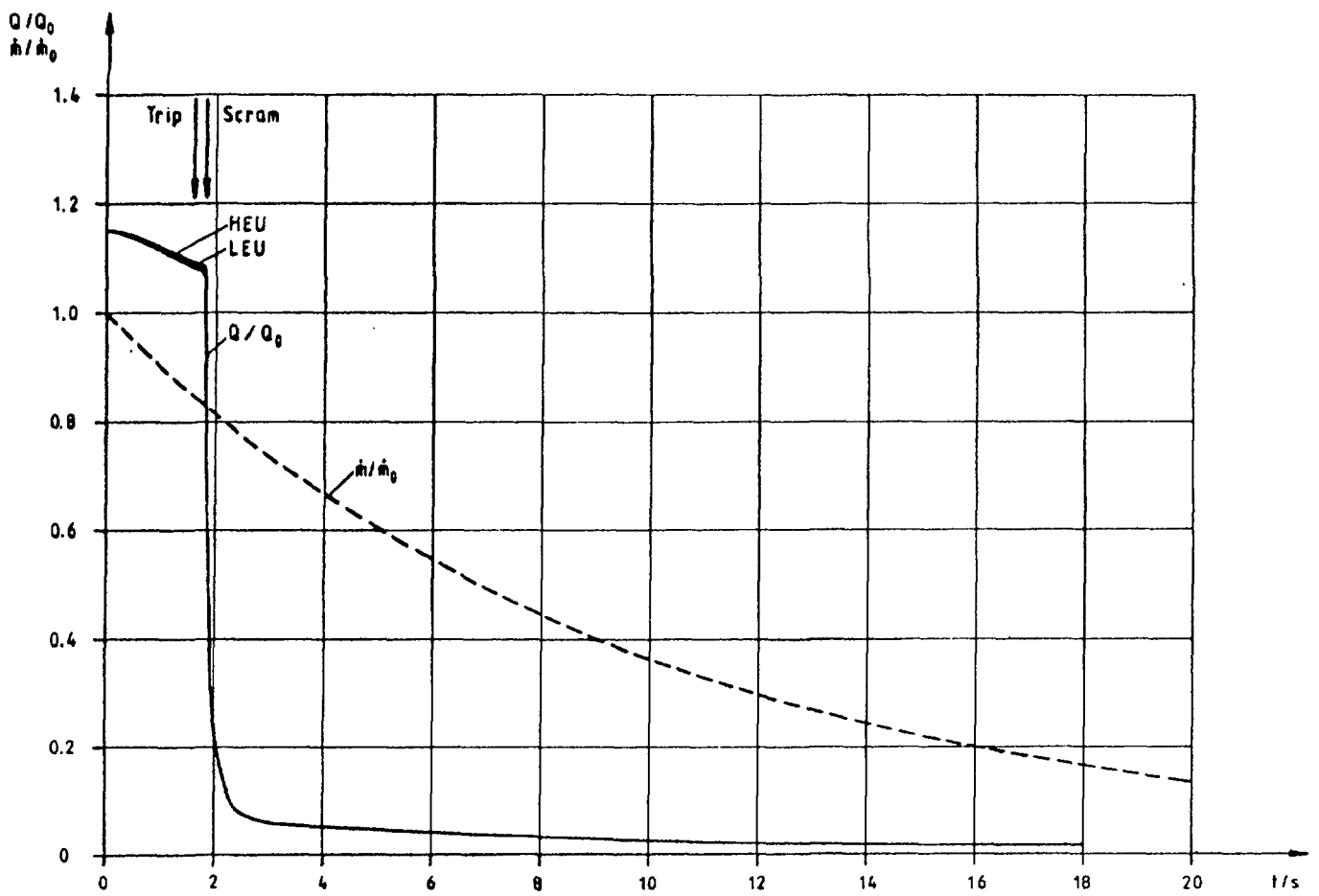
Table 5: Control Rod Withdrawal Accident (Power Range)

Fuel	HEU	LEU
Reactivity Insertion Rate, c/s	18.9	19.8
Initial Power; MW	10	10
Trip Point, MW	11.5 (0.775)*	11.5 (0.765)
Flow Rate, m^3/h	1000	1000
Time Delay, s	0.2	0.2
Peak Power, MW	11.93 (0.975)	11.81 (0.965)
Total Energy Release to Time of Peak Power, Ws	$1.065 \cdot 10^7$	$1.051 \cdot 10^7$
Total Energy Release beyond 11.5 MW, Ws	$2.338 \cdot 10^6$	$2.319 \cdot 10^6$
Peak Fuel Temperature, °C	133.3 (0.975)	130.5 (0.965)
Peak Clad Temperature, °C	130.0 (0.975)	158.4 (0.965)
Peak Outlet Temperature, °C	52.9 (1.0)	52.8 (0.965)
Min. Bubble Detachment Parameter, cm^3 K/Ws	114.3 (0.975)	117.2 (0.965)

*) Quantities in parentheses indicate time (in seconds) at which values occur

The comparison of the HEU- and LEU-case shows that the coolant temperature, the clad temperature and the safety margin against flow instability are almost identical. The only exception is the maximum meat temperature, which is about 20 K higher for LEU because of the poor thermal conductivity of this fuel.

Inadvertent Control Rod Withdrawal

It is postulated that all control rods are withdrawn from the core with the nominal control rod drive speed while the pumps are in operation. Lacking specific data for the Generic Core the speed of the BER-II rod drives is taken, i. e. 0.207 cm/s. The transient is terminated by the trip period too low respectively neutron flux level higher than 5 % in the start-up range or by the N-16 adjusted neutron flux respectively neutron flux higher that 115 % in the power range. The delay time is 0.2 s in all cases.

Since the safety margin in the case of rod withdrawal in the start-up range is very large, detailed results will not be shown here.

The results for the rod withdrawal in the power range are given in Table 5. The initial power is 10 MW. Fig. 14 shows the relative neutron flux vs. time. The peak flux value is slightly higher for HEU than for LEU. The maximum coolant outlet temperature and the maximum clad temperature are again very similar, whereas the maximum fuel temperature is somewhat higher for LEU than for HEU as for the loss of flow accident. The minimum safety margin against flow instability is marginally larger for the LEU-case but both are far beyond critical values.
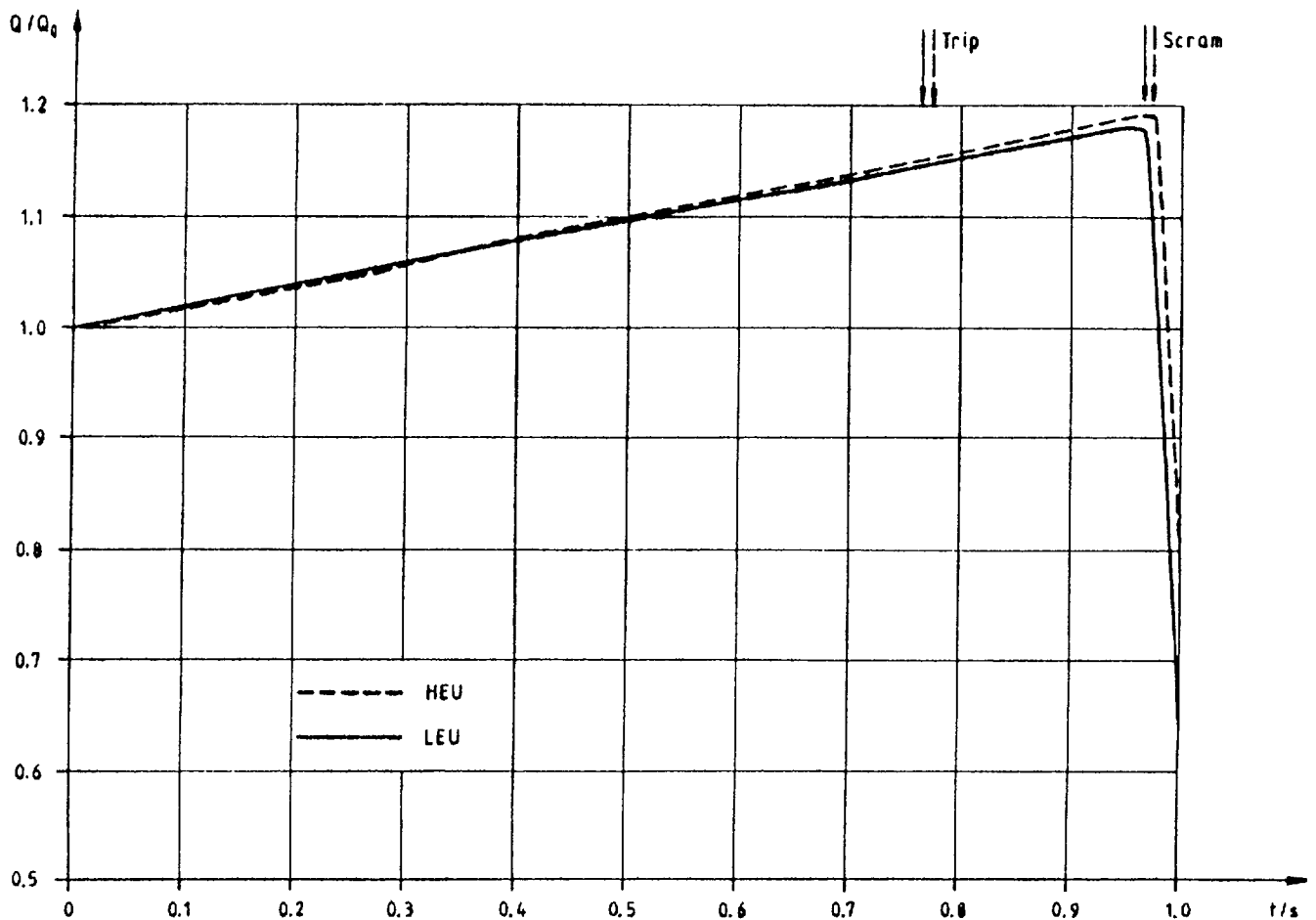
FIG. 14. Rod withdrawal accident.

Conclusion

The analysis of typical accidents to be considered shows that both cores using either HEU- or LEU-fuel perform satisfactorily as far as plate temperatures, coolant temperatures and flow stability are concerned. There are only marginal differences in the transient behaviour of the cores.

Reference

/ 1 /   R. H. Whittle, R. Forgan
         A Correlation for the Minima in the Pressure Drop
         versus Flow-Rate Curves for Subcooled Water Flowing
         in Narrow Heated Channels
         Nucl. Eng. and Des. 6 (1967)

Appendix A-2

SAFETY ANALYSES FOR HEU AND LEU EQUILIBRIUM CORES
AND HEU-LEU TRANSITION CORE
FOR THE IAEA GENERIC 10 MW REACTOR

J.E. MATOS, K.E. FREESE
RERTR Program,
Argonne National Laboratory,
Argonne, Illinois,
United States of America

Abstract

Analyses are provided for the key safety parameters and transient
behavior of the IAEA generic 10 MW reactor with HEU and LEU
fuels. The LEU fuel element design that was studied contains 23
plates with 0.5 mm thick U_3Si_2-Al fuel meat, a uranium density of
4.5 g/cm^3, and 390 g ^{235}U. The performance and safety
characteristics of equilibrium cores are studied first, followed
by detailed results for each step of a gradual transition from HEU
to LEU fuel.

1. INTRODUCTION

This appendix provides the results of a study of the key safety para-
meters and transient behavior of the IAEA generic 10 MW reactor with HEU and
LEU fuels. The performance and safety characteristics of equilibrium cores
with HEU and LEU fuels are studied first, followed by detailed results for
each step of a gradual transition from HEU to LEU fuel.

The design of the reactor is described in detail in IAEA-TECDOC-233
(Ref. 1), and a summary of the key features are shown in Table 1 and Fig. 1.
The 5 × 6 element core contains 23 MTR-type standard fuel elements and 5
control fuel elements. The core is reflected by graphite on two opposite faces
and is surrounded by water. One water-filled flux trap is located near the
center of the core and another near an edge. In these calculations, both flux
traps were replaced with 77 mm × 81 mm blocks of aluminum with 50 mm square
water holes in order to compute more realistic power peaking factors.

The HEU standard elements have 23 plates, UAl_x-Al fuel, and 280 g ^{235}U.
The LEU replacement elements that were studied have the identical geometry,
but contain 390 g ^{235}U and U_3Si_2-Al fuel with a uranium density of 4.45 g/cm^3
(40 vol% U_3Si_2).

The 10 MW benchmark reactor (Appendix G) that has been studied extensively
by a number of laboratories has an HEU fissile loading of 280 g and an LEU
fissile loading of 390 g. This provides the opportunity to compare results
between the benchmark reactor and the generic reactor by those laboratories who
have performed calculations only for the benchmark.

Table 1. IAEA Generic 10 MW Reactor and Fuel Element
Design Descriptions with HEU and LEU Fuels

Reactor Design Description

Reactor Type	Pool-Type MTR
Steady-State Power Level, MW	10
Number of Standard Fuel Elements	23
Number of Control Fuel Elements	5
Irradiation Channels	1 at Core Center 1 at Core Edge
Active Core Geometry	5 x 6 Positions
Grid Plate	8 x 9 Positions
Lattice Pitch, mm^2	77 x 81
Moderator, Coolant	H_2O
Reflectors	C, H_2O
Coolant Flow Rate, m^3/h	1000
Coolant Inlet Temperature, °C	38

Fuel Element Design Descriptions

Fuel Type	UAl_x-Al	U_3Si_2-Al
Uranium Enr., w/o $235U$	93	19.75
Element Dimensions, mm^3	76 x 80 x 600	76 x 80 x 600
Plate Thickness, mm	1.27	1.27
Water Channel Thick., mm	2.19	2.19
Plates/Standard Element	23	23
Plates/Control Element	17 + 4 Al Plates	17 + 4 Al Plates
Fuel Meat Dimensions, mm^3	0.51 x 63 x 600	0.51 x 63 x 600
Clad Material	Al	Al
Clad Thickness, mm	0.38 Inner Plates 0.495 Outer Plates	0.38 0.495
Uranium Density in Fuel Meat, g/cm^3	0.68	4.45
$235U$/Fuel Element, g	280 Standard 207 Control	390 288

2. CALCULATIONAL METHODS

2.1 Static and Burnup Calculations

The methods and codes used for cross section generation (EPRI-CELL) and for burnup calculations are described in Appendix A of Ref. 1. There are three exceptions: (1) all of the burnup (REBUS-3) and static diffusion theory (DIF3D) calculations were performed in three dimensions, (2) fueled and non-fueled regions of each standard and control fuel element were modeled separately, and (3) the fuel shuffling pattern was changed from the inside-out scheme used in Ref. 1 (one standard element was replaced per cycle) to an outside-in fuel shuffling pattern in which two elements were replaced per cycle.

2.2 Transient Calculations

The transient calculations described in this appendix were performed using the PARET code (Ref. 2). The code was originally developed for the analysis of the SPERT-III experiments for temperatures and pressures typical of power reactors. This code has been modified at ANL to include a selection of flow instability, departure from nucleate boiling (DNB), single and two-phase heat transfer correlations, and a properties library applicable to the low pressures, temperatures, and flow rates encountered in research reactors. A description of the current PARET code and a detailed comparison with the SPERT I experiments are provided in Ref. 2. A summary of the results can be found in the benchmark calculations in Appendix G-1.

FIG. 1. 10 MW reactor core.

The PARET code was also used to compute steady-state thermal-hydraulic safety margins. Values computed using PARET are nearly identical with those computed using the COBRA-3C/RERTR code.

3. EQUILIBRIUM CORES

The first objective was to compare the operating parameters and safety margins of the HEU and LEU equilibrium cores to ensure that these character-istics were satisfactory before beginning the mixed core calculations.

3.1 Burnup Results

Three-dimensional burnup calculations for the HEU and LEU cores were first performed using the REBUS-3 fuel cycle analysis code with half-core symmetry and eight axial depletion zones above the core midplane. The calculations were done using ENDF-B/IV cross section data generated using the EPRI-CELL code and five energy groups with the following upper energy boundaries: 10.0 MeV, 0.821 MeV, 5.53 keV, 1.855 eV, and 0.625 eV.

The planar models that were used to represent the standard and control elements are shown in Fig. 2. Each standard element was modeled as three

FIG. 2. Models for standard element and for control element with and without absorber blades (dimensions in cm).

separate regions - one region (6.3 cm × 8.1 cm) representing the fueled por-
tion of the element and two regions (each 0.7 cm × 8.1 cm) representing the
sideplates and the other non-fueled portions of the element. Each control
element without absorber blades was modeled in a similar manner, except that
two additional separate regions were included to represent the aluminum guide
plates and their associated water channels. Further additional regions were
added to model the control elements with the absorber blades inserted.

The end boxes on the top and bottom of each fuel element were represented
using a homogenized mixture of 25 v/o Al and 75 v/o H_2O extending 15 cm
above the fuel. A thickness of 20 cm of water was added above the axial end
boxes.

32

Table 2. Burnup Results for HEU and LEU Equilibrium Cores
with an EOC Excess Reactivity of 2.3% k/k.

	HEU	LEU
Cycle Length, days	21.4	30.6
U Ave. Discharge Burnup, % Standard/Control Elements	49.9/55.3	48.5/53.8
Peak-to-Average Burnup Standard/Control Elements	1.19/1.18	1.18/1.18
No. of Elements/Year 100% Duty Factor Standard/Control Elements	28.0/6.1	19.6/4.3

A burnup search was first performed to determine the cycle length in the equilibrium HEU and LEU cores that would yield an end-of-cycle (EOC) excess reactivity of 2.3% k/k. This EOC excess reactivity is intended to account for 1.5% k/k for experimental loads, 0.5% k/k for control reserve, and 0.3% k/k for the cold-to-hot reactivity swing. The main results of these calculations are shown in Table 2. The   U contents, average thermal (<0.625 eV) fluxes, and average power per element at BOC are shown in Fig. 3.

The cycle length was computed to be 21.4 days in the HEU core and 30.6 days in the LEU core because of the much higher fissile loading of the LEU elements. (A   U content of about 320 g per LEU standard element is required to match the cycle length and EOC excess reactivity of the HEU core.) The discharge burnups in the standard and control elements and the peak-to-average burnups are nearly the same in the two cores. Since the LEU core has a longer cycle length, about 24 standard plus control elements would be required per year instead of about 34 elements in the HEU core if both reactors were operated with a 100% duty factor.

3.2 Nuclear Power Peaking Factors

In these 3D calculations, the total power peaking factor is defined as the product of two components: (1) a radial factor defined as the average power in each element divided by the average power in the core, and (2) an element factor defined as the peak power in each element when the control rods are 50% withdrawn divided by the average power in that element.

Appendix G-1, Section 5.3, in the safety-related benchmark calculations shows that the axial power bulge toward the bottom of the core with the control absorbers partially-withdrawn is largest when the control absorbers are withdrawn 50%. The power peak is located at a height of about 20 cm from the bottom of the active core or about 1/3 of the way up from the bottom of the fuel. Generally, the peak axial power densities in the limiting standard and control fuel elements are about 15% larger with the absorbers 50% withdrawn rather than 100% withdrawn.

^{235}U LOADINGS, G

	A	B	C	D	E	F
1	C	C	C	C	C	C
HEU / LEU	275 / 384	256 / 357	177 / 248	217 / 304	257 / 358	276 / 384
3	235 / 328	196 / 276	174 / 247	151 / 217	145 / 205	236 / 330
4	216 / 303	118 / 167	173 / 244	(○)	164 / 232	181 / 255
5	216 / 303	198 / 278	177 / 250	155 / 221	123 / 174	197 / 277
6	(○)	249 / 347	180 / 251	237 / 331	258 / 360	276 / 384
7	C	C	C	C	C	C

CORE FISSILE
LOADINGS BOC

HEU: 5713 G ^{235}U

LEU: 8015 G ^{235}U

LEU/HEU = 1.40

AVE. THERMAL FLUX x 10^{14}

	A	B	C	D	E	F
	C	C	C	C	C	C
	0.38 / 0.28	0.47 / 0.34	0.59 / 0.42	0.57 / 0.41	0.47 / 0.34	0.35 / 0.26
	0.47 / 0.33	0.65 / 0.45	0.78 / 0.53	0.82 / 0.57	0.66 / 0.47	0.44 / 0.31
	0.50 / 0.35	0.78 / 0.53	0.81 / 0.56	(1.52 / 1.33)	0.76 / 0.54	0.52 / 0.36
	0.46 / 0.33	0.60 / 0.42	0.74 / 0.51	0.79 / 0.55	0.69 / 0.48	0.47 / 0.33
	(0.74 / 0.67)	0.44 / 0.32	0.54 / 0.39	0.52 / 0.37	0.45 / 0.33	0.34 / 0.25
	C	C	C	C	C	C

AVE. POWER PER ELEMENT, KW

	A	B	C	D	E	F
1	C	C	C	C	C	C
HEU / LEU	333 / 324	393 / 383	334 / 330	397 / 394	389 / 383	313 / 308
3	349 / 342	405 / 403	426 / 432	385 / 407	303 / 306	331 / 325
4	343 / 338	284 / 293	440 / 446	(○)	388 / 404	293 / 296
5	313 / 316	379 / 377	411 / 415	382 / 402	267 / 274	290 / 290
6	(○)	353 / 351	312 / 310	397 / 392	374 / 367	302 / 295
7	C	C	C	C	C	C

FIG. 3. Uranium-235 content, average thermal (<0.625 eV) flux, and average power per element in HEU and LEU equilibrium cores at BOC.

The radial, element, and total nuclear power peaking factors at BOC for the HEU and LEU equilibrium cores are shown in Fig. 3a. The total peaking factors with all five absorbers 50% withdrawn are within about 10% of each other, but the limiting value in core position C2 is slightly smaller in the LEU core.

Radial Power Peaking Factors
(Absorbers 50% Withdrawn)

HEU / LEU

	A	B	C	D	E	F
1	C	C	C	C	C	C
2	1.01 / 0.97	1.11 / 1.07	1.11 / 1.10	1.07 / 1.06	1.03 / 1.01	0.90 / 0.87
3	1.05 / 1.01	1.10 / 1.09	1.15 / 1.16	1.05 / 1.12	1.01 / 1.02	0.92 / 0.90
4	0.98 / 0.97	0.95 / 0.99	1.22 / 1.24	◯	0.96 / 1.01	0.81 / 0.82
5	0.90 / 0.91	1.00 / 1.00	1.10 / 1.11	1.04 / 1.09	0.87 / 0.90	0.80 / 0.80
6	◯	0.96 / 0.95	1.01 / 1.00	1.05 / 1.04	0.97 / 0.95	0.85 / 0.83
7	C	C	C	C	C	C

Element Power Peaking Factors
(Absorbers 50% Withdrawn)

HEU / LEU

	A	B	C	D	E	F
1	C	C	C	C	C	C
2	1.98 / 2.11	2.07 / 2.06	2.21 / 2.20	1.93 / 1.90	2.23 / 2.23	2.10 / 2.28
3	1.84 / 1.99	1.99 / 2.02	1.71 / 1.81	1.76 / 1.85	2.14 / 2.19	2.03 / 2.21
4	1.82 / 1.93	1.92 / 1.93	1.67 / 1.81	◯	1.97 / 2.08	1.79 / 1.98
5	1.85 / 1.91	2.13 / 2.14	1.79 / 1.90	1.80 / 1.91	2.09 / 2.15	1.94 / 2.13
6	◯	2.07 / 2.03	2.22 / 2.19	1.98 / 1.95	2.29 / 2.27	2.16 / 2.32
7	C	C	C	C	C	C

Total Power Peaking Factors
(Absorbers 50% Withdrawn)

HEU / LEU

	A	B	C	D	E	F
1	C	C	C	C	C	C
2	2.00 / 2.05	2.29 / 2.21	2.46 / 2.42	2.07 / 2.02	2.29 / 2.24	1.88 / 1.99
3	1.93 / 2.02	2.20 / 2.21	1.96 / 2.11	1.86 / 2.07	2.15 / 2.23	1.87 / 2.00
4	1.79 / 1.87	1.83 / 1.90	2.04 / 2.24	◯	1.89 / 2.10	1.45 / 1.63
5	1.67 / 1.73	2.13 / 2.14	1.97 / 2.10	1.87 / 2.08	1.83 / 1.94	1.55 / 1.70
6	◯	1.99 / 1.93	2.23 / 2.20	2.09 / 2.03	2.22 / 2.16	1.84 / 1.92
7	C	C	C	C	C	C

FIG. 3a. Radial, element, and total nuclear power peaking factors in HEU and LEU equilibrium cores at BOC with control absorbers 50% withdrawn.

It is worthwhile noting that the element factor was computed using fluxes calculated at the edge of the mesh interval with highest power and not the fluxes at the center of the mesh interval with highest power. Normally, there is a sharp rise in power density near one corner of the fueled region in the limiting element. Power peaking factors based on power densities computed at the centers of mesh intervals depend on the mesh spacing that is selected and underestimate the peaking. Power peaking factors based on power densities computed at the edges of the mesh intervals are nearly independent of the mesh spacing.

3.3 Thermal-Hydraulic Safety Margins

The three steady-state thermal-hydraulic safety margins that are most important for plate-type reactors are the margin to onset of nucleate boiling (ONB), the margin to onset of flow instability, and the margin to departure from nucleate boiling (DNB).

For the following input parameters,

			Nuclear Peak Factors		HEU	LEU
Inlet Temperature:	38°C					
Inlet Pressure	:	1.7 bar	Radial × Local	:	1.64	1.61
Flow Rate	:	1000 m³/h	Axial	:	1.5	1.5
			Total Nuclear	:	2.46	2.42
			Total Engineering Hot-Channel Factor:		1.58	1.58

the data in Table 3 show that the margins to ONB using the Bergles and Rohsenow correlation, the minimum values of the flow instability parameter ($\eta = v \cdot \Delta T_s/q''$), and the margins to DNB using the Mirshak correlation are satisfactory and nearly the same in the two cores. The parameters v, ΔT_s, and q'' are the local values of the coolant velocity, coolant subcooling and heat flux, respectively. The slightly larger margins in the LEU equilibrium core are a direct result of its slightly smaller total nuclear power peaking factor.

Table 3. Steady-State Thermal Hydraulic Safety Margins
for HEU and LEU Equilibrium Cores

	HEU	LEU
Margin to ONB	1.55	1.58
Minimum η, cm³ K/Ws	230	234
Margin to DNB (Mirshak Correlation)	5.17	5.26

3.4 Control Rod Worths

In order to validate the methods used for computing control rod worths with diffusion theory, 3D Monte Carlo and diffusion theory calculations (Ref. 3) were run for the fresh HEU and LEU cores for three configurations of the fork-type Ag-In-Cd control rods: (1) all five rods fully-withdrawn, (2) all five rods fully-inserted, and (3) the rod of maximum worth fully-withdrawn and four rods fully-inserted. The diffusion theory calculations were performed using internal boundary conditions derived using data from the Monte Carlo calculations for the cases with all five rods inserted and using effective diffusion parameters obtained from blackness coefficients for the case with the rod of maximum worth fully-withdrawn. The results of these validation calculations are shown in Table 4.

Table 4. METHODS COMPARISON - Monte Carlo vs Diffusion Theory
Reactivity Worth of Control Rods in **Fresh** HEU and LEU Cores

Control Rod Configuration	Monte Carlo k_{eff} (1σ)	$-\Delta\rho$, %	Diffusion Theory k_{eff}	$-\Delta\rho$, %
		HEU		
Five Rods Out	1.2152 ± 0.0032	-	1.2159	-
Five Rods In	1.0253 ± 0.0030	15.24 ± 0.39	1.0262	15.20
Max. Worth Rod Out	1.1002 ± 0.0032	8.60 ± 0.39	1.0996	8.70
		LEU		
Five Rods Out	1.1922 ± 0.0031	-	1.1903	-
Five Rods In	1.0296 ± 0.0031	13.25 ± 0.36	1.0309	12.99
Max. Worth Rod Out	1.0838 ± 0.0033	8.39 ± 0.36	1.0813	8.47

Table 5. Control Rod Worths in HEU and LEU Equilibrium Cores at BOC

Control Rod Configuration	BOC HEU Core k_{eff}	$-\Delta\rho$ %	$	BOC LEU Core k_{eff}	$-\Delta\rho$ %	$
Five Rods Out	1.0810	-	-	1.0767	-	-
Five Rods In	0.8897	19.89	26.22	0.9105	16.95	23.18
Max. Worth Rod Out	0.9623	11.42	15.05	0.9719	10.01	13.69
Five Rods 50% Out	1.0052	6.98	9.20	1.0101	6.12	8.37

The control rod worths that were computed using diffusion theory with the HEU and LEU equilibrium cores at BOC are shown in Table 5. The BOC cores are xenon-free, but contain equilibrium concentrations of samarium and lumped fission products.

The rod worths are smaller in the LEU core mainly because of the harder neutron spectrum caused by its much higher fissile loading. Both the HEU and LEU cores are predicted to be supercritical with the five rods 50% withdrawn.

As a note of interest, Attachment 1 shows a comparison of rod worths in the xenon-free BOC core, the BOC core with equilibrium xenon, and the EOC core. Although the calculations in Attachment 1 were done for a fuel shuffling pattern in which five fuel elements were replaced per cycle (as opposed to two elements per cycle) they illustrate the principle that the control rods have their minimum reactivity worth in the xenon-free BOC core.
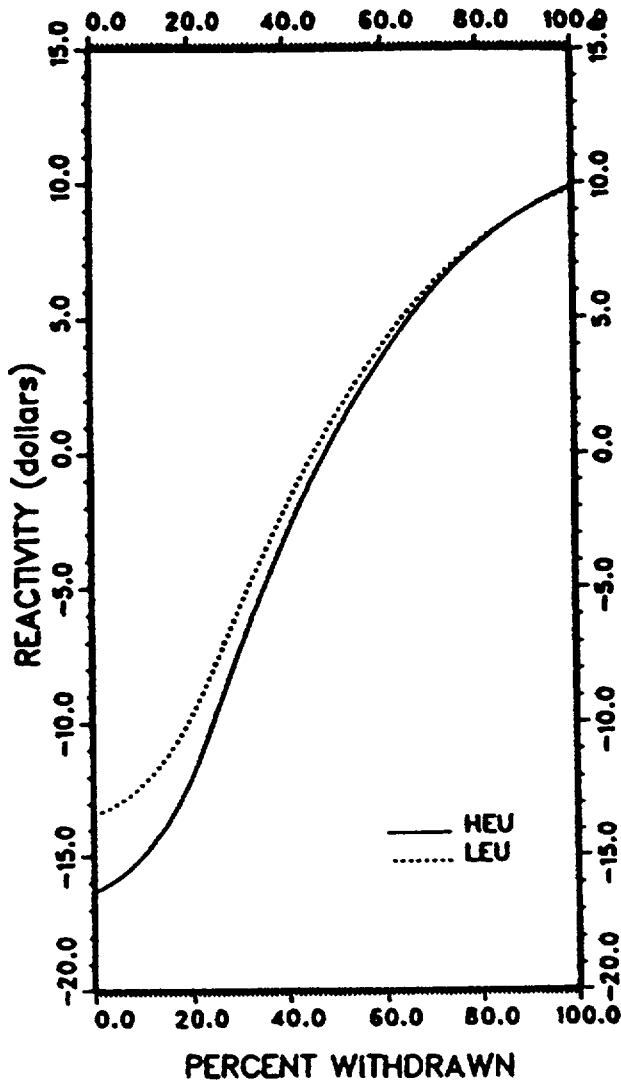
FIG. 4. Reactivity vs rod position.

3.5 Reactivity Worth Profiles

Profiles of reactivity worth in dollars versus percent withdrawal of the tips of the five absorbers are shown in Fig. 4 for the BOC, cold, xenon-free equilibrium cores with no experimental loads. The shapes and magnitudes of the two curves are very similar in the important operating range with the absorbers more than 50% withdrawn, even though the total LEU absorber worth is smaller by about 12%. As a result, critical absorber positions for various operational states of the reactor would be nearly the same in both cores.

3.6 Reactivity Balance Tables

As stated previously, the cycle lengths in the 3D burnup calculations were chosen so that each core had an EOC excess reactivity of 2.3% $\delta k/k$ to account for experimental loads (1.5% $\delta k/k$), a control reserve (0.5% $\delta k/k$), and the cold-to-hot reactivity swing (0.3% $\delta k/k$). The remaining components of the reactivity balance table are the reactivity loss due to burnup and the reactivity loss due to the buildup of equilibrium xenon. These data at BOC are shown in Table 6.

Table 6.   Reactivity Balance Tables for the HEU and LEU Equilibrium Cores at BOC

Reactivity Component	$\Delta\rho$, %		$\Delta\rho$, $	
	HEU	LEU	HEU	LEU
Burnup	1.90	1.65	2.50	2.26
Xe Poison	3.30	3.17	4.35	4.34
Experiments	1.50	1.50	1.98	2.05
Control Reserve	0.50	0.50	0.66	0.68
Cold-to-Hot Swing	0.30	0.30	0.40	0.41
Total Excess Reactivity	7.50	7.12	9.89	9.74
Total Excess React. × 1.5	11.25	10.68	14.84	14.61

Measured in $, the reactivity balance tables for the HEU and LEU cores are nearly the same, even though the LEU core has a cycle length of 30.6 days and the HEU core has a cycle length of 21.4 days. The main reason is that the slope of the burnup vs. time curve is smaller with LEU fuel than with HEU fuel (see IAEA-TECDOC-233, Appendix C). The total excess reactivity is multiplied by a factor of 1.5 in Table 6 for convenience in assessing one definition of the shutdown margin.

3.7 Shutdown Margins

Three examples of shutdown margins at BOC are shown in Table 7, based on the data in Tables 5 and 6 for the control rod worths and reactivity balances. One shutdown margin is based on the total excess reactivity and all rods in; the second is based on the total excess reactivity multiplied by a factor of 1.5 and all rods in, and the third is based on the total excess reactivity and the rod of maximum worth fully-withdrawn.

Table 7. Shutdown Margins in HEU and LEU Equilibrium Cores at BOC

Basis	$\Delta\rho$, % HEU	LEU	$\Delta\rho$, $ HEU	LEU
Total Excess Reactivity and All Rods In	12.39	9.83	16.33	13.44
Total Excess React. × 1.5 and All Rods In	8.64	6.27	11.38	8.57
Total Excess Reactivity and Max. Worth Rod Out	3.92	2.89	5.16	3.95

These shutdown margins are 18 - 25% smaller (measured in dollars) in the LEU core than in the HEU core, but are fully adequate to guarantee the safety of the facility. A shutdown margin of 1% $\delta k/k$ is considered to be acceptable with the rod of maximum worth fully-withdrawn.

3.8 Transient Analysis for HEU and LEU Equilibrium Cores

Selected transients were studied within three broad categories: (1) loss-of-flow transients, (2) uncontrolled slow reactivity insertions that may occur during reactor startup, and (3) rapid reactivity insertions that may occur due to failure or malfunction of a core component or misoperation of the reactor.

The basic kinetics parameters and isothermal reactivity feedback coefficients for the HEU and LEU equilibrium cores are shown below.

Parameter	HEU	LEU
Generation Time Λ, μs	54.6	42.4
Delayed Neutron Fraction β_{eff}, %	0.7587	0.7311
Water Temp. Only	0.1046	0.0737
Water Density Only $\quad \delta\rho/\delta T \times 10^{-3}$	0.0806	0.1051
Fuel Temp. Only $\qquad (38-50°C)$	0.0006	0.0247
Void Coefficient $\delta\rho/\%$ Void (0 - 10% Void)	0.0021	0.0027

The fuel properties that were used in these calculations are:

	Thermal Conductivity, W/mK	Heat Capacity* J/cm³K
HEU UAl$_x$-Al Fuel Meat	158	1.985 + 0.0010T
LEU U$_3$Si$_2$-Al Fuel Meat	50	1.929 + 0.0007T
6061 Aluminum Clad	180	2.069 + 0.0012T

*T in K.

The transients that were analyzed and the results obtained using the PARET code (Ref. 2) are summarized in the following paragraphs.

● Loss-of-Flow: Exponential flow decay with a time constant of 1.0 s from a power level of 12 MW. Trip setting at 85% of nominal flow. Time delay of 200 ms before shutdown reactivity insertion of -$10/0.5s. Engineering hot-channel factor of 1.58.

The peak temperatures reached at the clad surface were 114°C with HEU fuel and 113°C with LEU fuel. These values are far below the solidus temperature of 582°C for 6061 alloy cladding.

● Slow Reactivity Insertion: Ramp rates of 16 ¢/s for HEU and 14 ¢/s for LEU from power levels of 1 W and 10 MW. Trip setting at 12 MW and 25 ms time delay before shutdown reactivity insertion of -$10/0.5s. Ramp rates correspond to maximum insertion rates (Fig. 3) of 75.7 ¢/cm for HEU and 66.1 ¢/cm for LEU with maximum ORR rod withdrawal speed of 0.212 cm/s. Engineering hot-channel factor of 1.58.

From an initial reactor power of 1 W, the peak temperatures reached at the clad surface were 84°C with HEU fuel and 81°C with LEU fuel. From an initial reactor power of 10 MW, the corresponding peak clad temperatures were 102°C and 101°C, respectively. Again, these values are far below the temperature needed to initiate melting of the cladding.

Profiles of power, reactivity, and temperatures as a function of time for these transients would be very similar to those shown for the benchmark calculations in Appendix G-1.

● Reactivity Insertion Limits for Clad Melting: Steps and 0.5 s ramps from a power level of 1 W with and without scram at 12 MW. Time delay of 25 ms before shutdown reactivity insertion of -$10/0.5 s for cases with scram.

Table 8. Summary of Limiting Reactivity Insertions from a Power Level of 1 W
to Initiate Melting of 6061 Alloy Cladding at a Surface Temperature
of 582°C for HEU and LEU Equilibrium Cores.

	Limiting Reactivity Insertion, $	
Scram	HEU	LEU
Step Insertions, $		
Yes	2.3	2.9
No	2.3	2.9
Ramp Insertions, $/0.5s		
Yes	3.3	8.1
No	2.8	7.9

As noted in Ref. 4 and shown in Ref. 2, the results for the HEU core with
a hot-channel factor of 1.0 would be in very good agreement with the SPERT I
experimental data. Thus, our preference for these transients is to compute
the limiting reactivity insertions with a hot-channel factor of 1.0 and reduce
this value for purposes of conservatism. The results are shown in Table 8.

All of the limiting reactivity insertions are larger in the LEU equili-
brium core because of its significant prompt Doppler coefficient and larger
void coefficient.

In order to generalize the results somewhat, the calculations for the
step reactivity insertion (with scram) necessary to initiate clad melting were
repeated for several values of the prompt neutron generation time (Λ) and the
thermal conductivity of the fuel meat. The results for varying only Λ in the
HEU and LEU equilibrium cores are shown in Fig. 5 and those for varying only
the thermal conductivity of the fuel meat are shown in Fig. 6.

The linear variation with Λ in Fig. 5 is not surprising since the inverse
period $\alpha \approx (\rho-1)\beta/\Lambda$ for step insertions (ρ measured in dollars). With HEU
fuel, the limiting reactivity inertion is about \$2.3 for $\Lambda \sim 55$ μs and about
\$2.8 for $\Lambda \sim 150$ μs. With LEU fuel, the corresponding values are about \$2.9
for $\Lambda \sim 42$ μs and \$3.3 with $\Lambda \sim 150$ μs.

The step insertions necessary to initiate clad melting are approximately
constant for fuel meat thermal conductivities greater than about 40 W/mK with
HEU fuel and about 60 W/mK with LEU fuel. For thermal conductivities smaller
than these values, the limiting reactivity insertions decrease as shown in Fig. 6.

3.9 Radiological Consequences

Radiological consequence analyses (see Appendix D-1 and Ref. 5) for these
HEU and LEU cores show that there are no significant differences between HEU
and LEU fuels for the same hypothetical accidents. LEU fuel gives essentially
the same doses as HEU fuel. The buildup of plutonium in the LEU fuel does
not significantly increase the radiological consequences and the dose to
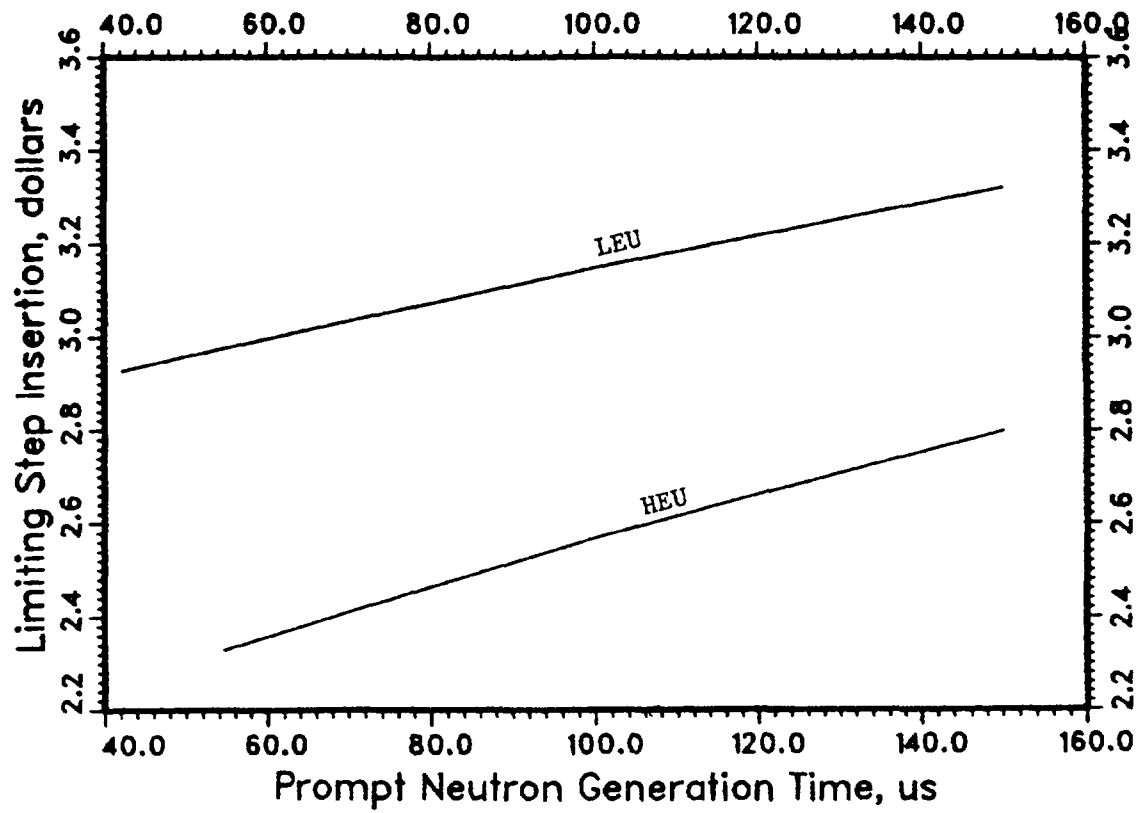the thyroid is the limiting dose.

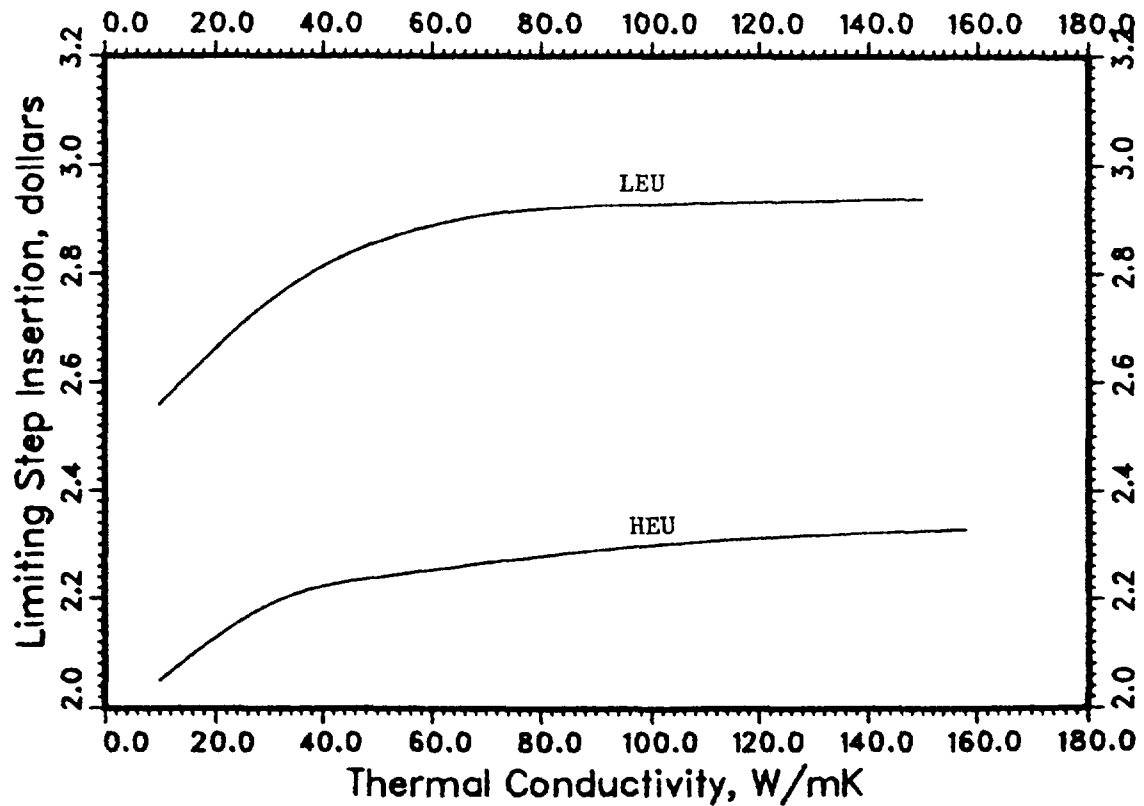FIG. 5. Step reactivity insertion to initiate clad melting vs prompt neutron generation time.

FIG. 6. Step reactivity insertion to initiate clad melting vs thermal conductivity of fuel meat.

3.10 Spent Fuel Storage

Studies of spent fuel storage (see Appendix N-3.1 and Ref. 6) show that these LEU elements could be safely stored in the pool using the same racks that are currently used with HEU fuel.

3.11 Fuel Cycle Costs

A detailed model and the results for fuel cycle cost estimates with HEU and LEU fuels can be found in Refs. 7 and 8.

The major variables in the fuel cycle are the prices for natural uranium, enrichment services, fuel fabrication, shipping, and reprocessing. There are many nuances associated with each of these variables. For example, a few of the factors that affect fuel fabrication costs are the number of fuel elements ordered, fuel element specifications, inspection procedures, the type and volume percent of the dispersed phase, and currency exchange fluctuations.

In Ref. 8, the annual fuel cycle costs are parameterized linearly as a function of the LEU/HEU fuel fabrication cost ratio. The coefficients of the lines are shown to be nearly independent of the input price assumptions as long as these prices are in a reasonable range and as long as the HEU and LEU fuel cycle costs are computed in a consistent manner. The coefficients are also independent of the reactor power level and duty factor.

For the HEU and LEU fuel elements considered in this appendix, the annual fuel cycle cost would be lower with the LEU fuel element if the LEU/HEU fuel fabrication cost ratio were less than about 1.6. If the fabrication cost of the LEU element were larger by a factor of 2.3, the total LEU fuel cycle cost would be larger by about 15%.

4. MIXED CORES

Most research reactor operators are planning to convert their cores from HEU to LEU fuel by gradually replacing their HEU elements with LEU elements. This section presents results for the key operational and safety parameters for each step of a gradual transition from HEU fuel to LEU fuel.

Over the years, many reactors have been safely operated with numerous mixed cores composed of elements with different geometries, different fissile loadings, different enrichments, or a combination of these. The same principles and safety considerations apply to the current conversions from HEU to LEU fuel.

For the same element geometry, the most important variable is the relative fissile loading of the current and replacement elements and the most important safety parameters are the shutdown margins and the margin to ONB.

Since the HEU elements in this study contain 280 g ^{235}U and the LEU elements contain 390 g ^{235}U, nuclear power peaking will be larger in mixed cores of these elements than in the individual equilibrium cores and the margins to ONB will be smaller as a result. Shutdown margins will also be smaller in both the mixed cores and the LEU equilibrium core because the neutron spectrum is harder in the more highly loaded LEU elements.

4.1 Procedures

Two sets of calculations are shown here, starting from the EOC ^{235}U loadings of the HEU xenon-free equilibrium core, for each of the 14 cycles that are needed to replace the 28 element core. In the first set, HEU elements were replaced with HEU elements using a standard calculational fuel replacement pattern in order to determine typical operating parameters and safety characteristics. One control element was discharged in each of cycles 4, 6, 8, 12, and 13 when it reached an average ^{235}U burnup of 55-60%.

In the second set, HEU elements were replaced with LEU elements, but the replacement pattern was different from the HEU case in order to minimize power peaking in the LEU control elements.

Before beginning the neutronics calculations, it is prudent to determine the maximum total nuclear power peaking factor that will yield an acceptable margin to ONB. Since the calculations for the mixed cores are performed sequentially, the adequacy of the margin to ONB and the limiting shutdown margin must be checked after each cycle. If one choice of LEU element positions does not satisfy the safety criteria, others must be tried until a successful solution is found.

Using the thermal-hydraulic input parameters shown in Section 3.3 for the equilibrium cores, the maximum acceptable total nuclear peaking factor (including axial peaking) with the five absorbers 50% withdrawn would be 3.18 if the minimum acceptable margin to ONB is assumed to be 1.2 in this example. The value of the flow instability parameter, η_{min}, that corresponds to this peaking factor would be 130. The smallest acceptable value for the shutdown margin with the rod of maximum worth fully-withdrawn was assumed to be 1% $\delta k/k$.

4.2 LEU Replacement Pattern

Conceptually, the core for the LEU replacement was divided into two regions: (1) an outer region consisting of 15 standard elements on the periphery of the core plus the standard element in location B6, and (2) an inner region consisting of the 7 remaining standard elements plus the 5 control elements. The LEU replacement pattern for all 14 mixed cores is shown in Fig. 7. Triangles indicate LEU elements and a tick mark in one corner indicates the element with the largest total nuclear power peaking factor.

Fresh LEU standard elements were always introduced in locations A2 and F6. Replacement of the outer core was completed by first replacing rows 2 and 6 (Cores 1-5 in Fig. 7) and then columns A and F plus the element in B6 (Cores 6-8). In the inner core, the standard elements in B3 and E4 were replaced first (Core 9), leaving the 5 HEU control elements with an adjacent HEU standard element. These control-standard element pairs were then replaced counterclockwise in successive cycles beginning with Core 10 and ending with Core 14.

4.3 Results

Table 9 shows a cycle-by-cycle comparison of key operational and safety characteristics for the typical HEU core and the mixed core with HEU and LEU fuel. The main results for the mixed cores (Fig. 7) are summarized below:

● All of the shutdown margins and margins to ONB are fully adequate and satisfy the reasonable safety criteria that were assumed for these example calculations.
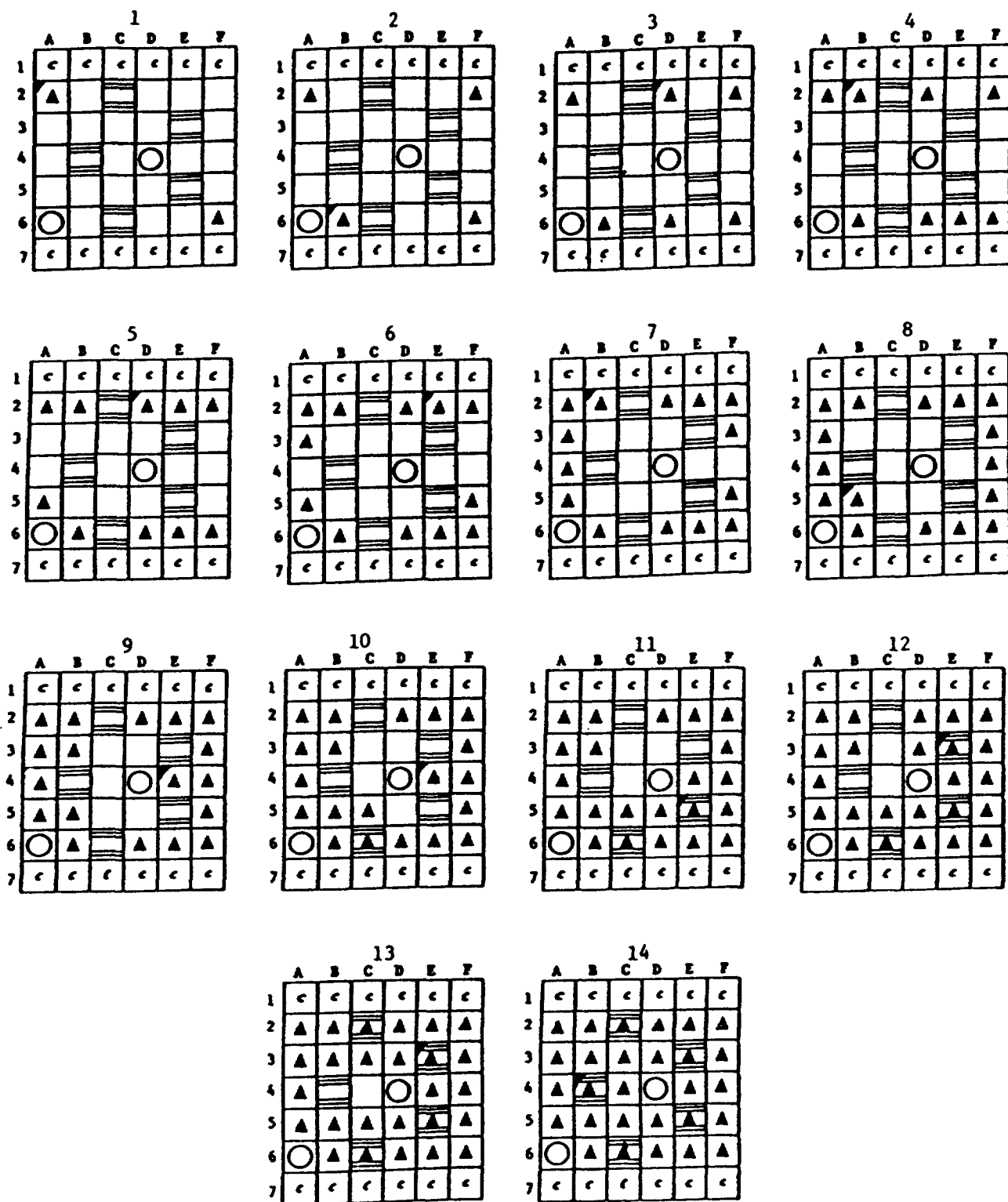
44

FIG. 7. LEU replacement pattern for each of the 14 cycles needed to convert the HEU core. Triangles indicate LEU elements. Tick mark in corner indicates element with largest nuclear power peaking factor.

45

Table 9. Cycle-by-Cycle Comparison of Key Operational and Safety Characteristics for a Typical HEU Core and a Mixed Core of HEU and LEU Fuel. The Fuel Replacement Patterns are <u>Different</u> for the Two Cases (See Text).

Cycle No. and Replacement Fuel	Cycle Length, Days	Total Excess Reactivity, % BOC	Total Excess Reactivity, % EOC	Shutdown Margins at BOC (no Xe), % Based on Total Excess Reactivity, All Rods In	Based on Total Excess React. x 1.5, All Rods In	Based on Total Excess Reactivity, Max. Rod Out	Total Nuclear Peaking Factor (5 Rods 50% Out), Factor	Location	Margin to ONB
1 - HEU	21.4	7.59	2.40	12.17	8.38	3.76	2.42	B2	1.58
LEU	21.4	7.64	2.48	12.05	8.23	3.68	2.45	A2	1.56
2 - HEU	21.4	7.26	2.04	12.78	9.15	4.61	2,36	E2	1.62
LEU	21.4	7.38	2.24	12.47	8.78	4.38	2.69	B6	1.42
3 - HEU	21.4	7.26	2.04	12.66	9.03	4.43	2.44	D2	1.56
LEU	21.4	7.41	2.36	12.12	8.43	4.06	2.98	D2	1.28
4 - HEU	21.4	7.36	2.13	12.47	8.79	3.66	2.57	C6	1.48
LEU	21.4	7.50	2.50	11.69	7.94	3.57	2.93	B2	1.30
5 - HEU	21.4	7.40	2.19	12.42	8.72	3.75	2.49	C6	1.53
LEU	21.4	7.51	2.57	11.64	7.89	3.73	2.79	D2	1.37
6 - HEU	21.4	7.37	2.14	12.72	9.03	4.25	2.62	C2	1.46
LEU	21.4	7.37	2.47	11.54	7.86	3.61	2.71	E2	1.41
7 - HEU	21.4	7.33	2.11	12.63	8.96	4.19	2.48	C6	1.54
LEU	21.4	7.44	2.59	11.21	7.49	3.29	2.90	B2	1.32
8 - HEU	21.4	7.41	2.19	12.66	8.96	4.34	2.58	C2	1.48
LEU	30.6	7.39	1.90	11.21	7.51	3.54	2.87	B5	1.33
9 - HEU	21.4	7.27	2.05	12.75	9.12	4.56	2.49	C2	1.53
LEU	21.4	6.82	2.07	11.66	8.25	4.07	3.07	E4	1.24
10 - HEU	21.4	7.02	1.79	13.02	9.52	4.80	2.34	C6	1.63
LEU	30.6	7.36	2.10	10.76	7.08	2.92	2.89	E4	1.32
11 - HEU	21.4	7.11	1.88	12.88	9.33	4.71	2.36	E6	1.62
LEU	30.6	7.51	2.38	10.36	6.61	3.12	2.94	E5	1.30
12 - HEU	21.4	7.04	1.79	13.06	9.54	4.87	2.63	C6	1.45
LEU	30.6	7.60	2.60	9.95	6.15	3.24	2.89	E3	1.32
13 - HEU	21.4	7.23	1.99	12.89	9.28	4.23	2.71	C2	1.41
LEU	30.6	7.58	2.68	9.69	5.90	3.04	2.77	E3	1.38
14 - HEU	21.4	7.30	2.08	12.63	8.98	3.83	2.65	C2	1.44
LEU	50.0	7.97	2.19	8.83	4.85	1.76	2.75	B4	1.39
15 - HEU	21.4	7.25	2.02	12.69	9.06	4.04	2.44	C2	1.56
LEU	30.6	6.96	2.11	10.22	6.75	3.01	2.59	B4	1.47
16 - HEU	21.4	7.31	2.10	12.63	8.98	4.11	2.37	E2	1.61
LEU	30.6	6.86	2.00	10.34	6.91	3.25	2.46	B4	1.55

• Cores 1-7 were run with the same cycle length (21.4 days) as the HEU equilibrium core since the excess reactivity added by introducing the HEU elements on the periphery of the core was relatively small. Note that the margins to ONB are smaller than in either the HEU or LEU equilibrium cores because the total nuclear peaking factors are larger in the mixed cores.

• Core 8, which completed replacement of the outer core, was run for 30.6 days (the cycle length expected when the full LEU equilibrium core is reached) in anticipation of the faster buildup of excess reactivity when partially burned LEU elements are introduced into the inner core positions.

• Core 9 had the lowest margin to ONB (1.24) of all the mixed cores. The limiting element in position E4 is adjacent to a water-filled flux trap and had a ^{235}U content of 298 g - the highest burnup LEU element available.

• Cores 10-13 were run for 30.6 days since sufficient excess reactivity for burnup was available during replacement of the inner core. The HEU control elements which were replaced had average ^{235}U discharge burnups of 60-70%.

• Core 14, which completed the LEU replacement, had the highest excess reactivity at BOC and the smallest shutdown margin (1.76% $\delta k/k$) with the rod of maximum worth fully withdrawn. This full LEU core was operated for 50 days to run down the excess reactivity to a value near that expected for the LEU equilibrium core and to maximize the burnup in two LEU elements that need to be replaced for next cycle.

• Cores 15 and 16 have characteristics similar to those of the LEU equilibrium core.

There are many possible variations in the sequence just described. All of them are valid if the safety criteria are shown to be satisfactory.

4.4 Transient Analysis for Mixed Cores of HEU and LEU Fuel

Selected transients were recomputed for two of the mixed cores: Core 9 (Fig. 6) because it has the largest total nuclear power peaking factor and Core 3 because it has the largest nuclear peaking factor in a core composed mostly of HEU fuel with essentially no Doppler coefficient or enhanced void coefficient.

The kinetics parameters and reactivity feedback coefficients were computed for Core 9 and also for Core 14, which has the highest ^{235}U content and the hardest neutron spectrum. The results are shown below.

Kinetic Parameters and Reactivity Feedback Coefficients for Core 9 and Core 14.

Parameter	Core 9	Core 14
Generation Time $\Lambda, \mu s$	49.7	41.3
Delayed Neutron Fraction β_{eff}, %	0.7495	0.7334
Water Temp. Only 	0.0813	0.0698
Water Density Only $\delta\rho/\delta T \times 10^{-3}$	0.0954	0.1043
Fuel Temp. Only (38-50°C)	0.0101	0.0268
Void Coefficient $\delta\rho/\%$ Void (0 - 10% Void)	0.0024	0.0027

Table 10. Summary of Limiting Reactivity Insertions from a Power Level of
1 W to Initiate Melting of 6061 Alloy Cladding at a Surface
Temperture of 582°C for Core 3 and Core 9 in Fig. 7.

Scram	Limiting Reactivity Insertion, $	
	Core 3	Core 9
Step Insertions, $		
Yes	2.1	2.2
No	2.0	2.2
Ramp Insertions, $/0.5s		
Yes	2.7	3.8
No	2.4	3.5

The Core 14 values are very close to those of the LEU equilibrium core.
Core 3 data were not recomputed since they would be nearly identical with
those for the HEU equilibrium core. In Core 9, the prompt neutron generation
time and Doppler coefficient are about 40% of the way between the values for
the HEU and LEU equilibrium cores and the void coefficient is about half way
between. The data are not proportional to the relative numbers of HEU and
LEU elements in Core 9 because the smaller number of HEU elements near the
center of the core have a greater importance than the larger number of HEU
elements on the periphery.

The reactivity insertion limits for clad melting that were computed for
Core 3 and Core 9 are shown in Table 10.

In Core 3, the kinetics parameters and reactivity feedback coefficients
of the HEU core were used, but the total nuclear peaking factor was increased
from 2.46 to 2.98. This resulted in decreases of $0.10 - 0.20 for the step
insertions and $0.40 - 0.60 for the ramp insertions relative to the HEU
equilibrium core values.

In Core 9, computed values of the kinetics parameters and reactivity
feedback data were used along with a total nuclear peaking factor of 3.07.
The limiting reactivity is slightly larger than in Core 3 for step insertions,
and is considerably larger for ramp insertions because of the larger Doppler
and void coefficients.

Thus, the limiting mixed core for transients in this example is Core 3
because of the increased power peaking with a few highly loaded LEU elements
in the HEU equilibrium core.

REFERENCES

1. Guidebook on "Research Reactor Core Conversions from the Use of Highly
    Enriched Uranium to the Use of Low Enriched Uranium Fuels,"
    IAEA-TECDOC-233 (August 1980).

2. W. L. Woodruff, "A Kinetics and Thermal-Hydraulics Capability for the
    Analysis of Research Reactors," Nuclear Technology 64, 196 (1984) and
    "The PARET Code and the Analysis of the SPERT I Transients,"
    ANL/RERTR/TM-4, CONF-821155 (September 1982), pp. 560-579.

3.   M. Bretscher, "Blackness Coefficients, Effective Diffusion Parameters, and Control Rod Worths for Thermal Reactors - Methods and Applications," Proceedings of the 1984 International Meeting on Reduced Enrichment for Research and Test Reactors, Argonne National Laboratory, Argonne, Illinois, 15-18 October 1984, ANL/RERTR/TM-6, CONF-8410173 (July 1985), pp. 388-410.

M. Bretscher, "Blackness Coefficients, Effective Diffusion Parameters, and Control Rod Worths for Thermal Reactors," ANL/RERTR/TM-5 (September 1984).

4.   J. E. Matos, K. E. Freese, and W. L. Woodruff, "Comparison of Safety Parameters and Transient Behavior of a 10 MW Reactor With HEU and LEU Fuels," Proceedings of the International Meeting on Reduced Enrichment for Research and Test Reactors, 24-27 October 1983, Tokai, Japan, JAERI-M 84-073 (May 1984), pp. 270-288.

5.   W. L. Woodruff, D. K. Warinner, and J. E. Matos, "A Radiological Consequence Analysis with HEU and LEU Fuels," ANL/RERTR/TM-6, CONF-8410173, (July 1985), pp. 472-490.

6.   R. B. Pond and J. E. Matos, "Nuclear Criticality Assessment of LEU and HEU Fuel Element Storage," JAERI-M 84-073 (May 1984), pp. 416-425.

7.   J. E. Matos and K. E. Freese, "Fuel Cycle Cost Comparisons With Oxide and Silicide Fuels," Proceedings of the International Meeting on Research and Test Reactor Core Conversions from HEU to LEU Fuels, Argonne National Laboratory, Argonne, Illinois, 8-10 November 1982, ANL/RERTR/TM-4, CONF-821155, (September 1983), pp. 517-542.

8.   J. E. Matos and K. E. Freese, "A Fuel Cycle Cost Study With HEU and LEU Fuels," ANL/RERTR/TM-6, CONF-8410173 (July 1985), pp. 223-233.

Results are provided in this Attachment for the reactivity worth of the control rods, the prompt neutron generation time, the effective delayed neutron fraction, and the reactivity feedback components for three states of the reactor:

BOC: Xenon-free core; beginning of equilibrium cycle
Zero Sm and lumped fission products in fresh elements
Equilibrium Sm and lumped fission products in burned elements

BOC*: Same as BOC, but with equilibrium Xe in all fuel elements

EOC: End of equilibrium cycle
Equilibrium fission product concentrations in all fuel elements

The calculations were performed for HEU and LEU equilibrium cores in which five fuel elements were replaced per cycle. Two fuel elements were replaced per cycle for all of the calculations shown in the text.

The purpose is to show that the limiting state of the core from a safety point of view is at BOC.

Table A1. Diffusion Theory Control Rod Worths at BOC, BOC*, and EOC in HEU and LEU Equilibrium Cores With Five-Element Replacement Pattern.

Control Rod Configuration	$\Delta\rho$ [a], %				$\Delta\rho$ [a], $		
	BOC	BOC*	EOC		BOC	BOC*	EOC
				HEU			
Five Rods In	18.64	18.88	20.90		24.59	24.91	27.54
Max. Worth Rod Out	11.94	12.13	13.40		15.75	16.00	17.65
				LEU			
Five Rods In	16.03	16.22	17.61		21.78	22.04	24.22
Max. Worth Rod Out	10.43	10.58	11.46		14.17	14.38	15.76

[a]Relative to five rods fully-out.

Table A2. Λ and β_{eff} at BOC, BOC*, and EOC for HEU and LEU Equilibrium Cores With Five-Element Replacement Pattern.

	Λ, μs			β_{eff}		
	BOC	BOC*	EOC	BOC	BOC*	EOC
HEU	50.7	50.9	57.5	0.00758	0.00758	0.00759
LSI	40.1	40.2	44.3	0.00736	0.00736	0.00727
LOX	41.2	41.4	45.0	0.00741	0.00741	0.00733

Table A3. Slopes of Reativity Components (38°C → 50°C) at BOC, BOC*, and EOC. HEU and LEU Equilibrium Cores with Five-Element Replacement Pattern.

Effect		HEU Core BOC	BOC*	EOC
Water Temperature		0.0903	0.1078	0.1344
Water Density	$\delta\rho/\delta T \times 10^{-3}$	0.0793	0.0826	0.0837
Fuel Temperature	(38 – 50°C)	0.0006	0.0006	0.0005
Total		0.1702	0.1910	0.2186
Void Coeff. $\delta\rho/\%$ Void (0-10% Void)		0.0021	0.0022	0.0022

Effect		LEU Core BOC	BOC*	EOC
Water Temperature		0.0646	0.0773	0.0943
Water Density	$\delta\rho/\delta T \times 10^{-3}$	0.1021	0.1051	0.1093
Fuel Temperature	(38 – 50°C)	0.0240	0.0249	0.0258
Total		0.1907	0.2073	0.2294
Void Coeff. $\delta\rho/\%$ Void (0-10% Void)		0.0027	0.0028	0.0029

Appendix A-3

**TYPICAL SAFETY ANALYSES FOR
UZrH FUEL — 10 MW CORE**

GA TECHNOLOGIES, INC.,
San Diego, California,
United States of America

Abstract

Typical safety analyses are provided for a 10-MW TRIGA LEU reactor using the 16-rod UZrH (45 wt-%) fuel cluster. Results include data on the prompt negative temperature coefficient and heat transfer parameters along with analyses for a start-up accident and a loss-of-flow accident.

1. 10-MW TRIGA-LEU FUEL AND REACTOR DESIGN DESCRIPTION-SUMMARY

The parameters describing a 10-MW TRIGA-LEU reactor which uses the 16-rod UZrH fuel cluster are summarized as follows:

Fuel Cluster: TRIGA-LEU 45 wt-% U in UZrH (76 mm x 80 mm x 559 mm)

Fuel rods per cluster: 16

Nominal fuel rod dimensions:

      Fuel O.D.: 13.0 mm

      Clad O.D.: 13.7 mm (Incoloy)

      Fuel height: 559 mm

Fuel loading: 274 gm U (20% enriched)/rod

             4.38 Kg U (20% enriched)/cluster

             877 gm U-235/cluster

             ~0.8 wt-% Erbium as burnable absorber

Number of fuel clusters in the core: 30

Number of control rods: 4 or 5

Reflector: Water

Core volume (liters): 105

U-235 Content/core (Kg): 26.3

Core Geometry: 6 x 6 arrangement

Grid plate: 6 x 9 positions (normal conversion)

Desired average burnup of U-235 in the fuel cluster discharged from the
    core: >40%

Burnup status of the core: equilibrium core

Average core burnup (%):   ~25

Fuel Shuffling: introduction of new fuel clusters into the core center

Thermal-hydraulic data:

      Average power density (Kw/liter):   95

      Coolant flow rate: 5000 GPM, 1135 M^3/hr (1.9 x 10^7 cc/min)

      Core inlet temperature: 38°C

2. FUEL DESIGN DESCRIPTION

The TRIGA fuel uses a uranium-zirconium hydride fuel material in which the hydrogen moderator is homogenously contained within the fuel material. It is this feature which leads to the large prompt negative temperature coefficient of reactivity and the inherent safety of TRIGA reactors. Although each fuel rod is actually a fuel-moderator rod, it will be referred to simply as a fuel rod.

Figures 1, 2, and 3 show the general layout of the fuel rod and the 16-rod fuel cluster. The fuel cluster consists of 16 fuel rods arranged in a 4 by 4 square array. The cluster is contained within a rectangular aluminum shroud with inner dimensions forming a 6.805-cm (2.679-in.) square. The shroud serves two principal functions:

1. It provides structural support and protection.

2. It confines the coolant flow for each array to a fixed channel, making it unnecessary to provide a cooling flow shroud around the complete core and thus allowing greater flexibility to the core size and shape.

The shroud is attached to an aluminum bottom fitting which fits into the reactor grid plate. The shroud also supports a top separator and two intermediate separators which maintain the spacing between fuel rods. Two circular holes are located in the shroud wall near the top of the shroud which are used for handling the cluster. Rectangular holes are located in the shroud wall near the top of the fuel rods to provide an alternate flow path for coolant in the unlikely event that the top of the fuel cluster is blocked by some foreign object.

54
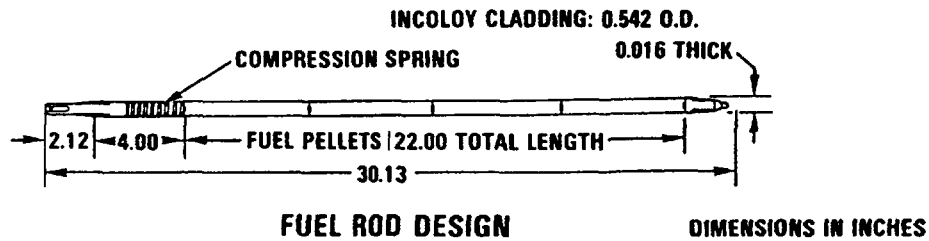
Fig. 1. TRIGA fuel rod for 16-rod cluster
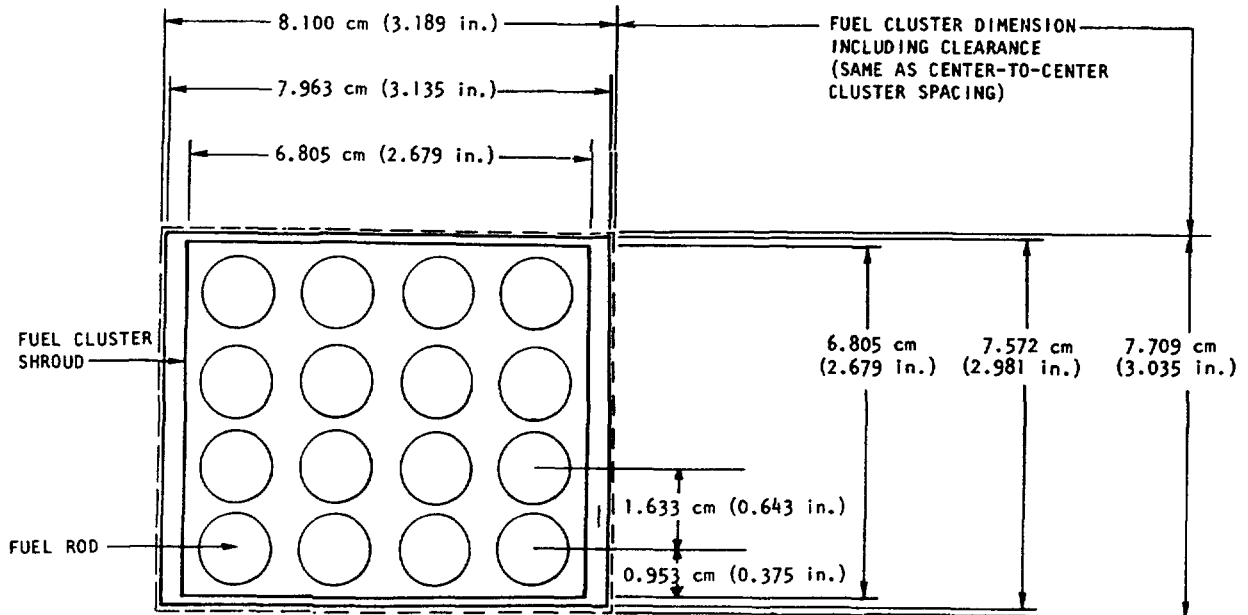
Fig. 2. General layout of 16-rod fuel cluster

There is an ~10-cm (4-in.) section at the top of each fuel rod which is included as a flow-straightening section for the coolant and allows free differential expansion of the fuel and cladding. A spring is installed to ensure that the fuel pieces remain in position. Stainless steel end fittings are heliarc welded to both ends of the cladding.

The hydrogen-to-zirconium atom ratio of the fuel material is approximately 1.6. The fuel pieces are ground to a high polish and exact tolerances in order to fit closely into the cladding. During final assembly, the clearance area between the fuel rod and the cladding is filled with helium at about 1/10th of atmospheric pressure before final welding. The close tolerances and helium backfill increase the heat transfer across the fuel-clad interface and result in lower fuel centerline temperature.

55
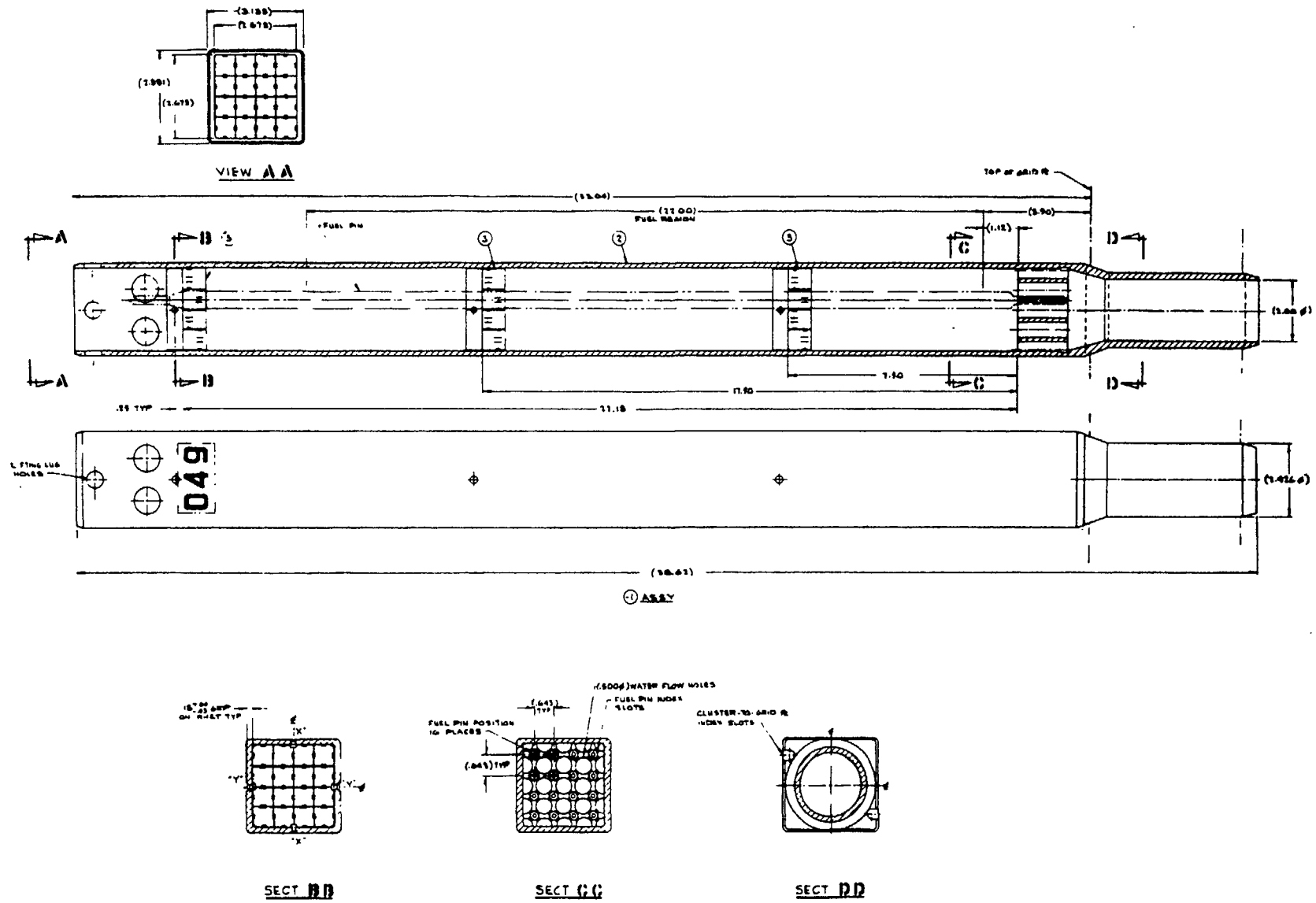
Fig. 3.   Details of 16-rod fuel cluster

Instrumented fuel rods have three thermocouples inserted in the fuel. The sensing tips of the thermocouples are located on the axial centerline of the fuel section and spaced about 2.54 cm (1.0 in.) below the core horizontal midplane. In other respects the instrumented fuel rod is identical to the standard rod.

The individual fuel rods are designed so that any single rod can be removed from its fuel cluster at any time.

Shown in Fig. 4 is the core configuration for a reference 10-MW reactor.
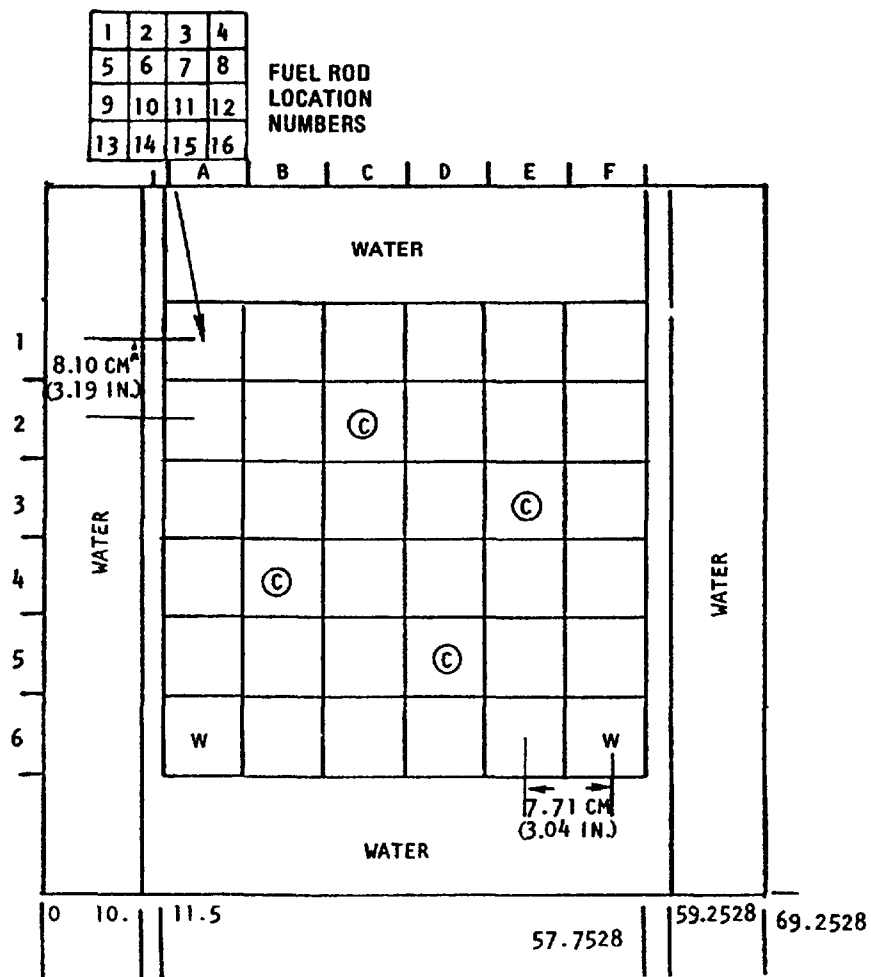
Fig. 4. Core arrangements and typical dimensions for 10-MW TRIGA geometry

3. NUCLEAR DESIGN CHARACTERISTICS

3.1. REACTIVITY REQUIREMENTS

Table 1 summarizes many of the core design parameters and characteristics. On initial startup of the core, it is estimated that about 4% to 5% excess reactivity is necessary to compensate for equilibrium xenon, the reactivity loss due to heating of the fuel and the buildup of Sm-149 during the initial few weeks of full-power operation. Since the reactivity loss due to samarium results from the buildup of a stable isotope, it builds up to an equilibrium value (rather quickly) and remains at that value during core life. Thus, the reactivity change in going from zero to full power does not include the reactivity loss due to Sm-149.

TABLE 1

SUMMARY OF CORE DESIGN PARAMETERS AND CHARACTERISTICS

Reactivity requirements, δk ($)	
Xenon (equilibrium)	~2.8% ($4.00)
Samarium (equilibrium)	0.8% ($1.14)
Cold-to-hot reactivity change[a]	0.8 - 1.3% ($1.14 - $1.86)
Total	~4.4 - 4.9% ($6.29 - $7.00)
Operational reactivity change[b]	~3.6 - 4.1% ($5.14 - $5.86)
β_{eff} (δk)	0.0070
ℓ(microsec)	~25 (beginning-of-life) ~32 (end-of-life)
Maximum fuel temperature	640°C
Recommended excess reactivity at beginning-of-life, δk	>6.0% ($8.57)
Recommended control system worth, δk	
With maximum-worth rod stuck out	>6.5%[c] ($9.29)

[a]Based on a peak fuel temperature of 640°C and an average core temperature of 255°C.

[b]Samarium not included.

[c]It is possible to use an existing control system when converting a core. GA Technologies Inc. has a control system designed for use with this core having a worth of about 8% with the maximum worth rod stuck out. It consists of 4 rods arranged as shown in Fig. 4. Each rod is 6.87 in. O.D. and contains B_4C compacts.

TABLE 2
NEUTRON ENERGY GROUP STRUCTURE

Group	Lethargy Interval	Energy Interval (eV)
1	-0.4 - 2.8	$14.9 \times 10^6 - 6.08 \times 10^5$
2	2.8 - 7.0	$6.08 \times 10^5 - 9.12 \times 10^3$
3	7.0 - 16.0	$9.12 \times 10^3 - 1.125$
4	16.0 - 16.98	1.125 - 0.420
5	16.98 - 18.08	0.420 - 0.140
6	18.08 - 19.11	0.140 - 0.050
7	19.11 -	0.050 - 0.002

3.2. CALCULATIONAL METHODS

Neutron cross sections used in the analyses are generated for seven neutron energy groups. The lethargy and the energy for each each of the seven broad groups are given in Table 2.

All neutron cross sections for energies above thermal (>1.125 eV) are generated using the GGC-5 code where fine-group (approximately 100-group) cross sections, stored on tape for all commonly used isotopes, are averaged over a spatially independent flux derived by solution of the B-1 equations for each discrete reactor region composition. This code and its related cross section library predict the age of each of the common moderating materials to within a few percent of the experimentally determined values. The resonance integral method of Nordheim is used to generate cross sections for resonance materials.

The core thermal cross sections are generated using the multigroup cross section code GTF. GTF computes the spatially dependent thermal spectra at each mesh point in the cell, using the discrete ordinates method and the fine-group (58-point) cross section data contained in the thermal portion of the GGC-5 code.

Scattering kernels are used to describe properly the interactions of the neutrons with the chemically bound moderator atoms. The bound hydrogen

kernels for hydrogen in water were generated by the THERMIDOR code, while those for hydrogen in zirconium hydride were generated by SUMMIT. These scattering models have been used to predict adequately the water and hydride (temperature-dependent) spectra as measured at the GA Technologies' linear accelerator.

The unit cell description used in the generation of the thermal cross sections for the core is given in Table 3. The fuel and clad dimensions represent the rod exactly, but the water dimension has been specified such that it represents 1/16 of the water associated with a fuel cluster (including the shroud clearance). The aluminum shroud will not affect the spectrum so is not included in the calculation.

The epithermal core spectrum was calculated using the homogenized fuel cluster atom densities as given in Table 4.

TABLE 3
UNIT CELL DESCRIPTION

Region	Radius (cm)	Nuclide	N (Atoms/b-cm)
Er-U-ZrH$_{1.6}$	0.6475	H	0.044004[b]
		Zr	0.029282[b]
		Er-166	7.747×10^{-5}
		Er-167	5.319×10^{-5}
		U-235	0.001885
		U-238	0.007539
Incoloy clad[a]	0.6885	SS	0.0969
Water	0.98195	H	0.0668
		Oxy	0.0334

[a]Composition assumed to be 20 wt-% Cr, 2 wt-% Mn, 68 wt-% Fe, and 10 wt-% Ni (stainless steel) with stainless steel atomic density (0.0843 atoms/b-cm) increased by 15% to give thermal neutron absorption equivalent to Incoloy.

[b]$N_H/N_{Zr} \neq 1.6$ because some Zr combines with carbon impurity to form ZrC and some H combines with Er to form ErH$_{1.6}$ or ErH$_2$.

TABLE 4
HOMOGENIZED FUEL CLUSTER DESCRIPTION

Region	Volume Fraction	Nuclide	N (Atoms/b-cm)
$Er-U-ZrH_{1.6}$	0.3378	H	0.01486
		Zr	0.009892
		Er-166	2.617×10^{-5}
		Er-167	1.797×10^{-5}
		U-235	6.366×10^{-4}
		U-238	2.547×10^{-3}
Incoloy clad	0.0436	SS	0.00422
Water	0.3946	H	0.02636
		Oxy	0.01318
Al shroud	0.2240	Al	0.01351

3.3. POWER PEAKING

Power peaking in the core is analyzed on the basis of the following component values:

1. $\bar{P}_{rod}/\bar{P}_{core}$: rod power factor, the power generation in a fuel rod relative to the core average power generation.

2. $(\hat{P}/\bar{P})$ axial: axial peak-to-average power ratio (Fig. 5).

3. $(\hat{P}_{rod}/\bar{P}_{rod})$ radial: rod-peaking factor, the peak-to-average power on a radial plane within a fuel rod (Fig. 6).

Since maximum fuel temperature is the limiting operation parameter for the core, the peaking factor of greatest importance is $\bar{P}_{rod}/\bar{P}_{core}$. The maximum value of this factor, the hot-rod factor [$(\bar{P}_{rod}/\bar{P}_{core})$ max = hot-rod factor], determines the power generation in the hottest fuel rod. When combined with the axial power distribution, the hot-rod factor is used in the thermal analysis for determination of the maximum fuel temperature. (The radial power distribution within the rod has a small effect on the peak temperature.) Results of the thermal analysis show that, for nominal design conditions, hot-rod factors can be as high as about 2.3 before the design maximum operational fuel temperature of 750°C is reached.
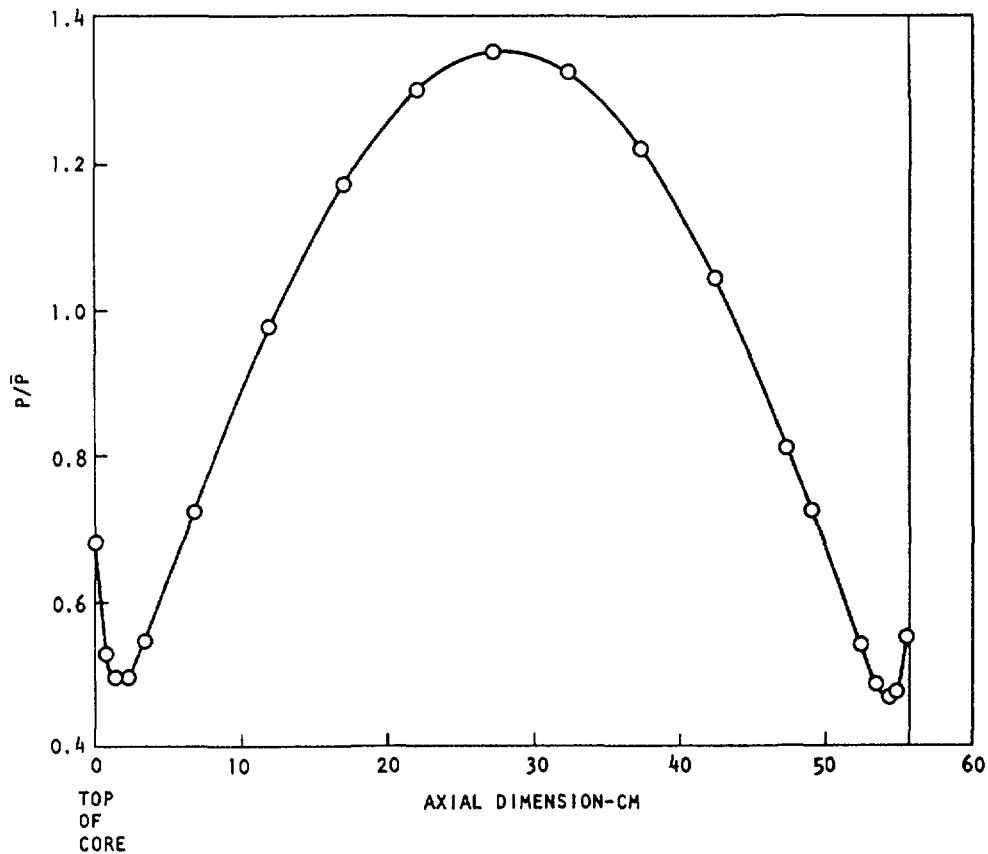
Fig. 5. Relative axial power distribution (400°C)

4. PROMPT NEGATIVE TEMPERATURE COEFFICIENT

The basic parameter which provides the great degree of safety in the operation of a TRIGA reactor system is the prompt negative temperature coefficient. This temperature coefficient (α) allows great freedom in steady-state operation, since the effect of accidental reactivity changes occurring from experimental devices in the core is minimized.

The prompt negative temperature coefficient for the 10-MW TRIGA-LEU core is based on the same core spectrum hardening characteristic that occurs in a standard* TRIGA core. The spectrum hardening is caused by heating of the fuel-moderator elements. The rise in temperature of the hydride increases the probability that a thermal neutron in the fuel element will gain energy from an excited state of an oscillating hydrogen atom in the lattice. As the neutrons gain energy from the ZrH, the thermal neutron

---

*A standard TRIGA core contains U-ZrH fuel with no erbium. The uranium enrichment is 20%, and the fuel element (rod) diameter is about 3.8 cm (1.5 in.) with a core water volume fraction of about 0.33.
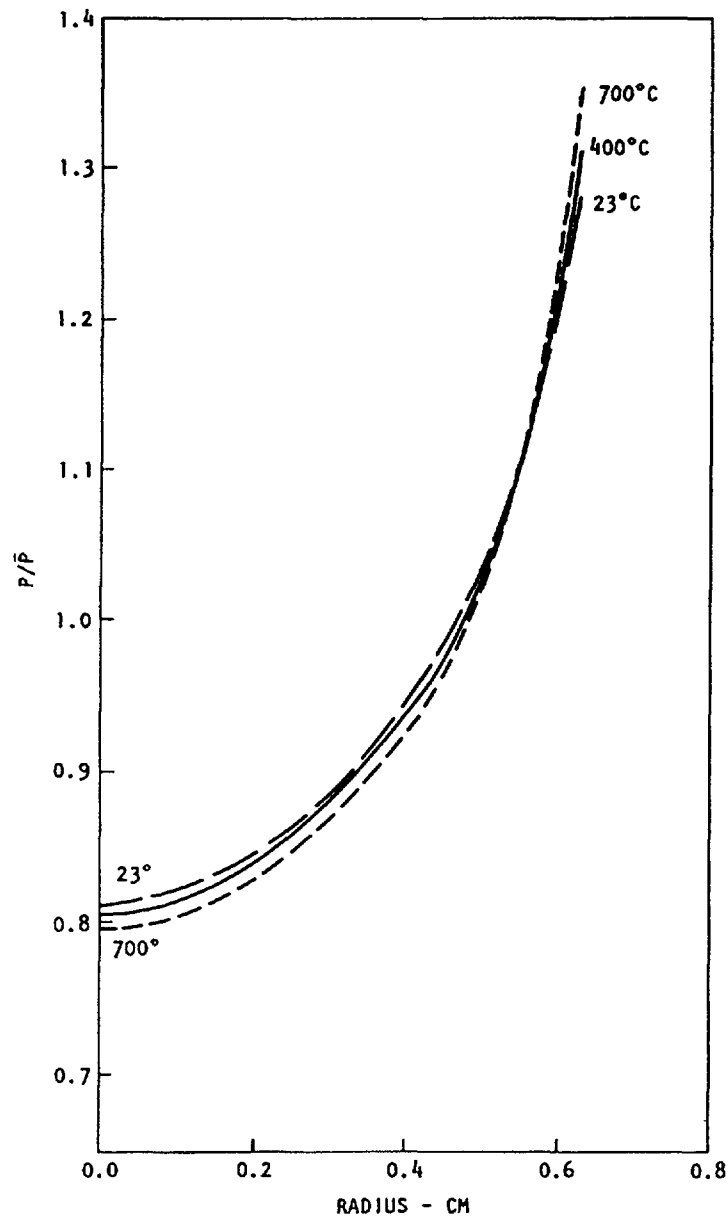
Fig. 6. Relative radial power distribution in fuel rod at various temperatures

spectrum in the fuel element shifts to a higher average energy (the spectrum is hardened), and the mean free path for neutrons in the element is increased appreciably. For a standard TRIGA element, the average chord length is comparable to a mean free path, and the probability of escape from the element before being captured is significantly increased as the fuel temperature is raised. In the water the neutrons are rapidly rethermalized so that the capture and escape probabilities are relatively insensitive to the energy with which the neutron enters the water. The heating of the moderator mixed with the fuel in a standard TRIGA element thus causes the spectrum to harden more in the fuel than in the water. As a result, there is a temperature-dependent disadvantage factor for the unit cell in which the

ratio of absorptions in the fuel to total cell absorptions decreases as fuel element temperature is increased. This brings about a shift in the core neutron balance, giving a loss of reactivity.

In the 10-MW TRIGA-LEU fuel, the temperature-hardened spectrum is used to decrease reactivity through its interaction with a low-energy resonance material. Thus, erbium, with its double resonance at ~0.5 eV, is used in the 10-MW TRIGA-LEU fuel both as a burnable poison and as a material to enhance the prompt negative temperature coefficient. With the smaller diameter fuel rod used in the 10-MW TRIGA, the ratio of the absorption probability to the neutron leakage probability is greatly increased relative to the standard TRIGA fuel because the U-235 density in the fuel rod is about seven times greater and also because of the use of erbium. When the fuel-moderator material is heated, the neutron spectrum is hardened, and the neutrons have an increasing probability of being captured by the low-energy resonances in erbium. This increased parasitic absorption with temperature causes the reactivity to decrease as the fuel temperature increases. The neutron spectrum shift, pushing more of the thermal neutrons into the Er-167 resonance as the fuel temperature increases, is illustrated in Fig. 7 where cold and hot neutron spectra are plotted along with the energy-dependent absorption cross section for Er-167. As with a standard TRIGA core, the temperature coefficient is prompt because the fuel is intimately mixed with a large portion of the moderator; thus, fuel and solid moderator temperatures rise simultaneously, producing the temperature-dependent spectrum shift.

For the reasons just discussed, more than 50% of the temperature coefficient for a standard TRIGA core comes from the temperature-dependent disadvantage factor, or cell effect, and ~20% each from Doppler broadening of the U-238 resonances and temperature-dependent leakage from the core. These effects produce a temperature coefficient of ~-9.5 x 10^{-5}/°C, which is essentially constant with temperature. On the other hand, for the 10-MW TRIGA-LEU core, the effect of cell structure on the temperature coefficient is small. Over the temperature range from 23°C to 700°C, slightly more than half of the coefficient comes from temperature-dependent changes in ηf within the core, and ~90% of this effect is independent of the cell structure. Almost all of the remaining part of the prompt negative temperature coefficient is contributed by Doppler broadening of the U-238 resonances.

64
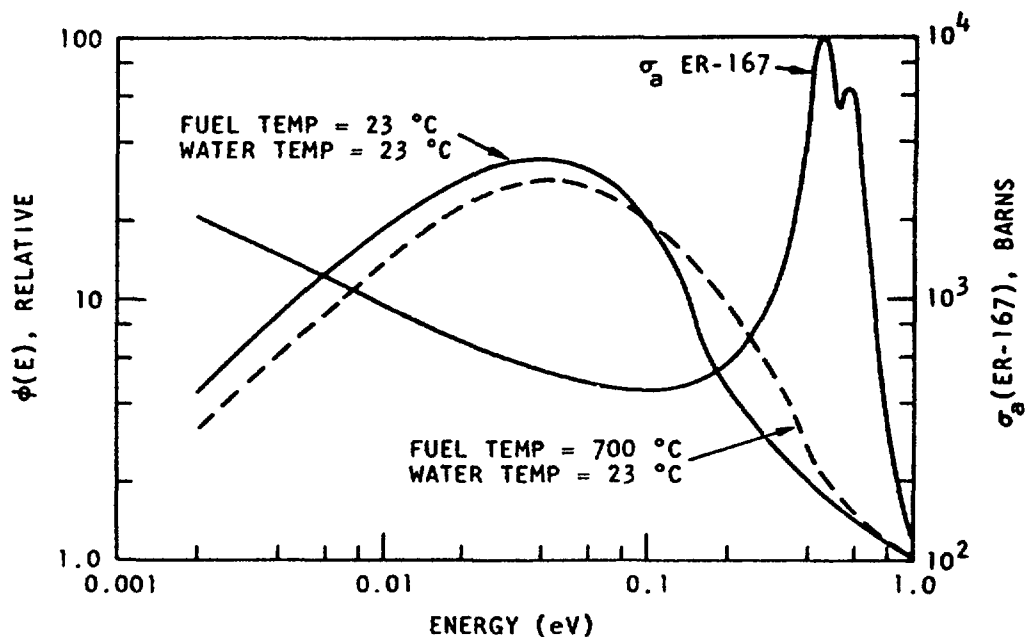
Fig. 7. Thermal neutron spectra versus fuel temperature relative to σ_a versus energy for Er-167

The calculation of the temperature coefficient for standard TRIGA and 10-MW TRIGA-LEU cores requires a knowledge of the differential slow neutron energy transfer cross section in water and zirconium hydride, the energy dependence of the transport cross section of hydrogen as bound in water and zirconium hydride, the energy dependence of the capture and fission cross sections of all relevant materials, and a multigroup transport theory reactor description which allows for the coupling of groups by speeding up as well as by slowing down.

Qualitatively, the scattering of slow neutrons by zirconium hydride can be described by a model in which the hydrogen atom motion is treated as an isotropic harmonic oscillator with energy transfer quantized in multiples of ~0.14 eV. More precisely, the SUMMIT model uses a frequency spectrum with two branches: one for the optical modes for energy transfer with the bound proton, and the other for the acoustical modes for energy transfer with the lattice as a whole. The optical modes are represented as a broad frequency band centered at 0.14 eV and whose width is adjusted to fit the cross-section data of Woods. The low-frequency acoustical modes are assumed to have a Debye spectrum with a cutoff of 0.02 eV and a weight determined by an effective mass of 360.

This structure then allows a neutron to thermalize by transition in energy units of ~0.14 eV so long as its energy is above 0.14 eV. Below 0.14

eV, the neutron can still lose energy by the inefficient process of exciting acoustic Debye-type modes in which the hydrogen atoms move in phase with one another. These modes therefore correspond to the motion of a group of atoms whose mass is much greater than that of hydrogen, and indeed even greater than the mass of zirconium. Because of the large effective mass, these modes are very inefficient for thermalizing neutrons; but for neutron energies below 0.14 eV, they provide the only mechanism for neutron slowing down. (In a TRIGA core, the water provides for ample neutron thermalization below 0.14 eV.) In addition, in the ZrH it is possible for a neutron to gain one or more energy units of ~0.14 eV in one or several scatterings from excited Einstein oscillators. Since the number of excited oscillators present in a ZrH lattice increases with temperature, this process of neutron speeding up is strongly temperature-dependent and plays an important role in the behavior of ZrH-moderated reactors.

The temperature coefficient at the beginning of life for the 10-MW TRIGA-LEU core increases as a function of fuel temperature because of the steadily increasing number of thermal neutrons being pushed into the Er-167 resonance. This temperature-dependent character of the temperature coefficient of a TRIGA core containing erbium is advantageous in that a minimum reactivity loss is incurred in reaching normal operating temperatures, but any sizeable increase in the average core temperature results in a sizably increased prompt negative temperature coefficient to act as a shutdown mechanism. The end-of-life coefficient is less temperature-dependent than the beginning-of-life coefficient because of the sizable loss of Er-167 and the resulting increased transparency of the approximate 0.5-eV resonance region to thermal neutrons. Temperature coefficient values are shown in Fig. 8, which depicts the approximate shape and relationship of the beginning-of-life and end-of-life curves.

5. HEAT TRANSFER ANALYSIS

The heat generated in the fuel is conducted through the fuel, across the fuel-cladding interface, and through the cladding to the coolant. Although most of the temperature drop from the center of the fuel rod to the coolant takes place in the fuel, a significant drop occurs in the fuel-cladding interface. Special attention was given, therefore, to this fuel-cladding interface in the design of the fuel rod.
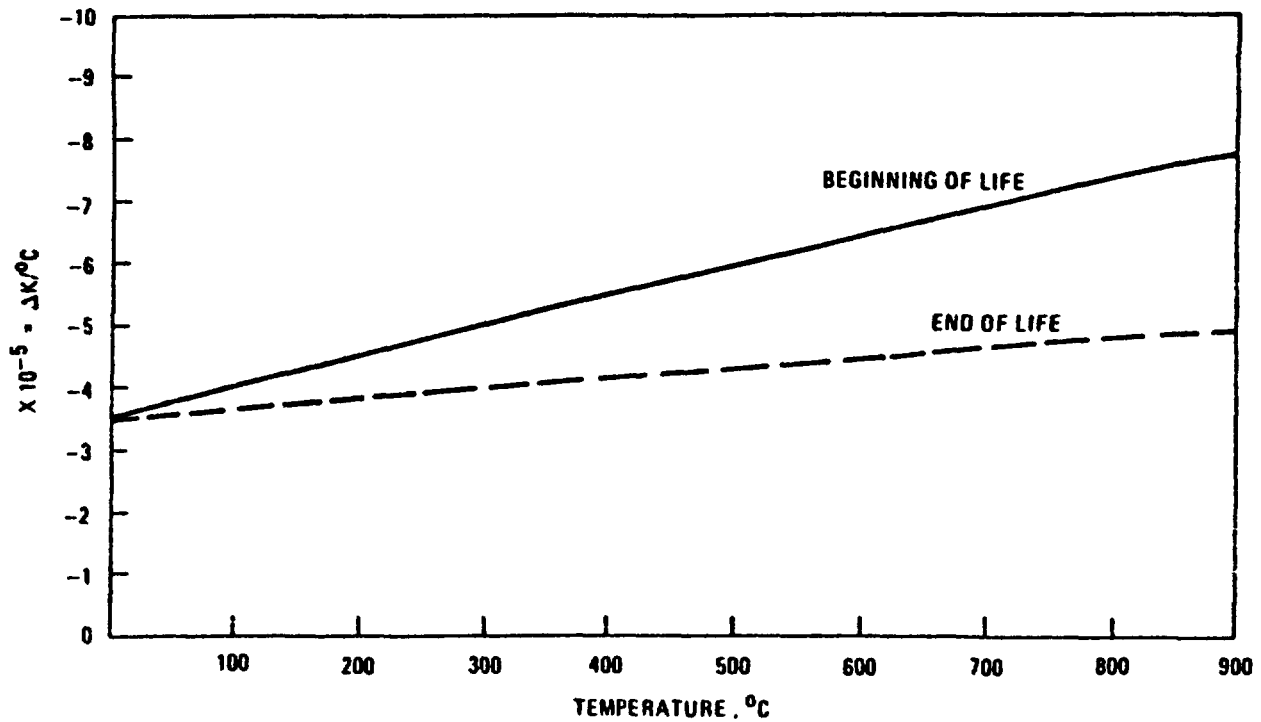
Fig. 8. Relative temperature coefficient as a function of temperature for beginning of life and end of life

The TIGER computer code was used to perform the thermal-hydraulic analysis of the steady-state reactor core. This code was originally developed by Westinghouse for the analysis of pressurized water reactors; hence, correlations applicable to 10-MW TRIGA conditions were added to the core. The TIGER code is a finite difference solution of the one-dimensional momentum and energy transport equations. The output from the code includes the axial variations of flow rate, velocity, pressure drop, bulk coolant and surface temperatures, and DNB* ratio.

The forced convection heat transfer coefficient h was determined with the Dittus-Boelter correlation as recommended by Tong and Weisman:

$$Nu = 0.023 \ Re^{0.8} \ Pr^{0.4} \quad , \tag{1}$$

where Nu, Re, and Pr are the Nusselt, Reynolds, and Prandtl numbers, respectively, based on the bulk water properties. Various refinements to Eq. 1 are possible by considering film properties; however, these were not

_____

*Departure from nucleate boiling (ratio of critical heat flux to calculated heat flux).

considered necessary and Eq. 1 was used, although it is somewhat conservative. Similarly, the pressure loss calculations were based on bulk properties, which also is conservative. Although Eq. 1 was derived from experiments in tubes, it has been shown, as discussed by Tong, that it is valid for fuel cluster geometries provided the equivalent hydraulic diameters of the subchannels are used. In fact, for the fuel rod pitch-to-diameter ratios in the 10-MW TRIGA, the leading coefficient in Eq. 1 is actually smaller than some published values, and hence conservative. In forced convection the heat flux and the wall and bulk temperatures are related by

$$q_{fc} = h \ (T_w - T_b) \quad , \tag{2}$$

where q_{fc} = forced convection heat flux (Btu/hr-ft^2),

h = force convection heat transfer coefficient (Btu/hr-ft^2-°F),

T_w = wall temperature (°F),

T_b = coolant bulk temperature (°F).

At certain pressure and temperature conditions an incipient heat flux, q_i, exists at which isolated vapor nucleations occur on the cladding surface. The correlation used with the Dittus-Boelter relationship (Eq. 1) to predict q_i was reported by Bergles and Rohsenow as follows:

$$q_i = 15.60 \ p^{1.156} \Delta T_s^\alpha \quad , \qquad \alpha = 2.30 \ p^{-0.0234} \quad , \tag{3}$$

where p = absolute pressure (psia),

T_s = degree of superheat (°F) (the surface temperature minus the saturation temperature),

q_i = incipient heat flux (Btu/hr-ft^2).

At heat fluxes above q_i more nucleation sites are created on the cladding surface so that the heat is removed partly by forced convection and partly by local, subcooled nucleate boiling. Eventually, at still higher heat fluxes, the surface is uniformly covered by a dynamic bubble-layer and the heat is removed by fully developed, subcooled nucleate boiling. The correlation used for this mode of heat transfer is due to McAdams et al:

68

$$q_{fd} = 0.074 \ \Delta T_s^{3.86} \quad , \tag{4}$$

where q_{fd} is the heat flux for fully developed, subcooled nucleate boiling (Btu/hr-ft^2). In the transition region, between forced convection and fully developed, subcooled nucleate boiling, Eqs. 2 and 4 were interpolated by a scheme due to Bergles and Rohsenow. Since the heat flux is specified for the TRIGA fuel rod, Eqs. 1 to 4 and the interpolation scheme can determine the surface temperature. This is done in TIGER.

In the fully developed nucleate boiling regime it is possible to increase the heat flux further without an appreciable change in the surface temperature, until the bubble motion on the surface becomes so violent that a hydrodynamic crisis occurs with the formation of a continuous vapor film on the surface. This is termed departure from nucleate boiling (DNB) and the heat flux is the critical heat flux (CHF). The ratio of the CHF to the actual heat flux is the DNB ratio. In subcooled boiling the CHF is a function of the coolant velocity, the degree of subcooling, and the pressure. The correlation used to predict CHF is due to Lund which was developed from empirical data gathered from an experiment conducted on a test assembly that conformed to the actual fuel bundle in terms of dimension, flow, and heat flux. The critical heat flux is given by

$$q_c = 0.5 \ f_c \ \rho \ V_g \ C_p \ (T_c - T_o) \quad , \tag{5}$$

where f_c = friction factor for the channel between fuel rods

   = $0.55 \ Re_g^{-0.37}$

Re_q = Reynolds number for the interrod channel

   = $2\rho V_g D_r \ (S-1)/\mu_{sat}$

V_g = interrod channel velocity

   = $V \ [1.0 - 0.98 \ e^{-2.2(S-1)}]$

S = pitch-to-diameter ratio

D_r = rod diameter, ft

V = average velocity, ft/hr

ρ = density, lb/ft^3

μ_{sat} = viscosity at saturation temperature, lb/ft hr

C_p = constant pressure specific heat, Btu/lb°F

T_o = temperature at outlet of cooling channel, °F

T_c = critical wall temperature, °F

The critical wall temperature is given by

$$T_c = T_{sat} (1 + 6 \sqrt{\theta_c})$$

where T_{sat} = saturation temperature

$\theta_c = q_c \sigma_{sat} / p \mu_{sat} h_{fg}$

σ_{sat} = saturation surface tension, lb/ft

p = absolute pressure, lb/ft^2

and h_{fg} = heat of vaporization, Btu/lb

The design flow rate has a lower limit determined by the value of the CHF at that flow rate; the larger the flow rate the larger will be the CHF and hence the safety margin. The flow rate also has an upper limit which is determined by the maximum allowable pressure drop through the bundle to avoid cavitation in the flow system. In TIGER, pressure losses are calculated using the friction perimeter and area of the cluster with the standard Blasius formula for turbulent pipe flow. In addition, there are provisions for head loss coefficients along the flow channel to account for the presence of spacer grids. The values used in TIGER for the head loss coefficients were derived from measured pressure drops through a fuel element cluster that was hydraulically equivalent to the 10-MW TRIGA fuel cluster. In the 10-MW TRIGA design there is a large range of feasible flow rates between the upper and lower limits.

The contact pressure or the interface gap between the fuel rod and the clad are computed by TIGER, given the temperature distribution and the initial (cold) gap. Assuming a parabolic temperature distribution, which closely approximates the temperatures in the fuel, the expansion of the fuel material is calculated as a nonlinear function of the temperature. The cladding expansion is proportional to the average cladding temperature. When the power generation in the fuel increases, a temperature distribution is reached where the fuel expands more than the cladding, narrowing the initial interface gap until contact occurs between the fuel and cladding. At this point the fuel and cladding may interact and develop a contact pressure between the fuel and cladding which can increase until the yield stress of the cladding is reached, beyond which no further increase in pressure occurs.

The results of the thermal-hydraulic analyses, using the design conditions in Table 5, are summarized in Fig. 9. The abscissa is the axial dis-

TABLE 5
DESIGN CONDITIONS USED FOR THERMAL ANALYSIS OF THE 10-MW TRIGA REACTOR

Fuel pellet diameter, cm (in.)	1.29 (0.508)
Cladding outside diameter, cm (in.)	1.37 (0.540)
Heated length, cm (in.)	55.9 (22.0)
Inlet temperature, °C (°F)	37 (98.6)
Bulk coolant temperature rise @ 5000 gpm, °C (°F)	7.7 (13.8)
Inlet pressure, kPa (psia)	174 (25.2)
Core pressure drop @ 5000 gpm, kPa (psia)	68.9 (10)
Cluster flow area per rod, cm^2 (in.^{2})	1.37 (0.213)
Cluster hydraulic diameter, cm (in.)	0.91 (0.36)
Cluster mass velocity, kg/sec-m^2 [lb (mass)/hr-ft^2] (equivalent to 5000 gpm per 30 clusters)	4780 (3.526 x 10^6)
Inlet pressure loss coefficient (converting one velocity head)	3.2
Spacer pressure loss coefficient (each)	0.4
Outlet pressure loss coefficient (converting one velocity head)	0.8
Hot rod factor	1.8
Core average heat flux, W/cm^2 [Btu/hr-ft^2]	86.4 ±4.4 [2.74 ±0.14) x 10^5]
Initial fuel-cladding radial gap, µ (in.)	22.2 ±9.5 (0.00087 ±0.00037)
Fuel-cladding surface roughness, µ (µin.)	0.813 ±0.203 (32 ±8.0)
Cladding thermal conductivity, W/m °C (Btu/hr-ft-°F)	16.8 ±0.7 (9.7 ±0.4)
Fuel thermal conductivity @ 1000°F W/m °C (Btu/hr-ft-°F)	21.6 ±2.6 (12.5 ±1.5)
Fuel-cladding gap helium gas conductivity, W/m °C (Btu/hr-ft-°F)	0.199 ±0.026 (0.115 ±0.015)
Fuel-cladding gap helium gas partial pressure, kPa (psia)	10.1 (1.47)
Cladding thermal expansion coefficient, °C^{-1} (°F^{-1})	(17.2 ±0.5) x 10^{-6} [(9.53 ±0.28) x 10^{-6}]
Cladding hardness to yield stress ratio	6.4 ±0.6
Fuel linear thermal expansion coefficient, °C^{-1} (°F^{-1})	(4.18 ±0.22) x 10^{-6} [(2.32 ±0.12) x 10^{-6}]
Fuel second-order thermal expansion coefficient, °C^{-2} (°F^{-2})	19.2 x 10^{-9} (5.94 x 10^{-9})
Cladding yield strength, MPa (ksi)	251.5 (36.5)
Cladding elasticity modulus, MPa (ksi)	188,000 (27,400)
Fuel elasticity modulus, MPa (ksi)	75,900 (11,000)

tance from top to bottom of the heated length of the cluster. The ordinates
are heat flux, fuel temperature, cladding temperature, and water temperature.
The results are shown for the hot channel with a hot-rod factor of ~1.8.
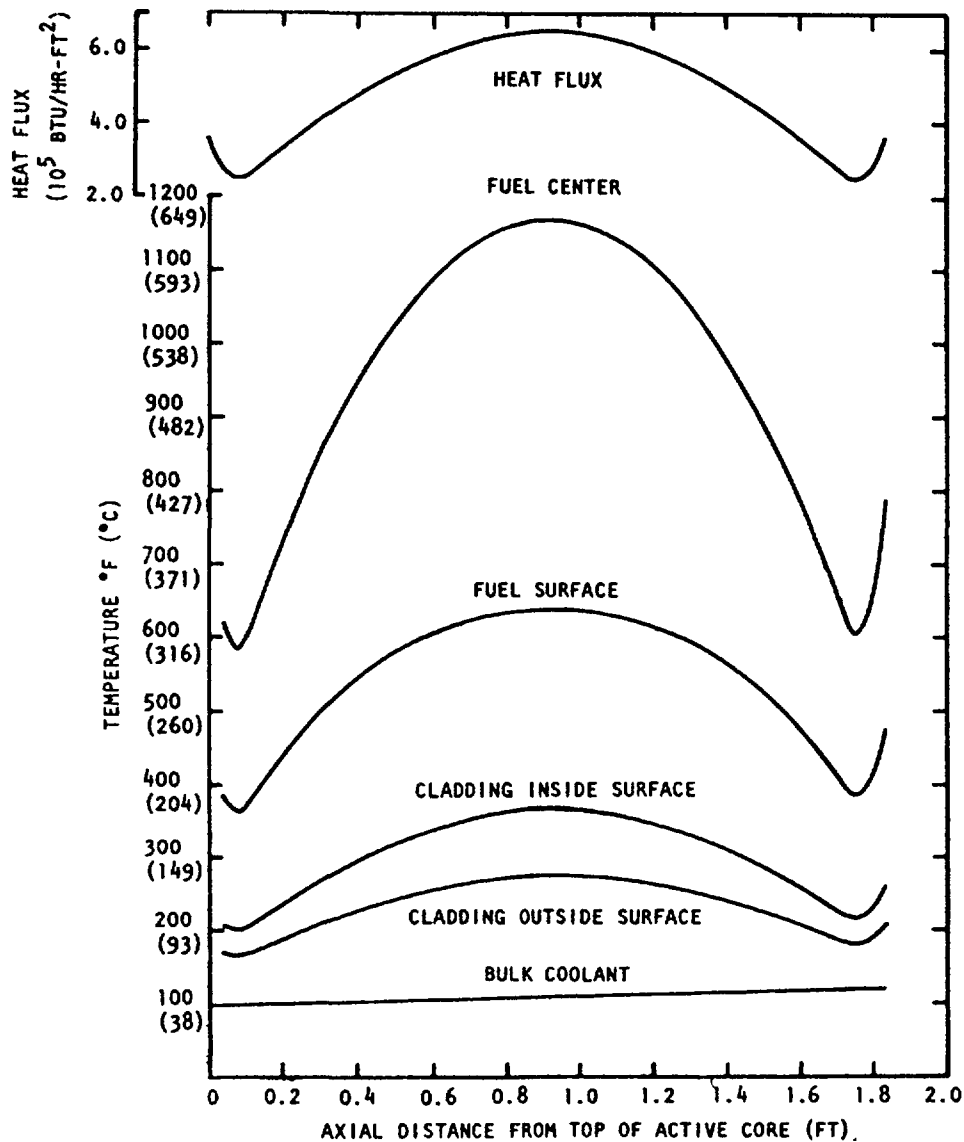
Fig. 9. Axial temperature profiles of the 10-MW TRIGA-LEU design (hot channel, hot-rod factor ∿1.8)

As can be seen from Fig. 9, the peak heat flux occurs at the horizontal mid-plane of the core, and the DNB ratio is a minimum at this location. Only a small amount of local subcooled nucleate boiling is predicted for the hottest rods, and this may occur over the central region between the two spacers.

As discussed earlier, the largest temperature increase is in the fuel and at the fuel-cladding interface. At the horizontal mid-plane of the individual fuel rod, the beginning-of-life (BOL) radial gap between the fuel and cladding is 0.0005 in. and the gap is filled with helium. This results in an interface conductance of approximately 2400 Btu/hr-ft^2. As the fuel burns up, radiation-induced swelling will cause this gap to close, and this

72
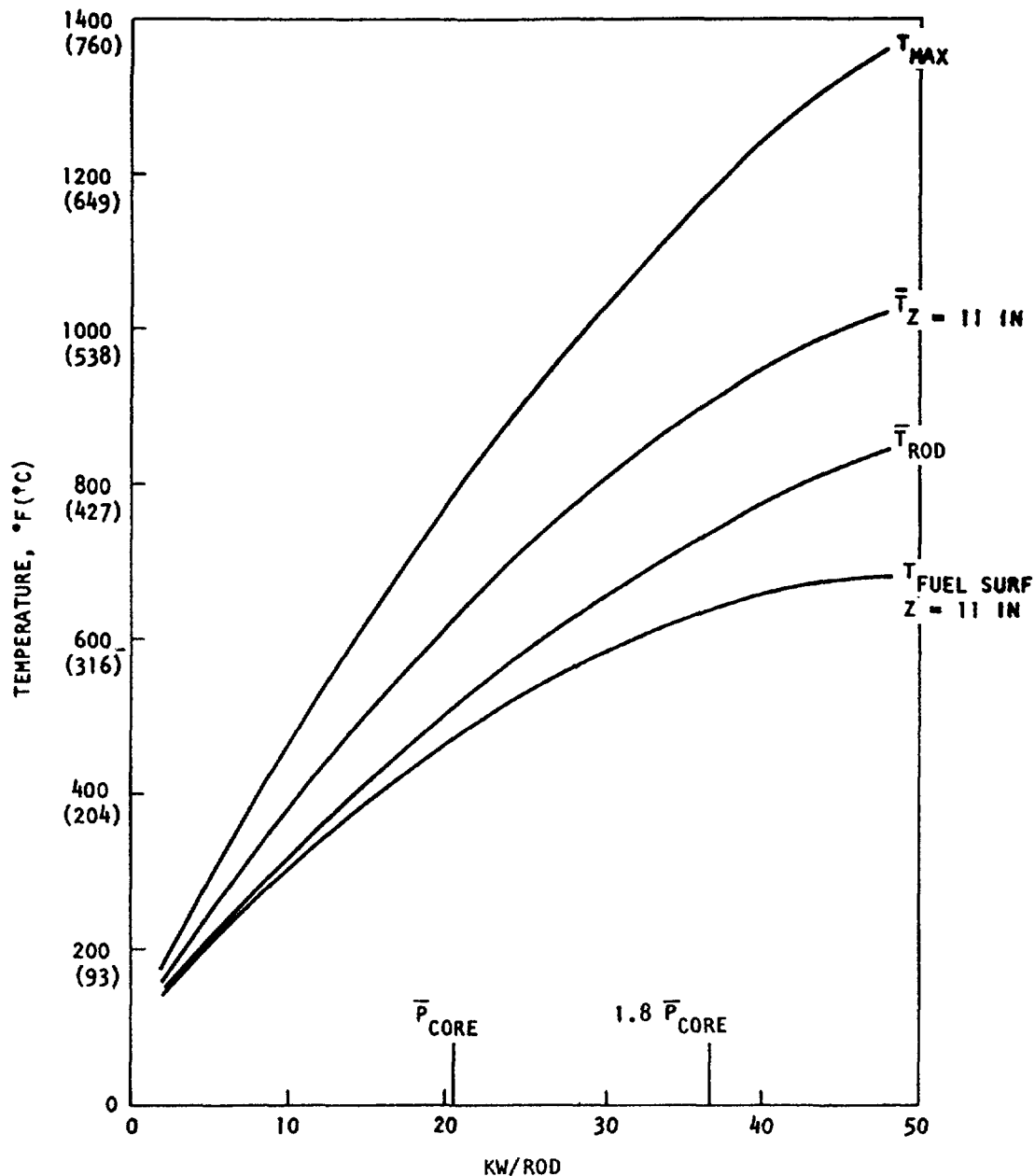
Fig. 10. Temperature as a function of kW/rod

will reduce the peak fuel temperatures. The calculated peak fuel temperature at BOL is 640°C, which is well below the design maximum of 750°C.

Figure 10 shows the variation in temperature within a fuel rod as a function of rod power density.

The effects of design variables and off-standard conditions have been evaluated to determine the amount of margin existing in the design point selected for the steady-state reactor core. The results of the thermal-hydraulic tests correlating critical heat flux and flow rate for minimum clearance between rods have been used in the design analysis summarized in
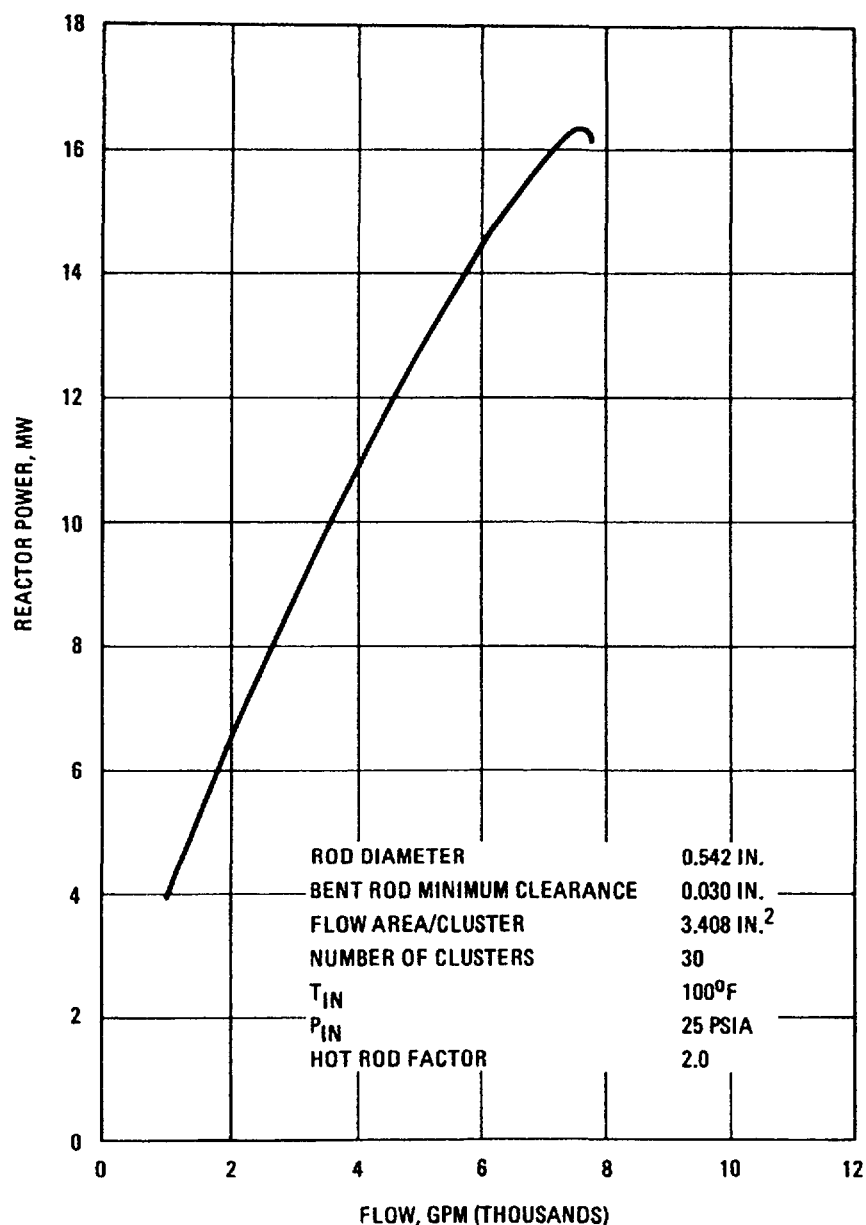
Fig. 11. Critical heat flux power versus flow for 16-rod clusters

Fig. 11. For the limiting design conditions described in Fig. 11, including fuel rods bent to give only a 0.0762-cm (0.030-in.) clearance, the critical heat flux is a factor of 1.3 greater than the operational heat flux at 10 MW [coolant flow rate of 18,900 liters/min (5000 gpm), hot-rod factor of 2.0]. It is also seen from Fig. 11 that a flow rate of about 8300 liters/min (2200 gpm) will allow 5-MW operation with a critical heat flux about 1.4 times the operational heat flux. Thus, existing reactor systems with the lower flow rate can be upgraded to TRIGA fuel and can operate at about 5 MW until additional cooling capability is installed to permit 10-MW operation.

6. REACTIVITY ACCIDENT

A start-up accident has been evaluated where the entire rod bank travels out of the core at 3.9 in./min (10.0 cm/min) until a scram occurs.

Calculations described in this section were done with the BLOOST-7 Code and the following conditions prevailed:

1. Nuclear parameters were those for end-of-life core.

2. The thermal characteristics were those shown in the previous section with the addition that the specific heat of the fuel material was represented by C_p = 151 + 0.307 W(t)/sec-°C-rod.

3. Flow characteristics were representative of natural convection flow induced by the removal of the accident-generated heat. Higher fuel and clad temperatures result from this condition as opposed to assuming forced flow conditions.

4. One of the redundant power scrams was assumed to be activated at 12 MW (20% above the maximum power of 10 MW - this allows for tolerance in the normal set point of 110% of power for each range).

5. A fuel temperature scram was assumed to be achieved at a temperature about 40°C above its normal operating value (in this case 680°C, as the maximum fuel temperature is predicted to be 640°C).

6. There was a 0.2 sec delay between reaching the scram point and initiation of scram rod movement.

7. The maximum-worth rod does not scram.

8. Control rods drop back into the core with constant acceleration, based on a drop time of 1 sec from full out to full in.

9. $\bar{P}_{max}$ = 1.9.

10. T_o = 37°C (98.6°F).

11. The period scram does not operate.
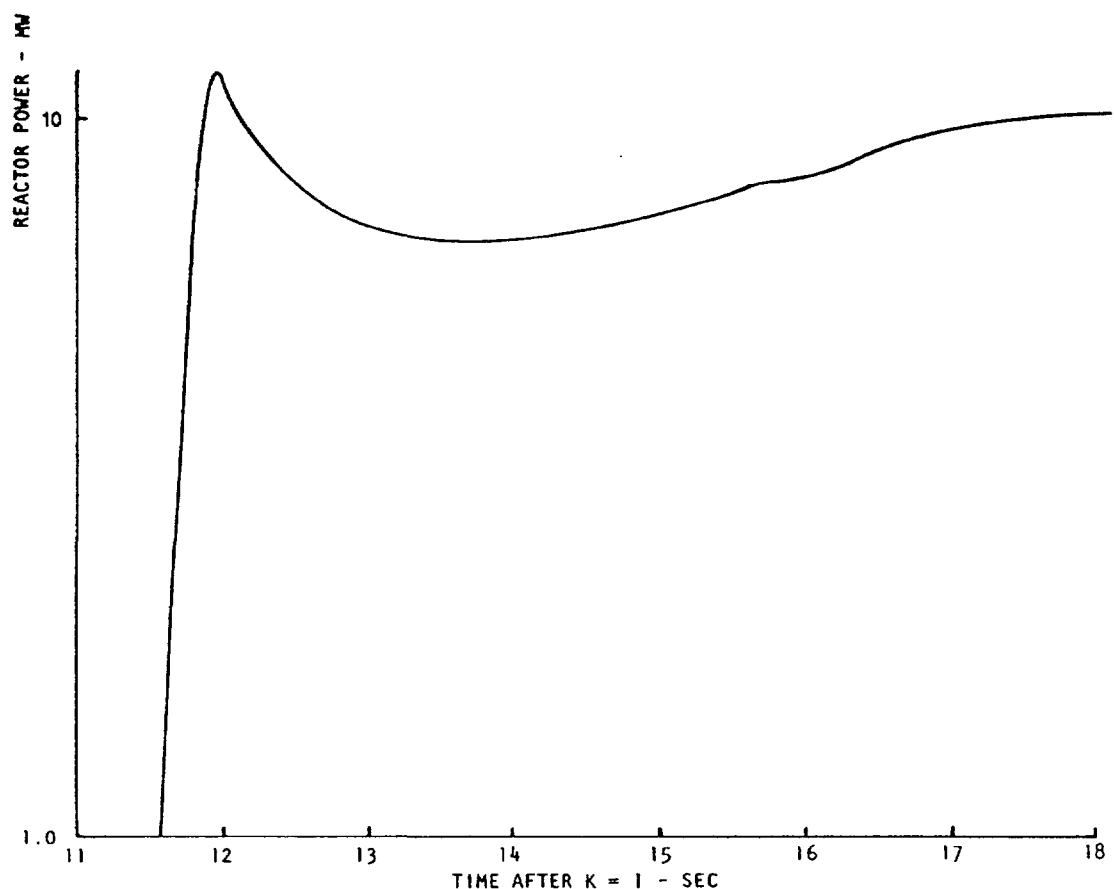
Fig. 12. 10-MW TRIGA rod runout accident, power versus time

In this accident, the entire rod bank withdraws from the full-in position at the normal rate of 3.9 in./min (10.0 cm/min) constant velocity; 5.6-min withdrawal time for 22-in. (55.85-cm) length. The excess reactivity in the core with all rods out is 7.8%. When the power scram is activated the maximum-worth rod continues to withdraw but all other rods fall to the full-in position.

The calculational results are shown in Figs. 12 and 13, where power and the maximum fuel temperature in the maximum-power fuel rod are plotted as a function of time. The peak power is about 11.6 MW (with the minimum period being about 0.1 sec). The reactivity insertion is slow enough that sizable fuel temperatures are generated before the reactivity insertion is completed, and the temperature coefficient limits the maximum excess reactivity to about 0.7% 6k.

As the peak power (11.6 MW) does not exceed the assumed scram point (12 MW), the ramp continues until the fuel temperature at the thermocouple

76
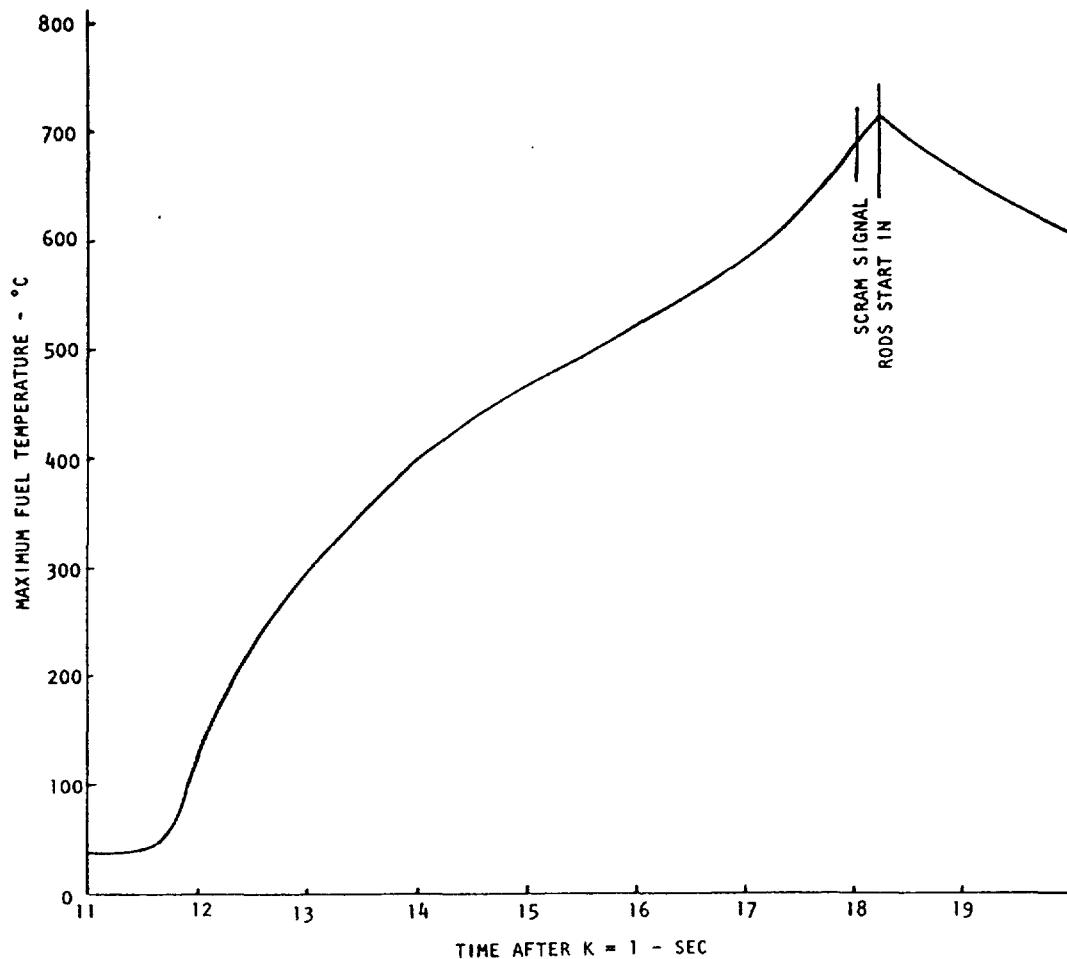
Fig. 13. Rod bank runout accident, maximum fuel temperature versus time
for maximum-power rod

reaches 680°C. At about 17 seconds after the beginning of the excursion,
the maximum fuel temperature would be about 600°C. This is the temperature
of the fuel in the maximum power density rod when operating at about 3 MW
with natural convection flow. Above this temperature, it is difficult to
reject any additional heat, so both the fuel and clad temperature increase
at a greater rate. Although there would be bulk boiling in the channel, the
fuel temperature remains low enough to preclude damage because a temperature
scram would limit the fuel temperature to about 700°C. This is about 240°C
below the fuel temperature safety limit (when fuel and clad are at the same
temperature) of 940°C.

The assumption that the power level scram is set at 120% of full power
is overly conservative. The scram point should be no more than 105 to 110%
of full power. If this were the case, the transient would be terminated
during the initial power increase. The maximum fuel temperature would never

77

exceed about 350° to 400°C under these conditions. Also, not only would the 5% power rod withdrawal inhibit by-pass relay have to malfunction for this accident to happen with natural convection cooling but also necessary for malfunction to occur would be scrams on primary pump operation, primary flow, and flapper valve closed, all of which are operational above 5% of full power. Thus, even though the accident produces no fuel element damage, it is highly unlikely to occur and is used as an upper-limit assessment of the rod withdrawal accident in that if the accident occurred under forced-flow conditions the results would be less severe.

7. LOSS-OF-FLOW ACCIDENT

When the reactor is shut down from power under normal operation, the main coolant pumps will continue to be operated for a short time until the fuel temperature declines to a near-ambient value. Should the pumps fail or
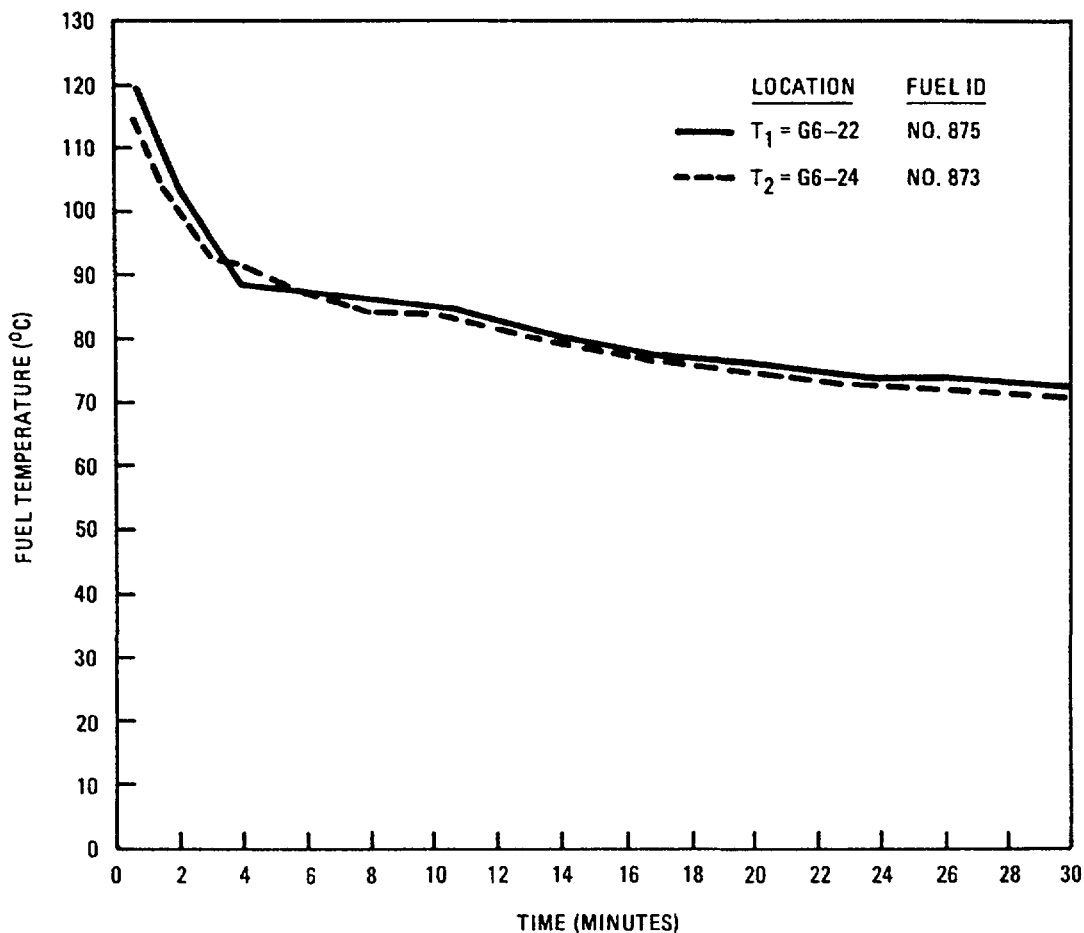
Fig. 14. Fuel element temperatures after power scram from 14MW and shut down of all cooling pumps

be shut off because of an emergency during full-power operation, the reactor would scram on a loss-of-flow signal. Experiments conducted on other force-flow-cooled TRIGA reactors show that the flow coast down takes several seconds and then the flow reverses direction to the natural convection mode very quickly and smoothly, with essentially no interruption in the fuel temperature decay rate. Thus, the afterheat from the shut-down reactor will be removed by natural convection following pump failure or emergency shutdown.

7.1. FLOW COAST-DOWN TESTS (14-MW TRIGA)

After a 120-hr run at full power and with the inventory of fission products generated therein, the flow coast-down tests were conducted to study the effect on fuel rod temperatures. The instrumented fuel rods were Nos. 873 and 875 located in the hottest core locations.

In the test, the reactor was scrammed from full power and all cooling pumps (two in use) were scrammed simultaneously. The fuel temperatures were monitored frequently during the ensuing period. The fuel temperatures fell continuously. At 16 minutes, the fuel temperature was 80°C. See Fig. 14 for results.

Appendix B

SAFETY ANALYSIS —
PROBABILISTIC METHODS

Abstract

Methods are presented as a guide to probabilistic safety
analysis, although they do not refer in any way to the
differences between HEU and LEU fueled cores.

Appendix B-1

PROBABILISTIC METHODS IN SAFETY ANALYSIS AND LICENSING

T.J. MOSS, D.B. McCULLOCH
Lucas Heights Research Laboratories,
Australian Atomic Energy Commission
  Research Establishment,
Lucas Heights, New South Wales,
Australia

Abstract

A brief general review of the background related to the use of PRA in design and licensing is given along with a brief discussion of the requirements for a comprehensive PRA approach to safety assessment and review for licensing purposes.

1. BACKGROUND

Probabilistic Risk Assessment (PRA) techniques provide a full alternative, or a supplementary approach to the deterministic accident analysis methods historically used almost exclusively in reactor safety assessment and licensing procedures.

With increasing experience of reactor design and operation, the deterministic approach, demanding as it often did, that design be dictated heavily by the requirement to protect against a highly improbable "Maximum Credible Accident (MCA)" scenario, began to be questioned. It became increasingly apparent that other less dramatic possibilities might, when weighted by the likelihood of the event, represent larger real risks and possibly pose an entirely different set of design demands.

Probabilistic Risk Assessment (PRA) provided a welcome means of addressing the difficulty. It provided the designer with a suitable means of enumerating a wide range of accident scenarios and establishing their relative importance to system performance goals. However, although PRA was initially widely acclaimed as a powerful additional tool for both design and licensing authorities, the incorporation of formal PRA and quantitative goals in the licensing process has not proved easy. While the advantage of a more balanced overall approach to safety aspects of design is generally acknowledged, the demands on effort, skill and experience for the design and operating groups, and for the licensing authority itself, are very

substantial. It is not a route to be followed lightly, without full cognisance of the commitment required.

The well-publicised "Reactor Safety Study" - WASH 1400,[1] sponsored by the USNRC and published in 1975, was one of the earliest major PRA studies of reactor safety. It addressed the risks posed by operation of a whole envisaged generation of PWR and BWR (power generating) reactors. It was a pioneering work, ambitious in scope and design, carried out against a background of well defined objectives and priorities. Not surprisingly, therefore, it was subject to many detailed criticisms, culminating in the "Lewis Report"[2] commissioned by the USNRC and published in 1978.

The Lewis report, while critical of specific methods and results, was generally favourably disposed to prospects for further development and application of PRA technology in the reactor field. Nevertheless, the USNRC has not formally incorporated PRA into the legal framework of licensing. Rather, it has recommended the use of PRA as an aid to the licensing process, but to an extent based on negotiation between technically highly sophisticated reactor vendors, power utilities and a large licensing authority with substantial technical experience in the field.

In considering the use of PRA as an aid to licensing, the benefits should be carefully weighed against the costs and implications of its use. The effort required to apply PRA to any type of reactor is heavy, and demands special skills and experience. The effort may not be significantly less for a single research reactor than for a generation of power reactors (see Section 3). The costs for application to a research reactor may therefore well be considered prohibitive. On the other hand, limited use of PRA techniques may provide a more balanced overall assessment of the safety of the system, and be of significant benefit in terms of the quality of the information on which licensing and design decisions are based.

2.   GENERAL PROCEDURES FOR A PRA

The general procedure for application of PRA techniques to a particular system is summarised by the following broad steps. It should be noted that the entire process, or parts of it, may take place several times during design, licensing and operation.

(i)   The details of the system being known, a set of initiating events is identified. Accident sequences developed from these are evaluated, usually using approximate methods. The resulting consequences, with their estimated frequency of occurrence, quantify the risk or hazard, and enable the significant events to be

determined. The set of initiating events should be as complete as possible, and may be progressively modified and updated in the light of results as the study proceeds.

(ii) A set of bounding cases for the events deemed likely to be of concern should be selected for detailed analysis.

(iii) A detailed failure model (using fault trees, logic diagrams supported by Failure Modes and Effects Analysis (FMEA), or other suitable analytical procedure) is produced which identifies those components, systems and human actions capable of influencing the path and results of the event in question.

(iv) The overall system is evaluated for its susceptibility to common cause events and an attempt may be made to quantify that susceptibility. Great care is required, as common cause effects can often dominate the performance of highly redundant systems.

(v) Probabilities are assigned to the failure modes or component failures relevant to the chosen failure model.

(vi) Overall system performance and hence final event frequencies are computed.

(vii) If a suitable model exists, the consequences of the event are modelled, for example, from a knowledge of the appropriate source term, release characteristics and the meteorology of the particular site.

(viii) Accident frequencies versus consequences for the system in question can now be plotted.

(ix) The derived performance may be compared against any required criteria.

Reference to NUREG/CR-2300,[3] is recommended for more detailed and definitive guidance.

3.   EFFORT REQUIRED IN PRA

In relation to power reactors, NUREG 2300 (para 2.1.3) defines three levels of PRA in terms of effort and depth.

(1) Systems analysis.

(2) Systems and containment analysis.

(3) Systems, containment and consequence analysis.

Estimates of man-time for these studies are given as

Level 1	51 - 89 man-months
Level 2	75 - 288 man-months
Level 3	80 - 298 man-months.

There are no obvious reasons why PRA studies for research reactors (other than for the simplest ones) should be substantially less demanding than those for power reactors. Furthermore, they are more likely to deal with a novel system having fewer analytical precedents; it is consequently likely that the higher estimates given above may be more appropriate.

4. CONCLUSIONS

Probabilistic Risk Analysis studies can significantly augment the detailed technical knowledge of a reactor system's safety performance.

The cost to the operator/licensee can be high both in effort and, in the case of a new technology which does not have a formally established framework for its application, in delays in licensing.

In making a decision to choose licensing techniques lacking well established precedents, it is important to consider carefully the differences between large nuclear power programs for which PRA has appeared increasingly attractive and the much different circumstances of the construction or alteration of a (usually single) small research reactor, possibly of an essentially unique type. Potential benefits in the research reactor case may be too marginal compared with those obtained from simpler assessment approaches, to justify the much greater costs of a full, formal PRA approach.

However, the use of PRA in design and as a voluntary aid to the licensing process allows for far greater flexibility of application. Provided that PRA-based conclusions are not allowed to cloud well established precedents or to undermine the tightly-knit process of control offered by a coherent set of codes and standards, then PRA offers valuable and attractive possibilities for more effective design and a more coherently argued and balanced safety case. The depth and extent of PRA in this context can be tailored to the real capabilities and needs of the particular organisation(s) concerned.

REFERENCES

[1] USNRC (U.S. Nuclear Regulatory Commission) [1975] - Reactor Safety Study. An Assessment of Accident Risks in U.S. Commercial Power Plants, WASH 1400 (NUREG-75/014), Washington, D.C.

[2] USNRC [1978] - Risk Assessment Review Group Report to the U.S. Nuclear Regulatory Commission, NUREG/CR-0400, Washington, D.C.

[3] USNRC [1983] - PRA Procedures Guide (A Guide to the Performance of Probabilistic Risk Assessments for Nuclear Power Plants), NUREG/CR-2300, Washington, D.C.

Appendix B-2

SAFETY ANALYSIS — PROBABILISTIC METHODS

C. BAGLIN
GEC Energy Systems Limited,
Whetstone, Leicester,
United Kingdom

Abstract

A simple example of the probabilistic method in accident analysis
is applied to a flow blockage accident in a downflow pool reactor
to illustrate the general concepts of this approach.

1. INTRODUCTION

A reactor presents a whole spectrum of risks ranging from normal
operation activity releases through anticipated transients up to major
accidents. An assessment of only the worst accident that might occur
does not give a proper measure of the real risk. Nor does it
necessarily give an upper limit for this risk since the frequency of the
accident is as important as its consequence.

The probability method seeks to quantify the frequency as well as the
consequence of the whole spectrum of accidents.

The starting point is to assume a plant failure or maloperation, the so
called initiating event. This event can set up an accident sequence
that can follow several paths dependent on the subsequent performance of
several items of plant and the operator.

The full safety evaluation then comprises a spectrum of events with
associated probabilities and consequences. A probability/consequence
diagram can then be drawn, as in Fig. 1 in which the probability is
given as reactor years between releases and the consequence is given as
dose to the public in units of dose limit. Dose limit is the annual
dose limit recommended by the ICRP for members of the public i.e. 0.5
rem/year.

It is then necessary to compare these results with some safety
criterion. Farmer (1) in the 1960s proposed the use of the lime AB in
Fig. 1 which joins points of equal risk in terms of dose per year; or
some modification of such a lime to bias it against large releases. The
British licensing authority, the NII, now applies a criterion based on
the above and shown in Fig. 2, again the consequences are given in terms
of dose limit and ERL. ERL is the emergency reference level as defined
by the British Medical Research Council i.e. 10 rem whole body.

2. CASE CONSIDERED

As an example of the method we have applied it to a flow blockage
accident in a downflow pool reactor. Since the the reference reactors
of the guide book do not specify a protection system we have based the
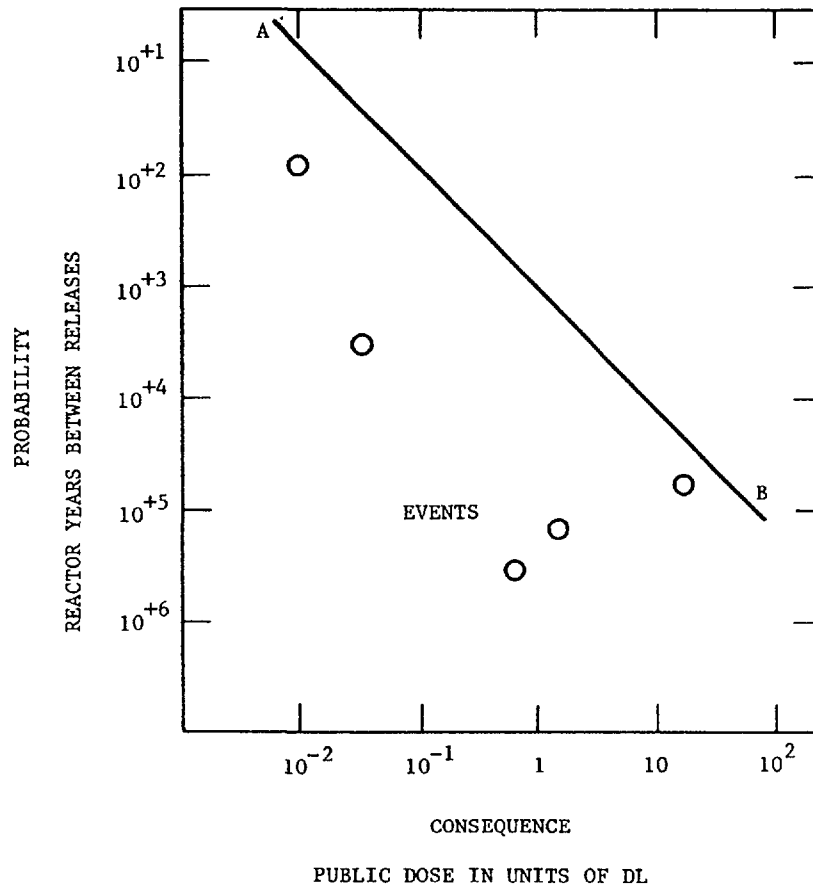
FIG. 1. Probability–consequence diagram.

protection system for this example on a modern installation at a European research reactor.

The first trip parameter for this accident is excess rate of flux decrease, the second parameter is high coolant activity in the core outlet flow. Containment isolation is activated by the same sensors as well as stack off-gas activity high.

3. ACCIDENT SEQUENCES

Following the initiating event partial or total failures of the protection system, shutdown system, containment isolation system, etc lead to the set of alternative routes shown on Fig. 3. The design intent is the top path and the worst combination is the lower path. Each route has a different probability and a different consequence. It would of course be possible to extend this event tree to cover variations in weather, wind direction etc.

4. PROBABILITY OF THE INITIATING EVENT

There are two approaches to this problem.

Firstly the considerable operating experience of reactors could be examined for the event in question and a global frequency determined. The difficulties with this approach are: for rare events the historical
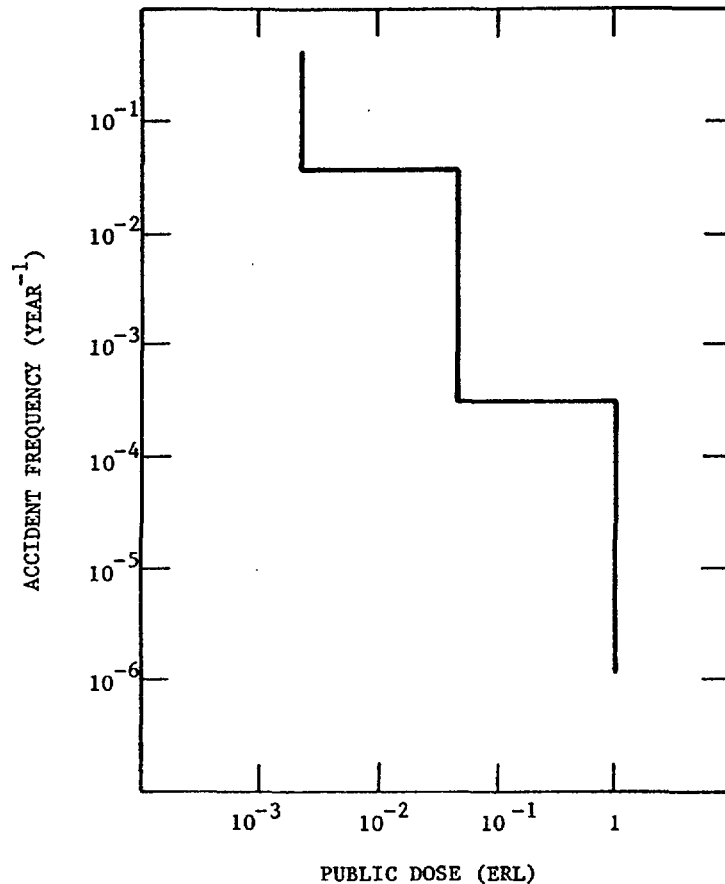
FIG. 2. Accident criteria currently adopted in the United Kingdom by NII.

record is fairly short, no two reactors are identical, the experience for some reactors is poorly reported and reliability improves as experience from previous events is fed into operating procedures.

Secondly by considering the frequency of operations that could produce the event and probabilities of component failure that could produce the event and event probability may be synthesised. The difficulty here is asigning probabilities to human error.

Both approaches will be applied to our example.

NSIC publish abnormal reactor operating experiences for US reactors. In a survey of experiences for the years 1966 - 1974 (2) it was found that 2 flow blockages had occurred. In one other case part of the primary circuit internals had broken away giving a potential flow blockage. The experiences reported cover about 700 reactors years. Thus an estimate for the frequency of flow blockage would be 3/700 per reactor year.

Operations which would introduce foreign bodies into the primary circuit are:

primary circuit maintenance, 1/year, bridge and control rod mechs. maintenance 1/year.
fuel handling 1/month.
crane operations above core 1/week.
foil irradiations 1/week.

```
        INITIATING              REACTOR              CONTAINMENT

          EVENT                   TRIP               ISOLATION


                                                    ┌──── AUTO CI ─────────
                                                    │
                          HI  dⵁ/dt  TRIP ──────────┼──── MANUAL CI ───────
                          ┌                         │
                          │                         └──── NO CI ───────────
                          │
                          │                         ┌──── AUTO CI ─────────
                          │                         │
   ───────────────────────┤      COOLANT    ────────┼──── MANUAL CI ───────
                          │  ACTIVITY TRIP           │
                          │                         └──── NO CI ───────────
                          │
                          │                         ┌──── AUTO CI ─────────
                          │                         │
                          └────  NO TRIP  ──────────┼──── MANUAL CI ───────
                                                    │
                                                    └──── NO CI ───────────
```
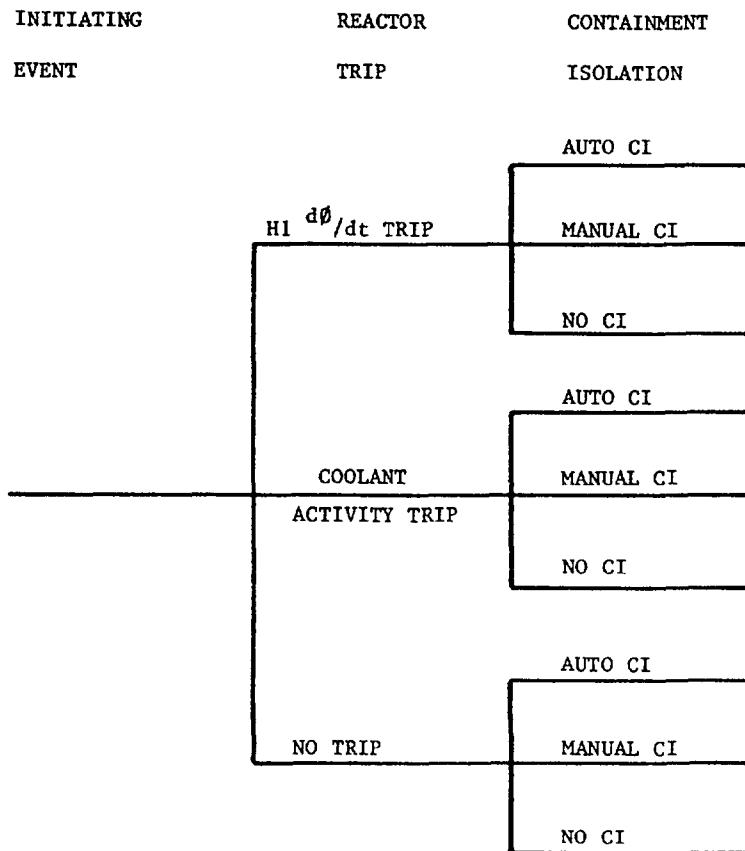
FIG. 3. Event tree.

conservative estimates may now be made of the probabilities of introducing or failing to detect foreign bodies. The following values are indicative only.

Clearly most of the operations are done shutdown and foreign bodies on the core should be seen on a pre start up visual check. Such a check could be skimped say once in a hundred times. It would not reveal transparent objects, or loose parts in the flow circuit.

The former are common enough = gloves, tape, poly sheet etc, say 1 in 10 bodies introduced are transparent and the rate of introduction from the careful above-core operations is 1 in 1000. The latter could be introduced by the maintenance operation at say 1 in 100.

In service failures of strainers, pumps, control rod mechs etc. could produce foreign bodies during power operation. Such failures will have probabilities in the range $10^{-4} - 10^{-2}$.

Using this data one could assess the probability of flow blockage as:

maintenance introduced.
body in circuit (1/year x $\frac{1}{100}$ = $\frac{1}{100}$ years^{-1}

transparent object (1/year + 1/month + 2/week) $\frac{1}{1000}$ x $\frac{1}{10}$ = $\frac{1}{100}$ years^{-1}

90

opaque object missed.
by visual check (1/year+1/month+2/week) x $\frac{1}{1000}$ x $\frac{1}{100}$ = $\frac{1}{1000}$ years^{-1}

In service failure (4 items of plant) x $\frac{1}{1000}$ = $\frac{4}{1000}$ year^{-1}

Total $\frac{2.5}{100}$ year^{-1}

From this crude example data the probability of the initiating event for the reactor under consideration is between 3/700 and 3/100. We will adopt a value of 1/100.

5. PROTECTION SYSTEM RELIABILITY

The classic approach is to consider random component failure and use the laws of probability to calculate the system reliability.

It has long been recognised that the assumptions on which such an analysis is based cannot be entirely true and will begin to invalidate the results as the failure probability becomes very small. In particular the assumptions that all failures are independent, all testing is perfect and the system contains no design errors are suspect. Such effects will be common to several redundant channels and are usually referred to as common mode (CM) failures.

In recent years however so much emphasis has been placed on CM failure that, for example, the NRC will not accept random failure calculations for reactor trip reliability (3). Where system failure from random faults is several orders of magnitude lower than CM system failure such a position is justified; but not all protection systems are as highly redundant as those considered by NRC and the use of fail safe designs and diversity can do much to reduce CM failure.

THere are several ways of dealing with CM failures. The simplest is to regard them as a degradation of a redundant system which places an upper limit on the claimable reliability of the system. The NII for example will not accept that a protection system could have a failure per demand of $<10^{-5}$ without diversity of equipment, initiation and action.

A more satisfying approach is to identify common mode failures, establish failure rates and combine them with random failures in a total analysis. NCSR have used such an approach (4).

The failure probability of the system is given by

$$F_s = F_o(1 - \sum P_n) + P_1 F_1 + \cdots P_n F_n$$

where:

F_o = failure probability of system for no CM faults.

P_n = probability of the Nth CM fault.

F_n = failure probability of system when Nth CM fault is present.

CM failure may also be incorporated directly into a fault tree representation of the system.
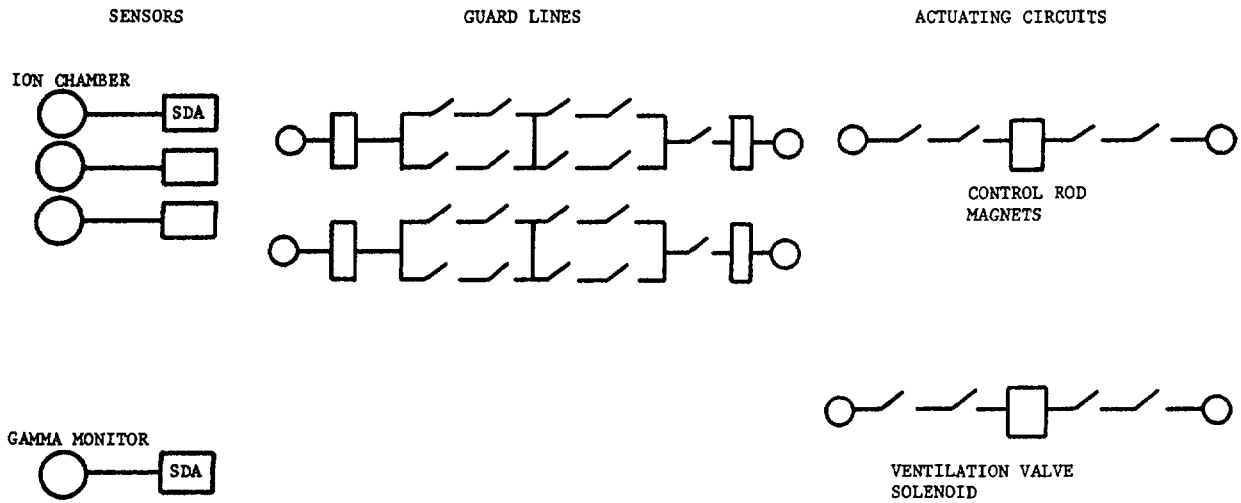
FIG. 4. Protection system.
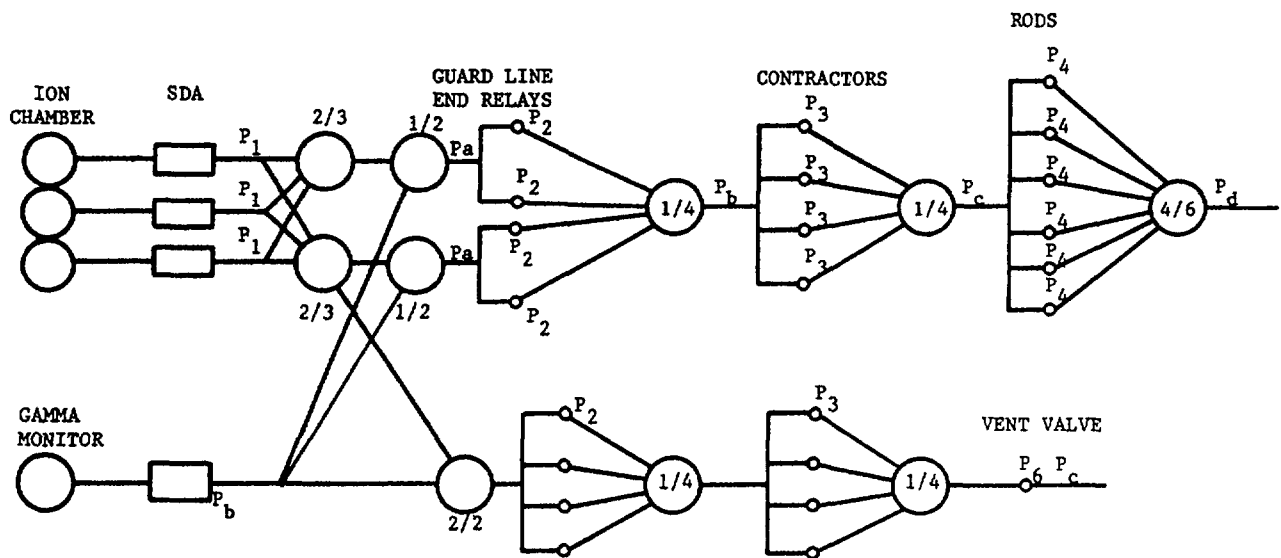
FIG. 5. Protection system logic.

The probability of a random component failure is

$$P = 1 - e^{-\Theta\tau}$$

where Θ = failure rate
τ = test interval

The relevant failure rate is the unrevealed fail to danger rate; other failures either announce themselves or produce a spurious trip.

Figures 4 and 5 show a simplified version of the relevant part of the protection system for our example. Shut down is achieved if 4 of the 6 rods insert.

Random failure rates, obtained from a reliability data bank and test intervals for the various equipments are shown in table 1.

Typical common mode failures to danger i.e. neglecting those which are covered by fail safe design such as shorts, power loss etc. are shown in table 2.

Several studies (5, 6, 7) of CM failures suggest that the CM failure rate is ˜ 0.01 per sub system year and that design and maintenance are the dominating causes. Most of the failures were fail to danger but most were partial i.e. the complete sub system was no invalidated. We will use this rate for each of the sub systems:

flux channels
guard lines
CI valve
and 0.005 for the rod system.

We then have, using the nomenclature on Fig. 5:

A. Failure of H1 $\frac{d\phi}{dt}$ trip

Random $P_d = 3P_1^2 + P_2^4 + P_3^4 + 20P_4^3$

substituting the component failure probabilities from table 1.

$P_d = 2.3 \times 10^{-5}$

The sum of the sub system CM failure probabilities is 7.5 x 10^{-4}

Total failure probability = 7.7 x 10^{-4}

TABLE 1

EQUIPMENT	FAILURE RATE (UNREVEALED DANGER) PER 10^6 hrs	TEST INTERVAL	FAILURE PROBABILITY
ion chambers	0.1	continuous	0
S.D.A.'s	14	1 week	P^1 2.4 x 10^{-3}
Relays	0.1	1 week	P^2) P^3) negligable
control rods	10	1 month	P^4 6.7 x 10^{-3}
monitor	14	1 week	P^5 2.4 x 10^{-3}
ventilation valve	10	1 month	P^6 6.7 x 10^{-3}

TABLE 2

EQUIPMENT	CM FAILURES
sensors	miscalibration, loss of sensitivity.
logic	sticking relays, faulty repair/test.
rods	external hazards, maintenance, corrosion.

B. Failure of auto C.I

Random failure.

$$P_e = P_a + P_5 + P_2^4 + P_3^4 + P_6$$
$$= 3P_1^2 + P_5 + P_2^4 + P_3^4 + P_6$$
$$= \underline{9.1 \times 10^{-3}}$$

CM failure $= \underline{4 \times 10^{-4}}$

Thus the final overall probability for the worst event on the fault tree is: initiating event x trip failure x CI failure.

$$10^{-2} \quad x \quad 7.7 \times 10^{-4} \times 9.5 \times 10^{-3}$$

i.e. 7.3×10^{-8} and the probability of an untripped flow blockage accident is 7.7×10^{-6}.

6. Activity Release

In the two flow blockage accidents reported the melting in the blocked assembly was extensive. It would therefore be prudent to assume complete melting of all the elements which are blocked. The isotopic fractions available for release from the building may be taken from ANSI/ANS 15-7.

The release rate from the building should be the leak rate incorporated in the technical specifications or that plus the ventilation flow depending on the success or failure of containment isolation.

7. Consequences

The radiological consequences can be assessed from atmospheric diffusion of the contaminated containment atmosphere making assumptions about weather conditions. The dose commitments should be assessed in the 3 zones specified in ANSI/ANS 15-7 i.e. within the site boundary, the rural zone and the urban zone.

References

1. Reactor Safety and Siting F.R. Farmer Nucl. Safety, 8(6) 1967.

2. Abnormal Reactor Operating Experiences ORNL-NSIC 64
                                           ORNL-NSIC 103
                                           ORNL-NSIC 121

3. Anticipated Transients without scram NRC Report NUREG 0460 NTIS 1978.

4. A study of Common Mode Failures Edwards and Watson
   SRD R 146 1979 Appendix 2
   UKAEA.

5. Reactor Safety Study WASH 1400

6. Common Mode Failure Considerations E.P Epler
   Nuclear Safety 10(1) 1969.

7. Edwards and Watson (op cit) Appendix 3.

APPLICATION OF PROBABILISTIC ANALYSIS TECHNIQUES
TO A TYPICAL 10 MW MTR

F.R. ALLEN
Safety and Reliability Directorate,
United Kingdom Atomic Energy Authority,
Culcheth, Warrington, Cheshire,
United Kingdom

Abstract

A detailed example is presented of the way in which probability analysis techniques may be applied to a typical 10 MW MTR. The steps necessary to enable an assessment of the probability and consequences of an accident sequence are outlined. Some detailed examples are given of the ways in which probabilities for particular accidental occurrences may be assessed from an analysis of the components of a system and a knowledge of their individual failure characteristics.

1. **Introduction**

    This document presents an example of the way in which probability analysis techniques may be applied to a typical 10 MW MTR. It outlines the steps necessary to enable an assessment to be made of the probability and consequences of an accident sequence. Some detailed examples are given of the ways in which probabilities for particular accidental occurrences may be assessed from an analysis of the components of a system and a knowledge of their individual failure characteristics.

2. **Outline of the Fault Sequence Analysed**

    The fault sequence analysed is that of loss of reactor coolant due to a pipework failure in the reactor coolant circuit. The reactor is cooled by the D_2O moderator which is circulated through the core in an essentially unpressurised circuit. Loss of this D_2O could lead to fuel overheating and melting giving fission product release. To prevent this, various safeguards are provided. If the fuel did melt, the activity would not be released directly to the environment, but would have to cross various barriers, the most significant of these being the containment building with its extract clean-up system which, if operating correctly, will reduce the activity released to an acceptable level.

The fault sequence may be summarised as below.

Fault No	Fault	Result of Fault Chain
1	Pipework failure leading to loss of D_2O from circuit.	Potential for loss of core cooling.
2	Failure of engineered safeguards designed to protect against loss of coolant accidents.	Actual loss of core cooling. Release of fission products within reactor containment.
3	Failure of containment extract system to contain the activity released by 1 + 2.	Release of activity to the environment.

The various steps in this fault sequence are considered in detail in the following sections. Section 3 deals with the probability of pipework failure and the probability of failure of the engineered safeguards designed to prevent loss of coolant. Section 4 deals with the containment extract and clean-up system, and assesses the probability of failure of this system to trap the activity. Finally, Section 5 considers briefly the amount of activity which would be released in the various circumstances considered, and compares this with the Farmer criterion for acceptable risks.

3. **Analysis of Pipework Failure and Engineered Safeguards against Loss of Coolant**

3.1 Introduction

The reactor is cooled by D_2O which is circulated from the Reactor Aluminium Tank (RAT) through heat exchangers and back to the tank. The D_2O in the RAT is doubly contained, but leakage from the external circuit spills into the Plant Room and is lost to the circuit except for the action of sump pumps which can return D_2O from the Plant Room back to the tank.

Leaks in excess of the sump pump capacity could empty the RAT and cause the fuel elements to dry out. Even if the reactor is shut down, decay heat in the fuel elements could result in their melting unless the fuel plates are kept covered by D_2O. In extreme emergency H_2O can be introduced into the RAT, but an assessment of the H_2O system is outside the scope of this study, which is to assess the probability of occurrence of a D_2O leak which will dry out the fuel elements.

3.2 Description of System

A simplified diagram of the D_2O circuit is shown in Figure 1. The circuit is completely contained in the Plant Room which is situated directly below the RAT.

The four downcomers protrude into the RAT, level with the top of the fuel plates. D_2O is drawn from the upper levels of the RAT into a common suction header. From there it is drawn by three main pumps in parallel through non-return valves to the common discharge header from where it is pumped through three heat exchangers in parallel into the fuel element header box in the RAT by way of the risers. From the fuel element header box the D_2O passes through the centre of the fuel elements to the top levels of the RAT. The
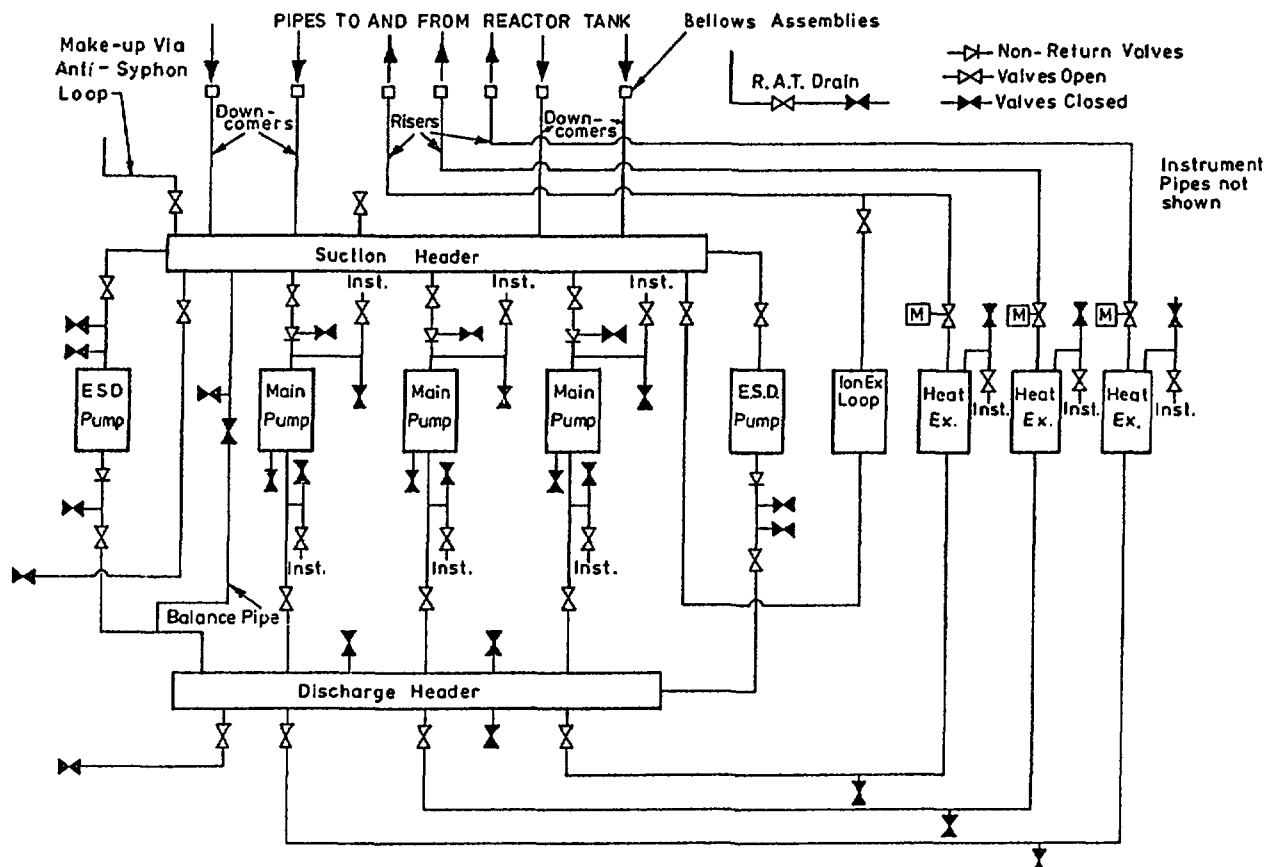
FIG. 1. D₂O circuit as assessed.

three heat exchanger outlet valves are motorised to enable remote, automatic operation.

During reactor operation the Emergency Shutdown (ESD) pumps are not in operation, reverse flow being prevented by their non-return valves. During reactor shutdown, the main pumps are switched off and circulation is maintained by the ESD pumps to dissipate decay heat.

A small proportion of the circulated D_2O by-passes the fuel elements through the ion-exchange loop to maintain water quality.

The D_2O level is maintained by the liquid level pumps from the storage tank into the suction header, the overspill returning to the storage tank by way of a weir pipe. D_2O cannot leak back to the make-up tank because of the anti-syphon loop. The RAT can be drained through the drain line direct to the tank.

3.3 Protection

A certain amount of leakage can be returned to the RAT by the sump pumps. It is assumed in this assessment that the capacity of a single small pump is 20 gal/min, (90 l/min), and from tests it has been calculated that the combined output of both is 34 gal/min (150 l/min). Leaks up to this size can be accommodated by these pumps. The pumps are manually started.

In addition there is a 100 gal/min (450 l/min) pump which increases the leak rate which can be accommodated by the sump pumps, thereby reducing the

number of leak sources with leak rates exceeding sump pump capacity. It also provides additional pump redundancy for leaks less than 34 gal/min. This pump is started automatically when a significant leak from the reactor tank to the sump is detected. Make-up from the make-up tank affords a small measure of protection in the case of small leaks in that it will slightly extend the time available for remedial action to be taken. The motorised heat exchanger valves enable that part of the system upstream of the valves to be isolated from the risers. These are closed automatically when a significant leak from the reactor tank is detected. Detection is by a set of probes which trip when the level of D_2O in the tank falls by 10 cm.

3.4 Reliability of Protection System

3.4.1 Sump Pumps

The probability of failure of a sump pump is the probability of its failing to start and run for sufficient time to repair the leak or remove the fuel from the reactor. The SRS Data Bank (2) gives the failure rate for typical pumps as 0.4 per year. Assuming the fuel can be removed in 4 days, the probability of a pump failing to operate satisfactorily for 4 days is:-

$$P_{PR} = 0.4 \times 4/365 = 4.4 \times 10^{-3}$$

and with the probability of failure to start when demanded of 5×10^{-3}, the probability of pump failure is:

$$P_P = (4.4 + 5) \times 10^{-3} = 9.4 \times 10^{-3}$$

(see also section 3.7)

3.4.2 Motorised Valves

The motor driven valves require power both to open and close. The generic failure[2] rate for all faults is about 0.2 f/y. It is not unreasonable, and is possibly pessimistic, to assume that half the failures are failure to close. The failure rate for the valves is therefore 0.1 f/y. This does not include failure of the power supplies to the valves, which make a negligible contribution to the total failure probability.

It is assumed that the valves will be tested for operation at each shutdown. The probability of failure on demand for the three valves is therefore:

$$D_H = 3 \times 0.1 \times \frac{1}{12} \times 0.5 = 1.3 \times 10^{-2}$$

3.4.3 Automatic Operation of Valves and Pump

The largest potential leaks in the system will drain the RAT to a dangerous level in about 2 minutes. For the motorised valves to give adequate protection their closure must be automatically initiated. Similarly, to obtain full benefit of the additional pump, it too should be started automatically. The pump will be capable of 100 gal/min (450 l/min) delivery, which will protect against leaks which will drain the RAT to a dangerous level in about 5 minutes.

The automatic system is designed to good reactor practice, such as using majority vote systems, and is adequately maintained and tested. A probability of failure on demand of 5×10^{-3}, is assumed in this assessment.

3.5 Sources of Dangerous Leaks

3.5.1 Large Pipework

The D_2O circuit consists of 7, 9 and 10 in (175, 228, 254 mm) nominal-bore pipework connecting the heat exchangers and main pumps to the RAT through bellows. The emergency shutdown pumps are connected into the main circuit by 6 in and 4 in (152 and 102 mm) pipes, and the partial-dump pipe is also 6 in (152 mm) nominal-bore. Except for a drain in the discharge header and the liquid-level make-up into the suction header, which are of 2 in (51 mm) n.b., the ancillary pipe connections into the main circuit for ion exchanger, drain points etc are 1½ in, 1 in, ¾ in and ½ in (38, 25, 19 and 13 mm) n.b., with ½ in (13 mm) connections being most numerous.

For a leak of greater than the sump pump's capacity to occur would require a catastrophic failure of a pipe with no forewarning such as minor leakage. The maximum internal pressure is about 36 lb/in² (250 KN/m³) in the discharge header, producing a stress in the pipe wall of about 600 lb/in² (4.1 KN/m³). The weight of the valves will also contribute to stress in the pipework. With the low stresses in the pipework it is difficult to visualise any mechanism which could cause catastrophic failure under normal loading. Furthermore, with short lengths of pipe rigidly supported, if a failure should occur the pipes would remain in position, limiting the size of leak unless the supporting structure failed. This is considered to be of negligible probability. In this assessment it is assumed that weld failure in the large pipework would result in a leak not exceeding 20 gal/min (90 l/min).

3.5.2 Small Pipework

The smaller pipework, 2 in (51 mm) diameter and below, is subjected to less stress due to internal pressure than the larger pipes, but, owing to the lower stiffness of the pipe runs, is more likely to be subjected to cyclic stresses due to vibration. The greatest stress concentration would occur at the positions where the pipe is rigidly fixed, e.g. where it is welded into the main circuit.

For the joints of 2 in (51 mm) diameter pipes to the main circuit, the 2 in pipe is welded directly to the large bore pipe. For joints for 1 in, ¾ in and ½ in (25, 19 and 13 mm) n.b. pipe a boss is welded into the larger pipe forming a socket into which the smaller pipe is welded. Thus there are two welds associated with each boss. If, as in most joints, the smaller pipe is a short stub terminating in a valve, there is a third weld between the stub and the flange to which the valve is attached. The flow restriction due to the short stub is negligible, and in the assessment the leak rate due to the flange weld failure is considered to be the same as for the pipe to boss weld failure. The leak rates from these weld failures are:-

Size of Branch Inches n.b.	Orifice Size (ins)	Leak Rate, gal/min Discharge Header	Suction Header
2	Pipe dia. 2.13	240	187
1	Outer dia. 2.13	240	187
1	Pipe bore 1.22	79	61
¾	Outer dia. 1.88	187	145
¾	Pipe bore 0.97	50	39
½	Outer dia. 1.63	140	109
½	Pipe bore 0.72	27	21

TABLE 1. SOURCES OF LEAKS DOWNSTREAM OF HEAT EXCHANGER VALVES

Part of Circuit	Leak Source	Qty	Leak Rate Per Source gal/min	Total Failure Rate f/y	
				Higher	Lower
Heat exchangers to risers	1 in (2.5mm) boss outer weld	1	20	3.3×10^{-6}	1×10^{-6}
	i in (2.5mm) pipe weld	2	61	6.6×10^{-6}	2×10^{-6}
	Instrument pad weld	4	32	1.3×10^{-5}	4×10^{-6}
	Circumferential weld	18	<20	6×10^{-5}	1.8×10^{-6}
RAT Drain	1 in (2.5mm) nb pipe	1.5 ft	38	6.6×10^{-7}	1.5×10^{-7}
	1 in (2.5mm) nb pipe	1.5 ft	27	6.6×10^{-7}	1.5×10^{-7}
	Instrument pipe	15 ft	7	6.6×10^{-6}	1.5×10^{-6}
Bellows	Bellows and gland in series	3	<20	1.1×10^{-4}	0

A summary of leak sources has been compiled and an example is given in Table 1. They have been classified according to their positions in the circuit for the convenience of the later part of the assessment.

3.6 Failure Rates

The D_2O pipework differs from most of the power reactor systems for which failure data have been collected in that it sustains only low pressure. Furthermore, in the main circuit there are a large number of welds in relation to the length of pipe run, and in the event of fracture there is negligible disruptive force to separate the components. The major pipework is more akin to a series of lightly stressed low-pressure vessels. The failure rate of the large pipework is therefore based on weld-failure data.

In the smaller pipework the weld/pipe run relationship is more representative of the normal systems, and pipework-failure data are used.

Owing to the paucity of data on low-pressure systems failure rates for this assessment are obtained from systems operating at higher pressures. Economics dictate that pressure equipment is usually designed to be no more than adequate, with sufficient safety margin, for its duty, with the result that failure rates are not greatly dependent on operating pressure. In the D_2O pipework it is probable that factors other than internal pressure, such as general robustness, dictated the thickness of material, and it would be expected that in consequence the safety margin is higher and that the failure rates used in this assessment tend to be pessimistic.

3.6.1 Welds

Two sources give failure rates for welds. Two entries in the Data Bank[2] quote failure rates of 2×10^{-5} and 6.6×10^{-5} faults/year per weld for all modes of failure. WASH 1400[3] quotes 2.6×10^{-5} faults/year per weld for serious leaks in low-pressure containment. "Serious" is not defined, but complete rupture is not implied.

102

Gibbons and Hackney[4] in a survey of piping failures show that of 399 failures reported 19 were complete severance, none of which were preceded by known leakage. In all only 25 failures occurred without detected leakage. About 38% of all failures and 42% of severance failures were associated with welds.

In Smith's and Warwick's survey[1] of pressure vessels, out of a total of 69 failures in service of unfired components, 8 were disruptive, presumably with no known prior leakage, 24 faults were detected by leakage and the remainder were disclosed by visual inspection or non-destructive testing. It is not known, of course, whether the faults disclosed by inspection would have developed into leaks or disruptions. About 85% of all faults and 50% of disruptive faults were associated with welds.

On the D_2O main circuit, with its low internal pressure, only complete severance would cause a dangerous leak. From Ref 4 only about 5% and from Ref 1 only about 11% of all failures caused severance. Both of these surveys were from general commercial plant, in which constant monitoring for leaks would not be expected. It does not seem unreasonable to assume that on the D_2O circuit, where continuous sensitive leak monitoring is carried out, the failure rate for disruptive failures for welds is at most 5% of all failure modes, and even this would be a pessimistic assumption.

From the data sources the failure rates for all modes for welds lie between 2×10^{-5} and 6.6×10^{-5} f/yr per weld. In this assessment the failure rate for severance failures is assessed to be between

$$\theta_w = 2 \times 10^{-5} \times .05 = 1 \times 10^{-6} \text{ f/yr per weld}$$

and $\quad \theta_w = 6.6 \times 10^{-5} \times .05 = 3.3 \times 10^{-6}$ f/yr per weld

3.6.2 Pipework

As mentioned previously pipework failure rates as distinct from weld failure rates are used in this assessment for the smaller pipework. WASH 1400[3] gives a failure rate of 8.8×10^{-6} faults per year per section for ruptures in pipes less than 3 in (76 m) diameter where a section is defined as the average length (between 1.0 and 10.0 ft, or 0.3 to 3 m) of pipe between discontinuities such as valves and pumps. Each section can include several welds and flanges. The "sections" involved in the D_2O circuit are about 20 ft (6 m) long, which would result in a failure rate of 4.4×10^{-7} f/y ft (1.5×10^{-6} f/y m).

Gibbons and Hackney[4] do not give the population over which their survey was made, but Rudham[5] has deduced, by making certain assumptions, a failure rate of 1×10^{-7} f/y ft.

The Data Bank,[2] from a source concerning pipelines, gives a failure rate for all failures of 1.4×10^{-7} f/y ft for pipes of 5 to 10 in (127-254 mm) dia, operating over a wide pressure range of 20 to 1080 lb/in^2 (138 KN/m^3 to 7.4 MN/m^3). WASH 1400 gives data which suggest that the failure rate of pipe over 6 in (153 mm) dia is about one tenth of pipes from $\frac{1}{2}$ to 2 in (13 to 51 mm) dia. Applying this ratio, and also that for the relationship between total failure and rupture, to the failure rate given by the Data Bank, gives

$$1.4 \times 10^{-7} \times 10 \times 0.05 = 7 \times 10^{-8} \text{ f/y ft}$$

which does not differ widely from the failure rate deduced by Rudham. For this assessment the failure rate for rupture of small pipework is assumed to lie between Rudham's deduced value and that derived from WASH 1400, ie between

$$\theta_p = 1 \times 10^{-7} \text{ faults/y ft}$$

and $\quad \theta_p = 4.4 \times 10^{-7} \text{ faults/y ft}$

3.7 Failure Probabilities

It is assumed in this assessment that failures occur randomly in time, ie the failure rate is constant. The reactors are past the early-life failure state, and it is assumed that components are operating in their constant useful life phase. This is true for plant where items have been in service for a long period, provided that a good standard of repair and maintenance has been adhered to.

With a constant failure rate the probability of failure in time t is given by:

$$P_F = 1 - e^{-\theta t}$$

where θ is the failure rate.

If a system consists of a number of components, the failure of any of which will fail the system

$$P_F = 1 - e^{-(\theta_1 + \theta_2 \ .. + \theta_n)t}$$

where θ_1, θ_2 ... are the failure rates of the components.

If $(\theta_1 + \theta_2 \ ... \ \theta_n)t$ is much less than unity, the expression is closely approximated by:

$$P_F = (\theta_1 + \theta_2 \ ... \ + \theta_n)t$$

For components which can be in the unrevealed failed state, eg non-return valves which can be seized in the open position, and whose failure is not apparent until a test or demand is made, the maximum probability of the component's being in the unrevealed failed state is:

$$P = 1 - e^{-\theta T}$$

where T is the interval between tests.

The probability of failure to operate on random demand is:

$$D = \frac{1}{T} \int_0^T (1 - e^{\theta t}) \ dt,$$

which reduces to:

$$D = \frac{\theta T}{2}$$

for single components with no redundancy if θT is much less than unity.

If in a multi-component system all components must fail to fail the system, the probability of system failure is:

$$P_{SYS} = P_1 P_2 \ldots P_n$$

where P_1, P_2, P_n are the probabilities of failure of each component. However, if the values of P_1, P_2 etc are low, the result is unrealistically low values for system failure, as common mode failures are ignored. When values of the order of 10^{-6} are reached, failures which have no connection with the mechanical performance of the component, such as a local fire, power failure or a systematic maintenance fault, may have a higher probability of occurrence.

Where the probability of failure of a number of protective devices in redundancy arrangement is calculated to be less than 10^{-6} a lower limit of 10^{-6} has been imposed. A lower limit of 10^{-8} has also been stated for the combined probabilities of leakage and of protection failure. However, it is emphasised that these limits exclude the probability of common mode faults which for redundant systems can increase the overall probability of failure to between 10^{-3} and 10^{-4}. In terms of the overall hazard a lower limiting value of 10^{-6} is considered more appropriate.

3.8 Assessment

The possible leaks can be classified according to the protection against dry-out afforded by the pumps, viz:

(i)   Over 100 gal/min (450 l/min) for which there is no pump protection.

(ii)   Between 100 and 34 gal/min (450 and 150 l/min) which cannot be returned to the RAT if the 100 gal/min pump or the automatic operation of the pump fail.

(iii) Between 34 and 20 gal/min (150 and 90 l/min) which cannot be returned to the RAT if the 100 gal/min pump and one of the 20 gal/min sump pumps fail.

Note: It is assumed that if the leak is less than 34 gal/min (150 l/min) there is sufficient time for the operator to start the small pumps if the auto start fails.

The leak sources can also be classified according to their position in the circuit, viz:

(i)   Those upstream of the heat exchanger valves which can be isolated from the risers and thus prevented from draining the centre of the fuel elements by closure of the heat exchanger valves.

(ii)   Those downstream of the heat exchanger valves which cannot be isolated from the risers. (These are listed in Table 1).

Thus there are 8 categories of leaks, and these are listed in Table 2, together with their probabilities of occurrence. Also listed in Table 2 are the protection against dry-out for each category, the probability of failure of the protection, and the probability of dry-out resulting from failure of each category.

TABLE 2. PROBABILITY OF DRY-OUT

Leak Size gal/min	Position in Circuit	Probability Leakage Per Year		Protection	Probability of Protection Frailure	Probability of Dry-Out Per Year	
		Higher	Lower			Higher	Lower
Over 100	1. Upstream of HEV's	1×10^{-4}	3×10^{-5}	1. Heat Exchanger valves with automatic initiation	1.8×10^{-2}	1.8×10^{-6}	5.4×10^{-7}
	2. Downstream of HEV's	NONE	NONE	NONE	-	-	-
100-34	3. Upstream of HEV's	3.9×10^{-5}	1.1×10^{-5}	1. Heat exchanger valves with automatic initiation. 2. 100 gal/min pump with automatic initiation.	5.1×10^{-3}	2×10^{-7}	5.6×10^{-8}
	4. Downstream of HEV's	7.3×10^{-6}	2.2×10^{-6}	1. 100 gal/min pump with automatic initiation.	1.4×10^{-2}	1×10^{-7}	3.1×10^{-8}
34-20	5. Upstream of HEV's	3.3×10^{-4}	9.9×10^{-5}	1. Heat exchanger valves 2. 100 gal/min pump · 3. Both 20 g/min pumps	2.3×10^{-6}	1×10^{-8}	1×10^{-8}
	6. Downstream of HEV's	1.4×10^{-5}	4.2×10^{-6}	1. 100 gal/min pump 2. Both 20 g/min pumps	1.8×10^{-4}	1×10^{-8}	1×10^{-8}
Below 20	7. Upsteam of HEV's	5.7×10^{-4}	1.3×10^{-4}	1. Heat exchanger valves 2. 100 gal/min pump 3. 20 g/min pump No 1 4. 20 g/min pump No 2	1×10^{-6}	1×10^{-8}	1×10^{-8}
	8. Downsteam of HEV's	1.8×10^{-4}	2×10^{-5}	1. 100 gal/min pump 2. 20 g/min pump No 1 3. 20 g/min pump No 2	1×10^{-6}	1×10^{-8}	1×10^{-8}
					TOTAL	2.1×10^{-6}	6.8×10^{-7}

The total probability of the D_2O level falling below the outlets in the fuel elements is assessed as between 2.1 x 10^{-6} and 6.8 x 10^{-7} per year.

3.9 Conclusions

The probability of leakage from the D_2O pipework which would cause dry-out of the fuel plates of the reactor is assessed to be between 2.1 x 10^{-6} and 6.8 x 10^{-7} per year.

4. Assessment of the Reactor Extract System

4.1 Introduction

The extract system considered normally operates in conjunction with the other ventilation input and extract systems to maintain a depression of $\frac{1}{4}$ in wg in the reactor hall. For emergency conditions of activity release within the hall the mode of operation changes to seal the building, decontaminate the extract air and return it to the reactor hall instead of discharging it up the stack. A schematic diagram of the system is shown on Fig 2.

The inlet system delivers 6,500 ft^3/min of air to the reactor hall and is extracted by the two extract systems of 4000 ft^3/min and 2500 ft^3/min capacity to the stack. Flow is trimmed by a damper to account for leakage and to maintain the depression. When an activity release is detected by the gamma monitors on the extract filters, the inlet and additional extract lines are isolated and air is recirculated via charcoal beds to reduce contamination
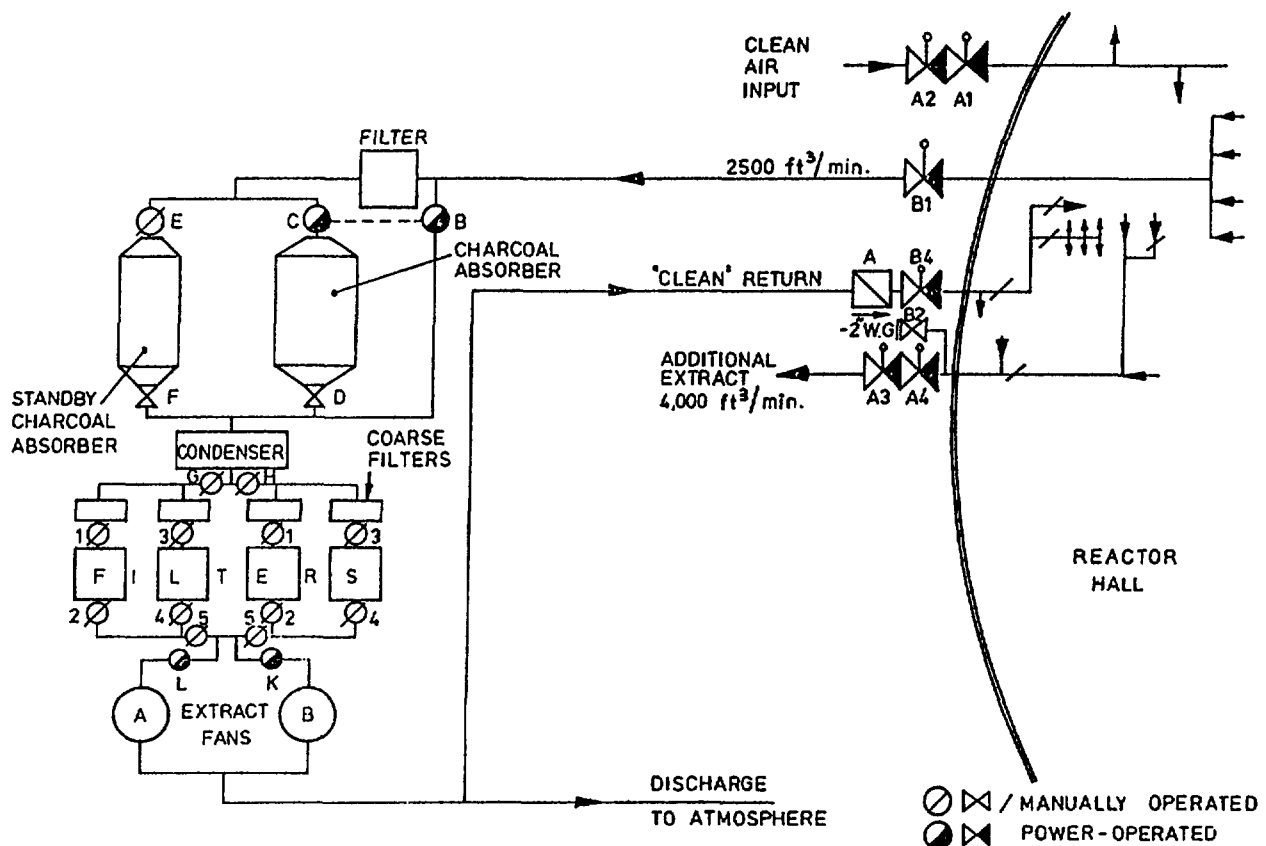
FIG. 2. Schematic layout of ventilation system.
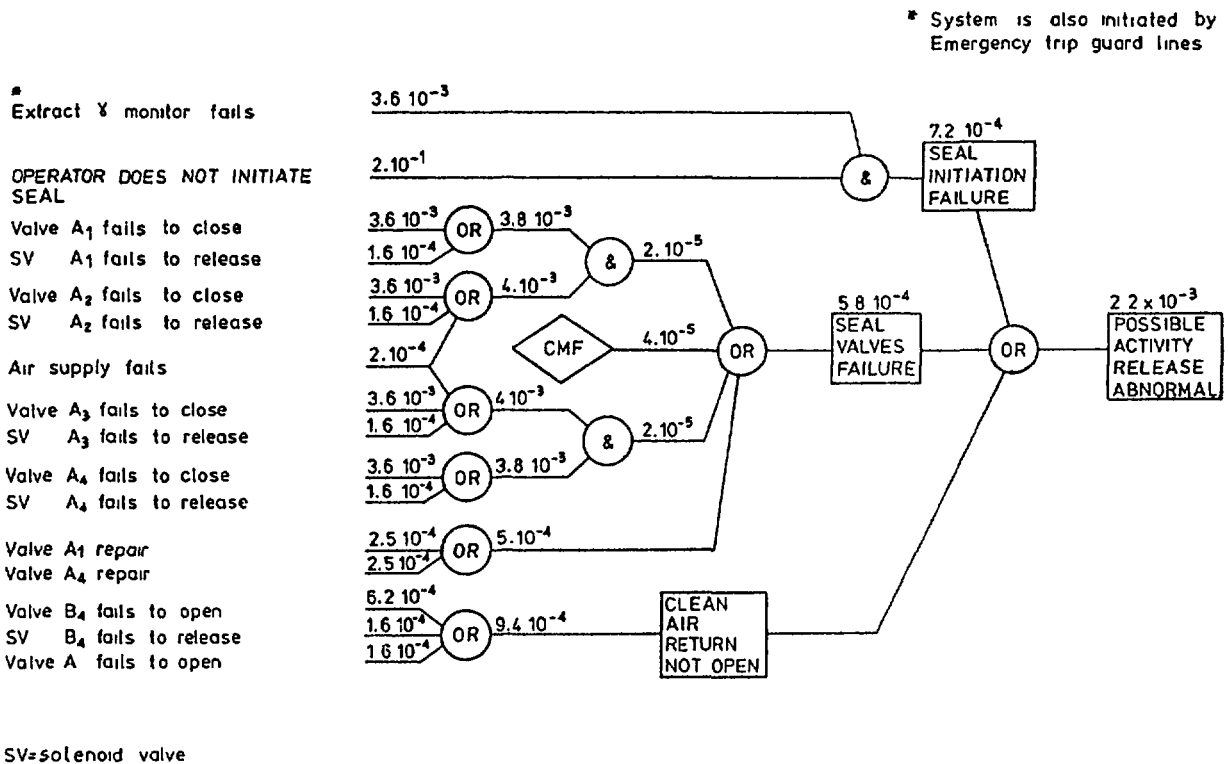
FIG. 3. Extract system failure logic (1).

in the reactor hall. Only a flow of air equal to the building leakage is dis-
charged to the stack and the depression is maintained at 2.5 in wg by a flap
valve in the decontaminated air return line to the reactor hall. The system
would then be required to operate for a period of perhaps up to a week to
adequately decontaminate the reactor hall air.

4.2 System Reliability

4.2.1 System Requirements

The failure logic for the various system failure modes is shown on Figs
3 and 4. With the exception of the inlet and outlet valves (A, B_1 and B_4)
and the charcoal bed control valves (B and C), redundancy of the main com-
ponents is applied, with one item selected for normal operation and one on
standby duty.

The initial requirement is for the inlet and additional extract lines
to be isolated by either or both of the two valves in each line. At the
same time valve B is closed and valve C is opened to allow extract air to
pass via the charcoal absorber column, and the valve B_4 in the decontaminated
air return line to the reactor hall must also be opened. The operator can
manually operate these valves to the emergency state if automatic initation
fails.

From the system operating requirements described above the reliability
of the building seal valves system can be expressed in terms of its proba-
bility of failure on demand, which for a demand rate much lower than the
test frequency is equivalent to the system unavailability. Failure to ini-
tiate and maintain a seal could lead to an unacceptable activity release as
indicated on Figure 3. An unacceptable release could occur if valve B_4 or
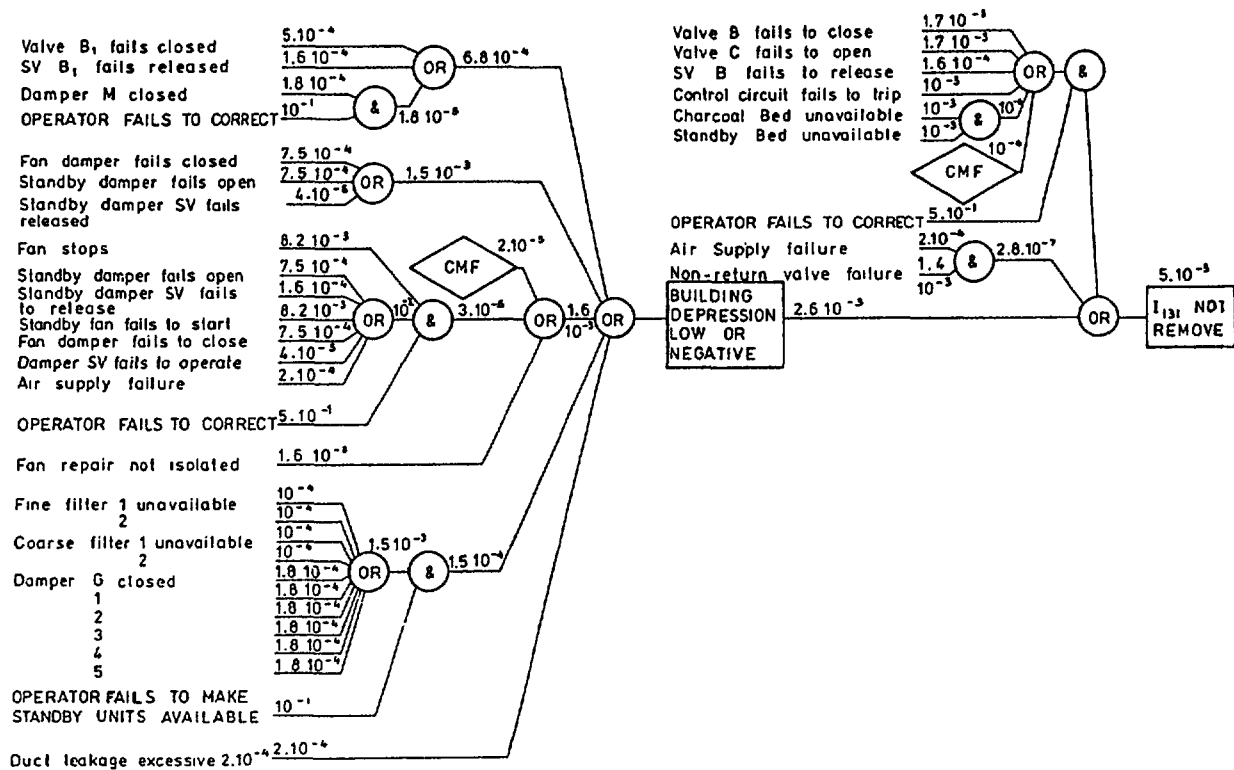
FIG. 4. Extract system failure logic (2).

valve A does not open on demand, so causing all extract air to be discharged to the stack and the building depression to be high.

Failures of valve B_1, fans, dampers or filter blockage will cause the containment depression to tend to zero or be negative. This condition, combined with the charcoal beds unavailability will make the system incapable of I_{131} removal.

4.2.2 Building Seal Valves

The two inlet and two outlet seal valves are identical gate valves, but differ in the method of actuation. The inner valves (A_1, A_4) are opened by a solenoid valve controlled pneumatic cylinder and mechanically latched. They are closed by solenoid (or manual) release of the latch and attached weights. The two outer valves (A_2, A_3) have two-way cylinders for pneumatic opening and closing and therefore rely on the air supply for emergency closure. The solenoid valves controlling the air can only be isolated from the air supply for maintenance in pairs for valves A_1, A_4 and A_2, A_3. The operation of the valves is tested daily from the manual control panels, but it is assumed that testing of the trip initiation from the APS or the gamma monitors will be at the normal shutdown intervals of 28 days.

The valves only control air flow at low pressure and are therefore only lightly stressed. Routine maintenance should alleviate any wear problems and therefore an average failure rate for this type of component will probably err on the pessimistic side. Although the extract system is external to the reactor hall these valves have some protection provided from the weather.

4.2.3 Isolation and Control Valves

Valves B and C which control the inlet and bypass to the charcoal bed are butterfly valves actuated from a common solenoid valve via individual pneumatic cylinders. Daily tests on these valves are specified in conjunction with the tests on the seal valves.

The control valve A which controls the reactor hall depression under emergency conditions at $2\frac{1}{2}$" wg is a simple mechanical flap valve. It is tested daily and with appropriate routine maintenance would be expected to have the low failure rate indicated.

Valves B_1 and B_4 are pneumatically actuated inlet and outlet isolation valves, B_1 being normally open, and therefore, only spurious closure can inhibit the system. For the solenoid valve in the normally energised state and air pressure being required to actuate the valves the failure rates for this event have been assessed as relatively low and insignificant. Valve B_4 however is normally closed, must open on demand, and remain open.

4.2.4 Emergency State Initiation

The closure of the building seal valve and the operation of the charcoal bed isolation and bypass valves is initiated by the gamma monitor instruments on the extract filter that is selected for operation, and also by the reactor Emergency Trip guard lines. The instrument on the filter not in use is bypassed by contacts indicating that the isolating damper is closed.

Duplicated contacts from the emrgency trip guard lines and the gamma monitors control each pole of the supply to the seal valve control relay.

4.2.5 Fans and Dampers

Two extract fans are provided, with one normally being operational and the other on automatic standby. They are manually changed over daily to test their functional capability and to equalise their operating times. The control circuits include interlocks with the associated inlet dampers' controls. In addition to fan failure the system can be subject to interlock and control circuit failure, operating fan damper closure, standby fan damper opening, or failures of their respective solenoid valves.

4.2.6 Filters

Four sets of coarse and fine filters for the removal of particulate matter operate in pairs, with one pair able to operate whilst the other is being replaced. Filters are checked daily by inspection of manometers on the plant that indicate the pressure drop across them. The isolating dampers are fitted with microswitches for remote position indication. The significant failure modes of the filter arrangement are probably unavailability due to replacement, which should not be coincident for the two sets due to operational procedures, and the incorrect setting of dampers. This could occur either during operation or replacement of filters causing blockage of the system or excessive leakage, both conditions being immediately revealed to the operator. If filter changing is staggered in time and done as in the operating procedures then coincident blocking should not occur.

4.2.7 Charcoal Beds

The efficiencies of the charcoal beds for the absorption of iodine is measured annually at normal working conditions on the plant and also by a

laboratory test at high humidity on a small sample of charcoal. There is
a known gradual deterioration of the material which normally will only re-
quire renewal at approximately 10 year intervals. This is dependent on the
results of the annual tests for which limits have been set for the decontami-
nation factors for both the main and standby beds. The test results are
generally very much in excess of these values. The system design is such
that valves B and C cannot both be in the closed state to allow the standby
bed to become operational whilst the main bed is opened for renewal. This
work is done during times when there is negligible risk of an activity re-
lease in the reactor hall.

4.2.8 Maintenance

With the possible exception of filter replacement and instruments, the
repair of failed items will almost certainly be of long duration, such that
if the failure occurs during an emergency period the item could remain in
an unavailable state throughout the remainder of that period. This will par-
ticularly apply to large plant items for which complete spare items are not
available, such as fans and valves.

4.2.9 Indications and Alarms

An important measurement for revealing and identifying failures of the
active extract system is that of building depression. At present there is
an indication of differential pressure across the airlock doors that will be
frequently observed during normal usage.

A trip of the active extract fans occurs when a high depression is generated
by separate pressure switches.

Adequate indications and alarms are provided for the main components of
the system, ie fans, valves, dampers, in the plant room and control room and
use of these in association with the appropriate controls is incorporated in
the routine test procedures.

4.3 Reliability Quantification

4.3.1 Reliability Models

For quantitative assessment of reliability it is usually assumed that all
failures are random independent events and that repair of failed items is
perfect. This implies that the failure rate (θ) is constant and is the charac-
teristic of the exponential distribution. For systems where redundancy is
applied to improve reliability dependent (common-mode) failures must also be
considered.

The probability (P) of failure of an item in some specified time interval
(t) is given by:-

$$P = (1 - e^{-\theta t})$$

which for most cases can be simplified to, when $\theta t \ll 1$

$$\underline{P = \theta t}$$

111

TABLE 3. MODELS FOR COMPONENTS UNAVAILABILITY

Components Arrangement	Failure logic Function	Repair Process		Component Unavailability U_I or U_D	System Unavailability U_s	Comment
		Immediate /Deferred	Independant /Dependent			
Series	OR	Immediate	Independent	$\theta.t_r$	$\sum \theta.t_r$	t_r = repair time θ = failure rate
		Deferred	Independant	$\dfrac{\theta.t_o}{2}$	$\sum \dfrac{\theta.t_o}{2}$	t_o = operating period
Redundant	AND	Immediate	Independent	$\theta.t_r$	$\theta^n.t_r^n$	n = No of redundant components
			Partly Dependent	$\theta.t_r$	$\theta^n t_r^n + K.k.\theta.t_r$	k = No of dependent components K = dependent failure fraction of θ
		Deferred	Independent	$\dfrac{\theta.t_o}{2}$	$\dfrac{\theta^n.t_o^n}{n+1}$	
			Partly Dependent	$\dfrac{\theta.t_o}{2}$	$\dfrac{\theta^n.t_o^n}{n+1} + K.k.\theta.t_r$	

For redundancy systems having m from n voting and r failures for system failure

$$P_s = \binom{n}{r} \cdot P^r$$

The reliability expressed in terms of the unavailability (U) for failures that are immediately revealed and repaired in a time (t_r) is

$$U_I = \theta \cdot t_r$$

If the repair is unrevealed until some proof test, or repair is deferred to allow plant operation to continue until some scheduled shutdown and the period between such events (τ) or (t_o) respectively, the unavailability is:

$$U = \frac{\theta\tau}{2} \quad \text{OR} \quad U = \frac{\theta \cdot t_o}{2}$$

If the repair time is not insignificant with respect to the test interval then

$$U = \frac{\theta\tau}{2} + \theta t_r = \theta \left(\frac{\tau}{2} + t_r\right)$$

For redundancy systems

$$U_s = \frac{\binom{n}{r} U^r}{r + 1}$$

An exception to the product rule of probabilities occurs when repair of redundant items is not independent as previously described. The system is unavailable when certain components are being repaired due to lack of fault isolation, and such events can be considered as common-mode failures. If some fraction (K) of all failures have this repair dependency then for a 1 from 2 system with deferred repair the unavailability is:-

$$U_s = \frac{\theta^2 t_o^2}{3} + 2.K\theta.t_t$$

On the failure logic diagrams the OR functions are summated terms and the AND functions are product terms. All the above expressions are probabilities of events and can be combined as shown.

4.3.2 Reliability Data

The primary failure rate data has been obtained either directly or derived from the NCSR Reliability Data Bank. Where it was considered appropriate, account was taken of particular conditions at the reactor to modify the data that was available. Restoration time estimates have been based on repair time estimates supplied from the reactor. Estimates of operator reliability performance have been assessed from the procedures described in the operating instructions and from general experience.

TABLE 4. COMPONENTS RELIABILITY DATA

COMPONENT	FAILURE MODE	FAILURE REVEALED OR UNREVEALED R OR U	FAILURE RATE $\theta f/10^6$hrs	REPAIR TIME t_r hrs	PROOF TEST OR INSPECTION INTERVAL τ hrs	REPAIR IMMEDIATE OR DEFERRED (I OR D)	DEPENDENT FAILURE FRACTION K	UNAVAILABILITY $U_I = \theta.t_r$	$U_D = \frac{\theta.\tau}{2}$	$U_D = \frac{\theta t_o}{2}$
FAN A, B	LOW FLOW	R	20	100	24	D	0.8			$7.2.10^{-3}$
FAN DRIVE	STOPPED	R	50	20	24	I	-	10^{-3}		
FAN DAMPER, K, L	OPEN	R	15	50	24	I	0.5	$7.5.10^{-4}$		
	CLOSED	R	15	50	24	I	0.5	$7.5.10^{-4}$		
SOLENOID VALVE	FAILS TO RELEASE	U	10	4	24	I	0.5	$4.0.10^{-5}$	$1.2.10^{-4}$	
	RELEASED	R	10	4	24	I	0.5	$4.0.10^{-5}$		
SEAL VALVE A_1, $_4$	OPEN	U	10	50	24	D	0.5	5.10^{-4}		$3.6.10^{-3}$
	CLOSED	R	10	50	24	I	0.5	$5.0.10^{-4}$		
SEAL VALVE A_2, A_3	OPEN	U	10	50	24	D	-			$3.6.10^{-3}$
	CLOSED	R	10	50	24	I	-	$5.0.10^{-4}$		

TABLE 4. (cont.)

ISOLATION VALVE B	OPEN	U	10	50	720	D	-			$3.6.10^{-3}$
	CLOSED	R	10	50	720	I	-	$5.0.10^{-4}$		
ISOLATION VALVE B$_4$	OPEN	U	10	50	24	I	-	$5.0.10^{-4}$	$1.2.10^{-4}$	
	CLOSED	R	10	50	24	I	-	$5.0.10^{-4}$	$1.2.10^{-4}$	
ISOLATION VALVE B	OPEN	U	15	100	24	I	-	$1.5.10^{-3}$	$1.8.10^{-4}$	
	CLOSED	R	15	100	24	I	-	$1.5.10^{-3}$		
ISOLATION VALVE C	OPEN	U	15	100	24	I	-	$1.5.10^{-3}$	$1.8.10^{-4}$	
	CLOSED	U	15	100	24	I	-	$1.5.10^{-3}$	$1.8.10^{-4}$	
CONTROL VALVE A	OPEN	U	5	20	24	I	-	$1.0.10^{-4}$	$6.0.10^{-5}$	
	CLOSED	U	5	20	24	I	-	$1.0.10^{-4}$	$6.0.10^{-5}$	
GAMMA MONITOR	FAILURE TO TRIP	U	10	5	720	I	-		$3.6.10^{-3}$	
FILTER	UNAVAILABLE	R	100	1	-	I	-	$1.0.10^{-4}$		
CHARCOAL BED	UNAVAILABLE	U	20	50	$8.8.10^{3}$	D	-	$1.0.10^{-3}$		
DUCT	LEAK	R	10	20		I	-	$2.0.10^{-4}$		
AIR SUPPLY	LOW PRESSURE	R	20	10	-	I	-	$2.0.10^{-4}$		
NON-RETURN VALVE	OPEN	U	4	10	-	D	-			$1.4.10^{-3}$
MANUAL DAMPER	OPEN	U	5	50	720	I	-			$1.8.10^{-4}$
	CLOSED	U	5	50	720	I	-			$1.8.10^{-4}$

4.3.3 Common-Mode Failure

The active extract system for the reactor has redundancy applied to most of its main components and will therefore be subject to dependent failures of these due to common causes. Directly applicable experience of CMF is limited[7], but when independent failure probability for redundancy systems are less than, say, 10^{-4}, some qualitative analysis at least is necessary to identify possible CMF and then to estimate their significance to the quantitative analysis. The CMF to which redundant components of the active extract system are vulnerable are discussed below.

(a) **Seal Valves**

The main possible causes of CMF are expected to be due to imperfect maintenance or severe environmental effects. Gland tightness or other cause of sticking, foreign matter in the valve body with their close location to each other, or mechanical damage are possible, but not only modes of failure of the valve, its actuator or the solenoid valves. For the two outer valves the air supply is a common service required for closure and for the two inner valves the non-release of air from the cylinder, solenoid sticking or latch seizure are examples of possible CMF. A probability of failure on demand due to CMF is estimated at 4.10^{-5}.

(b) **Fans and Dampers**

There are several common features of the power and control circuits for the fan drive. Although there are automatic changeover arrangements between the normal and guaranteed supplies, they are common together with the main isolator switch and distribution board. With common components and common design and construction of the control circuits there are therefore many possible causes of CMF. No definite causes of CMF of the fans have been identified, but the possibility cannot be ignored due to them being identical in design, their close proximity to each other and common maintenance procedures. A CMF probability of 10^{-4} has been estimated.

The dampers are actuated by 2 way cylinders and pistons from a 5 port solenoid valve. Common maintenance or environmental influences could cause CMF of these components and failure of the air supply could have similar consequences. A CMF probability of 2.10^{-5} has been estimated.

(c) **Filters and Dampers**

The major possible causes of CMF are expected to be errors during maintenance procedures or maintainability problems. Certain environmental effects could also occur, but in each case the failure is likely to be immediately revealed. The possibility of maintenance error is considered to be remote because of the relative simplicity of operations and the procedures tend to eliminate certain effects that could occur with such plant. A CMF probability of 10^{-5} is thought to be appropriate.

116

(d) Emergency Initiation Circuits

Comments have been made in a previous section regarding the possibility of CMF due to dependencies in the circuit's design. Maintenance or operator error are other possible causes of CMF that have been identified.

4.4 Summary Discussion

The quantified reliability of the system has been derived on the logic diagrams of figures 3 and 4 in terms of the unavailability of the various functional requirements of the system, which is equivalent to the probability of failure on demand. The seal valve system and the line recirculating air back to the reactor hall has an unavailability of $2.2.10^{-3}$, or an abnormal release of activity can be expected once in approximately 450 demands. The most significant contributors to unreliability, although not dominant, are the gamma monitor, and the valve B_4 in the clean air return line. Repair of valves A_1 and A_4 is also significant, but these events are under the control of the operators and can be considered as not independent of fuel handling operations. Procedures could therefore take account of this repair problem.

The system unavailability for iodine removal is 5.10^{-3}. This means that there will be a failure to remove the activity once in every 200 demands. Common significant contributors are the isolation valve B_1, the fan dampers and the dependent repair of fans. The charcoal bed valves, B and C, are significant for iodine removal.

Main components such as the fans, dampers and seal valves have been duplicated for the system to be able to tolerate single independent failures. However, it has been shown that certain failure modes of components can cause the system to be unavailable or that the system could become unavailable during repair. Several of these events have been identified as significant contributors to system unavailability.

5. Comparison of Possible Releases of Activity with the Farmer Criterion

5.1 Introduction

5.1.1

In the approach based on probability analysis, the chain of events leading up to and beyond certain accident conditions is analysed by statistical techniques to give the probability that the eventual outcome of that chain of events will occur. These probabilities are always small for major accident conditions which might have a probability of 10^{-6} per year, ie it would be expected to occur once in a million years. In addition, the consequences of the chain of events are calculated, and these are weighed against the probability of their occurring. This may be done by reference to a criterion of acceptability. Such criteria have been proposed by Farmer (8) and Kinchin (10). The analysis of the faults as they occur in the plant is similar in both cases, but using the Kinchin criterion, the effect of the possible discharges on the actual surrounding population distribution, taking into account weather conditions on a statistical basis, is also assessed. The analysis presented here has been carried out in terms of a Farmer diagram, which plots consequences (usually in terms of curies of I^{131} released) against probability, and has a line dividing "acceptable" from "unacceptable" release/probability combinations.

A similar method was extensively used by Rasmussen (9) who plots actual lives or cost of damage incurred against their probability for nuclear plants and other natural and man-made risk sources.

5.1.2

The object of this section is to apply this recently developed technique to the assessment of the reactor in the area of loss of coolant through pipework failure. In order to simplify the presentation, reference will be made to the Farmer criteria as proposed for power reactors other than in near-urban sites, as is appropriate for the rural situation around the reactor.

5.2 Probability Studies

5.2.1

The probability of loss of the D_2O coolant due to a pipework failure has been calculated in Section 3 to be between 2.1×10^{-6} and 6.8×10^{-7} per year. These figures are arrived at using statistical failure rates for the pipework, and also considering the capacity of the protective equipment installed (sump pumps etc.) and the failure rate of this also. Further, because of the dearth of data on systems so lightly stressed as those in the reactor, pessimistic values have been taken for failure rates. It will be seen, therefore, that these probabilities represent an over-estimate of the probability of fuel melting occurring.

5.2.2

A full consideration of the consequences of the melting of fuel in the core must take into account the containment building and the extract system. The containment is regularly maintained and subject to Lloyd's surveyors inspection and is extremely unlikely to suddenly develop a gross leak. The overall probability of the failure of the extract system to remove I_{131} on demand has been assessed in Section 4 to be 7.2×10^{-3}.

5.3.1

The consequence of a failure leading to fuel melting will be the release of fission products from the fuel to the environment. The most hazardous fission product in this respect is I_{131}. The total inventory of I_{131} in the core is 1.9×10^5 Ci, and this represents an upper limit to any possible release. Actual releases would be expected to be less than this, for the reasons given below.

5.3.2

It is extremely unlikely that all the core would in fact melt. Some heat would be removed by steam.

However, this is very difficult to quantify. It will be assumed that all the core melts when cooling is lost. This will result in the release figures quoted being over-estimates.

5.3.3

Some fission products would be retained in the melted fuel by entrainment and also by chemical combination. Extensive work has been done on oxide fuel/fuel clad combinations which indicate that, under conditions where over 99% of

118

I_{131} is released from the fuel itself, 60% to 90% is retained by reaction with the clad (varying with temperature and clad material). It will be assumed that in this case 50% of the I_{131} in the core is retained by the cladding and 50% escapes into the reactor tank.

5.3.4

A considerable fraction of the iodine released from the fuel would plate out on the internal surfaces of the reactor structure or in the reactor shell, or dissolve in the D_2O. It is assumed as an upper limit that 10% of the iodine is released in the form of methyl iodide, 90% being elemental iodine. The elemental iodine is easily absorbed in the D_2O, on other reactor components and in the extract system charcoal traps.

The 10% of iodine released as methyl iodide is therefore assumed to be the limiting species.

5.3.5

The main charcoal absorber of the extract system is provided to retain iodine, especially methyl iodide, and is doped with potassium iodide to improve its efficiency. It is regularly tested both in situ and by laboratory tests on samples and is capable of providing decontamination factors for methyl iodide well in excess of the figure of 28 which is the current working limit (typical values are over 1,000). 90% of the main bed flow is recirculated and only 10% discharged, giving an effective DF of 280. The standby absorber, working on reduced flow, is capable of decontamination factors well in excess of 280. The decontamination factor assumed for the limiting species (methyl iodide) is therefore 280. This will result in the release to atmosphere being over-estimated.

5.3.6

The total core inventory of I_{131} given in 5.3.1 is reduced by the factors given above to give the actual release from the containment building under extreme conditions.

This is pessimistically calculated to be

$$1.9 \times 10^5 \times 0.5 \times 0.1 \times \frac{1}{280} = 34 \text{ Ci } I_{131}$$

This will therefore be the absolute upper limit of the possible release to the environment if the extract filtration system functions correctly.

Complete failure of the extract system would lead to releases of up to 2×10^4 Ci I_{131}, since some 90-95% I_{131} would still be retained by the fuel and in the D_2O and reactor structure. This release would be reduced by operator action to seal the building manually.

5.4 Comparison with Farmer Criteria

5.4.1

The probability of fuel melting as a result of loss of coolant has been pessimistically assessed at 2.1×10^{-6} per year as an upper limit. If this were to lead to a total core inventory release, it would still be just inside the Farmer criteria (A in Fig. 5). However, the effect of the extract system operation is to bring it well within the acceptable region (B in Fig. 5).

119
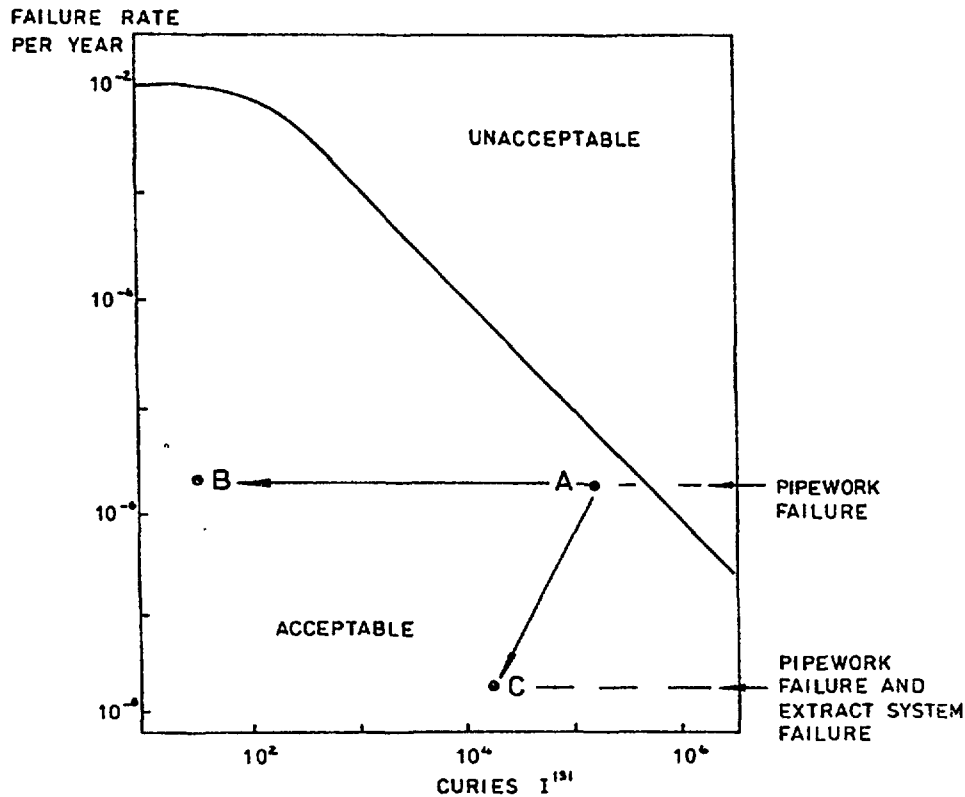
FIG. 5. Accident sequences plotted on a Farmer diagram.

5.4.2

The assessed failure rate of 7.2×10^{-3} demands for the extract system is sufficient to bring the release in the event of a D_2O leak and the co-incident failure of the extract system well within the acceptable level (C in Fig. 5).

5.5 Conclusions

5.5.1

Failure of the D_2O circuit leading to a core melt-down would release much less than the upper estimate of 34 Ci of I_{131} to the environment provided the extract system functioned correctly. This figure is well within the Farmer criteria at the upper limit of the failure rate of 2.1×10^{-6}. Release of the total core inventory would be just within the criterion. Co-incident failure of both extract system and reactor extract system would lead to releases of up to 2×10^{4} Ci I_{131}. The reliability of the extract system would be sufficient to meet the criteria for this level of release.

REFERENCES

1. SMITH, T.A., and WARWICK, R.G. - SRD R 30. The Second Survey of Defects in Pressure Vessels built to High Standards of Construction and its Relevance to Nuclear Primary Circuits.

2. The Systems Reliability Service Data Bank - SRS, Culcheth.

3. WASH 1400 - Reactor Safety Study: An Assessment of Accident Risks in US Commercial Nuclear Power Plants, Appendix III - Failure Data - US Department of Commerce.

4. GIBBONS, W.S. and HACKNEY, B.D. - GEAP 4574 - Survey of Piping Failures for the Reactor Primary Coolant Pipe Rupture Study.

5. RUDHAM, R.C. - Private communication.

6. GREEN, A.E. and BOURNE, A.J. - Reliability Technology.

7. EDWARDS, G.T. and WATSON, I.A. - A Study of Common-mode Failures. SRD R 146, SRD, Culcheth, July 1979.

8. FARMER, F.R. Siting Criteria - A new approach - IAEA Conference Containment and Siting, Vienna - April 1976. SM - 89/34.

9. Reactor Safety Study WASH 1400 (NUREG 75/014). US Nuclear Regulatory Commission, October 1975.

10. Assessment of Hazards in Engineering Work.

    KINCHIN, G.H., Proc. Ins. Civ. Eng. I, 1978, 64, August, pp 431-8.

    also

    Design Criteria, Concepts and Features important to Safety and Licensing.

    KINCHIN, G.H., ANS/ENS Meeting on Fast Reactor Safety Technology, Seattle, 1979.

Appendix C
METHODS FOR PREVENTING LOCA

Abstract

The probability for a total or partial Loss-of-Coolant
Accident (LOCA) is normally reduced to very small values
by incorporation of engineered safety features into the
design.

The protective measures taken against LOCA are described
for several reactors with very different designs: two
light water swimming-pool-type reactors (DEMOCRITOS and
SAPHIR), a light water tank-type reactor (HFR-Petten),
and two heavy water tank-type reactors (DIDO and PLUTO).

Appendix C-1

ENGINEERED SAFETY FEATURES AGAINST LOCA FOR THE 'DEMOCRITOS' REACTOR

N.G. CHRYSOCHOIDES
Physics Laboratory,
Athens University of Agricultural Sciences

J.N. ANOUSSIS, C.A. MITSONIAS, C.N. PAPASTERGIOU
Department of Reactors,
Democritos Nuclear Research Center,
Greek Atomic Energy Commission

Athens, Greece

Abstract

"DEMOCRITOS" is a 5 MW swimming-pool type reactor. One safety concern of this type of reactor is a LOCA due to rupture either of a pipe of the primary cooling system or of an experimental beam tube. Existing engineered safety features against LOCA are described along with further solutions that are being considered.

1. The "Democritos" research reactor is a swimming pool 5 MW reactor using MTR fuel elements. Its design is typical of many swimming pool reactors, built in the early 60's.

   One safety concern of this type of reactor is a Loss of Coolant Accident due to rupture either of a pipe of the primary cooling system or of an experimental beam tube. The minimum time required to uncover the core, following such a rupture, depends on the reactor design and for the case of the "Democritos" reactor, it is of the order of 30 minutes.

   As a result of such an accident a core meltdown may occur, the extent of which depends on the operating history of the core and the power of the reactor.

   A core meltdown may start, after a LOCA, at a reactor with operating power 1.5-2.0 MW, according to calculations reported by ANL in early drafts of this guidebook. However, according to calculations reported in Appendix G-6 with lag times until core uncovering of the same order of magnitude, this power level may rise over 5 MW.

2. With the present design and layout the existing engineered safety features of the "Democritos" reactor are:

a. **Butterfly automatic valves**: These valves installed at the primary coolant outlet and inlet (No. 4 in Fig. 1) are actuated from the low water level signal (12" below the normal level).

Thus, a LOCA can be prevented in case that the pipe rupture takes place farther than the valves.

① Reactor Core
② Beam tubes
③ Beam tube cover
④ Butterfly valve
⑤ Steel liner
⑥ Dividing wall
⑦ Valve
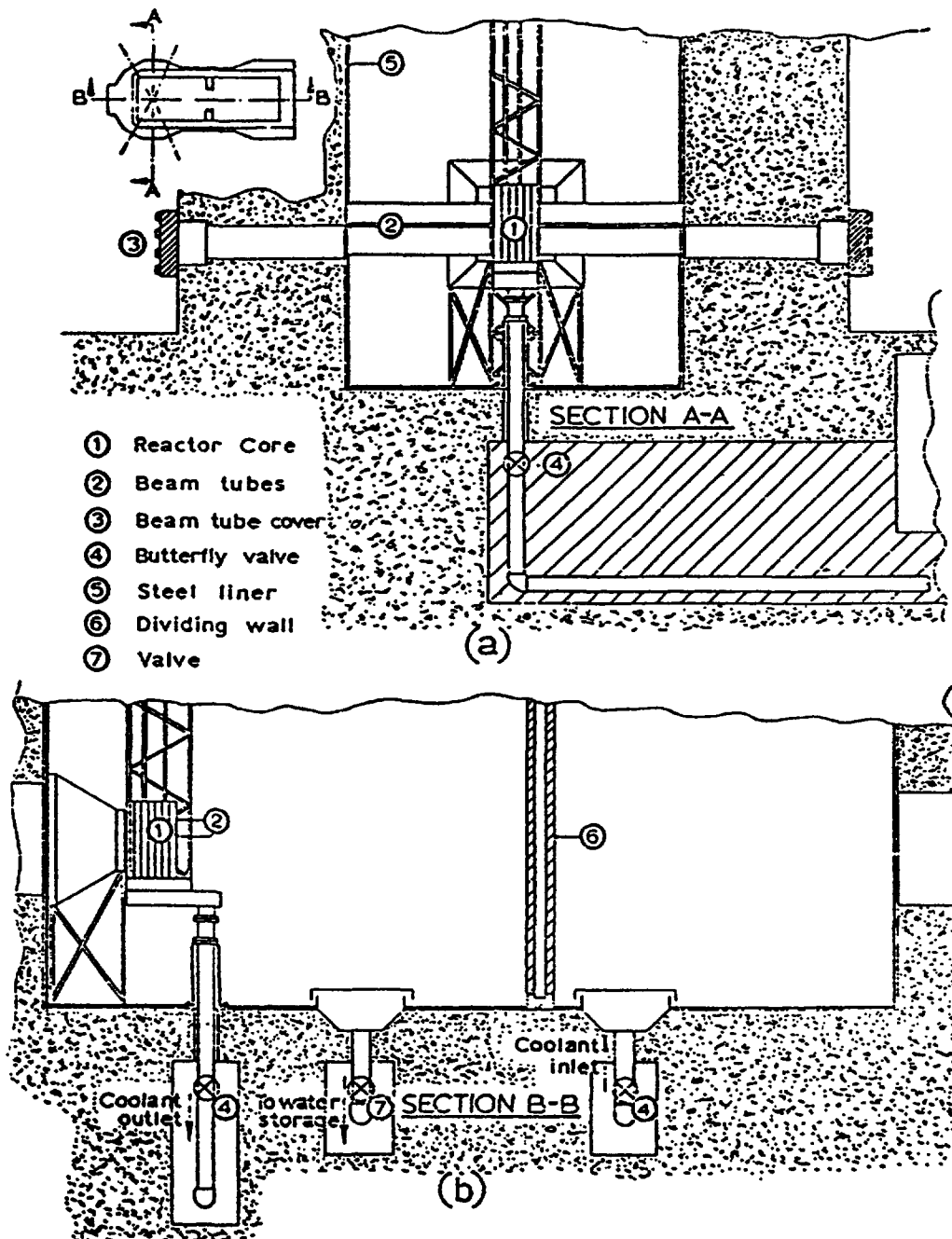
FIG. 1. Vertical cross-sections of the 'Democritos' reactor pool with associated facilities.

126
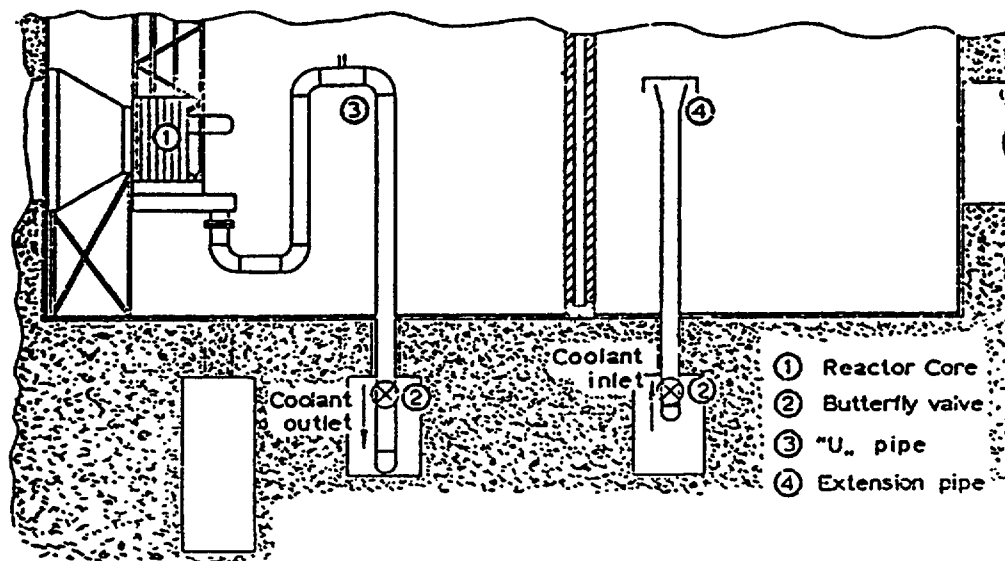
FIG. 2. Modification of cooling system inlet and outlet.

b. **Beam tube protection:** The collimators installed in the tubes used
for beam experiments are designed to minimize a pool water leakage
in case of a beam tube rupture.

When a beam tube is not in use, a suitable steel cover is fastened on
the outer side of the pool wall against the beam tube. It should be
noticed here, that the lowest level of four out of the six tubes
is above the core midplane and so total uncovering of the core due to
a rupture of these beam tubes is not possible.

Cross sections of the reactor pool with the reactor core, the beam
tubes and the coolant outlet and inlet for the "Democritos" reactor
are shown in Fig. 1 (a and b).

3. At the "Democritos" reactor, even with the present operating mode (up to
10 hours operation daily) additional safety measures against LOCA are
planned to be taken. Similar measures could be applied to other swimming
pool reactors.

To prevent a LOCA in case of a guilotine-type rupture in a pipe of the
primary cooling system, taking place between the pool and the butterfly
valves, the following solutions are considered.

a. **Modification of the cooling system inlet-outlet:** A U-pipe can be
installed at the coolant outlet, as well as an extension of the
coolant inlet pipe inside the pool (Fig. 2). In case of a severe
break of the type described above, the drainage of the pool ceases

127
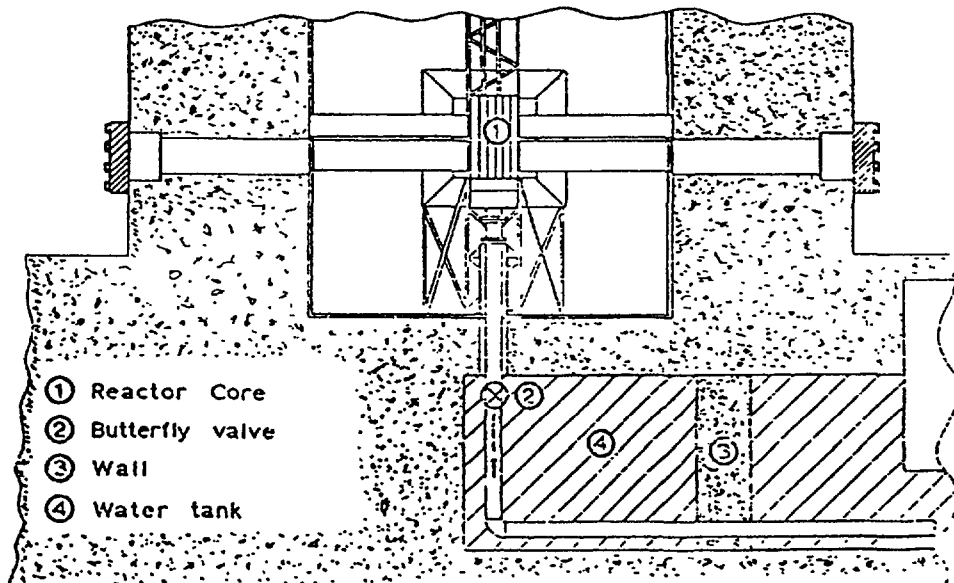
FIG. 3. Water tank construction under the reactor pool.

① Reactor Core
② Butterfly valve
③ Wall
④ Water tank

FIG. 4. Water spray system.

① Reactor Core
② E.C.C.S.
③ Tank
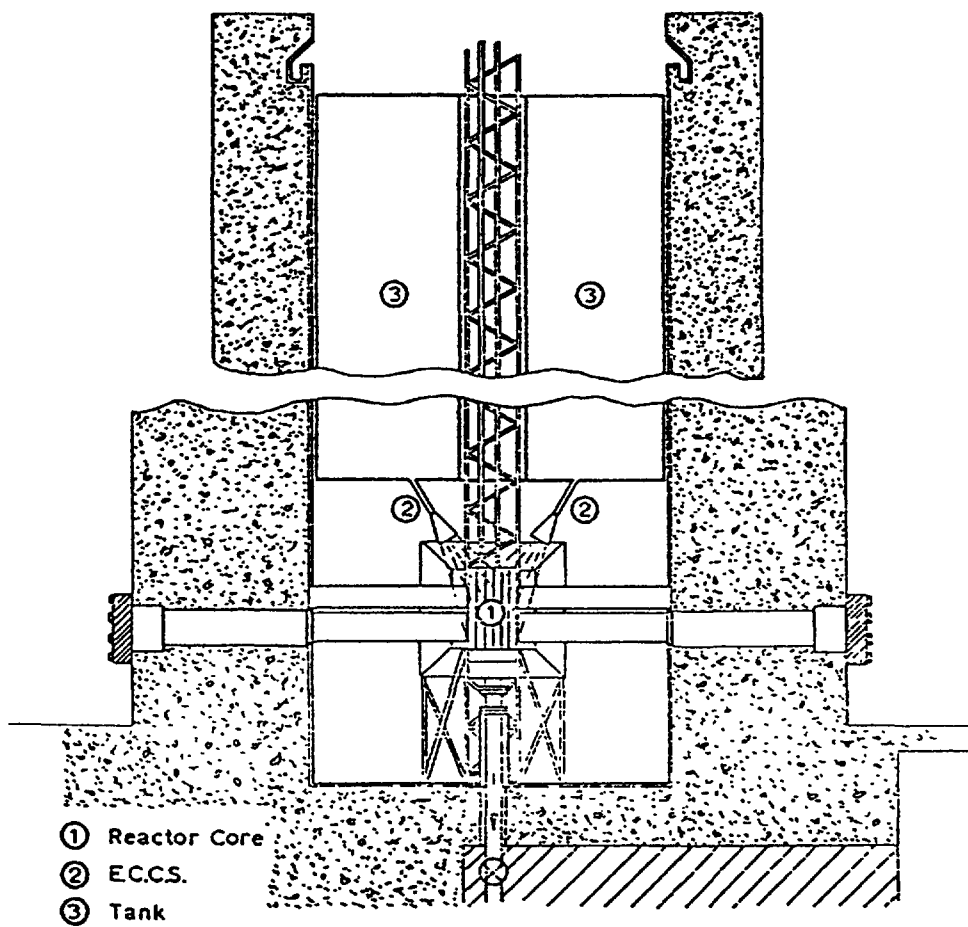
when the water level reaches either the end of the inlet pipe or the upper level of the U-pipe (where an opening exists, preventing any further drainage due to the siphon phenomenon) depending on where the rupture appears. The upper level of the U-pipe and the end of the inlet pipe should be above the top of the core to prevent any core uncovering.

b. **Construction of water tanks under the reactor pool:** These tanks are easily constructed by building suitable walls or installing steel doors which block the existing channels, as shown in Fig. 3 for the case of the coolant outlet.

By this construction the valves are enclosed in the tanks and a pool drainage is prevented in case of a cooling system pipe rupture occurring between the pool bottom and the valves, because the capacity of these tanks is very small in comparison with the pool capacity.

c. **Installation of water spray system:** A special tank installed inside the reactor pool can provide water supply for the spray system (Fig. 4). The water in this tank is at the same level with the pool water prior to the rupture.

When the pool water has lowered down to the level at which the core begins to uncover, the spray system is actuated using the water supply of the special tank. The tank capacity can be in the range of 15-20 m^3, but provision can be taken for its continuous supply by tap water. The lag time can be thus prolonged as much as it is considered necessary.

Appendix C-2

ENGINEERED SAFETY FEATURES AGAINST LOCA
FOR THE SAPHIR REACTOR

H. WINKLER
Eidgenössisches Institut für Reaktorforschung,
Würenlingen, Switzerland

Abstract

SAPHIR is a 10 MW swimming-pool research reactor whose usual core contains 28-35 fuel elements. The most serious accident in this type of reactor is a LOCA which can occur either by a serious rupture in the primary cooling system or a break of a beam tube. Some of the engineered safety features against LOCA taken at SAPHIR are described.

1. Introduction

SAPHIR is a 10MW Swimming Pool research reactor using 23 plate MTR-Elements containing 280 g U-235 each. Its usual core contains 28 to 35 fuel elements with a burn-up of up to 60% of the initial U-235 content.

Constructed in 1956 it operated at 1 MW_{th}. The power was increased to 5MW in 1969 and to 10MW in 1983.

The most serious accident in this type of reactor is a loss of coolant water. These types of accidents can occur either by a serious rupture in the primary cooling system or a break of a beam tube.

In the following some of the engineered safety features against LOCA taken at SAPHIR are described.

2. Total Loss of Coolant Accident

At the construction of SAPHIR the total loss of coolant water through a rupture of the cooling system has been taken into account.

In Fig. 1 the layout of the cooling system in the pool is given. The piping is constructed in such a way that the lowest pipe (sucking pipe) penetrates the pool wall 760mm above the top of the core and the return pipe is another 300mm higher.

A small pipe connected to the main cooling outlet pipe acts as anti-siphon device when the water level reaches the cooling pipe.

So if a serious rupture in the primary circuit occurs, the core is still completely under water (see Fig. 1)

Thus a total LOCA is impossible in the SAPHIR reactor if very strong earthquakes (more than strength 8,5 on Richter scale) are neglected.

131

3. Partial Loss of Coolant Accident

A partial LOCA can principally occur at SAPHIR if an open beam tube breaks. Different mesures against a serious loss of coolant water have been taken at SAPHIR.

Fig. 2 and Fig. 3 show the beam tube layout.

The most serious case is a break of the lower beam tube. Then the water level without any actions will be such that only 50mm of the core is covered with water.

The time required to reach this level is of the order of 45 min. In general this time is much longer because a total rupture of a beam tube is nearly impossible.

In order to prevent or to stop such an accident, three measures have been taken:

1.) The collimator is sealed by a 1,5mm thick aluminum membrane. So the beam tubes are normally tight.

2.) Shutter plugs in all beam tubes are installed with a collimator opening (aperture) of 40mm width and 80mm height. The beam shutter can be closed by actuation of an electric motor.

   Fig. 4 shows the layout of a radial beam tube with shutter plug.

3.) As a third barrier to coolant water loss, a slide-valves has been installed in the pool wall. It can be manually actuated by a hydraulic system such that the beam tube will be completely closed in about five minutes.

   Fig. 5 shows one part of the beam tube openings with the slide valves.

A probabilistic accident study of LOCA has given a probability of less than 10^{-6}/y for a loss of coolant water due to a broken beam tube. So a LOCA is considered as a hypothetical accident for SAPHIR.

FIG. 1. Pool (longitudinal section).

133

FIG. 2. Pool (cross-section).

347 fuel center

Ansicht von A
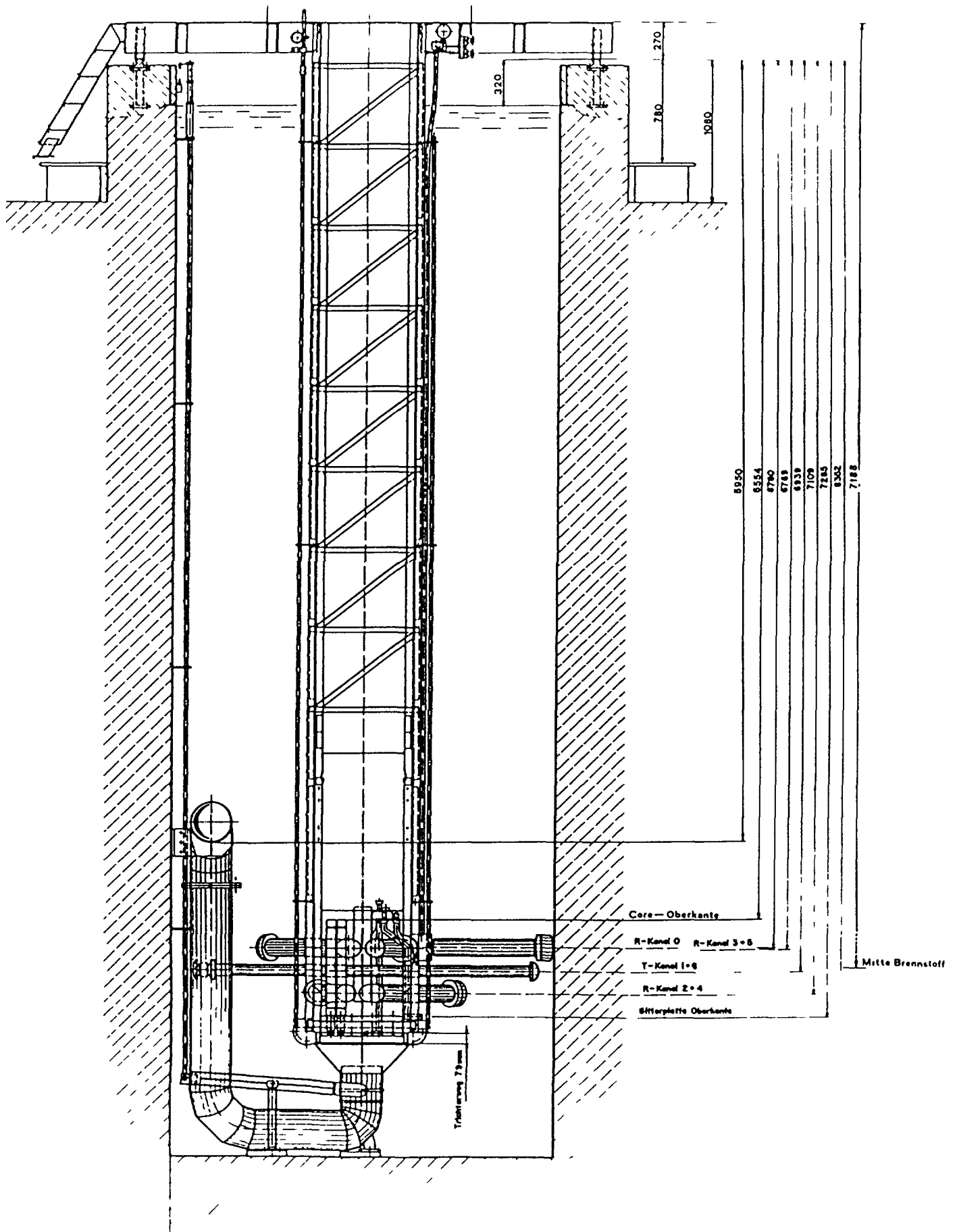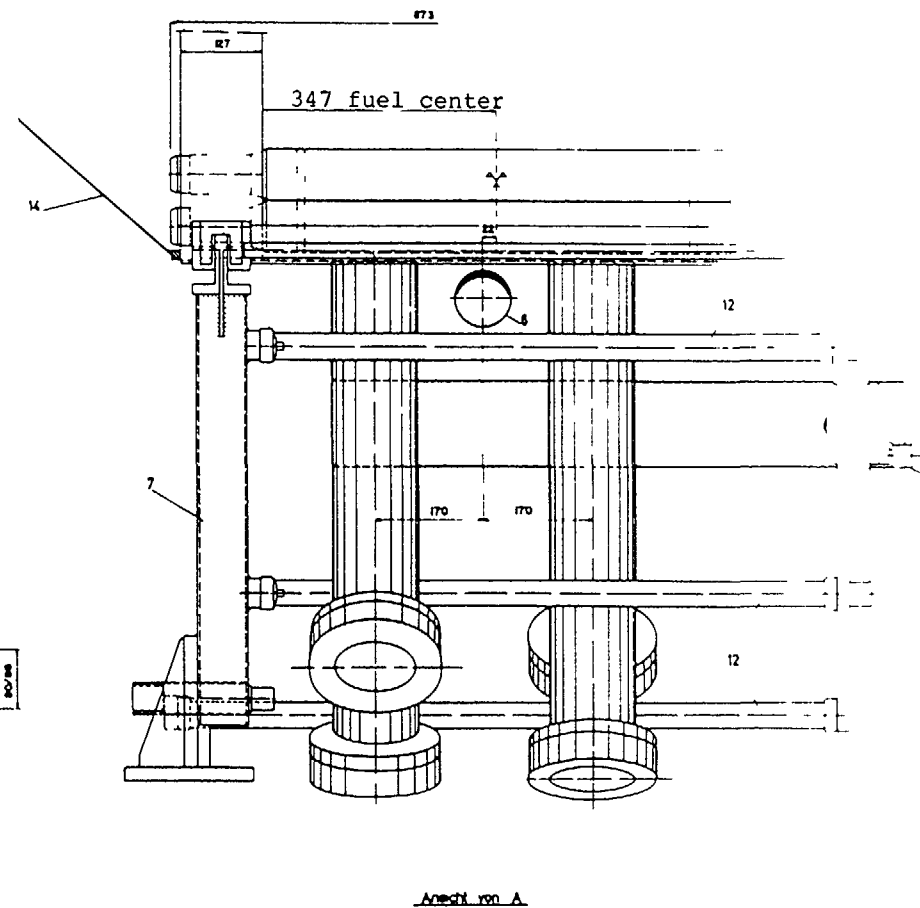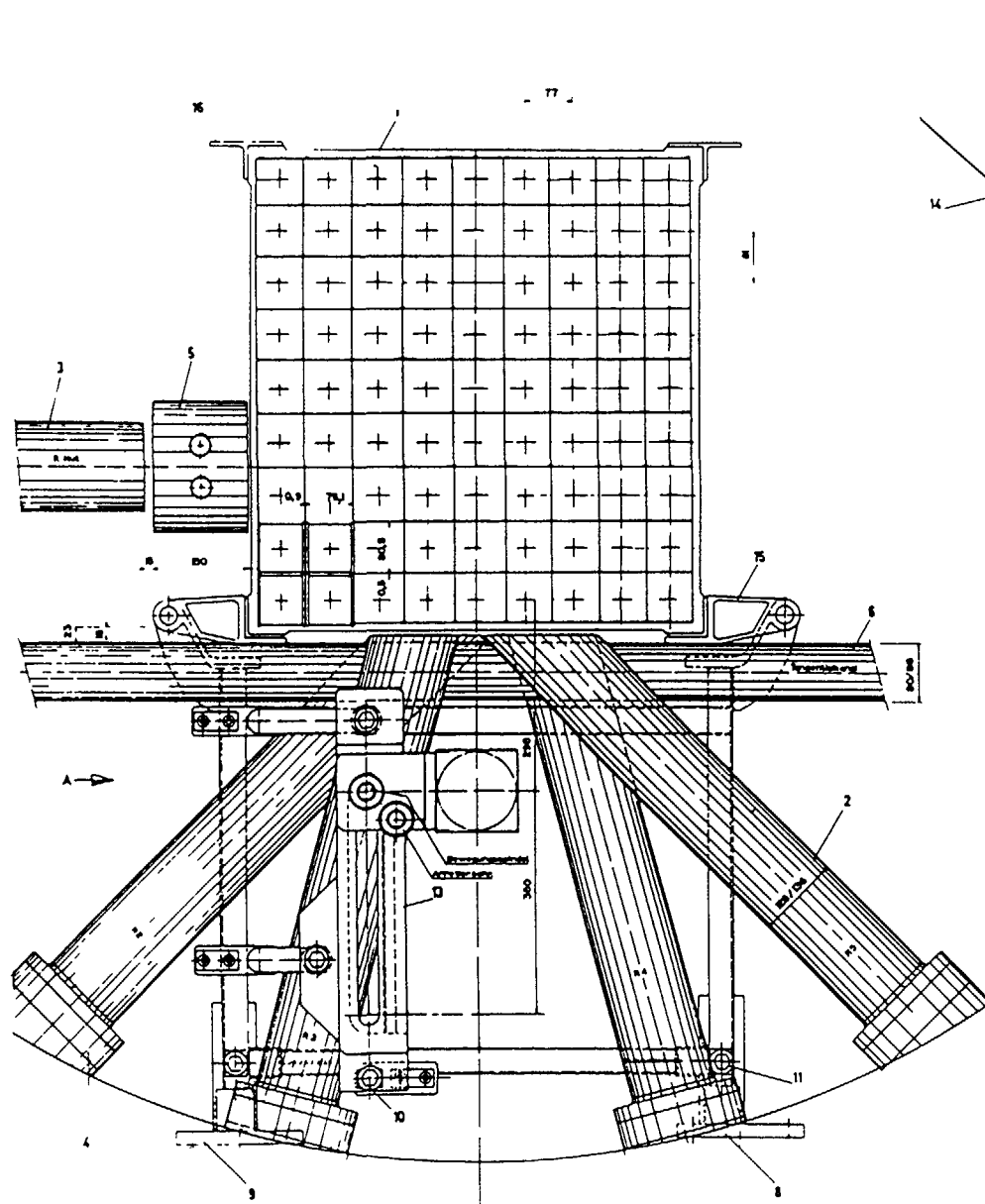
FIG. 3. Beam tube arrangement.
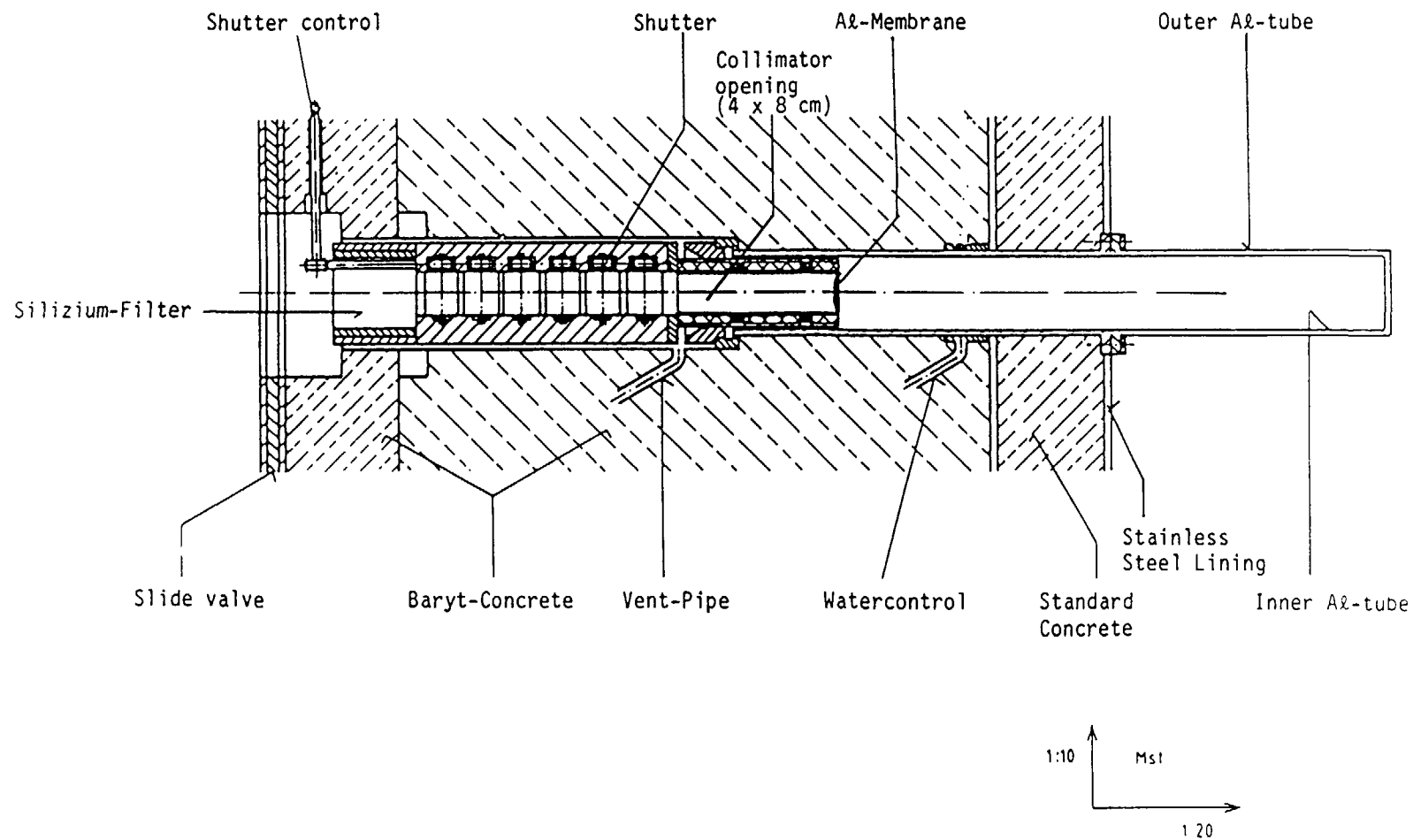
FIG. 4. Radial beam tube with shutter plug.
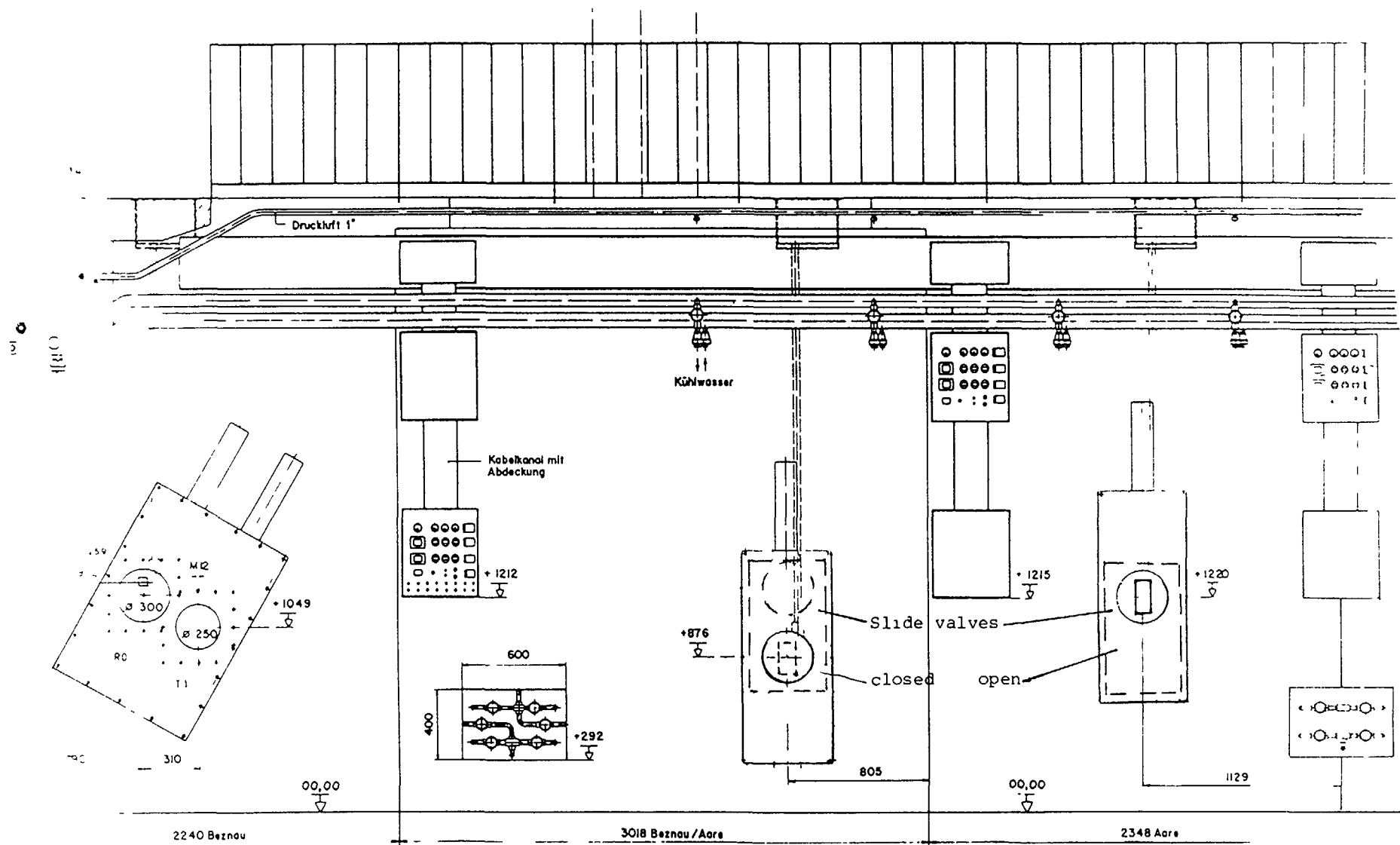
FIG. 5. Beam tube in experimental hall.

Appendix C-3

ENGINEERED SAFETY FEATURES AGAINST LOCA
FOR THE HIGH FLUX REACTOR — PETTEN

N.G. CHRYSOCHOIDES
HFR Division,
Commission of the European Communities,
Joint Research Centre,
Petten

A. TAS
Netherlands Energy Research Foundation,
Petten, Netherlands

Abstract

The High Flux Reactor - Petten is a 45 MW tank-type Materials Testing Reactor that is moderated and cooled by light water. The reactor core with its adjacent devices is contained in a closed vessel which is immersed in a pool of demineralized water. The engineered safety features against LOCA for both partial and complete uncovering of the core are described.

1. General

The High Flux Reactor (H.F.R.) - Petten is a 45 MW Materials Testing Reactor cooled and moderated by light water. The reactor is operated under contract by the Netherlands Energy Research Foundation (ECN) for the Commission of the European Communities (CEC) at Petten Establishment, in North Holland, which is one of the four Establishments of the Joint Research Centres of the CEC.

A general layout of the reactor, the pool and the ancillary equipment is shown in Fig. 1.

The reactor core with its adjacent devices is contained in a closed vessel which is immersed in a pool of demineralized water, having a depth of 4,2 m above the top of the vessel, Fig. 2.

Two power increases, from the original power of 20 MW, have been made so far since the reactor went first critical in 1961. Other changes and improvements have been also performed in the past, to fulfil the requirements of the clients (industries and institutes).

139
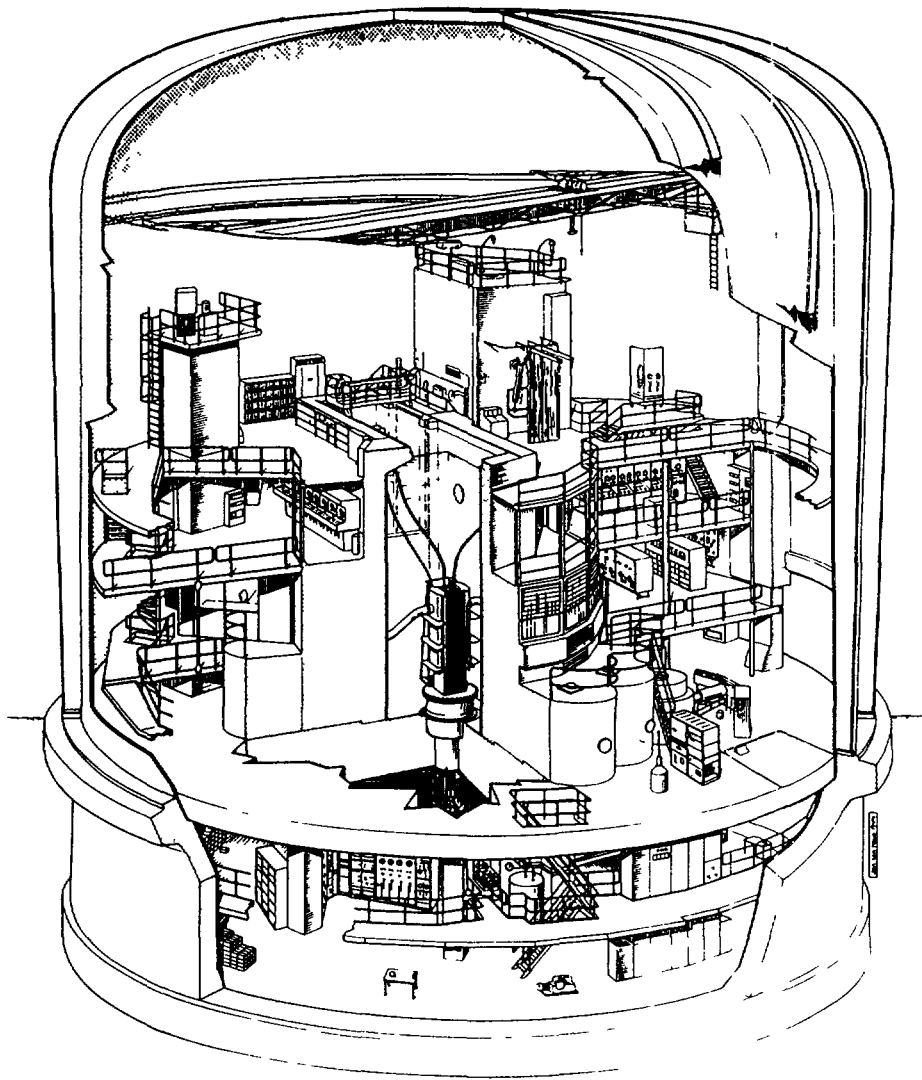
FIG. 1. High Flux Materials Testing Reactor (HFR), Petten.

In the original design of the HFR, measures were taken to prevent the reactor core from a total or partial loss of coolant.

During the replacement of the reactor vessel in 1984 additional improvements have been made, mainly towards the partial loss of coolant. The new reactor vessel, 5,5 m high, consists of cylindrical support, 1,6 m in diameter, a rectangular core box and an inlet plenum, Fig. 3.

Reactor cooling is provided by recirculating, in a closed circuit, demineralized water downwards in the reactor vessel through the core and through an external circuit with a delay tank, three main circulating pumps and the shell-side of the three water-to-water heat exchangers.

The new core lattice is a 9 x 8 array containing 33 fuel assemblies of the MTR type, 6 control members, 17 experimental positions and 16
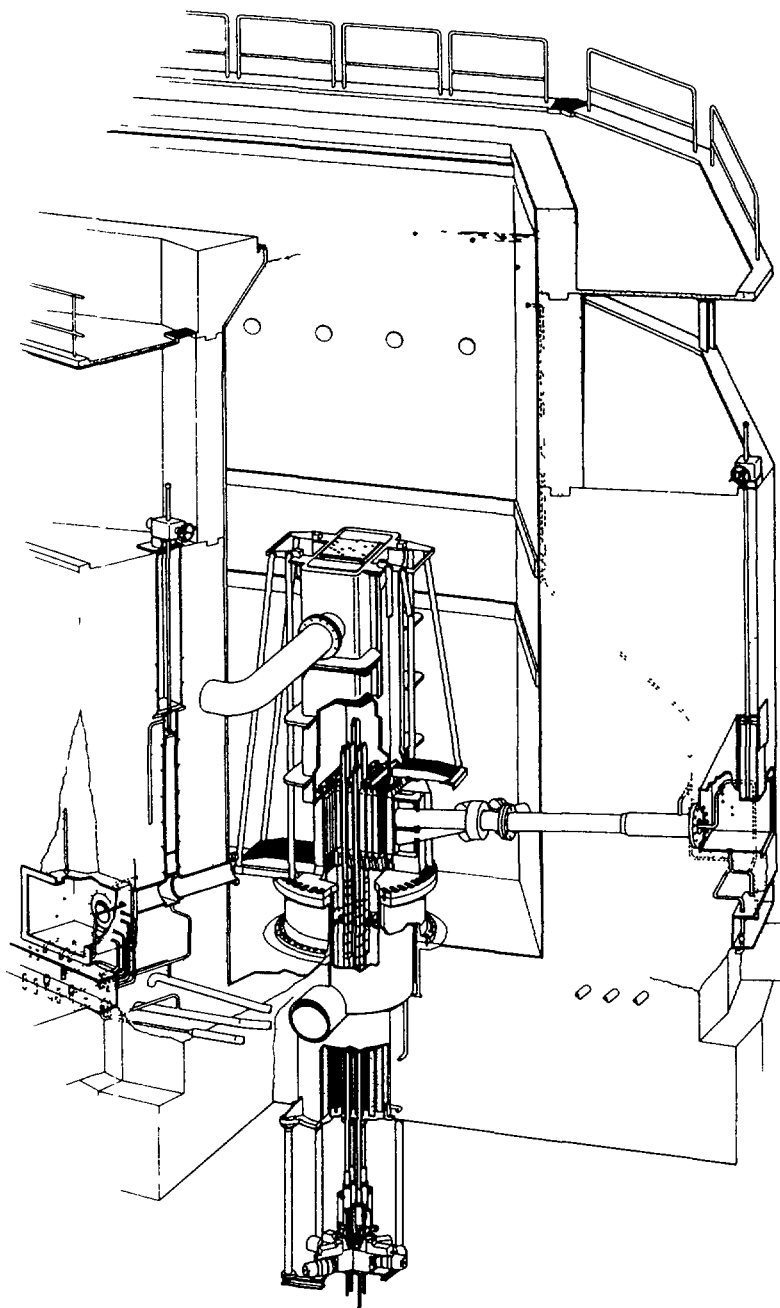
FIG. 2. Reactor vessel in pool.

berylium reflector elements.Out-side the core box and adjacent to its
East side, an additional row of 9 berylium elements is positioned,
completing the 9 x 9 array core lattice of the original reactor vessel.
Each fuel assembly contains 23 vertically arranged fuel plates. Each
plate consists of a layer of Al + U alloy meat, 0,51 mm thick clad with
0,38 mm thick aluminium for the inner plates and 0,57 mm thick aluminium
for the outer fuel plates. The uranium is about 93% enriched in ^{235}U and
each fresh fuel assembly contains 405g ^{235}U while the two flat side
plates contain together 1000 mg ^{10}B. The control of the reactor is
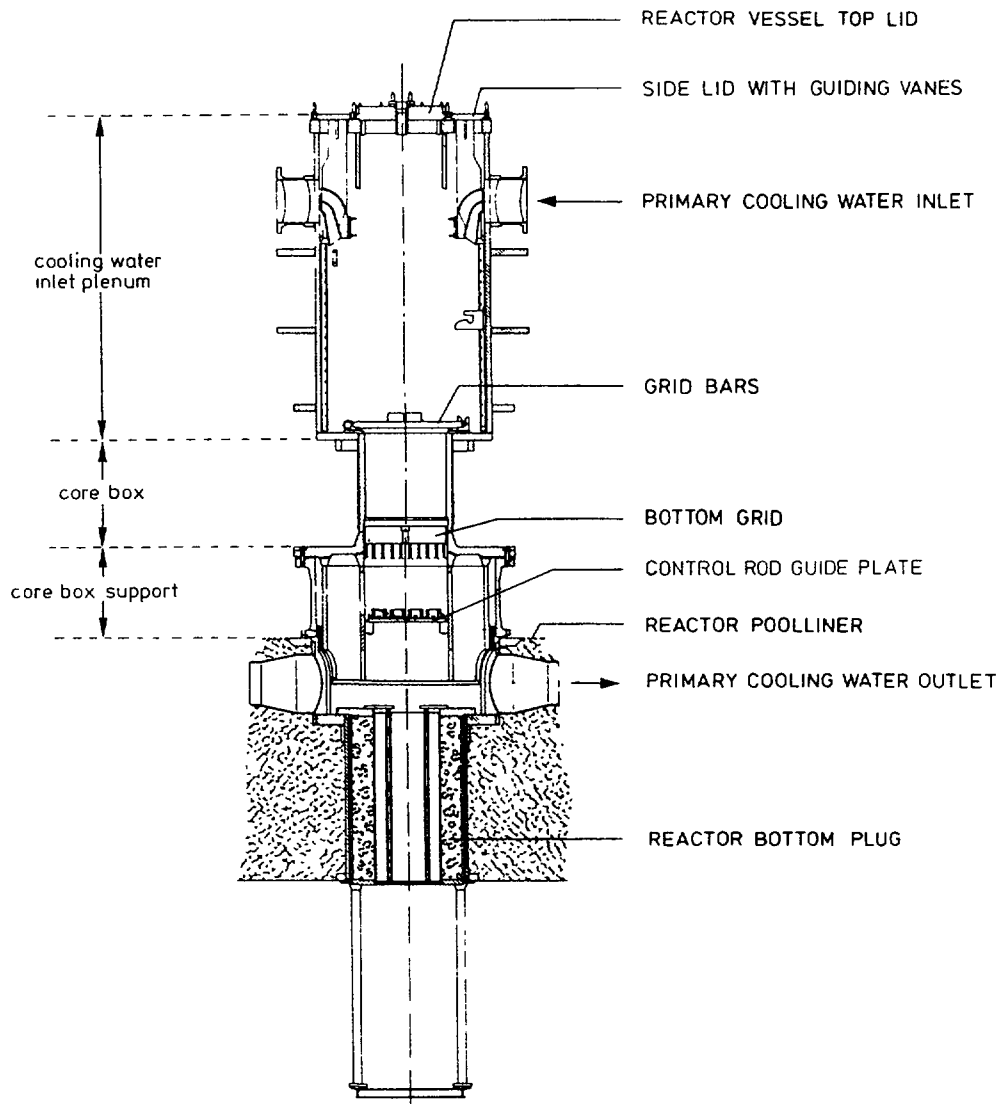
FIG. 3. The new reactor vessel.

achieved by six control members, each of which comprises a fuel section
surmounted by a cadmium section. Drive mechanisms below the reactor move
the control members upwards, displacing the cadmium with fuel.

2.   Engineered Safety Features Against Complete Core Uncovering

Fig. 4 presents a simplified flow diagram of the main cooling circuits
for normal operation and emergency situations, where the elevation of
the various components from the bottom pool liner of the reactor is also
shown.

The heat removal system of the reactor consists of a closed primary
cooling system which absorbs the reactor fission heat in the
reactor vessel and transfers it to an open secondary cooling system

142

FIG. 4. Flow diagram of the main cooling circuits.

PUMPS 1,2,3 : PRIMARY COOLING PUMPS 4300 m³/h
PUMP 4 : SHUT.DOWN COOLING PUMP 230 m³/h
PUMP 5 : EMERGENCY SHUT-DOWN PUMP 230 m³/h
PUMP 8,8A : POOL COOLING PUMPS 280 m³/h
S.PUMPS 1,2,3,4 : SECONDARY COOLING PUMPS 2700 m³/h

—— PRIMARY COOLING
—— SECONDARY COOLING
—— POOL COOLING
----- EMERGENCY COOLING
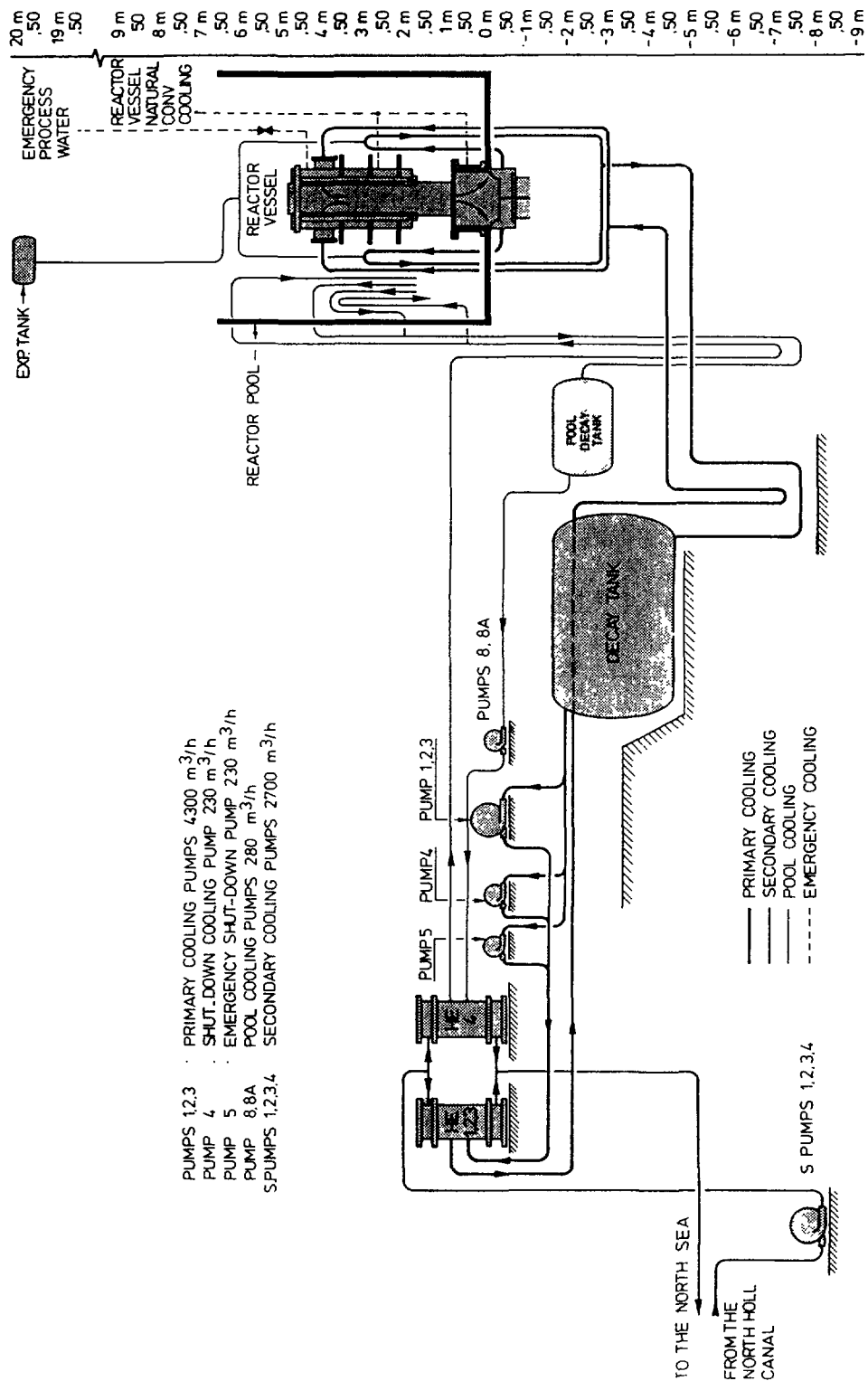
which pumps water out of the North Holland Canal, through the tubes
of the main heat exchangers and finally dumps the heat into the
North Sea.

The heat generated in the pool either by convection from the reactor
vessel or by absorption of radiation from the reactor core, is removed
by a separate pool cooling system which pumps the pool water through two
pipes leaving the pool at elevations of approx. 4,5 m and 2 m from the
bottom pool liner, the second pipe being extended vertically in the pool
up to the primary inlet pipe level forming a U-shape with a vacuum break
system. The water circulates then through a pool decay tank and a heat
exchanger and returns to the reactor pool at elevations approx. 6,5 m
and 0,3 m from the bottom pool liner, the second being again extended
vertically in the pool, in a manner similar to the outlet pipe.
"Uncovering of the reactor vessel from the pool water, below the primary
inlet level in the case of a major break of the pool cooling piping
system, is prevented by the high elevation and the U-type of these
pipes".

In case of a major break in the primary cooling system, the reduced flow
will scram the reactor.

"Uncovering of the core in the vessel is prevented, by the U-type
primary cooling pipes (with a vacuum break system), leaving the vessel
outlet", Fig. 5.

In such an event, the Emergency Cooling System can be manually
initiated, to cool the core down and make up losses of water in the
vessel due to vaporization process. This sytem consists of an Emergency
Cooling Assembly, providing pool water to the reactor vessel for the
natural convection of the core and of an Emergency Process Water System,
in the event that more cooling water is required than presented by the
volume of the water in the pool.

3.   Engineered Safety Features Against Partial Core Uncovering

Eight horizontal beam tubes (H.B.), 17,5 cm in diameter each and two
beam tubes, 25 cm in diameter each, are terminated at the East and South
walls of the core box. The ten beam tubes (HB 1 to 10) are placed in
three levels:
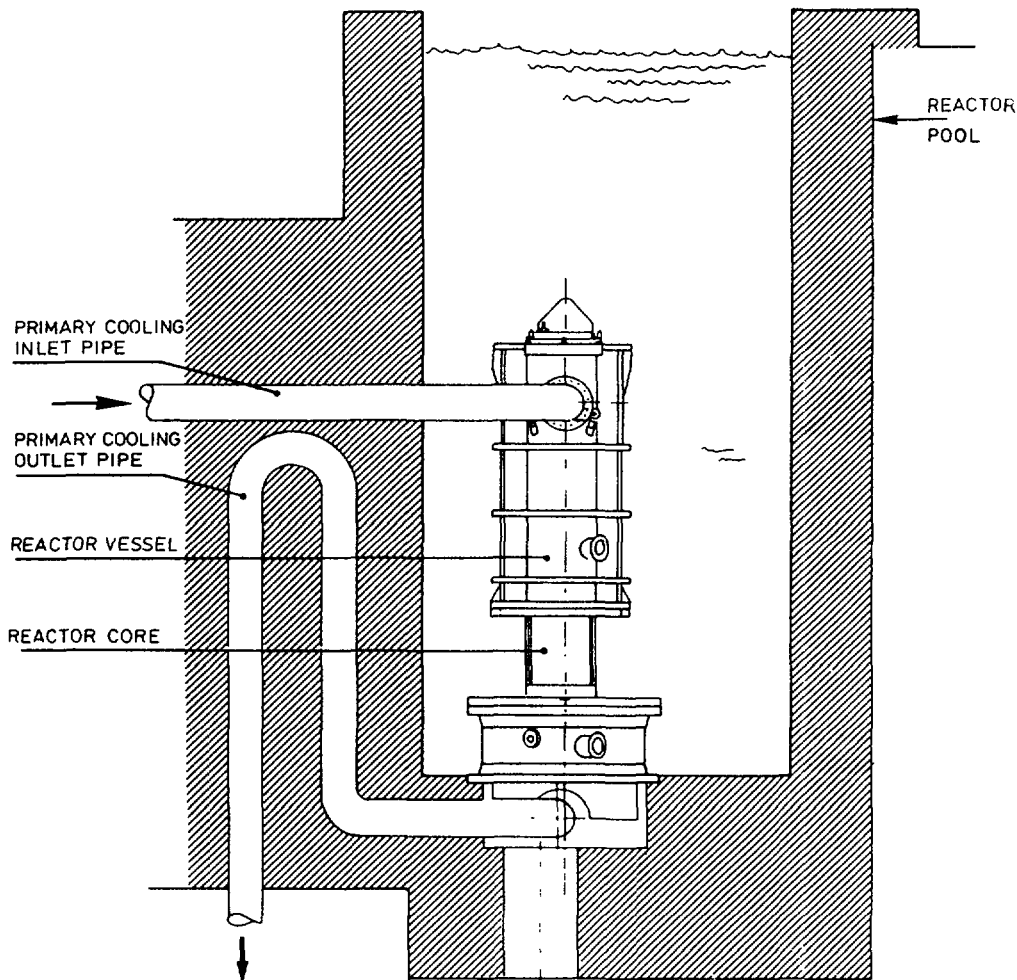
FIG. 5. Cross-section through reactor vessel and pool walls.

- five 17,5 cm HB's at 11,5 cm above the centre line of the reactor core,
- three 17,5 cm HB's at 11,5 cm below the core centre line
- and the two 25 cm HB's at 15 cm below the centre line.

A large experimental facility, (originally HBO and now HB 11 + 12), is terminated on the North wall of the core box, Fig. 6 and 7.

In the original design: "The tubes were penetrating the vessel wall and welded on the vessel and the core box walls, to prevent any water leakage from the vessel through the tubes", Fig. 6(a) and 7(a).

In the new vessel design, the following improvements, regarding the beam tubes, have been incorporated:

- An aluminium protection cover, 5 mm thick, will be bolted at the external pool wall side of each beam tube as a second barrier to
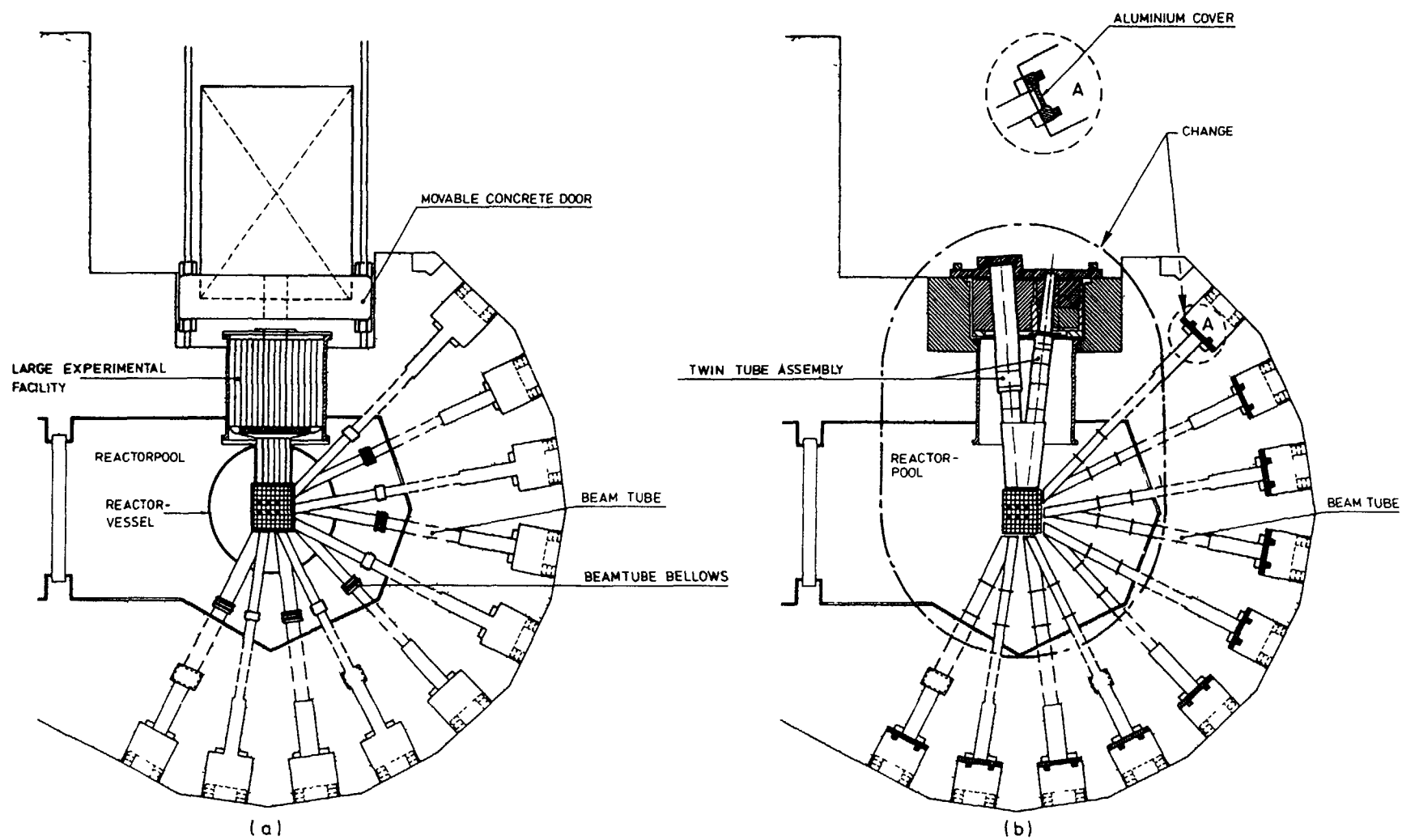
FIG. 6. Schematic horizontal cross-section through reactor vessel and beam tubes: (a) original design; (b) improved design.

Legend:

- ▨ FUEL ELEMENT
- ▩ CONTROL ROD
- ◉ CORE EXPERIMENTAL POSITION
- + BERYLLIUM REFLECTOR ELEMENT
- HB HORIZONTAL BEAM TUBES
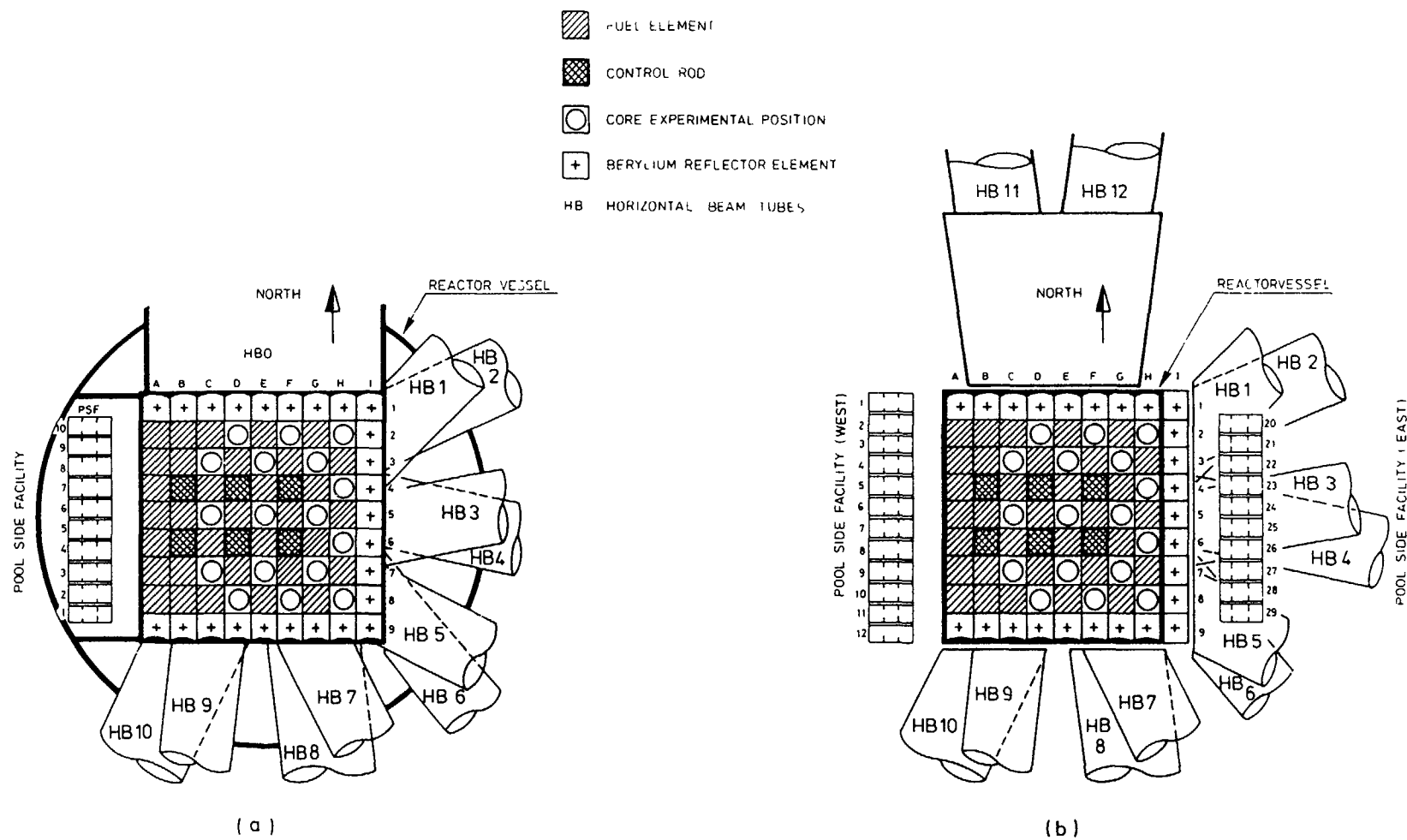
FIG. 7. Schematic horizontal cross-section through reactor core and experimental facilities: (a) original design; (b) improved design.

any pool water leakage through the tube, while the HBO will be replaced by a twin tube assembly with similar second barrier protection, Fig. 6(b).

- The beam tube bellows will be eliminated, improving thus the integrity of the tubes, Fig. 6(b).

- The beam tube ends will not be welded to the reactor vessel but sealed and terminated at about 5 mm from the core box walls, thus preventing any direct leakage of the primary vessel water through the tubes, Fig. 7(b).

Appendix C-4

ECCS USED IN DIDO AND PLUTO

R. PANTER
Atomic Energy Research Establishment,
United Kingdom Atomic Energy Authority,
Harwell, Didcot, Oxfordshire,
United Kingdom

Abstract

DIDO and PLUTO are heavy water tank-type reactors with power levels of 25.5 MW. Measures are described that protect against failure of the smaller pipes in the primary system, and more importantly, against weld failure at the junction to a large pipe rather than in the small pipe itself.

The requirement for an ECCS has been re-considered from time to time as the operating power or fuel element design has been changed. More recently, probability techniques have been used to decide whether the protection meets current standards – an example of the application of this technique being included at Appendix B-2 of this guidebook.

The original arrangement included spray rings in each fuel element, supplied through the fuel element plug, a self-seal coupling at the plug top, and individual flexible pipes. The supply of either D_2O or H_2O required manual valving operation. It was felt that this system was too complex to be reliable, and that the fine spray holes were extremely vulnerable to dirt in the system.

The reactor tank is not penetrated by the beam tube liners, and is within a secondary containment, such that after tank failure the fall in water level will not expose the fuel elements.

The reactor design is such that any leakage from the reactor tank, secondary containment or the D_2O pipework must drain into the plant room sump. If the maximum credible leak rate can be assessed, a sump pump of adequate capacity and adequate redundancy, will allow the coolant level to be kept near normal, and normal cooling to be maintained. The spray system was therefore discontinued, and a pair of sump pumps, capable of operation on mixed water and air, provided to return any leakage to the reactor tank. The assessment at the time was that the large pipes would not fail catastrophically so the system was intended to deal with a fracture of one of the 1/2-in. nominal bore pipes – which are not rigidly supported.

FUEL
ELEMENT

D₂O RISERS
(INLET)

DOWNCOMERS

SUCTION
HEADER

DELIVERY
HEADER

REACTOR
ALUMINIUM
TANK (R.A.T.)

D₂O
DOWNCOMERS

R.A T INLET
HEADER

EXPANSION
BELLOWS

ISOLATING
VALVES
(ACTUATORS
NOT SHOWN)
HEAT
EXCHANGERS
SHUTDOWN
PUMP (2)

MAIN D₂O
PUMPS
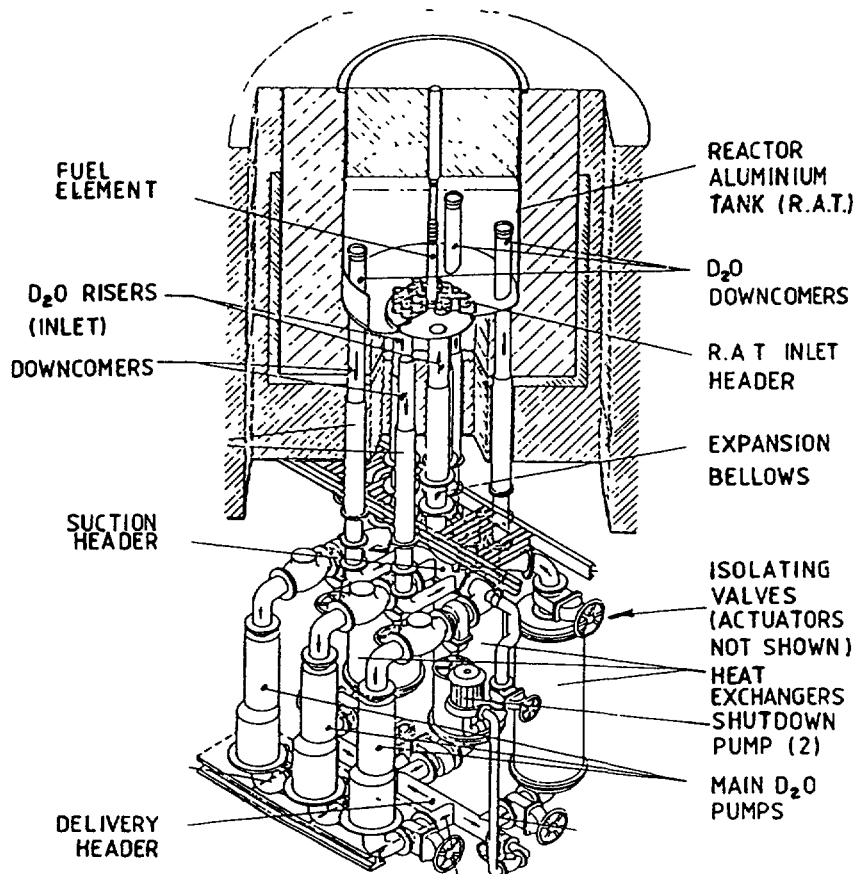
FIG. 1. D_2O system.

Following the latest increase in reactor power to 25.5 MW, the re-assessment of the low probability but potentially serious fault conditions was undertaken. The probability assessment of both the main pipework failure and the ventilation clean-up plant was necessarily pessimistic, because the available failure rate data was for higher pressures and less rigid assemblies, but it was decided that some improvement should be made. Examination of the analysis showed that a rather larger size of break could occur, if a weld failure occurred at the junction to the large pipe rather than in the small pipe itself, but that the length of pipework at risk could be much reduced by closing of isolating valves.

The new proposal therefore followed the earlier principle of using a sump pump, but the larger leak rate requires action in less than a minute, so automatic operation is provided that if tank level falls and water is in the sump, the isolating valves are closed (15 sec.) and sump pump started, returning water through a 0.5 MW capacity cooler to the reactor tank. For small leaks, where rapid action is not necessary, operator action to start a sump pump will avoid the automatic isolation, and allow normal cooling circulation to continue.

150
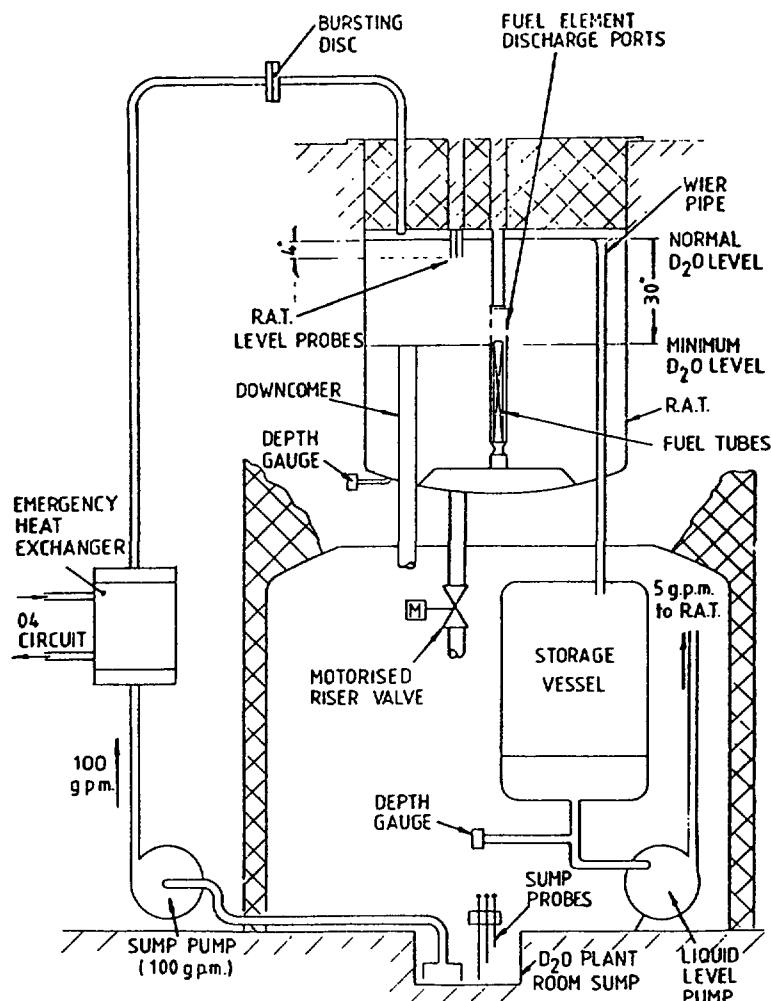
FIG. 2. Diagrammatic arrangement of emergency cooling system.

It is not possible to envisage every possible combination of faults, so light water injection is also provided, as an alternative emergency cooling method. Several alternative power supplies are provided, with careful routeing to avoid vulnerability to common mode failures.

By these several methods we believe that adequate cooling could be provided indefinitely, though we would expect to unload the fuel to alternative cooled storage as quickly as possible.

The reactor design and the system which has been installed are illustrated in Figs. 1 and 2. A more detailed description of the new ECCS features can be found in the reference below.

Reference

R. Panter, "Installation of an ECCS for the DIDO and PLUTO MTRs," IAEA-SR-77/11 and paper presented at the Seminar on Research Reactor Operation and Use, Jülich, Federal Republic of Germany, 14-18 September 1981.

Appendix D

RADIOLOGICAL CONSEQUENCE ANALYSES

Abstract

Methods and examples relevant to conversion from HEU to LEU
fuel are presented for analysis of the radiological conse-
quences of postulated accidents for several different types
of research reactors and according to various national
practices. Simple hand calculations may be adequate in many
cases. However, a more detailed evaluation using sophisti-
cated computer codes will often result in substantial
reductions in dose estimates. The plutonium buildup in LEU
fuel does not significantly increase the radiological
consequences.

Appendix D-1

RADIOLOGICAL CONSEQUENCE ANALYSIS

W.L. WOODRUFF, D.K. WARINNER, J.E. MATOS
RERTR Program,
Argonne National Laboratory,
Argonne, Illinois,
United States of America

Abstract

A model for estimating the radiological consequences from a hypothetical accident in HEU and LEU fueled research and test reactors is presented. Simple hand calculations based on fission product yield table inventories and non-site specific dispersion data may be adequate in many cases. However, more detailed inventories and site specific data on meteorological conditions and release rates and heights can result in substantial reductions in dose estimates. LEU fuel gives essentially the same doses as HEU fuel. The plutonium buildup in the LEU fuel does not significantly increase the radiological consequences. The dose to the thyroid is the limiting dose.

1. Introduction

A common approach in Safety Analysis Reports (SARs) for research and test reactors is to assume that a hypothetical accident results in the release of some portion of the inventory of radioactive materials from the fuel to the containment/reactor building and, eventually, in the release of a portion of these materials to the atmosphere. The consequences to the surrounding population are usually evaluated in terms of estimated radiological doses from the materials released.

A uniform model and methodology based on U.S. Nuclear Regulatory Commission (USNRC) Regulatory Guides for estimating radiological doses from hypothetical accidents in research and test reactors is presented. The method incorporates fission product inventories and dose conversion factor data to calculate doses. The model accounts for the containment/reactor building leakage and for the decay of the fission products before leakage to the atmosphere. It also includes the dispersion of airborne material by diffusion factors (χ/Q) based on release height, wind velocity, atmospheric stability, and diffusion parameters.

The following sections describe the details of the model and provide results of sample calculations for the generic 10 MW reactor described in IAEA-TECDOC-233[1] and in Appendix A-2 of this guidebook. Various approximate methods are also considered with varying degrees of conservatism. The sensitivity of the results to the isotopic content of the inventory (including plutonium) is also considered.

It is important to note that the IAEA generic 10 MW reactor is used as an example, and the method and results should not be taken as a guide for all reactors. The inventory for the peak power element is chosen here for convenience. The results may then be scaled to illustrate the consequences for the release from a single plate, multiple plates, or multiple elements. These

results do not include the effects of filter systems, washdown spray systems, or any other engineered safety features that may be present in reactor designs. Neither do the results take into account any reductions in release fractions as suggested by recent evidence from TMI-2.

1.1 Calculational Model

The calculation of dose estimates may be split into two categories, an internal (inhalation) dose and an external (immersion) dose. The internal dose to organ k from isotope i may be expressed as

$$D_i^k = \chi/Q(t)\; Q_i(t)\; BR(t)\; DCF_i^k,\qquad\qquad (1)$$

and the external whole body dose from isotope i may be given by

$$D_i^{Ext} = \chi/Q(t)\; Q_i(t)\; DCF_i^{Ext},\qquad\qquad (2)$$

where

$\chi/Q(t)$ is the atmospheric diffusion factor, s/m^3,

$Q_i(t)$ is the inventory of isotope i released over time t, Curies (Ci),

$BR(t)$ is the breathing rate for the receptor during the time t, m^3/s,

DCF_i^k is the dose conversion factor for organ k and isotope i, rem/Ci,, and

DCF_i^{Ext} is the dose conversion factor for external beta and gamma radiation from isotope i, rem/Ci per s/m^3.

The total dose to organ k or to whole body is then the sum over all isotopes in the inventory released in the time interval t. The diffusion factor, the inventory released, and the breathing rate may vary with time. The components in Eqs. (1) and (2) may be determined with varying degrees of detail and conservatism to fit the safety requirements of a given reactor.

1.2 Source Terms and Leakage Rates

The total activity of isotope i released over time τ, $Q_i(\tau)$, is obtained from the following equation, given in Ref. 2,

$$Q_i(\tau) = F_p F_B\; q_i\; \frac{\lambda_\ell}{\lambda_\ell + \lambda_r}\left[1 - e^{-(\lambda_\ell + \lambda_r)\tau}\right],\qquad\qquad (3)$$

where

F_p = fractional release from fuel to building,

F_B = fraction remaining airborne and available to be released from the building to the atmosphere,

q_i = quantity of isotope i in reactor core at time of accident, Curies,

λ_ℓ = leak rate parameter, sec^{-1}, and

λ_r = radioactive decay constant, sec^{-1}.

Isotope release rates depend on reactor fission product inventory, paths and rates of leakage from the primary system to the containment, and paths and rates of leakage from the containment or reactor building to the atmosphere. The leakage rates depend strongly on system design and containment or

reactor building design. In addition, the leak fraction of a given radio-
nuclide depends on its chemical form. The noble gases, krypton and xenon,
will be free to escape completely; solid, non-volatile fission products
will remain in place. Iodine is volatile, and it is normally assumed that a
significant fraction escapes.

The inventory of fission products and other radionuclides in a reactor
depends on a number of parameters including the fissile material, the reactor
design and materials, the operating neutron flux levels and distributions,
the power history, and the fuel management scheme. In the past, many SARs for
research and tests reactors have relied mainly on fission yield tables,
conservative estimates of total fissions at the end of a fuel cycle, and
hand calculations to determine fission product inventories. The inventory
of fission products and other radionuclides in a ^{235}U-fueled reactor can be
estimated by

$$q_i = 0.84^* \ \gamma_i \ P_o(1-e^{-\lambda_r T_o}),$$ (4)

in which

q_i is the amount of isotope i contained in the fuel
after T_o, Curies,

P_o is the fuel power level, watts,

γ_i is the ^{235}U fission yield of isotope i,

λ_r is the radiological decay constant for the isotope, s^{-1}, and,

T_o is the time interval during which the fuel has been at power P_o, s.

Various computer codes are available which can provide more accurate q_i
results. The ORIGEN computer code[3] provides such an improvement utilizing
extensive libraries of cross sections, yields, decay constants and branches
for many nuclides. A power history (consisting of any number of arbitrarily
sized time steps at constant power) may be imposed to the given reactor core
composition, and the code computes the concentrations of all significant
nuclides as a function of irradiation time. The code then estimates the con-
centrations of nuclides remaining after specific decay times (as supplied by
the user) following irradiation.

With holdup in the containment, this q_i source may not be the only
source of the ith radionuclide. Many nuclides are produced by precursors at
some time after the time of release. One technique for accounting for this
precursor contribution is to analyze the decay chain leading to the ith
radionuclide and determine a correction factor which increases q_i to approxi-
mate this additional precursor contribution. The calculation then proceeds as
if the entire amount were available to leak from the fuel, to the containment/
reactor building, and to the atmosphere. This method is outlined in Ref. 2.

1.3 Atmospheric Dispersion

The radionuclide inventory at the time of a postulated fuel damaging
accident can be calculated by ORIGEN. The integrated source term for each
significant radionuclide can then be estimated, given a containment/reactor
building leakage history. The next step is to account for atmospheric dis-
persion as the fission products are transported from the release point to the
receptor location. The method used is credited to O. G. Sutton and is outlined

---

* $\dfrac{3.1 \times 10^{10} \ \text{fissions/s/W}}{3.7 \times 10^{10} \ \text{Disintegrations/s/Ci}} \approx 0.84 \ \text{Ci/W}$

in Ref. 4. Diffusion factors (χ/Q) are determined based on release height, wind velocity, air stability, and the distance from release to receptor locations. Tables and curves of χ/Q factors, as functions of these variables, are compiled in U.S. Nuclear Regulatory Commission (USNRC) Regulatory Guides 1.3[5] and 1.4.[6] A more recent guide for site specific χ/Q values is provided in USNRC Regulatory Guide 1.145.[7] Values used in the remainder of this section were taken from those tables for power reactors.

1.4 Dose Conversion Factors

Application of the diffusion factor (χ/Q) to the integrated source term for the ith radionuclide (Q_i) yields the expected integrated concentration at the receptor site. The effects of this radioactive material on a person, located at the receptor site for a given exposure time, depend on the intake and retention of the various nuclides, the possibility of concentration in body organs, and the radiological half life of the nuclides.

A significant element from this human biology standpoint is iodine, which concentrates in the thyroid gland. Each radioisotope of iodine will affect the thyroid in a characteristic manner depending on both its behavior as a radionuclide and as an element taken into, utilized by, and eventually elim- nated from the human body. During its stay in the thyroid, the radioactivity of each iodine isotope can result in energy deposited—and damage done— to the gland. This effect, measured in rem, is estimated by using dose conver- sion factors (DCF). DCF data are available from a number of sources for external whole body immersion and for internal whole body, bone, lung, thyroid, etc. An extensive tabulation of DCFs for a large selection of isotopes and an assortment of internal organs is available in Ref. 8. These data are used in subsequent calculations in this section.

1.5 Breathing Rate Data

For the calculation of inhalation doses the breathing rate of the receptor during the time of exposure must be specified. The breathing rate data for man in these analyses are taken from USNRC Regulatory Guides 1.3[5] and 1.4[6] The first eight (8) hours of the exposure are taken to be an active period with a breathing rate of 3.47×10^{-4} m^3/s. The interval from eight to twenty four (8-24) hours is considered to be a resting period with a rate of 1.75×10^{-4} m^3/s. For time periods greater than one day, a breathing rate of 2.32×10^{-4} m^3/s is used.

2. Application of Methods

Some applications of the models and methods are provided for illustration and for the comparison of LEU and HEU fuel. The following definitions and guidelines of the USNRC 10 CFR part 100[9] are used for this study:

"(1) An exclusion area of such size that an individual located at any point on its boundary for two hours immediately following onset of the postulated fission product release would not receive a total radiation dose to the whole body in excess of 25 rem or a total radiation dose in excess of 300 rem to the thyroid from iodine exposure.

(2) A low population zone of such size that an individual located at any point on its outer boundary who is exposed to the radioactive cloud resulting from the postulated fission product release (during the entire period of its

passage) would not receive a total radiation dose to the
whole body in excess of 25 rem or a total radiation dose
in excess of 300 rem to the thyroid from iodine exposure."

These values of 25 rem for whole body and 300 rem for thyroid exposure,
along with values of 150 rem for bone and 75 rem for lung doses, were once
considered the maximum once-in-a-lifetime doses for radiation workers. As
noted in 10 CFR 100, these values should not be considered acceptable limits
for doses to the public under accident conditions but may be used as reference
values for evaluations of reactor sites.

USNRC 10 CRF part 20 also provides standards for radiation protection
which may be used for assessing the consequences of a postulated accident.
These standards generally do not include limits by individual organ.

Ideally one would like to use a simple yet conservative method which
would demonstrate that even with conservative assumptions the reactor would
not present a significant risk to the public. In some cases, however, these
simple methods may be too conservative and it will be necessary to do more
detailed calculations with more complex models. The sensitivity of some of
the options are considered in the following discussion.

2.1 Simple Example

In order to demonstrate the application of some of the methods, a simple
example is useful. Consider a single isotope of iodine, ^{131}I. Calculate the
dose to the thyroid from an inventory of 1000 Ci, assuming a 25% release to the
containment/building and a 1%/day leakage rate to the atmosphere at ground
level. The activity of ^{131}I released, Q_i, over time τ can be determined
from Eq. (3), where

$$q_i = 1000 \text{ Ci},$$
$$\lambda_\ell = 0.01/d = 1.157 \times 10^{-7} \text{ s}^{-1},$$
$$\lambda_r = 1.00 \times 10^{-6} \text{ s}^{-1} \ (T_{1/2} = 8.04d), \text{ and}$$
$$F_p F_B = 0.25$$

τ	^{131}I Released, Ci
0-2h	0.207
2-8h	0.613
8-24h	1.56
1-4d	5.91
4-30d	16.2
Total	24.5

After 30 days 24.5 Ci (9.8%) of the 250 Ci available have been released to
the atmosphere. If the half life of ^{131}I were long or the decay while in the
containment were neglected, 25.9% would have been released after 30 days.
Credit for decay of the isotope before leakage from the containment can result
in a significant reduction in the activity released to the atmosphere. The
dose to the thyroid can be estimated by using Eq. (1) with DCF = 1.44×10^6

rem/Ci and with the atmospheric diffusion factor data from USNRC Regulatory Guide 1.4[6] for a ground level release as follows:

τ	BR, m^3/s	χ/Q, s/m^3 500 m	1000 m	5000 m
0-8h	3.47×10^{-4}	2.08×10^{-3}	6.40×10^{-4}	6.00×10^{-5}
8-24h	1.75×10^{-4}	4.95×10^{-4}	1.50×10^{-4}	1.20×10^{-5}
1-4d	2.32×10^{-4}	1.72×10^{-4}	5.30×10^{-5}	4.10×10^{-6}
4-30d	2.32×10^{-4}	4.00×10^{-5}	1.20×10^{-5}	8.80×10^{-7}

for distances from the source of 500, 1000, and 5000 m:

τ	Thyroid Dose, rem 500 m	1000 m	5000 m
0-2h	0.216	6.63×10^{-2}	6.22×10^{-3}
0-30d	1.60	0.491	4.22×10^{-2}

The dose is significantly reduced at larger distances from the point of release by dispersion.

This simple example also illustrates how hand calculations can be done for selected isotopes. It may be sufficient to make conservative estimates of doses based on only hand calculations for the most important contributors. Such calculations are considered later in this section.

2.2 Source Estimates and the ORIGEN Code

The ORIGEN code[3] can provide a powerful capability for estimating the inventory of fission products and actinides in the reactor fuel after a specified irradiation history. The fuel cycle history may be represented by a sequence of power and shutdown cycles of variable power level and duration. The burnup/buildup is represented spatially by a point model. The entire core or fuel element is limited to a uniform power distribution over each cycle.

The nuclear data library for the code is intended for the treatment of ^{235}U and ^{239}Pu fuels in both fast and thermal spectra and ^{233}U in a thermal spectrum. The user may set a flag in the input by reactor type for LWR (Light Water Reactor), HTGR (High Temperature Gas-cooled Reactor), MSBR (Molten Salt Breeder Reactor), or LMFBR (Liquid Metal Fast Breeder Reactor), and three parameters may be set for the thermal, resonance, and fast flux data. The LWR library is probably the best choice for thermal research reactors. However, since the enrichment in the LEU fuel for research reactors is substantially higher than that of a typical LWR, it is useful to compare the cross-section data in ORIGEN for applications to research reactors. The burnup/buildup from ORIGEN has been compared to that obtained from the EPRI-CELL (CINDER) cross section generation code.[10] The ORIGEN and EPRI-CELL data are compared in Table 1. The largest differences are in the capture cross-sections for ^{238}U and the plutonium isotopes.

The data from EPRI-CELL may be used in the ORIGEN code by overriding the library data at run time. This option has been used in all subsequent analyses. Since only the plutonium production is affected, the HEU dose

160

Table 1. ORIGEN LWR Cross-sections Compared With EPRI-CELL Cross-Sections for the IAEA Generic 10 MW Reactor With HEU and LEU Fuels.

| Isotope | $\sigma_{n,\gamma}(b)$ | | | $\sigma_{n,f}(b)$ | | |
| | ORIGEN LWR | EPRI-CELL | | ORIGEN LWR | EPRI-CELL | |
		HEU	LEU		HEU	LEU
^{235}U	92.6	80.3	76.8	412.6	407.5	379.3
^{236}U	41.1	42.0	45.1	2.4	0.8	1.0
^{238}U	5.4	32.8	10.1	0.4	0.4	0.5
^{239}Pu	473.1	362.2	382.7	1136.0	740.0	748.5
^{240}Pu	611.8	1124.4	1178.7	1.8	2.5	2.9
^{241}Pu	416.3	-	285.0	1149.0	-	844.4
^{242}Pu	237.8	-	150.1	0.1	-	2.2

| Isotope | $\sigma_{n,2n}(b)$ | | |
| | ORIGEN LWR | EPRI-CELL | |
		HEU	LEU
^{235}U	0.0220	0.0094	0.0110
^{236}U	0.0095	0.0090	0.0105
^{238}U	0.0220	0.0186	0.0217
^{239}Pu	0.0073	0.0039	0.0046
^{240}Pu	0.0051	0.0015	0.0018
^{241}Pu	0.0116	-	0.0309
^{242}Pu	0.0109	-	0.0079

results are unchanged. The doses from the highest power element in the 10 MW generic HEU reactor after 100 full power days (FPD) of irradiation are compared for LEU fuel at a hypothetical 500 m site boundary in Table 2. Even for this LEU case the changes are less than 5% and essentially only the bone dose is affected. The thyroid dose dominates and is unchanged by the cross-section data used. The effects of plutonium buildup on dose will be considered in more detail later in this section. The influence of cross-section changes on the doses determined with the inventories from the ORIGEN code are quite small, and the original library for LWR applications is adequate for most cases one would consider.

The inventory of fission products is strongly influenced by the irradiation history of the reactor. The maximum inventory for a given isotope may not be at the end of the maximm irradiation time for the fuel. The duty cycle

161

Table 2. LEU Doses With and Without ORIGEN Cross-section Changes
at 500 m Site Boundary

Organ	Dose, rem (Change,%)		
Bone	Original ORIGEN	Modified	ORIGEN
2 h	0.1484	0.1546	(+4.2)
30 d	1.404	1.425	(+1.5)
Lung			
2 h	0.2028	0.2035	(+0.3)
30 d	1.630	1.636	(+0.4)
Thyroid			
2 h	4.510	4.526	(+0.4)
30 d	26.91	26.98	(+0.3)
Whole Body (internal)			
2 h	1.601-02	1.616-02	(+0.9)
30 d	0.1213	0.1228	(+1.2)
Whole Body (external)			
2 h	5.439-02	5.429-02	(-0.2)
30 d	0.1864	0.1865	(+0.1)

of the reactor can also have a substantial effect on this inventory. Table 3 illustrates the inventory of a selection of isotopes under varying irradiation conditions. The approximate half lives of these isotopes are also provided. The table shows many of the kryton and xenon isotopes peaking early in the irradiation history (~4 days), while the iodine isotopes have a peak inventory at about 100 full power days of irradiation. The inventories corresponding to a five day week with eight hours per day of operation are shown after one week and after six (6) weeks (~10 days at full power total). These inventories are substantially below even the four day continuous irradiation at full power case. Accurately accounting for the operating history of the reactor can result in an important reduction in the peak inventory for a reactor.

The inventory of the peak power element in the generic 10 MW reactor after continuous operation at full power for 100 days has been taken as a conservative standard for much of the subsequent analyses. This may not be the peak inventory condition for other reactors with other choices of fuel but can serve as a useful basis for comparison.

2.3 Dose Estimates and Isotopic Components

A simple Fortran code[11] has been written which computes dose estimates for bone, lung, thyroid, and whole body for inhalation using Eq. (1) and the whole body gamma and beta dose for immersion using Eq. (2). The χ/Q data must be input. The inventory is determined from Eq. (3), where the factors F_P, F_B, and λ_ℓ are input and the source q_i may be read from a file generated by the ORIGEN code or input from another source of data. Dose conversion factors and decay constants for ~290 isotopes are tabulated in a library from Ref. 8. The precursor source to the iodine isotopes is approximated in the following fashion:

The inventories of the precursors for each iodine isotope are simply summed, e.g.

$$^{131}In \rightarrow\ ^{131}Sn \rightarrow\ ^{131}Sb \rightarrow\ ^{131m}Te \rightarrow\ ^{131}Te \xrightarrow{\lambda}\ ^{131}I,$$
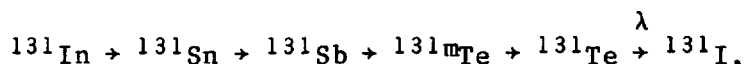
where the In, Sn, Sb, and ^{m}Te are assumed to instantly decay to Te to form the iodine precursor source, q_{po}, and

$$q_p(\tau) = q_{po}\,(1 - e^{-\lambda\tau}), \tag{5}$$

where λ is the decay constant for Te and τ is the elapsed time after release. No credit is taken for holdup in decay of the precursors to Te. This contribution is then lumped in with the fission product inventory of iodine.

The code computes doses after exposures of 2 hours and 30 days (~infinite) at distances from the reactor as specified in the input. The code provides edits of activity by isotope released to the building and released to the atmosphere over 2 hours, 2-4 hours, 4-8 hours, 8-24 hours, 1-4 days, and 4-30 days. The dose by organ is also broken down into percent contribution by isotope, which can be useful in determining the relative importance of each component. It can be shown that only a limited number of isotopes need to be considered in calculating a reasonable estimate for the dose, and while a computer code is convenient, it is not essential.

For illustrative purposes the generic 10 MW reactor has been selected for dose computations. No attempt will be made to postulate the accident conditions that might lead to the assumed releases for the cases considered. An attempt is made, however, to choose realistic examples that can be scaled to other conditions. In all cases only the fuel element with the highest power level at the beginning of equilibrium cycle is considered, and in most cases the "worst case" inventory for 100 full power days of irradiation is used as shown in Table 3. The HEU case has 280 g of ^{235}U in the element, and the LEU element contains 390 g of ^{235}U.

Although only the inventory for a single element is considered, the doses computed can be scaled up or down as more or less damage to the fuel is postulated. This single element can also be thought of as representing partial releases from several elements.

Now that the inventory is established, further assumptions must be made regarding the release to the containment, the fraction available for release to the atmosphere, and the leakage rate to the atmosphere. One common set of assumptions is to assume that 100% of the noble gases, 50% of the halogens, and 1% of the solids in the inventory are released into the containment, and to assume that only 50% of the halogens remain available for release to the atmosphere. A leakage rate to the atmosphere of 1%/day is assumed for most of the sample cases. The variation in leakage rate with the change in pressure

163

Table 3. Volatile Fission-Product Activities after Full-Power-Operation
Runs of 1) 5d at 8h/d; 2) 4d; 3) 21d; 4) 100d, and 5) 300d

| Nuclide | $T_{1/2}$ (Knolls Chart) 1977 | ORIGEN-Calculated Activities at shutdown, 10^3 Curies | | | | | |
| | | 5-d,8h/d | | | | | |
		After 5d 0.74 MWD	After 6 weeks 4.34 MWD	4d 1.77 MWD	21d 9.31 MWD	100d 44.34 MWD	300d 133.0 MWD
^{83m}Kr	1.86 h	0.0200	0.0200	2.80	2.77	2.74	2.38
^{85m}Kr	4.48 h	0.0500	0.0496	6.87	6.84	6.77	5.84
^{85}Kr	10.72 y	1.08×10^{-5}	3.23×10^{-5}	9.71×10^{-4}	0.00539	0.0258	0.0744
^{87}Kr	76 m	0.132	0.132	13.4	13.3	13.1	11.3
^{88}Kr	2.84 h	0.163	0.163	18.8	18.7	18.5	15.9
^{89}Kr	3.15 m	0.246	0.246	24.6	24.4	24.1	20.6
^{131m}Xe	11.92 d	3.72×10^{-5}	2.28×10^{-4}	0.00317	0.0443	0.103	0.103
^{133m}Xe	2.19 d	0.00692	0.00281	0.577	1.04	1.04	0.896
^{133}Xe	5.25 d	0.125	0.0898	10.4	32.7	35.3	31.0
^{135m}Xe	15.3 m	0.0406	0.0389	5.76	5.71	5.68	5.15
^{135}Xe	9.09 h	0.0232	0.0211	3.83	3.62	2.84	0.742
^{138}Xe	14.2 m	0.329	0.329	32.8	32.6	32.3	28.0
^{131}I	8.041 d	0.0442	0.0388	4.08	12.4	14.8	14.1
^{132}I	2.29 h	0.131	0.0636	13.1	22.2	22.3	20.4
^{133}I	20.8 h	0.287	0.143	33.8	35.3	35.1	30.6
^{134}I	52.6 m	0.355	0.355	40.1	39.8	39.5	34.3
^{135}I	6.585 h	0.218	0.206	33.3	33.1	32.8	28.6

within the building is not included. No credit is taken for filtering, wash-down, or other engineered safety features that might be included in some designs.

After release to the atmosphere, other assumptions may be made in order to describe the dispersion of the plume in the atmosphere before reaching the receptor site. Without site specific data on wind speed and atmospheric stability conditions, the conditions suggested in USNRC Regulatory Guide 1.4 for a ground level release may be assumed. This χ/Q data assumes a wind speed of 1 m/s and Pasquill type F (stable) atmospheric conditions for the first eight hours following release. These are the same conditions assumed for the previous example, and χ/Q values at 500, 1000, and 5000 m distances are listed in Section 2.1. These assumptions are used in many of the cases considered.

Doses for the generic 10 MW reactor with HEU and LEU fuel are compared in Table 4. The doses for release from the highest power element after 100 full

Table 4. Doses at 500 m Site Boundary for Generic 10 MW
Reactor 100 FPD Peak Element With HEU and LEU Fuel*

	HEU	LEU	Guideline Doses (rem) from 10 CFR 100
Bone Dose, rem			
2 h	0.138	0.155	150
30 d	1.305	1.467	150
Lung Dose, rem			
2 h	0.199	0.204	75
30 d	1.600	1.636	75
Thyroid Dose, rem			
2 h	4.419	4.526	300
30 d	26.38	27.03	300
Whole Body (internal), rem			
2 h	0.0155	0.0162	25
30 d	0.117	0.123	25
Whole Body (external), rem			
2 h	0.0531	0.0543	25
30 d	0.181	0.187	25
Burnup, MWD	44.34	45.11	

*Assuming 100% of noble gases, 25% of halogens, and 1% of
other are available for release from the containment, and a
leakage rate from the containment of 1%/day (using Regula-
tory Guide 1.4 χ/Q values).

power days at a 500 m site boundary are given at 2 hours and after 30 days.
Doses after 100 FPD are chosen for comparison in this example because the
activity of the radioiodines is a maximum (see Table 3).

When the differences in the power levels (the highest power element in
the LEU core was calculated to have ~2% higher power than in the HEU core)
are discounted, the LEU and HEU doses are very similar and well below the
guideline doses from 10 CFR 100. The LEU inhalation dose for bone and whole
body are slightly higher due to the presence of more plutonium. This differ-
ence is considered in more detail later. In either case the largest dose is
to the thyroid, and 5 rem after 2 hours or 27 rem after 30 days are both well
below the 300 rem guideline dose for the thyroid.

The isotopes that make significant contributions to the dose in specific
organs are tabulated in Table 5 for the HEU case. Only the iodines contribute
to the thyroid dose with 66% of the dose contributed by ^{131}I. The iodine con-
tributions from precursors is ~5% of the total for this case. The bone dose
contributors are dominated by ^{144}Ce, ^{89}Sr, and ^{91}Y. The lung and internal
whole body doses are similar and each show ^{144}Ce and ^{131}I as major contributors.

Table 5. Isotopic Contributions to the Thyroid, Bone, and Lung Doses, the Whole Body Internal (Inhalation) Dose, and the Whole Body External (Immersion) Dose.

Isotope	Dose, %	Isotope	Dose, %	Isotope	Dose, %
Thyroid Dose					
I-131	66.	I-135	4.8	I-134	0.4
I-133	25.	I-132	3.5		
Bone Dose					
Ce-144	25.	Zr-95	4.3	Pu-239	0.5
Sr-89	24.	Pr-143	1.9	Nd-147	0.5
Y-91	23.	Ce-141	1.6	Pm-147	0.4
Ba-140	7.8	Pu-238	1.1		
Sr-90	7.8	Nb-95	0.6		
Lung Dose					
Ce-144	17.	Ce-141	2.8	I-132	1.0
I-131	16.	Ru-103	2.6	La-140	0.8
Y-91	12.	Pr-143	2.4	Nd-147	0.7
Zr-95	11.	Nb-95	2.2	Sr-90	0.7
Ba-140	11.	I-135	1.3	Mo-99	0.6
Sr-89	8.5	Te-132	1.1	Ce-143	0.4
I-133	5.4	Ru-106	1.1		
Whole Body Internal (Inhalation) Dose					
I-131	27.	Y-91	6.7	Pr-143	1.0
Ce-144	15.	I-135	2.5	Te-132	1.0
Zr-95	13.	Nb-95	2.1	La-140	0.5
I-133	8.4	I-132	1.9	Mo-99	0.5
Sr-89	7.5	Sr-90	1.7	Nd-147	0.4
Ba-140	7.0	Ce-141	1.5		
Whole Body External (Immersion) Dose					
I-131	27.	I-134	6.3	Kr-85m	1.4
Kr-88	15.	Kr-87	4.9	La-140	1.1
Xe-133	11.	I-131	4.1	Xe-137	0.6
I-135	10.	Xe-135	1.7	Zr-95	0.5
I-133	9.8	Xe-138	1.6	Ba-140	0.3

The largest contributors to the external whole body dose are ^{132}I and ^{88}Kr. A large percentage of the doses are contributed by a limited number of isotopes. This makes the use of source data generated from fission product yield tables a reasonable approximation. The inventory from experiments and the operating history of the reactor may shift the importance of the various isotopes to dose.

2.4 Yield Table Approximation

The inventory of fission products in the fuel can be approximated by using Eq. (4). If adequate fission product yield data are available and a constant reactor power is an acceptable approximation for the irradiation, then data for only a few selected isotopes should provide a reasonable estimate for the release source. For long irradiation times the exponential term in Eq. (4) can be neglected and the resulting inventory is the maximum corresponding to an infinite irradiation time. Such an estimate should give a conservative approximation for the source.

The yield fractions and infinite irradiation fission product inventory data for selected isotopes are provided in Table 6 based on yield tables from Ref. 12. Only the first 29 isotopes are considered as important contributors to the direct inventory based on the results from the previous section. The last 19 isotopes of In, Sn, Sb, and Te are included primarily to account for iodine precursor contributions. The dose conversion factors for these 29 isotopes from Ref. 8 are listed in Table 7. Equations (1)-(3) and (5) may be used to estimate the dose directly without the need for computer codes.

Dose estimates based on these cumulative yield data for the HEU core are compared with dose estimates from ORIGEN after 100 FPD of irradiation in Table 8. Also shown are the cumulative yield results for infinite irradiation time using the source data from Table 6 directly. For an irradiation time of 100 FPD, the cumulative yield data agree remarkably well with the corresponding ORIGEN results. However, the infinite irradiation time yield results substantially overestimate the bone dose. The differences in the cumulative yield data for 100 FPD and infinite irradiation times are largely due to the difference in the ^{90}Sr inventory. At infinite irradiation times, the ^{90}Sr contribution is ~84% of the total bone dose, while for a 100 day irradiation only ~7% of the bone dose is due to ^{90}Sr buildup.

The infinite irradiation cumulative yield method can provide a conservative estimate for the dose. The yield table data do not include the buildup of actinides. The importance of plutonium buildup in the LEU fuel is considered in a later section.

2.5 Site Specific Data and Sensitivity of Dose Estimates

The cumulative yield method provides a convenient way of presenting the dose per unit power. The results may be generalized to any power level. The dose levels correspond to a single element at the highest power again with assumed release fractions of 100% for the noble gases, 25% for the halogens, and 1% for all others. The levels may be scaled to fractional or multiple element cases. The term site boundary has been purposely used in the previous comparisons so that the results may be interpreted either as doses at the exclusion area boundary or at the outer boundary of the low population zone for the reactor using USNRC definitions. The sensitivity of these dose data to changes in distance from the source, leakage rate, and other accident or site specific conditions will now be considered.

The variation in dose/MW to the thyroid and whole body with leakage rate from the containment and distance from the source of release is illustrated in Fig. 1. These data are for a ground-level release and for non-site specific conditions. The χ/Q data at distances of 500 and 1000 m are those listed in section 2.1 from Regulatory Guide 1.4.[6] The doses vary strongly with both the leakage rate and distance from the source.

Table 6. Isotopic Yields and Source Data

Isotope, i	Yield, γ_i	Decay Const., s^{-1}	$Q_i^*/MW \times 10^{-4}$
Kr-85m	0.01290	4.30-05	1.084
Kr-87	0.02556	1.50-04	2.147
Kr-88	0.03541	6.90-05	2.974
Sr-89	0.04822	1.60-07	4.050
Sr-90	0.05772	7.58-10	4.848
Y-91	0.05931	1.70-07	4.982
Zr-95	0.06519	1.20-07	5.476
Nb-95	0.06520	2.30-07	5.477
Mo-99	0.06074	2.90-06	5.102
Ru-103	0.03029	2.00-07	2.544
Ru-106	0.00402	2.17-08	0.338
I-131	0.02892	1.00-06	2.429
Te-132	0.04297	2.50-06	3.609
I-132	0.04313	8.40-05	3.623
I-133	0.06693	9.30-06	5.622
Xe-133	0.06696	1.50-06	5.625
I-134	0.07794	2.20-04	6.547
I-135	0.06293	2.90-05	5.286
Xe-135	0.06535	2.10-05	5.489
Xe-137	0.06122	3.00-03	5.142
Xe-138	0.06238	8.10-04	5.240
Ba-140	0.06202	6.30-07	5.210
La-140	0.06207	4.80-06	5.214
Ce-141	0.05787	2.50-07	4.861
Ce-143	0.05963	5.80-06	5.009
Pr-143	0.05963	5.90-07	5.009
Ce-144	0.05493	2.82-08	4.614
Nd-147	0.02270	7.30-07	1.907
Pm-147	0.02270	8.37-09	1.907
In-131	0.00029	2.30+00	0.0244
Sn-131	0.00932	1.10-02	0.7829
Sb-131	0.02577	5.00-04	2.165
Te-131m	0.00391	6.40-06	0.3284
Te-131	0.02567	4.60-04	2.156
Sn-132	0.00576	1.70-02	0.4838
Sb-132m	0.01165	4.10-03	0.9786
Sb-132	0.01633	2.80-03	1.372
Sn-133	0.00180	4.70-01	0.1512
Sb-133	0.02208	4.80-03	1.855
Te-133m	0.04054	2.10-04	3.405
Te-133	0.02999	9.20-04	2.519
I-133m	0.00153	7.70-02	0.1285
Sb-134m	0.00228	7.70-01	0.1915
Sb-134	0.00468	6.70-02	0.3931
Te-134	0.06932	2.70-04	5.823
I-134m	0.00365	3.20-03	0.3066
Sb-135	0.00148	4.10-01	0.1243
Te-135	0.03247	3.60-02	2.727

$^*Q_i = 0.84 \gamma_i \times 10^6$, Ci/MW (infinite irradiation time).

Table 7. Isotopic Dose Conversion Factors

| Isotope | Inhalation, rem/µCi | | | | External Whole mrem/yr |
	Bone	Thyroid	Lung	Whole Body	Body µCi/mℓ
Kr-85m	–	–	–	–	3.75+09
Kr-87	–	–	–	–	1.88+10
Kr-88	–	–	–	–	2.09+10
Sr-89	4.14-02	–	1.79-01	1.16-02	4.95+09
Sr-90	1.11+01	–	1.19+00	2.22-01	1.68+09
Y-91	3.35-01	–	2.11-01	8.96-03	5.26+09
Zr-95	6.17-02	–	1.97-01	1.60-02	7.63+09
Nb-95	1.31-02	–	6.45-02	4.47-03	7.26+09
Mo-99	–	–	1.20-02	6.62-04	5.15+09
Ru-103	1.56-03	–	7.56-02	7.71-04	4.98+09
Ru-106	2.04-02	–	1.16+00	2.85-03	1.06+08
I-131	–	1.44+00	2.07-02	2.63-03	5.22+09
Te-132	3.20-03	2.47-03	3.14-02	1.97-03	2.43+09
I-132	–	5.31-02	8.88-04	1.29-04	2.50+10
I-133	–	3.92-01	5.06-03	5.74-04	9.84+09
Xe-133	–	–	–	–	1.72+09
I-134	–	2.49-02	3.63-04	4.24-05	2.71+10
I-135	–	1.22-01	1.97-03	2.86-04	1.83+10
Xe-135	–	–	–	–	5.11+09
Xe-137	–	–	–	–	1.79+10
Xe-138	–	–	–	–	1.34+10
Ba-140	8.94-02	–	1.48-01	7.22-03	4.61+09
La-140	4.75-03	–	1.67-02	8.35-04	2.52+10
Ce-141	1.97-02	–	4.17-02	1.65-03	2.32+09
Ce-143	3.97-03	–	1.00-02	3.38-04	6.53+09
Pr-143	2.28-02	–	3.60-02	1.13-03	2.90+09
Ce-144	1.20+00	–	1.01+00	6.50-02	1.08+09
Nd-147	1.48-02	–	2.84-02	1.16-02	3.76+09
Pm-147	1.88-01	–	6.71-02	6.92-03	6.28+08

In the next sequence of cases the leakage rate is held fixed at 1%/day, and the influence of building wake effects at ground level and of various stack heights are considered. The non-site specific data from Regulatory Guide 1.3[5] are used with 1/2 the cross-sectional area of the building assumed to be 1000 m^2 for the wake correction factor. The thyroid dose/MW is shown in Fig. 2 for ground-level releases with and without the wake correction factor and for releases at effective stack heights of 50, 100, and 150 m. The ground-level release data without a wake correction are consistent with the data in Fig. 1. The wake correction factor near the building reduces the dose to 1/3. The stack releases assume full fumigation conditions for the first one-half hour after release. The effective stack heights are also assumed to be more than two and one half times the height of adjacent solid structures. The above ground-level release results in a further reduction in the dose.

Table 8. Comparison of Doses with Fission Product Inventories from ORIGEN Code vs. Yield Tables for Generic 10 MW Reactor with HEU Fuel.

		Dose at 500 m Site Boundary, rem[*]				
		Inhalation			Whole Body	
Case	Time	Bone	Lung	Thyroid	Internal (Inhalation)	External (Immersion)
ORIGEN	2 h	0.1384	0.1987	4.419	1.549-02	5.305-02
100 FPD	30 d	1.305	1.600	26.38	0.1171	0.1812
Cumulative Yields	2 h	0.1373	0.1999	4.463	1.567-02	5.718-02
100 FPD	30 d	1.309	1.632	26.70	0.1195	0.2015
Cumulative Yields	2 h	1.712	0.4859	4.463	5.230-02	5.730-02
Infinite Irrad.	30 d	17.47	4.541	26.70	0.4943	0.2030

[*]Using peak element, 0.4434 MW, in 10 MW HEU generic reactor with a 1.0%/d leak rate and the release of 100% of Noble gases, 25% of halogens, and 1% of all other to containment.
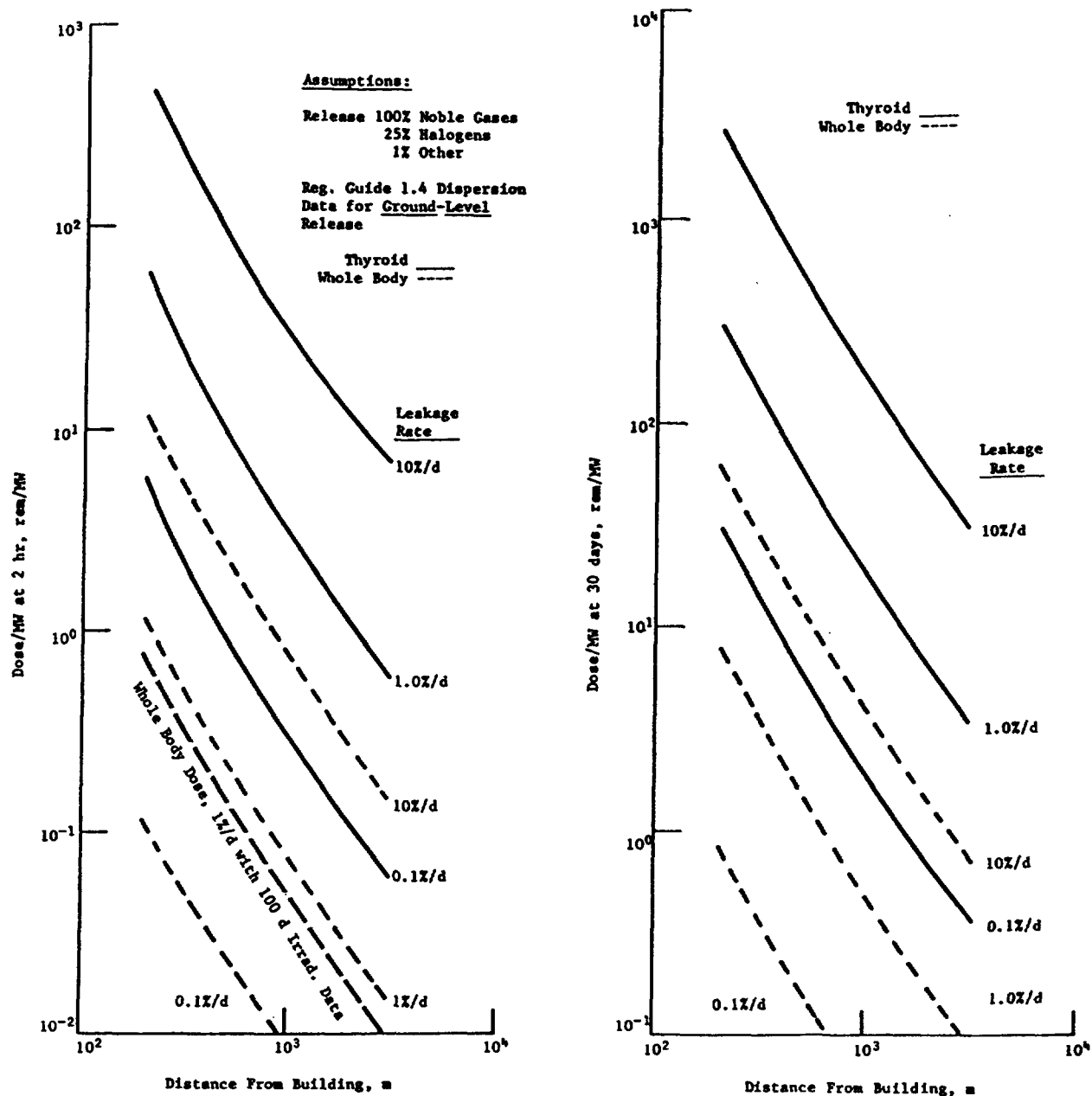
Fig. 1. Dose/MW Variation With Leakage Rate and Location

The maximum dose after 30 days (Fig. 2) does not occur at the nearest distance from the source but at some distance from the release point. The location of the peak dose is determined by the χ/Q for each stack height.

Although there are no site specific meteorological data for the generic reactor, the changes in dose that can be expected by using site specific data can be indicated by some examples. The dose received is directly proportional to the χ/Q values for the specific atmospheric conditions. Thus, the comparison can be limited to χ/Q values. The dispersion models from Regulatory Guide 1.145[7] will be used for this comparison with a 0-2 hour time interval and a distance from the source of 500 m. Data for both a ground-level release and release from an effective stack height of 50 m are presented in Table 9. The non-site specific data are also shown for comparison. For a ground-level release under Pasquill class F conditions the diffusion factor value is simply reduced to 1/4 if the wind speed is really 4 m/s at the site rather

171
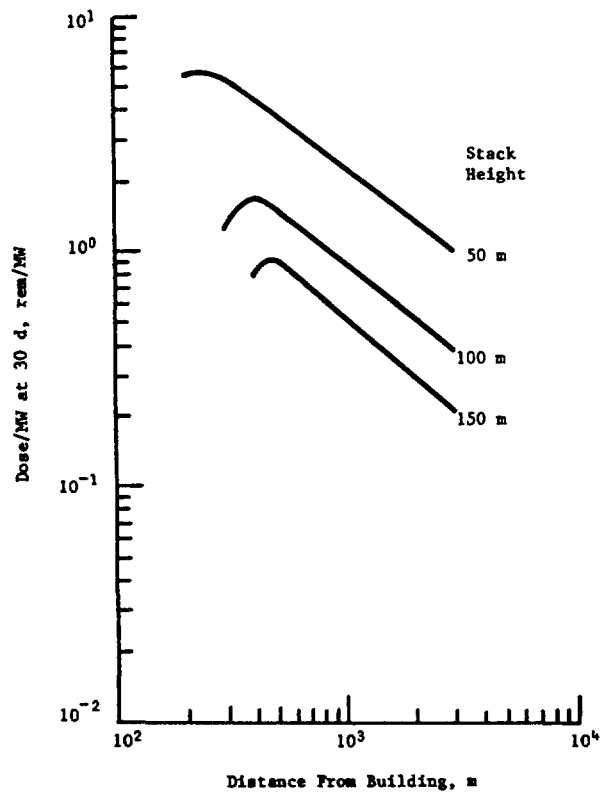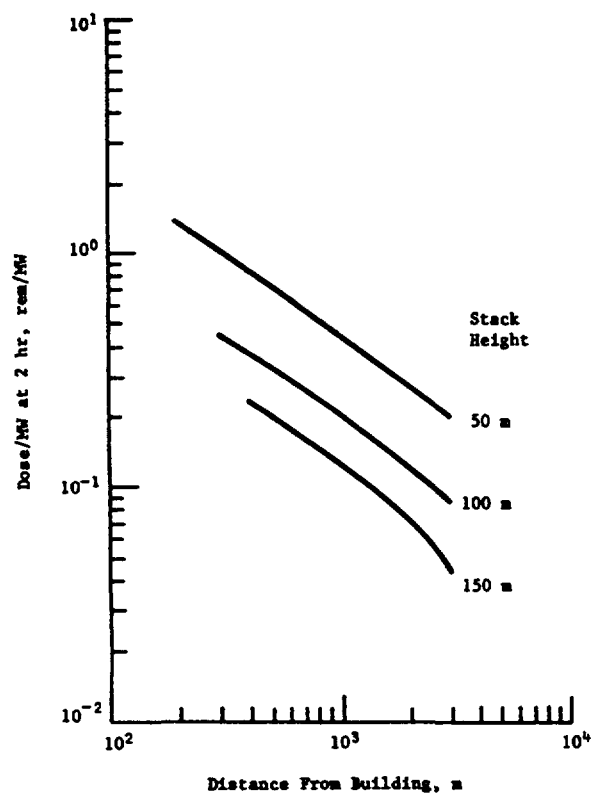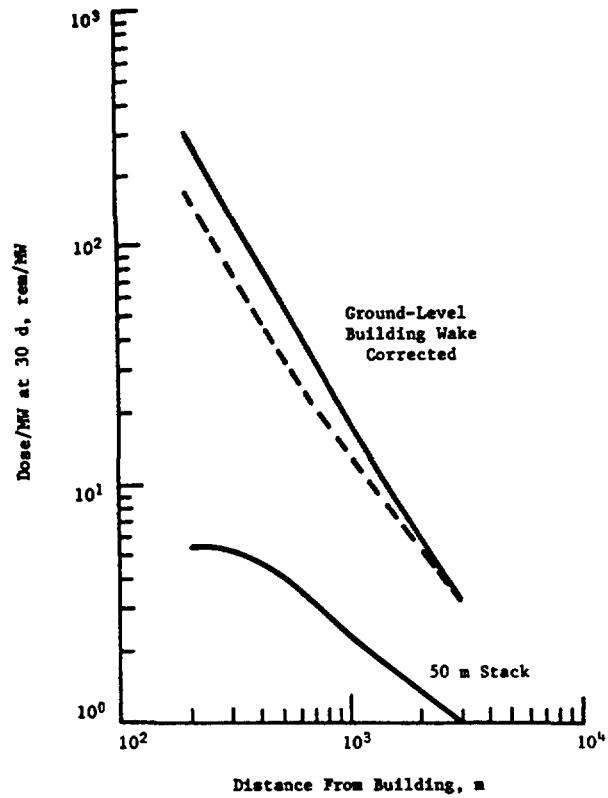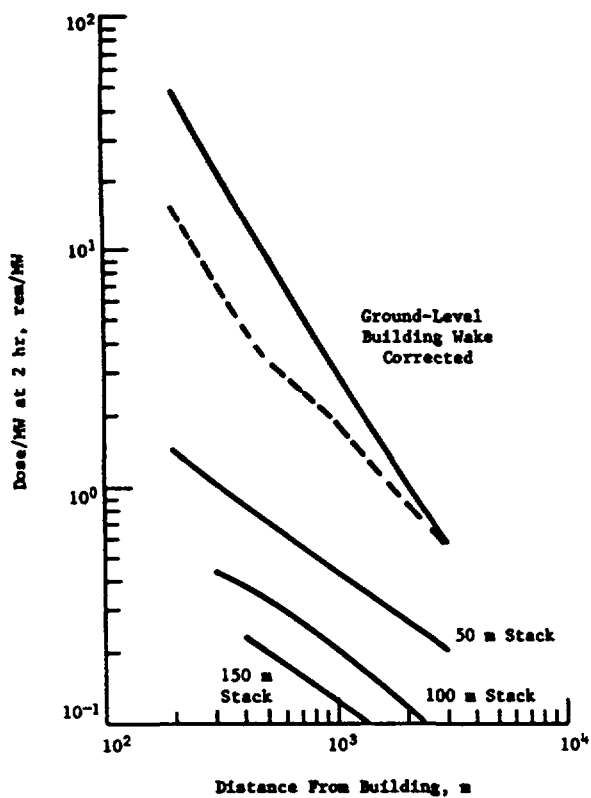
Fig. 2. Thyroid Dose/MW Variation with Stack Height

Table 9. χ/Q Data with Site Specific Conditions.

Ground-level Release

Non-site Specific	χ/Q, s/m^3
Pasquill Class F, 1 m/s	2.1 - 03*
With Wake Effect Correction	7.0 - 04

Site Specific

Class F (stable), 4 m/s	1.8 - 04
Class C (slightly unstable), 8 m/s	1.8 - 05

Release from 50 m Stack

Non-site Specific

With Fumigation	4.0 - 04
Without Fumigation	5.9 - 05

Site Specific

Class A, 8 m/s	2.6 - 06
Class B	6.0 - 06
Class C	7.5 - 06
Class D	1.3 - 06
Class E	1.1 - 07
Class F	~0.0

*Value used in previous calculations at 500 m.

than 1 m/s, as assumed for the non-site specific case. This value is reduced by a full order of magnitude with class C conditions and a wind speed of 8 m/s. With releases from a stack of 50 m, this factor can be further reduced. A range of χ/Q values are shown for Pasquill classes A-F and a wind speed of 8 m/s. The values increase from unstable to more stable atmospheric conditions until class D, after which the values decrease. At the 500 m location the χ/Q value for class F is essentially zero. The peak location for the class F curve is well beyond 500 m. The class C curve has a peak near the 500 m location. These data show the same trends suggested by the curves

173

Table 10. Plutonium Buildup and Dose in Peak Power (0.4511 MW) Element for Generic 10 MW Reactor with 390 g ^{235}U per Fresh Standard LEU Fuel Element.

Irrad. Time, FPD	Burnup, MWD	^{235}U Atom % Burnup	390 g ^{235}U LEU Peak Power (0.4511 MW) Element							
			Mass, g					Dose, rem at 2 h (30 d)		
			Pu-238	Pu-239	Pu-240	Pu-241	Pu-242	Bone	Lung	Thyroid
100	45.1	14.4	–	4.38	0.26	0.03	----	0.155 (1.47)	0.204 (1.64)	4.53 (27.0)
200	90.2	28.2	0.02	7.80	0.94	0.25	0.01	0.258 (2.43)	0.251 (2.10)	4.55 (27.2)
300	135.3	41.8	0.07	10.3	1.81	0.74	0.07	0.365 (3.61)	0.280 (2.39)	4.52 (27.2)
400	180.4	54.6	0.18	11.9	2.74	1.53	0.24	0.532 (5.32)	0.304 (2.64)	4.51 (27.1)
500	225.5	66.7	0.41	12.9	3.52	2.49	0.60	0.774 (7.81)	0.328 (2.89)	4.48 (27.0)
600	270.6	77.7	0.81	13.4	4.09	3.46	1.23	1.13 (11.4)	0.358 (3.20)	4.45 (26.9)

in Regulatory Guide 1.3.[5] The corresponding doses that would be determined with site specific data can be substantially reduced compared to the non-site specific data.

2.6 LEU Fuel and Doses with Plutonium Buildup

With HEU fuel the content of ^{238}U is small and the production of plutonium and other actinides is negligible. The LEU fuel will have a content of ~80% ^{238}U and a greater potential for the buildup of plutonium with burnup. While the LEU fueled reactors can be expected to show an increase in dose due to this plutonium buildup, the consequences may still be insignificant.

In order to compare results with HEU and LEU fuel, the 10 MW generic reactor with LEU fuel is used again with the same release fractions, non-site specific conditions, and site boundary assumptions as before. Table 10 shows the buildup of ^{239}Pu and ^{241}Pu in grams as predicted by the ORIGEN code and the corresponding doses to bone, lung, and thyroid at the 500 m site boundary after two hours and after 30 days for irradiations times up to 600 FPD (78 atom percent burnup in ^{235}U). The 100 FPD data is identical to that for the LEU case shown in Table 4. In that comparison the bone dose for the LEU core is slightly higher than the HEU core. The bone and lung doses increase with increased irradiation time and burnup, while the thyroid shows a peak for 200 FPD and decreases slightly at higher burnups. At 600 FPD and 78% burnup, the fuel is well beyond the normal burnup limits for the fuel, and the bone dose is still substantially below that for the thyroid.

It is also interesting to look at the changes in importance of the major contributors to the bone dose with burnup as shown in Fig. 3. After 45 MWD (100 FPD), Ce-144 at 22% dominates with Pu-238 contributing less than 1% of the dose. Ce-144 continues to have the highest percent through 150 MWD with Pu-238 and Pu-241 steadily increasing. At 200 MWD, the Pu-238 becomes the largest contributor (25%). The Pu-238 continues to increase, while Pu-239, Pu-240 and Pu-241 reach peak values and begin to decrease with burnup. The contribution of Pu-242 is negligible throughout the burnup range.

In an effort to put the effects of plutonium on dose in perspective, it is useful to compare the peak doses by organ to some reference limits:

	Dose, rem		
Organ	Peak	Reference	Margin
Thyroid	27.2	300	11.0
Bone	11.4	150	13.2
Lung	3.20	75	23.4

The thyroid margin is lower than either the bone or lung margins even with an unrealistically high burnup of 78%. The thyroid dose is still the limiting factor in the LEU core. However, the thyroid dose may not be the limiting dose under all operating conditions and experiment inventories. The whole body internal and external dose for this extreme case is less than 0.6 rem at the site boundary after 30 days. This is well within the 3.0 rem per calender quarter limit for occupational dose to the whole body of USNRC 10 CFR part 20.

Core Irradiation Time, FPD
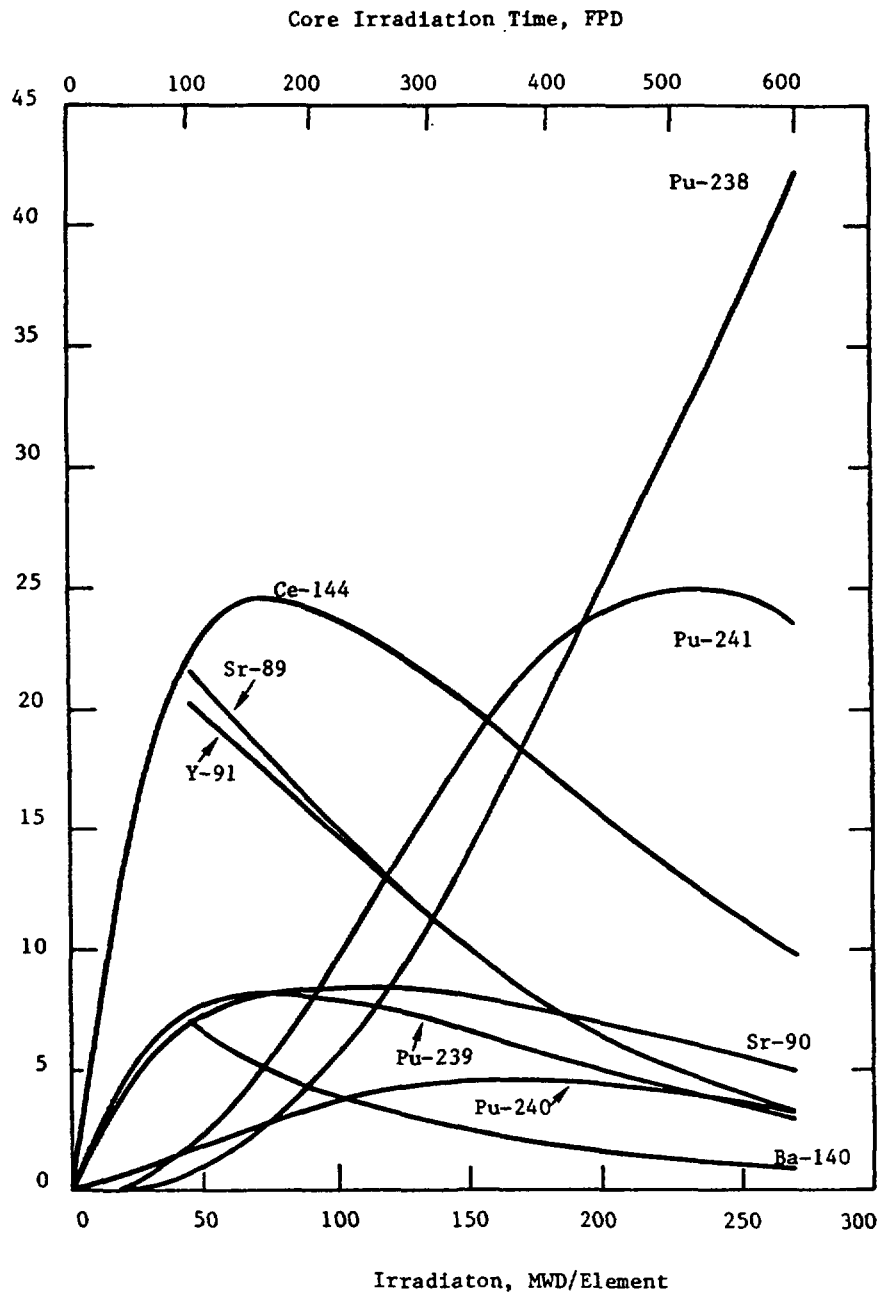
Fig. 3 Percentage Contribution of Various Isotopes
to Bone Dose as a Function of Burnup with
LEU Fuel in IAEA Generic 10 MW Reactor.

3. Summary

Models and methods with varying degrees of detail and conservatism have
been considered. If the safety requirements for a reactor can be satisfied by
using a simple but conservative model, there is no need for more detailed
models or methods. At the same time it should be recognized that more detailed
evaluations can substantially reduce the dose estimates for a given accident.

A detailed inventory of fission products and actinides in the reactor
fuel may be useful. The operating history (duty factor, fuel cycle, etc.) can
substantially affect the radiological consequences. Accounting for the at

176

power and down-time history can significantly reduce the source term for the release.

In some applications fission product yields can be used to estimate the reactor inventory to sufficient accuracy. Only a limited number of isotopes are important contributors to the dose, and most can be neglected. Assuming an infinite irradiation time for the fuel provides a conservative estimate. This method does not normally account for the production of actinides, but this component is not essential to the more limiting thyroid dose.

The assumed leakage rate from the containment and the assumed local meteorological conditions play a strong role in estimating the radiological consequences of an accident. Credits for elevated releases and site specific wind speed and atmospheric conditions can result in order of magnitude reductions in the dose estimates.

No attempt has been made to assess the effectiveness of any filtering system, washdown spray system, or other engineered safety features that may be included in some reactor designs. Such systems may provide additional safety margins. These must be assessed individually. Also, no attempt has been made to alter the release fractions assumed through out this section. However, there is growing evidence that the iodine release fraction could be substantially reduced. The model used here does not account for the finite transit time from the point of release to the receptor site, for the finite passage time of the radioactive cloud past the receptor, or for any evacuation procedures that might limit the exposure time. The full evaluation of the radiological consequences must be tailored to the characteristics and requirements of each individual reactor.

References

1. "Research Reactor Core Conversion From the Use of Highly Enriched Uranium to the Use of Low Enriched Uranium Fuels Guidebook," IAEA-TECDOC-233, IAEA, Vienna (1980); Appendix A, pp. 81-240.

2. J. J. DiNunno, et al., "Calculation of Distance Factors for Power and Test Reactor Sites," TID-14844, U.E. AEC (March 1962).

3. "ORIGEN-79: Isotope Generation and Depletion Code - Matrix Exponential Method," CCC-217, Oak Ridge National Laboratory Radiation Shielding Information Center (Sepember 1979).

4. "Meteorology and Atomic Energy - 1968," TID-24190 (July 1968).

5. U.S. Nucler Regulatory Commission, "Assumptions Used for Evaluating the Potential Radiological Consequences of a Loss of Coolant Accident for Boiling Water Reactors," Regulatory Guide 1.3, Revision 2 (June 1974).

6. U.S. Nuclear Regulatory Commission, "Assumptions Used for Evaluating the Potential Radiological Consequences of a Loss of Coolant Accident for Pressurized Water Reactors,"Regulatory Guide 1.4, Revision 2 (June 1974).

7. U.S. Nuclear Regulatory Commission, "Atmospheric Disperson Models for Potential Accident Consequence Assessments at Nuclear Power Plants," Regulatory Guide 1.145 (August 1979).

8. G. G. Killough and L. R. McKay, "A Methodology for Calculating Radiation Doses from Radioactivity Rebased to the Environment," ORNL-4992 (March 1976).

9. U.S. Nuclear Regulatory Commission Rules and Regulations 10 CFR Part 100, "Reactor Siting Criteria."

10. B. A. Zolotar, et. al., "EPRI-CELL Code Description," Advanced Recycle Methodology Program System Documentation, Part II, Chapter 5 (October 1975).

11. W. L. Woodruff and R. J. Cornella, "DOSER - A Code for Radiological Consequence Analysis," Argonne National Laboratory Internal Memorandum, February 20, 1984.

12. "Compilation of Fission Product Yields," NEDO-12154-3B (1980).

Appendix D-2

RADIOLOGICAL CONSEQUENCE ANALYSIS

C. BAGLIN
GEC Energy Systems Limited,
Whetstone, Leicester

F.R. ALLEN
Safety and Reliability Directorate,
United Kingdom Atomic Energy Authority,
Culcheth, Warrington, Cheshire

United Kingdom

Abstract

An overview of the methods used by the Safety and Reliability Directorate of the UKAEA for conducting a radiological consequence analysis is described. For the assessment of accidental releases of radioactive material to the atmosphere, it would be normal in the UK to use the TIRION or WEERIE suites of computer codes. A general description of the models used in the TIRION code (Gaussian-plume, constant weather) is provided along with a simpler and quicker method of obtaining public doses by using prepared solutions to the diffusion equation plus dose conversion factors.

1. Introduction

Reactor accident evaluations require predictions of the consequences of potential releases of radioactive material. A full consequence model would describe:

1) The transport and diffusion of released material in the atmosphere and in water.

2) The deposition of activity on the ground.

3) The processes whereby people in the area may receive radiation doses - e.g. inhalation.

4) The processes that may reduce radiation doses - e.g. bans on milk consumption.

5) The biological effects of radiation doses on the human body.

6) The socio-economic impacts.

A general description of consequence modelling is given by Kaiser (1).

Such models have been used for several years and several computer codes have been written and several more are under development. Despite this however there are many areas where judgement is required from the modeler.

179

Benchmark problems are currently being analysed under the sponsorship of CSNI with the general aim of improving consequence predictions (2).

There is a degree of uncertainty attached to many of the parameters and thus a statistical approach may be the best way to give meaningful results. Beattie and Bell (3) describe a method of allowing for the frequency of different weather conditions.

2. TIRION Code

For the assessment of accidental releases of radioactive material to the atmosphere it would be normal in the U.K. to use the TIRION or WEERIE suites of computer codes.

These contain models of all the important physical processes between the release from the containment and the dose commitment to the individual. Both are available from NEA.

TIRION (4) is a Gaussian-Plume, constant weather code. It contains the following models.

Release Model

Given the nuclides involved, the release period, the initial activities and any hold up period, this model calculates the total activity released for each nuclide allowing for decay and daughter build up.

Dispersion Model

The model used for atmospheric dispersion is the Gaussian Plume diffusion model incorporating Pasquill weather categories A – F.

Dry Deposition

This model allows ground deposition from the cloud dependent on parameters such as chemical form, vegetation cover, distance. The source depletion method in which a dry deposition velocity is assigned is used.

Radioactive Decay

Decay and daughter build up during the diffusion time are calculated by this model.

Building Wakes

This model allows for the effect wake dilution and gives reasonable estimates of the effect on downwind concentrations but does not lead to accurate values within the wake.

Lift-Off

Determines whether or not a ground level plume will lift off the ground.

Plume-Rise

Determines the trajectory of a rising plume based on initial momentum, initial temperature and radioactive heating of the cloud.

Plume-Breakup

Determines the termination of plume rise.

Inversion Lids

The presence of a strong overhead inversion inhibits the upward diffusion of material. This model sets the vertical concentration below the lid uniform. User specifies the height of the lid.

Inhalation Dose

The total dose commitment after time t is calculated using breathing rates and the ICRP lung model.

External Radiation Dose

This model calculates the cloud dose using triple integration over the whole cloud and, where it is shown to be within 10%, the faster infinite cloud approximation.

Consequence of Absorbed Doses

This model includes various dose-risk relationships which may be used to estimate the probability of health consequences.

Number of Casualties

Given a sectored population distribution this model calculates the number of casulties.

Deposited Activity

This model determines dose rates from deposited material and the area for which resuspension of actinides is unacceptable for a series of times after the accident. It will also determine the area within which milk contamination will be unacceptable.

3. Parametric Solutions

A simpler and quicker method of obtaining public doses is to use pre-prepared solutions to the diffusion equation plus dose conversion factors.

In the U.K. the National Radiological Protection Board have published a report which gives the air concentration of a nuclide at ground level for unit release as a function of downwind distance (5). Stack height, weather conditions and release duration are included as parameters.

The basic dispersion model used is similar to that in TIRION but, as yet, the modifying effects of plume rise, dry deposition, etc. are not modeled.

Dose conversions may be obtained from the Medical Research Councils publication of emergency reference levels for selected fission products (6). These are derived from the ICRP lung model.

As an example we may take the release of 10 Ci of I^{131} from a 50m high stack over a 2 hour period for a 500m site boundary.
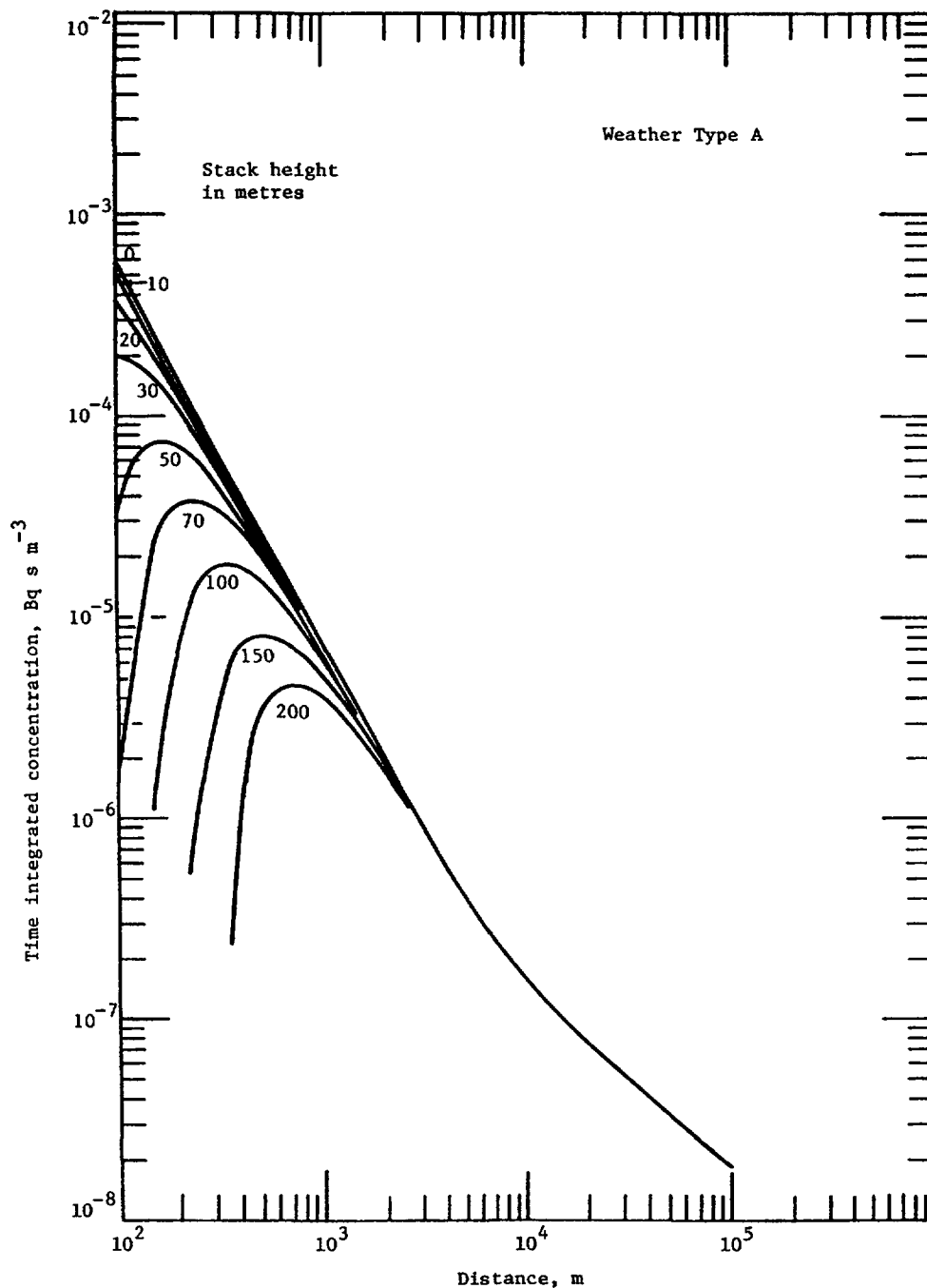
Figure 1. On-axis ground level time integrated concentrations
as a function of effective release height for a
short (30 min) release of unit activity in
Weather A conditions

Figure 1, taken from Ref. 5, gives the time integrated air concentration
for a 30 minute release in the worst weather conditions. It will be
seen that at 500m the concentration is 2.4×10^{-5} Ci s m^{-3} per Ci
released. The modifying factor for the longer release (2 hours) is
given in Ref. 5 as 0.76.

Thus the time integrated concentration at the site boundary for the actual
release is:

$$2.4 \times 10^{-5} \times 0.76 \times 10 \text{ Ci s m}^{-3}$$

182

Reference 6 gives the time integral concentration to produce a dose commitment of 30 rem to the thyroid as 0.043 Ci s m^{-3} for the child.

Thus the child dose due to the postulated release is:

$$\frac{2.4 \times 10^{-5} \times 0.76 \times 10 \times 30}{0.043} = 127 \text{ m rem}$$

4. Acceptability

The acceptability of the consequences calculated as indicated above may be assessed by comparison with the criteria adopted by the country or licensing body concerned. In the United Kingdom there are various criteria currently available. A basic requirement, based on ICRP recommendations, is that all radiation doses (both in routine operation and under emergency conditions) should be as low as reasonably achievable. In the case of accident conditions, various published criteria exists, for example, the Farmer criterion for acceptable releases (7) or the Kinchin criterion for acceptable consequences (8). In addition the Nuclear Installations Inspectorate have published their criteria (9) for requiring a detailed analysis and justification of operation. These are discussed in Appendix B-2.

References

1. Kaiser, A. D., et. al., "Environmental Transport and Consequence Analysis," ANS/ENS Topical Meeting on Risk Assessment, Port Chester, New York, September 1981.

2. Aldrich, D. C., et. al., "International Standard Problem for Consequence Modelling : Results," ANS/ENS Topical Meeting on Risk Assessment, Port Chester, New York, Septmber 1981.

3. Beattie, J. R. and Bell, G. C., "A Possible Standard of Risk for Large Accidental Releases," IAEA-SM-169/33.

4. Fryer, L. S., "A Guide to TIRION 4," SRD R 120 1978. United Kingdom Atomic Energy Authority.

5. Clarke, R. H., "A Model for Short and Medium Range Dispersion of Radionuclides Released to the Atmosphere," NRPB - Z91 1979.

6. Criteria for Controlling Radiation Doses to the Public After Accidental Escape of Radioactive Material, Medical Research Council (HMSO 1975).

7. Farmer, F. R., "Reactor Safety and Siting," Nuclear Safety 8(6) 1976.

8. Kinchin, G. H., "Design Criteria, Concepts and Features Important to Safety and Licensing," ANS/ENS International Meeting on Fast Reactor Safety Technology, August 19th-23rd, 1979, Seattle, Washington, U.S.A.

9. Safety Assessment Principles for Nuclear Power Reactors, HM Nuclear Installations Inspectorate, HMSO.

Appendix D-3

ESTIMATION OF RADIOLOGICAL DOSES
FROM RESEARCH REACTOR ACCIDENTS

J.N. ANOUSSIS, N.G. CHRYSOCHOIDES
Department of Reactors,
Democritos Nuclear Research Center,
Greek Atomic Energy Commission,
Athens, Greece

Abstract

A model for calculating radiological consequences from research reactor accidents is described. The model covers all steps of the chain, Source term + Air concentration of radioactivity + Absorbed dose and is purposely simple for use when additional computer codes are not available. All approximations used lie on the conservative side. Minimum necessary data required for the relevant calculations are also given. The Gaussian dispersion model is used for the air concentration of radioactivity and its conversion to dose is made by using the appropriate conversion factors for specific points of impact, radionuclides and exposure time intervals of interest.

The described model and methodology was already applied in the SAR example (Appendix E-6 of the present guidebook) with results in good agreement with the ones derived in similar cases.

1. INTRODUCTION

Although the accidents in research and test reactors are in many ways dissimilar, many of the models,methodologies and much of the data are commonly used for evaluating the radiological impact and consequences of the accidents. The general information providing estimated radiological doses for an individual remaining at specified points of impact and for various time intervals is presented in this paper.

The accidental airborne releases of radionuclides contribute to the following radiological doses. External whole body dose (gamma) due to submersion in the exhaust air plume (cloudshine), external whole body (gamma) dose due to the activity deposited on the ground (groundshine), internal irradiation originating from radionuclides inhaled with the air,resulting in both critical organ and whole

body doses, external β-radiation from the exhaust air plume (skin dose mainly) and internal irradiation due to consumption of contaminated food.

In order to determine the total dose of the whole body or of a certain critical organ the contributions of all relevant radionuclides via the exposure pathways have to be summed for the individual-receptor whom we consider a member of the critical group to quarantee more conservatism in the estimates.

In practice not all of the before-mentioned doses are important as far as their contribution to the total dose is concerned, as it will appear in the proceeding sections. The importance of doses and their relative significance strongly depends on the kind of accident considered, the fission products inventory of the core, the extent of fuel failure and hence the amount of radionuclides released to the atmosphere, the distribution of release rate, the meteorological conditions of the reactor region etc.

This report doesn't intend to give a complete analysis of the radiological consequences due to a reactor accident, but to provide the minimum necessary data and knowledge required for a rough estimation of doses through the prementioned ways that an individual may be exposed to irradiation, with emphasis on what is applicable to research and test reactors.

2. SOURCE TERMS

A fully detailed and precise calculation of the amount of fission products present in a reactor core lies out of the scope of this paper. A good number of computer codes calculate the activities of all fission product radionuclides as a function of irradiation time and also the activities at specific times after shutdown. Ref.$\overline{/1/}$ is a good example for such a code and refs $\overline{/2/}$,$\overline{/3/}$ are typical tables for fission product data.

An approximate formula giving the activity $A_i(t)$ of an isotope i at time t after the start of irradiation (t=0) whose fission yield isYand its decay constant is λ_i irradiated for time period T in P (Megawatts of thermal power) can be written $\overline{/4/}$ as :

$$A_i(t) = 0.82 \cdot Y.P. (1-e^{-\lambda i T}).e^{-\lambda_i(t-T)} \tag{1}$$

Realistic off-site radiological doses can be caused only by radionuclides with a high degree of mobility. The isotopic data

186

considered here is limited thus to noble gases and the volatile group which is likely to be released in significant quantities in the event of fuel melting, with halogens, Te, Cs and Sr being the most important contributors. From the non volatile group most isotopes are relatively involatile even at fuel melting and they are likely to be released in significant quantities in the event of fuel vaporization or in some cases by chemical reactions.

2.1 Assumptions for Radionuclide Release from the Reactor Building

If the fuel failure is subject to radionuclide transport directly to the air and actual data do not exist the following assumptions can be used.

(a) Iodines:Twenty-five percent of the equilibrium radioactive iodine inventory developed from maximum full power operation of the core are immediately available for leakage to the reactor building in the direct proportion to percent of fuel failure $/5/$, $/6/$.

(b) Noble gases: One hundred percent of the equilibrium radioactive noble gas invetory developed from maximum full power operation is immediately available for leakage to the reactor building in direct proportion to percent of fuel failure $/5/$,$/6/$

(c) Solid fission products:Less than 1% $/6/$.

From the above radionuclides hold up in the reactor,the leakage to the environment is possible taking into consideration the reduction due to radioactive decay during hold up and the reduction due to Engineered Safety Features. The reactor building leaks at the leak rate incorporated in the technical specifications for the duration of the accident.

2.2 Realistic Mode of Release of Radioactive Effluents

In most accidentsin research reactors the radioactive effluents will be released to atmosphere through the stack after passing the appropriate filters in a specified air flow rate provided by the emergency ventilation system. This flow rate is suitably converted to a reactor building leak rate,λ_L.

Suppose the reactor building inventory for an isotope i is $C_i(t)$ (Curies), its decay constant is λ_i and $C_i(o) = C_{io}$ at t =0. It is obvious that,

$$\frac{dC_i(t)}{dt} = -\lambda_i C_i(t) - \lambda_L C_i(t)$$

the solution of which is ,

$$C_i(t) = C_{io} \, e^{-(\lambda_i + \lambda_L)t}$$

The release rate from the reactor building is $Q_i'(t) = \lambda_L C_i(t)$. The radioactivity released in time interval (t_1, t_2) is then,

$$Q_i(t_1, t_2) = \int_{t_1}^{t_2} Q_i'(t)dt = \int_{t_1}^{t_2} \lambda_L C_{io} \, e^{-(\lambda_i + \lambda_L)t} \, dt =$$

$$= \frac{\lambda_L C_{io}}{\lambda_i + \lambda_L} \cdot \{ e^{-(\lambda_i + \lambda_L)t_1} - e^{-(\lambda_i + \lambda_L)t_2} \} \qquad (2)$$

This activity will be reduced due to Engineered Safety Features (eg. filters) as before mentioned.

3. EXTERNAL CLOUD DOSE

3.1 Gama Dose

The dose rate to air over a point submerged in an infinite radioactive cloud can be derived using the energy argument that the amount of energy produced per unit volume must be equal to the amount absorbed per unit volume. This is true when the dimensions of the cloud are much greater than the relaxation length of gammas.

Application of the energy argument yields for the gamma dose rate D_γ' in air /4/,

$$\gamma \, D_{air}' = \frac{X \, (3.7 \times 10^{10}) \, \overline{E}_\gamma \, (1.6 \times 10^{-6})}{1293.100} \quad \left(\frac{rad}{sec}\right) \qquad (3)$$

where

$\overline{E}_\gamma$: average gamma energy per disintegration $\left(\frac{MeV}{dis}\right)$

1.6×10^{-6} = erg/MeV

X = Concentration of gamma emitter in air $\left(\frac{Ci}{m^3}\right)$

$3.7 \times 10^{10} = \frac{dis}{Ci.sec}$, $1293 = \frac{gr}{m^3}$ of air and $100 \frac{erg}{gr.rad}$

188

At ground level the dose rate to air amounts to $\frac{1}{2}$ of the above gamma dose rate (because the cloud occupies the infinite half-space above the ground level). To convert this to dose rate to tissue multiplication by 1.11 is required to account for higher electron densities in tissues than in air /4/.

Thus, for a receptor at ground level taken into consideration that rad=rem for γ' s, the gamma dose rate eventually becomes,

$$\dot{D}'_\gamma = 0.25 \ \overline{E}_\gamma \ \dot{X} \ (\frac{rem}{sec}) \tag{4}$$

and if the receptor remains exposed for time τ

$$D_\gamma = 0.25 . \ \overline{E}_\gamma \ \int_0^\tau \dot{X} dt \ (rem) \tag{5}$$

The appropriate $\overline{E}_\gamma$ is given in Ref./7/. For $\dot{X}$ calculation at ground level it is assumed that the exhaust plume will diffuse both laterally and vertically in a Gaussian distribution and at first a complete reflection will occur on the ground.

3.2. Activity Concentration in Air from a Continuous Short Release (less than 2 hrs)

Activity Concentration in the air at place (x,y,z) can be calculated /8/, /9/, /10/ from:

$$X_{(x,y,z)} = \frac{Q'}{2\pi\sigma_y\sigma_z\overline{u}} \ e^{-\frac{y^2}{2\sigma_y^2}} \ \left[e^{-\frac{(z-h)^2}{2\sigma_z^2}} + e^{-\frac{(z+h)^2}{2 \ \sigma_z^2}} \right] \tag{6}$$

where,

x,y,z : Cartesian coordinates in the diffusion direction (x) as well as perpendicular to the direction of diffusion, horizontally (y) and vertically (z).

Q' : emission source strength (Ci/sec)

$\overline{u}$: mean wind speed (m/sec)

h : effective emmission height (m)

σ_y,σ_z : horizontal and vertical standard deviation of material in the plume (m).

The centerline near- to-ground activity concentration is obtained from equation (6) for $y = z = 0$

$$X_{(x,0,0)} = \frac{Q'}{\pi \bar{u} \sigma_y \sigma_z} \; e^{-\frac{h^2}{2\sigma_z^2}} \tag{7}$$

The quantity X/Q' (effluent concentration/source strength) in $\frac{sec}{m^3}$ usually called, dilution factor, can be calculated from eq. (7) for a given wind speed effective emission height, and σ_y, σ_z which depend on source distance x, weather stability and emission height h. σ_y and σ_z can be found on Fig. A.2, A.3 /9/ as function of weather stability, source distance and emission height.

The time integrated concentration X_{INT} in $Ci-sec/m^3$ over a period of time $\tau < 2h$ is obtained from Eq. (7).

$$X_{INT} = \int_\tau X_{(x,0,0)} dt = \frac{Q}{\pi \sigma_y \sigma_z \bar{u}} \; e^{-\frac{h^2}{2\sigma_z^2}} \tag{8}$$

where,

$$Q = \int_\tau Q' dt \tag{9}$$

The time integrated near- to-ground concentration under the diffusion axis $(y=z=0)$ related to the unit of the released activity i.e.

$$X_{INT}/Q = \frac{1}{\pi \sigma_y \sigma_z \bar{u}} \; e^{-\frac{h^2}{2\sigma_z^2}} \tag{10}$$

is defined as short- term average diffusion (or dilution) factor $(\frac{sec}{m^3})$ in time interval τ and can be used for emissions in time τ in the event of constant meteorological conditions.

3.3 Gamma Dose Due to a Continuous Short-term Release

Substitution of eq. (10) into eq. (5) yields the total whole body gamma dose received by an individual immersed in a semi-infinite plume of uniform cocnentration in time τ.

190

$$_\gamma D = 0.25 \; \bar{E}_\gamma (X_{INT}/Q)_\tau \int_\tau Q'dt \qquad (11)$$

Summing the total released activities over all isotopes the total gamma dose received over τ is given as,

$$_\gamma D(\tau) = 0.25 \; (X_{INT}/Q)_\tau \; \sum_i \; \bar{E}_{\gamma_i} \; Q(\tau)_i \qquad (12)$$

Where

$D_\gamma(\tau)$: whole body gamma dose over τ (rem)

(X_{INT}/Q): atmospheric dispersion factor over τ (sec/m^3)

$Q(\tau)_i$: total activity of isotope i, released in τ (Curies)

To select the appropriate X_{INT}/Q value for the aforementioned calculations two methods are commonly used.

(a) If there is adequate on-site meteorological data statistical distributions of atmospheric dispersion may be deduced from data accumulated. For time periods of interest, τ, cumulative distributions may be prepared and X_{INT}/Q not exceeded X-percent of the time can be selected. It is a matter of scientific judgment to decide which per cent can be considered conservative for max. consequences in an accident and which is realistic specially for long term releases.

(b) Lacking Site Specific data, conservative estimates of atmospheric dispersion are recommended in refs /5/ and /11/ for different time periods of interest up to 1 month.

3.4 Gamma Dose due to a Continuous Long Term Release

For a long term release (time period greater than 2 hr but less than 24 hrs) the plume should be assumed to meander and spread uniformly over a sector of φ radians. X_{INT}/Q value of plume centerline at ground level is now /9/.

$$X_{INT}/Q = \frac{(2/\pi)^{1/2}}{x\bar{u}\varphi\sigma_z} \; e^{-\frac{h^2}{2\sigma_z^2}} \qquad (13)$$

where: x = distance from emission point to receptor (m)

For $\varphi = \frac{2\pi}{16}$ radians $= 22.5^{0*}$ /11/ eq. 13 becomes

$$X_{INT}/Q = \frac{2.032}{x.\bar{u}\sigma_z} \; e^{-\frac{h^2}{2\sigma_z^2}} \qquad (14)$$

$X_{INT/Q}$ can be calculated from eq. (14) for a given wind speed, emission height, distance from the source. Again, σ_z from ref. /9/ if the weather stability is known.

Ref./5/ recommends diffusion parameters (Pasquill condition F, wind speed $1m$ /sec variable direction within a 22.5^0 sector) and for periods exceeding 24 hr (1-4 days) it recommends less conservative atmospheric parameters to be used and even less for periods greater than 4 days.

Thus, The Whole Body Gamma Dose for a long period release T, can be calculated from eq. (12) modified as,

$$_{\gamma}D(T) = 0.25 \sum_j (X/Q)_j \sum_i \bar{E}_{\gamma_i} Q_{ij} \qquad (15)$$

where:

$(X/Q)_j$: average atmospheric dilution factor during the jth time interval (sec/m^3).

Q_{ij} : equivalent release of nuclide i during the jth time interval (Curies).

Other symbols as before mentioned.

3.5 Distribution of Gamma Dose to Organs

If it is desired to know how the external gamma dose due to immersion in an infinite cloud is distributed to various organs of interest, refs /13/ and /14/ contain suitable tables to convert the activity concentration of photons in a cloud to doses absorbed by 22 different organs of the human body. This conversion is also possible in the case of exposure in a contaminated ground, which will be considered in Section 5.

---

* 16 corresponds to the main wind directions. Ref. /12/ recommends 12 directions and hence an aperture angle of 30^0.

3.6 Beta Dose Estimation

The beta dose (mainly surface or skin dose) due to the exposure of an individual in the semi- infinite cloud of beta emitters for time T is derived similarly as in the gamma dose case

$$_\beta D(T) = 0.23 \sum_j (X/Q)_j \sum_i \bar{E}_{\beta_i} Q_{ij} \qquad (16)$$

where,

$\bar{E}_\beta$: average beta energy per disintegration $(\frac{MeV}{dis})$

other symbols as before mentioned.

Appropriate values for $\bar{E}_\beta$ are given is Ref. /7/.

3.7 Comments on External Cloud Dose

Equations derived for external dose due to immersion in a radioactive cloud were based on the semi-infinite cloud model. If the dimensions of the cloud are small compared to the range of gamma rays in air, the doses are smaller than those estimated before. If corrections are desired to be made, correction factors whose values depend on the dimension of the cloud, expressed in σ_z and z, must be used. The method of calculation is described in /2/ where also a table of finite-cloud dose correction factors can be found.

Eqs (5), (12), (15) and (16) were used to give the external dose. If all parameters except integrated concentration $(\frac{Ci-s}{m^3})$ are lumped together they can constitute a dose conversion factor (rem per $\frac{Ci-sec}{m^3}$) for immersion in contaminated air. So external dose is estimated by multiplying the integrated concentration by the appropriate dose conversion factor for the radionuclide of interest (Tables in refs /2/ /12/ /13/).

The most important contribution to the external cloud dose are the Krypton and Xenon isotopes and especially Kr-83m, Kr-85m, Kr-87, Kr-88, Xe-131m, Xe-133m, Xe- 133, Xe-135, Xe- 135m.

Information for determining the effective emission (stack) height from the actual height is provided in App. B /5/.

When the emission height is smaller than 2.5 times the building height, the building wake effect must be taken into consideration by substituting /5/ Σ_y and Σ_z for σ_y and σ_z respectively everywhere σ_y and σ_z appear is the before mentioned equations.

$$\Sigma_y: \quad (\sigma_y^2 + CA/\pi)^{1/2}$$

$$\Sigma_z: \quad (\sigma_z^2 + CA/\pi)^{1/2}$$

C : .5 arbitrary constant

A : building cross section normal to wind (m^2)

The emission height may be set equal to zero. /5/

4. INTERNAL (INHALATION) DOSE

4.1 Thyroid Dose due to Inhalation of Contaminated Air

The relation given in Vol. I. App. F-1 of the present guidebook for the Thyroid dose calculation is modified for not constant dispersion parameters during the inhalation time period of interest T,

$$_{Thyr}D(T) = \sum_j R_j \, (X_{INT/Q})_j \sum_i Q_{ij} \, (CF)_i \quad (rem) \tag{17}$$

where

R_j :average breathing rate during the time interval j $(\frac{m^3}{sec})$

$(CF)_i$:dose conversion factor for isotope i $(\frac{rem}{Ci})$

  other symbols as already used.

Breathing rates can be taken from ref. /15/, while suitable tables for dose conversion factors in rems per Ci inhaled can be found for example in references /2/, /12/, /16/ .

The integration time in such tables is usually a 50 year period, so what is actually calculated is the dose commitment to thyroid for the inhaled activity.

It is adequate to consider only iodines, being the important contributions to thyroid dose through the pathway of inhalation in a reactor accident.

4.2 Doses to other Organs than Thyroid

The same form of eq. (17) can be used for the dose to any organ due to inhalation of an isotope, by using the appropriate dose conversion factor, again provided by refs /2/ /12/ and /16/, in which the dose conversion factor of radionuclides is given apart for the various organs of interest also for the whole body dose. Here, again, dose commitment are considered.

194

From health physics point of view important radionuclides in a research reactor accident Sr-89, Sr-90, Ce-144 (bones and lungs) and Cs-137 (whole body) can be considered.

4.3 Conversion of Organ Doses to Whole Body Ones

If it is desired to convert the doses of the various organs of the human body to an equivalent whole body dose which would give the same health risk, the weighting factors recommended by ICRP /17/ should be used. An effective whole body dose is thus derived which is the sum of the weighted doses of the organs under consideration.

5. GROUND DEPOSITION DOSE

5.1 Whole Body Gamma Dose

The isotopes assumed as contributing predominantly to the gamma dose due to external irradiation from a contaminated ground plane, are the iodines. In dry weather the rate at which an isotope deposits on the ground is proportional to its concentration in the cloud /8/.

$$\omega = \upsilon_g \cdot X \qquad (18)$$

where,

ω : activity deposition rate $(Ci/m^2 . sec)$

υ_g : ground deposition velocity $(\frac{m}{sec})$

X : concentration of isotope in the cloud $(\frac{Ci}{m^3})$

The rate of change of accumulated activity, R, equals the deposition rate minus the elimination rate,

$$\frac{dR}{dt} = \omega - \lambda_e R \qquad (19)$$

where,

λ_e : elimination constant $= \lambda_f + \lambda_i$

λ_i : decay constant due to radiological decay.

λ_f : decay constant due to other processes.

195

For deposition onto foliage that leads to an ingestion dose, λ_f correspond to a half life of about 14 /8/ days because of weathering or dilution by new plant growth. For ground deposition, λ_f can be considered insignificant, to be on the conservative side.

The solution of eq. (19) if at t = 0 R = 0, is:

$$R_\tau = \frac{\omega}{\lambda_e} \ (1- e^{-\lambda}e^\tau)$$ (20)

Eq. (20) yields the accumulated activity in $\frac{Ci}{m^2}$ on the ground in time interval τ.

In equilibrium (rate of production provided by constant deposition equals the decay rate), the saturated accumulated activity Rs in time τ is

$$R_s = \frac{\omega}{\lambda_e} = \frac{(X/Q)_\tau Q_\iota U_g}{\lambda_e}$$ (21)

where,

Q_τ : released activity in time τ

$(X/Q)_\tau$: average dilution factor in time interval τ

Computation of external whole body dose $_dD$ from deposited radionuclides is performed assuming a uniform semi-infinite plane source:

$$_dD = R_\tau \ Fd$$ (22)

where, Fd is the dose conversion factor in mrem/hr per Ci/m^2. Fd is derived for the various isotopes from a consideration of the dose rate to air, 1 meter above the ground plane and the penetration of the radiation into the body. The total body dose is computed at a penetration depth of 5 cm (beta or skin dose at a depth of $7mg/cm^2$). Tables of Fd for the various isotopes is given in refs /16/(Table E-6,/13/ and also in ref /4/ for 1 and 7 days of exposure.

Values for U_g have been listed by Slade /9/ Typical U_g for elementary iodines is 10^{-2} m/sec while corresponding U_g for the organically bound iodine is two orders of magnitude smaller /12/.

196

5.2 Beta (Skin) Dose

Eq. (22) can also give   the beta (or skin) dose provided the right dose conversion factors for beta emitting isotopes are used. Refs /16/ and /13/ include values of dose conversion factors also for this kind of exposure.

Ref. /13/ calculates dose conversion factors (for photons only) for 22 body organs of interest from irradiation from a contaminated ground.

5.3 Internal Dose from Contaminated Food

Appropriate dose factors /2/, /12/, /16/ convert the activity ingested to dos commitment for each radionuclide of interest. But to estimate the activity ingested by contaminated food or water, many specific factors as local feeding habits, time of the year, consumption of food etc. should be taken into consideration and the way of calculation is not of a general nature. It lies, therefore, out of the scope of this paper.

6. COMMENTS CONCERNING ALL PREMENTIONED DOSES

6.1 Depletion of Radioactive Cloud

In all dose calculations of preceding sections no depletion of radioactive cloud was taken into consideration during the transit of the plume from emission point to the receptor. Although this omission leads to more conservative results, for a more precise calculation cloud depletion will be required to be considered. The cloud depletion can be due to:

a) Radioactive decay*   in transit. By using an average wind speed $\bar{u}$, the concentration of the isotope i at a distance x will be modified by exp $(-\lambda_i \frac{x}{\bar{u}})$

b) Dry deposition.   The cloud is depleted due to dry fallout and the fraction, f, of the cloud remaining airbone at distance x downwind is /4/

$$f = \exp\left[- \frac{u_g}{\bar{u}} (\frac{2}{\pi})^1/_2 \quad \sigma_z^{-1} \exp{(-\frac{h^2}{2\sigma_z^2})}\right] \qquad (23)$$

where all symbols as already used.

---

* Radioactive decay was taken into account during the release time only (eq. 2), and while the radionuclides were confined into the reactor building.

c) __Wet deposition:__   The depletion of cloud activity due to
rainout is difficult to quantify precisely.

A simple way of handling /4/ gives

$$f = exp \left[- W (t- t_0) \right]$$ (24)

where

   W   : washout coefficient $(\frac{m}{sec})$

   $(t-t_0)$:time elapsed since the onset of precipitation.

6.2 Relative Significance of Doses

The cloud dose(including the external gamma dose received over the
whole body from gamma- emitters, skin dose from beta emitters and internal dose
from inhaling radionuclides as the cloud passes) constitutes the early
exposure and dominates in determining the consequences in terms of radiation
illness or number of fatalities, if any, that will result from a research
reactor accident.

The chronic exposure due to ground contamination caused by settling
of radioisotopes from the passing cloud, is much less important than the early
exposure, but since if may last for years in case of long-lived isotopes it
may became very significant, when the dose is delivered over a long period of time

For a research reactor accident, however, the radioactive inventory
is not such that would create very severe deposition on one hand and on the
other ample time often would be available so that this kind of exposure
should be controlled by evacuation from contaminated areas and by
decontamination measures, which will mitigate the consequences drastically.
Th ese arguments apply even more for doses received from the ingestion of
contaminated food and water due to deposition of radioactive elements on
foliage or water and from inhalation from resuspended aerosol particles.

6.3 Collective (Population) Dose

The doses which were derived in preceding sections   must now
be calculated for distances of interest. A short time (2 hr)   dose
at exlusion   zone boundaries will be necessary (for evacuation
procedure purposes) and integrated long time doses at specific distances
of the low population zone. (Vol. I, App. F-1 of the present guidebook).

For a complete assessment of the consequences, in terms of health
effects on population surrounding the reactor site, the collective dose
D_{col} (in man-rem) must be estimated.

198

$$\text{Col}^D = \sum_{N=1}^{16} \sum_{x=0}^{r} \text{Dx.POP}_{x,N} \cdot f_N \qquad (25)$$

where,

Dx   : Dose at given distance x

r   : Desired upper limit of distance considered

$\text{POP}_{x,N}$: number ot people living at distance x in sector N of aperture angie $\varphi = 22,5^o$

f_N : fraction of time the wind blows toward sector N.

Eq. (25) can b e now treated by the appropriate dose-risk relationship to give number ot different health effects to be considered.

REFERENCES

/1/ ORIGEN-/9 "Isotope Generation and Depletion Code - Matrix Exponential Method" ccc-217. Oak Ridge National Laboratory, Radiation Shielding Information Center (Sept'79).

/2/ U.S. NRC "Reactor Safety Study" WASH-1400 (NUREG 75/104) App. VI, 1975.

/3/ J.R. Beattie "An Assessment of Environmental Hazards from Fission Product Releases", U.K. Atom. Energy Author.Rep., AHSB (5), R-64, 1961.

/4/ E. Lewis "Nuclear Power Reactor Safety", Wiley Interscience, 1977.

/5/ American National Standard, Research Reactor Site Evaluation ANSI/ANS-15.7 1977 (N379).

/6/ J.J.DiNunno F.D. Anderson, R.E. Baker, R.L. Waterfield "Calculation of Distance Factors for Power and Test Reactor Sites" TID-14844 U.S.A.E.C., 1962.

/7/ Table of Isotopes, Sixth Edition by C.M. Lederer, J.M. Hollander, I. Perlman, University of Calif., Lawrence Rad. Lab. 1966.

/8/ J.R. Lamarsh "Introduction to Nuclear Engineering"Addison-Wesley Publishing Company, 1975.

/9/ D.L. Slade (Ed) "Meteorology and Atomic Energy"U.S. AEC Report, TID-24190 1968.

/10/ IAEA-SS-No 50-5 G-53 "Atmospheric Dispersion in Nuclear Power Plant Siting", Safety Guide 1980

/11/Regulatory Guide 1.3 Rev. 2 "Assumptions Used for Evaluating the
Potential Radiological Consequences of a Loss of Coolant Accident for
B.W.R."U.S.A.E.C., 1974.

/12/Allgemeine Berechnungsgrundlage für die Strahlenesposition bei
Radioaktiven Ableitungen mit der Abluft oder in Oberflächengewässer"
Rd. Schr. de BMI v. 15.8.79-RS II 2-515603/2.

/13/D.C. Kocher "Dose-Rate Conversion Factors for External Exposure to
Photon and Electron Radiation from Radionuclides Occuring in Routine Releases
from Nuclear Fuel Cycle Facilities"Health Physics Vol. 38, 1980.

/14/J.W. Poston and W.S. Snyder "A Model for Exposure to Semi-infinite Cloud
of a Photon Emitter"Health Physics V. 26, 1974.

/15/ ICRP 23 "Report of the Task Group on Reference Man"Pergamon Press 1975.

/16/ Calculation of Annual Doses to Man from Routine Releases of Reactor
Effluents for the Purpose of Evaluating Compliance with Part 50" App.I.,
Regulatory Guide 109, Rev. 1 USNRC, 1977.

/17/ ICRP Publication 26 "Recommendations of the International Commission
on Radiological Protection (1977).

RADIOLOGICAL CONSEQUENCE ANALYSIS
FOR A HIGH POWER CANADIAN RESEARCH REACTOR

D.J. AXFORD
Chalk River Nuclear Laboratories,
Atomic Energy of Canada Limited,
Chalk River, Ontario,
Canada

Abstract

Some of the factors to be considered in a radiological consequence analysis for a high power Canadian research reactor are described. Methods of determining the inventory of fission products and some of the factors affecting the fission product release are considered. Atmospheric dispersion factors are also described. Simple formulae and correction factors are given for calculating whole body external doses for gamma radiation from a cloud of noble gas fission products.

1. INTRODUCTION

In order to evaluate the effectiveness of the fission product cleanup system and to place an upper limit on the maximum potential for exposure of both members of the public and personnel on site, a number of accidents are postulated which release significant fractions of the inventory of fission products from the reactor core or from individual fuel assemblies. Most of these accidents would require a chain of several failures with a very low overall probability of occurrence. Some of these incidents are historical in nature and are considered even though modifications have been made to systems to prevent a recurrence with the result that the probability of a similar accident occurring is very remote.

Many research reactors are housed in either a standard industrial building or a special low leakage industrial building which is exhausted through a fission product cleanup system to a reactor exhaust stack - often referred to as a vented containment. For normal operations the building would have a fairly high rate of exhaust with the airflow being directed from areas of potentially low contamination levels to areas of progressively higher levels of contamination. Airflow would normally be into the building through leakage and in most cases inlet fans supply conditioned air to the building. In the event of an accident the building supply fans would be stopped and the exhaust fans would exhaust any released radioactivity through the fission product cleanup system to atmosphere. In some cases the entire exhaust flow passes through the fission product cleanup system. In other cases an emergency ventilation and fission product cleanup system would be activated by high radiation levels and automatically placed on line at a reduced flowrate. The small quantities passing through the cleanup system would be dispersed in the atmosphere by the reactor stack.

The time for one building air change through the fission product cleanup system will vary for each reactor and could be from a few minutes to a few hours. The duration of the fission product release is assumed to be similar. Many accident analyses also consider the additional consequences of a coincident failure of the ventilation system. In this case fission products could be released at ground level over a similar period of time depending upon the building design.

The calculation of the radiological consequences of a postulated accident involves the determination of the fission product inventory, the release from the fuel, the calculation of the time dependent release from the reactor building, atmospheric dispersion, and the resultant individual and population doses received as a result of the release of radionuclides.

2. INVENTORY OF FISSION PRODUCTS

For each specific accident considered in the consequence analysis the inventory of fission products in the reactor core or the fuel assembly would be determined. This can be done with the aid of a computer program such as FISSPROD-2 [1] or any other suitable computer code. The most significant radionuclides are normally the radioiodines and the noble gases. However, the significance of any postulated releases of other fission products such as cesium or strontium would have to be examined to confirm this conclusion. In addition for a heavy water reactor the potential doses from any release of tritium would have to be reviewed. For the radioiodines, normal practice is to consider only the Iodine-131 and apply a factor of two to account for the other radioiodines and tellurium. The most important noble gases usually considered are Kr-85m, Kr-87, Kr-88, Xe-133 and Xe-135. Other noble gas fission products have either a very short half life in terms of transport times to the exposed individual or they have a very low gamma energy for whole body irradiation. Despite the fact that some of the specific radionuclides are skin limiting the total external exposure is usually whole body limiting and it is normal practice in an accident analysis to neglect skin doses.

3. FISSION PRODUCT RELEASE

The fractional release of fission products from the fuel element or reactor core will be dependent on various factors such as the type of fuel and the cladding as well as the type of accident postulated. The subsequent release to the reactor building will be dependent upon the transport mechanisms within the primary cooling system for a whole core incident. Radioiodines will plateout on various surfaces both in the primary cooling system piping and within the building. In many accidents where the release is associated with water most of the radioiodines will be dissolved in the water. The remainder will be largely removed by the fission product cleanup system. The chemical form of the radioiodines would be taken into account in determining the amount of plateout and dissolution and of the efficiency of the charcoal adsorbers in the fission product cleanup system. The bulk of the noble gases released from the fuel will be transported by the building ventilation system to the reactor stack and be dispersed in the atmosphere.
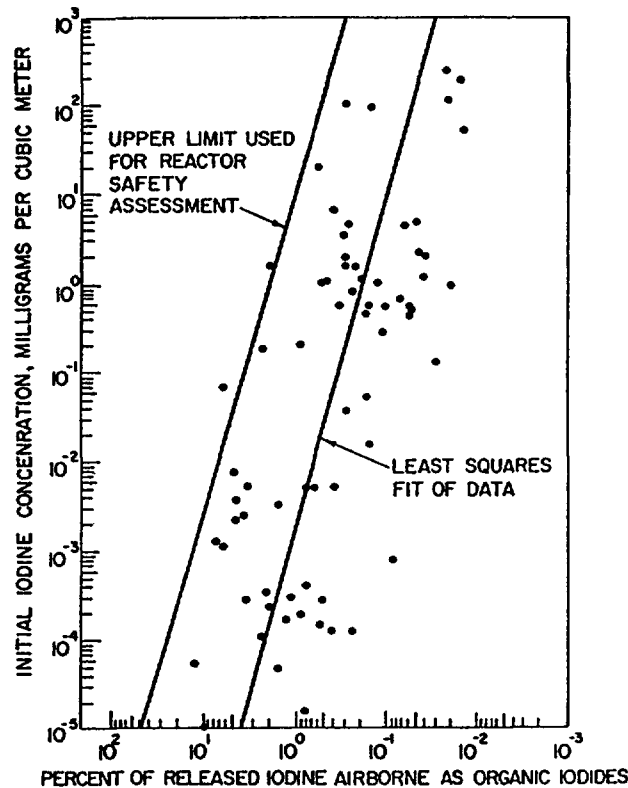
FIG. I ORGANIC IODIDE FORMATION FOLLOWING IODINE RELEASE UNDER CONDITIONS RELATING TO LOCA FOR WATER COOLED REACTORS

3.1 Chemical Form of Radioiodines

The penetrating forms of radioiodine likely to occur in the reactor building atmosphere following an accident are inorganic hypoiodous acid (HOI) and organic (predominantly CH_3I) compounds. Considerable experimental and theoretical work has been done in the US and the UK to study the formation mechanism of organic iodides and determine the percent conversion of the elemental iodine to CH_3I under accident conditions and this mechanism is relatively well understood. The mechanisms for the formation of HOI are not as well understood however it is likely that the large scale containment experiments conducted in the US did in fact include all forms of penetrating iodine in the measurements made. This data has been summarized by Postma and Zavadoski [2] and is shown in Figure 1. The percentage formation of penetrating forms of radioiodine is taken from the upper limit of all the data which is about an order of magnitude greater than the least squares fit of the data. For specific cases where very high radiation fields are present the radiolytic formation of penetrating forms of radioiodine would also have to be considered but this is not normally the case for a research reactor.

3.2 Radioiodine Removal Processes

The plateout of elemental radioiodine on the reactor building surfaces may be significant depending on the building exhaust rate. Plateout is a time dependent process with an exponential removal half life that ranges from a few minutes to a few hours. This safely applies down to an atmospheric concentration of about 1% of the initial concentration.

203

Plateout of organic iodides is not significant. Various models are available for determining plateout half life.

Data for iodine partition in water when the release occurs under water is well known. Values ranging from 96 to 99% retention of radioiodine in the water are commonly assumed.

The efficiency of the charcoal adsorbers for both elemental and penetrating forms of radioiodine is also well known and several methods of specifying conservative values are used. Typically a properly designed adsorber with a 5 cm thick bed of activated charcoal would be expected to remove in excess of 99% of both the elemental and penetrating forms of radioiodine.

4. ATMOSPHERIC DISPERSION

Airborne radionuclides released to the atmosphere will disperse due to the effects of atmospheric turbulence and advective transport. The amount of dispersion depends, amongst other things, on the meteorological conditions, duration of the release, height of release, building wake effects, the buoyancy of the airborne effluent, and on the distance downwind. The standard Gaussian distribution is used to determine the concentration in the cloud using the simplified method proposed by Pasquill [3] or some other model such as proposed by Smith [4], Hosker [5], or Slade [6].

4.1 Meteorological Conditions

For an accidental release into the atmosphere the worst weather conditions occurring 10% of the time are assumed or if this is not known meteorological dispersion that is equivalent to stable Pasquill category F as modified by Bryant [7] is assumed [8]. In considering individuals at locations relatively close to an elevated release point the worst situation would occur during unstable weather such as Pasquill category A/B conditions and this would be used in the assessment. It is assumed that the weather condition persists for the duration of the release which as noted above could be from a few minutes to a few hours.

4.2 Effective Stack Height

The effective stack height is determined by considering downwash and entrainment effects and buoyancy and momentum rise due to efflux velocity. The elevation of the point of interest must also be considered.

When the release is from a stack, some of the emitted material can be drawn downward into the low pressure region on the lee side of the stack. This effect, called downwash, is noticeable when the efflux velocity is comparable to or smaller than the mean windspeed [9]. Another change in the height of the release is due to the fact that the discharged effluent might be caught in the aerodynamic cavity on the lee side of nearby buildings. When the effective release height is less than 1.5 times the height of nearby buildings no credit is taken for the stack. When the release height is between 1.5 and 2.5 times the height of nearby buildings the effective stack height is reduced by the method given by Bryant [7]. For release heights greater than this no correction is made.

Plume rise is a function of both buoyancy and momentum. For hot stacks where emissions are warmer than about 50°C, buoyancy is an important factor and can be determined by the method given by Bryant [7] or Slinn [11]. For cold stacks where the effluent is discharged at an appreciable velocity the momentum effects are usually the most important and in many instances for tall reactor exhaust stacks dominate the other effects.

The other major factor to consider is the elevation of the stack in relation to the boundary especially for sites located in hilly terrain. A conservative correction for stack height can be made by direct subtraction of the height difference [7].

4.3   Building Wake Effects

When the release height is less than 1.5 times the height of nearby buildings which are located closer to the release point than 3 times the height of the buildings, the assumption is made that the effluent will be caught in the turbulent wake downwind of the buildings [9]. This turbulent wake has the effect of creating a volume source rather than a point source. Various methods of accounting for this effect are given by Barry [10], and Slade [6]. When the release height is greater than 2.5 times the height of adjacent buildings the effect can be safely ignored. For release heights in between a smooth extrapolation as given by Bryant [7,9] is acceptable.

5.   DOSE CALCULATION

The radiation dose to the operating staff, to the most exposed non-operating person on-site, to a person situated at the boundary, and to the person most at risk living in the nearest dwelling is estimated for each of the accidents. Operational emergency procedures are in place to ensure that operational doses are kept to a minimum for any postulated severe accident sequence. Each high power research reactor has an exclusion boundary within which public access is limited. In addition, because of local topography an individual remote from the boundary may be most at risk. The dose assessment model assumes that on-site emergency stay-in and evacuation procedures are put in effect to minimize on-site doses but assumes that no off-site dose reduction procedures are followed in time to reduce the exposure from the passing cloud of fission products. The dose contribution received from inhabiting contaminated areas off-site or from ingestion of contaminated milk or foods is not normally included as appropriate procedures would be put into effect to alleviate these effects by evacuation of personnel or confiscating the contaminated foods subsequent to passage of the cloud of radionuclides.

5.1   Dose Conversion Factors

Whole body external doses for gamma radiation from a cloud of noble gas fission products can be derived from the relationship

$$D_\gamma i = 0.25 \ \overline{E}_\gamma \ \Psi$$

where $\underline{D}_\gamma i$ is the gamma dose in rem to an individual,
$\overline{E}_\gamma$ is the average energy per disintegration in MeV, and
Ψ is the exposure in Ci·s/m^3.
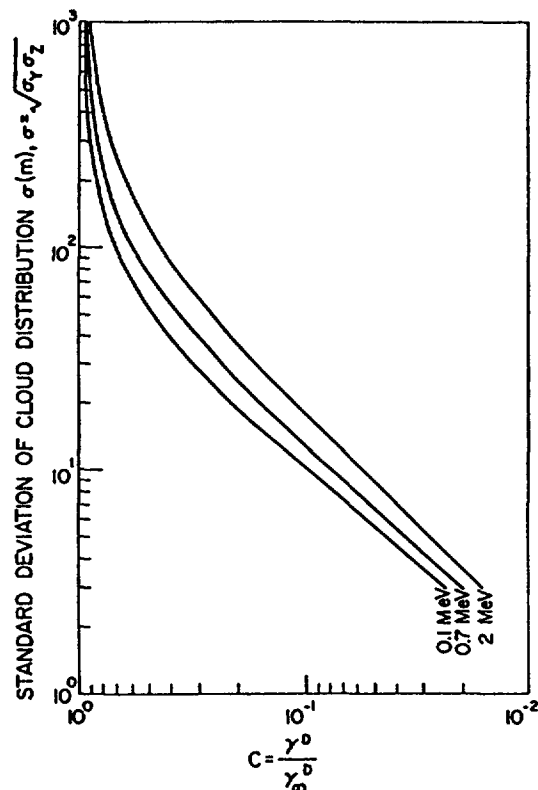
FIG. 2 RATIO OF GAMMA DOSE AT CENTRE LINE IN A
FINITE CLOUD OF GAMMA-EMITTING RADIONUCLIDES TO
AN INFINITE CLOUD WITH THE SAME CENTRE LINE
CONCENTRATIONS (REF. 9)

This relationship assumes a semi-infinite cloud at ground level and a substantial correction factor, $C = \gamma^D/\gamma^D_\infty$, can be applied to account for the finite dimensions of the cloud close to the release point. Thus the relationship for calculating individual(i) gamma doses from a finite cloud of passing gaseous fission products is $D_\gamma i = 0.25 \bar{E}_\gamma \psi C$. Values for this correction factor are given in Figure 2. Values for the lateral σy and vertical σz standard deviation of the cloud dimensions can be obtained from the specific Gaussian distribution model used in the calculation. For the population dose calculation this whole body dose is summed over the population extending out to the point where the individual dose is 1% of the boundary dose (b). In this calculation an additional correction factor must be applied to correct for those off the centreline of the passing cloud. Thus the relationship for calculating the population (p) gamma dose is

$$D_\gamma p = 0.25 \sum_{D_\gamma i \text{ at } b}^{D_\gamma i \text{ to } 1\%b} \bar{E}_\gamma \psi C^1$$

where C^1 is the combined correction factor for the finite dimensions of the cloud and the location of the receptor in relation to the centreline of the plume. Values of C^1 for an average noble gas energy of 0.7 MeV are given in Figure 3.

Thyroid doses are calculated for both infants and adults using the following dose conversion factors based on the integrated cloud concentration [9]. These doses are for Iodine-131 and include the contribution from the other isotopes of iodine and tellurium.

206
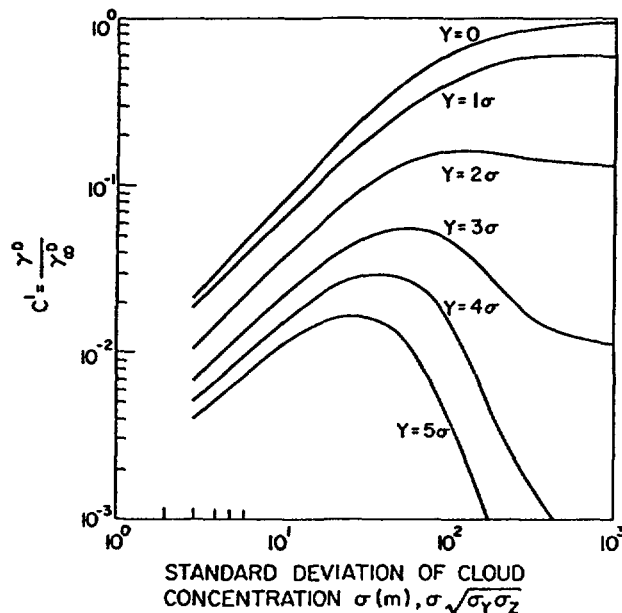
FIG. 3 RATIO OF THE GAMMA DOSE AT ANY LOCATION
IN A FINITE CLOUD TO THE GAMMA DOSE IN AN
INFINITE CLOUD FOR 0.7 MeV GAMMA PHOTONS (REF. 9

1 Ci·s/m^3 = 1630 rem infant

1 Ci·s/m^3 = 552 rem adult

1 Ci·s/m^3 = 726 rem average population dose based on the
projected Canadian population distribution for the year 2000.

The whole body dose conversion factor for the release of tritiated
water vapour is 1 Ci·s/m^3 = 42 mrem [9]. This includes the contribution
from inhalation plus the amount absorbed through the skin from immersion in
the cloud. The population dose would be calculated in a similar manner to
that for noble gases.

Dose conversion factors for other radionuclides can be obtained
from the draft CSA standard if necessary [9].

5.2   Activity Release Limits

The doses calculated as a result of each of the accident sequences
would be compared to the appropriate site criteria. The overall risk of
operation of the facility would be determined by comparing the probability
of each of the accident sequences with the respective doses resultant from
each accident to determine acceptability.

In Canada the Atomic Energy Control Board (AECB) is the regulatory
body responsible for all matters related to atomic energy. Detailed safety
criteria including radiation dose limits have been established by the AECB
for CANDU nuclear power reactors. For reactor accidents, both the frequency
of occurrence and the maximum consequences to the public are specified.
Similar criteria for research reactors have not been formalized but the
basic philosophy is that the risk to the public from the operation of a

207

TABLE 1

AECB GUIDELINES FOR ACCIDENT CONDITIONS

Situation	Maximum Frequency	Individual Dose Limit	Total Population Dose Limit
Single Failure*	1 per 3 years	0.5 rem whole body	10^4 man-rem whole body
		3 rem thyroid	10^4 thyroid rem
Dual Failure**	1 per 3000 years	25 rem whole body	10^6 man-rem whole body
		250 rem thyroid	10^6 thyroid rem

* Single failure is the complete failure of one of the process systems (for example: loss of regulation, or loss of coolant accident).

** Qual failure is the coincident failure of one of the process systems and the safety system which would normally intervene to terminate the incident (for example: loss of regulation coincident with failure of the shutdown system, or loss of coolant coincident with failure of emergency cooling).

research reactor should not be greater than the risk from operation of a CANDU nuclear power reactor. The radiation dose limits for members of the public for CANDU nuclear power reactors as established by the AECB are given in Table 1 [12,13].

Knowing the appropriate atmospheric dispersion parameters and the dose conversion parameters a set of derived release limits for accidental releases is established for both individual members of the public and for the population as a whole. For remote locations typical of many nuclear research reactor centres the individual dose is controlling. The safety analysis for a nuclear power plant must demonstrate that the total probability for all single process failures leading to the single failure dose limits is less than once in three years, and for all dual failures leading to the dual failure dose limits is less than once in 3,000 years.

In some instances, particularly for research reactors with a large exclusion area remote from major population centres, it is often adequate to specify radiation dose limits for the operating staff. This in turn ensures that radiation doses to off-site members of the public following a postulated accident will be acceptable. One accepted set of radiation dose limits for the operating staff is 10 rem whole body and 25 rem thyroid [14] with a maximum frequency of occurrence at once in the lifetime of the facility. These radiation dose limits are consistent with recommendations of the ICRP which for example discuss planned special exposures where the dose commitments do not exceed twice the relevant annual limits [15], emergency operations during or immediately after an accident where doses in excess of twice the annual limits may be acceptable [16], and accidental exposures of radiation workers where doses in excess of twice the annual limits would have to be reviewed by a competent medical authority.

REFERENCES

[1] Walker, W.H., "FISSPROD-2: An Improved Fission Product Accumulation Program", August 1975, AECL-5105.

[2]   Postma, A.K., Zavadoski, R.W., "Review of Organic Iodide Formation Under Accident Conditions in Water-Cooled Reactors", WASH-1233, October, 1972.

[3]   Pasquill, F., "The Estimation of the Dispersion of Windborne Material", Met. Mag. 90, 33 (1961).

[4]   Smith, F.B., "A Scheme for Estimating the Vertical Dispersion of a Plume from a Source Near Ground Level", Proc. of the Third Meeting of the Expert Panel on Air Pollution Modelling, NATO-CCMS Report #14, Brussels (1972).

[5]   Hosker, Jr., R.P., "Estimates of Dry Deposition and Plume Depletion Over Forests and Grassland", in "Physical Behaviour of Radioactive Contaminants in the Atmosphere", IAEA STI/PUB/354 (1974) 291.

[6]   Slade, D.H., Editor, "Meteorology and Atomic Energy, 1968", USAEC TID-24190, 1968.

[7]   Bryant, P.M., "Methods of Estimation of the Dispersion of Windborne Material and Data to Assist in Their Application", UKAEA Report AHSB(RP) R42, May 1964.

[8]   Hurst, D.G., and Boyd, F.C., "Reactor Safety and Licensing Requirements", 72-CNA-102, 1972.

[9]   Canadian Standards Association, "Guidelines for Calculation of Radiation Doses to the Public from a Release of Airborne Radioactive Material Under Accident Conditions in a Nuclear Facility", Draft CSA Standard N288.2, July 1981.

[10] Barry, P.J., "Estimation of Downwind Concentration of Airborne Effluents Discharged in the Neighbourhood of Buildings", AECL-2043, 1964.

[11] Slinn, W.G.N., "Simple Model for Buoyant Plumes Based on the Conservation Law", BNWL-1850 (Pt. 3), 1974.

[12] Hake, G., Barry, P.J., and Boyd, F.C., "Canada Judges Power Reactor Safety on Component Quality and Reliable System Performance", AECL-3974, September 1971.

[13] Boyd, F.C., "Containment and Siting Requirements in Canada", Paper #SM-89/22, IAEA Symposium on Containment Siting of Nuclear Power

[14] Barry, P.J., "Maximum Permissable Concentrations of Radioactive Nuclides in Airborne Effluents from Nuclear Reactors", AECL-1624, June 1963.

[15] Recommendations of the International Commission on Radiological Protection, ICRP Publication 26, 1977, paragraph 113.

[16] Recommendations of the International Commission on Radiological Protection, ICRP Publication 9, September 17, 1965, paragraphs 100-102.

FUNDAMENTAL CALCULATIONAL MODEL FOR THE DETERMINATION OF THE RADIOLOGICAL EFFECTS, INSIDE AND OUTSIDE A RESEARCH REACTOR, AFTER HYPOTHETICAL ACCIDENTS, WITH RELEASE OF HIGH AMOUNTS OF FISSION PRODUCTS FROM THE CORE

INTERATOM*
Bergisch Gladbach,
Federal Republic of Germany

Abstract

A fundamental calculational model is presented for determination of the radiological effects, inside and outside a research reactor, after hypothetical accidents, with release of high amounts of fission products from the core. Conservative calculation methods are used to solve the problem. The reference reactor for the model assumption is a pool type (light water) reactor. Models are presented for the following processes: source term, containment and activity enclosure, time dependent activity behaviour in the reactor building, radiation exposure in the reactor plant, and radiological exposure in the environment.

1 General

In this paper the method of determination of the radiological effects, inside and outside a research reactor, which result from an accident with release of activity from the core to the coolant is presented in the form of a fundamental calculation model. For the calculation of radiological consequences it is assumed that the blockage of cooling channels of a fuel element due to unusual objects will occur. As a result of this incident the fuel plates become overheated and the volatile fission product inventories are released instantaneously.

Conservative calculation methods are used, to solve the problem. The reference reactor for the model assumption is a pool type (Light Water) reactor.

Certain modifications are necessary in some points for other research reactor types.

In determining the radiological effects in the environment of the reactor it is assumed that these plants are located in research centers. The immediate surroundings can therefore be isolated after an accident.

In determining the radiological impact on the public resulting from the emission through the stack (dispersion into the atmosphere), it is assumed that members of the public are remaining at the most unfavourable distance in relation to the radioactive plume during the complete emission period.

2   Calculation Model

The calculation model discussed here includes

- a description of a comprehensive calculation programme for the determination of the fission product inventories, taking into account the irradiation history (ORIGEN)

- a detailed description of the transport of relevant fission product groups released from the fuel through the various retention barriers into the reactor building, and their behaviour with respect to time

- a model for taking into account the ventilation and filtering systems

- a model for determining the escape time dose for the personnel

- a model for determining the external radiation from the reactor building

- a model for calculating the atmospheric dispersion (χ -values), taking into consideration the emission height, the wind direction and wind velocity, atmospheric stability classes and their diffusion parameters

- a concept for the calculation of derived dose conversion factors based on the ICRP 26 and 30 to calculate the effects of released airborne radioactive materials for the downwind distance (point of maximum ground level concentration).

A common approach in Safety Analysis Reports (SAR) for research and test reactors is the assumption of the release of a part of radioactive fission product core inventory to the pool water. The pool is an effective barrier for the non gaseous fission products. Therefore only a small part of these fission products will be released to the air of the containment.

The dose calculation involves the following procedure:

- Fission product inventories available for release are determined

- Fission product inventories released from fuel to the containment (source term) are estimated conservatively

- The containment/reactor building air extraction rate is modelled under conservative assumptions to calculate post-accident fission product release to the environment

- Atmospheric dispersion is modelled by applying the Pasquill equations to estimate the dispersion factors

- The radiological exposure inside and outside the plant by direct radiation is estimated

- Time integrated concentration levels over the exposure period at the most unfavourable distance are converted to radiation dose by applying dose conversion factors.

3 Calculations of Fission Product Inventory of the Reactor Core

The fission product inventory in the core of a reactor depends on many data. The inventory can only be determined accurately with a computer programme.

For this purpose the ORIGEN-Code, with its numerous libraries and sub-programmes, is used. The following important parameters are

- Yields

- Cross-sections

- Decay constants

- Branches (Decay chains)

- Proportions of resonance neutron flux

- Proportions of fast neutron flux

- Power histogram with appropriate time intervals

The ORIGEN programme calculates the time dependent concentration of all nuclides in the fuel.

4 Source Term

The radiological source term describes the amount of the nuclides which will be released to the containment. The transport mechanism is split up

into two succeeding phases; the respective release fractions are indicated with f_1 and f_2

- Release from fuel into coolant: f_1

- Release from coolant into containment: f_2

The following relevant nuclide groups are considered:

- Noble gases

- Iodine (elementary and organic)

- Intermediate volatile groups Cs, Rb, Te

The data for the release fractions are listed in table 1.

Table 1   Release Factors for Nuclide Groups

	f_1	f_2	$f_1 * f_2$
Noble gases	1	1	1
Iodine elementary	0,25	10^{-4}	$2,5 \cdot 10^{-5}$
Iodine organic	0,25	10^{-2}	$2,5 \cdot 10^{-3}$
Cs, Rb, Te	0,1	10^{-4}	10^{-5}

f_1 : release fraction from fuel into coolant
f_2 : release fraction from coolant into containment
f_1*f_2: instantaneaous source term to containment atmosphere

The product $f_1 \cdot f_2$ is conservatively assumed to be an instantaneous source term to the containment atmosphere.

5   Containment and Activity Enclosure

The following calculation models refer to the barrier concept of research reactors in the FRG.

The following systems have an influence as activity barriers to a more or less extent:

No.	Component for activity enclosure	Noble gases	Halogens	Other fission products
1	Fuel and cladding of fuel	-	+	+
2	Pool water and primary loop	-	++	++
3	Primary loop purification	-	+	+
4	Reactor containment enclosure	+	++	++
5	Ventilation system (filtration)	-	++	++

+ small influence
++ strong influence
- neglected

The following numbers are associated with the above numbers.

1. Fuel and cladding of fuel

    The release factors are defined in chapter 4 (Values in Table 1)

2. Pool Water and primary loop

    The retention factors "f_2" of the water layer has been measured under accident conditions.

3. Primary loop purification

    The "purification system" reduces the non-gaseous materials, which are released into the primary water, to a considerable extent. This reduction has not been taken into consideration.

4./5. Reactor Containment enclosure and ventilation system

    In case of an accidental radioactivity release the air supply and the air extraction is closed and the

underpressure is maintained at the value of
normal operation by an automatically regulated
air extraction from the reactor building through
a (redundant) charcoal filter line.

The isolation of the normal operational venti-
lation is induced by the radioactivity monitor.

For the underpressure a value is chosen due to
avoid uncontrolled leakages from the reactor
building even in case of high wind speeds.

5.1 Modelling of Time Dependent Activity Behaviour in the Reactor Building (RB)

For the assumption that an instantaneaous release will
occur, the following model is be applied for calcula-
tion of time dependent airborne activity in the RB. The
influence of the parent daughter activities may be neg-
lected. The closing time for automatic containment
closure, is neglected too. The airbore activity in the
RB is calculated by:

$$K_c (t) = Q_o e^{-\lambda_c t}$$

$K_c (t)$:   time dependent airborne activity in RB in Bq

Q_o: Source term in Bq, see chapter 4

λ_c: Containment cleaning constant in h^{-1}

$$= \lambda_r + \lambda_{pl} + \lambda_1$$

λ_r: radioactive decay constant in h^{-1}

λ_{pl}:   plate-out constant[*] in h^{-1}

λ_1:   Containment venting rate[*]

t: time since accident in h

---

[*] typical values for:

λ_{pl}: Aerosols, 0.05 h^{-1}

λ_{pl}: J_2, ≤ 2 h^{-1}

λ_1: vented Containment, ≤ 0.07 h^{-1}

The time integrated activity release to the environ-
ment via the filters (aerosol and iodine charcoal
filters) and the stack can be expressed for any
isotope:

$$\int_0^\infty K_c\ (t)\ \cdot \lambda_1\ dt\ =\ \frac{Q_o\ \cdot \lambda_1\ (1 - \eta\ )}{\lambda_c}$$

η : efficiency of the ventilation filters
$\quad$ = 99 % for aerosols and CH_3J (organic)
$\quad$ = 99.9 % for J_2 (elementary)
$\quad$ = 0 % otherwise

6 Radiation Exposure in the Reactor Plant after Accidents

For calculation of the radiological effects on the
personnel (escape time dose) the radiation exposure
values in the reactor plant can be determined using
the following calculation method.

6.1 Gamma Submersion
(Model of the hemispherical Source without build-up)

In this calculation, a hemispherical source of radius
"R" and an activity concentration "K" is applied. The
radius "R" can be calculated from the actual space
volume. The build-up for air within rooms of the RB can
be neglected. The γ-dose rate in the RB for any iso-
tope is calculated by:

$$\dot{D}_\gamma\ =\ g_\gamma\ \cdot\ 2\pi\ \cdot\ K\ \cdot\ \frac{1 - e^{-\mu R}}{\mu}$$

$\dot{D}_\gamma$ = γ-dose rate in Sv/s

g_γ : Dose factor for γ-submersion in $\dfrac{Sv\ \cdot\ m^2}{Bq\ \cdot\ s}$
$\quad$ see table 2

μ : Averaged absorption coefficient; $\bar{\mu}\ \simeq\ 10^{-2}\ m^{-1}$ for γ
$\quad$ in air

218

Table 2. Dose Factors for γ-Submersion g_γ

Nuclide	g_γ $/\frac{Sv \cdot m^3}{Bq \cdot s}/$	Nuclide	g_γ $/\frac{Sv \cdot m^3}{Bq \cdot s}/$
H 3	0	Sr 91/Y 91	$4.3 \cdot 10^{-15}$
C 14	0	Zr 95	$3.0 \cdot 10^{-15}$
N 13	$4.3 \cdot 10^{-15}$	Nb 95	$3.2 \cdot 10^{-15}$
N 16	$1.2 \cdot 10^{-14}$	Mo 99	$6.5 \cdot 10^{-16}$
N 17	$1.4 \cdot 10^{-16}$	Tc 99m	$4.9 \cdot 10^{-16}$
O 15	$4.3 \cdot 10^{-15}$	Ru 103	$2.5 \cdot 10^{-15}$
O 19	$4.1 \cdot 10^{-15}$	Ru 106/Rh 106	$8.4 \cdot 10^{-16}$
F 18	$4.3 \cdot 10^{-15}$	Ag 110m	$1.1 \cdot 10^{-14}$
Na 22	$8.9 \cdot 10^{-15}$	Sb 124	$7.3 \cdot 10^{-15}$
Na 24	$1.4 \cdot 10^{-14}$	Sb 125	$2.2 \cdot 10^{-15}$
P 32	0	I 129	$4.6 \cdot 10^{-16}$
Ar 37	0	I 131	$1.7 \cdot 10^{-15}$
Ar 41	$4.9 \cdot 10^{-15}$	I 132	$8.9 \cdot 10^{-15}$
Cr 51	$1.2 \cdot 10^{-16}$	I 133	$2.3 \cdot 10^{-15}$
Mn 54	$3.5 \cdot 10^{-15}$	I 135	$9.2 \cdot 10^{-15}$
Fe 55	0	Xe 131m	$4.1 \cdot 10^{-16}$
Fe 59	$4.6 \cdot 10^{-15}$	Xe 133m	$3.8 \cdot 10^{-16}$
Co 58	$3.5 \cdot 10^{-15}$	Xe 133	$3.8 \cdot 10^{-16}$
Co 60	$9.5 \cdot 10^{-15}$	Xe 135m	$1.9 \cdot 10^{-15}$
Zn 65	$3.8 \cdot 10^{-15}$	Xe 135	$1.0 \cdot 10^{-15}$
Kr 83m	$5.9 \cdot 10^{-16}$	Xe 137	$6.5 \cdot 10^{-16}$
Kr 85m	$9.4 \cdot 10^{-16}$	Xe 138	$3.5 \cdot 10^{-15}$
Kr 85	$9.2 \cdot 10^{-18}$	Xe 139	$1.8 \cdot 10^{-15}$
Kr 87	$4.1 \cdot 10^{-15}$	Cs 134	$6.8 \cdot 10^{-15}$
Kr 88	$9.2 \cdot 10^{-15}$	Cs 137/Ba 137m	$2.4 \cdot 10^{-15}$
Kr 89	$7.6 \cdot 10^{-15}$	Cs 138	$8.4 \cdot 10^{-15}$
Kr 90	$7.0 \cdot 10^{-15}$	Ba 140	$9.5 \cdot 10^{-16}$
Rb 88	$2.7 \cdot 10^{-15}$	La 140	$8.1 \cdot 10^{-15}$
Kr 88/Rb 88	$1.2 \cdot 10^{-14}$	Ce 141	$3.8 \cdot 10^{-16}$
Sr 89	0	Ce 144	$1.2 \cdot 10^{-16}$
Sr 90	0	Pr 144	$1.1 \cdot 10^{-16}$
Y 90	0	Ce 144/Pr 144	$2.3 \cdot 10^{-16}$
Sr 90/Y 90	0	Np 239	$5.1 \cdot 10^{-16}$
Sr 91	$4.3 \cdot 10^{-15}$	Pu 238	$1.8 \cdot 10^{-16}$
Y 91	$1.4 \cdot 10^{-17}$	Pu 239	$2.0 \cdot 10^{-17}$
		Pu 240	0
		Pu 241	0
		Am 241	$1.2 \cdot 10^{-16}$
		Am 243	$1.9 \cdot 10^{-16}$
		Am 244	$3.5 \cdot 10^{-15}$
		Cm 242	0
		Cm 243	$5.1 \cdot 10^{-16}$
		Cm 244	0

The value g_γ is fixed $= 0$, if $g_\gamma < 2.7 \cdot 10^{-18} \frac{Sv \cdot m^2}{Bq \cdot s}$

The dose, which a person absorbs by staying in the reactor plant during a residence time "T" is given by:

$$D_{\gamma} = \frac{\dot{D}_{\gamma}}{\lambda_c} (1 - e^{-\lambda_c T})$$

6.2 Beta Submersion

To determine the beta exposure of the tissue for any isotope the dose rate is calculated by:

$$\dot{D}_{\beta} = K_c \cdot g_{\beta}$$

$\dot{D}_{\beta}$: ß-submersion dose rate in Sv/s

K_c: airbore activity concentration in Bq/m^3

g_{β}: ß-dose factors in $\frac{Sv \cdot m^3}{Bq \cdot s}$

The escape time dose in the reactor plant is calculated by:

$$D_{\beta} = \frac{\dot{D}_{\beta}}{\lambda_c} (1 - e^{-\lambda_c T})$$

T: excape time in s

λ_c: containment cleaning constant in s^{-1}

The ß-dose factors for the tissue are given in table 3.

6.3 Inhalation

The inhalation dose of any nuclide is calculated from its radioactivity concentration in the air by:

$$D_i = \dot{q} \cdot g_i \int_o^T K_c(t) \, dt$$

D_i: Inhalation dose in Sv

$\dot{q}$: breathing rate in m^3/s (= $3,3 \cdot 10^{-4} \, m^3/s$)

g_i: Inhalation dose factor in Sv/Bq; see chapter 8

$K_c(t)$: Radioactivity concentration in Bq/m^3

Table 3. β-Dose Factor for Tissue

Nuclide	g_β $/\dfrac{Sv \cdot m^3}{Bq \cdot s}/$	Nuclide	g_β $/\dfrac{Sv \cdot m^3}{Bq \cdot s}/$
H 3	0	Sr 91/Y 91	$7.3 \cdot 10^{-12}$
C 14	$1.9 \cdot 10^{-14}$	Zr 95	$4.6 \cdot 10^{-13}$
N 13	$3.0 \cdot 10^{-12}$	Nb 95	$2.7 \cdot 10^{-14}$
N 16	$2.1 \cdot 10^{-11}$	Mo 99	$2.3 \cdot 10^{-12}$
N 17	$1.2 \cdot 10^{-11}$	Tc 99m	0
O 15	$5.1 \cdot 10^{-12}$	Ru 103	$1.2 \cdot 10^{-13}$
O 19	$1.2 \cdot 10^{-11}$	Ru 106/Rh 106	$9.2 \cdot 10^{-12}$
F 18	$1.2 \cdot 10^{-12}$	Ag 110m	$2.6 \cdot 10^{-13}$
Na 22	$8.6 \cdot 10^{-13}$	Sb 124	$2.1 \cdot 10^{-12}$
Na 24	$3.5 \cdot 10^{-12}$	Sb 125	$2.6 \cdot 10^{-13}$
P 32	$4.3 \cdot 10^{-12}$	I 129	$1.9 \cdot 10^{-14}$
Ar 37	0	I 131	$9.2 \cdot 10^{-13}$
Ar 41	$2.7 \cdot 10^{-12}$	I 132	$2.7 \cdot 10^{-12}$
Cr 51	0	I 133	$2.5 \cdot 10^{-12}$
Mn 54	0	I 135	$1.8 \cdot 10^{-12}$
Fe 55	0	Xe 131m	$4.9 \cdot 10^{-14}$
Fe 59	$4.6 \cdot 10^{-13}$	Xe 133m	$2.4 \cdot 10^{-13}$
Co 58	$1.1 \cdot 10^{-13}$	Xe 133	$3.2 \cdot 10^{-13}$
Co 60	$2.7 \cdot 10^{-13}$	Xe 135m	$4.1 \cdot 10^{-13}$
Zn 65	$8.1 \cdot 10^{-15}$	Xe 135	$1.7 \cdot 10^{-12}$
Kr 83m	0	Xe 137	$1.1 \cdot 10^{-11}$
Kr 85m	$1.3 \cdot 10^{-12}$	Xe 138	$6.2 \cdot 10^{-12}$
Kr 85	$1.2 \cdot 10^{-12}$	Xe 139	$1.9 \cdot 10^{-11}$
Kr 87	$7.8 \cdot 10^{-12}$	Cs 134	$8.4 \cdot 10^{-13}$
Kr 88	$2.3 \cdot 10^{-12}$	Cs 137/Ba 137m	$1.1 \cdot 10^{-12}$
Kr 89	$1.5 \cdot 10^{-11}$	Cs 138	$9.4 \cdot 10^{-12}$
Kr 90	$6.8 \cdot 10^{-12}$	Ba 140	$1.4 \cdot 10^{-12}$
Rb 88	$1.4 \cdot 10^{-11}$	La 140	$3.8 \cdot 10^{-13}$
Kr 88/Rb 88	$1.6 \cdot 10^{-11}$	Ce 141	$6.5 \cdot 10^{-13}$
Sr 89	$3.5 \cdot 10^{-12}$	Ce 144	$2.2 \cdot 10^{-13}$
Sr 90	$8.9 \cdot 10^{-13}$	Pr 144	$8.1 \cdot 10^{-12}$
Y 90	$5.9 \cdot 10^{-12}$	Ce 144/Pr 144	$8.4 \cdot 10^{-12}$
Sr 90/Y 90	$6.7 \cdot 10^{-12}$	Np 239	$6.5 \cdot 10^{-13}$
Sr 91	$3.5 \cdot 10^{-12}$	Pu 238	0
Y 91	$3.8 \cdot 10^{-12}$	Pu 239	0
		Pu 240	0
		Pu 241	0
		Am 241	0
		Am 243	0
		Am 244	$5.6 \cdot 10^{-13}$
		Cm 242	0
		Cm 243	$1.7 \cdot 10^{-13}$
		Cm 244	0

The value g_β is fixed $= 0$, if $g_\beta < 2.7 \cdot 10^{-15} \dfrac{Sv \cdot m^3}{Bq \cdot s}$

Considering the time dependence of the radioactivity concentration the escape time dose amounts to

$$D_i = \frac{\dot{q}\, g_i}{\lambda_c} \cdot K_c \, (1 - e^{-\lambda_c T})$$

λ_c: Containment cleaning constant in s^{-1}
T: Escape time in s

The results of the calculation should only be taken as guide values, because they are considerably exaggerating for two reasons:

a) The activity release is usually not instantaneous but is time delayed (water seal)

b) Filter masks are available in the control areas of every reactor plant, so that inhalation of radioactive materials will not be the main exposure path.

7 Radiological Exposure in the Environment

7.1 Atmospheric Dispersion

The procedure to account for atmospheric dispersion when the fission products are transported from the release point to the receptor location is given. This method describes the release during the first 7 days, which are important for the radiological consequences. It is in accordance to "Pasquill's" diffusion model. Essentially, this model determines dilution factors taking into account the release height, wind direction and -velocity, air stability and the distance from release to receptor locations.

The following conservative calculation principles are based:

- The most unfavourable diffusion categories are supposed

- The most unfavourable distance is taken into account

- Time intervals after the begin of the release are considered with conservative dispersion factors.

7.1.1 Accident Dispersion Factors "χ" for the Activity Concentration near to Ground Level

These accident dispersion factors are determined for the calculation of the beta submersion exposure and inhalation.

Time interval	k	χ_k / $\frac{s}{m^3}$ /
up to 8 hours	1	$\max \{ \chi(A \ldots F) \}$
8 to 24 hours	2	$\max \{ (1/2) \chi(C \ldots F) \}$
24 to 72 hours	3	$\max \{ (1/4) \chi(C \ldots F) \}$
3 to 7 days	4	$\max \{ (1/8) \chi(C \ldots E) \}$

where

$\max \{ \chi(A \ldots F) \}$ is the most unfavorable short-term diffusion factor " χ "near ground level for the diffusion categories "A" till "F" with y = 0

and

$$\chi = \frac{1}{\pi \sigma_y \cdot \sigma_z \cdot u} * \exp\left(-\frac{H_e^2}{2\sigma_z^2}\right) * \exp\left(-\frac{y^2}{2\sigma_y^2}\right)$$

where

H_e : the effective emission height in m
"H_e" is usually the construction height of the stack if this height is greater than two times the height of the surrounding buildings. Otherwise special corrections are necessary.

u : the wind speed at the effective emission height in m/s, see below

σ_y σ_z: the dispersion parameters in m, see table 5

x : the source distance in m

y : the vertical distance in relation to the direction of diffusion in m

223

Table 4. Extract from Safety Series No. 9.

Basic Safety Standards for Radiation Protection. All Values in Bq

Fission Product: IODINE			CAESIUM		
Radionuclide		Inhalation b	Radionuclide		Inhalation b
I 129	ALI	3×10^5 (1×10^6) Thyroid	Cs 125	ALI	5×10^9
			Cs 127	ALI	4×10^9
I 130	ALI	3×10^7 (7×10^7) Thyroid	Cs 129	ALI	1×10^9
I 131	ALI	2×10^6 (6×10^6) Thyroid	Cs 130	ALI	7×10^9
			Cs 131	ALI	1×10^9
I 132	ALI	3×10^8 (6×10^8) Thyroid	Cs 132	ALI	1×10^8
I 132m	ALI	3×10^8 (7×10^8) Thyroid	Cs 134	ALI	4×10^8
I 133	ALI	1×10^7 (3×10^7) Thyroid	Cs 134m	ALI	5×10^9
			Cs 135	ALI	4×10^7
I 134	ALI	2×10^9			
			Cs 136	ALI	2×10^7
I 135	ALI	$6 \times 10^7)$ (2×10^8) Thyroid	Cs 137	ALI	6×10^6
			Cs 138	ALI	2×10^9

b = All Compounds of Iodine   b = All compounds of caesium

The ALI-values for stochastic effects are given in parenthesis between the ALI and the tissue or organ name.

The dispersion parameters can be represented as power functions of the source distance (see table 5).

Table 5   Atmospheric Dispersion Parameters as a Function of Source Distance "x" and Dispersion Coefficients "p_y" and "q_y"

$$\sigma_y = p_y \cdot x^{q_y}$$

$$\sigma_z = p_z \cdot x^{q_z}$$

Effective Height of Emission H_e	Weather-Category	Dispersion Coefficient			
		p_y	q_y	p_z	q_z
50 m	A	1.503	0.833	0.151	1.219
	B	0.876	0.823	0.127	1.108
	C	0.659	0.807	0.165	0.996
	D	0.640	0.784	0.215	0.885
	E	0.801	0.754	0.264	0.774
	F	1.294	0.718	0.241	0.662
100 m	A	0.170	1.296	0.051	1.317
	B	0.324	1.025	0.070	1.151
	C	0.466	0.866	0.137	0.985
	D	0.504	0.818	0.265	0.818
	E	0.411	0.882	0.487	0.652
	F	0.253	1.057	0.717	0.486

Definition of the Weather Categories

A: extreme unstable conditions
B: moderate unstable conditions
C: slightly unstable conditions
D: neutral conditions
E: slightly stable conditions
F: moderately stable conditions

The following procedure is used for determining the average wind velocity:

$$u = u_1 \left(\frac{H_e}{z_1}\right)^m \qquad \text{for } H_e \geq 10 \text{ m}$$

and

$u \quad = \quad u_1 \qquad \text{for } H_e < 10 \text{ m}$

u   :   average wind velocity in m/s

u_1 :   wind velocity in m/s for the height of $z_1 = 10$ m, see table 6

m   :   exponent of the vertical profile of wind velocity, see table 6

Weather Category	A	B	C	D	E	F
u_1 for $z_1 = 10$ m	0.9	1.3	1.7	2.0	1.2	0.4
m	0.09	0.20	0.22	0.28	0.37	0.42

7.1.2 Accident Gamma Submersion Factors "χ_Γ"

The accident gamma submersion factors are determined to calculate the dose for the exposure from gamma radiation from the exhaust air.

The following accident atmospheric gamma submersion factors are applied for the various time intervals:

Time Interval	K	$\chi_k^\Gamma \ / \ \dfrac{s}{m^2} \ /$
up to 8 hours	1	max $\{ \chi$ (A ... F)$\}_\Gamma$
8 to 24 hours	2	max $\{$ (1/2) χ (C ... F)$\}$
24 to 72 hours	3	max $\{$ (1/4) χ (C ... F)$\}$
3 to 7 days	4	max $\{$ (1/8) χ (C ... E)$\}$

where:

max $\{ \chi$ (A ... F)$\}$ is   the most unfavorable short-term diffusion factor for gamma submersion in the diffusion categories A till F

and

$$\chi_\Gamma = \int\int\int_{-\infty}^{+\infty} \frac{B \ (\mu r) \ \exp \ (-\mu r)}{2 \Gamma r^2 \delta_y \delta_z \cdot u} \ \exp \ (- \frac{y^2}{2 \delta_y^2} - \frac{(z - H_e)^2}{2 \delta_z^2}) \ dXdYdZ$$

226

The symbols used in this equation stand for:

μ : attenuation coefficient for gamma radiation of 1 MeV in air = $7.65 \cdot 10^{-3}$ m^{-1}

r : distance between the receiving point and the coordinates of the source point of gamma radiation in m

$$= \sqrt{(x-X)^2 + (y-Y)^2 + (z-Z)^2}$$

x, y, z : coordinates of the receiving point (y = 0 and z = 0)

X, Y, Z : coordinates of the source point of gamma radiation

σ_y, σ_z : dispersion parameters in m

B (μr) : dose build-up factor in air
B (μr) = $1 + 0.00765 \cdot r + 0.0000082 \cdot r^2$

u : wind speed at the effective height of emission in m/s

H_e : effective height of emission in m

The calculation has to be done for a gamma energy of 1 MeV.

7.2 Gamma Submersion

The gamma submersion dose in the time period k for any isotope is calculated from:

$$D_\gamma^k = A^k \cdot \chi_\gamma^k \cdot g_\gamma$$

D_γ : Gamma submersion dose in Sv in the time period k

A : Activity release in Bq in the time period k

χ_γ : Accident Gamma Submersion factor in s/m^2 in the time period k, see chapter 7.1.2

g_γ : Dose factor for γ-submersion in

$$\frac{Sv \cdot m^2}{Bq \cdot s}$$, see table 2

7.3 Beta Submersion

The beta submersion dose in the time period k for any isotope is calculated from:

$$D_\beta^k = A^k \cdot \chi^k \cdot g_\beta$$

D_β : Beta submersion dose in Sv in the time period k

A : Activity release in Bq in the time period k

χ : Accident dispersion factor in s/m^3 in the time period k, see chapter 7.1.1

g_β : Beta dose factor in $\frac{Sv \cdot m^3}{Bq \cdot s}$, see table 3

7.4 Inhalation

The inhalation dose in the time period k for any isotope is calculated from:

$$D_i^k = A^k \cdot \chi^k \cdot \dot{q}^k \cdot g_i$$

D_i : Inhalation dose in Sv in the time period k

A : Activity release in Bq in the time period k

χ : Accident dispersion factor in s/m^3 in the time period k, see chapter 7.1.1

228

$\dot{q}$: breathing rate for adults
- for $k = 1$ $(0 - 8$ h$)$: $3.3 \cdot 10^{-4}$ m^3/s
- for $k \geq 2$ $(> 8$ h$)$: $2.3 \cdot 10^{-4}$ m^3/s

g_i : Inhalation dose factor in Sv/Bq, see chapter 8

7.5 Ingestion

It is unusual to calculate the ingestion dose after hypothetical accidents because it is guaranteed by the administrative authority that the intake of radio-nuclides via the ingestion path can be avoided.

Therefore, a model for calculation of radiological consequences for this pathway is out of the scope of this paper.

7.6 Direct Radiation from the Reactor Building

The direct radiation from the reactor building is caused by two important parts:

- airborne (gaseous) activities

- plate out activities on structures, walls

The airborne activity is reduced in the case of "vented containment" by plate-out and circulated air purification (chapt. 5.1). A filtered exhaust air flow maintains underpressure to avoid leakage through the RB to the environment.

The deposited activity is determined by taking into account the plate-out effect and the exhaust air flow rate.

For the research reactors under consideration here, with a water layer of 6 - 7 m, i. e. with a high retention capacity for elementary iodine and inter-mediate volatile fission products $(f_2 \sim 10^{-4})$ in the

pool water, the proportion of gaseous fission products is dominant in the reactor building.

If it is assumed that members of the public are not remaining in the immediate environment of a reactor building after an accident, the radiation exposure through gammas can be estimated as follows.

The approximation by a shielded point source leads to the following dose rate calculation outside of the reactor building:

$$\dot{D}_\gamma (x, t) \simeq Q_o e^{-\lambda_c t} \cdot \frac{B}{x^2} \cdot g_\gamma \cdot e^{-\mu(x - x_L)}$$

$\dot{D}_\gamma$	:	γ-dose rate in Sv/s
Q_o	:	see chapter 5.1
λ_c	:	see chapter 5.1
B	:	Build-up factor for the shielding material
x	:	distance between point of the release to the receptor in m
g	:	see chapter 6.1
μ	:	see chapter 7.1.2
x_L	:	thickness of air layer which is equivalent to the wall of the reactor hall in m

In the case of a 30 m high reactor building (volume source) only a slight error results at 100 m distance using this formula.

The dose for an exposure time "τ" after the accident can be calculated by integration from zero to infinity as follows:

$$D_\gamma = Q_o \frac{B}{x^2} e^{-\mu(x-x_L)} \cdot \left(\frac{1 - e^{-\lambda_c \tau}}{\tau} \right)$$

230

8   Inhalation Dose Conversion Factor

The inhalation dose conversion factor g_i, used in
the chapters 6.3 and 7.4 have been derived from the
data for annual limit on intake for workers (ALI-values)
taken from IAEA safety series Nr. 9. Table 4 shows
an extract of these data.

The ALI-value of any nuclide is corresponding to the
ICRP dose limit for workers which amounts to

-   0.05 Sv if stochastic effects are dominant
    (effective dose equivalent), or

-   0.5 Sv if non-stochastic effects are dominant,
    (organ dose)

In case of dominant non-stochastic effects the organ
of reference is indicated in Table 4. In this case, the
figures in paranthesis are the ALI-values for stochastic
effects corresponding with the annual effective dose
equivalent limit of 0.05 Sv.

On the basis of these relations the inhalation dose
conversion factors are defined as follows

-   dose conversion factor for the Effective Dose
    Equivalent

$$g_i = g_i^{EDE} = \begin{cases} \dfrac{0.05\ Sv}{ALI} & \text{if stochastic effects are dominant} \\[2ex] \dfrac{0.05\ Sv}{(ALI)} & \text{if non-stochastic effects are dominant} \end{cases}$$

-   dose conversion factor for Organ doses

$$g_i = g_i^{O} = \frac{0.5\ Sv}{ALI} \quad \text{if non-stochastic effects are dominant}$$

g_i^{EDE}, g_i^O :   Inhalation dose conversion factor in Sv/Bq

ALI, (ALI)   :   Annual limit on intake in Bq.

9   Dose Calculation

When applying the outlined methods on evaluation, sometimes a lot of data have to be involved and a lot of results must be superposed to get the final result for the dose.

Therefore, dose calculation in the reactor building and in the environment are managed by extended computer programmes including

- superposition of dose contributions of nuclides

- superposition of dose contributions of time periods

- evaluation of atmospheric diffusion

- etc.

Besides the well-known computer code ORIGEN, the new computer codes AUBI and AREAN are very helpful to solve practical problems, starting from the source term to the RB.

232

Appendix D-6

RADIOLOGICAL CONSEQUENCE ANALYSIS FOR UZrH FUEL

GA TECHNOLOGIES, INC.,
San Diego, California,
United States of America

Abstract

Methods and sample calculations are presented for a radiological consequence analysis for UZrH fuel failure in a TRIGA reactor. The analysis summarizes results for the fission product release due to failure of a single fuel-rod cladding in water and design basis fission product releases for failure of all fuel rods in a 16-rod cluster in air and in water. Fission product inventories and release fractions, building release and downwind doses are described and compared to design basis dose criteria.

1. SUMMARY

The failure of a single fuel-rod cladding, due to material deficiencies, with the consequent release of fission products is an event that has a small but significant probability and, over the life of the core, it is to be expected that such a failure could occur during normal operation. Based on past experience these occurrences would be very rare and, because of the small amounts of activity released, the greatest problem is locating the failed rod and not the radiological consequences. The consequences of this anticipated fission product release are assessed and summarized in Table 1.

To provide a design basis for the building and ventilation system, an accident is postulated in which all the fuel rods in a single 16-rod cluster fail while in air. The conditions postulated for the analysis and the consequences predicted for this design basis accident are summarized in Table 2.

These failures were analyzed using the following assumptions:

1. The fuel rods that fail have operated at an average power density twice as great as the average power density in the core.

2. The core has operated continuously for a total of 5000 MWd.

233

TABLE 1

ANTICIPATED FISSION PRODUCT RELEASE
SINGLE-ROD FAILURE IN WATER WITH TRIGA RELEASE FRACTION

Fraction of core involved per incident	1 rod (0.21% of core)
Assumed relative power density	2.0
Fraction of fission products available for release to pool:	6.3×10^{-4}
Noble gases	100%
Halogens	25%
Fraction of fission products released from pool water:	
Noble gases	100%
Organic halogens (10% of total)	100%
Elemental and particulate halogens (90% of total)	1%
Condition of ventilation system	Normal
Exhaust rate from stack	31,500 m^3/hr
Maximum downwind doses (at 250 m):	
Whole body gamma dose	0.11 mrad
Thyroid dose	1.2 mrem

3. For the anticipated release (single-rod failure), experimentally determined fission product release data for $U-ZrH_{1.6}$ fuel was used. At the temperature conditions of the hottest fuel rod, experiments (Ref. 1) indicate that the fraction of the volatile fission products that escape from the fuel material would be about 6.3×10^{-4}.

4. For the design basis release, it is assumed that there is no retention of volatile fission products in the $Er-U-ZrH_{1.6}$.

5. One hundred percent of the noble gases in the fuel-clad gap are released from the fuel cluster and subsequently are transferred directly to the reactor hall. Twenty-five percent of the halogens in the fuel-clad gap are released from the fuel cluster (with the remainder assumed to plate-out on the relatively cool clad). Of the halogens that escape for the anticipated (single-rod failure) release, 10% are assumed to form organic compounds which escape the pool water. Only 1% of the balance is undissolved in the pool

TABLE 2
DESIGN BASIS FISSION PRODUCT RELEASE
16-ROD CLUSTER FAILURE IN AIR WITH TOTAL RELEASE

Fraction of core involved	3.3% (single cluster)
Relative power density in failed cluster	2.0
Fraction of fission products released from fuel to reactor room:	
Nobel gases	100%
Halogens	25%
Condition of ventilation system	Emergency
Filter efficiency for noble gases	0%
Filter efficiency for halogens	99%
Exhaust rate to stack	850 m^3/hr
Maximum downwind doses (at 250 m):	
Whole body gamma dose	2.0 rad
Thyroid dose	2.6 rem

water and appears in the reactor room air. The net halogen release to the reactor room and potentially to the outside is 2.725%. All other fission products remain in the pool or are otherwise unable to escape from the reactor room. For the design basis release (in air) fully 25% of the halogens are released to the reactor hall. All other fission products are assumed unable to escape from the reactor room because of plate-out on cool surfaces.

These assumptions for the design basis release conform to the USAEC Regulatory Guides 3 and 4 (Ref. 2 and 3) dealing with the design basis analysis of fission product releases for boiling-water and pressurized-water reactors.

6. For the analysis of the anticipated (single-rod failure) release it is assumed that the quantities of fission product gases are so small that they are undetected in the reactor room air; therefore, the normal ventilation system remains operative, discharging 31,500 m^3/hr from the stack. It is assumed that in the design basis release the released gases are immediately detected and cause the ventilation system to operate in the emergency mode. The discharge is through an activated charcoal trap. It is

assumed that this trap removes 99% of the halogens and none of the noble gases. The discharge rate from the stack is 850 m^3/hr.

The assumption that the anticipated release does not activate the emergency ventilation mode is overly conservative as the concentration of fission products in the reactor room from the single-rod failure model would be over 1 mCi/m^3 (which would be detectable by the fission product detector). This concentration results because total release of the fission products in the gap is assumed for the anticipated release model. Experience has shown that only a fraction of these fission products actually reach the reactor room (with the rest presumably plated-out on the clad). A release of about ten times less than the anticipated release might not be detectable, however, so this assumption is conservative by about that factor, i.e., 10.

The assumption for the design basis release as to the trap efficiency is conservative by at least a factor of 10. The removal of halogens by activated charcoal traps can be accomplished easily with efficiencies greater than 99.9%. Although it is assumed here that no noble gases are removed by the traps, it is probable that, depending on the trap design, 10% to 90% of the noble gases would be condensed.

7. Atmospheric dispersion of the released fission product gas cloud was consistent with the model defined in the USAEC Regulatory Guide 3 (Ref. 2) in which dilution factors are presented as a function of time and distance. It was assumed the point of discharge was 50 m above ground level.

8. Two additional fission product release conditions were also analyzed. Shown in Table 3 are the results for a modified design basis release where the fuel cluster is in water rather than air and an experimentally based fission product release fraction for the fuel of 6.3×10^{-4} is used. Table 4 gives the results for a modified design basis release where the fuel cluster is in water rather than air. The assumption for this case, that there is no retention of fission products in the fuel, implies that the fuel involved is at temperatures approaching the melting point of U-ZrH. This is inconceivable because the fuel cluster is in water.

236

TABLE 3
MODIFIED DESIGN BASIS FISSION PRODUCT RELEASE
16-ROD CLUSTER FAILURE IN WATER WITH TRIGA RELEASE FRACTION

Fraction of core involved	3.3%
Relative power density in failed cluster	2.0
Fraction of fission products released from fuel	6.3×10^{-4}
Fraction of fission products released from pool water:	
Noble gases	100%
Organic halogens (10% of total)	100%
Elemental and particulate halogens (90% of total)	1%
Condition of ventilation system	Emergency
Filter efficiency for noble gases	0%
Filter efficiency for halogens	99%
Exhaust rate to stack	850 m^3/hr
Maximum downwind doses (at 250 m):	
Whole body gamma dose	1.1 mrad
Thyroid dose	0.18 mrem

TABLE 4
MODIFIED DESIGN BASIS FISSION PRODUCT RELEASE
16-ROD CLUSTER IN WATER WITH TOTAL RELEASE

Fraction of core involved	3.3% (single cluster)
Relative power density in failed cluster	2.0
Fraction of fission products released from fuel:	
Noble gases	100%
Halogens	25%
Fraction of fission products released from pool water:	
Noble gases	100%
Organic halogens (10% of total)	100%
Elemental and particulate halogens (90% of total)	1%
Condition of ventilation system	Emergency
Filter efficiency for noble gases	0%
Filter efficiency for halogens	99%
Exhaust rate to stack	850 m^3/hr
Maximum downwind doses (at 250 m):	
Whole body gamma dose	1.8 rad
Thyroid dose	0.29 rem

2. FISSION PRODUCT INVENTORY

The noble gas and halogen fission product inventory in the core was calculated assuming a burnup of 5000 MWd occurring in 1.4 calendar years. This results in equilibrium quantities of all isotopes except for the long-lived Kr-185. The cluster that was assumed to have failed operated at a power density twice that of the average in the 30-cluster core; i.e., at 670 kW/bundle. Table 5 lists the inventory of noble gases and halogens in the entire core.

It was assumed that, at the time of the fuel integrity failure, a fraction of the ith isotope in this inventory was released to the reactor hall instantaneously. This fraction w_i is

$$w_i = (p/N) \ e_i \ x \ f_i \ x \ g_i \quad ,$$

where p/N = the relative power density in the failed cluster = 2/30,

e_i = the fraction released to the fuel-clad gap,

f_i = the fraction of the ith isotope released to the pool,

g_i = the fraction of the ith isotope released to the reactor room.

For the anticipated release the value of e_i is 6.3×10^{-4}, whereas for the design basis release it is assumed to be equal to 1.

For release in water the values of f_i and g_i are:

	f_i	g_i
Noble gases	1.00	1.0
Halogens	0.25	0.1 + (0.01 x 0.9) = 0.109
Others	0.0	0.0

The value of g_i for the halogens arises from the assumption that 10% of the halogens form organic compounds which are insoluble in water and 90% of the halogens are in elemental or particulate form of which all but 1% are retained in the water. For the analysis of releases in air the value g_i for the halogens is also 1.

238

TABLE 5

NOBLE GAS AND HALOGEN FISSION PRODUCT INVENTORY IN CORE

Isotope	Decay Constant (hr^{-1})	Core Inventory (Ci)
Br-83	3.02×10^{-1}	4.08×10^4
Br-84	1.31×10^0	8.21×10^4
Br-85	1.39×10^1	8.57×10^4
I-131	3.58×10^{-3}	2.37×10^5
I-132	3.07×10^{-1}	3.54×10^5
I-133	3.34×10^{-2}	5.74×10^5
I-134	7.93×10^{-1}	6.44×10^5
I-135	1.04×10^{-1}	5.36×10^5
I-136	2.90×10^1	5.19×10^5
Kr-83 m	3.66×10^{-1}	4.08×10^4
Kr-85 m	1.59×10^{-1}	8.57×10^4
Kr-85	7.67×10^{-6}	2.00×10^3
Kr-87	5.35×10^{-1}	2.16×10^5
Kr-88	2.50×10^{-1}	3.08×10^5
Kr-89	1.31×10^1	3.90×10^5
Kr-90	7.55×10^1	4.34×10^5
Kr-91	2.54×10^2	2.94×10^5
Xe-131 m	2.41×10^{-3}	1.89×10^3
Xe-133 m	1.26×10^{-2}	1.379×10^4
Xe-133	5.50×10^{-3}	5.79×10^5
Xe-135 m	2.67×10^0	1.61×10^5
Xe-135	7.62×10^{-2}	2.01×10^5
Xe-137	1.07×10^1	5.01×10^5
Xe-138	2.45×10^0	4.68×10^5
Xe-139	6.08×10^1	4.71×10^5
Xe-140	1.56×10^2	3.23×10^5

3. BUILDING RELEASE

Two modes for the release of the fission product gases from the building were considered. They were:

1. Removal by the emergency ventilation system through an activated charcoal trap.

2. Removal by the normal ventilation system.

239

The first of these modes is the one for which the system is designed. A detector in the reactor hall will sense the presence of fission product gases and will cause the following to occur:

1. The main supply fan and exhaust fan shut down.

2. The emergency ventilation exhaust fan is energized.

3. All the exhaust air is diverted through activated charcoal filters.

In the analysis the charcoal filters are assumed to have an efficiency of 0% for noble gases and 99% for the halogens.

The contaminated air from the reactor hall is discharged at a rate of 850 m^3/hr from a stack 50 m above ground level. Only the bottom one-fifth of the reactor hall volume is assumed to be involved in the air circulation (i.e., the top four-fifths is stagnant)*. The effective room volume, then, is about 3000 m^3 and the ventilation rate is 850/3000 = 0.28 air changes/hr.

In the normal ventilation mode, which is assumed for the anticipated release, the room air is discharged directly to the stack at a rate of 31,500 m^3/hr. The ventilation rate, then, is 31,500/3000 = 10.5 air changes/hr.

4. DOWNWIND DOSES

The ground level dilution factor as a function of downwind distance from the point of discharge is shown in Fig. 1. This is based on an envelope of Pasquill diffusion categories as found in Ref. 4. The wind velocity is assumed to be 1 m/sec.

The calculation of whole body gamma doses and thyroid doses downwind from the point of release was accomplished through the use of the computer code GADOSE (Ref. 5). In this code the set of differential equations describing the rate of production of an isotope through the decay of its precursors and the rate of removal through radioactive decay and removal by

---

*This assumption is based on standard engineering practice for handling air in large rooms. It also results in a conservatively high release rate.

240
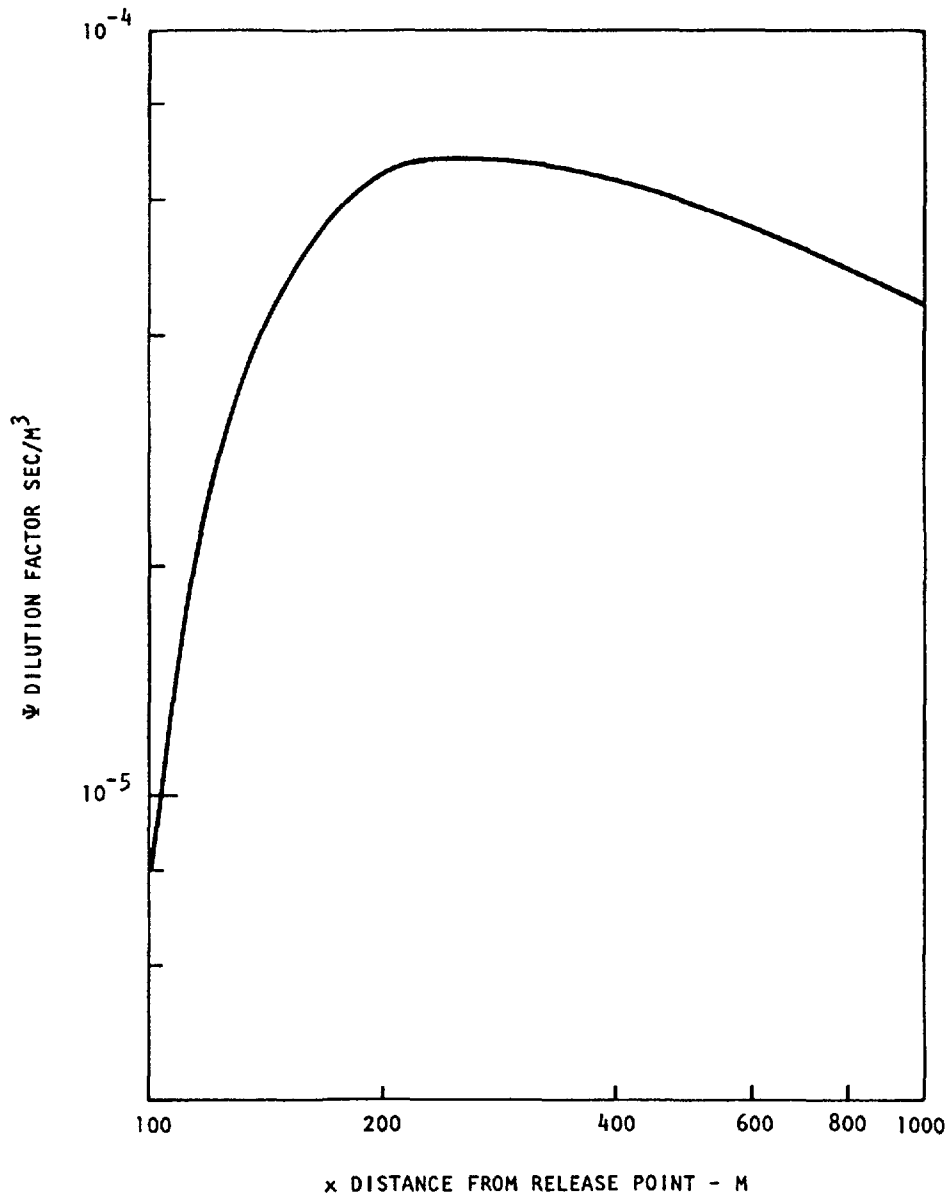
Fig. 1. Elevated release atmospheric dilution factors release point
elevation = 50 m

the ventilation system is integrated for each member of the chain. The release rate q_i to the environment for the ith isotope at time t in hours is:

$$q_i(t) = g_i \; Q_i(t) \; \ell \times 3600 \quad ,$$

where $Q_i(t)$ = the concentration of the ith isotope in Ci/m^3,

ℓ = the building leakage rate in m^3/hr,

$g_i = 1 - E_i$,

E_i = the filter efficiency for the ith isotope.

241

The concentration downwind at a distance x for the ith isotope is calculated from

$$Q_i'(t,x) = q_i(t-\tau) \times \Psi(x)e^{-\lambda_i \tau} \quad ,$$

where τ = the transit time from the release point to the dose point (hr),

λ_i = the decay constant for the ith isotope,

Ψ = the dilution factor at the distance x (sec/m^3).

The dilution factor is taken from USAEC Regulatory Guide 3, assuming a 50-m stack height, and is plotted in Fig. 1.

The whole body gamma ray dose rate for the ith isotope D_{w_i} at the distance x and time t is calculated, assuming a semi-infinite cloud, through the expression:

$$D_{w_i}(t, X_i) = 900 \; \bar{E}_i Q_i'(t,x) \quad ,$$

where $\bar{E}_i$ = the average gamma ray energy per disintegration in MeV and the constant includes the attenuation coefficient for air as well as the conversion factors required.

Interval dose rates, in this case the dose rate to the thyroid, are calculated by:

$$D_{th_i}(t,x) = 3600 \; B \times Q_i'(t,x) \times K_i \quad ,$$

where B = the breathing rate (m^3/sec),

and K_i = the internal dose effectivity of the ith isotope (rem/Ci).

The values for the breathing rate are given in Table 6 and are taken from USAEC Regulatory Guide 4 (Ref. 3).

The average gamma ray energy per disintegration and the internal dose effectivity for each isotope considered are given in Table 7.

The decay products of these isotopes are also included in the calculation; however, their contribution to the dose rates are small and therefore the data for these isotopes were not included in the table.

242

TABLE 6
ASSUMED BREATHING RATES

Time (hr)	Breathing Rate (m^3/sec)
0 to 8	3.47×10^{-4}
8 to 24	1.75×10^{-4}
over 24	2.32×10^{-4}

TABLE 7
AVERAGE GAMMA RAY ENERGY AND INTERNAL
DOSE EFFECTIVITY FOR EACH FISSION PRODUCT ISOTOPE

Isotope	$\bar{E}_i$(MeV)	K_i(rem/Ci)
Br-83	0.92×10^{-2}	
Br-84	1.87	
I-131	0.40	1.486×10^6
I-132	1.96	5.288×10^4
I-133	0.56	3.951×10^5
I-134	3.02	2.538×10^4
I-135	1.77	1.231×10^6
I-136	2.91	
Kr-83 m	0.8×10^{-3}	
Kr-85 m	0.16	
Kr-85	0.4×10^{-2}	
Kr-87	1.07	
Kr-88	2.05	
Kr-89	2.40	
Xe-131 m	0.82×10^{-2}	
Xe-133 m	0.37×10^{-1}	
Xe-133	0.29×10^{-1}	
Xe-135 m	0.46	
Xe-135	0.25	
Xe-137	1.22	
Xe-138	1.57	

5. DESIGN DOSE RATE CRITERIA

The criteria used to assume that the building, ventilation system, and fission product handling system designs are adequate are those presented in the United States Code of Federal Regulations, 10CFR100. This code, dealing with siting criteria for nuclear power plants, specifies that in a low-density population zone, immediately adjacent to the site boundary, it must be shown that there will never be a fission product release the consequences of which could result in a whole body gamma ray dose to the population of 25 rem or a thyroid dose to the population of 300 rem.

These values can be compared to the ICRP recommended limits for annual exposure to the general public of 0.5 rem/yr whole body gamma dose and 3 rem/hr thyroid dose.

6. ANTICIPATED FISSION PRODUCT RELEASE

During the lifetime of the core it can be anticipated that a few fuel rods might experience a failure of the clad. Experience with other TRIGA-type reactors indicates that such events are uncommon and their consequences are minor. The release of fission products from TRIGA fuel has been measured (Ref. 1) and the release fraction f can be expressed as:

$$f = 1.5 \times 10^{-5} + 3.6 \times 10^{3} \, e^{-1.34 \times 104/T_k} \quad ,$$

where T_k = the fuel temperature (°K).

The fraction of the fission products in the volume outside the fuel but inside the clad after a long period of operation is

$$f_T = \int_V f_T(v) dV/V$$

$$= \int_V \left[1.5 \times 10^{-5} + 3.6 \times 10^{3} \, e^{-1.34 \times 10^{4}/T_k(v)} \right] dV/V \quad ,$$

where $T_k(v)$ = the temperature in the differential fuel volume dV,
and   V = the fuel volume.

244

Using a temperature distribution calculated for a maximum-power-density rod in which the peak temperature was assumed to be 760°C (1400°F), the fission product release fraction is found to be 6.3 x 10^{-4}.

Assuming that the normal ventilation system continues to operate, the effects of the release of 100% of the noble gases and 25% of the halogens from the fuel-clad gap in the hottest rod was determined. The whole body gamma dose to an individual 250 m downwind from the stack, using the dilution factors from Fig. 1, would be

$$D_{wbg} = 1.1 \times 10^{-1} \text{ mrads} \quad ,$$

and the thyroid dose would be

$$D_{thy} = 1.2 \text{ mrem} \quad .$$

For persons remaining in the reactor room the doses would be less than

$$D_{wbg} = 20 \text{ mrad}$$

and

$$D_{thy} = 3.1 \text{ rem} \quad .$$

7. DESIGN BASIS FISSION PRODUCT RELEASE CONSEQUENCES

The integrated doses downwind of the reactor stack resulting from the design basis release described in Section 1. and summarized in Table 2 are plotted in Fig. 2. It can be seen that the maximum doses occur at a point approximately 250 m distant from the stack where the whole body gamma dose is seen to be less than 2.0 rad and the dose to the thyroid is 2.6 rem. Slightly less than 97% of these doses are accumulated in the first hour after the release. The doses at the site boundary (300 m) are slightly lower.
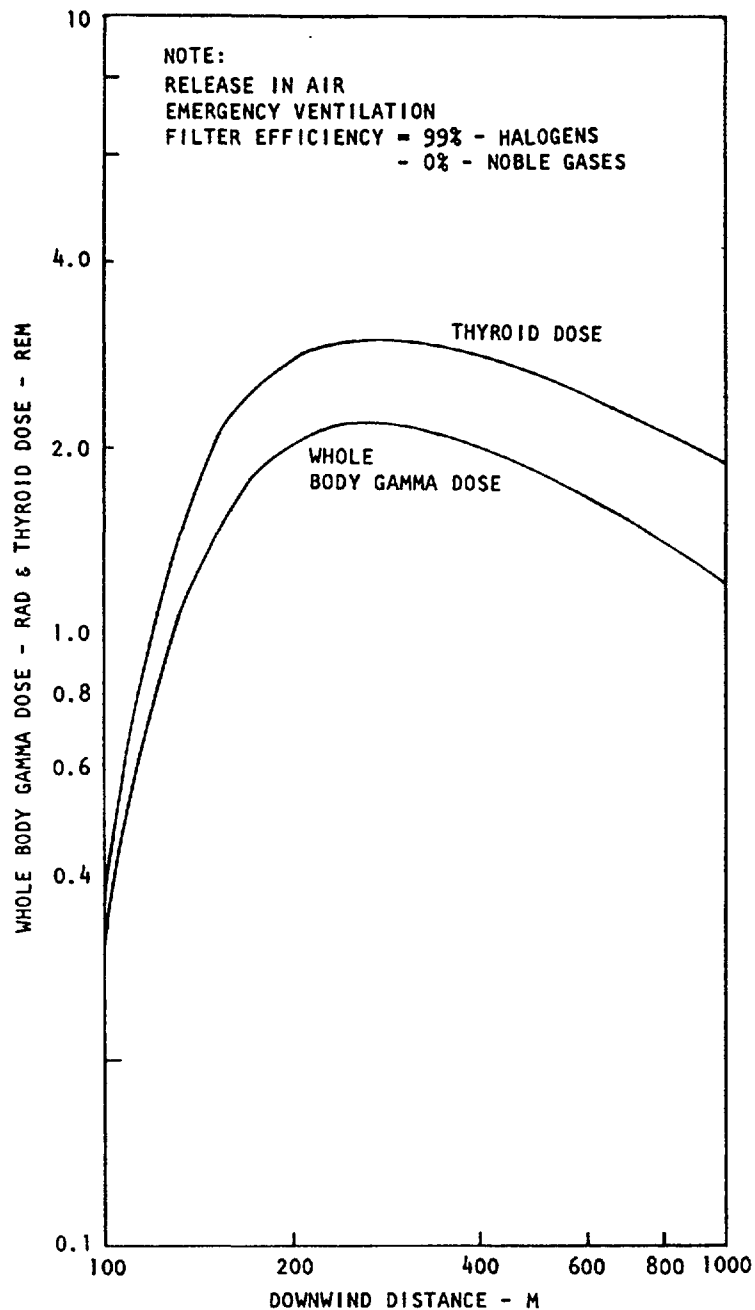
Fig. 2. Design basis fission product release - downwind dose versus distance

At a distance of 10 km the whole body gamma dose would be about 0.5 rad and the thyroid dose 0.7 rem.

It is important to recognize that the release fraction assumed in this analysis is extremely conservative (by at least a factor of 3 to 5) based on experiments such as SNAPTRAN.

246

REFERENCES

1. Foushee, F. C., and R. H. Peters, "Summary of TRIGA Fuel Fission Product Release Experiments," GA Technologies Inc. Report Gulf-EES-A10801, 1971.

2. "Assumptions Used for Evaluating the Potential Radiological Consequences of a Loss of Coolant Accident for Boiling Water Reactors," USAEC Regulatory Guide 3, 1970.

3. "Assumptions Used for Evaluating the Potential Radiological Consequences of a Loss of Coolant Accident for Pressurized Water Reactors," USAEC Regulatory Guide 4, 1970.

4. Slade, D. H. (ed.), "Meteorology and Atomic Energy," USAEC Reactor Development and Technology Division Report TID-24190, CFSTI, Springfield, VA. 1968.

5. Lee, E., R. J. Mack, and D. B. Sedgley, "GADOSE and DOSET – Programs to Calculate Environmental Consequences of Radioactivity Release," GA Technologies Inc. Report GA-6511 (Rev.), 1969.

Appendix E

EXAMPLES OF SAFETY REPORT AMENDMENTS

Abstract

Several example documents are provided to illustrate the
work that has been required, or is expected to be required,
in preparing a Safety Report amendment for a licensing
authority in order to obtain a license for core conversion.
The examples represent a spectrum of reactor types from
critical facilities to research reactors with power levels
between 2 and 70 MW. The changes addressed range from the
testing of prototype elements to full core replacement. One
reactor required changes to the associated plant as well.
The extent of the Safety Report amendments required varies
from case to case over a similarly wide range.

SAFETY REVIEW OF KUCA CONVERSION
FROM HEU TO MEU FUEL

K. KANDA, Y. NAKAGOME, M. HAYASHI
Research Reactor Institute,
Kyoto University,
Osaka, Japan

Abstract

An outline is provided of the items examined by the Japanese
Government in its safety review for conversion of the KUCA core
from HEU to MEU fuel. Results include a comparison of the
neutronic characteristics of the core with HEU and MEU fuels,
information on the integrity of MEU aluminide fuel, and an
analysis of the worst case accident that was considered.

1. Introduction

The Kyoto University High Flux Reactor (KUHFR) consist of two
separate cylindrical cores, 15 cm apart, which are light water moderated
and heavy water reflected. Because of the complex design, a detailed
engineering mock-up was necessary to verify calculated basic core
parameters. The Kyoto University Critical Assembly (KUCA) was utilized
for KUHFR design purposes to justify the reliability of calculations,
including experiments to determine the critical mass, flux
distributions, control rod worths, temperature coefficients, void
coefficient, etc.

KUCA consists of three cores : the A- and B-cores are operated with
solid moderator fuel only (similar to ZPR-9 and ZPPR), and the C-core is
operated with light water as the moderator and heavy water as the
reflector. The C-core was used for detailed KUHFR critical experiments
with HEU fuel from October, 1974 to October, 1977.

The Reactor Installation License for the KUHFR using HEU was
approved by the Japanese Government in September 1978.

If reduced enrichment fuel, MEU of approximately 45 % enrichment in
^{235}U, is to be utilized in the KUHFR, demonstration of MEU fuel assembly
integrity and strict safety examinations would be required by the
Japanese Government.

An application of safety review (Reactor Installation License) for
MEU fuel to be used in the KUCA was submitted to the Japanese Government
in March 1980, and licensed in August 1980. Subsequently, the

application for 'Authorization before Construction' was submitted and was authorized in September 1980. Immediately, fabrication of MEU fuel elements for the KUCA experiments by CERCA in France was started, and was completed in March 1981. The critical experiments in the KUCA with MEU fuel were started on a single-core in May 1981 as a first step.

The specifications of MEU fuel are described in Appendix K-5. The results already performed by using the KUCA are written in Appendix H-2.

Therefore, this section provides only the outline of items examined by the Japanese Government.

2. **Comparison of neutronic characteristics of the KUCA using HEU and MEU fuels**

Table 1 shows the neutronic characteristics for HEU and MEU fuels, and the computer codes used are also listed.

Table 1   Neutronic Characteristics (KUCA)

	HEU	MEU
fuel plate pitch (mm)	3.8	3.8
moderator	H_2O	H_2O
reflector	D_2O	D_2O
fuel meat	U-Al alloy	UAl_x-Al
enrichment	93.2	45
uranium content (w/o)	22.0	42
uranium content (g/cm^3)	0.6737	0.7575
minimum critical mass (g-^{235}U)	3524	4347
minimum critical mass (no. of plates)	266	266
k_{eff}	1.00204	1.00581
total rod worth	0.1481	0.1461

computer code :   2D-diffusion code

KAK, THERMOS and GGC-4

3-groups ;

1: 15 MeV $\sim$ 5.53 keV

2: 5.53 keV $\sim$ 0.683 eV

3: 0.683 eV $\sim$

3. Integrity of aluminide MEU fuel

In addition to mechanical examination on aluminide fuel, the integrity, mainly fission product release from aluminide fuel, was discussed. We refered the former data performed in Argonne National Laboratory - Idaho, some of which an shown in Figs. 1 ∼ 3. The authorities, however, required more reliable update data when alminide fuel is applied to the KUHFR. Therefore, we measured later the release of fission products using miniature fuel plate, which was a part of KURRI-ANL Joint Study. (See Appendix J-5.2)
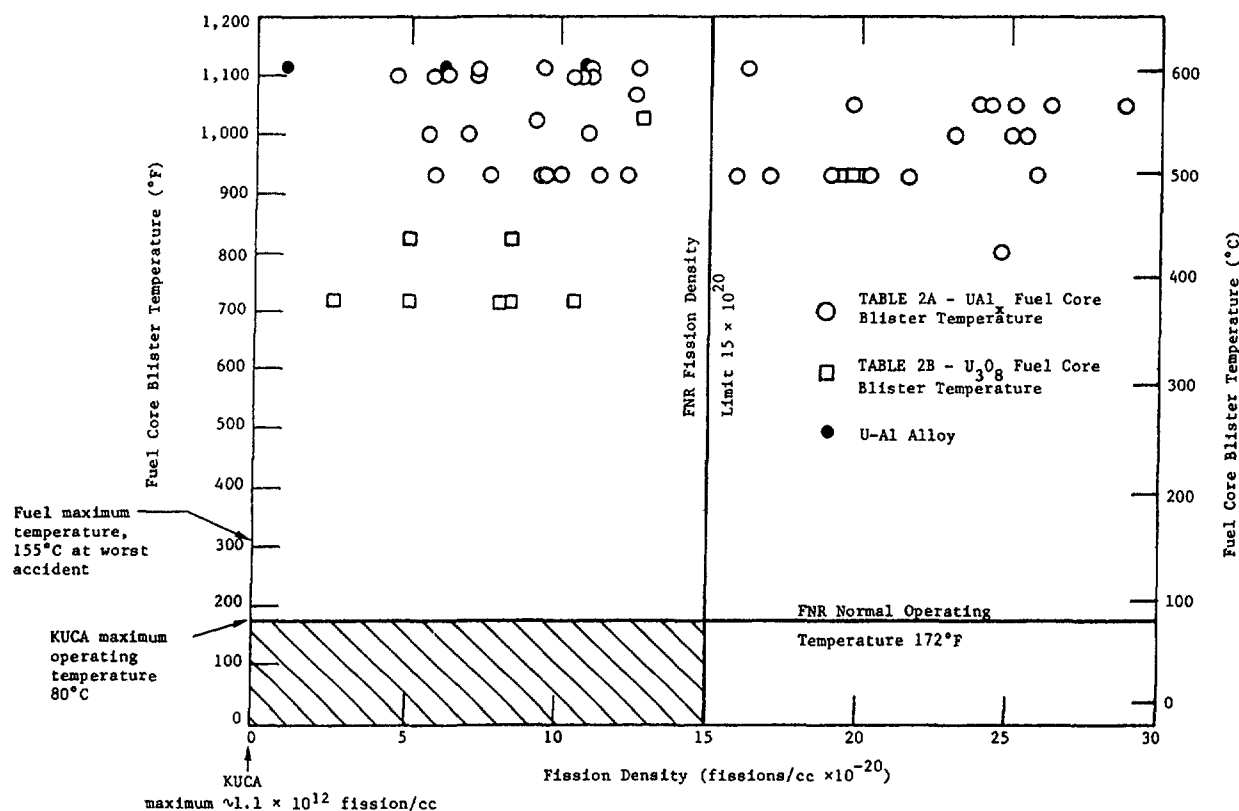
Fig. 1 Fuel Core Blister Temperatures (from Fig. 2, Appendix E-3)
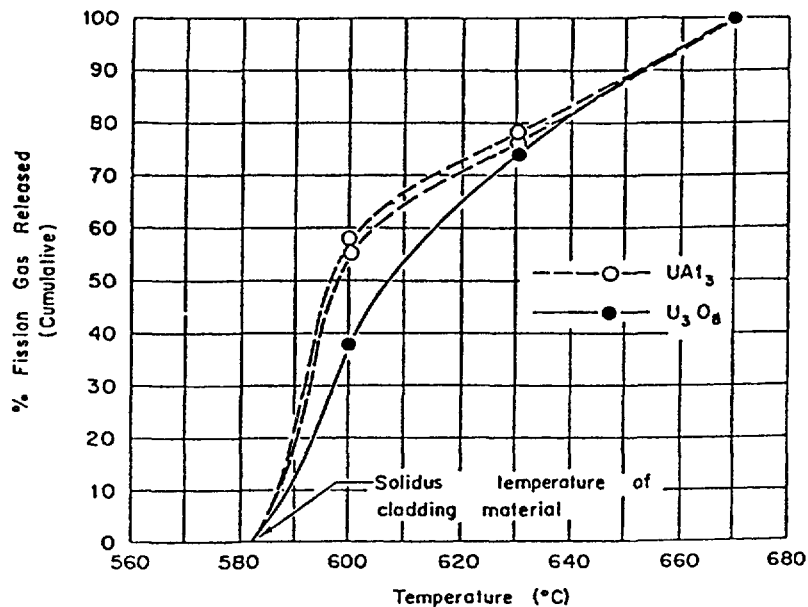
Fig. 2   Percent Fission Gas Released (cumulative) from Three Fuel Plates

M. J. Graber, M. Zukor and G. W. Gibson, "Fission Gas Release from Fuel Plate Meltdown", IDO-17218 (1966).
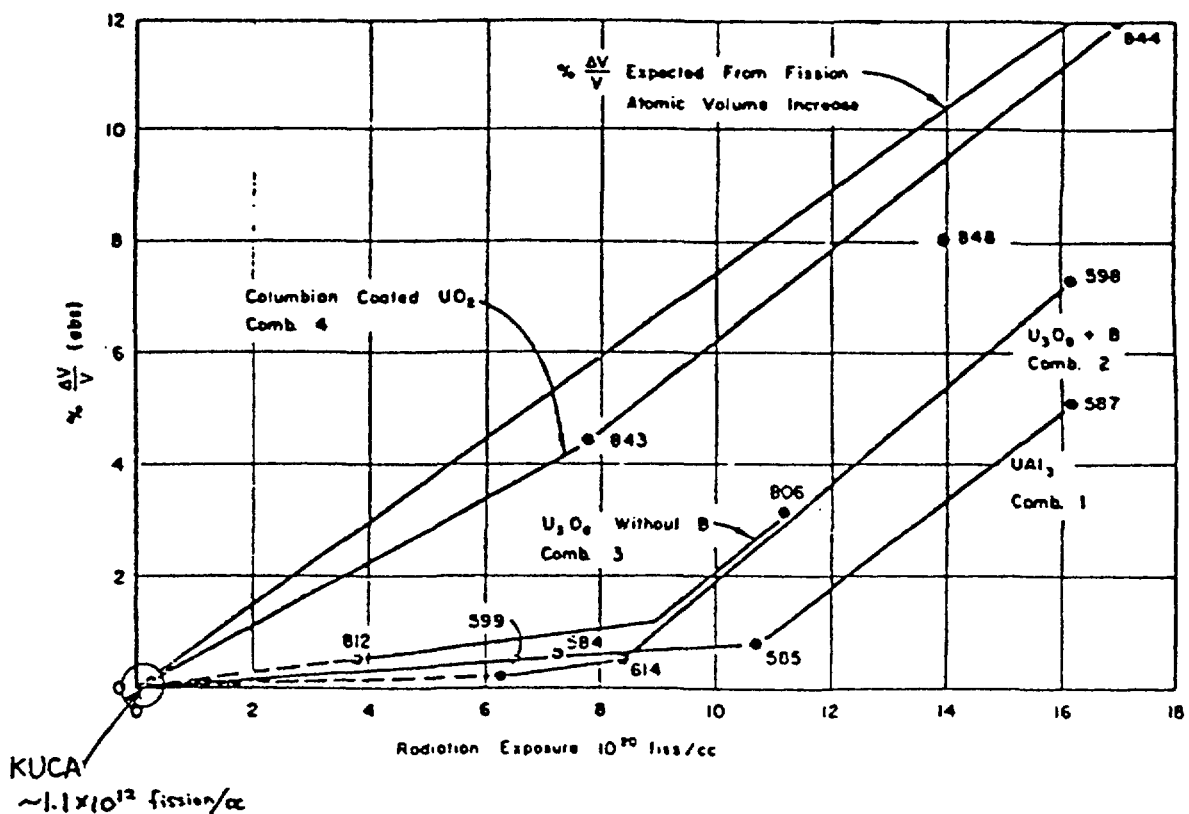
Fig. 3   Core Volume Behavior as a Function of Fission Density

V. A. WalRer, M. J. Graber, G. W. Gibson, "ATR Fuel Material Development Irradiation Results, PART II", IDO-17157 (1966).

254

4. Accident analysis

The sequence of the worst accident examined was as follows :

(1) The KUCA is operated at power level of 0.01 W.

(2) The reactivity insertion is done at 0.02 %Δk/k/sec.

(3) The maximum excess reactivity is 0.5 %Δk/k.

(4) The scram signals from the nuclear instrumentation are failed.

(5) The oprator notices the alarm from the radiation monitor at 1.2 kW level.

(6) In 20 sec after the alarm, the operator push the manual scram buttom.

(7) But all control and safety rods are stuck. Only the backup scram system, "Drain Valve Open" works in 10 sec.

The result of the accident calculation is shown in Table 2 with reference to other core compositions using HEU fuel. The maximum temperature, released energy and fuel temperature increase for the MEU core did not exceed the former calculations for HEU cores. Figure 4 shows an example of accident analysis for a light water core using HEU fuel, on the other hand, Fig. 5 that for the core using MEU.

Table 2   Worst accident analysis

	Core	Enrich-ment (%)	Max. power (KW)	Reliesed Energy (MW.sec)	Fuel Temperature Increase(°c) Ave. Max.		Total Reactivity Increase (%k/k)
L.W Moderator	3.5-0	93	308	3.4	92	166	0.5
	3.5-1.5-H_2O	93	620	6.7	91	164	0.5
	3.5-30-C	93	459	5.0	91	164	0.5
	BK38O_2(MEU)	45	296	2.8	86	155	0.5
Solid Moderator	1-CH_2-100	93	135	1.3	141	211	0.35
	1-C-800	93	139	1.4	151	227	0.35
	2-1-U	93	1,307	7.4	195	293	0.35
	2-1-Th	93	1,096	6.1	139	209	0.35
	2-2-U	93	1,623	10.8	219	329	0.35
	2-2-Th	93	1,400	9.3	154	231	0.35
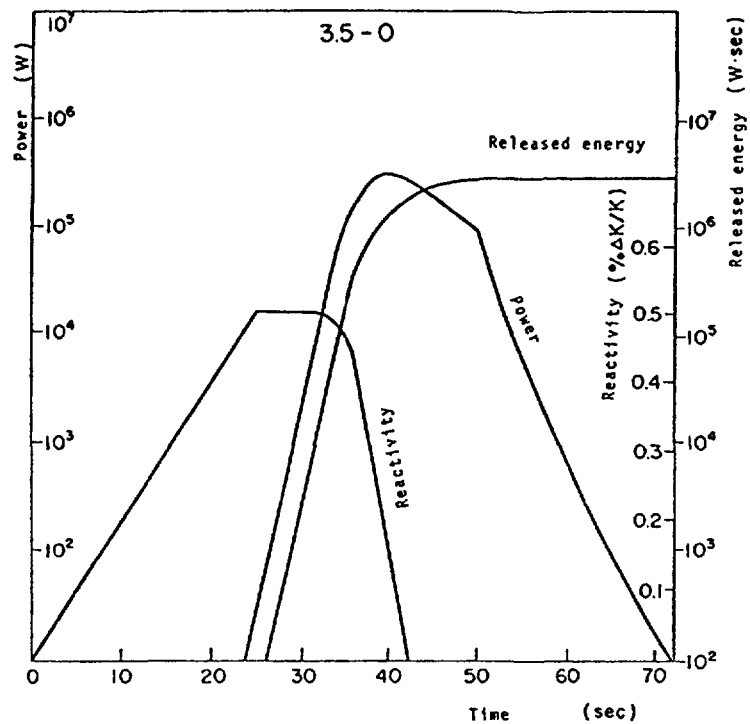
Fig. 4 Worst Accident Analysis for 3.5-0 Core
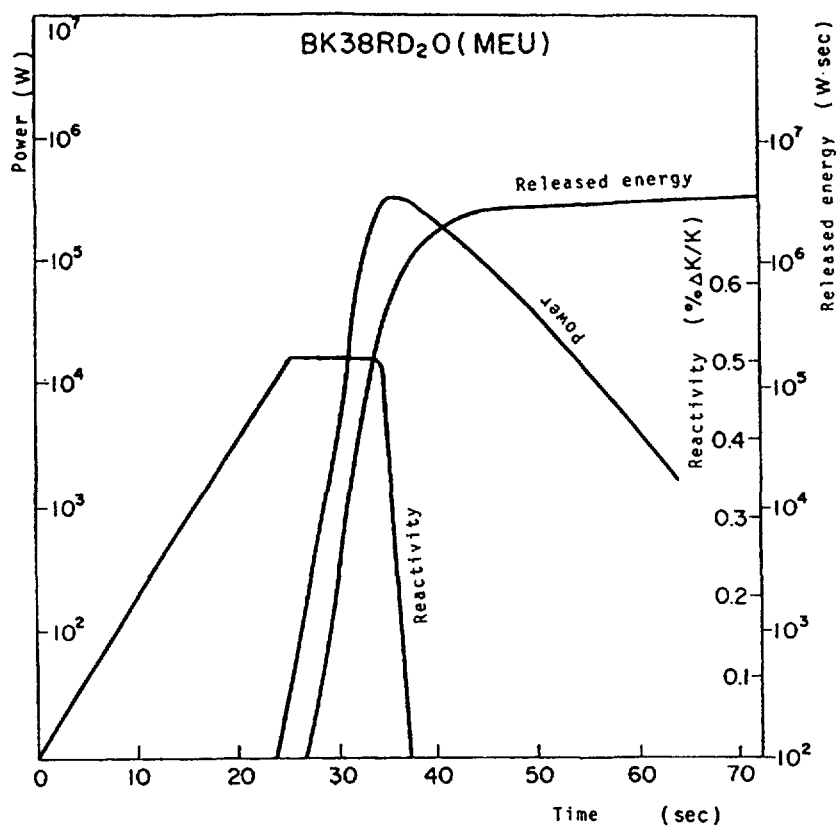
Fig. 5 Worst Accident Analysis for MEU-BK-38RD$_2$O Core

Appendix E-2

SAFETY ANALYSIS OF JMTRC CORE CONVERSION FROM HEU TO MEU FUEL

R. OYAMADA, T. NIIBO, Y. NAGAOKA
Japan Atomic Energy Research Institute,
Tokai-mura, Naka-gun, Ibaraki-ken,
Japan

Abstract

An outline is provided of main parts of the safety analysis for conversion of the JMTRC core from HEU to MEU fuel. Results include information on the fuel design, neutronic characteristics of the reactor core, postulated reactivity insertion accidents, and the maximum credible accident.

1. INTRODUCTION

The JMTRC is a 100 W swimming pool type critical facility, moderated and cooled by light-water, and a nuclear mock-up of the JMTR (50 MW).

Purposes of critical experiments in the JMTRC are to validate nuclear calculation codes used for analyzing the JMTR MEU core, and to obtain reactor characteristics of the JMTR MEU core. Items of the experiments are shown in Table 1.

For the JMTRC core conversion, we have prepared the application required for the safety review.

This paper provides outlines of main parts of the safety analysis.

2. FUEL DESIGN

2.1 Fuel Specification

Dimensions of the MEU fuel are the same as those of the HEU fuel, but U-235 content and cladding material are different from the HEU fuel. Table 2 shows the MEU fuel specifications as well as those of the current HEU fuel.

Three kinds of standard fuel elements different in U-235 content will be fabricated in order to simulate equilibrium core of the JMTR.

257

Table 1   Items of Critical Experiments in the JMTRC MEU Core

1. Minium critical core
   • Critical mass

2. Full core
   • Excess reactivity
   • Control rod worth
   • Power calibration (Reactor noise technique)
   • Space dependent mass coefficient
   • ℓp/β (Pulsed neutron technique)
   • Flux distribution and power calibration
   • Shut-down margin
   • Void coefficient
   • Temperature coefficient*

* If infeasible in the JMTRC either JRR-4 with the LEU fuel or JMTR is to be used for this item.

Table 2   Fuel Specifications

	HEU Fuel		MEU Fuel	
	Standard	Follower	Standard	Follower
Fuel type	Modified ETR	ETR	Modified ETR	ETR
Enrichment (Wt.%)	90	90	45	45
Plates/Element	19	16	19	16
U-235/Element (g)	A:279*(0.73)	F:195*(0.77)	MA:310*(1.62)	MF:205*(1.61)
	B:237 (0.62)		MB:280 (1.46)	
	C:195 (0.51)		MC:250 (1.31)	
Meat Dimension (mm)	0.50×59.5×752.5	0.50×47.6×743.5	0.50×59.5×752.5	0.50×47.6×743.5
Cladding Thickness(mm)	0.385	0.385	0.385	0.385
Plate Dimension (mm)	1.27×70.8×778	1.27×59.5×780	1.27×70.8×778	1.27×59.5×780
Water Gap (mm)	12×2.67	15×2.59	12×2.67	15×2.59
	2×2.92		2×2.92	
	4×3.02		4×3.02	
Element Dimension (mm)	76.2×76.2×1200	63.5×63.5×855	76.2×76.2×1200	63.5×63.5×855
Fuel Core Material	U-Al Alloy	U-Al Alloy	UAlx-Al Powder	UAlx-Al Powder
Cladding Material	Al(JIS A1100 or JIS A1200)	Al(JIS A1100 or JIS A1200)	AL-Mg Alloy or AL(JIS A6061)	Al-Mg Alloy or AL(JIS A6061)

* The figure in parentheses shows the uranium loading density (g/cm³) in the fuel meat.

2.2 Fuel Mechanical Integrity

Thermal-hydraulic problems are not severe. Only corrosion of the cladding material (aluminum) is needed to evaluate.

Corrosion of the cladding material was estimated to be at most 0.015 mm in thickness for service period of thirty years, based on data shown in Fig. 1. And this thickness change is negligible comparing with the nominal cladding thickness (0.385 mm).
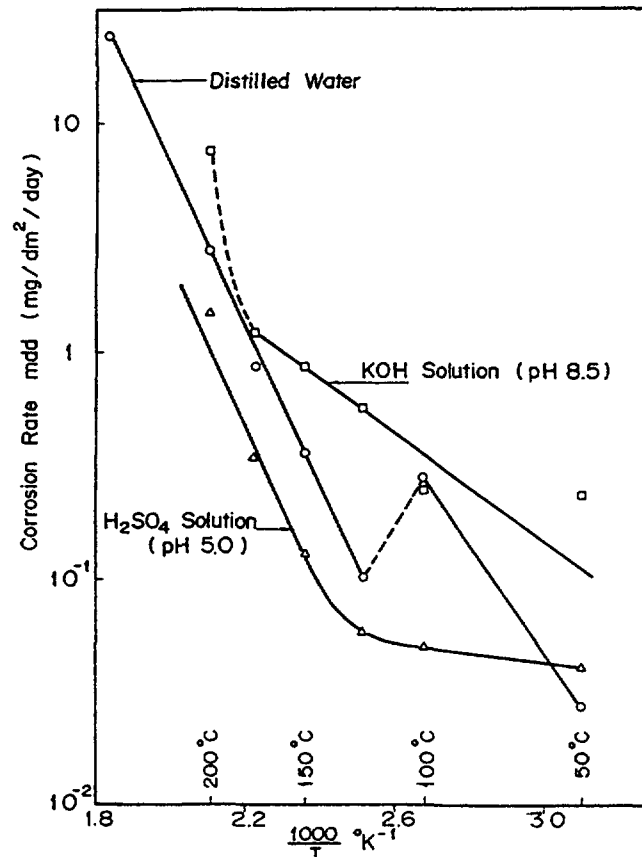
FIG. 1. Corrosion rate on aluminum (Ref.: Japan Soc. of Mech. Eng., Mechanical Engineering Handbook, fourth revised edition (1960) 5-76).

In addition, the quality of pool water is maintained in the range of pH 5.5 to 7.7 and over 5×10^5 ohm-cm in specific resistance.

3. NEUTRONIC CHARACTERISTICS OF REACTOR CORE

3.1 Neutronic Criteria

The neutronic criteria for the JMTRC operation are as follows ;

(1)	Thermal output	:	Max. 100 W
(2)	U-235 loading	:	Max. 8 Kg
(3)	Excess reactivity	:	Max. 15 %Δk/k
(4)	Shutdown margin	:	Less than or equal to 0.9 in K_{eff}
(5)	One rod-stuck margin	:	Subcritical when one rod with maximum reactivity is fully withdrawn.

3.2 Neutronic Characteristics

Neutronic characteristics were reviewed for the standard core and the maximum core with the MEU fuel elements. The former is a core configuration used in usual experiments and the latter is one which is the most severe core in terms of the neutronic criteria for safety review. Both core configurations are shown in Figs. 2 and 3. These reviews were made for the HEU cores as well in order to compare with the MEU cores.

The codes used for neutronic calculations are as follows ;

(1)	Thermal group constants	:	THERMOS
(2)	Fast group constants (3 groups)	:	GGC-4
(3)	Core calculation	:	CITATION (X-Y directions)
(4)	Kinetics parameters	:	KPARAM

The calculated results are summarized in Table 3.

4. POSTULATED REACTIVITY INSERTION ACCIDENTS

Reactor kinetics parameters are affected by the core conversion from the HEU fuels to the MEU fuels. It is therefore necessary to review the postulated reactivity insertion accidents. In the accident analyses, however the same values with some margin were used for both the HEU and the MEU core, considering the fact that calculational values show somewhat overestimation compared to experimental values.

FIG. 2. Standard core.

261

FIG. 3. Maximum core.
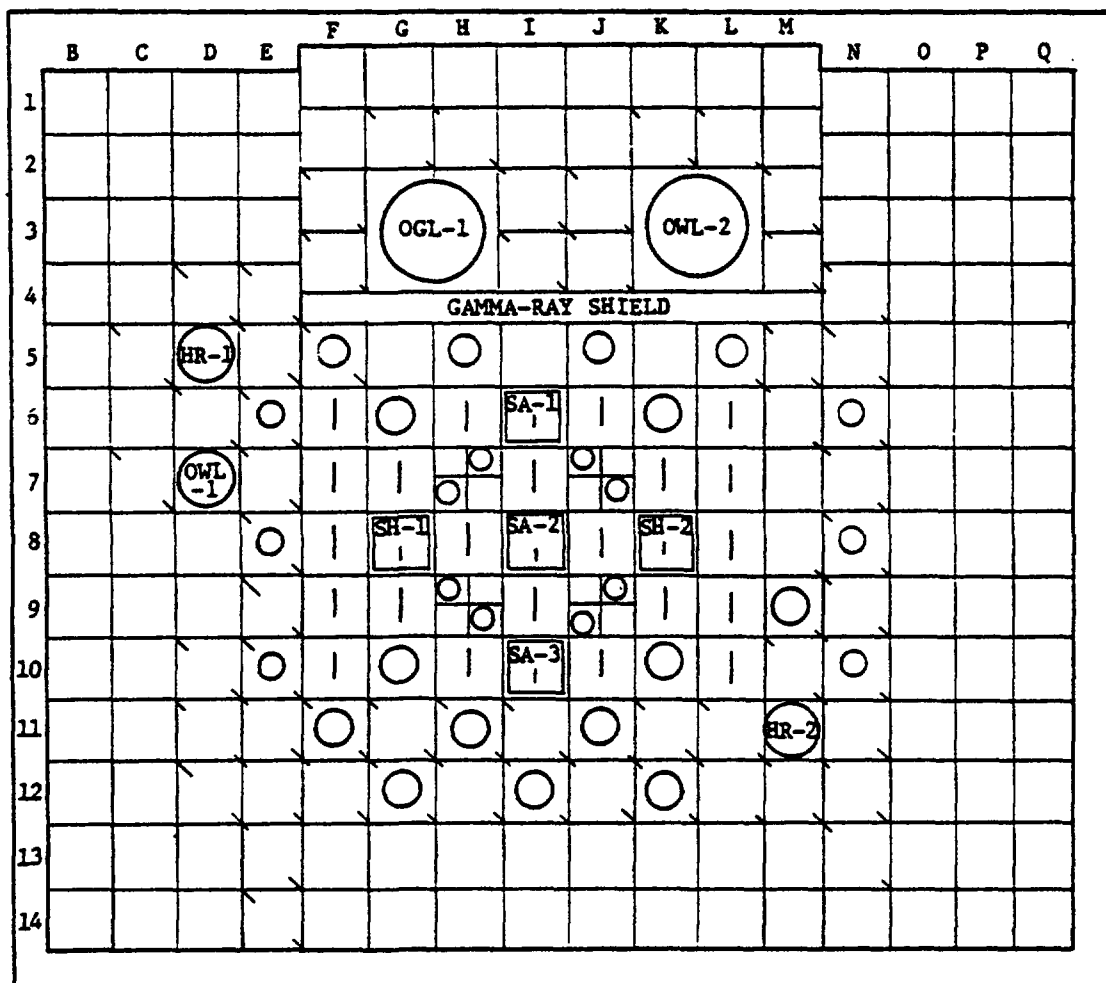
Remarks

	Fuel Element
	Control Rod with Follower Fuel
	Be Element
O	Mock-up of Capsule (φ 30)
	Al Element (1 irradiation hole)
O	Mock-up of Capsule (φ 36)
	Al Element (4 irradiation holes)
O	Mock-up of Capsule (φ 40)
	Mock-up of Loops and Hydraulic Rabbits

Table 3 Nuclear Characteristics

	HEU Fuel Core		MEU Fuel Core	
	Std. Core	Max. Core	Std. Core	Max. Core
Core Configuration				
No. of Standard A or MA	8(279)*	10(279)*	8(310)*	2(310)*
No. of Standard B or MB	12(237)	0(237)	12(280)	0(280)
No. of Standard C or MC	2(195)	16(195)	2(250)	24(250)
No. of Follower F or MF	5(195)	5(195)	5(205)	5(205)
U-235 Loading (kg)	6.4	6.9	7.4	7.6
Nuclear Characteristics				
Excess Reactivity($\%\Delta k/k$)	9.9	14.8	9.8	14.0
Total Rod Woth ($\%\Delta k/k$)	36.3	34.5	34.9	28.1
Shutdown Margin ($\%\Delta k/k$)	22.8	14.5	21.7	10.2
One Rod-stuck Margin (k_{eff})	0.870	0.935	0.877	0.962

* The figure in parentheses shows the U-235 Content (g) per
  fuel element.

The postulated reactivity insertion accidents in the JMTRC
are as follows ;

- Control rod withdrawal
    - Start up :
    ramp reactivity insertion rate of 0.05 $\%\Delta k/k/s$ from
    0.1 mW until safety system trip initistion
    - Rated power operation :
    ramp reactivity insertion rate of 0.05 $\%\Delta k/k/s$ from
    100 W until safety system trip initiation
- Failure of in-core experiment
    - Poison plate :
    step reactivity insertion of 0.2 $\%\Delta k/k$ at 100 W
    - Void elements (floating) :
    ramp reactivity insertion rate of 4.4 $\%\Delta k/k/s$ for the
    period of 196 ms at 7 W

Following assumptions are adopted in each accident analysis
described above ;

- Core : the maximum core (the most severe core in
          terms of the nuclear criteria)
- Safety system trip point : 120 W
- Time delay to scram : 40 ms of delay after power
          reaches the trip point which the scram is stared

263

Reactivity insertion transients were analyzed by the
EUREKA-PT code, which was developed by modifying the EUREKA
code for plate-type reactors, and has been demonstrated
reliability through the SPERT-III C core experiment analysis.
The code provides a coupled thermal, hydrodynamic and point
kinetics capability with continuous reactivity feedback.

The kinetics parameters of the cores with the HEU and the
MEU fuels used for the reactivity insertion transient analyses
are shown in Table 4.

Table 5 shows characteristic values for the fuel meat and
the cladding material.

Peak powers analyzed for each accident are presented in
Table 6. As can be seen in Table 6, the void elements accident
is the most severe one of the reactivity insertion accidents
for both the HEU and the MEU fuel cores in the JMTRC. Hence,
this accident was selected as the maximum credible accident and
further analyzed for radiological consequence, as described
in section 5.

Table 4   Kinetics Parameters used for Reactivity Insertion
           Transient Analyses

	Temp. Coef. (% k/k/°C)	Void Coef. (% k/k/%Void)	ℓ_p (s)	β_{eff}
HEU core	-0.8×10^{-2}*	-1.5×10^{-1}*	3.89×10^{-5}	7.16×10^{-3}
MEU core	-0.8×10^{-2}*	-1.5×10^{-1}*	3.59×10^{-5}	7.14×10^{-3}

* Considering the fact that   calculated   values show
  somewhat overestimation compared to experimental values,
  the same values with some margin were used for the
  accident analyses of both the HEU and the MEU cores.

Table 5   Characteristic Values for Fuel Meat and
           Cladding Material

	HEU Fuel		MEU Fuel	
	Fuel Meat	Cladding	Fuel Meat	Cladding
Density (g/cm³)	3.30	2.699	3.86	2.699
Heat Capacity (kcal/kg·°C)	0.174	0.215	0.136	0.215
Thermal Conductivity (kcal/m·h·°C)	146.88	174.96	74.52	174.96

Table 6 Peak Power Reached in Reactivity Insertion Accidents

	Control rod withdrawal		Failure of in-core experiment	
	Start up	Rated power ope.	Poison plate	Voild element
HEU core	1.1 kW	121 W	144 W	86.6 MW
MEU core	1.1 kW	121 W	144 W	172.0 MW

Figure 4 plots transient responses of the HEU and the MEU cores to the ramp reactivity insertion of 4.4 %Δk/k/s for the period of 196 ms, which is the results of the void elements accident analyses. Table 7 shows main results of the void elements accident analyses.
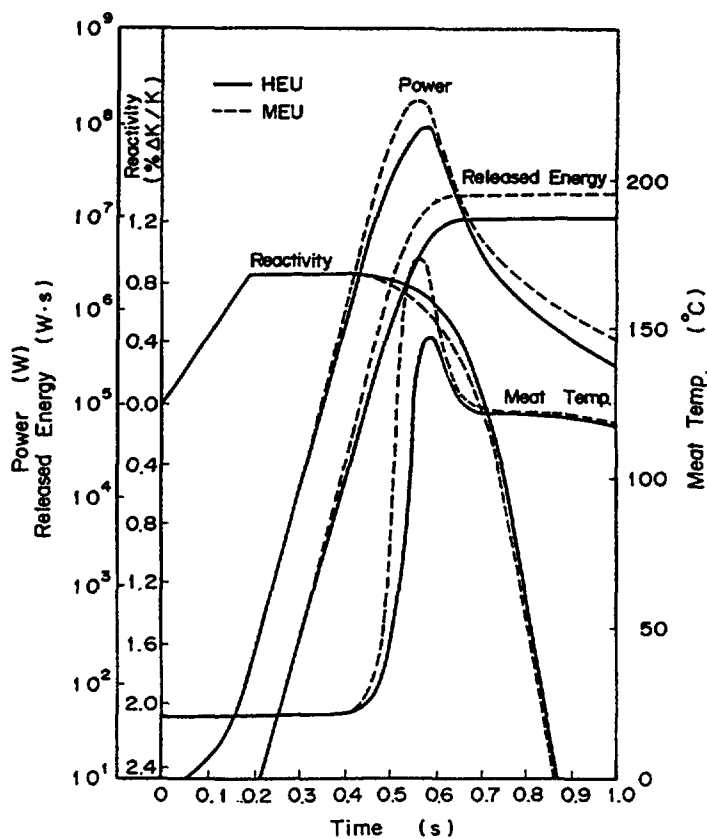
FIG. 4. Transient responses of HEU and MEU cores to ramp reactivity insertion of 4.4% ΔK/K/s in 196 ms.

Table 7   Results of Void Elements Accident Analysis

	Peak Power (MW)	Released Energy (MW.s)	Meat Temp. (°C) Average Spot	Meat Temp. (°C) Hot Spot
HEU core	86.6	9.4	101	149
MEU core	172.0	17.8	128	176

5. MAXIMUM CREDIBLE ACCIDENT

As described in section 4, void elements accident is the most severe one of the postulated reactivity insertion accidents in the JMTRC.

In order to evaluate the radiological consequence fully conservatively, following assumptions were made ;

(1) The reactor is operated at rated power of 100 W for infinite period.

(2) All fuels in the core are damaged by the accident.

(3) Of fission products (FP) accumulated after the infinite reactor operation time and during the reactor transient (released energy of 17.8 MW·s), 100 % of inert gas and 5 % of iodine are released to the reactor building, respectively through the pool water.

Schema of FP release at the maximum credible accident is shown in Fig. 5.

Effective continuous release time of FP from the reactor building was conservatively assumed to be one hour.

Activities of FP released to the atmosphere were estimated to be ;

Inert gas : 1.43×10^4 Ci (equivalent to 0.5 MeV γ-ray)

        : 1.79×10^4 Ci (equivalent to 0.5 MeV β-ray)

Iodine   : 4.58×10^{-1} Ci (equivalent to I-131)

The estimated maximum exposure dose for the public in the sorrounding area (the minimum distance from the reactor building is 1040 m) are as follows ;

External dose to the total body due to γ-ray :   121 mrem

External dose to the total body due to β-ray :   515 mrem

Internal dose to the thyroid due to iodine for child

                                    :   236 mrem

These values are negligible order for the tolerance values specified in the official notification and there is no problem.

FIG. 5. FP release in maximum credible accident.

Appendix E-3

SAFETY ANALYSIS — UTILIZATION OF LOW ENRICHMENT URANIUM (LEU) FUEL IN THE FORD NUCLEAR REACTOR

FORD NUCLEAR REACTOR/UNIVERSITY OF MICHIGAN
Ann Arbor, Michigan,
United States of America

Abstract

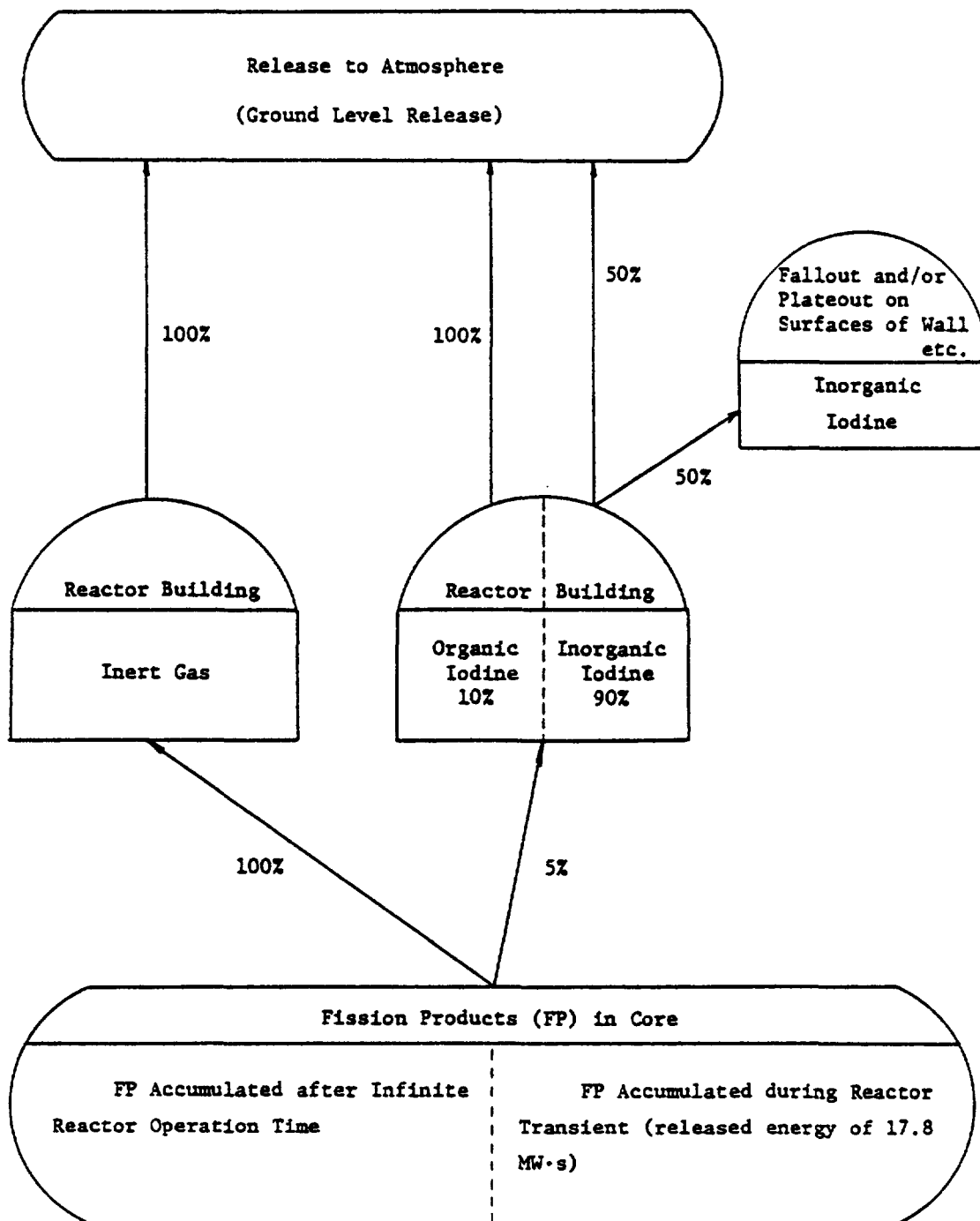This analysis reviews the safety aspects of utilizing low enrichment uranium (LEU-less than 20% enrichment) fuel in the Ford Nuclear Reactor (FNR). A brief description of the proposed fuel is followed by an examination of fuel swelling, high temperature blistering, and failure data for similar operational and test fuels under operating conditions similar to those in the FNR. Fuel specifications have been developed with technical requirements identical to those for reactors which use equivalent fuel. Heat transfer characteristics are not examined in detail because fuel and coolant flow channel dimensions are identical to those in present FNR fuel. Core physics analyses show some variation in fast and thermal neutron flux distributions within the core and in the reflector regions. The available data and the analyses performed indicate that no reduction in safety margins are expected from utilizing LEU fuel in the FNR core.

1. INTRODUCTION

As part of the national plan for development of high uranium density research and test reactor fuel to accomodate the use of low enrichment uranium (LEU) fuel, the Ford Nuclear Reactor (FNR) proposes to test the use of 19.5 wt% enriched uranium fuel in the form of uranium aluminide (UAl_x) or uranium oxide (U_3O_8) in place of the present 93 wt% uranium aluminide fuel.

The use of less than 20% enrichment fuel gives the potential benefit of reducing the probability of uranium-235 diversion. An additional benefit is a possible reduction in the cost of security requirements for both fuel fabrication and fuel handling and storage.

This report includes information on fuel which is physically similar to the proposed LEU fuel and which has been satisfactorily tested under operating conditions similar to those of the Ford Nuclear Reactor.

Core physics calculations indicate that utilization of LEU fuel in the FNR core will result in a decrease in thermal flux of 12-20% in the core region and a decrease of 6-10% in the reflector region.

2. FUEL DESCRIPTION

The proposed LEU fuel meat is to be intermetallic uranium aluminide (UAl_3, UAl_4, UAl_2) or uranium oxide (U_3O_8) cermet, both of which are licensed for use by the FNR, clad in 6061 aluminum.

Fuel element overall dimensions and internal dimensions will remain identical to the dimensions of fuel presently being used in the FNR at two megawatts. Plate thickness will be 0.060 inches. The meat will be 0.030 inches and cladding 0.015 inches. Two plate thicknesses are presently in use at the FNR. Uranium-aluminum alloy fuel plates are 0.060 inches thick with 0.020 clad-0.020 meat-0.020 clad. Aluminide fuel plates are 0.050 inches thick with 0.015 clad-0.020 meat-0.015 clad. The FNR has   operating experience with fuel plates which are 0.060 inches thick and which have 0.015 inch clad, and no problems have arisen.

The proposed meat thickness of 0.030 inches is dictated by an attempt to provide fuel with the same reactivity as present FNR fuel while reducing the enrichment from 93% to just under 20%. In order to provide the proper uranium-235 loading, the weight percent of the fissile compound in the fuel meat must be increased from the present 19.1 weight percent UAL_x or 16.8 weight percent U_3O_8 to approximately 56.5 weight percent UAL_x or 49.6 weight percent U_3O_8. Present uranium loading is 14.2 weight percent; the proposed loading is 42.0 weight percent.

3.   OPERATING CONDITIONS

Fuel swelling data and fuel blister data, which were obtained for fuel plates made of materials similar to those in the FNR and which were determined at fuel temperature, pressure, and pH conditions similar to FNR conditions, were extracted from the data contained in reports referenced in the Safety Analysis bibliography and are tabulated in TABLE 1 and TABLE 2. All available data points are included.

The aluminum powder used in the proposed FNR fuel and in the test cores is a blend of nearly pure aluminum. 1100 aluminum is pure aluminum. The various powder blends (PB-01, PB-04, PB-32, PB-36) are essentially pure aluminum of specific grain sizes. 5214 is spherical aluminum powder with .05% iron and a total of .08% iron plus silicon permitted. X8001 is a nickel alloy of aluminum which is only slightly harder than 1100.

4.   FUEL SWELLING

Table 1A provides UAL_x fuel swelling data. [1, 2, 3, 4, 5] Table 1B contains U_3O_8 fuel swelling data. 4Test temperatures are as close as possible to the FNR peak operating temperature of 172°F. All test data were obtained at significantly higher pressures. Figure 1 is a plot of the UAL_x and U_3O_8 data points. Also shown on Figure 1 is the FNR fission density limit of 15×10^{20} fissions/cc and the calculated swelling rate for 100% dense fuels.

With the exception of one data point, the measured swelling rate is below the calculated swelling rate. It is expected that the measured swelling rate would be less than calculated because some voids are expected in core compacts and voids generally tend to reduce swelling.

No fuel failures were observed for the fission density-fuel swelling combinations plotted on Figure 1. Therefore, all of the available fuel swelling data at operating conditions similar to those in the FNR indicate that UAL_x and U_3O_8 fuel can be safely used in the FNR without failure due to swelling and that no reduction in the safety margin is expected.

270

TABLE 1A. UAL$_x$ FUEL CORE SWELLING DATA

Reactor Sample ID	Clad	Core	Weight Percent UAL$_x$	Weight Percent U	Core Temp, °F (°C)	Operating Pressure PSIG	pH	Fission Density f/cc X 10^{20}	Volume Change %ΔV/V	Ref
FNR	6061	5214	19.1	14.2	172 (78)	9.2	5-7	15.0		
MTR										
113-1	6061	6061	46.7	34.7	239 (115)	50	5-7	7.5	7.5	1
113-2	6061	6061	46.7	34.7	239 (115)	50	5-7	10.1	6.8	1
113-3	6061	6061	46.7	34.7	239 (115)	50	5-7	9.4	6.2	1
113-4	6061	6061	46.7	34.7	239 (115)	50	5-7	9.8	3.7	1
113-5	6061	6061	46.7	34.7	239 (115)	50	5-7	13.5	7.3	1
113-6	6061	6061	46.7	34.7	239 (115)	50	5-7	14.1	7.3	1
113-7	6061	6061	46.7	34.7	239 (115)	50	5-7	14.5	5.5	1
ETR										
I-1-1095	6061	X8001	51.0	37.9	230 (110)	200	5-7	6.9	0.8	2
I-1-1097	6061	X8001	51.0	37.9	230 (110)	200	5-7	5.6	0.8	2
I-12-727	APM786	X8001	51.0	37.9	230 (110)	200	5-7	10.9	3.9	2
I-1-584	6061	X8001	51.0	37.9	302 (150)	200	5-7	7.2	0.6	2
I-69-1579	6061	MD101	60.0	44.6	302 (150)	200	5-7	16.5	3.6	2
I-71-1594	6061	MD101	77.0	57.2	302 (150)	200	5-7	24.7	1.1	2
I-69-1580	6061	MD101	60.0	44.6	338 (170)	200	5-7	9.4	1.8	2
I-70-1583	6061	MD101	65.0	48.3	338 (170)	200	5-7	11.0	1.2	2
I-70-1584	6051	MD101	65.0	48.3	338 (170)	200	5-7	16.2	4.9	2
ETR										
169-4	6061	X8001	61.9	46.0	228 (109)	200	5-7	26.3	2.0	3
169-5	6061	X8001	61.9	46.0	228 (109)	200	5-7	28.8	4.7	3
169-11	6061	X8001	52.0	38.7	228 (109)	200	5-7	23.1	4.7	3
169-12	6061	X8001	52.0	38.7	228 (109)	200	5-7	24.3	5.9	3
169-19	6061	X8001	43.0	32.0	228 (109)	200	5-7	19.7	4.7	3
169-36	6061	X8001	52.8	39.2	228 (109)	200	5-7	25.1	6.4	3
169-37	6061	X8001	52.7	39.2	228 (109)	200	5-7	25.5	6.0	3
169-38	6061	X8001	52.7	39.2	228 (109)	200	5-7	25.0	7.4	3
169-39	6061	X8001	52.7	39.2	228 (109)	200	5-7	23.9	5.7	3
HF IR										
32-4	6061	PB-32*	51.0	37.9	176 (80)	1000	5-7	17.9	8.8	4
34-2	6061	PB-36	53.0	39.4	190 (88)	1000	5-7	19.5	6.8	4
14-3	6061	PB-32	53.0	39.4	198 (92)	1000	5-7	20.2	7.4	4
15-4	6061	PB-32	63.0	46.8	203 (98)	1000	5-7	22.2	6.1	4
35-4	6061	PB-36	63.0	46.8	201 (94)	1000	5-7	21.4	4.8	4
25-4	6061	PB-32	64.0	47.6	205 (96)	1000	5-7	21.7	4.1	4
FR2 (Kalsruhe, Germany)										
1-4	1100	1100	50	37.1	158 (70)	50	5-7	5.8	2.0	5
2-4	1100	1100	50	37.1	158 (70)	50	5-7	16.9	4.5	5
3-4	1100	1100	50	37.1	158 (70)	50	5-7	12.2	4.0	5
4-1	1100	1100	50	37.1	158 (70)	50	5-7	9.4	3.5	5
5-3	1100	1100	45.5	33.8	158 (70)	50	5-7	9.4	3.5	5
6-4	1100	1100	45.5	33.8	158 (70)	50	5-7	7.6	4.0	5
7-2	1100	1100	50	37.1	158 (70)	50	5-7	15.8	5.0	5
8-2	1100	1100	45.5	33.8	158 (70)	50	5-7	15.8	4.0	5

* Aluminum Powder Blends

TABLE 1B. U_3O_8 FUEL CORE SWELLING DATA

| Reactor Sample ID	Clad	Core	Fuel Characteristics Weight Percent U_3O_8	U	Core Temp, °F (°C)	Operating Pressure PSIG	pH	Fission Density f/cc X 10^{20}	Volume Change % ΔV/V	Ref
FNR	6061	5214	16.8	14.2	172 (78)	9.2	5-7	15.0		
HFIR										
12-3	6061	PB-01*	47	39.7	192 (89)	1000	5-7	19.8	3.0	4
13-4	6061	PB-01	40	33.8	183 (84)	1000	5-7	18.1	3.8	4
22-4	6061	PB-04	50	42.3	187 (86)	1000	5-7	19.7	2.9	4
23-1	6061	PB-04	42	35.5	181 (83)	1000	5-7	18.1	3.1	4
ETR										
67-974	6061	PB-01*	40	33.8	401 (205)	200	5-7	17.9	4.7	4
67-982	6061	PB-01	40	33.8	383 (195)	200	5-7	18.0	5.1	4
67-986	6061	PB-01	40	33.8	392 (200)	200	5-7	18.1	6.2	4
56-899	6061	PB-01	50	42.3	302 (150)	200	5-7	11.7	1.4	4
56-957	6061	PB-01	50	42.3	302 (150)	200	5-7	22.4	7.6	4
3-893	6061	PB-04	45	38.0	347 (175)	200	5-7	15.5	2.0	4
68-997	6061	PB-04	49	41.4	347 (175)	200	5-7	19.7	3.6	4
68-1638	6061	PB-04	49	41.4	428 (220)	200	5-7	12.7	0.4	4
68-1633	6061	PB-04	49	41.4	419 (215)	200	5-7	12.7	0.4	4
68-1642	6061	PB-04	49	41.4	410 (210)	200	5-7	12.7	1.7	4
68-1605	6061	PB-04	49	41.4	329 (165)	200	5-7	19.9	3.0	4
68-1607	6061	PB-04	49	41.4	338 (170)	200	5-7	19.5	3.1	4

* Aluminum Powder Blends
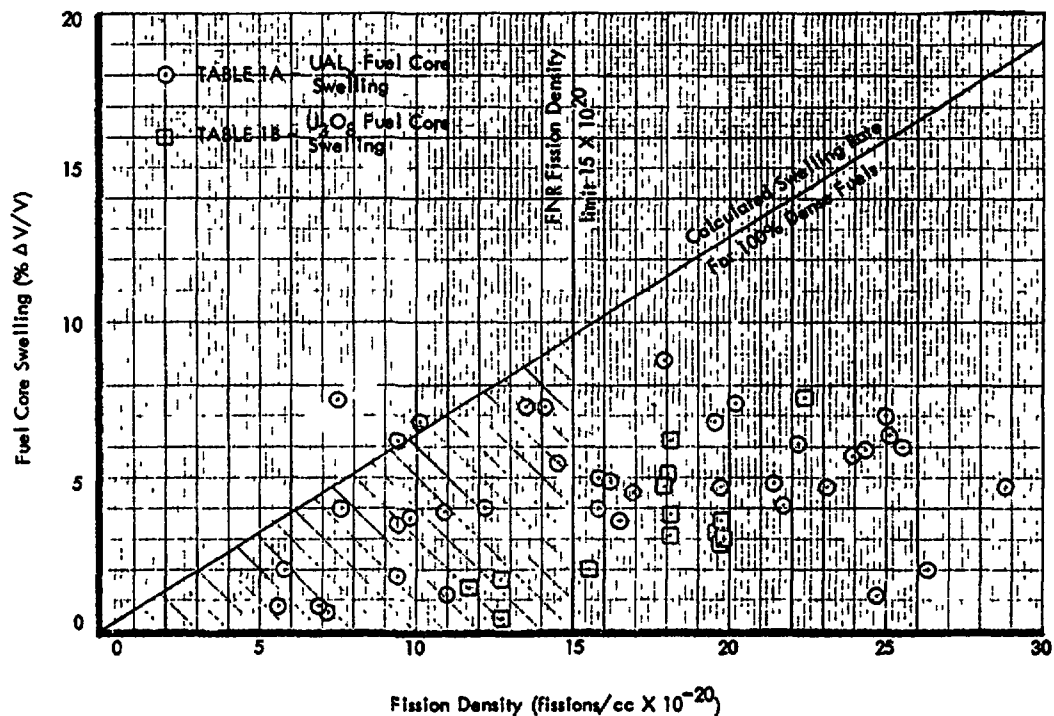
FIG. 1. Fuel core swelling.

5. FUEL BLISTERING

Table 2A provides UAL$_x$ fuel blister data. [1,2,3,5,7] Table 2B contains U$_3$O$_8$ fuel blister data. [1,8] Figure 2, a plot of fuel blister temperature versus fission density for the Table 2A and 2B data, shows that all blister failures occurred in fuel being operated at temperatures well above the FNR peak operating temperature of 172°F.

TABLE 2A. UAL$_x$ FUEL CORE BLISTER DATA

Reactor Sample ID	Clad	Core	Weight Percent UAL$_x$	U	Core Temp, °F (°C)	Operating Pressure PSIG	pH	Fission Density f/cc X 10^20	Blister Temp, °F (°C)	Ref
FNR	6061	5214	19.1	14.2	172 (78)	9.2	5-7	15.0		
ETR										
E-107	6061	X8001	54.0	40.1	403 (206)	200	5-7	10.4	1094 (590)	7
E-508	6061	X8001	54.0	40.1	403 (206)	200	5-7	10.7	1094 (590)	7
E-510	6061	X8001	54.0	40.1	403 (206)	200	5-7	11.0	1094 (590)	7
E-507	6061	X8001	54.0	40.1	403 (206)	200	5-7	11.2	1094 (590)	7
I-1-1095	6061	X8001	51.0	37.9	230 (110)	200	5-7	6.9	1004 (540)	2
I-1-1097	6061	X8001	51.0	37.9	230 (110)	200	5-7	5.6	1004 (540)	2
I-12-727	APM786	X8001	51.0	37.9	230 (110)	200	5-7	10.9	1004 (540)	2
I-69-1579	6061	MD101	60.0	44.6	302 (150)	200	5-7	7.2	1112 (600)	2
I-71-1594	6061	MD101	77.0	57.2	302 (150)	200	5-7	24.7	806 (430)	2
I-69-1580	6061	MD101	60.0	44.6	338 (170)	200	5-7	9.4	1112 (600)	2
I-70-1583	6061	MD101	65.0	48.3	338 (170)	200	5-7	11.0	1112 (600)	2
I-70-1584	6061	MD101	65.0	48.3	338 (170)	200	5-7	16.2	1112 (600)	2
I-71-1593	6061	MD101	77.0	57.2	338 (170)	200	5-7	12.6	1112 (600)	2
169-4	6061	X8001	61.9	46.0	228 (109)	200	5-7	26.3	1050 (565)	3
169-5	6061	X8001	61.9	46.0	228 (109)	200	5-7	28.8	> 1050 (> 565)	3
169-11	6061	X8001	52.0	38.7	228 (109)	200	5-7	23.1	1000 (538)	3
169-12	6061	X8001	52.0	38.7	228 (109)	200	5-7	24.3	1050 (565)	3
169-19	6061	X8001	43.0	32.0	228 (109)	200	5-7	19.7	1050 (565)	3
169-36	6061	X8001	52.8	39.2	228 (109)	200	5-7	25.1	>1050 (> 565)	3
169-37	6061	X8001	52.7	39.2	228 (109)	200	5-7	25.5	1000 (538)	3
169-38	6061	X8001	52.7	39.2	228 (109)	200	5-7	25.0	1000 (538)	3
169-39	6061	X8001	52.7	39.2	228 (109)	200	5-7	23.9	1050 (565)	3
MTR										
113-8	6061	6061	46.7	34.7	239 (115)	50	5-7	4.5	> 1100 (> 594)	1
113-9	6061	6061	46.7	34.7	239 (115)	50	5-7	5.7	> 1100 (> 594)	1
113-10	6061	6061	46.7	34.7	239 (115)	50	5-7	6.2	> 1100 (> 594)	1
113-11	6061	6061	46.7	34.7	239 (115)	50	5-7	7.2	> 1100 (> 594)	1
113-12	6061	6061	46.7	34.7	239 (115)	50	5-7	10.5	> 1100 (> 594)	1
113-13	6061	6061	46.7	34.7	239 (115)	50	5-7	9.2	1022 (550)	1
113-14	6061	6061	46.7	34.7	239 (115)	50	5-7	9.5	932 (500)	1
113-15	6061	6061	46.7	34.7	239 (115)	50	5-7	11.3	932 (500)	1
113-16	6061	6061	46.7	34.7	239 (115)	50	5-7	12.5	1067 (575)	1
113-17	6061	6061	46.7	34.7	239 (115)	50	5-7	20.3	932 (500)	1
FR2 (Kalsruhe, Germany)										
1-4	1100	1100	50	37.2	158 (70)	50	5-7	5.8	> 932 (> 500)	5
2-4	1100	1100	50	37.2	158 (70)	50	5-7	16.9	> 932 (> 500)	5
3-4	1100	1100	50	37.2	158 (70)	50	5-7	12.2	> 932 (> 500)	5
4-1	1100	1100	50	37.2	158 (70)	50	5-7	9.4	> 932 (> 500)	5
5-3	1100	1100	45.5	33.8	158 (70)	50	5-7	9.4	> 932 (> 500)	5
6-4	1100	1100	45.5	33.8	158 (70)	50	5-7	7.6	> 932 (> 500)	5
7-2	1100	1100	50	37.2	158 (70)	50	5-7	15.8	> 932 (> 500)	5
8-2	1100	1100	45.5	33.8	158 (70)	50	5-7	15.8	> 932 (> 500)	5
9-3	1100	1100	50	37.2	158 (70)	50	5-7	5.8	> 932 (> 500)	5
10-1	1100	1100	45.5	33.8	158 (70)	50	5-7	5.8	> 932 (> 500)	5
11-4	1100	1100	50	37.2	248 (120)	50	5-7	10.0	> 932 (> 500)	5
12-4	1100	1100	50	37.2	275 (135)	50	5-7	10.0	> 932 (> 500)	5

Reactor Sample ID	Clad	Core	Weight Percent UAL$_x$	U	Core Temp, °F (°C)	Operating Pressure PSIG	pH	Fission Density f/cc X 10^{20}	Blister Temp, °F (°C)	Ref
FNR	6061	5214	19.1	14.2	172 (78)	9.2	5-7	15.0		
FR2 (Kalsruhe, Germany)										
13-2	1100	1100	50	37.2	302 (150)	50	5-7	10.0	> 932 (> 500)	5
14-2	1100	1100	50	37.2	302 (150)	50	5-7	19.0	> 932 (> 500)	5
15-2	1100	1100	45.5	33.8	302 (150)	50	5-7	19.0	> 932 (> 500)	5
16-2	1100	1100	50	37.2	302 (150)	50	5-7	25.9	> 932 (> 500)	5
17-2	1100	1100	45.5	33.8	302 (150)	50	5-7	25.9	> 932 (> 500)	5
18-1	1100	1100	50	37.2	302 (150)	50	5-7	21.6	> 932 (> 500)	5
19-1	1100	1100	45.5	33.8	302 (150)	50	5-7	21.6	> 932 (> 500)	5
20-2	1100	1100	45.5	33.8	302 (150)	50	5-7	21.6	> 932 (> 500)	5

TABLE 2B. U_3O_8 FUEL CORE BLISTER DATA

| Reactor Sample ID	Clad	Core	Weight Percent U_3O_8	U	Core Temp, °F (°C)	Operating Pressure PSIG	pH	Fission Density f/cc X 10^{20}	Blister Temp, °F (°C)	Ref
FNR	6061	5214	16.8	14.2	172 (78)	9.2	5-7	15.0		
MTR										
1	6061	X8001	----	----	239 (115)	50	5-7	2.5	716 (380)	1
2	6061	X8001	----	----	239 (115)	50	5-7	5.0	716 (380)	1
3	6061	X8001	----	----	239 (115)	50	5-7	5.0	824 (440)	1
4	6061	X8001	----	----	239 (115)	50	5-7	8.0	716 (380)	1
5	6061	X8001	----	----	239 (115)	50	5-7	8.2	824 (440)	1
6	6061	X8001	----	----	239 (115)	50	5-7	8.3	716 (380)	1
7	6061	X8001	----	----	239 (115)	50	5-7	10.5	716 (380)	1
ETR										
68-1633	6061	PB-04*	49	41.4	419 (215)	200	5-7	12.7	1022 (550)	8
68-1638	6061	PB-04	49	41.4	428 (220)	200	5-7	12.7	1022 (550)	8
68-1643	6061	PB-04	49	41.4	410 (210)	200	5-7	12.7	1022 (550)	8
68-997	6061	PB-04	49	41.4	347 (175)	200	5-7	19.7	932 (500)	8
68-1605	6061	PB-04	49	41.4	329 (165)	200	5-7	19.9	932 (500)	8
68-1607	6061	PB-04	49	41.4	338 (170)	200	5-7	19.5	932 (500)	8

* Aluminum Powder Blends

274
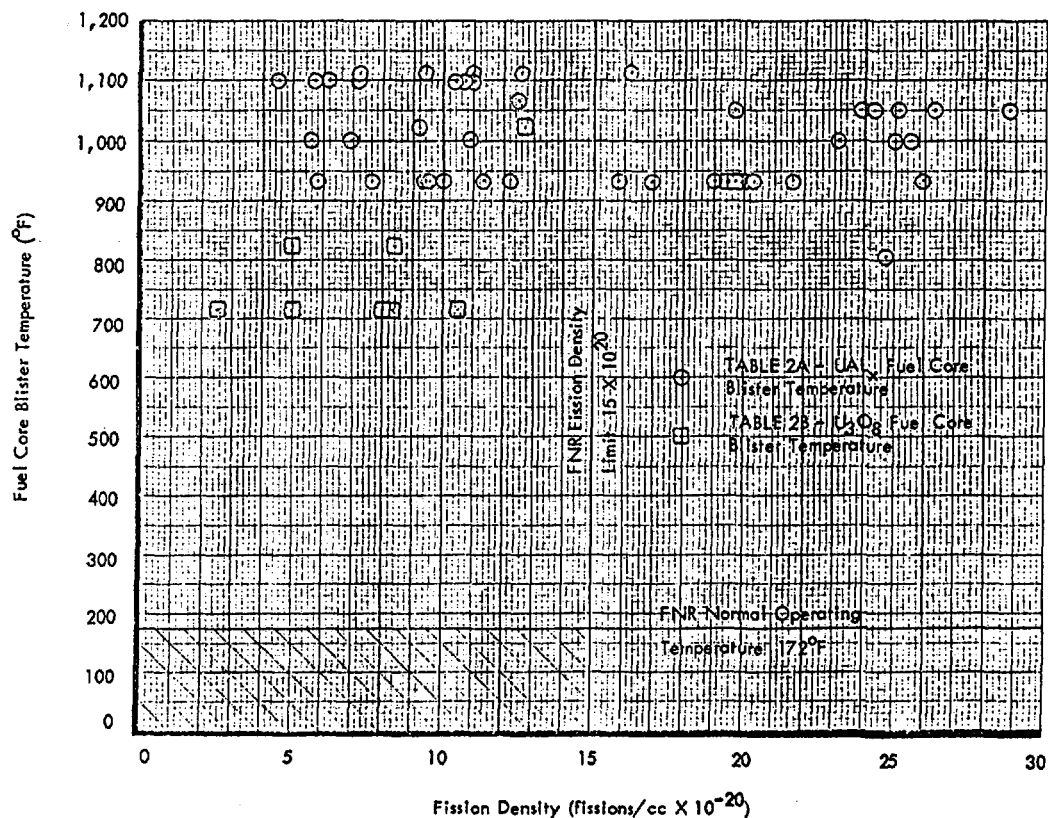
FIG. 2. Fuel core blister temperatures.

All of the available fuel blister data for UAL_x and U_3O_8 fuel which has been operated under conditions similar to those in the FNR indicate that UAL_x and U_3O_8 fuel can be safely used in the FNR without failure due to blistering and without reducing the safety margin.

6. FAILURE HISTORY

Table 3 provides a listing of reactor operating parameters for those reactors for which test data were provided in Table 1 and Table 2 and for the Ford Nuclear Reactor. Table 3 shows that the Advanced Test Reactor (ATR) routinely uses fuel with higher UAL_x loading than that proposed for FNR low enrichment uranium fuel. Similarly, the High Flux Isotope Reactor (HFIR) routinely uses fuel with U_3O_8 loadings equivalent to that proposed for the FNR.

The swelling and blistering data in Section 5 is for fuel cores with several aluminum alloys, but not 5214 alloy. The different core materials (powder blends, 1100, 6061, and X8001) show no significant effects on swelling and blistering characteristics. In addition, alloy 5214 is quite similar to 1100 as the list of constituents below indicates. Both essentially are pure aluminum powder.

275

TABLE 3A. TRAINING, RESEARCH AND TEST REACTOR OPERATING PARAMETERS

Parameter	Materials Testing Reactor (MTR)[1,23]	Engineering Test Reactor (ETR)[1,23]	Advanced Test Reactor (ATR)[1,23]	High Flux Isotope Reactor (HFIR)[9,23]	High Flux Beam Reactor (HFBR)[10,23]
Year placed in service	1952	1956	1967	1965	1965
Thermal power (MW)	40	175	40	100	40
Thermal power density (MW/l)	0.75	1.2	2.8	1.5	0.5
Fuel element meat volume (cc)	365	550	798	3475	870
U-235 per element (gm)	200	400	975	2600	315
U-235 burnup (%)	---	25	25	30.6	34
Peak fission density (fiss/cc)	---	1.8×10^{21}	2.3×10^{21}	1.9×10^{21}	1.24×10^{21}
Fuel element surface area (ft^2)	15	23	34	147	36
Heat flux (BTU/ft^2-hr)	3.5×10^5	5×10^5	4×10^5	2.5×10^5	3.8×10^5
Coolant flow rate (gpm)	24,000	44,000	16,000	17,000	16,6000
Fuel element materials:					
Cladding	1100 Al	1100 Al	6061 Al	6061 Al	6061 Al
Core	1100 Al	5214 Al	5214 Al	1100 Al	1100 Al
Core Fissile Compound (Weight %)	UAL_x 46.0	UAL_x 40.6	UAL_x 45.1 - 60.8	U_3O_8 25.6	U_3O_8 40.6
Core Uranium (Weight %)	34.2	30.2	33.5 - 45.2	21.6	34.3
Fuel Plate thickness (in)					
Clad	0.015	0.015	0.015	0.010	0.014
Core	0.020	0.020	0.020	0.030	0.023
Overall	0.050	0.050	0.050	0.050	0.051

TABLE 3B. FORD NUCLEAR REACTOR OPERATING PARAMETERS

Parameter	High Enrichment Fuel — Uranium Aluminum Alloy (U-Al)	High Enrichment Fuel — Uranium Aluminide (UAL_x)	Proposed Low Enrichment Fuel — Uranium Aluminide (UAL_x)	Proposed Low Enrichment Fuel — Uranium Oxide (U_3O_8)
Year placed in service	1958	1978	1980	Undetermined
Thermal power (MW)	2	2	2	2
Thermal power density (MW/l)	.025	.025	.025	.025
Fuel element meat volume (cc)	354	335	502	502
U-235 per element (gm)	140	140	167	167
U-235 burnup (%)	35	35	50	50
Peak fission density (fiss/cc)	1.5×10^{20}	1.5×10^{20}	2.6×10^{20}	2.6×10^{20}
Fuel element surface area (ft^2)	15	15	15	15
Heat flux (BTU/ft^2-hr)	3.68×10^4	3.68×10^4	3.68×10^4	3.68×10^4
Coolant flow rate (gpm)	980	980	980	980
Fuel element materials:				
Cladding	6061 Al	6061 Al	6061 Al	6061 Al
Core	1100 Al	5214 Al	5214 Al	1100 Al
Core Fissile Compound (Weight %)	Not Applicable	19.1	56.5	49.6
Core Uranium (Weight %)	14.2	14.2	42.0	42.0
Fuel plate thickness (in)				
Clad	.020	.015	.015	.015
Core	.020	.020	.030	.030
Overall	.060	.050	.060	.060
Coolant flow channel thickness (in)	.117	.125	.117	.117

276

Constituents	1100	5214
Maximum:			
Boron .	—	0.001%
Cadmium	—	0.002%
Copper	0.20%	0.20%
Iron	—	0.05%
Lithium	—	0.008%
Manganese	0.05%	
Silicon + Iron	1.00%	0.25%
Zinc	0.10%	0.10%
Others	0.15%	—
Minimum:			
Aluminum	99%	99.7%

The failure history for the Advanced Test Reactor in Section 6.1 provides extensive operational data. Advanced Test Reactor fuel cores are 5214 aluminum.

6.1 Uranium Aluminide (UAL_x)

To date, the Advanced Test Reactor has operated over 89,000 UAL_x fuel plates up to the depletion limit of 2.3 X 10^{21} fissions/cc. In all of these fuel plates, only one (and this one was found to have thinly rolled clad) allowed fission product leakage into the ATR coolant. The plate was operated to depletion.

The thin clad was attributed to "dogboning" in the fuel core which has been eliminated by sloping the edges of the core ingot before rolling.

To date, twenty-one 93% enrichment aluminide fuel plates with 5214 aluminum cores have been operated to partial depletion in the Ford Nuclear Reactor. The peak fission density among these elements is 1.27 X 10^{20} fissions/cc. Inspections for fuel damage are not specifically performed, but the plates have shown no evidence and given no indication of swelling, blistering, warping, or cracking.

6.2 Uranium Oxide (U_3O_8)

To date, the High Flux Isotope Reactor has operated over 76,000 U_3O_8 fuel plates up to the depletion limit 1.9 X 10^{21} fissions/cc with no failures. On two occasions, fuel plates developed suspected fission product leaks. In one case, the apparent leak was so insignificant that the element was operated to depletion. In the second case, the element was removed after 1500 MWD. Destructive tests showed no evidence of blisters, cladding separation, matrix cracking, or any defects indicative of incipient failure.

7. FUEL SPECIFICATIONS

7.1 Uranium Aluminide (UAL_x)

FNR fuel specifications have been developed in co-operation with the ATR staff at the Idaho National Engineering Laboratory and Atomics International (AI), the ATR fuel manufacturer. The UAL_x specification is identical to that specified by ATR. The present ATR fission density limit is 23 X 10^{20} fissions/cc.

The fuel swelling and blister data in the references and tables often refer to aluminide as UAL_3. The early intermetallic fuel development work in Idaho was for the fabrication and testing of UAL_3 material and so the early designation was UAL_3. During this early fuel testing work, it was recognized that aluminide was not purely UAL_3. In 1966, UAL_3 was identified as the major crystalline component with UAL_2 and UAL_4 present.[11] Current ATR fuel powder specifications require the UAL_3 content to be at least 50%.

The FNR fuel powder specification calls for uranium aluminide powder containing at least 50% UAL_3.

7.2 Uranium Oxide (U_3O_8)

U_3O_8 fuel specifications will be developed in co-operation with Oak Ridge National Laboratory (ORNL) and Brookhaven National Laboratory (BNL) should U_3O_8 fuel be used in the FNR.

8. HEAT TRANSFER CHARACTERISTICS

The proposed LEU fuel heat transfer characteristics will be essentially identical to those of alloy fuel which has been used in the FNR core since 1957 and still comprises the majority of the fuel elements in the core. Overall element dimensions, fuel plate dimensions, and coolant flow channel width and thickness are unchanged.

Peak fuel temperature in the hottest FNR fuel plate is calculated to be $172^\circ F$. The margin of operational safety will not be changed by the use of LEU fuel.

9. CORE PHYSICS

The core physics analysis of the proposed LEU fuel reflects two basic differences from the HEU fuel currently used in the FNR core: (1) the fuel loading will be increased from 140 grams to 167.3 grams of ^{235}U per 18-plate element to compensate for increased neutron absorption in ^{238}U and spectrum hardening, and (2) the fuel meat thickness will be increased from .020 inches to .030 inches, with clad thickness decreased from .020 to .015 inches, to maintain the same total fuel plate thickness while allowing for the larger amount of ^{238}U. The proposed LEU fuel specifications are selected so that the excess reactivity of a batch fresh core configuration is the same for both the current HEU fuel and the proposed LEU fuel.

9.1 Description of Calculational Methods

9.1.1 Computer Codes Used for Core Physics Analysis

All analysis was performed with the standard, well-verified production codes LEOPARD[12], EPRI-HAMMER[13], 2DB[14], ANISN[15], TWOTRAN[16], and VENTURE[17]. Brief descriptions of code capabilities are:

1) LEOPARD - a zero-dimensional unit-cell code using the MUFT/SOFOCATE scheme (54 fast and 172 thermal groups); has depletion capability; cross-section library consists of an early industrial data set.

278

2) EPRI-HAMMER - a one-dimensional integral transport theory code using 54 fast and 30 thermal groups; cross-section library constructed from ENDF/B-IV data.

3) 2DB - a two-dimensional multi-group diffusion theory code with depletion capability.

4) ANISN - a one-dimensional discrete ordinates transport theory code.

5) TWOTRAN-II - a two-dimensional discrete ordinates transport theory code.

6) VENTURE - a three-dimensional multi-group diffusion theory code

9.1.2 Code Modifications

The LEOPARD code originally performed a spectrum calculation for lattices consisting of cylindrical fuel rods. The code was modified to allow slab geometry and separate few-group edits for both lattice and non-lattice regions. The principal modification was in the calculation of thermal disadvantage factors by the ABH method for slab geometry[18].

The modified LEOPARD code compares satisfactorily with the EPRI-HAMMER code, an accurate, well-verified code used in the analysis of benchmark critical experiments.[19] A typical comparison of k_∞ and two-group parameters in Table 4 shows that despite the many engineering approximations in the LEOPARD code, it compares quite well with the more accurate HAMMER code. Differences in few-group constants are due primarily to differences in the cross-section libraries - HAMMER uses ENDF/B-IV data while LEOPARD uses an early industrial data set.

TABLE 4. COMPARISON OF LEOPARD AND HAMMER RESULTS FOR MTR-TYPE FUEL

	93% Alloy		19.5% UAl$_x$	
	LEOPARD	HAMMER	LEOPARD	HAMMER
k_∞	1.5477	1.5500	1.5150	1.5116
ϕ_1/ϕ_2	2.41	2.40	2.76	2.75
Age	51.5	49.9	49.1	47.5
D_1	1.434	1.372	1.424	1.360
Σ_{a1}	0.00204	0.00182	0.00358	0.00344
Σ_{r1}	0.0258	0.0257	0.0254	0.0253
$\nu\Sigma_{f1}$	0.00206	0.00223	0.00256	0.00274
D_2	0.284	0.272	0.280	0.269
Σ_{a2}	0.0597	0.0594	0.0676	0.0668
$\nu\Sigma_{f2}$	0.0948	0.0935	0.110	0.108

279

The 2DB code has been modified to allow a macroscopic depletion capability via interpolation of macroscopic cross sections as a function of depletion. In addition, the isotopic balance equations for xenon and iodine have been included to allow the correct xenon levels within the core as a function of position and time (and macroscopic absorption cross sections are appropriately modified). Other modifications to 2DB have been aimed at automating data handling (e.g., the link with LEOPARD to produce macroscopic cross sections as a function of depletion) and improving fuel shuffling and edit capabilities.

9.1.3 Basic Calculation Method

The LEOPARD and 2DB codes were used for routine calculations of core reactivity, depletion effects, and power and flux distributions. Special methods for control rods and core leakage flux are described in subsequent sections. For both HEU and the proposed LEU fuel, the following scheme was followed:

1) The LEOPARD code was used to generate few-group cross sections. For most applications, two energy groups (fast and thermal) were used, although four energy groups were chosen for several detailed calculations.

   The geometry chosen was a unit cell in slab geometry consisting of a lattice region and a non-lattice or extra region. The lattice region was composed of fuel meat, clad and water channel. For regular assemblies, the extra region consisted of the side plates, non-active portions of fuel plates, and inter-assembly water gaps, which were homogenized on a volume basis. For special* fuel assemblies, the central water hole was also included in the extra region.

   Few-group macroscopic cross-section sets were generated as functions of depletion for the lattice and non-lattice regions and the total assembly.

   For the water reflector and heavy water tank, the extra region was chosen as H_2O or D_2O with a .25% H_2O content with a volume fraction arbitrarily set equal to that of the lattice region.

   The extra region few-group cross sections obtained in this manner were used for the reflector and heavy water tank in the subsequent global calculation.

2) Global diffusion theory calculations were performed with the 2DB code. Three spatial mesh descriptions were used in x-y geometry: a homogeneous description, with a 2x2 mesh per assembly, was used for survey calculations, equilibrium core studies, and cycle length studies. A discrete representation, using a 6x6 mesh per assembly with the lattice and non-lattice portions of an assembly explicitly represented, was used for detailed analysis of power and flux distributions, temperature coefficient, and control rod reactivity worth. A discrete represen-

---

*Special is used in this section to designate control assemblies.

tation with a 12x12 mesh per assembly was used for verifying the adequacy of the 2x2 and 6x6 representations, and for comparison with the measured flux distributions.

Depletion was accounted for on the assembly level by interpolating macroscopic cross sections as a function of depletion (MWD/MT) for the particular assembly in question. The fuel shuffling capability in the 2DB code allowed actual FNR operation to be simulated. The axial buckling term for the 2DB code used to approximate transverse leakage was based on the active core height with a reflector savings correction.

9.1.4 Control Rod Worth Calculations

FNR control (shim) rods are boron stainless steel containing 1.5 w/o natural boron. They are essentially black to thermal neutrons and cause a drastic thermal flux depression when inserted. The presence of such strong localized absorbers necessitates the use of transport theory codes to adequately describe the large flux gradients. However, in a small high leakage core like the FNR, control rod effects are not strictly local; therefore whole core calculations are needed, but are prohibitively expensive for transport theory codes. To accurately treat both local and global effects, transport theory codes were used for assembly level calculations to develop effective diffusion theory constants for global calculations. The method developed is a variation of the "NGD blackness method"[20] and has proved quite accurate.

Few-group constants for the control rod and surrounding water were obtained from the EPRI-HAMMER code for a cylindricized special assembly. Due to the strong spectral/spatial coupling in the rod it was necessary to obtain few-group cross sections for three control rod regions - a surface layer .1 cm thick, a second layer .3 cm thick, and the central region. Since few thermal neutrons reach the central region, the control rod perimeter, rather than volume, was preserved in the geometric representation. Few-group constants for the special element lattice and side regions were obtained from the EPRI-HAMMER calculations for one half of a special element in slab geometry.

To accurately model the local effects of an inserted rod, the two-dimensional transport code TWOTRAN was used in fine-mesh calculations for a special assembly surrounded on all sides by one half of a regular assembly. Three regions of the rod and the surrounding water were explicitly represented, while the surrounding lattice regions were homogenized.

To develop effective few-group diffusion theory constants for use in global 2DB calculations, the 2DB code was used for the same geometry as in TWOTRAN calculations, except that the control rod and surrounding water were homogenized. Both fast and thermal absorption cross sections were varied until the 2DB calculation yielded the same relative absorption in the control region as the TWOTRAN result in each group. The resulting few-group constants for the control region were then used in global 2DB calculations. Although the flux distribution within the control region differs from the transport theory results, we believe the relative absorption in the control region and the flux in the surrounding fuel is accurately predicted in this scheme.

Control rod worth was then determined by comparing global 2DB calculations for the 6x6 mesh/assembly description with and without control rod inserted.

9.1.5 Calculational Methods for Temperature Coefficient of Reactivity and Xenon Reactivity Worth

Calculation of the temperature coefficient of reactivity and of reactivity worth of xenon poisoning was performed with global 2DB calculations with a 6x6 mesh/assembly description. The two-group cross sections for these 2DB cases were obtained from unit-cell calculations with the LEOPARD or the EPRI-HAMMER code, essentially following the basic scheme outlined in Section 9.1.3.

9.1.6 Equilibrium Core Model

Although the FNR core configuration and fuel shuffling pattern are, in practice, determined by operational requirements, an equilibrium core model was developed to-allow for meaningful comparison of operating characteristics for the HEU and the proposed LEU cores. Our equilibrium core model essentially simulates a typical FNR shuffling pattern. Fresh fuel assemblies are placed near the control assemblies at the core center and are moved outward as they deplete. This pattern maximizes the control rod reactivity worth. The shuffling pattern was varied until the fuel depletion per cycle at each assembly location obtained with global 2DB calculations closely matched that of the average FNR depletion at each location. The 2DB calculations performed over many cycles led to an equilibrium core model which, although not unique, is a realistic representation of the typical FNR operating cycle.

9.1.7 Ex-core Calculations

The ANISN and 2DB codes were used to calculate flux distributions in the H_2O and D_2O reflectors. Cross sections for the ANISN calculation were taken from the 100 group DLC -2 library and collapsed (with ANISN) to few groups. For 2DB calculations cross sections were generated by the LEOPARD code as explained in Section 9.1.3.

9.2 Comparison of Calculated and Experimental Results

The adequacy of the methods used for calculating core physics parameters for FNR core configurations has been established through comparing the calculated results with the data from several research and test reactors. In these verification efforts the calculated thermal flux and power distributions were compared with the experimental data obtained at the Bulk Shielding Reactor (BSR)[21], the High Flux Beam Reactor (HFBR)[22], and the FNR. The data for the BSR and HFBR cores were obtained at core configurations with MTR-type fuel elements similar to the FNR configurations.

9.2.1 Flux and Power Distributions

The measured thermal flux distributions and the core multiplication constants for the BSR loading 33 provide well documented experimental data[21] for a fresh critical core. The neutron flux distribution for this core was determined with x-y 2DB calculations utilizing a 6x6 and a 12x12 mesh per fuel assembly. Table 5 compares calculated and experimental results for the BSR and representative FNR configurations. Here the high neutron leakage causes the effective multiplication factor of the reactor to be sensitive to the input buckling value used to

TABLE 5. EXPERIMENTAL AND CALCULATED RESULTS FOR SEVERAL REACTOR CONFIGURATIONS

Case	Mesh/Group Structure	Core Reactivity		RMS Deviation[1] (thermal flux or assembly power)
		Measured	Calculated	
A (BSR #33)	6x6/2 group	1.006	1.009	11.3% [3]
	6x6/4 group	1.006	1.004	10.1% [3]
	12x12/2 group	1.006	1.012	7.8% [3]
B (FNR #67)	6x6/2 group	1.001	1.007 [2]	9.3% [4]
C (FNR 1977 critical)	2x2/2 group	1.000	1.000 [2]	---
	6x6/2 group	1.000	1.000 [2]	---

Notes
1. RMS deviation $= \sqrt{\dfrac{1}{N-1} \sum_{\lambda} \left(\dfrac{calc - exp}{exp}\right)^2_{\lambda}}$

2. Corrected for measured xenon worth

3. Thermal flux deviation at 17 locations

4. Assembly power fraction deviation at 42 locations

represent the leakage in the missing transverse direction. These calculations used an axial buckling of 2×10^{-3} cm^{-2}, which includes a calculated reflector savings.

Calculated results have been compared with the experimental data for a number of FNR core configurations. The assembly average power distribution in the Cycle 67 core was measured on March 17, 1971, with the core loading pattern presented in Figure 3. The power distribution was measured by thermocouples, with the coolant inlet temperature for each element measured inside the fuel element boxes and above the fuel plates, and the outlet temperature measured below the fuel plates in the element cone. From the assembly inlet and outlet temperatures, the power for each regular fuel element was calculated assuming equal coolant flow rate through each element. The assembly-average power distribution calculated by the 2DB code and the measured power distribution for the Cycle 67 core are presented in Figure 4. In this calculation the 2DB code predicted the core power distribution to within an rms deviation of 9.3%, as shown in Table 5.

The thermal flux distribution in the FNR Cycle 163B core was determined through flux maps obtained with a self-powered rhodium detector. The measurements were taken at the horizontal midplane of the core at the center of each regular fuel element. The core configuration for this cycle is shown in Figure 5, and a comparison of the calculated and measured thermal flux distributions is given in Figure 6. The calculated flux distribution shows good agreement with the measured distribution, with an rms deviation of 5.1%. Comparisons made for other fuel cycles show similar agreement between the measured and calculated results, with rms deviations in the range of 5 ~ 8%.
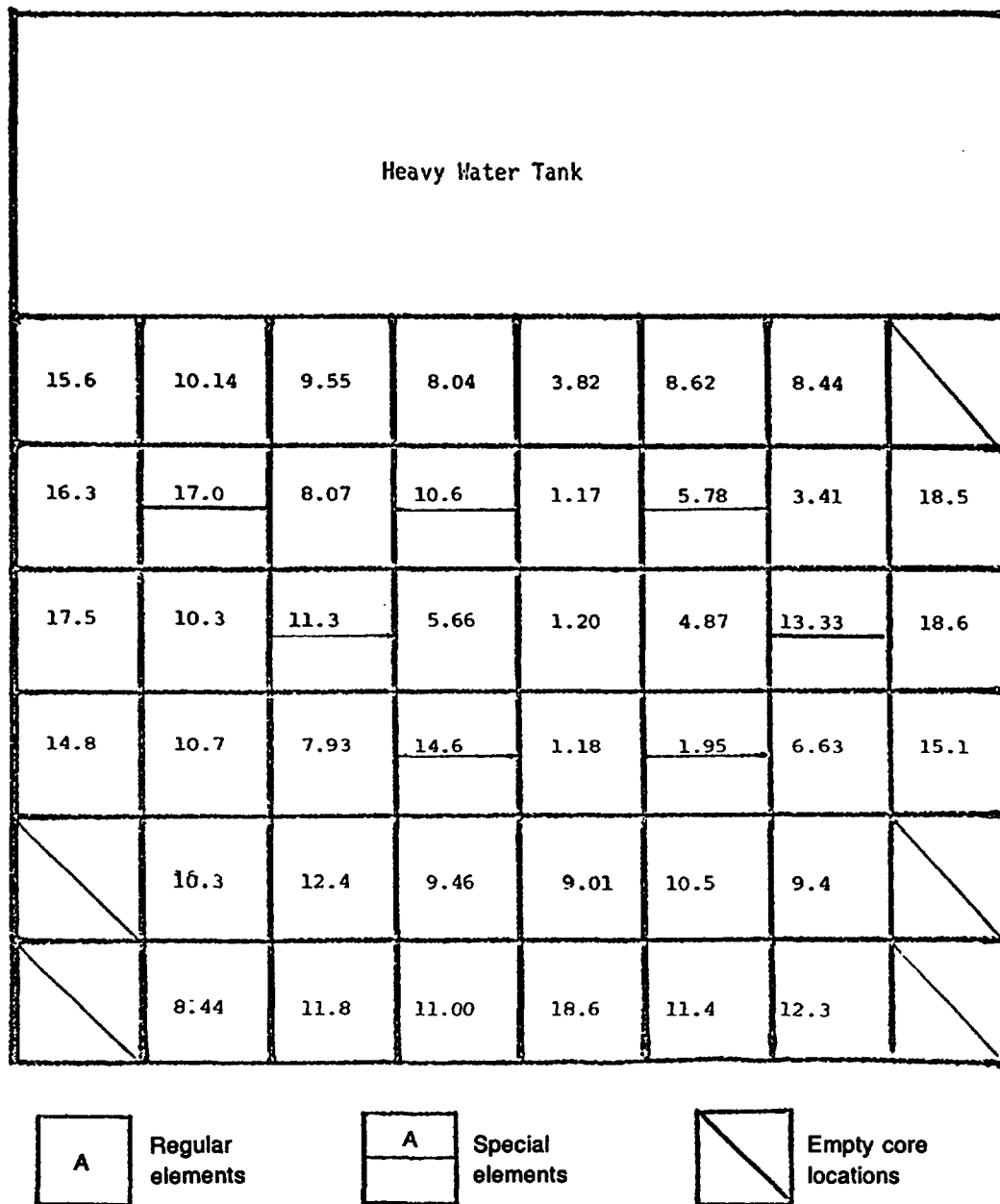
FIG. 3. Fuel burnup distribution for FNR cycle 67.

Heavy Water Tank

1.46 / 1.42	2.25 / 2.06	2.81 / 2.53	3.43 / 2.89	3.13 / 2.94	2.58 / 2.60	1.91 / 2.12	(empty)
1.80 / 1.76	1.26 / 1.28	3.73 / 3.46	2.06 / 2.02	4.12 / 4.00	1.83 / 1.97	2.32 / 2.76	1.41 / 1.72
1.93 / 1.82	3.14 / 2.85	1.96 / 1.95	4.64 / 4.17	3.69 / 4.08	3.75 / 3.77	1.26 / 1.49	1.66 / 1.82
1.95 / 1.83	2.66 / 2.55	3.50 / 3.39	1.74 / 1.90	3.86 / 4.26	1.94 / 2.07	2.30 / 2.71	1.58 / 1.77
(empty)	2.30 / 2.12	2.76 / 2.55	2.96 / 3.09		2.63 / 2.67	2.05 / 2.09	(empty)
(empty)	1.39 / 1.46	2.06 / 1.83	1.07 / .98	2.12 / 2.13	1.80 / 1.71	1.25 / 1.42	(empty)

A / B : Regular elements   A / B : Special elements   Empty core locations

A: Assembly power (%), measured
B: Assembly power (%), calculated   rms deviation = 9.3%

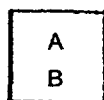FIG. 4. Experimental and calculated power distributions for FNR cycle 67.
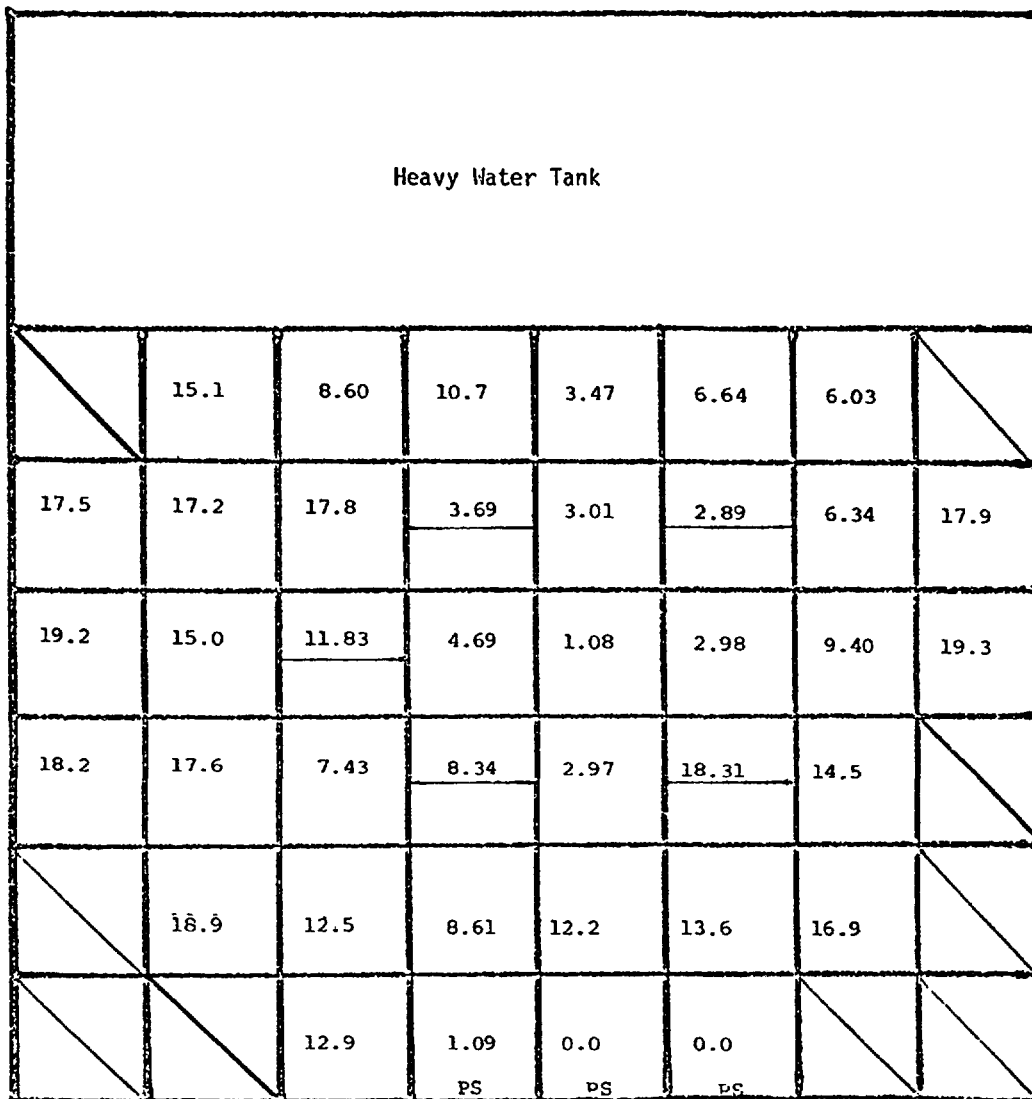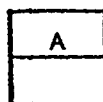
FIG. 5. Fuel burnup distribution for FNR cycle 163B.

	2.45	3.06	3.43	3.30	2.94	2.33	
	2.31	2.76	3.21	3.10	2.88	2.31	
1.96	2.94	3.79		4.04		2.82	1.96
2.01	2.82	3.83		4.17		2.84	1.98
2.20	3.30		4.53	4.28	3.92	3.06	2.33
2.15	3.20		4.69	4.35	4.05	3.00	2.11
2.08	3.06	3.79		4.28		2.94	
2.07	2.96	3.96		4.51		3.01	
	2.69	3.43	3.79		3.30	2.33	
	2.60	3.16	3.85		3.32	2.40	
		2.33	2.57	2.69	2.08		
		2.35	2.75	2.88	2.40		

Heavy Water Tank

A / B : Regular elements   A / B : Special elements   Empty core locations
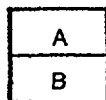
A: Assembly-average thermal flux, measured
B: Assembly-average thermal flux, calculated } rms deviation = 5.1%

FIG. 6. Experimental and calculated thermal flux distributions for FNR cycle 163B.

9.2.2 Ex-core Flux Distributions

Initial calculations to predict leakage neutron flux in the FNR D_2O tank concentrated on determining the accuracy of diffusion theory vs. transport theory calculations and on identifying critical parameters. Transport theory calculations performed in one-dimensional slab geometry with the ANISN code[15], and diffusion theory calculations performed with one- and two-dimensional codes were compared with experimental measurements for the FNR, BSR, and HFBR. The results indicate that because of the large thermal diffusion length in D_2O, diffusion theory can accurately predict the thermal flux distribution for considerable distances into heavy water. The calculations for D_2O reflectors were sensitive to the transverse buckling due to the small D_2O macroscopic absorption cross-section. In a 2DB model of the HFBR with R-Z geometry[22] diffusion theory accurately simulated the thermal flux profile at distances of .6-.8 meters into the D_2O reflector.

9.2.3 Control Rod Reactivity Worth

Control rod reactivity worth calculations were performed for the A, B, and C shim rods for FNR Cycle 67. The method for obtaining the rod worths was identical to that discussed in Sec. 9.1.4 except that the depletion of the fuel in the special fuel elements had to be accounted for. Accordingly, isotopic number densities for each of the special fuel element lattice regions were taken from a LEOPARD depletion calculation for a special element at the corresponding burnup points. These number densities were then used in place of BOL number densities, and the sequence of HAMMER calculations described in Sec. 9.1.4 was repeated. Full-core 6x6 2DB calculations were then performed with all rods out and then separate runs were made with each of the three rods inserted. The calculated and measured rod worths compared as follows:

	Rod worth (% $\Delta k/k$)	
Shim rod	Measured	Calculated
A	2.22	2.20
B	2.11	2.11
C	1.72	1.73
Total rod worth	6.05	6.04

The agreement is excellent and provides verification of the methods for computing control rod worth in small, high-leakage cores. While there still exist some uncertainties in the actual measured rod worth, the close agreement indicates that the basic approach is valid.

9.3 Comparison of HEU and Proposed LEU Fueled Cores

To provide a meaningful and comprehensive comparison of HEU and proposed LEU fuels, it is necessary to account for both the intrinsic fuel properties and the FNR operating conditions. For the purpose of comparing core phyiscs parameters, two core configurations were analyzed for both fuels. The first configuration corresponds to a

batch core consisting of fresh fuel assemblies, while the second con-
figuration is based on an equilibrium core. The batch core configura-
tion allows a comparison of undepleted HEU and LEU fuels, while the
equilibrium core allows comparison of depletion characteristics
and shutdown margin for conditions approximating typical FNR operation.

The following sections include a description of the model core con-
figurations and a comparison of core physics parameters.

9.3.1 Description of Batch and Equilibrium Core Models

The batch core model consists of 31 fresh fuel assemblies, with four
special assemblies at control rod locations. The configuration is
symmetric about the north/south midplane and was analyzed using
half-core calculations with a 6x6 mesh/assembly. Figure 7 illus-
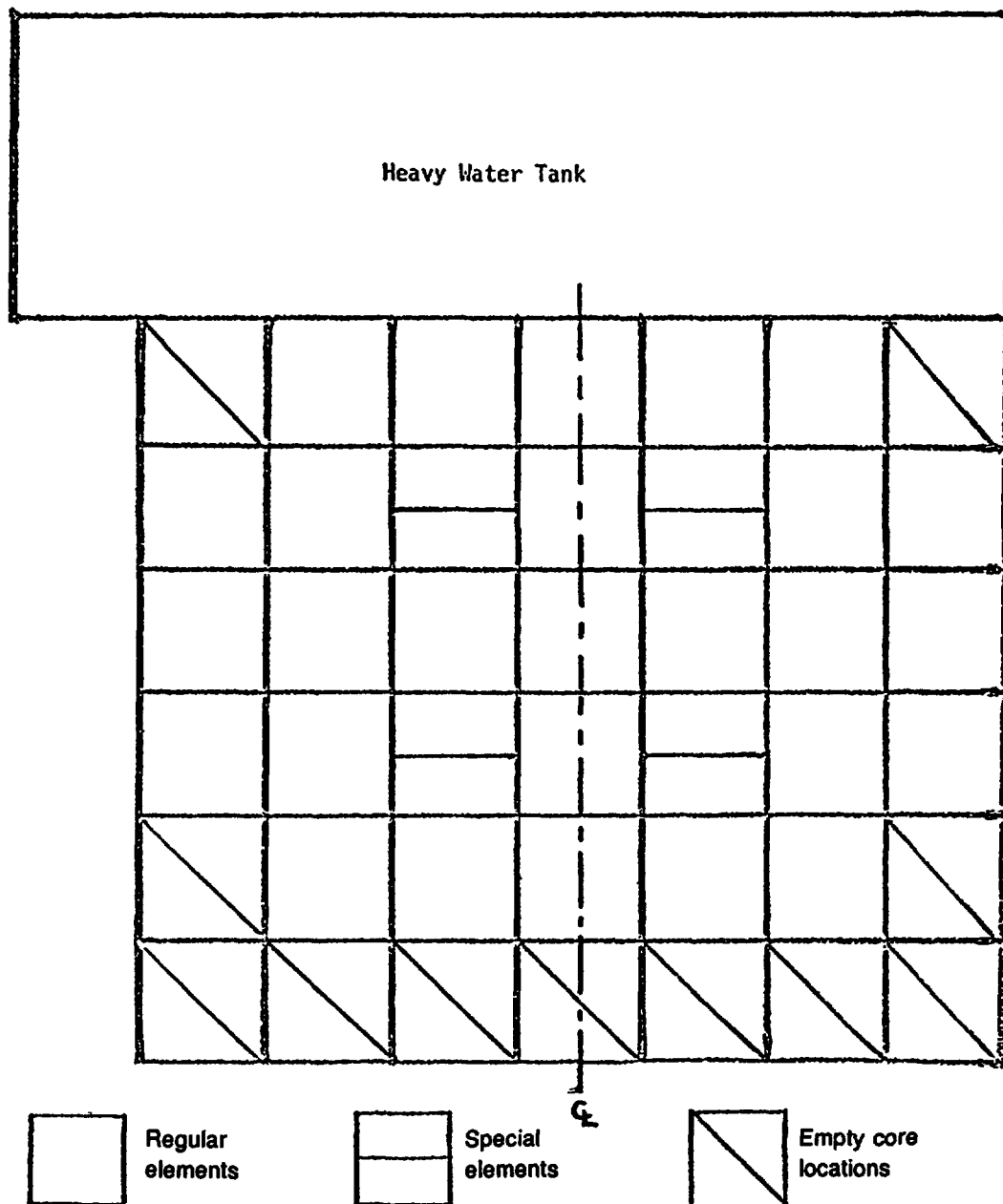trates this configuration.

FIG. 7. Batch core configuration.

The equilibrium core configuration shown in Figure 8 essentially simulates a typical FNR shuffling pattern, and is chosen so that the core loading and shuffling patterns repeat every sixth cycle. The core configuration consists of 39 fuel elements including six special fuel elements. The important criteria for choosing the core loading pattern are:

1. Fresh fuel elements are loaded into the central region of the core. This maximizes control rod worth and helps maintain the required shutdown margin. The fuel elements are moved outward in an in/out shuffling scheme as they deplete.

2. The fuel elements are loaded so as to equalize the worths of the three shim rods. Because the B and C Rods tend to be less reactive, the reactivity worth of these shim rods is increased by loading relatively fresh fuel into the vicinity of B and C Rods.. In contrast, more depleted fuel is loaded near the A Rod.
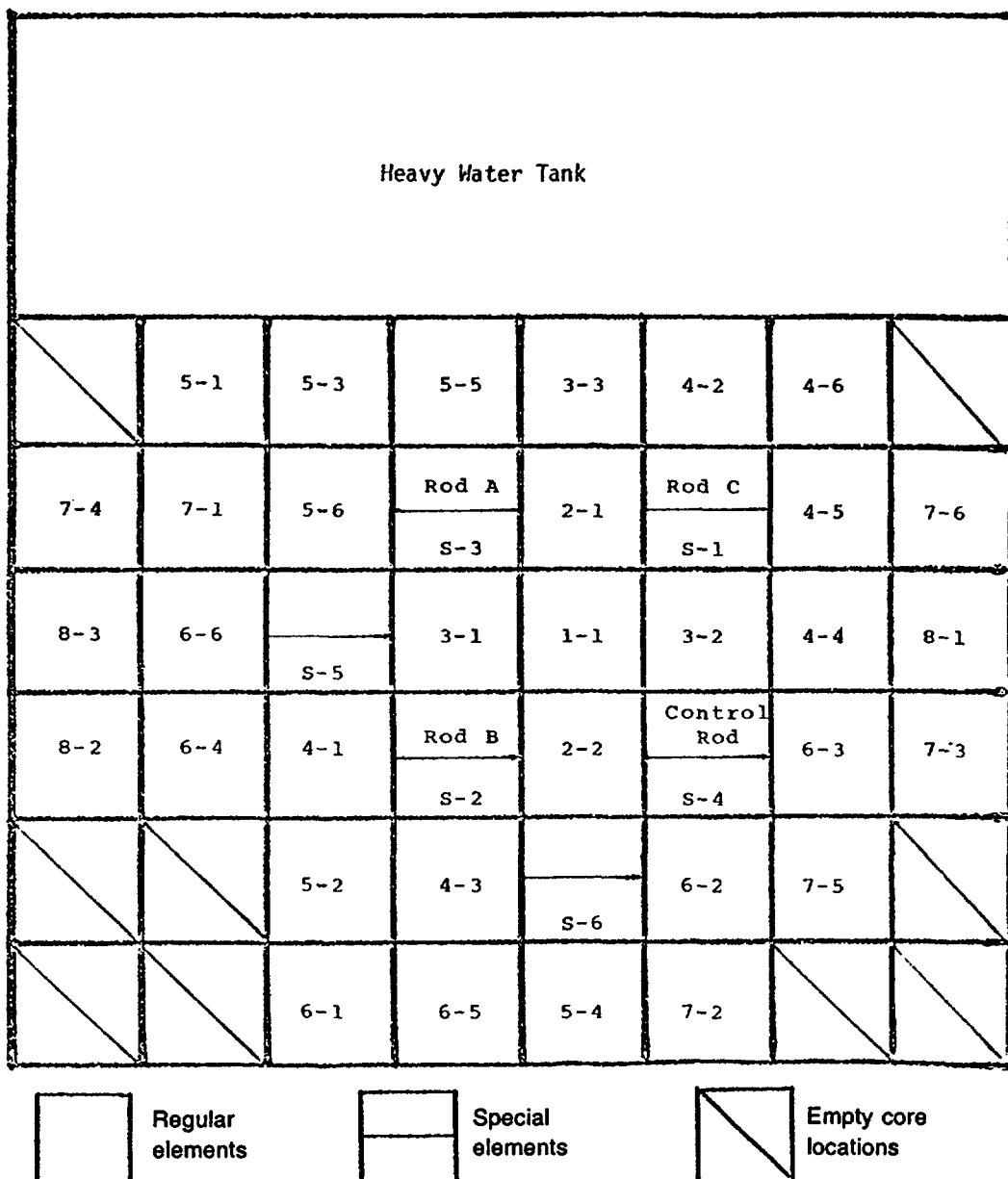

FIG. 8. Equilibrium core loading pattern.

With these core loading criteria, an equilibrium core burnup distribution is obtained with 2DB calculations, which repeats cyclically over a given time period. The fuel element shuffling pattern for the equilibrium core divides the 33 regular fuel element locations into eight loading zones as shown in Figure 8. Each regular element loading zone corresponds to core locations having nearly equal fuel burnup, although not necessarily equal burnup rates. New fuel is loaded into Zone 1 and depleted fuel is discharged from Zone 8. At the start of each cycle, one new element is loaded into Zone 1, and the element in Zone 1 is moved to Zone 2. Another element is moved from Zone 2 to 3, and continuing to Zone 8, with a depleted element being discharged from Zone 8. Because the core loading zones have a maximum of six elements, the core burnup distribution repeats every sixth cycle. The eight-zone shuffling pattern for the regular elements is shown in Table 6.

TABLE 6. REGULAR FUEL ELEMENT SHUFFLING SCHEME

Equilibrium Core Configuration
with 6 Cycles/Macro-cycle

Cycle	New Fuel	Core Loading Zone							
		1	2	3	4	5	6	7	8
1	→	1-1 →	2-1 →	3-1 →	4-1 →	5-1 →	6-1 →	7-1 →	8-1 →
2	→	1-1 →	2-2 →	3-2 →	4-2 →	5-2 →	6-2 →	7-2 →	8-2 →
3	→	1-1 →	2-1 →	3-3 →	4-3 →	5-3 →	6-3 →	7-3 →	8-3 →
4	→	1-1 →	2-2 →	3-1 →	4-4 →	5-4 →	6-4 →	7-4 →	8-1 →
5	→	1-1 →	2-1 →	3-2 →	4-5 →	5-5 →	6-5 →	7-5 →	8-2 →
6	→	1-1 →	2-2 →	3-3 →	4-6 →	5-6 →	6-6 →	7-6 →	8-3 →

Discharge

The shuffling pattern for the special fuel elements is somewhat different since there are six special element locations. A new special element is added and a depleted element is discharged only every sixth cycle. With this shuffling pattern a new special element is placed in Special-Zone 1 at the start of cycle 1. The element removed from Special-Zone 1 is placed in ex-core storage for one cycle and then placed in Special-Zone 2 at the start of cycle 2. The element from Special-Zone 2 is moved to storage before being placed into Special-Zone 3 at the start of cycle 3. The sequence continues until the start of cycle 6 when the element from storage is placed into Special-Zone 6 and a depleted special element is discharged from the core. This shuffling pattern for special elements is shown in Table 7.

TABLE 7. SPECIAL FUEL ELEMENT SHUFFLING SCHEME

Equilibrium Core Configuration
with 6 Cycles/Macro-cycle

Cycle	Storage		Core Loading Zone		Storage
1	New fuel	→	S-1	→	X_1
2	X_1	→	S-2	→	X_2
3	X_2	→	S-3	→	X_3
4	X_3	→	S-4	→	X_4
5	X_4	→	S-5	→	X_5
6	X_5	→	S-6	→	Discharge

While the reactivity decrease and core power distribution are nearly constant over each equilibrium cycle, the burnup distribution will repeat only every sixth cycle or over one macro-cycle. Any core parameter will be exactly the same at a given time into any macro-cycle.

To verify the practicability of the equilibrium cycle, Table 8 presents a comparison of the calculated equilibrium core parameters and actual core parameters based on the FNR operating experience during the past year. These comparisons indicate that the proposed equilibrium cycle represents a reasonably practical configuration, which may be used to compare the characteristics of the LEU and HEU designs for typical FNR operating conditions.

TABLE 8. COMPARISON OF THE EQUILIBRIUM CORE PARAMETERS WITH THE ACTUAL FNR PARAMETERS

	Equilibrium Core 93% Enrichment	FNR Experience (Oct. 78 - Sept. 79)
Average cycle length (days)	11	8.17*
Average reactivity swing between shuffles (% $\Delta k/k$)	-0.31	-0.40
Average number of shuffles/day	0.82	0.81
Average discharge burnup (%)		
Regular elements	17	17
Special elements	29	34
Calculated k_{eff}		
Range	1.022 ~ 1.026	1.020 ~ 1.032
Average	1.024	1.025
Control Rod Worth (% $\Delta k/k$)	(at beginning of cycle)	(at beginning of Cycle 67)
Shim Rod A	2.21	2.22
Shim Rod B	2.20	2.11
Shim Rod C	2.00	1.72
Total	6.41	6.05

*Includes periods of operation at 1MW power.

9.3.2 Comparison of Core Physics Parameters for HEU and Proposed LEU Fueled Cores

The major physics parameters which have been analyzed include the power defect of reactivity, xenon reactivity worth, control (shim) rod reactivity worth, cycle length, and shutdown margin. Differences in these parameters, as computed for the two model core configurations should provide a reasonable estimate of any effects of LEU fuel on FNR safety margins. These differences are compared for several equilibrium cores with differing cycle length and the batch core.

9.3.2.1 Temperature Coefficient of Reactivity and Power Defect Comparison

The isothermal temperature coefficient of reactivity was computed for the batch core model to be -8.4 pcm/°F for the HEU fuel and -12.6 pcm/°F for the LEU fuel. The large increase is due almost exclusively to fuel Doppler effects. For the HEU fuel, fuel Doppler effects are negligible due to the small amount of ^{238}U present. For the LEU fuel, the large amount of ^{238}U increases resonance absorptions in ^{238}U, resulting in much larger sensitivity to fuel temperature. The principal contribution to temperature coefficient of reactivity for both the HEU and LEU configurations is the effect of the reduction in moderator density on leakage and moderation.

The power defect of reactivity represents the total of all reactivity effects induced by taking the reactor from a cold zero-power condition to normal operating conditions. Due to the spatially nonuniform temperature and density changes involved, the power defect cannot be predicted solely on the basis of an isothermal temperature coefficient. Since the increased fuel Doppler effect is, however, the principal difference in the temperature effects between the HEU and the LEU designs, the change in power defect of reactivity is estimated in the present analysis on the basis of calculated temperature coefficients. Based on an average core temperature rise of 7°F, the power defect for the LEU fuel is estimated to be about .03% Δk/k larger in magnitude than for HEU fuel. For a typical FNR configuration, the excess reactivity required to overcome the power defect would thus change from a measured value of .21% Δk/k for HEU to .24% Δk/k for LEU.

9.3.2.2 Xenon Reactivity Worth Comparison

The xenon reactivity worths for the LEU and HEU equilibrium core configurations are compared in Table 9 and in Table 10 for the batch cores. For the cases considered the xenon worth is slightly lower for the LEU than the HEU fuel. There are two competing effects responsible for this decrease: First, the larger ^{235}U loading for the LEU core results in lower in-core thermal flux levels, with a greater (10-12%) xenon concentration. Second, the increased ^{235}U loading gives the LEU core a larger neutron absorption cross-section. As total core absorption is increased, the fractional absorption in xenon, and thus the xenon reactivity worth, is decreased. Although these two effects tend to cancel one another, the latter effect dominates and xenon reactivity worth is lowered by about .1% Δk/k.

TABLE 9. CORE PHYSICS PARAMETERS FOR EQUILIBRIUM CORE

	HEU		LEU		
	Regular	Extended	Equal Length	Equal Burnup	Equal Reactivity change
Cycle length (days)	11.0	13.0	11.0	13.0	15.0
Average discharge burnup (MWD/assembly)	19.2	22.8	18.6	21.8	25.3
Core average burnup at beginning of cycle (MWD/assembly)	10.7	12.6	10.6	12.6	14.6
Average reactivity change/cycle (% $\Delta k/k$)	- 0.31	- 0.38	- 0.23	- 0.26	- 0.32
Shim rod worth (% $\Delta k/k$)					
A Rod	2.21				2.20
B Rod	2.20				2.18
C Rod	2.00	2.06	1.82	1.86	1.95
Total	6.41				6.33
Excess reactivity required (% $\Delta k/k$)					
Xenon poisoning	2.24				2.08
Burnup effect	0.31				0.32
Power defect	0.21				0.24
Total	2.76				2.64
Shutdown margin (% $\Delta k/k$)	3.65				3.69

TABLE 10. CORE PHYSICS PARAMETERS FOR BATCH CORE

	HEU	LEU
Cycle length (days)	10.0	10.0
Reactivity change per cycle (% $\Delta k/k$)	- 0.31	- 0.22
Shim rod worth (% $\Delta k/k$)		
A Rod	2.37	2.26
B Rod	2.23	2.12
C Rod	2.37	2.26
Total	6.97	6.64
Excess reactivity required (% $\Delta k/k$)		
Xenon poisoning	2.50	2.40
Burnup effect	0.31	0.22
Power defect	0.21	0.24
Total	3.02	2.86
Shutdown margin (% $\Delta k/k$)	3.95	3.78

294

9.3.2.3 Control Rod Reactivity Worth Comparison

A comparison of the reactivity worths for shim rods A, B, and C is given in Table 9 for equilibrium cores and in Table 10 for batch cores. As expected, the rod worth is lower for the LEU cores. The greatest loss in total rod worth, .33% $\Delta k/k$, is seen for a batch core comparison. For the equilibrium cores, comparing the HEU regular cycle with the LEU cycle corresponding to an equal reactivity change shows a decrease of total rod worth of only .08% $\Delta k/k$, indicating that larger core-average burnup in the LEU core can mitigate the decrease in rod worth for the LEU core.

The decrease in rod worth is an expected result of the increased ^{235}U loading required for LEU fuel. When the loading of the principal core absorber (^{235}U) is increased, the control rods become less effective in competing with fuel for neutron absorption and the rod worth is decreased. Accordingly, fuel depletion should increase control rod effectiveness. This prediction is borne out by the equilibrium core calculations displayed in Table 9 and suggests that a longer LEU cycle could provide a means for increasing both control rod reactivity worth and shutdown margin.

9.3.2.4 Comparison of Depletion Characteristics

Depletion effects on reactivity for several equilibrium-core cycle lengths are presented in Table 9. Comparing the 11-day cycle for HEU and LEU cores shows that for equal cycle lengths, the rate of reactivity loss due to fuel burnup is 25% ~30% lower for the LEU core. This is primarily a direct consequence of the increased ^{235}U loading - for a given absolute loss of fuel mass, the fractional depletion and thus reactivity loss are decreased for higher fuel loading. In addition there is a secondary contribution due to the build-up of ^{239}Pu. While the reduction in the rate of reactivity decrease seen for equal length cycles would reduce the excess reactivity requirement, the reduction in control rod worth could result in a net decrease in shutdown margin. Another consequence of the equal-length fuel cycle is that fuel element discharge burnup is reduced, thus likely increasing fuel costs.

Since control rod worth calculations predict an increase in rod worth as fuel burnup is increased, two extended length cycles were investigated for LEU fuel: The first, with a length of 13 days, is intended to match fuel burnup with the 11-day HEU cycle. The second, with a length of 15 days, is intended to yield the same reactivity change per cycle as the 11-day HEU cycle. Results obtained for the two extended LEU cycles, as well as an extended HEU cycle for comparison, are included in Table 9.

Comparison of the 15-day LEU cycle with the 11-day HEU cycle shows that the fuel element discharge burnup is increased by 30%, and the cycle length is increased by 36%, while maintaining approximately equal reactivity change/cycle. These considerations suggest that fuel utilization is expected to be better for LEU fuel and that, over a long period of time, fuel costs could be lowered. This improvement in fuel utilization can be attributed to the small fissile plutonium buildup, increased fast fission due to ^{238}U, and spectrum hardening which reduces the reactivity effects of fuel depletion.

The most important consequence, however, of the extended 15-day LEU cycle is the effect on control rod reactivity worth. The extended cycle length increases the rod worth to a value approximately equal to the regular 11-day HEU cycle.

Since the 15-day LEU cycle offers distinct advantages over the 11- or 13-day LEU cycles, it has been analyzed in detail. Succeeding comparisons of LEU and HEU equilibrium core models will therefore compare the 11-day HEU cycle with the 15-day LEU cycle.

9.3.2.5 Comparison of Shutdown Margin

The most significant safety parameter related to core physics analysis is the shutdown margin. This parameter is obtained by subtracting the positive core excess reactivity required to overcome xenon poisoning, fuel depletion, and the power defect from the total control rod reactivity worth. The present Technical Specifications require that the shutdown margin be at least 3.0% $\Delta k/k$. Any difference between the estimated shutdown margin and the limiting value represents excess reactivity available for experiments.

For the LEU batch core, it is seen from Table 10 that the lower excess reactivity requirement is overshadowed by the decrease in control rod reactivity worth. The shutdown margin of 3.78% $\Delta k/k$ is lower than for the HEU core, but is still well above the 3% $\Delta k/k$ requirement. Additionally, with the most reactive rod fully withdrawn, the shutdown margin is 1.52% $\Delta k/k$, well in excess of the .75% $\Delta k/k$ required.

Comparing the HEU and LEU equilibrium core results shown in Table 9, it is seen that for cycles having equal reactivity change, the shutdown margin for the LEU core exceeds that for the HEU core. This rather surprising result is a consequence of the longer cycle length and a higher average fuel burnup in the LEU equilibrium core. With the HEU and LEU control rod worths nearly equalized, the relatively minor effect of lower xenon poisoning increases the shutdown margin slightly. The computed value of 3.69% $\Delta k/k$ is well in excess of the 3.0% $\Delta k/k$ requirement. Also, the shutdown margin with the most reactive control rod fully withdrawn in 1.49% $\Delta k/k$, well above the .75% $\Delta k/k$ required.

9.3.3 Comparison of Flux and Power Distributions

Calculated power distributions for both HEU and LEU cores are compared in Figures 9 and 10 for batch cores and equilibrium cores, respectively. Examination of these figures reveals only minor changes between LEU and HEU cores. The largest change in assembly power, a 3% relative increase, occurs for special element locations. Additionally, there is a small shift in the power distribution away from the heavy water tank and toward a slightly improved overall symmetry about the center. There is no evidence of changes which would require detailed thermal-hydraulic analysis; in fact, the ratio of peak to average assembly power is slightly reduced.

FIG. 9. Assembly power distribution for batch core.
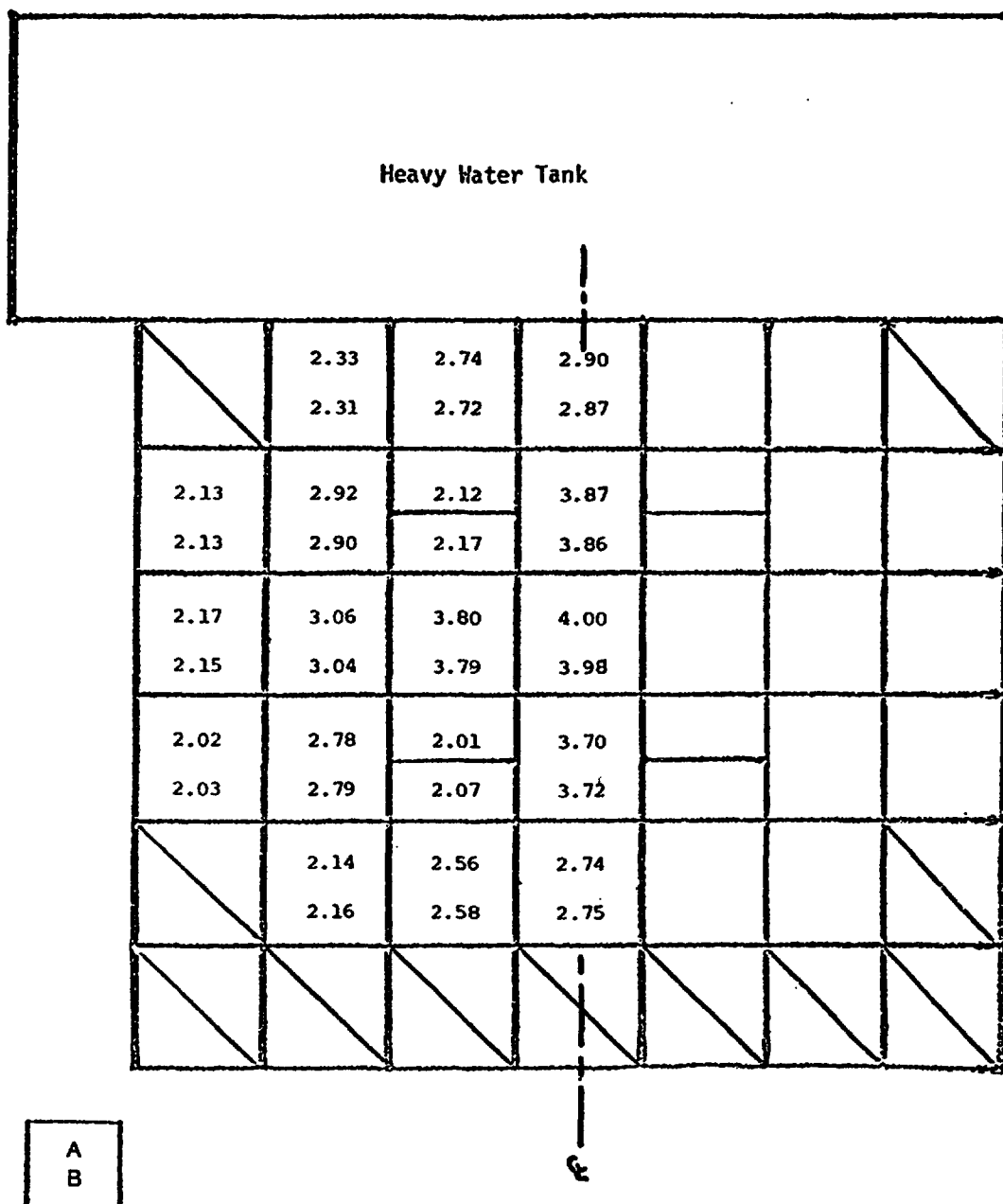
A: Assembly power (%), HEU core
B: Assembly power (%), LEU core

297

Heavy Water Tank

	A / B	A / B	A / B	A / B	A / B	A / B	
(empty)	2.130 / 2.098	2.593 / 2.562	2.983 / 2.977	3.116 / 3.118	2.765 / 2.781	2.358 / 2.373	(empty)
1.775 / 1.741	2.397 / 2.341	3.426 / 3.394	2.172 / 2.206	4.124 / 4.139	2.202 / 2.269	2.860 / 2.857	1.954 / 1.956
1.726 / 1.680	2.697 / 2.652	1.893 / 1.905	4.288 / 4.286	4.306 / 4.290	3.910 / 3.901	3.004 / 2.969	1.963 / 1.938
1.569 / 1.551	2.450 / 2.438	3.281 / 3.281	2.202 / 2.258	4.225 / 4.252	1.925 / 1.949	2.729 / 2.699	1.900 / 1.879
(empty)	(empty)	2.473 / 2.496	2.966 / 3.000	1.525 / 1.554	2.679 / 2.676	2.197 / 2.184	(empty)
(empty)	(empty)	1.598 / 1.639	1.864 / 1.900	2.009 / 2.039	1.765 / 1.774	(empty)	(empty)

| A / B | Regular elements | A / B | Special elements | | Empty core locations |

A: Assembly power (%), HEU 11-day cycle
B: Assembly power (%), LEU 15-day cycle

FIG. 10. Assembly power distribution for equilibrium core.

The calculated thermal flux distributions are compared in Figure 11 for batch cores and Figure 12 for equilibrium cores. A major difference between HEU and LEU fuel is apparent from these figures: since for a well moderated core the power is approximately proportional to the product of the macroscopic fission cross-section and thermal flux, an increased fuel loading results in a corresponding reduction in thermal flux for a given power. This effect is readily apparent in Figures 11 and 12, where the thermal flux in regular fuel elements is seen to decrease by about 14%. For special fuel elements, the reduction in thermal flux is only about 9%. This mitigation in the thermal flux decrease results from the effect of the thermal flux peaking in the large waterhole. This peak is primarily dependent on the fast flux, which is not significantly different between the LEU and HEU fuels. Since the thermal flux level within the special element will be affected by the waterhole peaking, the overall effect is to mitigate the decrease in thermal flux. As noted for the power distribution, there is a slight shift in thermal flux away from the heavy water tank toward a slightly improved overall symmetry about the center. Figures 13 and 14 display thermal flux for traverses along the north-south core center lines. It should be noted that the centerline of the equilibrium core is bordered by two special assemblies, whereas the batch core centerline is through the centers of regular assemblies. The general reduction in thermal flux is apparent in both figures, and the mitigating effects of the special assemblies are evident in the equilibrium core traverse.

Calculations of the ex-core thermal flux in the heavy water tank have indicated that the thermal leakage flux will be reduced by 6~10%. While this is an important consideration for experimental usage, it has no impact on the core safety analysis.

9.3.4 Core Dynamic Characteristics

Of the physics parameter changes that would affect core dynamics, temperature coefficient and power defect, which is largely affected by temperature coefficient, are expected to be the parameters of greatest significance. Calculations indicate the magnitude of negative temperature coefficient increases from -8.4 pcm/$^{\circ}$F to -12.6 pcm/$^{\circ}$F, primarily due to ^{238}U Doppler. The transient safety characteristics of the core are expected to improve because of the larger negative temperature coefficient and power defect.

The calculated slight decrease in total rod worth still allows for shutdown margins well in excess of Technical Specification limits and sufficient excess reactivity for normal cycle operations. These and other core physics parameters will be verified in the demonstration experiment and measurement program.

The FNR Safety Limits and Limiting Safety System Settings are designed to ensure that fuel clad integrity is maintained. They are based on static combinations of reactor power, core inlet temperature, coolant flow rate, and pool height which prevent boiling in the hottest spot in the core. These limits and settings are not altered by the changes in core physics parameters.
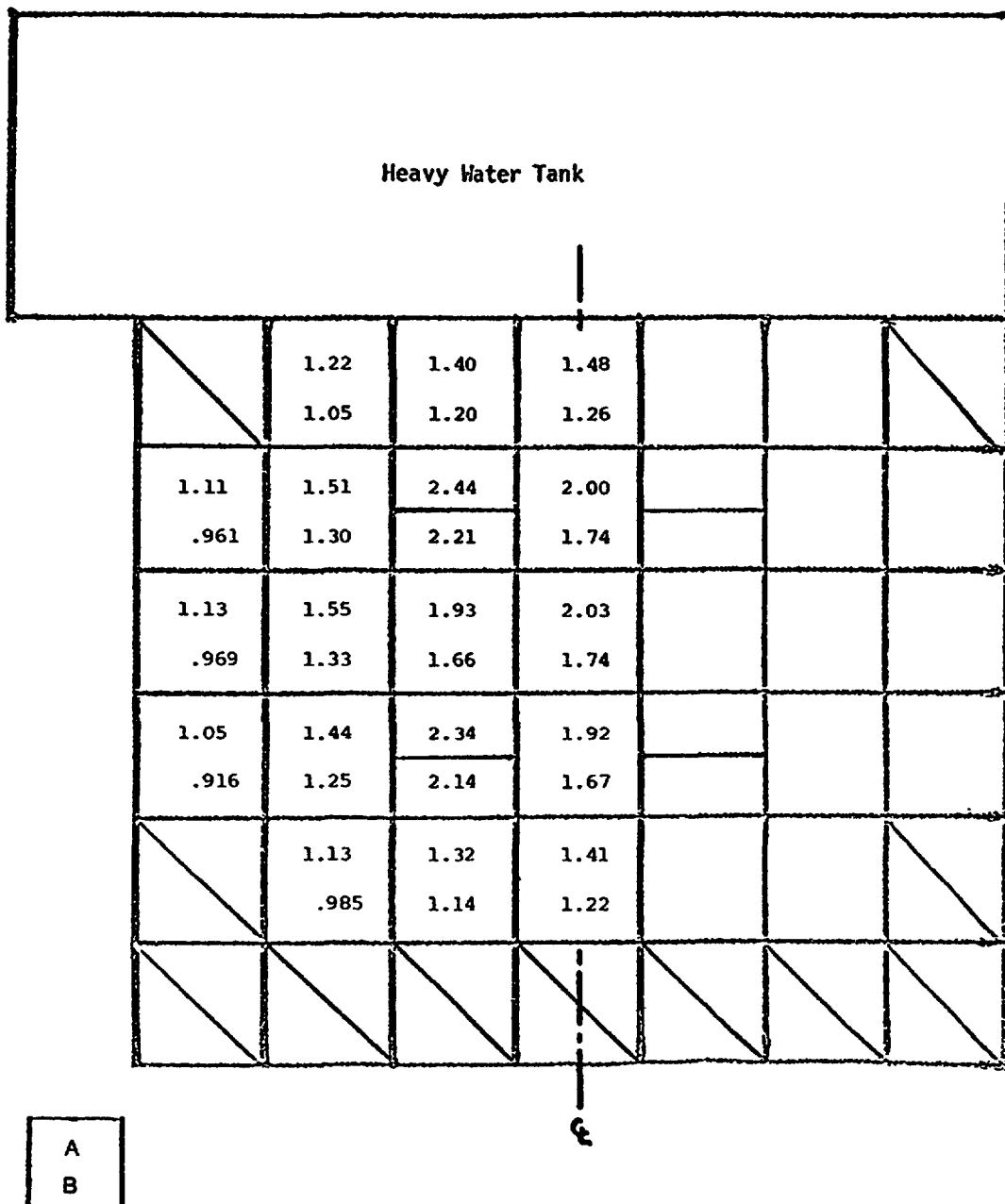
A: Assembly-average thermal flux (10^{13}n/cm^2·s), HEU core
B: Assembly-average thermal flux (10^{13}n/cm^2·s), LEU core

FIG. 11. Assembly-average thermal flux distribution for batch core.

Heavy Water Tank

	.993 / .858	1.18 / 1.01	1.36 / 1.17	1.35 / 1.16	1.26 / 1.09	1.07 / .934	
.853 / .735	1.11 / .963	1.53 / 1.32	2.22 / 2.02	1.80 / 1.57	2.05 / 1.86	1.29 / 1.12	.970 / .844
.842 / .720	1.23 / 1.06	2.10 / 1.91	1.88 / 1.62	1.79 / 1.54	1.68 / 1.45	1.32 / 1.13	.985 / .849
.779 / .675	1.13 / .974	1.50 / 1.30	2.18 / 1.98	1.82 / 1.59	2.07 / 1.89	1.28 / 1.11	.933 / .811
		1.18 / 1.02	1.34 / 1.16	1.82 / 1.67	1.29 / 1.11	1.06 / .929	
		.805 / .696	.916 / .792	.953 / .827	.896 / .784		

Legend:
- A / B — Regular elements
- A / B — Special elements
- Empty core locations

A: Assembly-average thermal flux (10^{13} n/cm$^2 \cdot$s), HEU 11-day cycle
B: Assembly-average thermal flux (10^{13} n/cm$^2 \cdot$s), LEU 15-day cycle

FIG. 12. Assembly-average thermal flux distribution for equilibrium core.
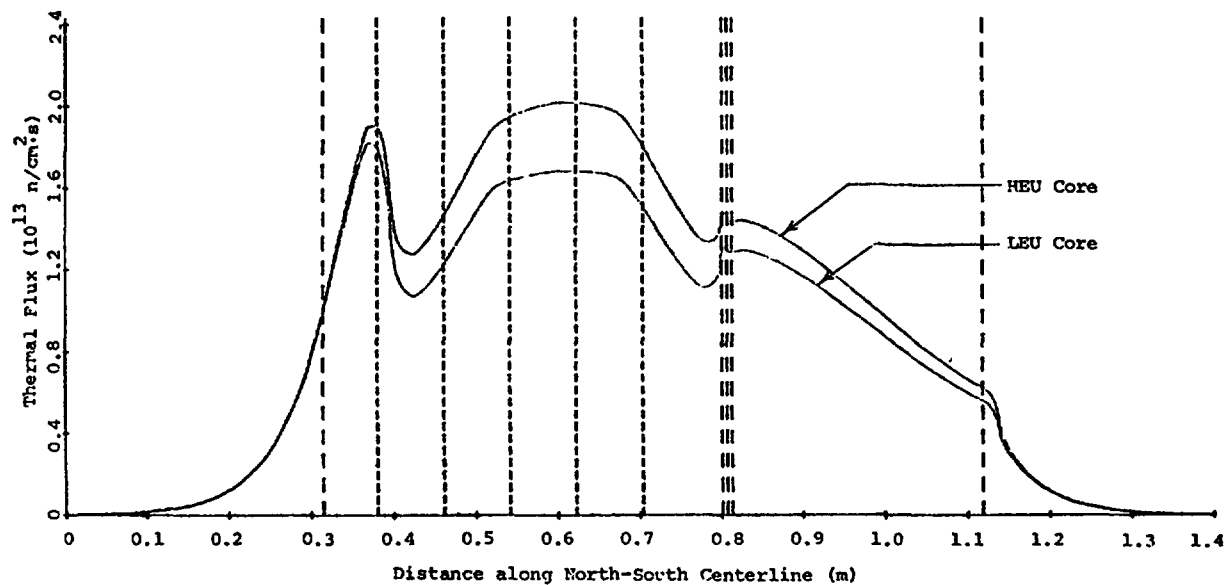
FIG. 13. Thermal flux distribution for batch core.

9.4 Summary of the Core Physics Analysis

Extensive effort has been devoted to the development of accurate calculational methods for the analysis of HEU and LEU fueled research reactors. These methods make use of existing well-verified computer codes wherever possible and have been verified through comparison with data from several different research reactor configurations. The accuracy of the computational methods is expected to be equally valid for the prediction of changes in core physics parameters due to the use of LEU fuel. To encompass all expected effects of the proposed LEU fuel, both a batch core model and an equilibrium core model were analyzed in detail and compared with the HEU fuel. The results of these comparisons serve to quantify predictions which can be made on physical grounds: decreasing the fuel enrichment from 93 w/o to 19.5 w/o and increasing the ^{235}U loading from 140 grams to 167.3 grams per 18-plate assembly result in a large decrease in the in-core thermal flux; a small decrease in xenon poisoning; a small increase in power defect due to increased Doppler effects; longer cycle length for a given reactivity change and higher discharge fuel burnup; a reduction in control rod worth, which may be offset by longer cycle; very little change in power distribution; and, most importantly, no significant change in the core shutdown margin.

While there are changes in core physics parameters for the proposed LEU fuel, there appear to be no reductions in any safety margins.

10. DEMONSTRATION EXPERIMENT AND MEASUREMENT PROGRAM

The demonstration experiments and measurements program will: 1) characterize the FNR in sufficient detail to discern and quantify neutronic differences between high and low enrichment cores, and 2) provide measurements to benchmark core physics calculations.
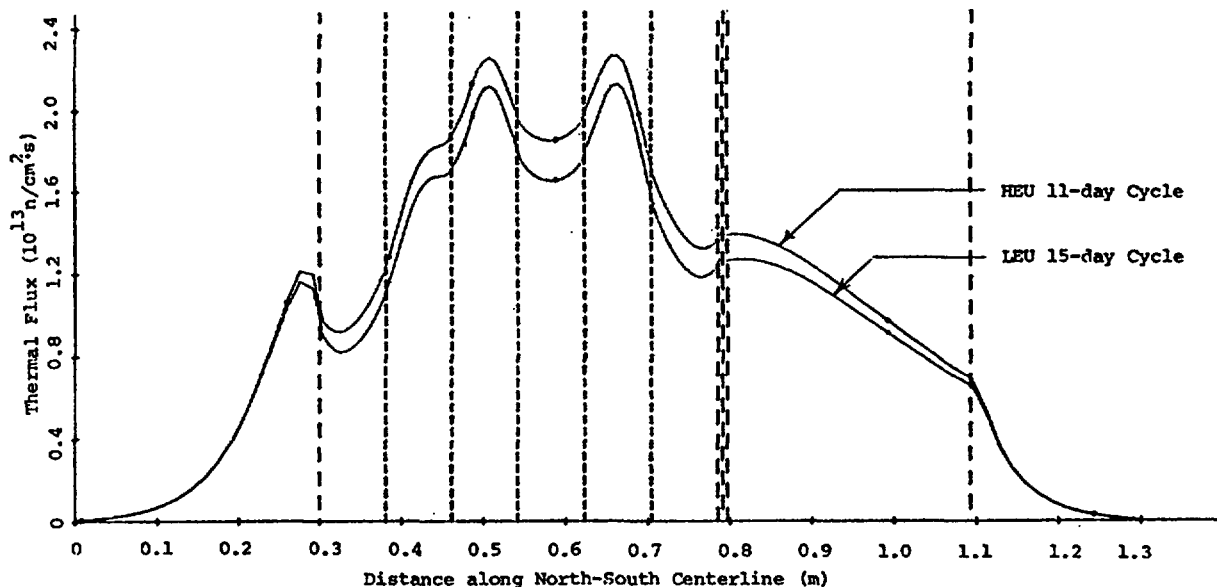
FIG. 14. Thermal flux distribution for equilibrium core.

The experiments chosen to accomplish this program are:

1. Wire activation measurements to provide absolute flux normalization.

2. Rhodium detector flux maps to provide absolute thermal (in-core and ex-core) fluxes.

3. Neutron diffraction measurements to determine the flux spectrum in the D_2O reflector.

4. Control rod worth measurements and power defect measurements.

5. Unfolding of foil activation measurements to determine the in-core flux spectrum.

10.1 Analysis of the Current High Enrichment Uranium Core

Experimental and analytical efforts are in progress which are designed to characterize the present FNR core. Spatial flux distributions are being measured with ^{103}Rh movable self-powered neutron detectors, with proper correction factors applied for epithermal neutrons. The measurement of fast neutron spectra are being made using the multiple threshold foil technique and the unfolding calculations (SAND-II and modified SAND-II codes) will be performed. In-core thermal flux spectra are being measured by standard activation foil techniques and Cd ratio methods, and the leakage spectra by crystal spectrometer method. In-core flux, correlated to changes in the reactor core config-urations, is being measured by partial-core ^{103}Rh flux maps and the leakage neutron flux levels in beam ports in preparation for partial loading of low-enrichment fuel elements. In addition, measurements of other reactor parameters including control rod worth and reactivity coefficients will be performed. We will also establish, to the extent possible, the accuracy of our measurement techniques so that we can obtain meaningful comparison between the high- and low-enrichment fuels and also with the calculated results.

303

10.2   Testing and Measurements on the Low-Enrichment FNR Core

Detailed measurements of flux distribution and other reactor parameters for partial- and full-core low-enrichment configurations of the FNR core will be performed. The measurements will be performed in accordance with the techniques established in section 10.1. The need for any modifications in the measurement techniques or detector calibrations for the low-enrichment environment will be determined prior to the full-core loading. The measurements will include in-core and ex-core maps, spectra, and other standard reactor physics parameters.

REFERENCES

1.   G.W. Gibson, "The Development of Powdered Uranium Aluminide Compounds for Use as Nuclear Reactor Fuels," IN-1133, TID-4500, Idaho Nuclear Corporation, December, 1967.

2.   R.M. Brugger, "Metallurgy and Materials Science Branch Annual Report Fiscal Year 1970", IN-1437, Idaho Nuclear Corporation, November, 1970.

3.   R.R. Hobbins, "INC-16-2 Irradiation Experiment", Idaho Operations Office, U.S. Atomic Energy Commission, July 19, 1974.

4.   M.M. Martin, A.E. Richt, and W.R. Martin, "Irradiation Behavior of Aluminum Base Fuel Dispersions," ORNL-4856, Oak Ridge National Laboratory, May, 1973.

5.   W. Dienst, S. Nazare, and F. Thummber, "Irradiation Behavior of UAL$_x$ Dispersion Fuels for Thermal High Flux Reactors," Journal of Nuclear Materials, 64, 1977.

6.   W.C. Francis, ANNUAL PROGRESS REPORT OF REACTOR FUELS AND MATERIALS DEVELOPMENT FOR FY 1965, USAEC Report IDO-17154, Idaho Operations Office, U.S. Atomic Energy Commission, February, 1966.

7.   G.W. Gibson, M.J. Graber, V.A. Walker, and W.C. Francis, "Results of ATR Sample Fuel Plate Irradiation Experiment", IDO-16958, Idaho Operations Office, U.S. Atomic Energy Commission, March 23, 1964.

8.   D.J. Rucker, "Fuels and Materials Development Program Quarterly Progress Report for Period Ending March 31, 1970", ORNL-4560, Oak Ridge National Laboratory, March, 1970.

9.   "Reactor Safety Evaluation of ORNL Proposal to Modify Fuel in ORR", Oak Ridge National Laboratory, February, 1977.

10.   P. Tichler, "Review of Proposed Increase in Fuel Element Loading and Fuel Burnup", Memorandum, Brookhaven National Laboratory, February, 1977.

11. V.A. Walker, M.J. Graber, and G.W. Gibson, "ATR Fuel Materials Development Irradiation Results - Part II," IDO-17157, Idaho Operations Office, U.S. Atomic Energy Commission, June, 1966.

12. R. F. Barry, "LEOPARD - A Spectrum Dependent Non-spatial Depletion Code", WCAP-3269-26, Westinghouse Electric Corporation (September 1963).

13. J. Barhen, W. Rothenstein. E. Taviv, "The HAMMER Code System", NP-565, Electric Power Research Institute (October 1978).

14. W. W. Little, Jr. and R. W. Hardie, "2DB User's Manual-Revision I", BNWL-831 REV1, Battelle Pacific Northwest Laboratory (February 1969).

15. W. W. Engle, Jr., "A User's Manual for ANISN, a One-Dimensionsl Discrete Ordinates Transport Code with Anisotropic Scattering", K-1693, Oak Ridge Gaseous Diffusion Plant (March 1967).

16. K. D. Lathrop and F. W. Brinkley, "TWOTRAN-II - An Interfaced Exportable Version of the TWOTRAN Code for Two-Dimensional Transport", Los Alamos Scientific Laboratory, LA-4848-MS (1973).

17. D. R. Vondy, T. B. Fowler, and G. W. Cunningham, "VENTURE: A Code Block for Solving Multigroup Neutronics Problems Applying the Finite-Difference Diffusion Theory Approximation to Neutron Transport", ORNL-5062 (1975).

18. M. H. Theys, "Integral Transport Theory of Thermal Utilization Factor in Infinite Slab Geometry", Nucl. Sci. Eng., 7, 58 (1960).

19. S. Jabbawy, J. Karni., W. Rothenstein, and S. Velner, "Water Moderated Reactor Analysis with ENDF/B Data", Nuclear Data in Science and Technology, Vol. II, p. 147, IAEA, Vienna (1973).

20. N. G. Demas, "Representation of Two-Dimensional Self-Shielded Poison Lumps in P-1 Calculations", WAPD-BT-21, Westinghouse Electric Corporation, pp. 29-32 (Nov. 1960).

21. E. B. Johnson, "Power Calibration for BSR Loading 33", CF-57-11-30, Oak Ridge National Laboratory (1957).

22. J. M. Hendrie, "Final Safety Analysis Report on the Brookhaven High Flux Beam Research Reactor", BNL-7661, Brookhaven National Laboratory (April 1964).

23. R.R. Burn, "Research, Training, Test, and Production Reactor Directory", United States of America, Order No. 250001, American Nuclear Society, LaGrange Park, Illinois, 1980.

305

BIBLIOGRAPHY

1. G.M. Adamson, "Fabrication of Research Reactor Fuel Elements", ORNL-TM-2197, Oak Ridge National Laboratory, June 1968.

2. ALCOA ALUMINUM HANDBOOK, Aluminum Company of America, Pittsburgh, 1962.

3. HANDBOOK OF ALUMINUM, Alcan Aluminum Corporation, Cleveland, 1970.

4. D.M. Alger and C. Julian, "UAl$_x$ Fuel in Research Reactors", Transactions of the American Nuclear Society, Chicago, June 10-14, 1973.

5. C. Allain, H. Aubert, and J. Laniesse, "Irradiation Dans Le Reacteur El 3 De Tubes En Uranium Faiblement Allie", Journal of Nuclear Materials, 31, Number 2, June 1969.

6. ALUMINUM WITH FOOD AND CHEMICALS, The Aluminum Association, New York, February 1969.

7. ALUMINUM STANDARDS AND DATA, The Aluminum Association, New York, December, 1969.

8. W.E. Berry, CORROSION IN NUCLEAR APPLICATIONS, John Wiley and Sons, New York, 1971.

9. J.H. Buddery, M.E. Clark, R.J. Pearce and J.J. Stobbs, "The Development and properties of an Oxidation-Resistant Coating for Uranium", Journal of Nuclear Materials, 13, No. 2, 1964.

10. B.L. Bramfitt and H.P. Leighly, "A Metallographic Study of Solidification and Segregation in Cast Aluminum-Uranium Alloys", Metallography, Vol. 1, No. 2, November 1968.

11. R.M. Brugger, "Metallurgy and Materials Science Branch Annual Report Fiscal Year 1970", IN-1437, Idaho Nuclear Corporation, November 1970.

12. J. Chamberlain, M.P. Johnson, J.R. Kench and A.G. Young, "The Influence of Microstructure on the Behaviour of Uranium Alloys During Temperature Cycling Creep Experiments", Journal of Nuclear Materials, 19, No. 2, 1966.

13. A.K. Chakraborty, R.S. Crouse and W.R. Martin, "Factors Affecting the Swelling During Degassing of Compacts Containing Uranium-Aluminum Inter-Metallics Dispersed in Aluminum", ORNL-TM-2800, Oak Ridge National Laboratory, March 1970.

14. P. Chiotti and J.A. Kateley, "Thermodynamic Properties of Uranium-Aluminum Alloys", Journal of Nuclear Materials, 32, No. 1, August 1969.

15. J.K. Dawson and R.G. Sowden, CHEMICAL ASPECTS OF NUCLEAR REACTORS, Butterworth and Co., London, 1963.

306

16. D.R. deBoisblanc, "Reactor Engineering Branch Annual Report Fiscal Year 1968", IN-1228, Idaho Nuclear Corporation, February 1969.

17. D.R. deBoisblanc, "Reactor Engineering Branch Annual Report Fiscal Year 1969", IN-1335, Idaho Nuclear Corporation, November 1969.

18. D.R. Dickinson, R.J. Lobsinger and R.B. Richman, "Corrosion of Aluminum-Clad Fuel Elements", TID-7642, Research Reactor Fuel Element Conference, Gatlinburg, Tennessee, September 1962.

19. W. Dienst, S. Nazare, F. Thummler, "Irradiation Behavior of UAl_x-Al Dispersion Fuels for Thermal High Flux Reactors", Journal of Nuclear Materials, 64, 1977.

20. J.O. Dittmer, "A Study of the Compressive Properties of Aluminum Clad Composite Nuclear Reactor Fuel Plates", Master's Thesis, Idaho State University, 1969.

21. E.A. Eldridge and H.W. Deem, "Report on Physical Properties of Metals and Alloys from Cryogenic to Elevated Temperatures", ASTM Special Technical Publication No. 296, American Society for Testing Materials, Philadelphia, April 1961.

22. H.E. Exner and G. Petzow, "Untersuchungen zur Stabilisierung von UAl_3 in Aluminiumreichen Kernbrennstoffen", Metal, No. 3, March 1969.

23. J.D. Fleming and J.W. Johnson, "Aluminum-U_3O_8 Exothermic Reactions", TID-7642, Research Reactor Fuel Element Conference, Gatlinburg, Tennessee, September 1962.

24. W.C. Francis, G.W. Gibson and W.P. Scarrah, "Some Results of Uranium Irradiations at the MTR/ETR", TID-7642, Research Reactor Fuel Element Conference, Gatlinburg, Tennessee, September 1962.

25. W.C. Francis, "Fuel Elements for Thermal Test Reactors - Performance at NRTS", AEC - Industry Meeting on Water Reactor Fuel Element Technology, Germantown, Maryland, January 1968.

26. FUEL ELEMENT FABRICATION, Volume 2, Proceedings of a Symposium in Vienna, Academic Press, New York 1961.

27. G.W. Gibson and D.R. deBoisblanc, "Uranium-Aluminum Alloy Powders for use as Nuclear Reactor Fuels", CONF-339-5, U.S. Atomic Energy Commission, October 1963.

28. G.W. Gibson, M.J. Graber, V.A. Walker and W.C. Francis, "Results of ATR Sample Fuel Plate Irradiation Experiment", IDO-16958, Idaho Operations Office, U.S. Atomic Energy Commission, March 23, 1964.

29. G.W. Gibson, "The Development of Powdered Uranium-Aluminide Compounds for use as Nuclear Reactor Fuels", IN-1133, Idaho Nuclear Corporation, December 1967.

30. J.C. Griess, H.C. Savage, J.G. Rainwater, J.L. English and T.H. Mauney, "The Corrosion of Aluminum Alloys Under Simulated ATR and HFIR Conditions", TID-7642, Research Reactor Fuel Element Conference, Gatlinburg, Tennessee, September 1962.

31. M.J. Graber, G.W. Gibson and W.C. Francis, "Annual Progress Report on Reactor Fuels and Materials Development for FY 1963", IDO-16934, Idaho Operations Office, U.S. Atomic Energy Commission, November 25, 1963.

32. M.J. Graber, W.F. Zelezny and G.W. Bison, "Annual Progress Report on Reactor Fuels and Materials Development for FY 1964", IDO-17037, Idaho Operations Office, U.S. Atomic Energy Commission, November 1964.

33. M.J. Graber and R.A. Moen, "The Effects of Compatibility on the Performance of Aluminum Fuel Plates Containing Various Fuel Dispersions", Transactions of the American Nuclear Society, Gatlinburg, Tennessee, June 21-24, 1965.

34. D.H. Gurinsky and G.J. Dienes, NUCLEAR FUELS, D. Van Nostrand Co., New York, 1956.

35. L.J. Harrison, "Mechanical Failures of MTR Fuel Assemblies", Nucleonics, Volume 21, No. 10, October 1963.

36. L.J. Harrison, "Heat Transfer from an Aluminum/Uranium Fuel Plate in a Subcooled Pool During a TREAT Transient", Transactions of the American Nuclear Society, Seattle, June 15-19, 1969.

37. H.H. Hausner and J.F. Schumar, NUCLEAR FUEL ELEMENTS, Reinhold Publishing Corp., New York, 1959.

38. R.R. Hobbins and M.J. Graber, "ATR Extended Burnup, XA003F Results and INC-16-1 Review", Idaho Operations Office, U.S. Atomic Energy Commission, 1974.

39. R.R. Hobbins, "INC-16-2 Irradiation Experiment", Idaho Operations Office, U.S. Atomic Energy Commission, July 19, 1974.

40. R.O. Ivins, "A Study of the Reaction of Aluminum Uranium Alloy Fuel Plates with Water Initiated by a Destructive Reactor Transient", CONF-39-70, U.S. Atomic Energy Commission, February 1963.

41. M. Jovanovic, "The Isothermal Growth of Secondary-Phase Particles in a Dilute Uranium Alloy", Journal of Nuclear Materials, 35, No. 2, May 1970.

42. C. Julian, "Evaluation of a 6.2 Kilogram U^{235} Core Loading for the Missouri University Research Reactor", University of Missouri, July 28, 1970.

43. A.R. Kaufmann, NUCLEAR REACTOR FUEL ELEMENTS, METALLURGY AND FABRICATION, John Wiley and Sons, New York, 1962.

44. R.T. King, E.L. Long, J.O. Stiegler and K. Farrell, "High Neutron Fluence Damage in an Aluminum Alloy", Journal of Nuclear Materials, 35, No. 2, May 1970.

45. J.H. Kittel, A.P. Gavin, C.C Crothers and R. Carlander, "Performance of Aluminum-Uranium Alloy Fuel Plates Under High Temperature and High Burnup Conditions", TID-7642, Research Reactor Fuel Element Conference, Gatlinburg, Tennessee, September 17-19, 1962.

46. D. Lazarevic, "Influence of Neutron Radiation on the Phase Composition of Low-Alloyed Uranium", RADIATION DAMAGE IN REACTOR MATERIALS, Volume 2, International Atomic Energy Agency, Vienna, June 1969.

47. J. Lehmann, P. Paoli and N. Azam, "Gonflement D'Alliages D'Uranium sous Irradiation", Journal of Nuclear Materials, Vol. 26, No. 2, May 1968.

48. J. Lehmann, P. Paoli and N. Azam, "Etude du Gonflement D'Alliages D'Uranium Sous Irradiation", Journal of Nuclear Materials, Vol. 27, No. 3, September 1968.

49. W.R. Martin and J.R. Weir, "Mechanical Properties of X8001 and 6061 Aluminum Alloys and Aluminum-Base Fuel Dispersion at Elevated Temperatures", ORNL-3557, Oak Ridge National Laboratory, February 1964.

50. M.M. Martin, J.H. Erwin and W.R. Martin, "Effect of Type and Concentration of Fuel on the Void Volume in Aluminum Dispersion-Type Fuel Plates", Transactions of the American Nuclear Society, Toronto, June 10-13, 1968.

51. M.M. Martin and A.E. Richt, "Effect of Void Volume on the Irradiation Performance of Aluminum-Base Dispersion-Type Fuel Plates", Transactions of the American Nuclear Society, Seattle, June 15-19, 1969.

52. M.M. Martin and W.R. Martin, "Fabrication Voids in Aluminum-Base Fuel Dispersions", ORNL-4611, Oak Ridge National Laboratory, October 1970.

53. M.M. Martin, A.E. Richt and W.R. Martin, "Irradiation Performance of Aluminum-Base Dispersion-Type Fuel Plates", Transactions of the American Nuclear Soceity, Miami, October 17-21, 1971.

54. M.M. Martin, A.E. Richt and W.R. Martin, "Irradiation Behavior of Aluminum-Base Fuel Dispersions", ORNL-4856, Oak Ridge National Laboratory, May 1973.

55. D.L. McElroy, R.S. Graves and J.P. Moor, "Physical Properties of Two-Phase Materials Used in Fuel Plate Cores", Canadian Journal of Physics, 45, 1967.

56. D.L. McElroy, "Physical Properties of Al Cermets", Oak Ridge National Laboratory, January 5, 1971.

57. Oak Ridge Reactor, "Reactor Safety Evaluation of ORNL Proposal to Modify Fuel in ORR", Oak Ridge National Laboratory, February 1977.

58. B.E. Paige, G.W. Gibson and K.L. Rohde, "The Effect of Silicon on Fabrication and Reprocessing of Aluminum Alloy Reactor Fuels", IN-1194, Idaho Nuclear Corporation, November 1968.

59. C.F. Reinke, "Irradiation and Postirradiation Annealing of Some Aluminum-Base Fuels", ANL-6665, Argonne National Laboratory, September 1963.

60. C.F. Reinke, "Postirradiation Annealing of Some Aluminum-Base Fuels", Transactions of the American Nuclear Society, Vol. 7, No. 1, Philadelphia, June 14-17, 1964.

61. A.E. Richt, C.F. Leitten, and R.J. Beaver, "Radiation Performance and Induced Transformations in Aluminum-Base Fuels", TID-7642, Research Reactor Fuel Element Conference, Gatlinburg, Tennessee, September 1962.

62. J.A.L. Robertson, IRRADIATION EFFECTS IN NUCLEAR FUELS, Gordon and Breach, New York, 1969.

63. D.J. Rucker, "Fuels and Materials Development Program Quarterly Progress Report for Period Ending June 30, 1968", ORNL-4330, Oak Ridge National Laboratory, June 1968.

64. D.J. Rucker, "Fuels and Materials Development Program Quarterly Progress Report for Period Ending September 30, 1968", ORNL-4350, Oak Ridge National Laboratory, September 1968.

65. D.J. Rucker, "Fuels and Materials Development Program Quarterly Progress Report for Period Ending December 31, 1969", ORNL-4520, Oak Ridge National Laboratory, December 1969.

66. D.J. Rucker, "Fuels and Materials Development Program Quarterly Progress Report for Period Ending March 31, 1970", ORNL-4560, Oak Ridge National Laboratory, March 1970.

67. D.J. Rucker, "Fuels and Materials Development Program Quarterly Progress Report for Period Ending September 30, 1970", ORNL-4630, Oak Ridge National Laboratory, September 1970.

68. O.J.C. Runnalls and R.R. Boucher, "Transformations in UAl_4 and $PuAl_4$ ", Transactions of the Metallurgical Society of AIME, Vol. 233, No. 7, New York, September 1965.

69. P. Tichler, "Examination of Reactor Safety Implications of Increased Fuel Loading and Extended Operating Cycle at the HFBR", Brookhaven National Laboratory, February 1977.

70. F. Thummler, H.E. Lilienthal and S. Nazare, "UAl_2-Al Instead of UAl_3-Al in Fuel Element Plates for Advanced Test-Reactors", Powder Metallurgy, Vol. 12, No. 23, London, 1969.

71. K.R. Van Horn, ALUMINUM, American Society for Metals, Metals Park, Ohio, 1967.

72. H.R. Voorhees and J.W. Freeman, "Report on the Elevated-Temperature Properties of Aluminum and Magnesium Alloys", ASTM Special Technical Publication No. 291, American Society for Testing Materials, Philadelphia, October 1960.

310

73. J.R. Weir, J.E. Cunningham and C.J. McHargue, "Metals and Ceramics Division Annual Progress Report for Period Ending June 30, 1974", ORNL-4970, Oak Ridge National Laboratory, October 1974.

74. R.E. Wison, "Kinetics of the Molten-Aluminum/Steam Reaction by the Levitation Method", Transactions of the American Nuclear Society, Vol. 6, No. 1, Salt Lake City, June 1963.

75. V.S. Yemel'Yanov and A.I. Yevstyukhin, THE METALLURGY OF NUCLEAR FUEL, Pergamon Press, New York, 1969.

76. W.F. Zelezny, G.W. Gibson and M.J. Graber, "A Microprobe Study of the Retention of the Fussion Gas Xenon in Irradiated Uranium Fuels Dispersed in Aluminum Clad Nuclear Reactor Fuel Plates", CONF-690910, United States Atomic Energy Commission, September 1969.

Appendix E-4

MODIFICATIONS REQUIRED BY THE
OSIRIS CORE CONVERSION

COMMISSARIAT A L'ENERGIE ATOMIQUE
Département de sûreté nucléaire,
Centre d'études nucléaires de Saclay,
Gif-sur-Yvette, France

Abstract

An outline is provided of the modifications required to substitute
low enriched Caramel fuel in place of highly enriched aluminide
fuel in the OSIRIS reactor core. A change in the fuel technology
and some modifications of the reactor itself were required.

PREAMBULE

The substitution in the OSIRIS reactor core of low enriched fuel
(LEU) in place of a highly enriched fuel (HEU) has implied :

- a change in the fuel technology,

- some modifications of the reactor itself.

The technical prescriptions notified to the operator by the licen-
sing authority (Ministry of Industry-Central Service of the Nuclear
Safety) lay down that the reactor must be maintained in conformity
with the safety report.

Therefore the HEU/LEU conversion in OSIRIS has required that the
operator sollicit an agreement. Documents in support of this request
were supplied as a complement to the existing safety report.

The conversion of ISIS, a neutronic model of the OSIRIS reactor,
was done previously, according to a similar procedure.

DOCUMENTS PROVIDED IN SUPPORT OF THE APPLICATION FOR CONVERSION LICENCE

The modification concerned only a part of the installation, mainly
the core assembly. To obtain the conversion licence, the operator
had to present :

- a complement to the safety report,

313

- a start-up program (at low and high power),
- a new version of the general operating rules.

It is to be noted that the licensing authority has recalled him to the necessity of providing a new "definitive safety report" within one year.

In the following, the data given in the complement with the elements quoted in the indicative plan -recalled in appendix- of French safety reports (preliminary, provisional and definitive), corresponding to the three following stages : construction, fuel loading and normal operation), are compared.

It is worth to notice that the functions affected by the fuel change have been reassessed from a safety point of view taking into account the new rules in force.

COMPARISON BETWEEN TYPICAL CONTENTS OF THE VOLUME III (SAFETY ANALYSIS) AND THE ELEMENTS PRESENTED IN THE COMPLEMENT TO THE SAFETY REPORT

1) Quality control

a) General rules of construction

The OSIRIS reactor was built in 1965, in compliance with procedures in force at that time. It was illusory to apply the prescriptions of the present quality code to the few components which were partially modified. The general former specifications have been kept with some improvements in order to obtain quality levels nearer to present ones.

b) Quality assurance

A quality organization was established by an industrial architect ensuring, either directly or through the instrumentality of approved organism, the second degree control of studies and construction.

This industrial architect has established a synthesis quality report.

2) *Tests intended to make sure of design validity concerning the*
   safety

   a) *Fuel elements*

   In addition to the experience acquired in loops or in
reactor, three prototype fuel elements, equipped with a specific
cladding failure detection, have been irradiated inside the former
core with metallic plates. One of them has undergone a destructive
examination in a hot cell.

   b) *Cladding failure detection*

   An irradiation of a small fuel element, manufactured
with a defectuous caramel has been carried out in an independent
cell of the EL3 reactor, in order to test the working of the clad-
ding failure detection. This irradiation has confirmed the good
behavior of the broken caramel in such accidental conditions and
of good detection.

   c) *Thermohydraulics*

   Tests in an outside-reactor loop (CAPRI) have confirmed
that corrugations of the "cramel" plates did not affect the coeffi-
cients, used in calculation codes and determined with smooth plates.
   Other tests have proved that, taking into account pres-
cribed limitations, the water flow value in the fuel elements would
be reached.

   d) *Control rods mechanisms*

   The weight increase of the control elements has required
a change of the command rod mechanisms. Their ability to move the
command rods has been checked on a trial rod. Moreover, the rod
drop time has been checked.

315

e) Neutronics

The test in the ISIS reactor of a "caramel" core configuration confirmed the calculation results, namely those relevant to the position, the value of the hot points and the efficiency of the control rods.

DETAILED SAFETY ANALYSIS (PREVENTION, SUPERVISION, MEANS OF ACTION)

a) Core

The presented document concerned in particular :
- The prevention and the supervision in normal operation :
    . Neutronic and thermal study,
    . Safety margins,
    . Neutronic controls and security,
    . Thermodynamic controls and security,
    . Claddind failures controls and security.

- The normal and abnormal transient conditions :
    . Transition to natural convection mode,
    . Loss of three primary pumps due to an electricity trip,
    . Sticking of a primary pump (This transient had not been taken into account during the safety study of the core with metallic plates, but is now systematically considered,
    . Rise of two rods at the maximal speed, as a result of a locking device failure.

As this type of fuel was used for the first time in a whole core, it was deemed necessary to install an automatic scram of the reactor after detection of a cladding failure. It is now recognized that this precaution is not fully justified.

b) Primary Cooling Circuit

The utilization of "caramel" fuel has entailed a substantial increase of the primary flow at the core entry, requiring among other things the utilization of new pumps.

This flow rate increase has implied :

. The modification of the existing installation,

. The checking of the compatibility of the non modified elements with the new parameters (in particular the difference of pressure at the core inlet).

The safety analysis carried out has evidenced that the core could become uncovered after the rupture of the primary circuit principal pipe. This has led to install a safety action which stops the pumps and scrams the reactor after detection of a low water level in the pool.

c) *Containment Hall - Ventilation Circuits*

For memory : The containment hall and the associated ventilation circuits have not undergone sensitive modifications except that the pumps ventilation was reinforced (by adding a cold battery) to take into account the increase of the installed power.

d) *Fuel handling and storage*

The reassessment of the criticality safety of fuel handling and storage has led to provide Cadmium sheets inside the racks between cells where the fresh fuel was stocked. New data on water-steam mixture reactivity coefficients were used.

The weight increase of the "caramel" fuel elements has required : - The mechanical reinforcement of the intact fuel storage racks,

- The mechanical test of storage racks under water.

TYPICAL ACCIDENTS AND ACCIDENTAL RELEASES

The typical accident considered is the fusion of the whole core under water at the end of an operating cycle, due to an hypothetical Borax accident.

The study has showed that the radiological effects of the accident considered were very similar for the "caramel" and UA1 fuels. So, the ventilation system, containment characteristics and health-physics monitoring, were not modified.

A N N E X

INDICATORY PLAN OF THE SAFETY REPORTS
(PRELIMINARY,PROVISIONAL,FINAL)

VOLUME I - INTRODUCTION AND GENERAL SURVEY

Chapter   I - Introduction

"   II - Site

"   III - General characteristics- Main technical alternatives

"   IV - Main safety principles

"   V - Summary of the safety analysis : radiological consequences of accidents for the site

"   VI - Storage, control and disposal of radioactive wastes

"   VII - Formation and training of the personnel

Appendices: - Table of characteristics

- General drawings

- Maps and tables concerning the site

VOLUME II - EQUIPEMENT OF THE POWER REACTOR AND OPERATION

Chapter   I - General survey

"   II - Engineering - Buildings

"   III - Nuclear steam supply system and associated safety circuits

a) Fuel

b) Reactor primary system

c) Fuel handling

d) Associated safety circuits

"   IV - Containment and associated safety circuits

"   V - Nuclear auxiliary equipment

"   VI - Secondary system

"   VII - General auxiliary equipment

"   VIII - Electrical auxiliary equipment

"   IX - Control

"   X - Core physics

"   XI - Operation

Appendices to the previous chapters (*)

(*) In these Appendices will be collected information concerning Industrial Property.

318

Chapter   I - Quality Assurance
        a) General rules of construction
        b) Quality control

"   II - Tests to ascertain that the choices regarding safety are valid

"   III - Detailed analysis of safety (prevention, supervision, means of action)

        a) Core
        b) Primary system
        c) Pressure vessel
        d) Containment
        e) Handling safety
        f) Secondary circuits safety
        g) Safety of associated facilities

"   IV - Typical accidents and accidental releases

"   V - Health physics
        a) Organization of personnel protection
        b) Control of radioactive releases (EURATOM Plan 16.11.60)

"   VI - Lessons drawn from pré-operational tests

319

Appendix E-5

THE POSSIBLE USE OF CERMET FUEL IN THE DIDO
AND PLUTO HEAVY-WATER RESEARCH REACTORS

T.D.A. KENNEDY
Atomic Energy Research Establishment,
United Kingdom Atomic Energy Authority,
Harwell, Didcot, Oxfordshire,
United Kingdom

Abstract

International restrictions on the supply of highly enriched uranium have resulted in the requirement to fuel research reactors with a lower-enrichment uranium fuel.

A study has been made of the feasibility of using low-enrichment fuels of a new type in the DIDO and PLUTO reactors. This work has been done as a contribution to the studies currently being carried out internationally on the implications of using lower-enrichment fuels in heavy-water-moderated research reactors.

The uranium content of the U/Al alloy at present used cannot be increased sufficiently to maintain the requisite U^{235} content without undesirable effects on the physical properties of the alloy. A different type of fuel will therefore be required to maintain the desired nuclear characteristics. A possible solution to the problem is the use of a cermet (U_3O_8/Al) fuel material.

Cermet fuel has poorer thermal conductivity than metallic fuel, and may also contain particles of the ceramic of a size that approaches the total thickness of the cermet core. We therefore have to consider both the average temperature of the centre of the fuel and whether large particles of the ceramic may be significantly hotter than the average.

This paper describes a preliminary study of the feasibility of this concept from the heat-transfer and safety viewpoints.

Calculations have been made for a cermet of 20%-enrichment 2.3g U/cm^3, used in a high-power element in a DIDO-type reactor. To accommodate the cermet, the cladding has been reduced in thickness to 0.318mm (0.0125 in) the core increasing to 1.044mm, but the fuel geometry is otherwise unchanged.

It is concluded that from the heat-transfer viewpoint there is no problem during normal operation or the maximum credible power transient in these reactors.
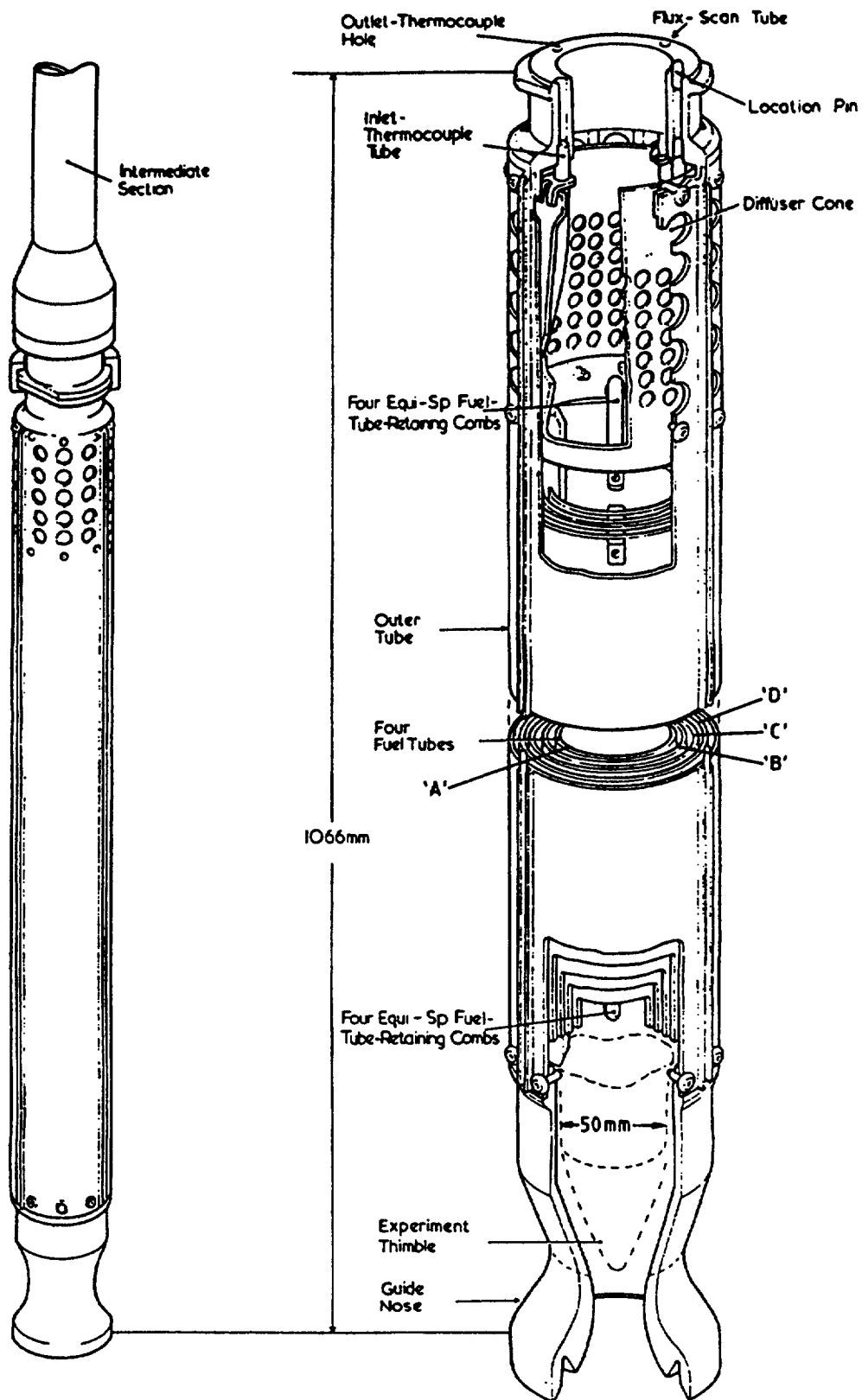
321

Fig. 1   DIDO/PLUTO MTR Fuel Element Mk 5/7

1. Introduction

The DIDO/PLUTO fuel elements currently used are of two main types. Both consist of a central cylindrical aluminium thimble surrounded by a number of concentric cylindrical fuel plates and, on the outside, an aluminium cylinder. The layout of a Mk 5/7 fuel element is shown in Fig.1. The inner-(Al)-tube/experiment-thimble has an outside diameter of 5.40 cm, and is used for housing in-core experiments. The other type of element, known as the S2 fuel element, is similar, but has more fuel tubes and a 2.86 cm outside-diameter central thimble. This paper investigates the thermal problems involved in replacing the U/Al-alloy (75% w/w U^{235}) fuel plates with U/Al-cermet (20% w/w U^{235}) plates, having the same outside dimensions to retain the same hydraulic characteristics. The investigation is limited to the Mk 5/7 fuel-element configuration. Cermet fuel plates have already been used in the Puerto Rico Nuclear Centre pool reactor (PRNC), and assumptions on cermet composition are based on information given by Kucera et al [1] for this reactor, which is a 5 MW(th) pool reactor. The interface conductance between cermet and cladding is an unknown quantity, since this type of fuel plate has not been manufactured in production quantities in the U.K. Experimental measurements will be required if this fuel is to be used; a poor contact at the interface could lead to high temperature differences and possible melting of the aluminium in the cermet.

2. Fuel-Plate Dimensions

Each PRNC fuel plate contains 10.67g of U^{235} at 20% enrichment at a total-uranium density of 2.3g $U/_{cm^3}$ (0.46g $U^{235}/_{cm^3}$).

The DIDO fuel elements contain 205g U^{235}, and if the cermet is of similar density to the PRNC fuel, would require a cermet volume of 466 cm³

The fuel loading in the four plates of a Mk 5/7 element has been optimised by Hopper[2], and the resulting dimensions are given in Table 1 below.

TABLE 1

Dimensions of Mk 5/7 Fuel Tubes and U^{235} Loading

Tube	U^{235} (g)	r_i (cm)	r_o (cm)	$\bar{r}$ (cm)
Thimble	–	2.540	2.699	2.620
'A'	43.8	3.010	3.178	3.094
'B'	49.3	3.487	3.655	3.571
'C'	55.8	3.965	4.133	4.049
'D'	56.1	4.442	4.610	4.526
Outer	–	4.837	4.992	4.915

The fuel loading in Table 1 results in the inner fuel tube 'A' having the highest fuel density, so calculations will be restricted to this tube as the worst case. In fact, the variation in fuel density from 'A' to 'C' is very small ($\sim$ 2½%), while tube 'D' requires $\sim$ 10% less fuel density.

The Mk 5/7 fuel is 'tapered' at top and bottom, so that the effective length is 18.5 in. (46.99 cm) instead of 24 in. (60.96 cm). The thickness of the cermet fuel in fuel tube 'A' is therefore 0.1044 cm.

To retain the existing 'A'-tube dimensions, this would allow 0.0318 cm (0.0125 in.) for the Al cladding. For tubes 'B' and 'C' the difference is very small, while for tube 'D' the fuel-core thickness required reduces to 0.091 cm (0.036 in.), allowing 0.038 cm (0.015 in.) for the cladding. Table 2 shows the radial dimensions of the cermet fuel.

TABLE 2

Dimensions of Cermet in Fuel Tubes

Tube	r_1 (cm)	r_2 (cm)
'A'	3.042	3.146
'B'	3.520	3.622
'C'	3.998	4.100
'D'	4.480	4.572

r_1 is the inner radius and r_2 the outer radius of the cermet in each tube

3. Fuel-Element Power

The average fuel-element-operating power is about 1 MW, but the flux shape and the presence of elements with up to 50% burn-up requires the highest-rated elements to operate at a power of about 1.25 MW.

The safety assessment of the reactor imposes two main requirements on the fuel elements - first that they will accept either a transient power ramp up to 1.3 times the operating power, i.e. to an element peak power of 1.63 MW, or a rapid whole-core heat input of 25 MJ. In both cases the transient is initiated from normal full-power operating conditions. In the simpler examinations it is assumed that no heat is transferred to the D_2O, but if this proves inadequate a more precise treatment may be necessary.

324

4. Steady Conditions for the Highest-Rated Fuel Element at 1.3 x Nominal Power (1.63 MW)

Approximately 10% of the fission heat from a DIDO/PLUTO MTR fuel element is deposited outside the fuel tubes, so the heat generation in the fuel tubes is $\sim$ 1.5 MW for a total heat output of 1.63 MW[2]. Fig.2 shows the heat-generation rate in fuel tube 'A' of a typical fuel element (D3 in DIDO) as a function of axial position. The maximum power density is seen to be 3020 W/cm^3. The fuel tubes are sufficiently thin that they may be treated as flat plates without significant loss of accuracy when calculating temperature distribution.
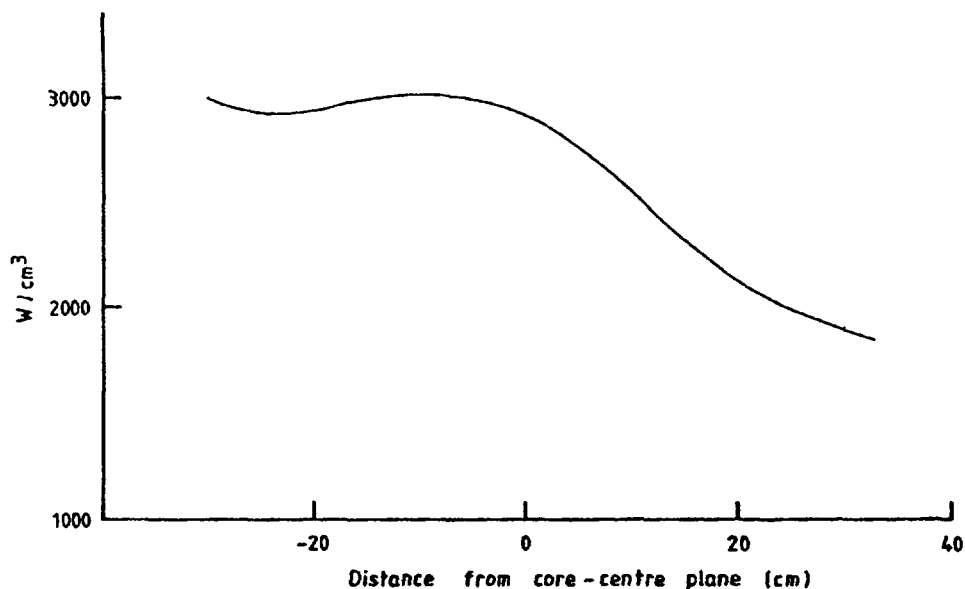
Fig. 2   Power Density in Fuel Tube 'A' for 1.5 MW from F.E.

Temperature difference from fuel-centre plane to fuel/cladding interface

$$\Delta T_c = \frac{I(t/2)^2}{2k_c} , \qquad (1)$$

where I = heat-generation rate

t = fuel-plate thickness

k_c = cermet thermal conductivity (Fig.3, taken from Ref.5)
(36.6% v/v U_3O_8)

t = 0.104 cm, k_c = 0.32 W/cmK;

$$\therefore \quad \Delta T_c = \frac{3020 \times 0.052^2}{2 \times 0.32} = 12K.$$

325

4.1 Temperature Difference Across Fuel/Cladding Interface (ΔT_{int})

The interface conductance (h_{int}) has been calculated (Appendix 1) as 1.42 $W/cm^2 K$.

$$A_s = 2\pi (r_1 + r_2) = 2\pi (3.042 + 3.146) = 38.88 \ cm^2/cm,$$

where A_s = interface surface area/unit length.

Maximum linear power rating,

$$Q_{max} = I_{max} (\pi (r_2^2 - r_1^2)) \tag{2}$$

$$= 3020\pi (3.146^2 - 3.042^2) = 6105.8 \ W/cm$$

$$\Delta T_{int} = \frac{Q_{max}}{A_s \cdot h_{int}} = \frac{6105.8}{38.88 \times 1.42} = 110.6 \ K.$$

4.2 Temperature Difference Across Cladding (ΔT_{cl})

$$\Delta T_{cl} = \frac{\phi \cdot t_{cl}}{k_{cl}} \tag{3}$$

$$\phi = \frac{Q}{A} = \frac{6106.0}{38.88} = 157.0 \ W/cm^2 = 1.57 \ MW/m^2$$

$$t_{cl} = 0.032 \ cm$$

$$k_{cl} = 2.4 \ W/cm \ K.$$

$$\therefore \ \Delta T_{cl} = \frac{157 \times 0.032}{2.4} = 2.1 \ K.$$

4.3 Temperature Difference Across D_2O Coolant Film (ΔT_f)

From the subcooled boiling correlation of Thom[3]:

$$(T_w - T_{sat}) = 22.65 \ \phi^{0.5} \ exp(- P/87) , \tag{4}$$

where T_w = wall temperature ($^\circ C$)

T_{sat} = saturation temperature of fluid ($104^\circ C$)

ϕ = surface heat flux ($1.57 \ MW/m^2$)

P = fluid pressure (1.1 bar).

$$\therefore \ T_w = 104 + 22.65 \ \sqrt{1.57} \cdot exp(- 0.01264) = 132.0^\circ C.$$

The D_2O temperature will be $50^\circ C$ at inlet and up to $74^\circ C$ at outlet, so equation (4) gives a max. heat-transfer coefficient (h_f) for the D_2O at $74^\circ C$.

$$h_f = \phi/\Delta T_f = 1.57/(132-74) = 0.0271 \ MW/m^2 K = 2.71 \ W/cm^2 K.$$

As this coefficient is of the same order as a single-phase coefficient to D_2O at high mass flux, the latter will be calculated from the Dittus-Boelter correlation:

$$(Nu) = 0.023 \ (Re)^{0.8}(Pr)^{0.4} \tag{5}$$

326

Total flow through fuel element, $\dot{m}_T$ = 17,300 g/s

D_2O flow area, A_T = $\pi[(13.01^2 - 2.699^2) + (3.487^2 - 3.178^2) + (3.965^2 - 3.655^2)$

$$+ (4.442^2 - 4.133^2) + (4.837^2 - 4.61^2)]$$

$$= 34.53 \text{ cm}^2$$

Mass flux, G_T = $\dot{m}_T/A_T$ = 17,300/34.53 = 501.0 g/cm^2 s

(Re) = $\dfrac{G_T \cdot d_e}{\mu}$; d_e = $\dfrac{4A_T}{s}$ = $\dfrac{4 \times 34.53}{2\pi(\Sigma(r_i + r_o))}$ = 0.5782 cm

μ = 5.5×10^{-3} g/cm s (viscosity of D_2O at 60°C)

k = 0.0063 W/cm K (thermal conductivity of D_2O at 60°C)

$\therefore$ (Re) = $\dfrac{501 \times 0.5782}{5.5 \times 10^{-3}}$ = 52,669

(Pr) = 3.6; $\therefore$ (Nu) = $0.023 \times 52,669^{0.8} \times 3.6^{0.4}$ = 229.9

h'_f = $\dfrac{(Nu) \cdot k}{d_e}$ = $\dfrac{229.9 \times 0.0063}{0.5782}$ = 2.505 W/cm^{2}K.

The boiling coefficient (Thom), h_f = 2.71 W/cm^{2}K, is slightly higher than the single-phase coefficient for D_2O at the maximum temperature of 74°C, and the maximum wall temperature of 132°C is therefore selected.

4.4 Overall Temperature Difference, Fuel Centre to D_2O (ΔT_T)

ΔT_T = $\Delta T_c + \Delta T_{int} + \Delta T_{cl} + \Delta T_f$ = 12.0 + 110.6 + 2.1 + 58.0 = 182.7 K

Max. fuel-centre temp., $\hat{T}_{UO}$ = $T_f + \Delta T_T$ = 74 + 182.7 = 256.7°C.

4.5 Fuel Mean Temperature (at max. fuel-temp. level)

$$\bar{T}_{UO} = \dfrac{\displaystyle\int_0^{t/2} \left(\hat{T}_{UO} - \dfrac{Ix^2}{2k_{UO}}\right) \cdot dx}{t/2} = \hat{T}_{UO} - \dfrac{I.(t/2)^2}{6k_{UO}}$$

$$= 256.7 - (3020 \times 0.052^2)/(6 \times 0.34) = 252.7°C.$$

5. Effect of 25 MJ Transient in Whole Reactor Core

5.1

In this transient, which is required to be withstood by the Harwell MTRs, it is assumed that 25 MJ of heat is added to the fuel plates instantaneously, i.e. with no heat transfer to the coolant. The initial conditions are for normal full-power operation. Thus, the conditions may be taken from the previous section for the inner fuel tube 'A' of a fuel element operating at 1.63 MW (1.3 × nominal full power

in the highest-rated fuel element). A 25 MJ whole-core transient would add 1.2 MJ to the highest-rated fuel element and (from the power distribution in the element given by Hopper [2] 247.4 kJ to fuel tube 'A'.

Calculation, assuming uniform heat distribution through plate and cladding, and with 10% of fission heat deposited outside the plate, shows a temperature rise of 444 K. As the maximum starting temperature was 257°C, this shows an apparent temperature of 700°C - above the melting temperature. The latent heat of fusion is sufficient to absorb this apparent excess, in melting about 15% of the aluminium in the cermet.

While this limited melting of the aluminium in the cermet would not constitute any safety hazard, the model on which it is based is unrealistic though generally pessimistic.
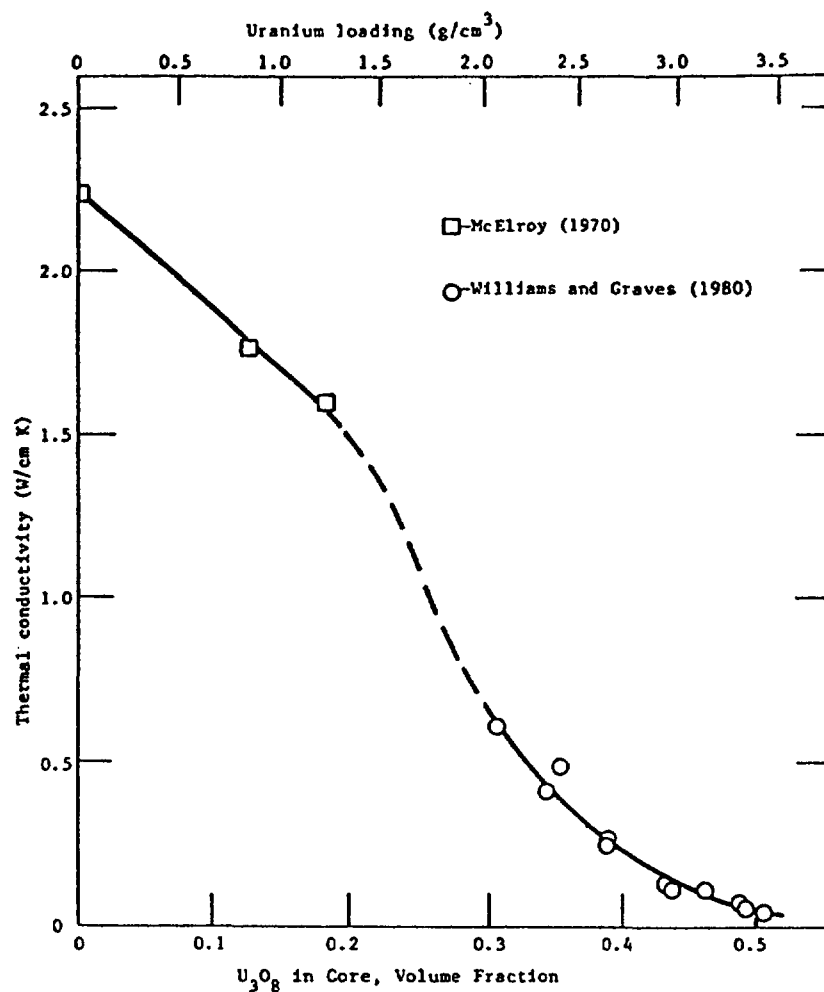
Uranium loading (g/cm^3)

□-McElroy (1970)

O-Williams and Graves (1980)

U_3O_8 in Core, Volume Fraction

Fig. 3 Thermal Conductivity of U_3O_8-Al Dispersions

5.2

A more realistic transient calculation takes account of heat transfer to the coolant during a ramped power increase, and of the distribution of heat within the fuel tube. To investigate this, a two-dimensional (r-z geometry) model of a fuel element was set up, using the finite-difference transient heat-transfer code, 2DT[7].

The model used is shown in Fig.4. It consists of six concentric annular tubes, the innermost and outermost tubes being of aluminium and the remainder being fuel tubes (Al/cermet/Al sandwich). D_2O coolant flows

HEAT - GENERATION RATES
IN FUEL TUBES (kW)
STEADY CONDITIONS

ZONE	'A'	'B'	'C'	'D'
1	30.7	34.6	40.3	43.5
2	52.9	59.6	69.6	74.5
3	55.8	63.0	73.4	78.7
4	55.6	62.5	73.0	78.2
5	50.1	56.4	65.8	70.5
6	41.2	46.4	54.2	58.6
7	21.6	24.4	28.4	30.4
TOTAL	307.9	346.9	404.7	434.4

FISSILE HEAT - 1493.9 kW
GAMMA HEAT (Al) - 6.1 kW
TOTAL HEAT - 1500 kW

COOLANT CONDITIONS
(STEADY STATE , 1500 kW)

No.	FLOW (kg/s)	H.T.Coeff (W/cm²K)	T_{IN} (°C)	T_{OUT} (°C)
1.	2.768	2.30	50	63.4
2	3.244	2.34	50	74.0
3	3.719	2.38	50	74.2
4	4.152	2.42	50	74.1
5	3.417	2.45	50	65.9

∎THE D_2O -COOLANT OUTLET
TEMPERATURES (T_{OUT}) ARE
COMPUTED BY THE PROGRAM
FOR THE CONDITIONS
OBTAINING. OTHER PARAMETERS
ARE INPUT INFORMATION.

EXTERNAL BOUNDARIES ARE
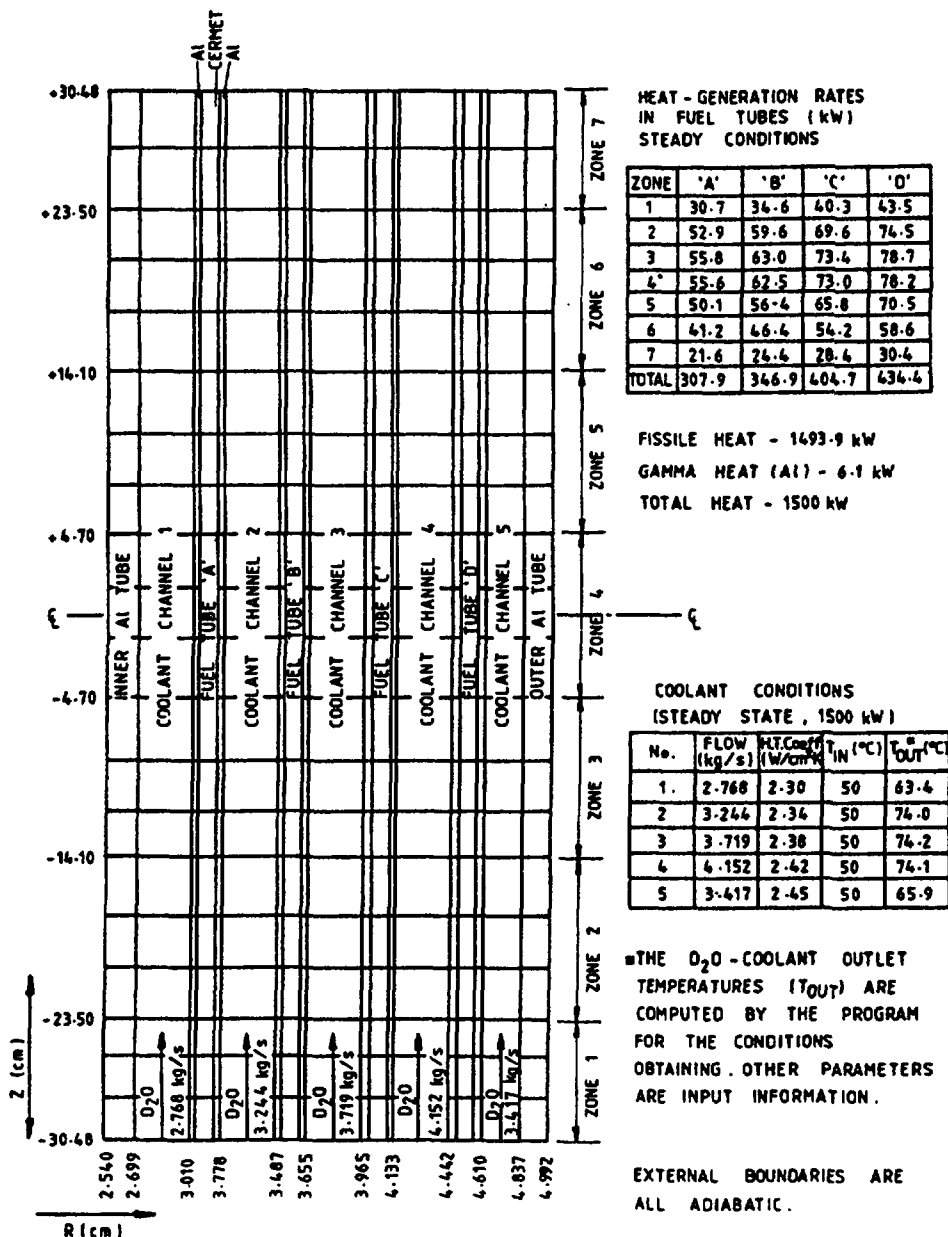ALL ADIABATIC.

Fig. 4   Computer Model of Fuel Element

upwards between the tubes. Heat transfer from the outside boundaries of the model is ignored; it will have a negligible effect, and any error in the model from this cause must be pessimistic. Steady conditions were computed for the model with 1.5 MW total heat generation from the fuel tubes and 17.3 kg/s total D_2O-coolant flow. The distribution of power among the fuel tubes[2] was 309.2 kW from 'A', 348.2 kW from 'B', 406.7 kW from 'C', and 436.0 kW from 'D'. The flow distribution up the coolant channels was taken from Lorenz[8]. The axial distribution of power in the fuel element is taken from a typical axial thermal-neutron flux profile in DIDO D3 fuel-element position[10] - as shown in Fig.2.

The maximum fuel temperature (nominal steady state) in the inner fuel tube 'A' was computed to be $247^{\circ}C$ at 3 cm above the core-centre plane. Corresponding cladding and D_2O temperatures were $129^{\circ}C$ and $65^{\circ}C$ (in the coolant channel on the outer side of the inner fuel tube 'A'). The model steady-state temperature distribution was then used for initial conditions for a one-second transient in which the power was increased exponentially so that an additional 1.2 MJ of heat was generated in the whole element, this corresponding to an additional 25 MJ in the whole core and to 247.4 kJ in the inner fuel tube 'A'. The computer program accepts heat-generation rates in the form:

$$I(r,z) = I_0(r,z)e^{m\tau} \text{, where } I_0(r,z) \text{ is the heat-generation rate at position}$$

(r,z) at time $\tau = 0$.

Assume that the heat-generation rates of all regions increase at the same rate. To find the value of m to give the required total heat production, Q_T, over the 1s transient,

$$Q_T = \int_{\tau=0}^{1} W \, d\tau = W_0 \int_0^1 e^{m\tau} \, d\tau = W_0 \frac{1}{m}\left[e^{m\tau}\right]_0^1 ,$$

where W is the total power produced by the fuel element. ($I(r,z)$ will vary with time in the same way as W.) In this case, $W_0 = 1.5$ MW, $Q_T = (1.5 + 1.2) = 2.7$ MJ ($\tau = 1.0$ s).

$$2.7 = \frac{1.5}{m}\left[e^m - 1\right]; \quad 2.7m = 1.5\left[e^m - 1\right]; \quad e^m = 1.8 m + 1;$$

$$m = 1.045868. \quad \therefore I(r,z) = I_0(r,z) \exp(1.045868 \, \tau).$$

This transient has a doubling time of 0.663 s, giving a power of 4.27 MW from the fuel element at the end of the one second. Fig. 5 shows the transient power increase and the consequent response of the highest fuel temperature in fuel tube 'A'. This is seen to reach $527^{\circ}C$ at the end of the transient, which is $133^{\circ}C$ below the melting point of aluminium. A doubling time of 0.663 s would be caused by a step addition of 0.6% $\delta k/k$. During the one-second transient postulated above, D_2O mean temperature would increase by $15^{\circ}C$, which, from the negative coefficient of
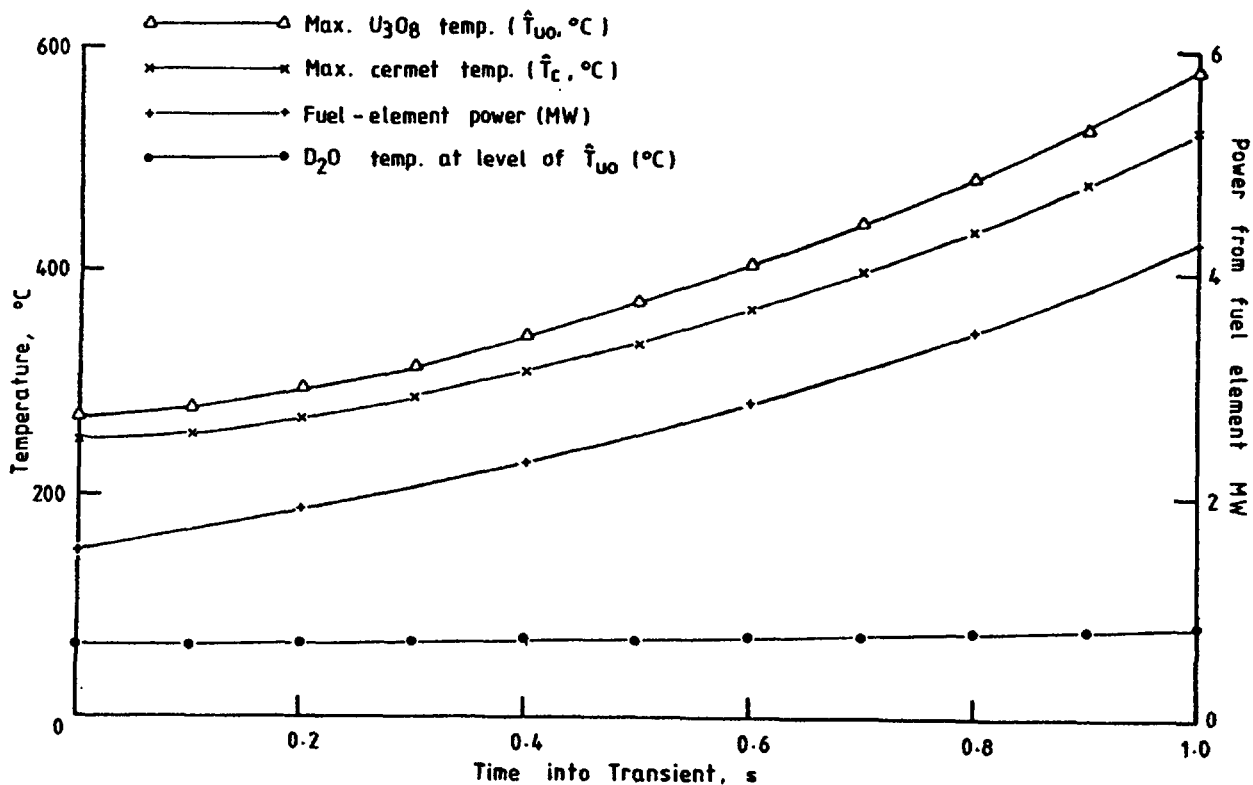
FIG. 5 TEMPERATURE RESPONSES TO CORE POWER TRANSIENT $(I = I_0 e^{1.045868\tau})$, WHERE τ = TIME IN s - FUEL TUBE 'A'

reactivity, would give -0.6% δk/k; thus, to sustain the transient, an additional 0.6% δk/k would have to be added over the one-second transient. The model assumed single-phase liquid heat-transfer coefficients to the D_2O of 2.3 to 2.45 $W/cm^2 K$ throughout the transient. In fact, the coefficients would increase at first as subcooled nucleate boiling increased (with increasing power), but might reduce drastically after about 0.5 s as the burn-out heat flux was exceeded. No bulk boiling would occur, and the short time and changing conditions would probably exclude film burn-out. This transient could not occur with the safety and control systems operated with the Harwell MTRs.

The maximum credible addition of reactivity to the Harwell MTRs is taken to be 1.2% δk/k at a maximum rate of 0.75% δk/k, controlled by the vertical control rods to give the power transient shown in Fig. 6 (worst case). The resulting maximum fuel-tube-'A' temperature is also shown. The fuel temperature peaks at 283°C, a rise of only 36°C, insufficient to give any safety problems.

331

6. Heat Transfer Within U_3O_8 Particles

The accompanying sketch shows the maximum-sized U_3O_8 particle which can be accommodated in the fuel plate. This is assumed to be a sphere having a diameter of 0.104 cm (i.e. the full width of the fuel plate).


The computed power produced by this sphere at steady state is 5.9W, or at the position of maximum power 7.1W. This causes a centre-to-surface temperature difference of 300 K and temperature drops across the fuel/cladding interface of 294 K, through the cladding of 6 K, and across the D_2O film of 46 K. The maximum U_3O_8 temperature is therefore 749°C.

Such a particle size (1040 μm) is much larger than the upper limit (149 μm) of the range of particle sizes reported by Kucera et al[1]. Although this large size does not lead to unacceptable temperatures, a more likely maximum size is 200 μm ($\equiv 0.02$ cm).

This leads to a centre-to-surface temperature difference of 11 K, and as such a particle would not significantly perturb the average heat flux from the cermet, the maximum U_3O_8 temperature may be derived, from the maximum cermet temperature, T_c, computed earlier (Section 3) of 247°C, as 258°C.

To assess the effect of the maximum transient power excursion, illustrated in Fig. 6, on a U_3O_8 particle of the size of a 200μm diameter sphere, a simple model was set up, consisting of a right cylinder of U_3O_8 (174.8 μm diameter) surrounded by a hollow right cylinder of aluminium (244 μm diameter). The model therefore contained the same proportion of U_3O_8 (36.6% v/v) to aluminium (63.4%) as the cermet. The U_3O_8 cylinder was of the same volume (4.19 x 10^{-6} cm³) as a 200 μm diameter sphere. The model was set up with an all-round boundary temperature of 247°C, representing the general cermet temperature computed in Section 3. The U_3O_8 was assigned a heat-generation rate of 12,000 W/cm³, corresponding to a fuel-element power of 1.5 MW.

Computer
Model of
$U_3 O_8$ Particle
in Cermet
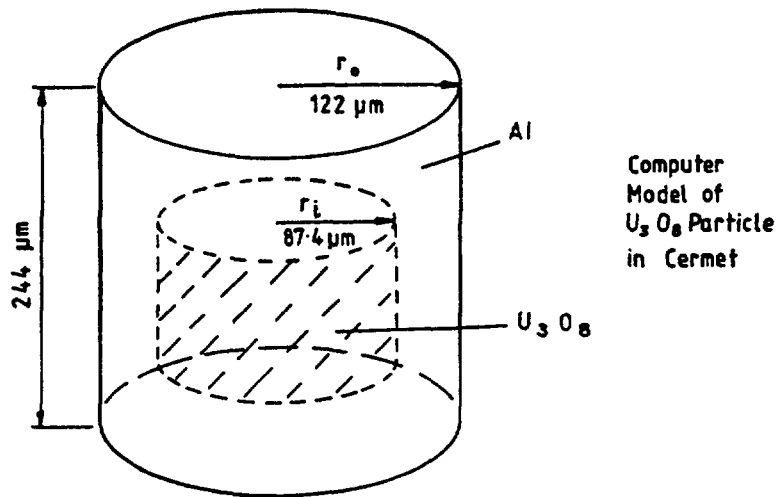
This model was then run to steady state, which showed a maximum U_3O_8 temperature of 258°C. From this initial condition, a transient of the form shown in Fig. 6 was applied to the model; the temperature history at the centre of the U_3O_8 particle is also shown in Fig. 6. The resulting maximum U_3O_8 temperature was 297°C at 0.37 s after the start of the transient. The exponential transient $(I = I_0 \exp(1.045868\ \tau))$ was also
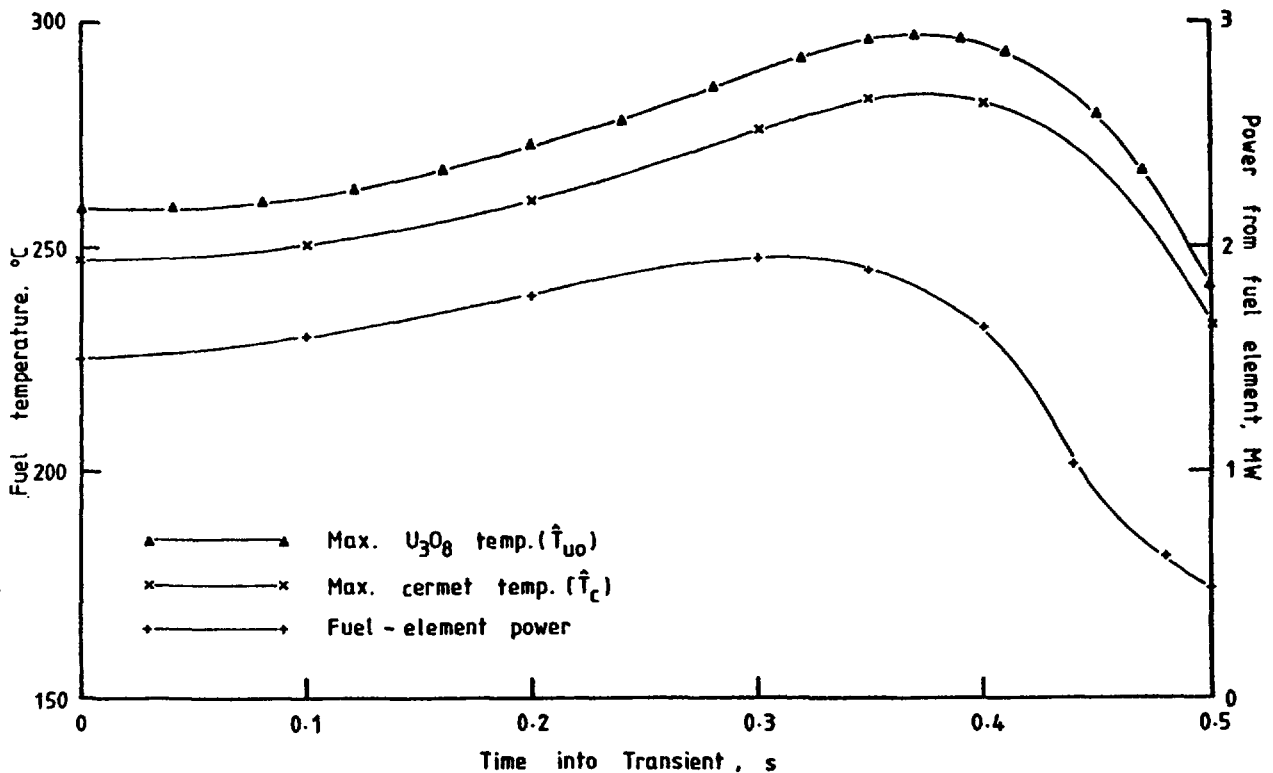
FIG. 6   FUEL - TEMPERATURE   RESPONSE   TO   CORE - POWER   TRANSIENT   (+0·75 %   δk / k   s⁻¹ ,
REACTOR   TRIP   AT   1·65 MW)

333

applied to the model for one second, with the results shown in Fig. 5. The maximum U_3O_8 temperature was then 582°C at the end of the one-second transient.

7. Conclusions

Provided that good bonding can be obtained between the cermet and the aluminium cladding, there appear to be no problems from a heat-transfer viewpoint to the use of U_3O_8/Al cermet fuel. Where information has been lacking, pessimistic assumptions have been made in the calculations, which nevertheless lead to maximum cermet temperatures below any which should cause problems. Experimental measurements of thermal conductivity should be made when the cermet is selected.   Local temperatures in the U_3O_8 particles within the cermet have been predicted, and present no problems in normal operation, nor for the maximum credible transient power excursion for the Harwell MTRs.

APPENDIX 1

Interface Conductance, U_3O_8-Al Cermet to Al

The conditions at this interface are not known, but because of the very high heat flux through it, contact must be good to prevent melting of the aluminium in the cermet. Main[9] gives methods of calculating interface conductance. The starting point is to assume three separate conductance paths in parallel:

$$h_T = h_f + h_s + h_r , \qquad (A1.1)$$

where subscripts T, f, s and r refer to total, fluid, solid and radiation respectively; h is the conductance (or heat-transfer coefficient in the case of h_T). In this case, h_r may be ignored, since any temperature above $600^\circ C$ at the interface will result in melting of the aluminium.

(a) Fluid Conductance, h_f

$$h_f = \frac{k_f}{d} , \qquad (A1.2)$$

where k_f is fluid conductivity, k_f (air) $= 0.0004$ W/cm K, and d is the effective gap thickness.

$$d = C(R_1 + R_2) + g_1 + g_2 , \qquad (A1.3)$$

where R_1, R_2 are surface roughnesses, C is the roughness-height factor (C = 1.5 for heavy contact), and g_1 and g_2 are temperature-jump distances.

Here assume $R_1 = R_2 = 25 \times 10^{-6}$ cm.

From Ref. (9),

$$g_1 = g_2 = \frac{(2 - \alpha)P_a}{\alpha P} Z , \qquad (A1.4)$$

and $Z \approx 3 \times 10^{-5}$ cm, $\alpha \approx 0.45$, $P = P_a = 1$ bar.

$$g_1 = g_2 = \frac{1.55 \times 3 \times 10^{-5}}{0.45} = 1.03 \times 10^{-4} \text{ cm}$$

$$d = 1.5 (2.5 \times 10^{-6} + 2.5 \times 10^{-5}) + 2 (1.03 \times 10^{-4})$$

$$= 2.81 \times 10^{-4} \text{ cm}$$

$$h_f = \frac{k_f}{d} = \frac{4 \times 10^{-4}}{2.81 \times 10^{-4}} = 1.42 \text{ W/cm}^2 \text{ K} .$$

(b) Solid Conductance h_s

This is very difficult to quantify, and since the value of h_f found above is adequate to prevent an excessive ΔT across the interface no attempt will be made to do so. For the U-Al-alloy fuel, the assumption is normally made that contact is complete, and hence $h_s = \infty$; in this case, the pessimistic assumption of no solid contact is made, so that $h_s = 0$.

REFERENCES

1. KUCERA, W.J., LEITTEN, C.F. and BEAVER, R.J., 'Specifications and procedures used in manufacturing U_3O_8-Al dispersion fuel elements for Core 1 of the Puerto Rico Research Reactor', O.R.N.L. 3458 (October 1963).

2. HOPPER, E.D.A., 'The design of new fuel elements for 25 MW operation of the Harwell reactors DIDO and PLUTO', AERE - R8947 (October 1977).

3. THOM, J.R.S., WALKER, W.M., FALLON, T.A. and REISING, G.F.S., 'Boiling in subcooled water during flow up heated tubes or annuli', Symposium on boiling heat transfer, I.Mech.E., Manchester (September 1965).

4. I.A.E.A. guidebook on the safety and licensing aspects of research reactor core conversions from H.E.U. to L.E.U. fuels - Appendix 'A', draft No.1 of U.S. contributions, I.A.E.A., Vienna (September 1980).

5. TOULOUKIAN, Y.S., 'Thermophysical properties of high-temperature solid materials', Purdue University (Collier MacMillan Ltd., London, 1967).

6. I.A.E.A. Technical Report No. 59, 'Thermal conductivity of uranium dioxide', I.A.E.A., Vienna (1966).

7. KENNEDY, T.D.A., '2DT, two-dimensional heat-transfer finite-difference computer program', AERE - R9210, Harwell (1978).

8. LORENZ, F.G.J., Private communication.

9. MAIN, F.K., unpublished information.

10. MOORE, P.G.F. and LAY, R.P., unpublished information.

Appendix E-6

CORE CONVERSION EFFECTS TO THE
SAFETY ANALYSIS OF RESEARCH REACTORS

J.N. ANOUSSIS, N.G. CHRYSOCHOIDES, C.N. PAPASTERGIOU
Department of Reactors,
Democritos Nuclear Research Center,
Greek Atomic Energy Commission,
Athens, Greece

Abstract

This paper has been prepared in accordance with the proposed SAR format contained in the Summary of this guide book, and incorporates several conclusions and results presented in various sections of the guide book. The paper could be considered therfore, as an application-example of the guide book for the preparation of a SAR of a research reactor in the case of its core conversion from the use of high to low enriched uranium fuel.

Although the 5 MW swimming pool "Democritos" research reactor (Greek Research Reactor-1) is used as an example for the various calculations of the SAR, the analysis is in many aspects of a more general nature (e.g. the analysis of MCA, DBA, Engineered Safety Features etc) and can be applied not only to this particular reactor but to other similar reactors as well. The Radiological consequences of the MCA and DBA are calculated as an application of the methodology presented in appendix D-3 "Estimation of Radiological Doses from Research Reactor Accidents". It is hoped that in this way, the present work can be of an assistance to several reactor operators. It should be noted though, that the present work is not in every sense a complete SAR to be submitted for licensing purposes, (e.g. no information on technical specifications, determination of safety limits or Q/A program, are included) but it contains the basic safety analysis considerations that a SAR for core conversion should include.

1. INTRODUCTION AND GENERAL DESCRIPTION OF FACILITY

The "Democritos" Greek Research Reactor (GRR-1) is a swimming pool, light water moderated and cooled heterogeneous reactor, presently operated at 5 MW with MTR type fuel elements using HEU.

The reactor, being operated by the Greek Atomic Energy Commission through the Nuclear Research Center "Democritos", went critical on July 27, 1961. The initial power of the reactor was 1 MW and the enrichment

of the fuel elements was 20% with high Uranium density of about 3 gr/cm^3 in the meat. During the first period of the operation of the reactor with the LEU fuel, several experiments were conducted and a number of reactor physics measurements were completed in order to study the reactor performance. Data from those measurements were very useful in evaluating the present core conversion from the use of HEU to the use of LEU and its safety consequences /1/.

After several years of operation, it was decided to increase the operating power of the reactor from 1 to 5 MW. Works started early in 1970 and included some major changes and modifications like complete replacement of the old cooling system with a new, consisting of primary and secondary circuit equipped with heat exchangers and cooling towers, replacement of the tile liner of the pool with a stainless steel one, installation of new power supply systems, change of the enrichment of the fuel elements to over 90% enrichment etc. The reactor started operating at 5 MW in July 27,1971.

The reactor is used now for reactor physics experiments, nuclear physics, neutron diffraction and spectroscopy work, cross section measurements, solid state physics and radiation damage studies, activation analysis, hot atom and nuclear chemistry and biological studies. It also serves for radio-isotope production on a rather large scale and as a source for sterilization purposes during the shutdown period. Finally, it provides basic experience and training for possible future power reactor installation and operation in Greece.

The "Democritos"Research Reactor is located at the "Democritos" Nuclear Research Center, about 12 km from Athens at the foot of mount Hymettus in the district of Aghia Paraskevi. It is constructed in the central region of seventyfive acres property which includes other laboratories and facilities as well.

The basic considerations for the safety analysis report, resulting from the scheduled core conversion back to LEU, are analyzed in some details in this report.

The analysis is based on a recent SAR for HEU core /2,3/. The format and contents of the present report are identical to the format of the above mentioned references and the format proposed in Chapter 1 of the Summary of ref. /3- A/ and /4-A/.

Only sections and subsections of the format ref. /4-A/ affected by core conversion will be discussed in this report while the other sections will just be mentioned in order to keep the integrity and continuation of the report.

20% enrichment is considered for the calculation of the LEU core.

The proposed LEU fuel heat transfer characteristics will be essentially identical to those of HEU U-Al alloy fuel which have been used so far in the GRR-1. Overall element dimensions, fuel plate dimensions,

coolant flow channel width and thickness as well as water coolant flow will be unchanged.

Material Incorporated by Reference (REFERENCE A):

The following topical reports presented by organizations other than the N.R.C. "Democritos", are given in support of this SAR.

1. NEUTRONIC CALCULATIONS FOR THE CONVERSION OF THE GRR-1 REACTOR FROM HEU TO LEU FUEL, by C. Papastergiou, GAEC and J. Deen ANL, Work performed at ANL, (Nov. 1981).

2. RESEARCH REACTOR CORE CONVERSION FROM THE USE OF HIGHLY ENRICHED URANIUM TO THE USE OF LOW ENRICHED URANIUM FUELS GUIDEBOOK   by IAEA-DEDOC-233 (1980).

3. RESEARCH REACTOR CORE CONVERSION, SAFETY AND LICENSING ISSUES (present Guidebook).

4. SAFE OPERATION OF RESEARCH REACTORS AND CRITICAL ASSEMBLIES, safety series No. 35, Vienna, (1984 edition).

2. SITE CHARACTERISTICS

The site characteristics, i.e. Geography, Demography, Nearby external facilities, Meteorology, Hydrology Engineering, Geology, Seismology and Geotechnical Engineering are described in details in reference /2/ and apply for the present SAR.

3. SAFETY PRINCIPLES AND GENERAL DESIGN CRITERIA

4. BUILDINGS AND STRUCTURES

The principal architecture and engineering design of the reactor structures, components equipment and systems which are important to safety are described in details in reference /2/ and apply for the present SAR as well.

5. REACTOR

The principal components of the reactor i.e. the reactor pool and its associated equipment, the reactor bridge and core, the control rods and drives, the control room and the cooling system are the same as for the case of the HEU fuels, reference /2/.

.2 Fuel System Design

The LEU fuel element specifications compared with the various HEU fuel elements ones used so far in the reactor are given in Table I.

The fuel element geometry for the LEU case is given in Fig. 1. The calculations for the fuel element specifications are based on the same BOL performance of the core as for the HEU fuel, reference $/\overline{1-A}/$.

TABLE I

LEU-Fuel Element Specifications in Comparison with HEU-Fuel Elements,Previously Used

	LEU	HEU		
		CERCA	U.S.Nuclear	NUKEM
FuelElement Cross Section (mm)	76.1 x 80.0	76.1x80.0	75.9x80.0	76.1x80.0
Fuel Element Active Height (mm)	600	596.5	597	600
Number of Plates/FE	18 plane	18 plane	18 curved	19 curved
Meat Thickness (mm)	0.76	.50	0.51	0.51
Meat Width (mm)	62.3	62.3	60	61.15
Cladding Thickness (mm)	0.38	0.51	0.38	0.38
Fuel Plate Thickness (mm)	1.52	1.52	1.27	1.27
Water Gap (mm)	2.9	2.9	3.12	2.95
Cladding Material	Al	Al	Al	Al
Meat Material	UAL_x-Al or U_3O_8-Al	UAL	U Al	U Al
Uranium-Loading/FE (gr)	1125 gr	194.37	189	200
U-235 Enrichment (%)	19.75	93.0	93	89.85
U-Density/Meat (gr/cm^3)	2.2	0.581	0.608	0.564
U-235-Loading/FE	222.2	180.83	176	180
U-Metal in Meat (w/o)	50.09 or 51.0	18.18		
Moderation Ratio (fresh fuel)	205	289		

The most important fact of these calculations is the resulting Uranium-density, which is 2.2 gr U/cm^3 for the designed burnup of 30% and the desired reactivity level. With this density, UAl_x-Al or U_3O_8-Al type fuel elements are available and well proven.

Fuel swelling data and fuel blister data for fuel plates made of materials similar to those in the GRR-1 and which were determined at fuel temperature,pressure and pH conditions, similar to the GRR-1 ones are given in references $/\overline{2-A}/$, $/\overline{4}/$ and in $/\overline{3-A}/$.
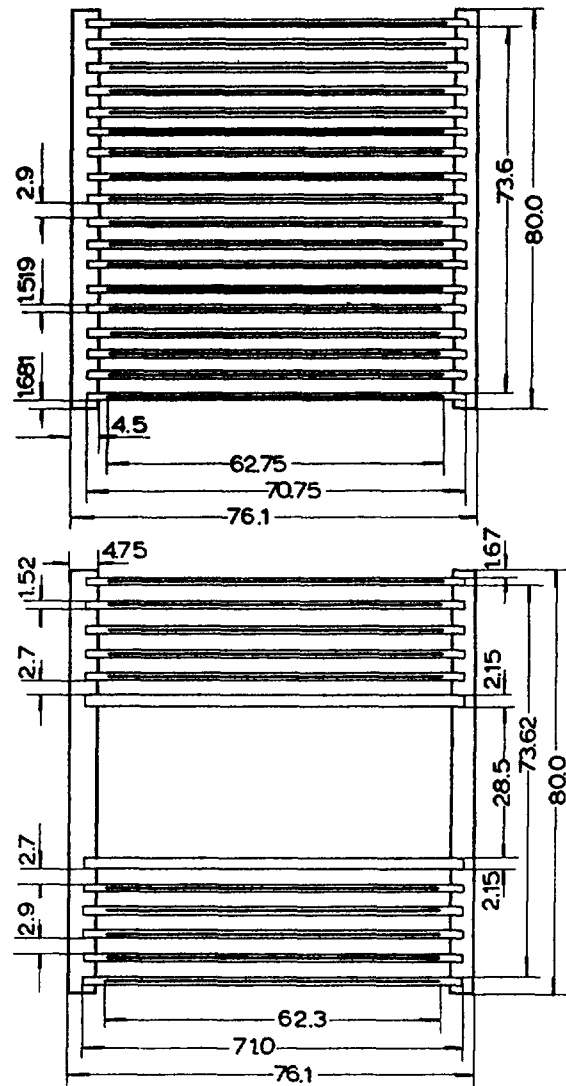
FIG. 1. Standard and control fuel element geometry of LEU fuel for the GRR-1 (dimensions in mm).

.3 Nuclear Design

For the conversion study two LEU fuel designs have been chosen with U densities 2.2 gr U/cm^3 of meat and 3.0 gr U/cm^3 of meat respectively /1- A/.At the present study the first of the above mentioned LEU design is considered. The geometry has been kept the same as for the HEU case (CERCA F.E.) regarding the overall fuel plate dimensions and water gap between plates as well.

The clad thickness decreased from 0.51 mm (HEU fuel) to 0.38 mm. This change made possible an increase of the fuel meat thickness from 0.50 mm (HEU fuel) to 0.76 mm (LEU fuel). Both the cladding and meat thickness chosen for the LEU fuel plates are currently being used by most fuel fabricators.

In addition to the meat thickness increase, an increase of the U-density from 0.581 gr U/cm^3 of meat to 2.2 gr U/cm^3 for the LEU fuel was possible using the dispersion technique (UAl$_x$-Al or U$_3$O$_8$-Al meat material) for the fuel plates fabrication.

These changes made possible the increase of the U loading per fuel element from 190-200 gr (HEU fuels) to 1125 gr (LEU fuel) and the increase of the U- 235 loading per fuel element from 180 gr (HEU fuels) to 222 gr (LEU fuel).

This last increase compensates the increased neutron absorption in U-238 and spectrum hardening for the LEU fuel.

The characteristics of the LEU fuel design compared with the equivalent ones of the HEU fuel designs, previously used are given at Table I.

a. Reactivity Requirements and Reference GRR-1 Core: The reactivity requirements had to be considered in order to set up the calculation for a reference operating core. Since the reactor is operating 10 hours a day, the xenon built-up after shutdown introduces a high negative reactivity. Calculations give for this reactivity a value of ρ =-3.2 % $\underline{/1-A/}$.

The worth of equilibrium xenon in the GRR- 1 core has been calculated to be - 2.7%.

Since equilibrium xenon is included in the fuel cycle calculations only an additional 0.5% $\Delta\rho$ is needed in the calculations to provide the -3.2%$\Delta\rho$ for xenon override. Taking into consideration also the reactivity worth of the experiments and the uncertainties of calculations one obtains.

Reactivity Allowances ($\Delta\rho$)

Experiments	3.8%
Xenon Override	0.5%
Calcualtion Uncertainties	0.8%
Total	5.1%

Therefore, the multiplication factor at EOC was set equal to k_{eff} = 1.054 for all equilibrium cycle studies. The 3.8% $\Delta\rho$ for experiments can be considered to include an allowance for the reactivity penalty of unflooded beam tubes.

The reference core consists of 30 standard and 5 control elements Fig. 2. The core constants have been calculated at ANL using the EPRI-CELL code. Diffusion calculations have been also performed with the DIF 3D code for this core with all fresh HEU elements. This BOL HEU core has a k_{eff}= 1.1759. It is clear that this is an extremely unrealistic situation, since a core with all fresh elements would attain criticality with much fewer assemblies.
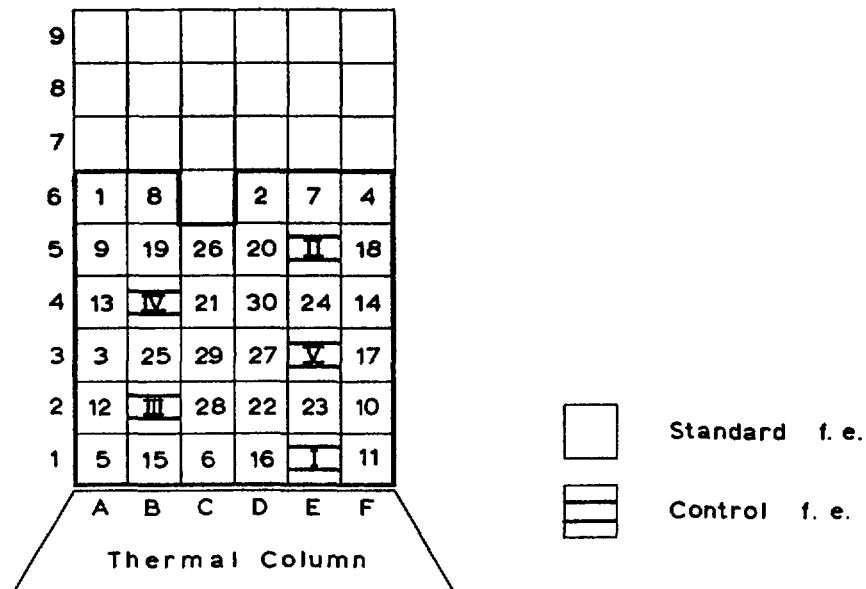
	A	B	C	D	E	F
9						
8						
7						
6	1	8		2	7	4
5	9	19	26	20	II	18
4	13	IV	21	30	24	14
3	3	25	29	27	V	17
2	12	III	28	22	23	10
1	5	15	6	16	I	11

Thermal Column

☐ Standard f. e.

▤ Control f. e.

FIG. 2. Shuffling pattern for the GRR-1 reference core.

The reference core has been chosen to be a 35 fuel element core in order to have the necessary reactivity margins for establishing an equilibrium fuel cycle /1-A/.

For the GRR-1 reference HEU core a 10 full-power-day (fp^d) cycle length has been calculated. The shuffling patern is shown in Fig. 2. One standard fresh fuel element is loaded at the beginning of each cycle (BOC) at position A-6, and one burned fuel element is discharged from position D-4. One control element is loaded every six cycles. This was simulated in REBUS code, used for the fuel cycle calculations at ANL, by loading 1/6 of a fresh control element in position E-1 and by discharging 1/6 of a control element from position E-5 each cycle.

The REBUS code has been used to calculate the equilibrium cycle length for the LEU core. The results for both LEU designs, UAL$_x$-Al and U$_3$O$_8$- Al with U-density 2.2 gr/cm^3 compared to HEU core ones, are given in Table II. It comes out that to match k_{EOC} for HEU and LEU cores a longer cycle length is calculated for LEU core i.e. 12 fpd instead of 10 fpd considered for the HEU core.

b.Flux, Power and Burn- up Distribution: Neutron fluxes for LEU core are shown in Fig. 3 and ratios of neutron fluxes (LEU/HEU core) are shown in Fig. 4. At these graphs the energy groups correspond to

group 1	E >	0.8208 MeV
group 3	1.8554 eV< E <	5.5308 KeV
group 5	0.0 eV < E <	0.6249 eV

TABLE   II.

Equilibrium Cycle Characteristics for Reference Design HEU   and   LEU MTR Fuel Elements

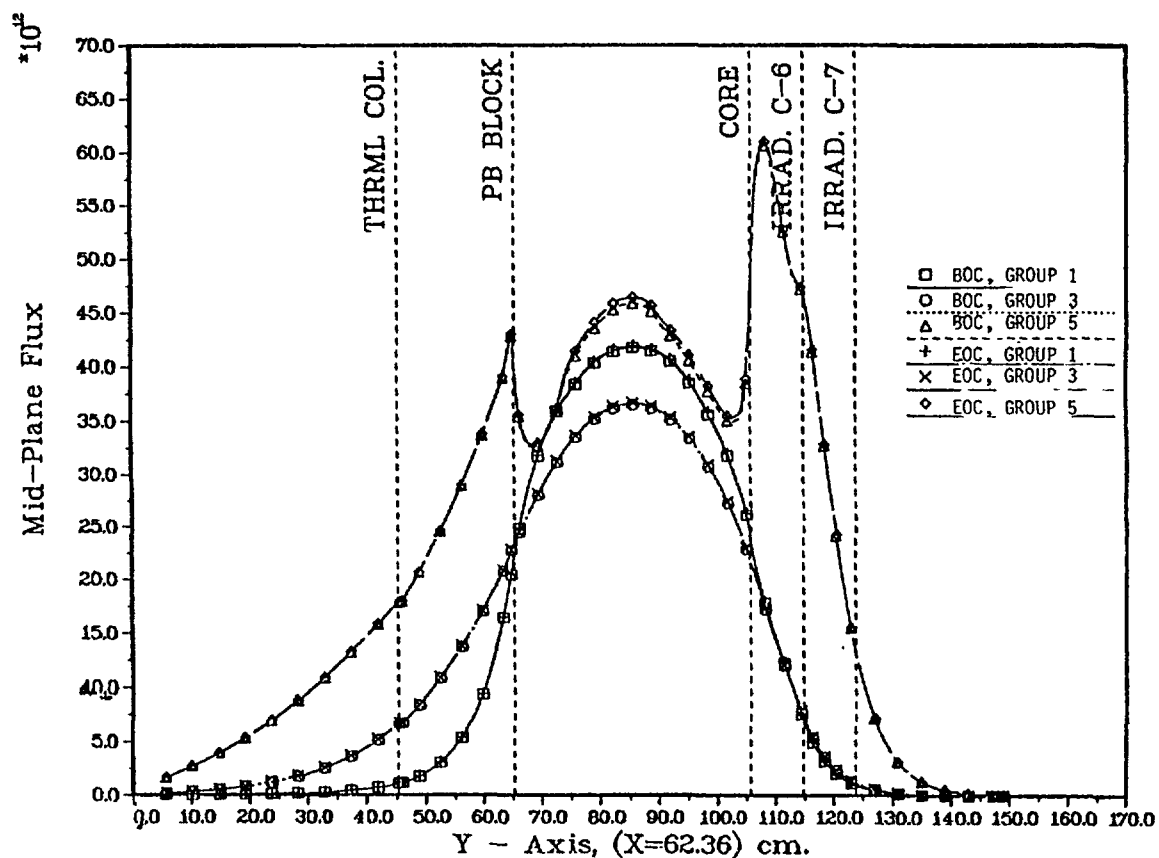|	HEU (93%) 180.8 g ^{235}U/el, ρ_U=58 gr/cm^3	LEU (19.75%) 222.2 g ^{235}U/el, ρ_U =2.2 gr/cm^3	
	UA1 Meat Design	UA1$_x$-Al Meat Design	U$_3$O$_8$-Al Meat Design
Cycle Length (fpd)	10.0	12.0	12.0
BOC k_{eff}	1.0619	1.0597	1.0636
EOC k_{eff}	1.0556	1.0544	1.0583
^{235}U Loading at BOC (g)	5091	6255	6255
^{235}U Loading at EOC (g)	5028	6181	6181
^{235}U Burned per Cycle (g)	63	74	74
Average Burnup at BOC (%)	14.1	14.1	14.1
Average Burnup at EOC (%)	15.2	15.1	15.1
Standard Element Discharge Burnup (%)	31.1	30.2	30.2

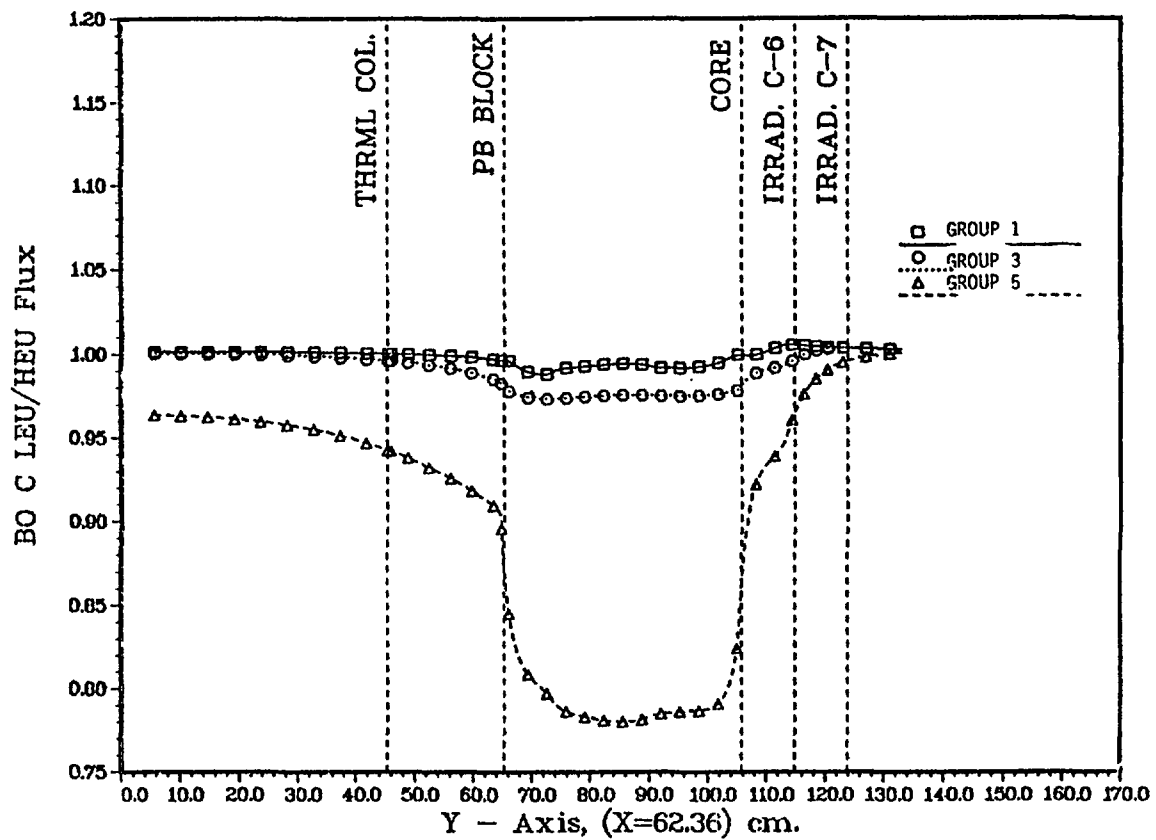FIG. 3. GRR-1 222g LEU BOC and EOC groups 1, 3 and 5 fluxes.

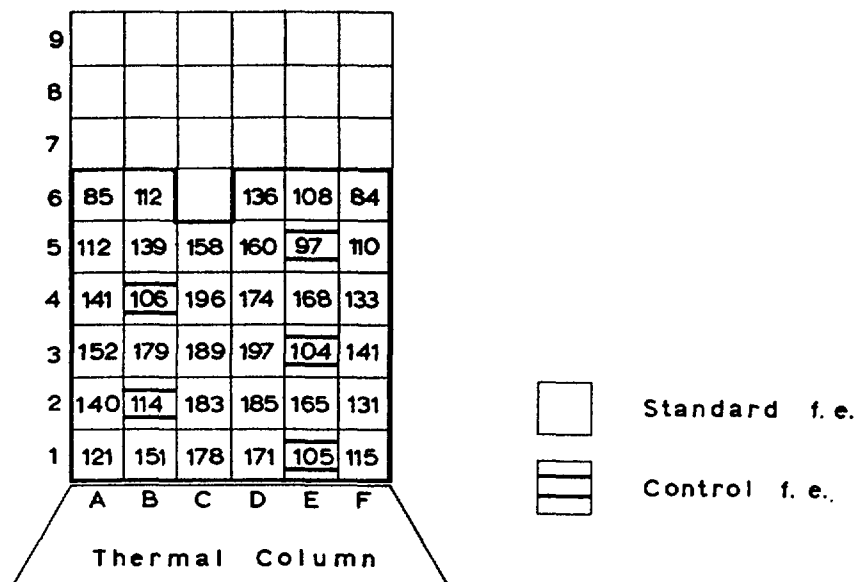FIG. 4. GRR-1 222g LEU/HEU ratios of groups 1, 3 and 5 fluxes.

FIG. 5. Power distribution in kW for LEU reference core at BOC (fuel cycle 12 fpd at 5 MW).

The power distribution for the LEU core is shown in Fig. 5 and the Burn- up distribution at EOC is shown in Fig. 6
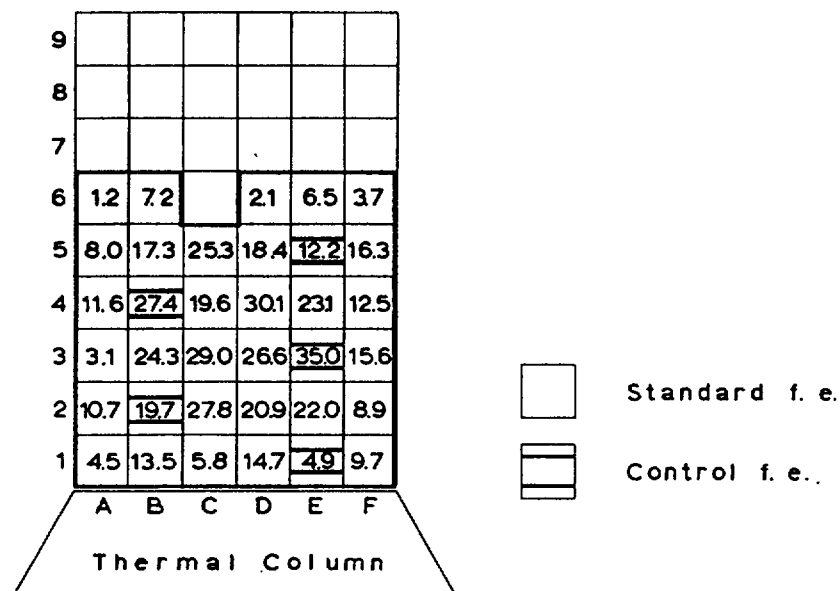

FIG. 6. Burnup distribution (%) at EOC for LEU reference core (fuel cycle 12 fpd at 5 MW).

c. <u>Prompt Neutron Generation Time and Delayed Neutron Fraction</u>: Using ten-group cross sections calculated by ERPI- CELL for an average burn-up state of the core and the two-dimensional diffusion code DIF 2D,real and adjoint fluxes were obtained. These fluxes were used by diffusion-perturbation theory calculations to determine the delayed neutron fractions β_{eff}, the prompt neutron lifetime (1) and the prompt neutron generation time $(\Lambda)\underline{/1-\Lambda/}$. The results of calculations for the LEU (UAL_x-Al) core,compared with the equivalent values for the HEU core are given in Tables III, IV.

TABLE III.
Delayed-Neutron-Dependent Parameters

Fuel	Enrichment	ρ_U g/cm^3	k_{eff}	β_{eff}	1(usec)	Λ(µsec)
HEU	93%	0.58	1.05787	0.006728	71.2	67.3
LEU	19.75%	2.2	1.05648	0.006584	60.8	57.6

346

TABLE IV.
Delayed Neutron Parameters

	HEU					
Family	1	2	3	4	5	6
$\bar{\lambda}$ (sec^{-1})	0.0127	0.0317	0.1160	0.3110	1.4	3.87
$\beta_{TOT} \times 10^{-4}$	2.6025	14.2662	12.6446	27.3967	8.6171	1.751

	LEU					
$\bar{\lambda}$ (sec^{-1})	0.0127	0.0317	0.1163	0.3115	1.399	3.8638
$\beta_{TOT} \times 10^{-4}$	2.5293	13.9594	12.3747	26.7536	8.4759	1.7473

d. Isothermal Reactivity Feedback Coefficients: The core k_{eff} has been calculated for various temperatures of the moderator and the fuel and for various moderator densities using DIF2D for both HEU reference and LEU (2.2 g/cm^3, UAl$_x$-Al) cores. Cross sections were generated by EPRI- CELL in ten groups for each nuclide. The calculations were performed using middle- of-cycle (MOC) burnup microscopic cross sections and BOC isotopic concentrations from REBUS-2.

i. Change of Moderator (H₂O) Temperature Only: THE EPRI-CELL library for hydrogen contains the temperatures 23°C, 77°C and 127° in the range of interest. Therefore, the calculations have been done for these water temperatures (T_{MOD}). The fuel temperature was kept constant at 20°C. Results of calculations are given in Table V and plots of k_{eff} and $-\Delta\rho$ vs temperature T_{MOD} are shown in Fig. 7 and 8.

TABLE V.

Reactivity Coefficients for Increasing Moderator Temperature

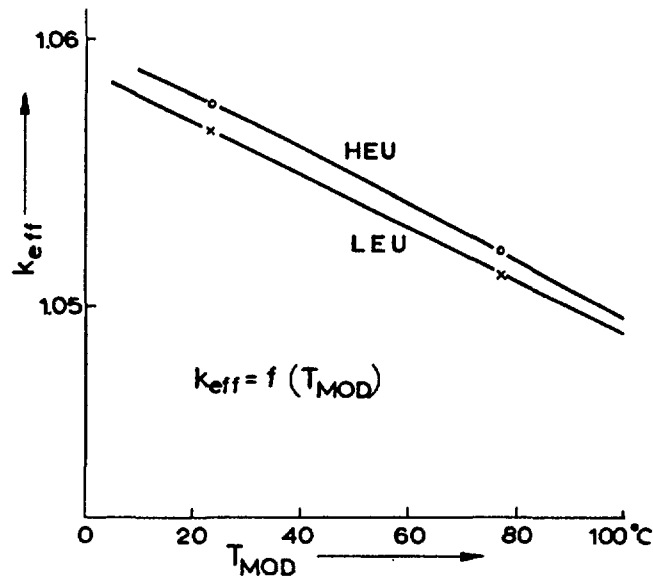| T_{MOD}(°C)	**HEU**		**LEU**	
	k_{eff}	$-\Delta\rho \times 1000$	k_{eff}	$-\Delta\rho \times 1000$
23	1.057859	0	1. 5648	0
77	1.052031	5.236	1.05117	4.782
127	1.046672	10.103	1.046335	9.178

FIG. 7. k_{eff} for change of water temperature (T_{MOD}) for HEU and LEU reference cores.
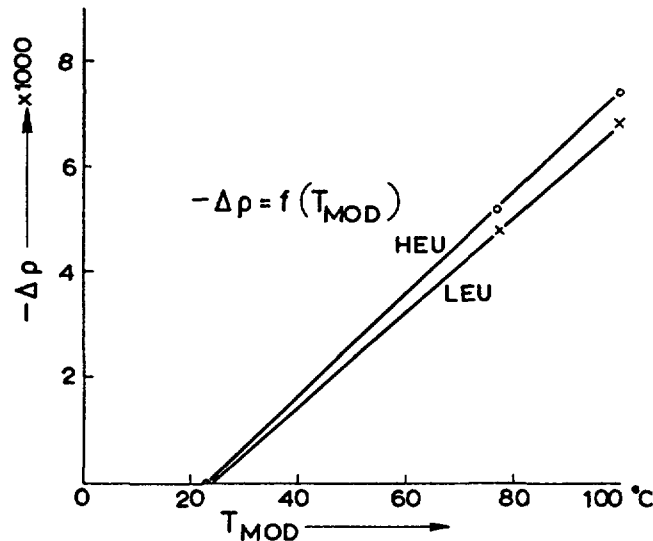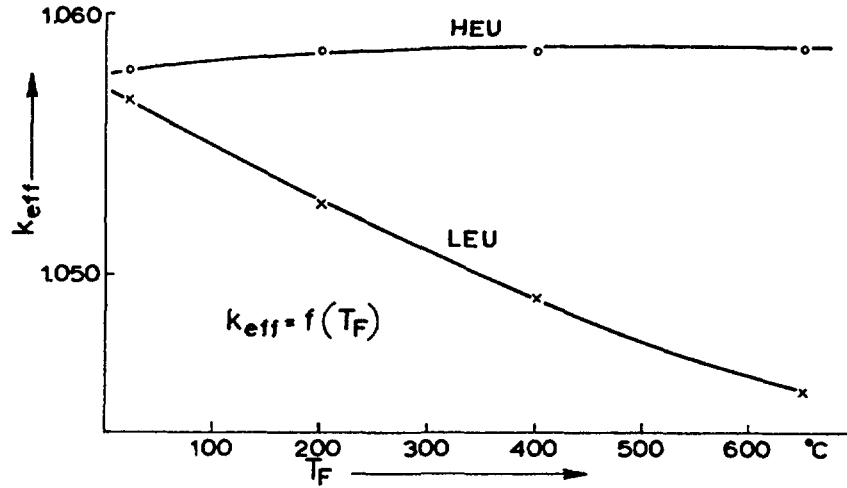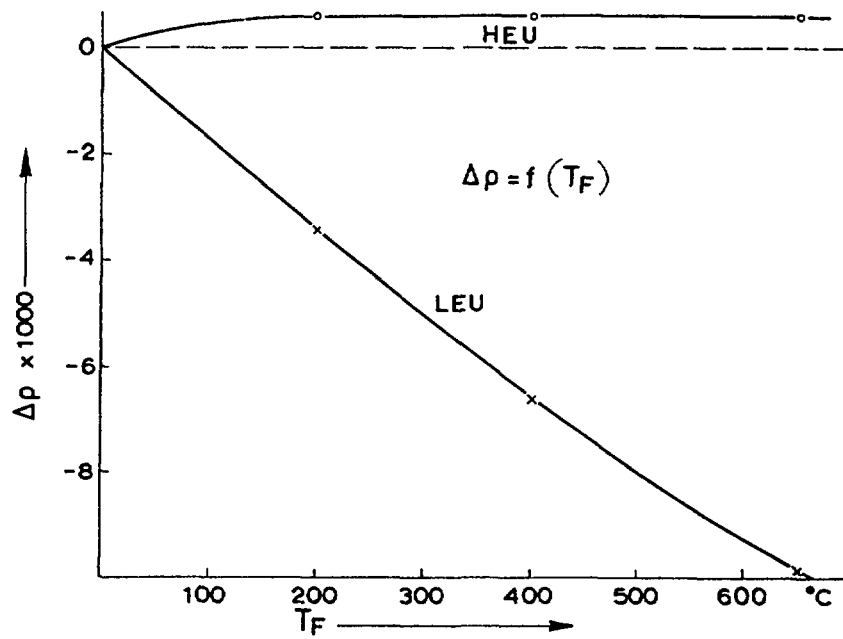

FIG. 8. $\Delta\rho$ for change of water temperature (T_{MOD}) for HEU and LEU reference cores.

ii. **Change of Fuel Temperature Only** : A series of calculations has been done for both cores under consideration for fuel temperatures T_F =20°C, 200°C, 400°C and 650°C. For these calculations, the water temperature (T_{MOD}) has been kept constant at 23°C. The results are given in Table VI and plots of k_{eff} and $\Delta\rho$ as a function of T_F are shown in the plots of Fig. 9 and 10. It is seen that the influence of temperature on k_{eff} (Doppler effect) is very small for the HEU case compared with the LEU case since the density of U-235 in the HEU fuel is low.

TABLE VI.

Reactivity Coefficients for Increasing Fuel Temperature

$T_F(^oC)$	HEU k_{eff}	$-\Delta\rho \times 1000$	LEU k_{eff}	$-\Delta\rho \times 1000$
20	1.057859	0	1.05648	0
200	1.058556	-0.6	1.052592	3.497
400	1.058549	-0.6	1.049106	6.654
650	1.058550	-0.6	1.045619	9.832

FIG. 9. k_{eff} for change of fuel temperature (T_F) for HEU and LEU reference cores.

FIG. 10. $\Delta\rho$ for change of fuel temperature (T_F) for HEU and LEU reference cores.

349

iii.**Change of Water Density Only- Void Coefficient:** Values of k_{eff} have
been calculated for various moderator densities using the DIF2D code
for both HEU and LEU cores. Extrapolation distances have been calcu-
lated for each case by R-Z geometry diffusion calculations. The water
densities (g/cm^3) for which the calculations have been done are 0.9986,
0.9974, 0.972, 0.958, 0.900 and 0.800. The two last densities represent
a whole- core void effect. All the calculations have been done keeping
the temperature of the moderator constant at $23°C$ in   order
to obtain the coefficient for change of water density only.
Results of the calculations are given in Table VII. Plots of
k_{eff} and Δp for water density (d_{MOD}) and k_{eff} and Δp vs void
are shown in Figs. 11-14.

TABLE VII.

Reactivity Coefficients for Decreasing Water Density of Whole-Core Coefficient

| Moderator Density (d_{MOD})	Void %	$\overline{D}_{ex}$(core) (cm)	$\overline{D}_{ex}$ (Ref.) (cm)	k_{eff}	$-\Delta p \times 1000$
0.9986	0.1	7.445	7.384	1.058830	0
0.9974	0.3	7.455	7.394	1.058581	0.222
0.972	2.8	7.627	7.554	1.054579	3.807
0.958	4.2	7.726	7.646	1.052185	5.964
HEU 0.900	10	8.167	8.056	1.041054	16.126
0.800	20	9.057	8.885	1.016677	39.159
0.9986	0.1	7.615	7.545	1.057709	0
0.9974	0.3	7.626	7.555	1.057392	0.283
LEU 0.972	2.8	7.803	7.720	1.052377	4.79
0.958	4.2	7.906	7.815	1.049409	7.477
0.900	10	8.364	8.239	1.035955	19.853
0.800	20	9.294	9.129	1.007725	46.894
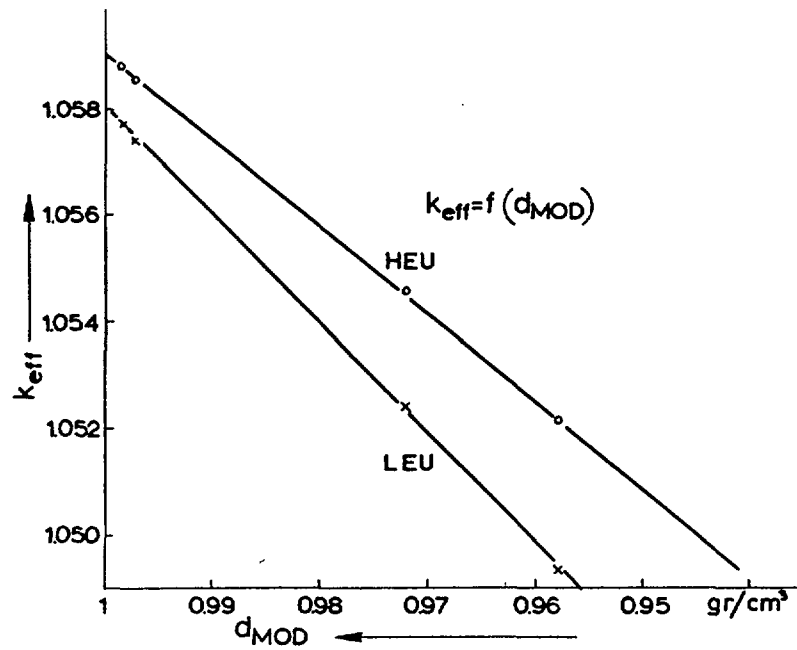
FIG. 11. k_{eff} for change of water density (d_{MOD}) for HEU and LEU reference cores.
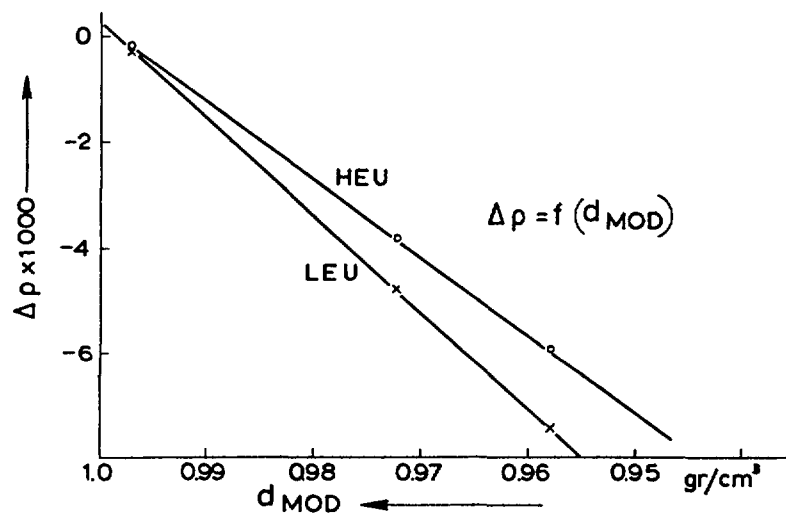

FIG. 12. $\Delta\rho$ for change of water density (d_{MOD}) for HEU and LEU reference cores.
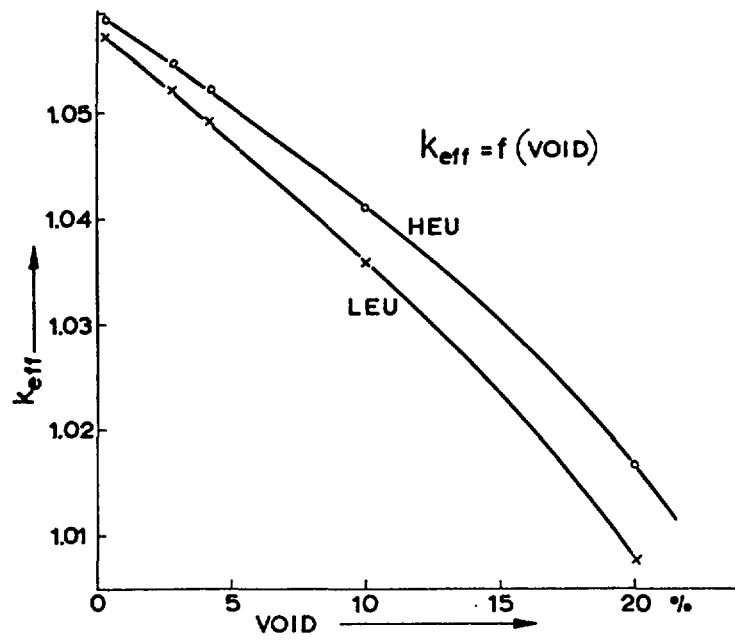
FIG. 13. k_{eff} for change of whole core void for HEU and LEU reference cores.
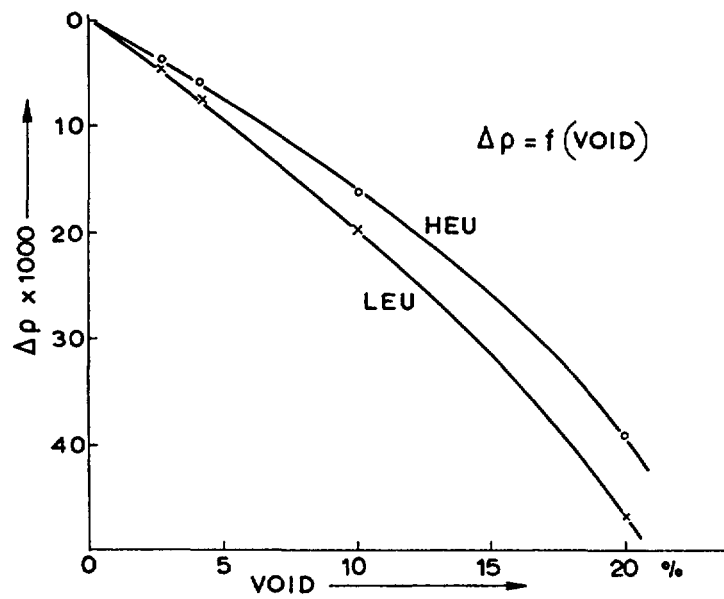

FIG. 14. $\Delta\rho$ for change of whole core void for HEU and LEU reference cores.

352

.4 Thermal and Hydraulic Design

 The heat generated in the reactor during the operation
is removed by the cooling system of the reactor. The main components
of the cooling system are the primary cooling system consisting of a delay
tank, pumps and heat exchangers and the secondary cooling system
consisting of pumps and cooling towers. The proposed LEU fuel elements
have the same geometry and heat transfer characteristics with the HEU
fuels used so far in the reactor, therefore, they will not affect
the thermal and hydraulic design.

.6 Mechanical Design of Reactivity Control Systems

 The reactivity control system of the reactor consists of the
drive mechanism which is an electromechanical device for the remote movement
of the rods, reference /2/. Shim safety rods are of Ag-Cd-In alloy with
composition of Ag:80%, Cd 5%, In 15% and a cross section of hollow
elliptical shape. Their length covers the active length of the fuel
elements. The same control system will be utilized for the LEU core
since the expected reactivity worth of the control rods is estimated
identical and the shut down margin will remain within required values.

6. REACTOR COOLANT SYSTEM AND CONNECTED SYSTEMS

 The reactor core is cooled by circulating the demineralized
water of the reactor pool through the core by means of the primary
cooling system. The primary system consists of a 20 m^3 delay tank,
two pumps of 225 m^3/hr capacity each and two heat exchangers. A total
flow rate of 450 m^3/hr is provided for 5 MW operation. The secondary
cooling system consists of two pumps which circulate tapwater from two
cooling towers to the two heat exchangers. Air circulates through each
cooling tower by means of an air blower. The reactor coolant system
and all connected water treatment systems will remain the same as with
HEU fuel, reference /2/.

7. ENGINEERED SAFETY FEATURES

 All engineered safety features employed in the reactor and
described in reference /2/ will be used in the LEU fuel case, including
the water storage pool of 250 m^3 for the ECCS. In addition, a structure
underneath the reactor pool to prevent uncovering of the core in case
of a severe loss of coolant water from the primary pipes, is under
consideration. (Paragraph 16, Decrease in reactor coolant inventory, ii,c).

8. INSTRUMENTATION AND CONTROLS

The nuclear design of the proposed new HEU core will not impose any change in the nuclear control and safety system as well as in the other instrumentation of the reactor and the radiation protection instrumentation described in reference /2/. It should be emphasised here that the existing system provides good means for early detection of any defected fuel element, a fact particularly important, when fuel elements with new technical specifications are to be used.

9. ELECTRIC POWER

No alteration of the electric power system of the reactor reference /2/, is necessary for the LEU core.

10. AUXILIARY SYSTEMS

All auxiliary systems like the various groups of ventilation units, the associated instrumentation, the communication and annunciation system,the lightning protection,compressed air and demineralized water systems are described in reference /2/. Particularly the present fuel storage and the fuel handling system is considered to be adequate for the new LEU fuel. There is place for 50 fresh fuel elements in the dry storage, 49 positions for used or spent fuel elements in the pool and 57 positions in a storage tank outside the pool, which can all receive LEU fuel elements. Fuel handling tools for fresh and used fuel elements will be the same as for HEU fuel and the same general safety consideration as far as their transfer operation is concerned will be applied.

11. EXPERIMENTAL USAGE

No change to the experimental facilities is forseen for the case of LEU fuel. The change of the neutron flux at each experimental position and the effect on the performance of the experiment will be evaluated for each individual case and will follow the same review procedure for approval, reference /2/.

354

12. RADIOACTIVE WASTE MANAGEMENT

The waste management system of the reactor for gaseous, solid and liquid waste is considered, in general, sufficient for handling the new LEU fuels.

The different value of the source term of the LEU fuel due to different amount of U in each fuel element will be taken into consideration in estimating the radiation dose rates during the M.C.A. and the physical security measures.

13. RADIOLOGICAL PROTECTION

Since it will not be any substantial change in the core design no change to the radiation design features is necessary for the new core.

The radiation protection intrumentation and the personnel protection and monitoring as described in reference /2/, is considered to be adequate for the LEU fuel.

14. CONDUCT OF OPERATIONS

The organizational structure, the operating procedures and the emergency plan are described in details in reference /2/. Additionally an improved physical security system is considered now which will be submitted under a separate cover.

15. TEST PROGRAM FOR CORE CONVERSION

The recommissioning program with the use of 5 experimental fuel elements in a mixed core and with full LEU core will be given as soon as the detailed "actual fabrication" specifications of the new fuel elements become available.

16. SAFETY ANALYSES

The analysis of the various accidents for the GRR-1 is presented in reference /3/. The presence of LEU fuel in the reactor core could affect the analysis of some of the accidents like for instance the loss of coolant accident, while the analysis of some other accidents like aircraft crash is independent of the kind of the fuel elements.

From the various possible accidents that can happen to this type of reactor, the Maximum Credible Accident (M.C.A.) is considered to be the partial blockage of the cooling flow which can cause a partial fuel melting and the release of fission products to the environment. The radiological consequences of such a type of accident depends on several factors like fission products inventory in each LEU fuel element, its position in the reactor core, the operating power etc. For demonstration purpose, the radiological doses resulting from the failure of fuel elements due to the partial blockage of the cooling flow are calculated and given in Tables IX and X per gram of failed fuel (U-235). From the above mentioned Tables, the doses corresponding to the total amount of the failed U-235 for each case can be calculated. In addition to the MCA, the Design Basis Accident (D.B.A.) for this type of reactor, with LEU fuels, is analyzed in order to determine the necessary engineered safety features to prevent such an accident to happen. For conservatism sake the Loss of Coolant Accident (LOCA) is considered as D.B.A. for this reactor, although LOCA accident for this type of reactor at 5 MW with LEU elements can not always lead to a core melt (partial or complete). For demonstration purpose the radiological consequences of such an accident are also calculated per gram of failed fuel (U-235)

.1 Decrease in Heat Removal by the Reactor Cooling System:

a. Primary Pumps Failure (Loss of Cooling Flow): During operation at 5 MW primary cooling system flow rate is maintained at 450 m^3/h by the two primary pumps.

Through protective circuits and interlocks a REACTOR REVERSE is initiated when the flow rate falls below 160 m^3/h. In the last case the reactor flapper opens providing cooling of the core through natural convection.

Through the above mechanism a loss of coolant flow does not affect the integrity of the fuel cladding, even at the inversion of the coolant flow.

To verify the above, a series of experiments with HEU, reference /5/, have been performed at the GRR-1. During these experiments, the reactor was operated at steady power 1 MW, 3 MW and 5 MW. Temperature monitored by thermocouples, installed into "instrumented" fuel elements, were recorded. The instrumented fuel elements were located at central positions of the core. A simulation of the loss of flow accident was performed by shutting the pumps down while the reactor was at steady operation. Shutdown of the pumps, as well as decrease of the flow rate initiated a reactor SCRAM.

The temperature rise in the fuel cladding material was maintained at low values for operation at 5 MW.

The average power density corresponding to the fuel element with the highest power generation in the HEU core during the experiments was 20.4 w/cm^2. The equivalent value for the LEU core (Fig. 5) was calculated to be 14.64 w/cm^2 corresponding to the fuel element at position D-3, giving a significant safety margin. The large difference of the above two power density values is due to the fact that the instrumented fuel element which was used during the experiments in the HEU case had zero burn-up, while in the LEU core the burn-up was 26.6 %, (Fig. 6)

b. Flow Blockage to One or More Fuel Assemblies: Among accidents, melting of fuel as a result of flow blockage in one or more fuel elements has the highest probability of occurence and has already happened in at least three reactors of the same general type as "Democritos" research reactor /6/, /19/, /20/, /21/.

This kind of accident can happen if a pliable object is accidentally introduced into the reactor pool and by being deposited on the top of a fuel element can cause blockage of coolant flow through it.

Such occurrences are likely to involve only small objects and small number of fuel elements, but unfortunately there seems to be no real upper limit to the size of objects that might be accidently introduced. In the LEU "Democritos" research reactor, its proposed core configurations with the 5 vertically rising control rod driving mechanisms can only allow blockage of alsmost eleven central fuel elements, (columns C and D), Fig. 2. In practice however, even in such a large-scale flow blockage, no more than part of one fuel element can melt before the negative reactivity inserted into the core from the fuel melting process decreases the reactor power drastically /22/, /23/.

.2 Reactivity Insertion and Power Distribution Anomalies

a. Startup Accident Giving Ramp Insertion of Reactivity. The "Democritos" GRR- 1 research reactor core is nearly identical to the SPERT- 1 core with respect to neutron generation time, temperature and void coefficients. The fuel-plate cladding and the water gaps between plates are of the same magnitude. Therefore, the physical results of a GRR-1 excursion can be predicted very closely on the basis of the SPERT-1 tests.

According to these tests, reactor periods shorter than 4 msec would be required to produce fuel melting of any consequence $\underline{/7/}$ For a reactor period of this order, reactivity insertion rates of 80$/sec-100$ /sec (50 $\frac{\Delta k}{k}$ %/sec - 65 $\frac{\Delta k}{k}$ %/sec) or more are required $\underline{/6/}$, $\underline{/8/}$.

For the GRR-1 there are no known or believable mechanisms that would give rise to insertion rates greater than $5 \times 10^{-2} \frac{\Delta k}{k}$ %/sec, which gives period much exceeding 4 msec and so, no fuel melting occurs $\underline{/6/}$.

At the maximum worth position of the rods, the maximum possible insertion rate is 3.18×10^{-2}% $\frac{\Delta k}{k}$ /sec (for 4 shim and 1 regulating rod).

Assuming a conventional startup accident (involving operator's error and failure of all the period protection systems), the reactivity insertion rate 3.18×10^{-2}% $\frac{\Delta k}{k}$ /sec will not give a reactor period less than 60 msec. But, even if we assume a reactivity insertion rate resulting in a partial fuel melting, superheated steam carrying fission products will not reach the surface of the water in the pool, approx. 7 meters above the core, therefore, overpressure in the reactor hall is not going to occur. This conclusion comes out of experiments conducted by General Electric, in which up to 90000 lb/hr of supper-heated steam was injected from a horizontal 14-inch pipe into water at temperature in the range 38°C - 65°C. All steam was observed to condense in depths of less than 1.83m (6 feet) $\underline{/9/}$, $\underline{/10/}$. Similar mockup experiments were performed for the TRITON swimming pool 5 MW reactor in France, with nearly the same conclusions.

b. Rod Withdrawal Accident: The location of the control rod electromagnets inside the reactor pool makes impossible the manual withdrawal of the control rods. Therefore, this accident is not going to be examined in the present analysis.

c. Core Loading Accident: An accident during loading of the core is considered to have very low probability to occur, because of the regulations which are strictly followed by the personnel, having a long experience on such manipulations.

During the loading usually three shim safety rods are fully inserted in the core. A fuel element may be added only into the outermost element position in each row, column or diagonal. This restriction limits the reactivity increase due to the accidentally drop of a fuel element to less than 1 % $\frac{\Delta k}{k}$.

From the reactivity allowance for 5 MW operation and the reactivity worth of the shim safety rods fully inserted in the core, comes out that a negative reactivity more than -2 % $\frac{\Delta k}{k}$ exists and the positive reactivity introduced by the drop of the fuel element is compensated easily.

d. **Fuel Element Drop**: A fuel element drop into the critical core is more severe accident than the described one in the core loading accident. But, the probability for such an accident to occur, is considered negligible because of the regulations set forth for any fuel movement.

According to these regulations any fuel element movement in the reactor pool, even far from the core, is prohibited when the reactor operates (critical core).

These manipulations take place by the reactor operators under the instructions and supervision of the reactor supervisor only when the reactor is subcritical.

In order to eliminate the probability of a deliberate fuel element drop into the core (sabotage action), the tools for this operations are kept always locked in the pool.

On the other hand, a modification of the hot storage racks, which is under construction, will make impossible the access to the used fuel elements to any unauthorized individual.

e. **Beam Tube Flooding**:   There are four 8 "diameter and two 12"x 12" beam tubes in the GRR-1. Provision has been taken for operating the tubes in the air filled condition.

The transition from the air filled to the water-filled state causes a positive change in reactivity given below.

Two 12"x 12" beam tubes	1.30% $\frac{\Delta k}{k}$
Four 8"diam. beam tubes	0.90% $\frac{\Delta k}{k}$
	2.20% $\frac{\Delta k}{k}$

Although, the instantaneous flooding of all beam tubes is considered as a quite unlikely event the introduction of a positive reactivity 2.2 % $\frac{\Delta k}{k}$ due to the flooding of all beam tubes by an improbable chain of malfunctions of an operator at a slow rate can be covered easily by the shut down margin of the safety rods , which is approx. 4% $\Delta k/k$.

f. Removal or Failure of In-pile Experiments: Experimental materials, placed inside the reactor, represent a potential means of impacting a sudden increase in reactivity, if they are removed while the core is critical, e.g. when a container with samples being irradiated, is for some reason damaged. The volume occupied by the container is then flooded by water and positive reactivity is introduced.

Measurements have been carried out in GRR-1 to determine the void effects of reactivity /11/. According to these measurements the void coefficient of reactivity for a central position in the core is approximately -10^{-3} % $\frac{\Delta k}{k}$/cm^3.

The large containers which are used for irradiaitons in the reactor occupy a volume of about 70 cm^3. Therefore, if a rupture occurs in such a container, placed in the most effective position of the critical core, the reactivity introduced is 0.70 % $\frac{\Delta k}{k}$. This step change causes a positive period longer than 50 sec, which can be easily compensated by the control system of the reactor.

The liquid nitrogen loop is a facility used for sample irradiation in the temperature of liquid nitrogen. The lower part of the loop is positioned in a hole of the grid plate, close to the core in the reflector.

Measurements have been carried out in GRR-1 to determine the reactivity introduced by the loop at various reflector positions. According to these measurements, the reactivity worth of the loop with liquid nitrogen and samples in it, in the most effective position, is approximately - 0.6 % $\frac{\Delta k}{k}$. Considering operation at 5 MW and sudden damage of the loop, i.e. flooding of the volume occupied by the loop by water and assuming that no mechanical damage of the fuel elements occurs and flooding takes place in a time interval Δt = 1 sec, the introduced positive reactivity and the released energy during the event can be determined. A reactor period T ≈ 144 msec in this case is derived and an energy release approx. 2.5 MW-sec is calculated.

Both of the above mentioned values are far below the safety limits for GRR-1.

.3 Changes in Inventory or Pressure of Reactor Coolant

a. Loss of Coolant Accident: The loss of coolant is a   very severe accident in a water cooled reactor.

A loss of coolant means from one point of view, removal of a very important part of the biological shielding of the reactor, which results in a great increase of radiation level around the reactor pool.

On the other hand the heat generated by gamma activity of fission products gives rise to the temperature of the fuel elements. This might cause severe damage at the fuel plate surface depending on the operating power history of the reactor and can even initiate a fuel melt down. Loss of coolant might occur after a rupture of the pool wall, a damage or rupture of an experimental beam tube or the thermal column and finally after a rupture of a pipe of the primary cooling system.

Since the power level of GRR-1 and the operating temperature and pressure are low, there is no supply of stored energy that could lead to a rapid and violent blow down as in the case of power reactors.

i. Engineered Safety Features Against LOCA:

The following Engineered Safety Features Against LOCA are incorporated in the present reactor design to prevent such an accident to occur. A more detailed discussion is included in Appendix C-1.

   a. Butterfly automatic valves are installed at the primary coolant outlet and inlet which are activated from the low water level signal in case of a primary pipe rupture.

   b. Sealed protective covers are provided on the beam tube ends when they are not used while the collimators installed in the beam tubes used for beam experiments are designed to minimize the pool water leakage in case of a beam tube rupture.

For further improvement of the engineered safety features, a construction of a pool water storage underneath the reactor pool is considered which will enclose part of the pipeline with the automatic valve in order to prevent drainage of the pool even in the case of a rupture of primary pipe, between the bottom of the reactor pool and the valve.

Modification of the coolant outlet to a U-pipe is also under consideration, to cease the drainage of the pool below the core level. Finally, a large water storage pool will be connected to a core spray system.

.4 Radioactive Releases for the M.C.A. per gram of Failed Fuel (U-235)

The assumptions for fission products releases in MCA are given below for each gram of failed burned fuel (U-235).

a.   Each gram contains 0.09% of total fission products inventory (assuming a mean burn-up of the equilibrium core of 15.1% the consumed U-235 is $(222.2 \times 30 + 5.123)$ $\frac{15.1}{100}$ = 1099.4 gr.

So 1 gram = $\frac{1}{1099.4}$ × 100 = 0.09% of the fission products inventory).

b.   100% release of noble gases and 50% of iodines, i.e. 0.09%
of noble gases and 0.045% of iodines are released into the water.

c.   10% /6/ of iodines and all noble gases in the water, i.e. 0.09% of
noble gases and 0.0045% of iodines will be released to the reactor building
over some period of time.

d.   Noble gases and iodines will then be released to the atmosphere
through the stack (effective height 50 m) after passing a system of absolute
and activated charcoal filters in an air flow rate of 1000 m³/h, provided by
the emergency ventilation system. The filters efficiency for Iodines was
conservatively taken as 95%. No absorption of Iodine on the walls and
internal components of the reactor was taken into consideration, although the
amount of Iodine absorbed and adhered is very high /12/.

.5 Estimation of Radiological Doses for the MCA

Under the prementioned assumptions, we calculate the total fission
products inventory, available for release to the atmosphere. Shutdown activity
for isotope i is calculated by the simplified formula /13/.

$$A_i = 0.865 \times 10^6 \ P \times Y_i (1-e^{-\lambda_{R_i} T}) \qquad (5)$$

where:

A_i	:	activity of isotope i at shutdown (Curies)
P	:	reactor power level (MW)
Y_i	:	total fission yield of isotope i in %
λ_{R_i}	:	radiological decay constant for the isotope i (sec^{-1})
T	:	operation time of the reactor (sec)

To calculate the maximum fission product inventory the average
burnup contained in the end-of-cycle equilibrium core, 15.1 %(Table II)
is multiplied by the nominal U-235 content to give the U-235 burned.
This   in turn is divided by 1.2 gr. U-235/MW-days and then by 5 MW to
give days of operation:

$$\frac{15.1}{100} \times (222.2 \times 30 + 123 \times 5) \ gr. \ U-235/1.2 \ g. \ U-235/MWD/5 \ MW = 183 \ days$$

362

Thus, about 200 full power (5 MW) days of preaccident operation
is assumed to produce the maximum fission product inventory. Out-of-this the
most important safety related volatile fission products activities are
calculated and tabulated in Table VIII togetherwith the activities available
to escape to atmosphere,per gram of failed U-235 fuel, according to the
prementioned assumptions.

TABLE VIII.

Volatile Fission Products Activities After 20u Full-Power Days of Operation
per gram of failed fuel (U-235).

Nuclide	Half Life /13/	Total Fission Yield /14/%	Activity at Shutdown/Curies	Activity Available for Release to AtmCi/gr of U-235
Kr-85m	4.36 h	1.33	5.752×10^4	5.177×10^1
Kr-87	1.3 h	2.56	1.107×10^5	9.963×10^1
Kr-88	2. 77 h	3.7u	1.600×10^5	1.440×10^2
Xe-131m	12 d	2.77	1.198×10^5	1.078×10^2
Xe- 133	5.27 d	6.77	2.928×10^5	2.635×10^2
Xe- 135m	15.6 m	2.0u	8.650×10^4	7.785×10^1
Xe- 135	9.13 h	6.70	2.898×10^5	2.608×10^2
I-131	8.u5 d	2.77	1.198×10^5	2.695×10^{-1}
I-132	2.4 h	4.13	1.786×10^5	4.018×10^{-1}
I-133	20.8 h	6.77	2.928×10^5	6.588×10^{-1}
I-134	52.5 m	7.19	3.109×10^5	6.995×10^{-1}
I-135	6.68 hr	6.70	2.898×10^5	6.520×10^{-1}

The releases of Table VIII are used for the dose calculations of an un-
protected individual remaining at the nearest to the stack exclusion
zone boundary (450 m) for 2 hours. As an exclusion zone in this case the
actual boundary of the N.R.C. "Democritos", which is a controlled
area, is considered. 450 m is the distance from the reactor stack to the
entrance gate. Any residential construction lies beyond this distance.

Another calculation at 1000 m distance for 30 days residence is
also included. In both cases thyroid doses from Iodine isotopes and whole
body gamma doses from noble gases are estimated.

a. Whole Body Gamma Dose : The dose rate D_γ' for whole body exposure
in a semi infinite cloud is given by reference /15/.

$$D_\gamma' = 0.25 \ E_{\gamma i} x i \qquad\qquad (6)$$

Where

D_γ' : rem/sec

$E_{\gamma i}$: average gamma energy/disintegration for isotope i (MeV/dis)

xi : concentration of gamma emitting isotope i in cloud (Ci/m^{-3})

Summing the total released activities over time τ and over all isotopes and multiplying by the atmospheric dispersion factors, we obtain the total dose received over τ (/3-A/).

$$D_\gamma (\tau) = 0.25 \ (X/Q)_\tau \ \Sigma \ E_{\gamma i} A(\tau)_i \qquad (7)$$

Where $D_\gamma(\tau)$: whole body dose over τ (rems)

$(X/Q)_\tau$: atmosphericdispersion factor over $\tau(sec/m^3)$

$A(\tau)_i$: total activity of isotope i,released in τ (Curies)

b. Thyroid Dose : In Vol.I App. D-1 reference /3-A/, the Thyroiddose in time τ, is aiven by

$$D_{Th} (\tau) = (X/Q)_\tau \ .R.\Sigma_i A (\tau)_i (CF)_i \qquad (8)$$

Where $D_{Th} (\tau)$: Thyroid dose over time $\tau(rem)$

$(CF)_i$: dose conversion factor (rem/Ci) for isotope i and

R : breathing rate (m^3/sec)

In both cases a and b integrated release of isotope i in τ, must be estimated.

This is given, reference /13/, and /3-A/:

$$A(\tau)_i = Ao_i \ \frac{\lambda_L}{\lambda_L + \lambda_{Ri}} \ (1-e^{-(\lambda_L + \lambda_{Ri})\tau}) \qquad (9)$$

where

A_{oi} : available for release activity at t=0 (where t=0 is the instant when the release of isotope i starts) (C_i)

λ_L : leakage parameter for the building (sec^{-1})

λ_{Ri} : decay constant of isotope (sec^{-1})

364

λ_L is determined for GRR-1 as following:

Since 1000 m^3/h are released to atmosphere through the stack

and the overall volume of the reactor is 14000 m^3 (i.e. $\frac{1000 \times 100}{14000} = 7.14$ %)

$$\lambda_L = 7.14\% \text{ /hr} = 1.984 \times 10^{-5} \text{ sec}^{-1}$$

X/Q values were taken from Regulatory Guide 1.3, /15/.

For the 2 hours dose $(X/Q)_{2h}$ was taken from Figure 1(A) of Ref. /15/.

Fig. 1(A) is the envelope of Pasquill diffusion categories for various stack heights and wind speed $1_m . sec^{-1}$, representing thus the most unfavorable weather conditions for the dispersion of radioactive plume to the atmosphere.

Dose conversion factors were taken from /3-7/ 1.48x10^6 rem/Ci, 5.35 x 10^4 rem/Ci, 4 x 10^5 rem/Ci, 2.5 x 10^4 rem/Ci and 1.24 x 10^5 rem/Ci for I-131, I-132, I- 133, I- 134 and I-135 respectively.

Breathing rate for a standard man was taken from I.C.R.P. /16/ to be,

$$R = 3.347 \times 10^{-4} \text{ } m^3/\text{sec for working-day and}$$

$$R = 2.32 \times 10^{-4} \text{ } m^3/\text{sec for average 24hr-day.}$$

Using now relations (7), (8) and (9). Thyroid and Whole Body Doses are calculated for 2hours exposure at 450 m from the point of release and the results are tabulated in Table IX, per gram of failed U-235 fuel.

TABLE IX.

Total Thyroid and Whole Body Doses at 450 m for 2 HR of Exposure per gram of failed fuel (U-235)

Nuclide	λ_{Ri} sec^{-1}	$A(2h)_i$ Curies	Thyroid Dose for 2 hr rem/gr of U-235	Whole Body Dose for 2 hr rem/gr of U-235
Kr-85 m	4.415 x 10^{-5}	5.524 x 10^0		1.608 x 10^{-5}
Kr-87	1.480 x 10^{-4}	8.257 x 10^0		1.702 x 10^{-4}
Kr-88	6.949 x 10^{-5}	1.517 x 10^1		4.709 x 10^{-4}
Xe-131 m	6.684 x 10^{-7}	1.431 x 10^1		3.500 x 10^{-5}
Xe-133	1.522 x 10^{-6}	3.488 x 10^1		4.238 x 10^{-5}
Xe-135 m	7.404 x 10^{-4}	2.022 x 10^0		1.578 x 10^{-5}
Xe-135	2.108 x 10^{-5}	3.226 x 10^1		1.210 x 10^{-4}
I-131	9.964 x 10^{-7}	3.574 x 10^{-2}	1.101 x 10^{-3}	
I-132	8.021 x 10^{-5}	4.090 x 10^{-2}	4.556 x 10^{-5}	
I-133	9.255 x 10^{-6}	8.458 x 10^{-2}	7.069 x 10^{-4}	
I-134	2.200 x 10^{-4}	4.756 x 10^{-2}	2.475 x 10^{-5}	
I-135	2.882 x 10^{-5}	7.855 x 10^{-2}	2.028 x 10^{-4}	
Total Dose			2.081 x 10^{-3} (2 mrem)	8.713 x 10^{-4} (0.9 mrem)

For the 30 days dose, Figures 1(A), 1(B), 1(C) and 1(D)
of Ref. /15/ were used for 8 hours, 8-24 hours, 24 hours-4days and
4 days- 30 days exposure time intervals repsectively.

Thus, relations (7) and (8) were modified as follows:

$$D_\gamma \; (30 \; \text{days}) = 0.25 \; \sum_j \; (X/Q)_j \; \sum_i \; \bar{E}_{\gamma i} A_{ij} \qquad (10)$$

and

$$D_{Th} \; (30 \; \text{days}) = R. \sum_j \; (X/Q) \; \sum_{ji} A_{ij} \; (CF)_i \qquad (11)$$

where

$(X/Q)_j$: average atmospheric dilution factor during the jth
time interval (0-8 hours, 8-24 hours, 1-4 days, 4-30 days)
(sec/m^3).

A_{ij} : equivalent release of nuclide i during the jth time
interval (Curies)
other symbols, as before mentioned.

The released activity over the aforementioned time intervals and
the resulting doses, were calculated and tabulated in Table X per gr of failed U-235
With respect to the results of Tables IX and X the following
comments should be made.

TABLE X.

Thyroid and Whole Body Dose at 1000 m for 30 Days of Exposure per gram of failed fuel(U-235)

Nuclide	Released Activity				Thyroid Dose				
	A_{i1} 0-8hr Ci	A_{i2} 8hr-1d Ci	A_{i3} 1d-4d Ci	A_{i4} 4d-30d Ci	D_{i1} rem	D_{i2} rem	D_{i3} rem	D_{i4} rem	
I-131	1.158×10^{-1}	9.843×10^{-2}	4.225×10^{-2}	1.919×10^{-4}	2.795×10^{-3}	8.449×10^{-4}	1.233×10^{-4}	1.67×10^{-7}	
I-132	7.520×10^{-2}	4.452×10^{-3}	1.404×10^{-5}	0	6.561×10^{-5}	1.382×10^{-6}	1.481×10^{-9}	0	
I-133	2.548×10^{-1}	1.580×10^{-1}	3.637×10^{-2}	0	1.662×10^{-3}	3.665×10^{-4}	2.869×10^{-5}	0	Total Thyroid dose 6.362×10^{-3} rem (6.5 mrem)
I-134	5.779×10^{-2}	5.788×10^{-5}	0	0	2.356×10^{-5}	8.393×10^{-9}	0	0	
I-135	2.003×10^{-1}	6.150×10^{-2}	3.971×10^{-3}	0	4.051×10^{-4}	4.423×10^{-5}	9.711×10^{-7}	0	

Nuclide	$\bar{E}_{\gamma i}$ /14/ MeV/dis	Released Activity				Whole Body Dose				
		A_{i1} Curies	A_{i2} Curies	A_{i3} Curies	A_{i4} Curies	D_{i1} rem	D_{i2} rem	D_{i3} rem	D_{i4} rem	
Kr-85m	0.181	1.351×10^{1}	2.478×10^{0}	6.376×10^{-2}	0	2.872×10^{-5}	2.803×10^{-6}	2.452×10^{-8}	0	
Kr-87	1.374	1.168×10^{1}	9.369×10^{-2}	0	0	1.886×10^{-4}	8.045×10^{-7}	0	0	
Kr-88	2.070	2.953×10^{1}	2.427×10^{0}	1.423×10^{-2}	0	7.183×10^{-4}	3.140×10^{-5}	6.258×10^{-8}	0	
Xe-131m	0.163	4.650×10^{1}	4.002×10^{1}	1.762×10^{1}	8.679×10^{-2}	8.906×10^{-5}	4.077×10^{-5}	6.103×10^{-6}	8.842×10^{-9}	
Xe-133m	0.081	1.124×10^{2}	9.364×10^{1}	3.852×10^{1}	1.526×10^{-1}	1.070×10^{-4}	4.741×10^{-5}	6.630×10^{-6}	7.723×10^{-9}	Total Body Dose 1.594×10^{-3} rem (1.5 mrem)
Xe-135	0.520	2.031×10^{0}	0	0	0	1.241×10^{-5}	0	0	0	
Xe-135	0.250	8.752×10^{1}	3.523×10^{1}	3.687×10^{0}	0	2.571×10^{-4}	5.505×10^{-5}	1.959×10^{-6}	0	

a.   In calculating   the above Tables, decay of fission products was only taken into account while they were confined into the reactor building and not during their transient to the receptor.

b.   For the isotope activity at shutdown 200 full-power days of pre-accident   operation was assumed.   This was a pessimistic assumption because the real operational schedule of GRR-1 (at least now) is up to 10 hours of operation per day on a 5 days per week basis. Taken this into account the activity of I-131 was calculated to be only about 30% of the activity given in Table VIII. The thyroid dose due to I-131 will be reduced accordingly.   The activity of isotopes with shorter than I-131 half-lives, will be reduced accordingly.   The activity of isotopes with shorter than I-131 half-lives, will be reduced even more.

c.   Beta exposure from the passing cloud will have a very small contribution to the whole body dose, (it will mainly cause skin dose) relatively to the gamma exposure, therefore, it was not calculated in the present report.   However, it will be included in Vol. II of the HEU Safety Analysis Report*of the GRR-1, in order to present a complete picture of the radiological consequences.

Doses from exposure to gamma rays emitted from within the reactor building, were also not included in the present report, since they have been estimated to be smaller than the ones presented on Tables IX and X, by at least one order of magnitude. They will, however, be considered in Volume II of th e SAR, together with a complete estimation of doses for various distances and sectors, integrated over the population distribution in each sector.

d.   Dose due to dry ground depositions of isotopes was estimated to be quite insignificant to be included in Tables IX and X , because noble gases do not deposit on the ground, iodine releases were very limited, while solid fission products were non-existent. (The filter efficiency for solid fission products is very high, 99,9% and the release of them from the damaged fuel elements to the water of the pool is only a few percent).

e.   The results of Tables IX and X must be multiplied by the actual amount of failed fuel (U- 235) to give the real radiological doses for a particular case of interest.   These doses are now to be compared to the site criteria established in 10CFR-100 /17/. According to /17/ thyroid doses at the two boundaries and over the time used in our calculations are required to be less than 300 rem. The whole body doses at the same locations and for the same periods, are not to exceed 25 rem. More

---

* Under preparation

conservative dose limits are the ones recommended by American National
Standard Research Reactor Site Evaluation (N. 379, 1977) ,being 5 rems
to the "Whole body"or 15 rems to "any organ"for 2hr-exposure at the site
boundary /18/.

.6 Radioactive Releases for the DBA per gram of Failed U-235 Fuel

The assumptions for release in the DBA are similar with
the ones in the MCA except the fact that since the core is now uncovered
the amount of Iodines available for release to atmosphere is 10 times
higher than in the MCA. (There is no water to retain the Iodines now).

Accordingly the thyroid doses, estimated in the same way as
before, will be 10 times higher than in the ones presented in Tables IX, X, (MCA
case).

For the noble gases assumptions will be the same as in the
MCA case and doses as the ones presented in Tables IX and X.

The comments in Section .5 are valid for this DBA
case as well.

ACKNOWLEDGEMENTS

REFERENCES

/1/   Comparison of Some Measurement in the Greek Research
        Reactor-1 (GRR-1) with 20% and 93% Enriched Uranium Fuel
        Elements, Rresented at the ANL Core Conversion Meeting Nov. 12-14
        (1980).
/2/   Safety Analysis Report of the Greek Research Reactor-1 (GRR-1),
        Vol. I, Athens (1981).
/3/   Basic Consideration for the Safety Analysis Report of the
        Greek Research Reactor-1 (GRR-1), DEMO 81/3 (1980).

/4/ Safety Analysis, Utilization of Low Enrichment Uranium (LEU)
Fuel in the FORD Nuclear Reactor, Prepared for the U.S. NRC
Oct. 1979.

/5/ Experimental Study of Some Thermohydraulic Characteristics of
the GRR-1, Internal Report prepared by the Reactor Department
N.R.C "Democritos" (1980).

/6/ 1969 Status Report on the Omega West Reactor with Revised Safety
Analysis LA-4192, July 1969.

/7/ M.R. Zeissler"Non-Destructive and Destructive Transient Tests
of the SPERT I- D Fully Enriched, Aluminium-plate-type Core"
Data Summary Report IDO-16886, Nov. 1963.

/8/ W.E. Nyer, in The Technology of Nuclear Safety Vol. 1, MIT
Press Cambridge Mass 1964 pp 440 F.

/9/ Hazards Evaluation in Support of Request for Amendment 6
Licence R-47 to Operate the Lynchbourg Pool Reactor at 1000 KW BAW-74
Suppl. 8, April 1962.

/10/ Holsmann E.G. Safeguard Report for Open Pool Reactor for State College
of Washington, 1959, GEAP-3100.

/11/ N.G. Chrysochoides, "Measurements of Void Effects on the Reactivity"
Chimika Chronica 30 A, Athens, 1965.

/12/ Sicherheitsbericht für FRG1/FRG2, GKSS Forschungszentrum
Geesthacht GMBH (1976).

/13/ J.J. DiNunno F.D. Anderson, R.E. Baker, R.L. Waterfield "Calcula-
tion of Distance Factors for Power and Tests Reactor Sites" TID-14844
U.S.A.E.C., (1962).

/14/ Chart of the Nuclides, Knolls Atomic Power Lab., Naval Reactors
USAEC-11th Edit. (1972).

/15/ Regulatory Guide 1.3 Revision 2 "Assumptions Used for Evaluating
the Potential Radiological Consequences of a Loss of Coolant Accident
for Boiling Water Reactors"USAEC (1974).

/16/ ICRP-23 (1974).

/17/ 10CFR-100, Reactor Siting Criteria (1979).

/18/ American National Standard-Research Reactor Site Evaluation
ANSI/ANS-15.7 (N 379),(1977).

/19/ A. Colomb et al:Nuclear Safety 5, 203 (1963)

/20/ R. A. Costner:Nuclear Safety 4, 144 (1963)

/21/ J.R. Buchanan:Nuclear Safety 3, 90 (1962)

/22/ M. Jacquemain et al.:Compte- rendu de 1' incident de fusion desplaques
d'un élément combustible à SILOE, CEA INT 760, 1968.

/23/ M. Baggenstos, H. Winkler et al.: Sicherheitsbericht für 10 MW des
Forschungsreaktors SAPHIR, Würenlingen, (1980).

Appendix E-7

SUMMARY — SAR AMENDMENTS FOR TESTING PROTOTYPE FUEL ELEMENTS IN THE FRG-2 REACTOR

W. KRULL
GKSS — Forschungszentrum Geesthacht GmbH,
Geesthacht, Federal Republic of Germany

Abstract

For the German research reactor FRG-2, a licensing procedure was necessary for testing prototype fuel elements with reduced enrichment. This summary lists the points that were discussed between the reactor operator, independent experts and the licensing authority.

For the German research reactor FRG-2 a licensing procedure was necessary for the tests of test and prototype fuel elements with reduced enrichment. These fuel elements have unchanged geometry, and unchanged specifications (homogeneity, water gap, meat area, accuracy of U-content etc.) 280 g U-235, UAl_x, 45 % enrichment; 270 g U-235, U_3O_8, 20 % enrichment and 323 g U-235, U_3Si_2, 20 % enrichment. Four of these fuel elements are instrumented with thermocouples.

The following points were discussed between the reactor operator, independent experts and the licensing authority:

1. fission product content,
2. Pu inventory,
3. temperature coefficients of reactivity,
4. loss of flow accident,
5. fissions/cm^3 limitations,
6. metallurgical behaviour of burned fuel plates,
7. irradiation time of a fuel element,
8. power distribution in a fuel element (esp. parallel to the fuel plates),
9. peaking factors, power distribution,
10. fuel cycle scheme,
11. reactivity addition,
12. reactivity values of control rods,
13. reactivity accidents,
14. criticality of fresh and spent fuel storage,

15. detection of defect fuel elements,

16. post irradiation experiments,

17. quality control (only for fuel fabrication),

18. startup and experimental program.

This licensing procedure was necessary for getting the permission for the performance tests of the test and prototype fuel elements.

Applying for a license for the whole core conversion all nuclear, thermodynamical and safety related aspects have to be considered. Besides this a review of the safety report has to be done and then the operator is obliged to compare the actual design with the present requirements for research reactors. The type of final licensing procedure /1/ will be decided in 1986.

REFERENCE

/1/ W. Krull: Experiences with Interpretation and Application of the German Atomic Energy Act for the German Research Reactors in Geesthacht FRG-1 and FRG-2, GKSS 80/E/16 (1980)

Appendix F

SAFETY SPECIFICATIONS

Abstract

General methodology and results for a specific reactor
(HFR Petten) are provided for determination of the power
limits for safety specifications with HEU and LEU fuel. LEU
elements with the same geometry as the HEU elements and LEU
elements with a reduced number of thicker plates are
considered.

DETERMINATION OF POWER LIMITS
FOR TECHNICAL SPECIFICATIONS

C. BAGLIN
GEC Energy Systems Limited,
Whetstone, Leicester,
United Kingdom

A. TAS
Netherlands Energy Research Foundation,
Petten, Netherlands

Abstract

An outline is provided of the considerations necessary to determine the maximum operating power, usually set by flow instability burnout, for core conversion from HEU to LEU fuel without changing the primary cooling circuit.

1. Case Considered

In converting a core to LEU there will be a strong incentive to retain the primary circuit without modification. This section outlines the considerations necessary to determine the maximum operating power for such a case.

2. Power Limitation

The limiting power will usually be set by flow instability burn-out. One formulation of this limit, using the bubble detachment parameter is

$$P_c = \frac{n \, LSV \, (T_s - T_i)}{F \left[\alpha \, \eta_c + \frac{4}{\rho C_p} \frac{L}{D_H}\right]} \tag{1}$$

where:

P_c	=	Critical power in element
n	=	Number of plates in element
L	=	Heated length
S	=	Heated width
V	=	Coolant velocity
T_s	=	Saturation temperature
T_i	=	Inlet Coolant Temperature
F	=	Horizontal peaking factor within element
α	=	Vertical peaking factor
η_c	=	Bubble detachment parameter
D_H	=	Channel hydraulic diameter

If all parameters except, n, D_H, and V are the same for the original fuel and the LEU fuel; we have:

$$P_c = \frac{C_1 n V}{C_2 + \frac{C_3}{D_H}}$$

(2)

3. Core Flow

The new core flow can be determined from the intersection of the pump characteristics and the circuit resistance. The latter comprises the piping, delay tanks, etc., plus the core resistance.

The LEU fuel will probably have reduced numbers of plates, reduced coolant flow area and hence higher pressure drops at the same flow rate. For example, for a constant water gap,

Core $\Delta P \propto 1/n^2$.

Figure 1 shows pump and circuit characteristics. The operating point will move from point 1 to point 2. Total circuit flow is reduced and core ΔP increased. Now,

$$V = \frac{2 W_2}{N n S D_H}$$

Where N = number of fuel elements. V can then be inserted in Eq. (2) to determine the critical element power. Typically, this power will be 5-10% lower than for the original core.

FLOW RESISTANCES

Total - New Core

Total - Old Core

Piping etc

PUMP Characteristic
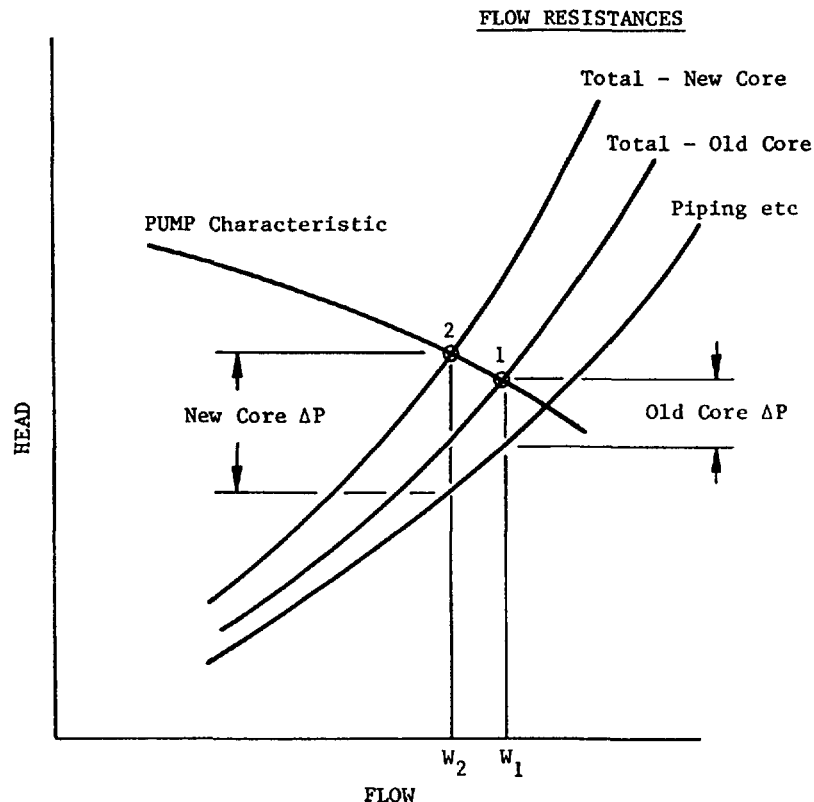
HEAD

New Core ΔP

Old Core ΔP

W₂ W₁

FLOW

FIG. 1. Reduction in core flow following fuel replacement.

This type of calculation will provide new values for the maximum operating power and the trip levels for power and flow.

There are some situations, e.g. materials testing reactors, where a loss of thermal flux of the size predicted above would be undesirable. One way of counteracting this would be, as is clear from Eq. (1), to use the actual day to day T_i, as determined by ultimate heat sink conditions, to allow the reactor to operate always at its maximum allowable power.

Appendix F-2

NOMINAL POWER LIMITS OF THE HFR FOR LEU ELEMENTS WITH A REDUCED NUMBER OF THICKER FUEL PLATES*

A. TAS
Netherlands Energy Research Foundation,
Petten, Netherlands

Abstract

A procedure is provided for determining the new power limits (based on the margin against flow-instability-induced burnout) for HEU to LEU core conversion cases in which the fuel element design is changed to include a reduced number of thicker fuel plates. Consequences of core conversion are investigated for a specific reactor (HFR Petten) for a variety of LEU fuel element design options.

1. INTRODUCTION

Core conversion from HEU to LEU requires an increase of the uranium contents, thus of the uranium density and/or the "meat" volume. Especially in the last case, that the geometry of the fuel element has been changed, a careful consideration of the consequences on the core flow and subsequently on the power limitation is required.

In this study the consequences on the power limits of the HFR for plate type fuel elements (with a reduced number of thicker fuel plates), compared to the present 23 plates UAl_x design has been investigated. The primary circuit has been considered as a boundary condition.

2. POWER LIMIT ASSESSMENT PROCEDURE AND CRITERIA

This study has been limited by a number of boundary conditions, viz.
o conservation of the main reactor operating parameters,
o conservation of all major components like core structure, control rods, heat exchangers, pumps,
o utilisation of a plate type fuel.
Within these limits the thermohydraulic aspects of fuel elements with a reduced number of (thicker) plates, have been investigated for the HFR Petten.

The thermal safety of an operational HFR core is assessed on basis of two criteria,
(I) the margin against flow-instability induced fuel plate burn-out
(II) the margin against film-boiling induced fuel plate burn-out.
In all practical cases of interest the first safety criterion will be determining for the maximum allowable power. The subsequent analyses will therefore be restricted to the calculation of the flow-instability margin, which is based upon the so-called "bubble-detachment" criterion. Bubble detachment in subcooled water

---

will only occur at a certain combination of process quantities. This condition can be represented by the following formula (see |3| and |4|) :

$$\eta_c \leqslant \frac{v \ (Ts - Tb)}{q} \tag{1}$$

in which :
v = coolant speed (cm/sec)
q = local heat flux density (W/cm^2)
η_c = critical bubble detachment parameter (η_c = 32 cm^3 °C/W.sec)
Ts = saturation temperature (Ts ~ 131 °C)
Tb = bulk temperature

Rewriting equation (1) in terms of practical fuel element/reactor data, the following expression for the critical reactor power, P_c, is obtained :

$$P_c = \min \quad {}^{1)} \left[\frac{(1 + \epsilon) \ n \ . \ L_H \ . \ S_H \ . \ v \ (Ts - Ti)}{\Pi \ . \ f_h \ . \ f_q \left\{ \alpha \ . \ \eta_c + \frac{4}{\rho.c} \ . \ \frac{L_H}{D_H} \right\} \ . \ F_u \ . \ F_s} \right]_i \tag{2}$$

in which :
ϵ = heat dissipation symmetry factor (for nominal case ϵ = 1)
n = number of fuel plates in element
L_H = heated length of plate
S_H = heated width of plate
v = coolant velocity
Ts = saturation temperature
Ti = coolant inlet temperature
Π = power fraction of element (i)
f_h = horizontal power distribution factor in element ($f_h = \frac{P_{max}}{P_{aver.}}$)

f_q = ratio of power dissipated to cooling channels to total fission power in plate
α = vertical power peak factor
η_c = critical value of bubble detachment parameter
ρ = density of coolant
c = specific heat of coolant
D_H = heated equivalent diameter : (D_H ~ 2 d) in which d = coolant gap width
F_u = total uncertainty factor (F_u = 1.64)
F_s = safety factor accounting for misloading errors and unscheduled power excursions (F_s = 1.20)
P_c = critical (maximum allowable) reactor power, related to the critical heat transfer conditions in a coolant channel of position (i).

Since a number of parameters values from eq. (2) are identical for both HEU and LEU elements, the following simplified formula can be derived :

$$P_c = \min \left[\frac{C1 \ . \ n \ . \ v}{\Pi \ . \ f_h \left\{ 1 + \frac{C2}{d} \right\}} \right]_i \tag{3}$$

in which :
C1 = 81600
C2 = 0.7 cm
Π . f_h represents the peak power in a horizontal plane per element.

Eq. (3) will be applied for thermal safety assessment of the LEU reference core in comparison to the HEU reference core.

1) $\min \left[------ \right]_i$ implies that the expression $\left[----- \right]$ must be evaluated for each fuel position (i) and that the minimum value found, must be applied for the determination of Pc.

For determining the effect of geometrical changes of the fuel elements on their cooling capacity, the following formula can be derived from eq. (3) if changes in power peaks are neglected :

$$\frac{P_c}{P_{c,ref}} = \frac{n}{n_{ref}} \cdot \frac{v}{v_{ref}} \cdot \frac{1 + \dfrac{C2}{d_{ref}}}{1 + \dfrac{C2}{d}}$$ (4)

in which :
ref : stands for reference element and C2 = 0.7 cm

3. POWER LIMITS

With formula (4) it is possible to analyse the effects of a changed fuel element geometry on the element core cooling capability. For this purpose fuel elements with a varying number of fuel plates with the standard meat thicknesses of 0.51 mm and 0.76 mm and three types of elements with very thick fuel plates have been investigated. In this investigation the differences in local power peaks have been ignored, moreover for the elements with the standard meat thicknesses it is assumed that the total core flow is not affected by geometrical changes of the fuel elements.

Table 1. Ratio of critical power $P_c/P_{c,REF}$ for several types of fuel elements

ELEMENT TYPE	MEAT TH. (CM)	CHANNEL WIDTH (CM)	$\dfrac{N}{N_{REF}}$	$\dfrac{V}{V_{REF}}$		$\dfrac{1 + 0.7/D_{REF}}{1 + 0.7/D}$	$\dfrac{P_c}{P_{c,REF}}$
23 PL HEU	0.051	0.218	1.000	1.000		1.000	1.00
23 PL LEU	0.051	0.218	1.000	1.000	1)	1.000	1.00
22 PL LEU	0.051	0.234	0.975	0.975	1)	1.055	0.984
21 PL LEU	0.051	0.251	0.913	0.952	1)	1.111	0.966
20 PL LEU	0.051	0.270	0.870	0.929	1)	1.172	0.95
19 PL LEU	0.051	0.291	0.826	0.908	1)	1.237	0.93
23 PL LEU	0.076	0.193	1.000	1.130	1)	0.910	1.03
22 PL LEU	0.076	0.209	0.957	1.092	1)	0.968	1.01
21 PL LEU	0.076	0.226	0.913	1.057	1)	1.028	0.99
20 PL LEU	0.076	0.245	0.870	1.024	1)	1.092	0.97
19 PL LEU	0.076	0.266	0.826	0.993	1)	1.160	0.95
18 PL LEU	0.076	0.289	0.783	0.964	1)	1.231	0.93
18 PL LEU	0.145	0.225	0.783	1.163	2)	1.024	0.93
16 PL LEU	0.145	0.260	0.696	1.091	2)	1.141	0.87
15 PL LEU	0.190	0.214	0.652	1.329	2)	0.986	0.85

N   Number of fuel plates per element
V   Coolant velocity
D   Coolant gap width
REF Stands for reference element (23 plates HEU element)

1) No influence of geometry of fuel element on primary flow assumed
2) Influence on primary flow calculated according to appendix, see Table 2.

Table 2. Influence of geometry of element on coolant velocity

Type fuel element	Heated area per element $10^{-4} m^2$	Cooling channel thickness $10^{-3} m$	Cooling channel cross section 1)	Total primary flow $m^3 h^{-1}$	Core primary flow $m^3 h^{-1}$	Pressure differences			Channel coolant velocity $m s^{-1}$
						pump $10^4 Nm^{-2}$	piping $10^4 Nm^{-2}$	core $10^4 Nm^{-2}$	
23 plates	17429 (ref.)	2.18 (ref.)	1675 (ref.)	4300	4100	33.5	23.3	10.2	6.80
15 plates	11367 (−35%)	2.14 (−2%)	1154 (−31%)	4000	3800	37.3	20.1	17.2	9.04 (+33%)
16 plates	12125 (−30%)	2.60 (+19%)	1513 (−10%)	4240	4040	34.5	22.7	11.8	7.42 (+9%)
18 plates	13640 (−22%)	2.25 (+3%)	1398 (−17%)	4175	3975	35.3	21.9	13.4	7.91 (+16%)

1) Core with 33 fuel elements, 6 control rods, 17 standard assemblies and 25 Be-elements.

From the results presented in Table 1 it is seen that for the elements with the standard meat thicknesses the reduction in heated area (in cases of less than 23 fuel plates per element) is largely compensated by the increased thickness of the water channels. This means that the resulting effect is about equal to the loss in coolant velocity in the coolant channels.

For the fuel elements with an appreciable increase in meat thickness and a significant decrease in total coolant channel cross section the influence on the primary flow has been taken into account, according to the procedure described in the appendix.

The average coolant velocity is equal to the primary flow divided by the total horizontal cross section of the coolant channels in the core. For the core configuration with 33 fuel elements, 6 control rods, 17 standard assemblies and 25 Be-elements this cross section is calculated for the four types of fuel elements, see table 2. For the present situation the nominal primary flow through the core is 4100 m^3/h, while the bypass flow through the former D_2O tank is maintained at 200 m^3/h. The calculated pressure difference over the core is 10.2 10^4 N/m^2 which is in good agreement with the measured value of 10.7 10^4 N/m^2. Using the primary circuit pressure drop equations and the characteristics of the primary pumps, the primary flow has been derived for cores with the alternative fuel elements. From this primary flow and the total horizontal cross section of the coolant channels in the core, the coolant velocity has been calculated, see Table 2. It is seen that the coolant velocity shows an increase of 33, 9 and 16% for the 15, 16 and 18 plates elements respectively. This increase is due to the considerable increase of pressure difference over the pumps and to a decreasing pressure difference over the piping at a decreasing primary flow, see Table 2.

In Table 1 the influence of the changed geometry of the 15, 16 and 18 plates elements are presented, taking into account the effects on the primary flow.

In all cases studied the influence of the introduction of LEU elements on the power peaking has neglected. In |5| a case study is presented in which this effect has also taken into account.

4. APPENDIX, CALCULATION OF COOLANT VELOCITY IN ALTERNATIVE FUEL ELEMENTS

The average coolant velocity in the core is equal to the primary flow divided by the total horizontal cross section of the coolant channels in the core.

For the core configuration with 33 fuel elements, 6 control rods, 17 standard assemblies and 25 Be-elements this cross section is calculated for the four types of fuel elements, see Table 2. In table 3 the cross sections are tabulated for each type of core element.

For each type of core the total flow can be calculated from the relations between flow and pressure difference over core and piping, together with the pump characteristics which give the relation between pressure difference over pump and flow.

The pressure difference over the primary pumps must be equal to the pressure differences over the core and the rest (piping) of the primary circuit. So

$$\Delta P_{pumps} = \Delta P_{core} + \Delta P_{piping} \tag{5}$$

In Figure 1 the pressure difference over the pumps is given as a function of the total primary flow.

Table 3. Coolant channel cross section for different types of core elements

| Type of core element	Coolant channel area in 10^{-4} m^2
23 plates fuel element (meat thickness 0.051 cm)	35.44
19 plates control element (meat thickness 0.051 cm)	34.84
15 plates fuel element alternative 1 (meat thickness 0.190 cm)	21.54
12 plates control element alternative 1 (meat thickness 0.190 cm)	24.47
16 plates fuel element alternative 2 (meat thickness 0.145 cm)	31.15
13 plates control element alternative 2 (meat thickness 0.145 cm)	31.41
18 plates fuel element alternative 3 (meat thickness 0.145 cm)	27.94
14 plates fuel element alternative 3 (meat thickness 0.145 cm)	29.90
standard assembly	5.97
Be-element	5.66
gap between core box walls and core elements	53.57
core with 33 elements with 23 plates, 6 control elements with 19 plates, 17 standard assemblies and 25 Be-elements	1675
core as above with 15 (12) plates fuel (control) elements	1154
core as above with 16 (13) plates fuel (control) elements	1513
core as above with 18 (14) plates fuel (control) elements	1398
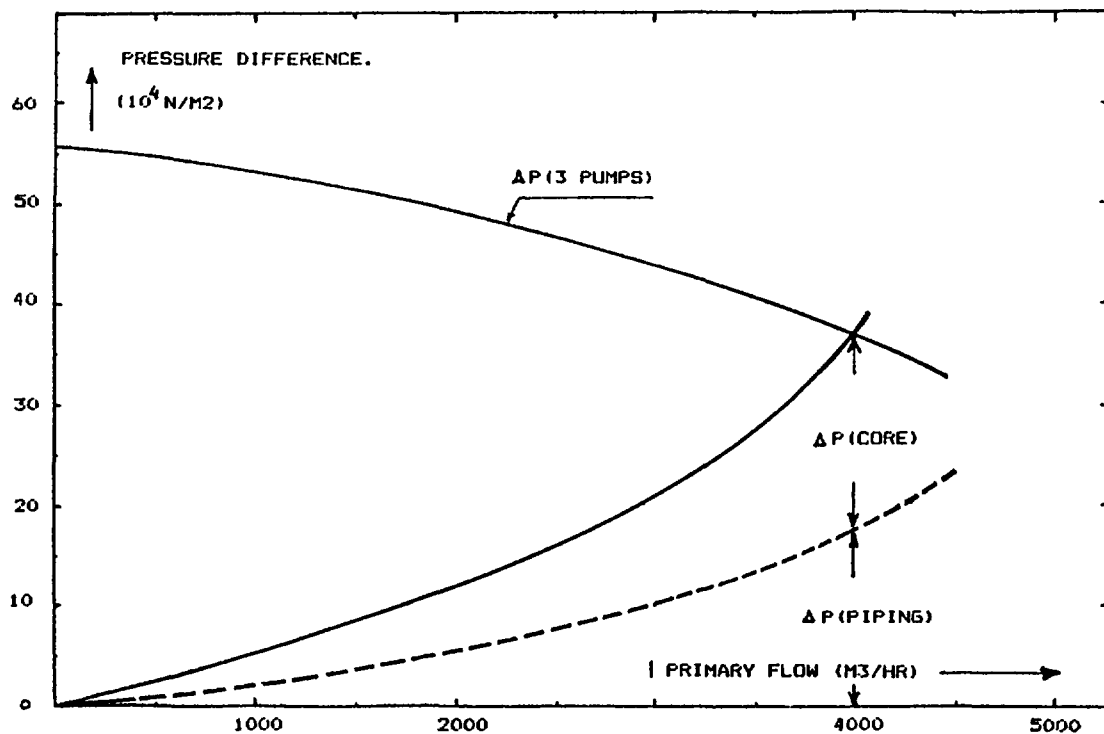
FIG 1   HYDRAULIC CHARACTERISTICS OF THE PRIMARY CIRCUIT OF THE HFR-PETTEN.

The pressure difference over a cooling channel in a fuel element, thus the pressure difference over the core is :

$$\Delta P_{core} = (\xi \frac{L}{D_H} + C_{w_{in}} + C_{w_{out}}) \tfrac{1}{2} \rho v^2 \tag{6}$$

in which :

L	= 0.62 m	is length of plate
D_H	= 2 d	is heated equivalent diameter
d(m)		is thickness coolant channel
ξ	= 0.3165 $Re^{-0.25}$	is Blasius formula
Re	= $\frac{v D_H}{\nu}$	is Reynolds number

v (m s^{-1})		is average coolant velocity in channel
$\nu = 0.553 \ 10^{-6} \ m^2 \ s^{-1}$		is kinematic viscosity
$C_{w_{in}} = 0.45$		is resistance inlet
$C_{w_{out}} = 1.00$		is resistance outlet
$\rho = 1000$ kg/m^3		is density of coolant

The pressure difference over the rest of the primary circuit can be approximated by

$$\Delta P_{piping} = C_p Q^2 \tag{7}$$

in which :

C_p   is a constant

Q ($m^3 \ s^{-1}$) is primary flow

For the present situation the nominal flow through the core is 4100 m^3/h, while the bypass flow through the former D_2O reflector is maintained upon 200 m^3/h. According to Fig. 1 the pressure difference over the pumps is 33.5 10^4 N/m^2 for a flow of 4300 m^3/h. The pressure difference over the core is for a flow of 4100 m^3/h according to (6) equal to 10.2 10^4 N/m^2 which is in good agreement with the measured value of 10.7 10^4 N/m^2.
From relation (5) it follows that the pressure difference over the piping is 23.3 10^4 N/m^2 for a flow of 4300 m^3/h. So relation (7) becomes

$$\Delta P_{piping} = 16.34 \ 10^4 \ Q^2 \tag{7a}$$

Using the relations (5), (6), (7a) and the characteristics of the primary pumps, Fig. 1, the primary flow can be calculated for the alternative fuel elements.

From this and the total cross section of the coolant in the core the average coolant velocity in the channels of these fuel elements can be calculated.

REFERENCES

|1| H. Röttger, A. Tas, P. von der Hardt, W.P. Voorbraak
High flux materials testing reactor HFR Petten
Characteristics of facilities and standard irradiation devices
EUR 5700e (1981)

|2| P. von der Hardt, A. Tas
Studies for a low-enriched MTR fuel cycle
Kerntechnik 20. Jahrgang (1978) No. 11

|3| R.J. Swanenburg de Veye
Operation of the HFR at 50 MW, system behaviour and safety analysis
RCN-int. 69-085

|4| A. Tas, G.J.A. Teunissen
Users report of HIP-TEDDI, a two dimensional, four group code for the
calculation of the neutron fluence in experiment positions and operating data
of the materials testing reactor H.F.R. at Petten.
EUR 6001 (April 1978)

|5| H. Pruimboom, A. Tas
Comparison of thermohydraulic and nuclear aspects in a standard core and a
typical LEU core for the HFR Petten, a case study
ANL/RERTR/TM-6, CONF-8410173

HOW TO ORDER IAEA PUBLICATIONS

■ An exclusive sales agent for IAEA publications, to whom all orders
and inquiries should be addressed, has been appointed
for the following countries:

CANADA
UNITED STATES OF AMERICA   UNIPUB, 4611-F Assembly Drive, Lanham, MD 20706-4391, USA

■ In the following countries IAEA publications may be purchased from the
sales agents or booksellers listed or through
major local booksellers. Payment can be made in local
currency or with UNESCO coupons.

ARGENTINA	Comisión Nacional de Energía Atómica, Avenida del Libertador 8250, RA-1429 Buenos Aires
AUSTRALIA	Hunter Publications, 58 A Gipps Street, Collingwood, Victoria 3066
BELGIUM	Service Courrier UNESCO, 202, Avenue du Roi, B-1060 Brussels
CHILE	Comisión Chilena de Energía Nuclear, Venta de Publicaciones, Amunategui 95, Casilla 188-D, Santiago
CHINA	IAEA Publications in Chinese: China Nuclear Energy Industry Corporation, Translation Section, P.O. Box 2103, Beijing IAEA Publications other than in Chinese: China National Publications Import & Export Corporation, Deutsche Abteilung, P.O. Box 88, Beijing
CZECHOSLOVAKIA	S.N.T.L., Mikulandska 4, CS-116 86 Prague 1 Alfa, Publishers, Hurbanovo námestie 3, CS-815 89 Bratislava
FRANCE	Office International de Documentation et Librairie, 48, rue Gay-Lussac, F-75240 Paris Cedex 05
HUNGARY	Kultura, Hungarian Foreign Trading Company, P.O. Box 149, H-1389 Budapest 62
INDIA	Oxford Book and Stationery Co., 17, Park Street, Calcutta-700 016 Oxford Book and Stationery Co., Scindia House, New Delhi-110 001
ISRAEL	Heiliger & Co. Ltd. 23 Keren Hayesod Street, Jerusalem 94188
ITALY	Libreria Scientifica, Dott. Lucio de Biasio "aeiou", Via Meravigli 16, I-20123 Milan
JAPAN	Maruzen Company, Ltd, P.O. Box 5050, 100-31 Tokyo International
PAKISTAN	Mirza Book Agency, 65, Shahrah Quaid-e-Azam, P.O. Box 729, Lahore 3
POLAND	Ars Polona-Ruch, Centrala Handlu Zagranicznego, Krakowskie Przedmiescie 7, PL-00-068 Warsaw
ROMANIA	Ilexim, P O. Box 136-137, Bucharest
SOUTH AFRICA	Van Schaik Bookstore (Pty) Ltd, P.O. Box 724, Pretoria 0001
SPAIN	Díaz de Santos, Lagasca 95, E-28006 Madrid Díaz de Santos, Balmes 417, E-08022 Barcelona
SWEDEN	AB Fritzes Kungl. Hovbokhandel, Fredsgatan 2, P.O. Box 16356, S-103 27 Stockholm
UNITED KINGDOM	HMSO, Publications Centre, Agency Section, 51 Nine Elms Lane, London SW8 5DR
USSR	Mezhdunarodnaya Kniga, Smolenskaya-Sennaya 32-34, Moscow G-200
YUGOSLAVIA	Jugoslovenska Knjiga, Terazije 27, P.O. Box 36, YU-11001 Belgrade

---

■ Orders from countries where sales agents have not yet been appointed and
requests for information should be addressed directly to:

**Division of Publications
International Atomic Energy Agency
Wagramerstrasse 5, P.O. Box 100, A-1400 Vienna, Austria**